

NMR Spectroscopy of Polymers in Solution and in the Solid State

ACS SYMPOSIUM SERIES **834**

NMR Spectroscopy of Polymers in Solution and in the Solid State

H. N. Cheng, Editor

Hercules Incorporated Research Center

Alan D. English, Editor

DuPont Central Research and Development



American Chemical Society, Washington, DC

QD 139 .P6N67 2003 c. 1

**NMR spectroscopy of polymers
in solution and in the**

Library of Congress Cataloging-in-Publication Data

NMR spectroscopy of polymers in solution and in the Solid State / H. N. Cheng, editor,
Alan D. English, editor.

p. cm.—(ACS symposium series ; 834)

Includes bibliographical references and indexes.

ISBN 0-8412-3808-1

1. Polymers—Analysis—Congresses. 2. Nuclear magnetic resonance spectroscopy—
Congresses

I. Cheng, H. N. II. English, Alan D., 1947- III. American Chemical Society. Division of
Polymer Chemistry, Inc. IV. American Chemical Society. . Meeting. (221st : 2001 : San
Diego, Calif.). V. Series.

QD139.P6 N67 2002
547 .7046—dc21

2002074775

The paper used in this publication meets the minimum requirements of American
National Standard for Information Sciences—Permanence of Paper for Printed Library
Materials, ANSI Z39.48-1984.

Copyright © 2003 American Chemical Society

Distributed by Oxford University Press

All Rights Reserved. Reprographic copying beyond that permitted by Sections 107 or
108 of the U.S. Copyright Act is allowed for internal use only, provided that a per-
chapter fee of \$22.50 plus \$0.75 per page is paid to the Copyright Clearance Center, Inc.,
222 Rosewood Drive, Danvers, MA 01923, USA. Republication or reproduction for sale
of pages in this book is permitted only under license from ACS. Direct these and other
permission requests to ACS Copyright Office, Publications Division, 1155 16th St.,
N.W., Washington, DC 20036.

The citation of trade names and/or names of manufacturers in this publication is not to be
construed as an endorsement or as approval by ACS of the commercial products or
services referenced herein; nor should the mere reference herein to any drawing,
specification, chemical process, or other data be regarded as a license or as a conveyance
of any right or permission to the holder, reader, or any other person or corporation, to
manufacture, reproduce, use, or sell any patented invention or copyrighted work that may
in any way be related thereto. Registered names, trademarks, etc., used in this
publication, even without specific indication thereof, are not to be considered unprotected
by law.

PRINTED IN THE UNITED STATES OF AMERICA

American Chemical Society
Library
1155 16th St. N.W.
Washington, D.C. 20036

In NMR Spectroscopy of Polymers in Solution and in the Solid State; Cheng, H., et al.;
ACS Symposium Series 834; American Chemical Society: Washington, DC, 2002.

Foreword

The ACS Symposium Series was first published in 1974 to provide a mechanism for publishing symposia quickly in book form. The purpose of the series is to publish timely, comprehensive books developed from ACS sponsored symposia based on current scientific research. Occasionally, books are developed from symposia sponsored by other organizations when the topic is of keen interest to the chemistry audience.

Before agreeing to publish a book, the proposed table of contents is reviewed for appropriate and comprehensive coverage and for interest to the audience. Some papers may be excluded to better focus the book; others may be added to provide comprehensiveness. When appropriate, overview or introductory chapters are added. Drafts of chapters are peer-reviewed prior to final acceptance or rejection, and manuscripts are prepared in camera-ready format.

As a rule, only original research papers and original review papers are included in the volumes. Verbatim reproductions of previously published papers are not accepted.

ACS Books Department

Preface

NMR spectroscopy is a vibrant and still rapidly growing field. Its utility as a research and as a problem-solving tool is well recognized. One of the most fruitful areas of its application is polymer science. The NMR spectroscopy field has attracted a large number of talented scientists and is constantly being refreshed by fundamental research and new improved methodologies. Because of the importance of polymers to industry, substantial investment has been made in NMR spectroscopy in industrial laboratories. Thus, excellent research work is being done not only in academia and in government laboratories but also in industry.

In view of the rapid advances being made in this field, we organized a three-day symposium at the 221st ACS National Meeting in San Diego, California, on April 3–5, 2001. The symposium was very successful, with 52 oral and poster papers and 45 presenters. Among the participants were leaders and active researchers in this field, with roughly equal representation from academia, industrial companies, and government laboratories. Thus, the presenters brought different skills and provided a balanced perspective as to the current practice of polymer NMR. Another feature of the symposium was its international nature; roughly 30% of the presenters came from outside the United States. Indeed, some of the best work in this field today is being done in Europe and Japan.

Because polymer NMR papers tend to be published in a number of different journals, we thought it would be beneficial to assemble the symposium papers into one book. This symposium volume is the result. Hopefully this book will be a useful reference work for students and practitioners of polymer NMR, as well as a practical handbook for many state-of-the-art NMR techniques. A total of 31 chapters are included herein, including an overview chapter (Chapter 1). For convenience, this book is organized into five sections: solid-state NMR of polymers, solution NMR of synthetic polymers, solution NMR of natural polymers, combined NMR-separation techniques, and dynamics of polymers in solution.

We are thankful to all the contributors of this volume, who not only took time to prepare the chapters but also observed the deadlines and followed the format of the symposium volume. Special thanks are due to Professor Peter Rinaldi who wrote an invited paper on 3D NMR (Chapter 8). We are also grateful to the ACS Books Department for agreeing to publish this symposium volume.

H. N. Cheng

Hercules Incorporated
500 Hercules Road
Wilmington, DE 19808–1599

Alan D. English

DuPont Central Research and Development
Experimental Station E356/103
Wilmington, DE 19880–0356

Prologue

Two topics both alike in pedigree,
In polymer science where we lay our scene,
From ancient art evolve fresh artistry,
Attaining a success that's unforeseen.

To the advancement of these same techniques
A lot of scientists dedicate their life,
Whose solid and solution work bespeaks
A field still flourishing and free of strife.

The lure of NMR, combined with love,
And popular usage and patronage,
Which, though impressive, has room to improve,
Is now this story with many a page;

The which if you with patient eyes attend,
What here shall miss, our toil shall strive to mend.

H. N. Cheng

A parody inspired by William Shakespeare's *Romeo and Juliet*.

Chapter 1

Advances in the NMR Spectroscopy of Polymers: An Overview

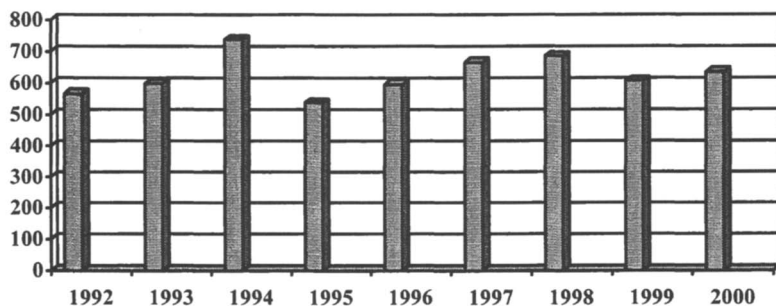
H. N. Cheng¹ and Alan D. English²

¹Hercules Incorporated Research Center, 500 Hercules Road,
Wilmington, DE 19808-1599

²DuPont Central Research and Development, Experimental Station,
Wilmington, DE 19880-0356

NMR spectroscopy is being used extensively to study both synthetic and natural polymers. Many techniques and methodologies have been developed, and these have been applied to a large number of polymeric systems. An overview is provided here of the recent advances in this field, covering both liquid-state and solid-state NMR. For illustration, pertinent examples are taken from selected publications in the literature and from the papers included in this symposium volume.

NMR spectroscopy is a well-known and popular technique for polymer characterization. The literature on this topic is vast and continues to grow. For example, according to Chemical Abstracts the number of publications containing “NMR” and “polymer” as the key words has hovered around 600 per year in the last few years.



In the past 4-5 years, quite a number of relevant review articles and books have appeared. These included general reviews on NMR of polymers (1-10), reviews on solid state NMR (11-15), solid state multidimensional techniques (16-19), spatially resolved techniques (20), solid state NMR studies of polymer dynamics and structure (21), hydrated polymers (22), vulcanized elastomers (23), crosslinked polymers (24), and polymer networks (25). Reviews have also been written on polymer gels (26-28), polymer colloids (29), polymer-surfactant systems (30), and polymers on surfaces (31).

In liquid state NMR, other than the general reviews noted above, reviews have appeared on chemical shift calculations (32) and on computer-assisted approaches (33). In addition, the NMR of polypropylene (34) and dienes and polyenes (35) has been specifically reviewed.

NMR imaging has been increasingly applied to polymeric materials. Several reviews have appeared (36-41).

In this article, an overview is given of this field, with an emphasis on the development of new or improved techniques and methodologies. In order to narrow the scope, only solution and solid state NMR techniques are covered. The polymeric systems chosen as examples are taken from the literature and particularly from the papers included in this symposium volume (42-71). Also included are selected preprints taken from the papers presented at the international symposium on High Resolution NMR Spectroscopy of Polymers held at the ACS National Meeting in April, 2001 in San Diego, CA (72-87).

Solution NMR

The use of solution NMR for polymer analysis has become routine in many laboratories. NMR is used to monitor the extent of a reaction, to check the purity of polymers, to identify unknown materials, and to study polymer

microstructure, dynamics, and interactions. Because of its wide usage, a large number of new or improved techniques and methodologies continue to appear. A summary of many of these developments is given below.

1. Multidimensional NMR

Since its introduction to polymer studies in the early 1980s, two-dimensional (2D) NMR (88) has continued to surprise and to delight NMR spectroscopists with the range and the depth of its problem-solving ability. This technique has become widely practiced and is commonly being used (89). In this volume Newmark has reviewed some of the standard 2D experiments and compared their performance (54). Brar *et al.* have applied 2D experiments to poly(vinyl alcohol) (53) and to acrylonitrile copolymers (52). Chai *et al.* have reported a 2D NMR study of polyurethane dendritic wedges (51). Xu *et al.* have used 2D NMR to assign the NMR spectra of ethylcellulose (65). In their spectral assignments of polypropylene, Segre *et al.* have obtained relevant 2D NMR data (55). 2D NMR has also been used in the papers by Martinez-Richa (59), Sachinvala *et al.* (64), and Yang *et al.* (58).

Three-dimensional (3D) NMR is an upcoming area that holds a lot of promise. Peter Rinaldi, who is an acknowledged leader in 2D and 3D NMR, has written a timely and authoritative review in a special Invited Paper (48). In addition, he and his coworkers have used 3D NMR and triple resonance methods to study poly(dimethylsiloxanes) (50), and fluoropolymers (49).

2. Hyphenated Techniques

One of the research trends in analytical chemistry is the combining of analytical techniques, and polymer chemistry is no exception. In fact, combined fractionation-NMR (off-line) has been around for many years (90). Recently, many papers have appeared, coupling NMR to SEC and LC, either off-line or on-line. An off-line SEC-NMR investigation of several copolymers has been reported by Montaudo *et al.* (68). On-line SEC-NMR studies have been made of polymer mixtures by Wu and Beshah (67), and of alginates by Neiss and Cheng (69). On-line HPLC-NMR has been used for oligomer analysis by Hiller and Pasch (66). On-line liquid chromatography critical adsorption point (LCCAP)-NMR has been employed to study tacticity distribution of poly(ethyl methacrylate) by Ute *et al.* (84).

In the literature, supercritical fluid chromatography (SFC)-NMR has been engaged for the analysis of plasticizers (91). Off-line capillary electrophoresis-NMR has also been reported, and a recent review is available (92).

3. Isotopic Labeling

Isotopic labeling is a very useful technique in NMR studies of polymers. For example, ^{13}C NMR studies of polymers and copolymers prepared using ^{13}C -enriched initiators have been carried out to obtain information about the chemo-, regio-, and stereo-selectivity of radicals derived from such initiators (93-95). In addition, ^{19}F and ^{31}P labeling has permitted the studies of chain ends obtained from ^{19}F and ^{31}P -containing initiators and chain transfer agents (72,95).

^{13}C and ^2H labeling has been one of the methods employed to study the reaction mechanism of cationic ring-opening copolymerization of trioxane and dioxolane (73). In the literature, specific ^{13}C labeling has been used for Ziegler-Natta and metallocene catalysis in order to probe reaction mechanism (96). Segre *et al.* have employed ^{13}C -enriched CO to quench propylene polymerization and to determine the structure of active chain ends (55).

Isotopic labeling can facilitate relaxation studies of polymers. In their relaxation studies, Blum and Durairaj have used ^2H labeling on their polyacrylates (70). Luther *et al.* have labeled their polyphosphazenes with ^{15}N in their work (71).

4. Theoretical Modeling

One of the advantages of NMR in polymer solution studies is the wealth of information available. A NMR spectrum may contain information on polymer microstructure, polymerization mechanism, side reactions, compositional heterogeneity, and (sometimes) molecular weight. Frequently, the challenge is to interpret the spectrum, to extract the relevant information, and to maximize the information content. One way whereby this can be accomplished is through theoretical modeling. This can be carried out, for example, for the polymer structure, polymerization statistics, and reaction kinetics.

The use of statistical models to interpret (and to rationalize) NMR tacticity and sequence data is well established (97,98). In this volume the enantiomorphic-site model has been used by Segre *et al.* in their studies of polypropylene at high fields (55). A two-site model has been employed by Shimozawa *et al.* to observe the effects of internal donors in propylene polymerization (56). Other models for polyolefins have been reported in the literature, e.g., the multi-site model (99), the dual catalytic-site/chain-end model (100), the perturbed model (101), the consecutive two-site model (102), the four-component model (103), and the chain end model (104).

A recent theoretical development is the use of NMR to study compositional heterogeneity. Two approaches can be used: 1) perturbed Markovian (continuous) model (105), and 2) multi-component (discrete) model (99). Neiss and Cheng have applied the discrete model to the SEC-NMR data of alginates (69). In an earlier work, the NMR data of alginates have also been fitted to a continuous model (106).

5. Computer-Assisted Methodologies

Computer methods have often been engaged for polymer microstructural studies (33). A common methodology is to use the computer to fit the observed data to a given theoretical model (model-fitting or analytical approach). Examples are the data treatment given in the papers by Segre *et al.* (55), Shimozawa *et al.* (56), and Neiss and Cheng (69). An alternative method is to simulate or to predict the observed data (simulation or synthetic approach). The data may be the NMR spectrum (107), NMR tacticity or sequence intensities (108), or the chemical composition distribution (109). Examples in the literature include polystyrene tacticity (using a statistical model) (110) and low-density polyethylene (using a kinetic model) (111).

Molecular modeling and conformational analysis has been used by Martinez-Richa *et al.* to determine the minimum-energy conformers in polyimides (59). Molecular modeling has also been employed for the conformational analysis of polyisocyanate model compounds (85). A review article on NMR conformational analysis has recently appeared (112).

In the identification of unknown polymers, it is often necessary to search an appropriate spectral library. Computer methods have been reported that help in this search (113,114). Many other papers have also reported the use of computers in various contexts, but space limitations preclude a comprehensive coverage here.

6. Relaxation Studies

The use of NMR relaxation in polymer solutions is well known (115). This is an excellent technique to study polymer chain dynamics (116), polymer/polymer, polymer/solvent, polymer/additive interactions (117), and phase transitions (118).

In this volume, Blum and Durairaj have used ^2H relaxation to probe the dynamics of deuterated polyacrylates in concentrated chloroform solutions (70). Luther *et al.* have carried out ^{15}N and T_1 relaxation studies to elucidate the interaction between lithium ions and ^{15}N -labelled polyphosphazenes (71).

Baianu and Ozu have used low-field relaxation data (together with high-resolution ^1H and ^{13}C spectra) to study the gelling mechanism of glucomannans in water (63).

7. Other Methods

Because of the need for spectral assignments, the *prediction of chemical shifts* remains an active area of research. Two popular methods are γ -gauche rotational isomeric state (RIS) model (119) and the empirical additive shift rules (120,121). For example, in their polyester work, Fawcett *et al.* have derived empirical additive shift rules that pertain to their polymeric system (57).

Diffusion measurements continue to be a recurring theme in the NMR literature. Quite a few papers have been published on diffusion in polymer solutions, mostly with the pulsed field gradient (PFG) technique (122). Diffusion-ordered spectroscopy (DOSY), a 2D method based on PFG, has been used on several polymer systems (123). A different approach to diffusion measurement has also been reported (124).

An exciting technique is *rheo-NMR*, being further developed by Callaghan (125). In this way the NMR behavior and rheology of complex fluids can be studied. An alternative method is the use of NMR *imaging* to study polymer rheology (126).

Another development is *nano-NMR*, which uses a probe containing a small-volume sample cell that rotates at ~ 2 kHz about the magic angle. This technique is suitable for studies of heterogeneous samples as well as for samples that are limited in quantity. This has been successfully applied to carbohydrates (83).

An interesting trend is the increasing use of *in situ NMR* to study polymerization kinetics, curing reactions, or to determine the comonomer reactivity ratios (127). *High-pressure*, high resolution ^1H NMR has been employed to study polymer/solvent interactions in poly(1,1-hydroperfluorooctyl acrylate) and its copolymer with styrene (128).

8. Application Areas

In view of its problem solving ability, it is not surprising that liquid-state NMR has been applied to a wide range of polymeric materials. A relatively comprehensive review of the different polymer types has recently appeared (1). A brief survey is given below.

a. Addition Polymers

These polymers have been widely studied by NMR. In general, there are several types of information available, depending on the polymer in question.

- stereochemistry, e.g., homopolymer tacticity
- regiochemistry, e.g., normal or inverted monomer addition
- comonomer sequence placement (in copolymers)
- compositional and tacticity heterogeneity
- molecular weight effects, e.g., chain end structures in low-molecular-weight polymers
- branching and crosslinked structures
- geometric isomerism, e.g., cis and trans isomers in polydienes

Addition polymers reported in this volume include fluoropolymers (49), polypropylene (55,56), polystyrene (66,67), polyacrylates (54,70), styrene-ethyl acrylate copolymer (66), styrene-methyl methacrylate copolymer (67,68), and acrylonitrile copolymers (52).

b. Condensation Polymers

Condensation polymers are easily amenable to NMR analysis. However, the information content is variable, depending on the polymer structures involved. There are several examples of condensation polymers in this volume:

- i. Polyesters (57)
- ii. Polyurethanes (51)
- iii. Polyimides (59)
- iv. Polysiloxanes (50)
- v. Phenolic polymers (60)

c. Ring-Opening Polymers

Examples given in this volume are the papers by Yang (on the cationic copolymerization of trioxane and 1,3-dioxepane) (58) and by Luther (on ¹⁵N-labelled polyphosphazenes) (71). Poly(ethylene oxide) is also included in the HPLC-NMR studies by Hiller and Pasch (66).

d. Natural polymers

The use of NMR for natural polymers is widespread. A large part of the effort has been directed towards proteins and polynucleotides. Two excellent examples are given in two preprints (81,82). Similarly, the polysaccharide area has its share of NMR studies. In this volume, Bush has expounded the origins of the flexibilities of complex polysaccharides (61). Huckerby *et al.* have carried out a careful structural investigation of keratan sulfates using NMR (62), and

Neiss and Cheng have studied the microstructure of alginates and related it to the action of enzymes (69). Baianu and Ozu have examined the gelling mechanism of konjac gum and its interactions with proteins (63). Other studies include bacterial exopolysaccharides (86) and oligosaccharides (83,87).

e. Polymer Reactions

Frequently the polymers found in nature or made commercially need some improvements in their end-use properties for specific applications. In such cases, modification reactions can be made on the polymers. A notable case is cellulose, which is insoluble in water and in most organic solvents. Suitable reactions are done industrially to convert it to esters or ethers. Sachinvala *et al.* have synthesized a number of di- and tri-substituted cellulose ethers and characterized them by NMR (64). Xu *et al.* have used 2D NMR to analyze ethyl cellulose, a commercial polymer (65). Newmark has used 2D NMR to study cellulose acetate butyrate (54). Other uses of NMR to study polymer reactions have been reviewed elsewhere (129).

Solid State NMR

1. General Comments

A variety of NMR methods can be used to characterize the structure and dynamics of polymers (both synthetic and naturally occurring) over a wide range of length and time scales. The length scales probed correspond to: 1) the primary chemical structure of the macromolecular chain (monomer content, sequencing, tacticity, etc.), 2) the secondary structure which is usually a two dimensional ordering such as a hydrogen-bonded sheet, and 3) the tertiary structure such as globular folding in proteins or the three dimensional crystal structure. Beyond these length scales, that are appropriate for individual molecules, are length scales that are characteristic of the morphology and/or phase structure.

Characterization of the polymer primary structure is best carried out using solution NMR methods due to the increased spectral specificity of 'solution' NMR methods as compared to solid state NMR methods. 'Solution' NMR methods here includes solutions, gels, dispersions, melts, etc. Any method involving dilution, dispersion, increased temperature, etc. that will introduce sufficient motion into the polymer chain such that the unwanted nuclear spin interactions can be averaged to their trace values (zero for dipolar, isotropic chemical shift for the chemical shift anisotropy, scalar coupling for the indirect dipolar interaction, and zero for quadrupolar), on a sufficiently short time scale,

will advance the ability to observe a 'solution' NMR spectrum. For many naturally occurring polymers and all thermoplastic synthetic polymers, solution NMR methods are the best approach. For a few naturally occurring polymers (45,46) and most thermosetting (43) synthetic polymers, it can be impossible to obtain a 'solution' NMR spectrum without significantly modifying the backbone structure. In these cases, even for the characterization of the primary chemical structure of the molecule, solid-state NMR methods may be required. A classic comparison of the information available from solution and solid state ^{13}C NMR methods is available (130). For determination of the primary chemical structure in the solid state the primary experiment utilized is the cross-polarization magic angle spinning (CP/MAS) ^{13}C NMR experiment. This experiment and a variety of other solid state NMR experiments are lucidly described in a book (131).

Investigations of the secondary or tertiary structure of polymers cannot be carried out with solution NMR methods because the very act of 'dissolution' destroys these structures. The chain conformation of a polymer that is intimately associated with another material, such as an inclusion complex (44), and the phase structure of a blend (42) are two examples of the importance of longer length scale structures requiring that the structure at all length scales be determined in the solid state.

Furthermore, characterization of the molecular dynamics must be carried out in the solid state if the objective is to understand the dynamic structure in the solid state (47). This information can be related to other relaxation methods such as anelastic and dielectric relaxation to develop an understanding of a variety of properties such as toughness, permeability, secondary/tertiary structure, and structure/property/processing relationships.

2. Experimental Techniques

Solid state NMR is a vibrant and exciting field where many new techniques appear regularly. An overview of some selected techniques is given here.

a. Techniques for Polymer Structure and Conformation

The solid state NMR spectrum tends to have broad lines because of chemical shift anisotropy and dipolar and quadrupolar couplings (11,15,130-134). The use of high-power dipolar decoupling, cross polarization (CP) and magic angle spinning (MAS) to produce high resolution ^{13}C spectra and to cut down on the instrument running time is well known (135). Likewise, the combined rotation and multi-pulse (CRAMPS) experiment can permit ^1H spectra with narrower linewidths to be obtained (136). Recently, with increasing

spinning rates (up to 50 KHz), MAS alone can sometimes produce relatively narrow lines in the ^1H solid state spectra (14,137).

For these high-resolution solid state spectra, many techniques analogous to those used in solution NMR can be applied. For example, 2D HETCOR experiments have been achieved using several pulse sequences (138). 2D double quantum correlation NMR (equivalent to 2D inadequate in solution and requiring ^{13}C -labelled spin pairs) has been found to be a good technique to study chain conformations in the solid state (139). Homonuclear ^1H - ^1H double quantum MAS experiment has been used to get detailed structural information for several chemical systems (140).

In addition, the rotational-echo double resonance (REDOR) is a powerful technique to determine distances between two hetero-nuclei (141). Methods have also been developed that permit the detection of torsional angles (142).

b. Techniques for Polymer Morphology

A major application of solid state NMR is the study of polymer morphology. Information potentially available includes the amount and orientation of crystalline phases in semi-crystalline polymers and the domain sizes in phase-separated polymeric systems. For the determination of crystallinity, a common method is to measure T_1 relaxation in ^1H NMR (or ^2H NMR for deuterated polymers). The relaxation data can often be resolved into two (or more) components, which may correspond to magnetization arising from crystalline and amorphous phases (11-15,130-134). The development of the maximum entropy regularization method has permitted more facile and less subjective analysis of the data (143). In optimal cases, multiple components can be identified.

An alternative approach is to determine the crystalline content from the solid state NMR spectra. For example, this can sometimes be done from ^{13}C NMR spectra with MAS or CP/MAS experiments. Another way to study semi-crystalline polymers is ^{129}Xe spectroscopy, whereby the degree of crystallinity, free volume, and the presence of micropores in polymeric materials may be ascertained (144).

NMR is particularly suited for the measurement of domain sizes in the range of 5 – 200 Å (145), which can be probed with a spin diffusion experiment, e.g., Goldman-Shen sequence (146) and dipolar filter pulse sequence (147). The use of multidimensional techniques to study length scales in heterogeneous polymers has been previously reviewed by Spiess (148).

c. Techniques for Polymer Dynamics

Among the most popular methods to study polymer dynamics are the

relaxation times, T_1 , T_2 , $T_{1\rho}$, and T_{CH} , and nuclear Overhauser effects (NOE) (11-15, 130-134). T_1 and NOE are sensitive to higher frequency motions (10^8 - 10^{12} s), whereas $T_{1\rho}$ and T_{CH} are sensitive to lower frequency motions (10^0 - 10^5 s).

A second group of techniques may be called "lineshape analysis." Simple methods entail the measurements of linewidths or second moments as a function of temperature. More sophisticated methods involve the analysis or the model fitting of spectral lineshapes. A prominent method is 1D ^2H lineshape analysis for deuterium-labeled polymers, which is sensitive to motions in the frequency range of 10^4 - 10^7 s (149). The 2D wideline separation NMR (WISE) experiment permits correlation of the ^{13}C high resolution spectrum with the wideline ^1H spectrum, which provides dipolar information (11, 150). The ^1H linewidth is a function of the frequency of the polymer motion relative to the time scale of dipolar couplings.

For low-frequency motions (10^0 - 10^4 s), the 2D ^2H exchange experiments are useful techniques (19). Other exchange experiments are also informative, e.g., the one-dimensional exchange spectroscopy by sideband alternation (ODESSA) (151), time-reversed ODESSA (152), and centerband-only detection of exchange (CODEX) (153). Many advanced techniques are given in a recent, excellent review by Brown and Spiess (14).

References

1. Cheng, H. N. *Structural Studies of Polymers by Solution NMR*, RAPRA Report 125, Rapra, Shewsbury, UK. (*Rapra Rev.* **2001**, 11(5), 1).
- 2.. Mirau, P. A. in *Appl. Polym. Sci.*; Craver, C. D. Carraher, C. E., Jr, Eds.; Pergamon, Oxford, **2000**, pp. 787-815.
- 3.. Ando, I.; Kobayashi, M.; Kanekiyo, M.; Kuroki, S.; Ando, S.; Matsukawa, S.; Kurosu, H.; Yasunaga, H.; Amiya, S. in *Exp. Methods Polym. Sci.* Tanaka, T. Ed., Academic Press, San Diego, **2000**, pp. 261-493.
4. Smith, P. B.; Pasztor, A. J., Jr.; McKelvy, M. L.; Meunier, D. M.; Froelicher, S. W.; Wang, F. C.-Y. *Anal. Chem.* **1999**, 71, 61R
5. Kurosu, H.; Yamanobe, T. *Nucl. Magn. Reson.* **1999**, 28, 364
6. Kurosu, H.; Yamanobe, T. *Nucl. Magn. Reson.* **1998**, 27, 337.
7. Fawcett, A. H. *Nucl. Magn. Reson.* **1997**, 26, 356.
8. Smith, P. B.; Pasztor, A. J., Jr.; McKelvy, M. L.; Meunier, D. M.; Froelicher, S. W.; Wang, F. C.-Y. *Anal. Chem.* **1997**, 69, 95R
9. *NMR of Polymers*; Bovey, F. A.; Mirau, P. A. Academic Press, San Diego, 1996.
10. *NMR Spectroscopy and Stereoregularity of Polymers*; Matsuzaki, K.; Uryu, T.; Asakura, T. Japan Sci. Soc. Press, Tokyo, 1996.

11. Mirau, P. A. *Solid State NMR of Polymers*, RAPRA Report 128, Rapra, Shewsbury, UK. (*Rapra Rev.* **2001**, 11(8), 1).
12. Aliev, A. E.; Law, R. V. *Nucl. Magn. Reson.* **2001**, 30, 214
13. Dybowski, C.; Bai, S. *Anal. Chem.* **2000**, 72, 1.
14. Brown, S. P.; Spiess, H. W. *Chem. Rev.* **2001**, 101, 4125.
15. *Solid State NMR of Polymers*; Ando I.; Asakura, T. Elsevier, New York, 1998.
16. Spiess, H. W. *AIP Conf. Proc.* **2000**, 519, 33.
17. Spiess, H. W. *Annu. Rep. NMR Spectrosc.* **1997**, 34, 1.
18. Spiess, H. W. *ACS Polym. Prepr.* 1997, 38(1), 768.
19. *Multidimensional Solid-State NMR and Polymers*; Schmidt-Rohr, K.; Spiess, H.W. ; Academic Press, San Diego, 1994.
20. Blumich, B.; Blumler, P.; Gasper, L.; Guthausen, A.; Gobbels, V.; Laukemper-Ostendorf, S.; Unseld, K.; Zimmer, G. *Macromol. Symp.* **1999**, 141, 83.
21. Horii, F.; Kaji, H.; Ishida, H.; Kuwabara, K.; Masuda, K.; Tai, T. *J. Mol. Struct.* **1998**, 441, 303.
22. McBrierty, V. J.; Martin, S. J.; Karasz, F. E. *J. Mol. Liq.* **1999**, 80, 179.
23. Mori, M.; Koenig, J. L. *Annu. Rep. NMR Spectrosc.* **1997**, 34, 231.
24. Whittaker, A. K. *Annu. Rep. NMR Spectrosc.* **1997**, 34, 105.
25. Smirnov, L. P. *Vysokomol. Soedin., Ser. A Ser. B* **2000**, 42, 1775.
26. Yasunaga, H.; Kobayashi, M.; Matsukawa, S.; Kurosu, H.; Ando, I. *Annu. Rep. NMR Spectrosc.* **1997**, 34, 39.
27. Matsukawa, S.; Y., H.; Zhao, C.; Kuroki, S.; Kurosu, H.; Ando, I. *Prog. Polym. Sci.* **1999**, 24, 995.
28. Cohen Addad, J. P. *Prog. Nucl. Magn. Reson. Spect.* **1993**, 25, 1.
29. Preuschen, J.; Rottstegge, J.; Spiess, H. W. *Colloids Surf., A* **1999**, 158, 89.
30. Stilbs, P. in *Polymer-Surfactant Systems*; M. Dekker; 1998. (*Surfactant Sci. Ser.* **1998**, 77, 239).
31. Blum, F. D. in *Colloid-Polym. Interact.*; Farinato, R. S.; Dubin, P.L., Eds.; pp. 207-223, Wiley, New York, 1999.
32. Ando, I.; Kuroki, S.; Kurosu, H.; Yamanobe, T. *Prog. Nucl. Magn. Reson. Spectrosc.* **2001**, 39, 79.
33. Cheng, H. N. *Polym. News* **2000**, 25, 114.
34. Busico, V.; Cipullo, R. *Prog. Polym. Sci.* **2001**, 26, 443
35. Takeuchi, Y.; Takayama, T. in *Chem. Dienes Polyenes*; Rappoport, Z., Ed.; Wiley, Chichester, UK, 2000, Vol. 2, pp. 59-196.
36. Demco, D.E.; Blumich, B. *Curr. Opin. Solid State Mater. Sci.* **2001**, 5, 195.
37. Watanabe, T. *Nucl. Magn. Reson.* **2001**, 30, 453.
38. Miller, J. B. *Prog. Nucl. Magn. Reson. Spectrosc.* **1998**, 33, 273.
39. Watanabe, T. *Nucl. Magn. Reson.* **1997**, 26, 447.
40. Parker, D. D.; Koenig, J. L. *Curr. Trends Polym. Sci.* **1996**, 1, 65.

41. Cheng, H. N.; Early, T. A. *Macromol. Symp.* **1994**, *86*, 1.
42. Mirau, P. A.; Yang, S. *ACS Symp. Ser.* (this volume), Chap. 2; also, *ACS Polym. Prepr.* **2001**, *42*(1), 47.
43. Thakur, K. A. *ACS Symp. Ser.* (this volume), Chap. 3; also, *ACS Polym. Prepr.* **2001**, *42*(1), 57.
44. Tonelli, A. E.; Lu, J.; Mirau, P. A. *ACS Symp. Ser.* (this volume), Chap. 4; also, *ACS Polym. Prepr.* **2001**, *42*(1), 53.
45. Tang, S.; Jacob, M. M.; Li, L.; Cholli, A. L.; Kumar, J. *ACS Symp. Ser.* (this volume), Chap. 5; also, *ACS Polym. Prepr.* **2001**, *42*(1), 19.
46. Asakura, T.; Ashida, J.; Yamane, T. *ACS Symp. Ser.* (this volume), Chap. 6; also, *ACS Polym. Prepr.* **2001**, *42*(1), 61.
47. Chujo, R.; Fukutani, K.; Magoshi, Y. *ACS Symp. Ser.* (this volume), Chap. 7; also, *ACS Polym. Prepr.* **2001**, *42*(1), 29.
48. Rinaldi, P. L. *ACS Symp. Ser.* (this volume), Chap. 8.
49. Assemat, O.; Rinaldi, P. L. *ACS Symp. Ser.* (this volume), Chap. 9; also, *ACS Polym. Prepr.* **2001**, *42*(1), 9.
50. Chai, M.; Rinaldi, P. L.; Hu, S. *ACS Symp. Ser.* (this volume), Chap. 10; also, *ACS Polym. Prepr.* **2001**, *42*(1), 15.
51. Chai, M.; Rinaldi, P. L.; Puapaiboon, U.; Taylor, R. T. *ACS Symp. Ser.* (this volume), Chap. 11; also, *ACS Polym. Prepr.* **2001**, *42*(1), 33.
52. Brar, A.S. *ACS Symp. Ser.* (this volume), Chap. 12; also, *ACS Polym. Prepr.* **2001**, *42*(1), 11.
53. Brar, A.S.; Kumar, R.; Yadav, A.; Kaur, M. *ACS Symp. Ser.* (this volume), Chap. 13; also, *ACS Polym. Prepr.* **2001**, *42*(1), 43.
54. Newmark, R. A.; Battiste, J. L.; Koivula, M. N. *ACS Symp. Ser.* (this volume), Chap. 14; also, *ACS Polym. Prepr.* **2001**, *42*(1), 17.
55. Busico, V.; Mannina, L.; Segre, A. L.; Van Axel Castelli, V. *ACS Symp. Ser.* (this volume), Chap. 15; also, *ACS Polym. Prepr.* **2001**, *42*(1), 6.
56. Shimozawa, K.; Saito, M.; Chujo, R. *ACS Symp. Ser.* (this volume), Chap. 16; also, *ACS Polym. Prepr.* **2001**, *42*(1), 28.
57. Andrews, G.P.; Fawcett, A. H.; Hania, M.I.M. *ACS Symp. Ser.* (this volume), Chap. 17; also, *ACS Polym. Prepr.* **2001**, *42*(1), 37.
58. Cui, M.-H.; Zhang, Y.; Werner, M.; Yang, N.-L.; Fenelli, S. P.; Grates, J.A. *ACS Symp. Ser.* (this volume), Chap. 18; also, *ACS Polym. Prepr.* **2001**, *42*(1), 21.
59. Martinez-Richa, A.; Vera-Graziano, R.; Likhatchev, D. *ACS Symp. Ser.* (this volume), Chap. 19; also, *ACS Polym. Prepr.* **2001**, *42*(1), 13.
60. Sahoo, S. K.; Liu, W.; Samuelson, L.; Kumar, J.; Cholli, A. L. *ACS Symp. Ser.* (this volume), Chap. 20; also, *ACS Polym. Prepr.* **2001**, *42*(1), 35.
61. Bush, C. A. *ACS Symp. Ser.* (this volume), Chap. 21; also, *ACS Polym. Prepr.* **2001**, *42*(1), 62.

62. Huckerby, T. N.; Brown, G. M.; Lauder, R. M.; Nieduszynski, I. A. *ACS Symp. Ser.* (this volume), Chap. 22; also, *ACS Polym. Prepr.* **2001**, 42(1), 78.
63. Baianu, I.C.; Ozu, E.M. *ACS Symp. Ser.* (this volume), Chap. 23; also, *ACS Polym. Prepr.* **2001**, 42(1), 65.
64. Sachinvala, N. D.; Winsor, D. L.; Niemczura, W. P.; Maskos, K.; Vigo, T. L.; Bertoniere, N. R. *ACS Symp. Ser.* (this volume), Chap. 24; also, *ACS Polym. Prepr.* **2001**, 42(1), 81.
65. Xu, Q.; Brickhouse, M.D.; Wang, H. *ACS Symp. Ser.* (this volume), Chap. 25; also, *ACS Polym. Prepr.* **2001**, 42(1), 83.
66. Hiller, W. G.; Pasch, H. *ACS Symp. Ser.* (this volume), Chap. 26; also, *ACS Polym. Prepr.* **2001**, 42(1), 66.
67. Wu, J.; Beshah, K. *ACS Symp. Ser.* (this volume), Chap. 27; also, *ACS Polym. Prepr.* **2001**, 42(1), 23.
68. Montaudo, M.S. *ACS Symp. Ser.* (this volume), Chap. 28; also, *ACS Polym. Prepr.* **2001**, 42(1), 69.
69. Neiss, T.G.; Cheng, H.N. *ACS Symp. Ser.* (this volume), Chap. 29; also, *ACS Polym. Prepr.* **2001**, 42(1), 76.
70. Blum, F. D.; Durairaj, R. B. *ACS Symp. Ser.* (this volume), Chap. 30; also, *ACS Polym. Prepr.* **2001**, 42(1), 71.
71. Luther, T. A.; Harrup, M. K.; Stewart, F. F. *ACS Symp. Ser.* (this volume), Chap. 31; also, *ACS Polym. Prepr.* **2001**, 42(1), 72.
72. Harwood, H. J.; Barkes, B. R.; Medsker, R. *ACS Polym. Prepr.* **2001**, 42(1), 2.
73. Yang, N.-L.; Dunn, P.; Werner, M.; Fenelli, S. P.; Grates, J. A. *ACS Polym. Prepr.* **2001**, 42(1), 4.
74. Grassi, A.; Trezza, E. *ACS Polym. Prepr.* **2001**, 42(1), 26.
75. Fawcett, A. H.; Burns, W.; Foster, A. B. *ACS Polym. Prepr.* **2001**, 42(1), 31.
76. Steckle, W. P.; Anglois, D. A.; Small, J. H. *ACS Polym. Prepr.* **2001**, 42(1), 41.
77. De Angelis, A. A.; Segre, A. L.; Capitani, D.; Crescenzi, V. *ACS Polym. Prepr.* **2001**, 42(1), 45.
78. Inglefield, P. T.; Jones, A.A.; Wen, W.; Wang, Y. *ACS Polym. Prepr.*, **2001**, 42(1), 49.
79. Wutz, C.; Samulski, E. T.; Tanner, M.; Brookhart, M. *ACS Polym. Prepr.*, **2001**, 42(1), 51.
80. Davis, R. D.; Mathias, L. J.; Jarrett, Jr.; W. L. *ACS Polym. Prepr.* **2001**, 42(1), 55.
81. Pardi, A.; Mollova, E.; McCallum, S.; Hanson, P.; Bondensgaard, K. *ACS Polym. Prepr.* **2001**, 42(1), 59.
82. Prestegard, J. H. *ACS Polym. Prepr.* **2001**, 42(1), 60.

83. Van Halbeek, H. *ACS Polym. Prepr.* **2001**, 42(1), 75.
84. Ute, K.; Janco, M.; Niimi, R.; Kitayama, T.; Hatada, K.; Berek, D. *ACS Polym. Prepr.* **2001**, 42(1), 67.
85. Wade, C. G.; O'Leary, D. J.; Roth, J.; Armstrong, K.; Thoburn, J.D.; Miller, D.C.; Pomerantz, A. *ACS Polym. Prepr.* **2001**, 42(1), 74.
86. Vliegthart, J. F. G.; Faber, E. J.; Kamerling, J. P. *ACS Polym. Prepr.* **2001**, 42(1), 63.
87. Serianni, A. S.; Carmichael, I. *ACS Polym. Prepr.* **2001**, 42(1), 80.
88. For example, (a) *Basic One- and Two-Dimensional NMR Spectroscopy*; Fiebolin, H. (translated by J. K. Becconsall), 3rd Ed., Wiley-CVCH, Weinheim, 1998. (b) *Spin Choreography: Basic Steps in High Resolution NMR*, Freeman, R.; Spektrum Academic Publishers, Oxford, 1997.
89. For example, (a) Cheng, H. N.; Lee, G. H. *Trends in Anal. Chem.* **1990**, 9, 285. (b) Mirau, P. A. *Bull. Magn. Reson.* **1992**, 13, 109. (c) Werstler, D.D. in *Comprehensive Polymer Science, Second Supplement*; Aggarwal, S.L.; Russo, S., Eds.; Elsevier, New York, 1996, p. 197.
90. For example, (a) Doi, Y. *Makromol. Chem., Rapid Comm.* **1982**, 3, 635. (b) Cheng, H. N. *Polym. Bull. (Berlin)* **1990**, 23, 889. (c) Cheng, H. N.; Kakugo, M. *Macromolecules* **1991**, 24, 1724.
91. Albert, K. *J. Chromatogr., A* **1997**, 785, 65.
92. Malik, A. K.; Faubel, W. *J. Capillary Electrophor. Microchip Technol.* **1999**, 6, 97.
93. Moad, G. *Ann. Rep. NMR Spectrosc.* **1994**, 29, 287.
94. Bevington, J. C. *Trends in Polymer Science* **1993**, 1, 68.
95. Harwood, H. J.; et al., *Makromol. Symp.* **1996**, 111, 25.
96. For example, (a) Tritto, I.; Donetti, R.; Sacchi, M.-C.; Locatelli, P.; Zannoni, G. *Macromolecules* **1999**, 32, 264. (b) Busico, V.; Cipullo, R.; Talarico, G.; Segre, A. L.; Caporaso, L. *Macromolecules* **1998**, 31, 8720.
97. Cheng, H. N. Polymerization and Statistical Models, in *Encyclopedia of NMR*, Grant, D. M.; Harris, R. K., Eds.; Wiley, New York, 1995, pp. 3713-3721.
98. *High Resolution NMR of Macromolecules*; Bovey, F. A.; Academic Press, New York, 1972.
99. Cheng, H. N. *Makromol. Chem., Theory Simul.* **1992**, 1, 415; and *Makromol. Chem., Theory Simul.* **1993**, 2, 901.
100. Cheng, H. N. *ACS Polym. Mater. Eng.* **1992**, 67, 35; also in *New Advances in Polyolefins*; Chung, T. C., Ed.; Plenum, New York and London, 1993, pp. 15-30.
101. For example, (a) Cheng, H. N. *Makromol. Chem., Theory Simul.* **1993**, 2, 561. (b) Cheng, H. N. *Macromolecules* **1992**, 25, 2351.
102. Cheng, H. N.; Babu, G. N.; Newmark, R. A.; Chien, J. C. W. *Macromolecules* **1992**, 25, 6980.

103. Cheng, H. N. *Macromol. Theory Simul.* **1994**, *3*, 979.
104. Randall, J. C. *Macromolecules* **1994**, *27*, 2120.
105. Cheng, H. N. *Macromolecules* **1997**, *30*, 4117.
106. Cheng, H. N. *Polymer Bulletin* **1999**, *43*, 247.
107. For example: (a) Cheng, H. N. *Macromol. Symp.* **1994**, *86*, 77. (b) Cheng, H. N.; Bennett, M. A. *Makromol. Chem.* **1987**, *188*, 2665.
108. For example: (a) Cheng, H. N. *Int. J. Polym. Anal. Charact.* **1997**, *4*, 71. (b) Cheng, H. N. *J. Appl. Polym. Sci.: Appl. Polym. Symp.* **1989**, *43*, 129.
109. Cheng, H. N.; Tam, S. B.; Kasehagen, L. J. *Macromolecules* **1992**, *25*, 3779.
110. Cheng, H. N.; Lee, G. H. *Int. J. Polym. Anal. Charact.* **1996**, *2*, 439.
111. Cheng, H. N.; Kasehagen, L. J. *ACS Polymer Prepr.* **1997**, *38*(1), 863.
112. Weller, C. T. *Nucl. Magn. Reson.* **1997**, *26*, 377.
113. Xu, J. in *Fuzzy Logic Chem.*; Rouvray, D. H., Ed.; Academic, San Diego, 1997, pp. 249-282.
114. Saito, K.; Ogawa, T. *Bunseki Kagaku* **2000**, *49*, 3.
115. For example, (a) Dais, P.; Spyros, A. *Prog. Nucl. Magn. Reson. Spectrosc.* **1995**, *27*, 555. (b) Bruschweiler, R. *Chimia* **1997**, *51*, 140. (c) Inglefield, P. T.; Jones, A. A. *Plast. Eng. (N.Y.)* **2000**, *56*, 43; (*Handbook of Polycarbonate Science and Technology*; M. Dekker).
116. For example: (a) Cavalieri, F.; Chiessi, E.; Paci, M.; Paradossi, G.; Flaibani, A.; Cesaro, A. *Macromolecules* **2001**, *34*, 99. (b) Yamazaki, S.; Noda, I.; Tsutsumi, A. *Polym. J. (Tokyo)* **2000**, *32*, 87.
117. For example, (a) Karali, A.; Dais, P.; Heatley, F. *Macromolecules* **2000**, *33*, 5524. (b) Mao, S.-Z.; Zhang, X.-D.; Dereppe, J.-M.; Du, Y.-R. *Colloid Polym. Sci.* **2000**, *278*, 264. (c) Meier, U.; Schlaepfer, C. W. *Ber. Bunsen-Ges.* **1998**, *102*, 1011.
118. For example, (a) Park, S. Y.; Cho, S. H.; Yuk, S. H.; Jhon, M. S. *Eur. Polym. J.* **2001**, *37*, 1785. (b) Spevacek, J.; Hanykova, L.; Ilavsky, M. *Macromol. Symp.* **2001**, *166*, 231.
119. Tonelli, A. E. *Annu. Rep. NMR Spectrosc.* **1997**, *34*, 185.
120. For example: (a) Paul, E. G.; Grant, D. M. *J. Amer. Chem. Soc.* **1964**, *86*, 2984. (b) Lindeman, L. P.; Adams, J. Q. *Anal. Chem.* **1971**, *43*, 1245.
121. For example: (a) Cheng, H. N.; Bennett, M. A. *Makromol. Chem.* **1987**, *188*, 135. (b) Cheng, H. N.; Bennett, M. A. *Anal. Chem.* **1984**, *56*, 2320. (c) Brosio, E.; Conti, F.; DiNola, A.; Delfini, M.; Segre, A. L. *Gazz. Chim. Ital.* **1977**, *107*, 237.
122. For example, (a) Masaro, L.; Zhu, X.X.; Macdonald, P.M. *Macromolecules* **1998**, *31*, 3880. (b) Abrahamsen-Alami, S.; Stilbs, P. J. *Colloid Interface Sci.* **1997**, *189*, 137. (c) Andersen, P. O.; Marstokk, O.; Nystrom, B.; Walderhaug, H. *Macromol. Chem. Phys.* **2001**, *202*, 1457. (d) Nilsson, S.; Thuresson, K.; Lindman, B.; Nystrom, B. *Macromolecules*

- 2000, 33, 9641. (e) Kopperud, H. B. M.; Walderhaug, H.; Hansen, F. K. *Macromol. Chem. Phys.* **1999**, *200*, 1839. (f) Walderhaug, H.; Nystrom, B. *Colloid Surf. A* **1999**, *149*, 1.
123. For example: (a) Chen, A.; Wu, D.; Johnson, Jr., C. S. *J. Amer. Chem. Soc.* **1995**, *117*, 7965. (b) Jerschow, A.; Mueller, N. *Macromolecules* **1998**, *31*, 6573. (c) Van Gorkom, L. C. M.; Hancewicz, T. M. *J. Magn. Reson.* **1998**, *130*, 125. (d) Hodge, P.; Monvisade, P.; Morris, G. A. Preece, I. *Chem. Commun. (Cambridge)* **2001**, 239.
124. Stamps, J. P.; Ottink, B.; Visser, J.M.; van Duynhoven, J. P. M.; Hulst, R. *J. Magn. Reson.* **2001**, *151*, 28.
125. Callaghan, P. T. *Rep. Prog. Phys.* **1999**, *62*, 599.
126. For example: (a) Uludag, Y.; McCarthy, M. J.; Barrall, G. A.; Powell, R. L. *Macromolecules* **2001**, *34*, 5520. (b) Arola, D. F.; Powell, R. L.; Barral, G. A.; McCarthy, M. J. *J. Rheol. (N.Y.)* **1999**, *43*, 9.
127. For example, (a) Ito, H.; Dalby, C.; Pomerantz, A.; Sherwood, M.; Sata, R.; Sooriyakumaran, R.; Guy, K.; Breyta, G. *Macromolecules* **2000**, *33*, 5080. (b) Ito, H.; Miller, D.; Sveum, N.; Sherwood, M. *J. Polym. Sci., Polym. Chem.* **2000**, *38*, 3521. (c) Martin, S. J.; McBrierty, V. J.; Dowling, J.; Douglass, D. C. *Macromol. Rapid Comm.* **1999**, *20*, 95. (d) Cutie, S. S.; Smith, P. B.; Henton, D. E.; Staples, T. L.; Powell, C. *J. Polym. Sci., Polym. Phys.* **1997**, *35*, 2029.
128. Dardin, A.; Cain, J. B.; DiSimone, J. M.; Johnson, Jr., C. S.; Samuelski, E. T. *Macromolecules* **1997**, *30*, 3593.
129. Cheng, H. N., Polymer Reactions, in *Encyclopedia of NMR*; Grant, D. M.; Harris, R. K., Eds.; Wiley, New York, 1995, pp. 3706-3713.
130. Yannoni, C. S. *Acc. Chem. Res.* **1982**, *15*, 201.
131. *Solid State NMR for Chemists*; Fyfe, C. A.; C.F.C. Press, 1983.
132. *High Resolution NMR of Synthetic Polymers in Bulk*; Komoroski, R. A., Ed.; VCH, Deerfield Beach, 1986.
133. *Solid State NMR of Polymers*; Mathias, L., Ed.; Plenum, New York, 1989.
134. *NMR in Solid Polymers*; McBrierty, V. J.; Packer, K. J.; Cambridge Univ. Press, New York, 1993.
135. Schaefer, J.; Stejskal, E. O. *J. Amer. Chem. Soc.* **1976**, *98*, 1031.
136. Taylor, R.; Pembleton, R.; Ryan, L.; Gerstein, B. *J. Chem. Phys.* **1979**, *71*, 4541.
137. Brown, S. P.; Schnell, I.; Spiess, H. W. *J. Amer. Chem. Soc.* **1999**, *121*, 6712.
138. (a) Caravatti, P.; Braunschweiler, L.; Ernst, R. R. *Chem. Phys. Lett.* **1983**, *100*, 305. (b) Burum, D. P.; Bielecki, A. *J. Magn. Reson.* **1991**, *94*, 645. (c) Van Rossum, B.-J.; Förster, H.; De Groot, H. J. M. *J. Magn. Reson.* **1997**, *124*, 516. (d) Lesage, A.; Sakellariou, D.; Steuernagel, S.; Emsley, L. *J.*

- Amer. Chem. Soc.* **1998**, *120*, 13194. (e) Saalwächter, K.; Graf, R.; Spiess, H. W. *J. Magn. Reson.* **1998**, *140*, 471.
139. Schmidt-Rohr, K. *J. Magn. Reson.* **1998**, *131*, 209.
140. (a) Geen, H.; Titman, J. J.; Gottwald, J.; Spiess, H. W. *Chem. Phys. Lett.* **1994**, *227*, 79. (b) Geen, H.; Titman, J. J.; Gottwald, J.; Spiess, H. W. *J. Magn. Reson. A* **1995**, *114*, 264. (c) Gottwald, J.; Demco, D. E.; Graf, R.; Spiess, H. W. *Chem. Phys. Lett.* **1995**, *243*, 314.
141. (a) Gullion, T.; Schaefer, J. *J. Magn. Reson.* **1989**, *81*, 196. (b) Gullion, T. *Magn. Reson. Rev.* **1997**, *17*, 83. (c) Fyfe, C.; Lewis, A.; Chezeau, J.; Grondey, H. *J. Amer. Chem. Soc.* **1997**, *119*, 12210.
142. (a) Feng, X.; Eden, M.; Brinkmann, A.; Luthman, H.; Erksso, L.; Graeslund, A.; Antzutkin, O.; Levitt, M. H. *J. Amer. Chem. Soc.* **1997**, *119*, 12006. (b) Hong, M.; Gross, J. D.; Griffin, R. G. *J. Phys. Chem. B* **1997**, *101*, 5869.
143. Chu, P. P. J.; Howard, J. J. *Macromol. Symp.* **1994**, *86*, 229, and references therein.
144. For example, (a) Nagasaka, B.; Omi, H.; Eguchi, T.; Nakayama, H.; Nakamura, N. *Chem. Phys. Lett.* **2001**, *340*, 473. (b) Meresi, G.; Wang, Y.; Bandis, A.; Inglefield, P. T.; Jones, A. A.; Wen, W.-Y. *Polymer* **2001**, *42*, 6153. (c) Junker, F.; Veeman, W. S. *Macromolecules* **1998**, *31*, 7010. (d) Morgan, D. R.; Stejkal, E. O.; Andrady, A. L. *Macromolecules* **1999**, *32*, 1897.
145. For example, (a) Mellinger, F.; Wilhelm, M.; Spiess, H. W. *Macromolecules* **1999**, *32*, 4686. (b) Jack, K. S.; Natansohn, A.; Wang, J.; Favis, B.; Cigana, P. *Chem. Mater.* **1998**, *10*, 1301. (c) Cheung, T. T. *P. ACS Polym. Prepr.* **1997**, *38*(1), 892.
146. Goldman, M.; Shen, L. *Phys. Rev.* **1966**, *144*, 321.
147. Egger, N.; Schmidt-Rohr, K.; Blümich, B.; Domke, W.-D.; Stapp, B. *J. Appl. Polym. Sci.* **1992**, *44*, 289.
148. Spiess, H. W. *Macromol. Symp.* **1997**, *117*, 257.
149. (a) Spiess, H. W. *Colloid Polym. Sci.* **1983**, *261*, 193. (b) Jelinski, L. W.; Dumais, J. J.; Engel, A. K. *Macromolecules* **1983**, *16*, 403. (c) Jackson, C. L.; Schadt, R. J.; Gardner, K. H.; Chase, D. B.; Allen, A. R.; Gabara, V.; English, A. D. *Polymer* **1994**, *35*, 1123.
150. Schmidt-Rohr, K.; Spiess, H. W. *Macromolecules* **1992**, *25*, 3273.
151. Gerardy-Montouillout, V.; Malveau, C.; Tekeley, P.; Olender, Z.; Luz, Z. *J. Magn. Reson. A* **1996**, *123*, 7.
152. Reichert, D.; Zimmermann, H.; Tekeley, P.; Poupko, R.; Luz, Z. *J. Magn. Reson.* **1997**, *125*, 245.
153. Reichert, D.; Bonagamba, T. J.; Schmidt-Rohr, K. *J. Magn. Reson.* **2001**, *151*, 129, and references therein.

Chapter 2

Solution and Solid-State NMR Characterization of Ethylene Oxide–Propylene Oxide Composites for Ultra-Low Dielectric Constant Applications

Peter A. Mirau^{1,*} and Shu Yang²

¹Agere Systems and ²Lucent Technologies, Bell Laboratories,
600 Mountain Avenue, Murray Hill, NJ 07972

*Corresponding author: mirau@bell-labs.com

High-resolution proton and silicon NMR has been used to study structure formation in solution mixtures of ethylene oxide/propylene oxide triblock copolymers and methyl silsesquioxane. These mixtures are precursors to ultra low dielectric constant films used in the fabrication of integrated circuits. The solution NMR results show that micelle formation is suppressed during solvent casting and curing of the films, and that miscibility is enhanced by the interactions of both the ethylene oxide and propylene oxide blocks of the triblock copolymer with the methyl silsesquioxane matrix.

The continued improvement of integrated circuits and the decreased size of new devices are the result of advances in materials chemistry, photolithography and device design. As the devices shrink, however, the distance between wires decreases and the performance is limited by increases in the circuit response time, power consumption and cross talk between the wires

(1). These problems can be minimized by using a packaging material with a lower dielectric constant (k). The current materials of choice, silicon dioxide, has a dielectric constant of 4 and will not be suitable for the next generation of devices with feature sizes below 100 nm. Most organic materials have dielectric constants greater than 3, so it is difficult to design ultra low- k materials without taking advantage of the low dielectric constant of air ($k=1$) by introducing pores (2,3). Pores can be created by the thermal treatments of composites containing high boiling point liquids (4) or polymers (3), where the organic material is either evaporated or burned away.

We have been exploring the possibility of using block copolymers as templates to control pore formation in composites that are precursors to ultra low- k films (5). Block copolymers are of interest since they are commercially available for a wide variety of monomers with well-controlled molecular weights and polydispersities, and it is possible to control the film morphology with the proper choice of monomer, molecular weight or architecture.

In the current studies we have prepared precursors to ultra low- k films using methyl silsesquioxane as the matrix and poly(ethylene oxide-*b*-propylene oxide-*b*-ethylene oxide) triblock copolymers as porogens. The triblock copolymers have been extensively studied, and the aggregation behavior and morphologies are known to depend on the block lengths and molecular weights (6). Methyl silsesquioxane, which has the empirical formula $\text{CH}_3\text{-SiO}_{1.5}$, is of interest as a matrix material because it has many of the favorable qualities required for low- k dielectrics, including good thermal stability, low moisture uptake and a relatively low dielectric constant (2.6-2.8) for the bulk films (3). We are hoping that the amphiphilic properties of the triblock copolymers will allow us to control the pore formation in the methyl silsesquioxane composites. The best films for low- k applications are expected to be those with small (nm-sized), isolated pores, since this morphology is expected to have the best mechanical strength and would provide little opportunity for metal diffusion from the surface.

Methods and Materials

The triblock copolymers of poly(ethylene oxide-*b*-propylene oxide-*b*-ethylene oxide) L101 ($\text{EO}_4\text{-PO}_{59}\text{-EO}_4$), P103 ($\text{EO}_{17}\text{-PO}_{60}\text{-EO}_{17}$), and F88 ($\text{EO}_{103}\text{-PO}_{39}\text{-EO}_{103}$) were obtained from the BASF Corp. The methyl silsesquioxane precursor was obtained from Techneglass as a neat solution or as a 30 wt% solution in a mixture in *n*-butanol and ethyl alcohol. The GPC analysis of the methyl silsesquioxane showed a number average molecular weight of 1668 and a polydispersity of 3.2.

The solution NMR experiments were performed at 500 MHz using a Tecmag Apollo NMR spectrometer. Hypercomplex pure-phase two-dimensional spin exchange spectra were measured using the $(90^\circ-t_1-90^\circ-\tau_m-90^\circ-t_2)$ pulse sequence (7,8).

Results

Proton NMR in solution has been used to study composite formation in mixtures of ethylene oxide/propylene oxide triblock copolymers and methyl silsesquioxane. The porous films for low constant applications are prepared (Figure 1) by mixing the polymers and methyl silsesquioxane in butanol followed by spin casting (5). The film is then heated to 120°C to condense the methyl silsesquioxane into a relatively rigid network. After the matrix has been cured, a high temperature treatment ($> 400^\circ\text{C}$) is used to remove the polymer and obtain the final porous film.

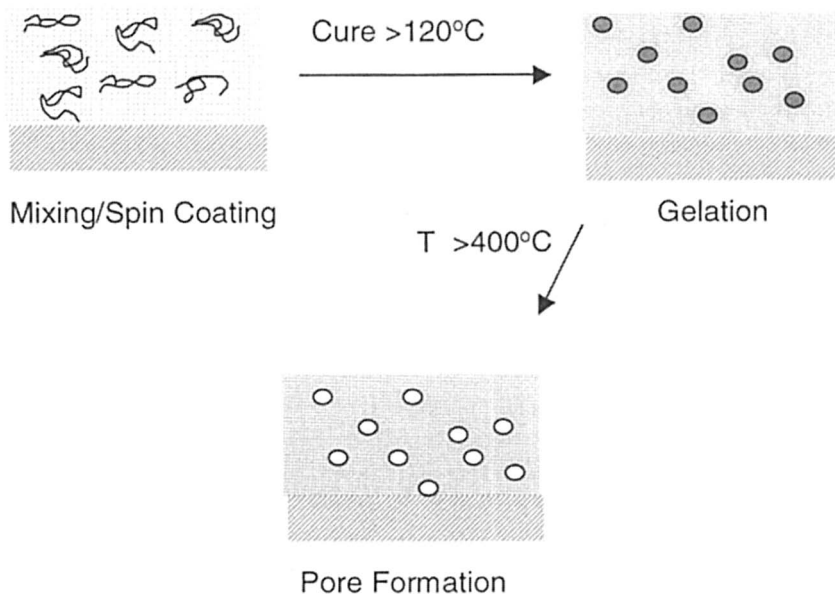


Figure 1. A schematic diagram showing casting and curing of the ultra low dielectric constant films. The films for devices are cast on silicon wafers.

The polymer and matrix components must be carefully chosen to obtain films with small, isolated pores. This can be accomplished by choosing

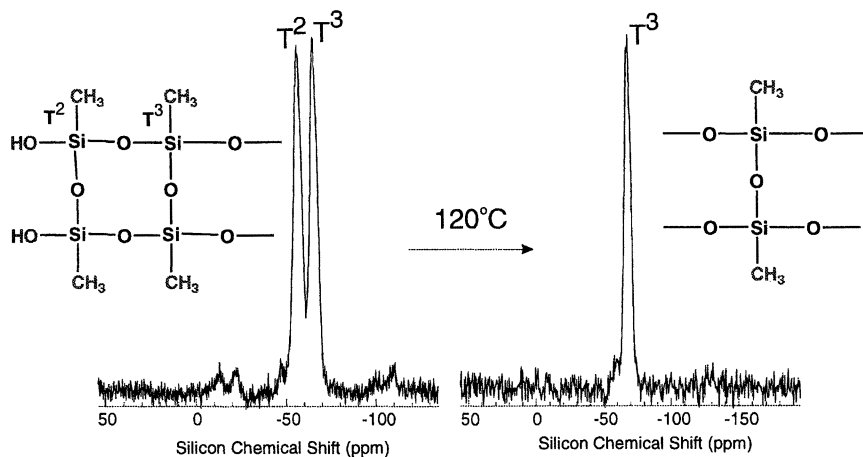


Figure 2. The solution (left) and solid-state (right) silicon NMR spectra of methyl silsesquioxane before and after heating to 120°C for 1 hour.

polymers that remain miscible with the methyl silsesquioxane as the film is cured. Polymer miscibility has been extensively studied and most mixtures of polymers are not miscible unless there are favorable interactions between the chains that drives miscibility (9). It is especially difficult to obtain miscible methyl silsesquioxane films because the film properties change significantly during the cure. This is illustrated in Figure 2, which shows the silicon spectra for the methyl silsesquioxane polymer before and after temperature treatment at 120 °C. Two peaks are observed in the silicon spectrum of the methyl silsesquioxane before heat treatment that can be assigned to the so-called T² and T³ sites, silicons attached to a methyl group with either two or three Si-O-Si bridging groups. These spectra show that the methyl silsesquioxane starting material contains high concentrations of hydrophilic hydroxyl groups and hydrophobic methyl groups. The polarity of the matrix changes substantially as the hydroxyl groups are lost during the cure, making it difficult to maintain the miscibility with the polymer as the film cures.

Much of the interest in ethylene oxide/propylene oxide block copolymers is due to the fact that these polymers are able to self-assemble in solution (6). The polymers can have complex phase diagrams (10) and have been used to template the formation of ordered structures in mesoporous silicas (11). The self-assembly of the triblock copolymers can be monitored by NMR, since the formation of micelles and other structures affects the chain dynamics and the NMR linewidths. This is illustrated in Figure 3 which shows the solution spectra for L101 (EO₄-PO₅₉-EO₄) in ²H₂O as a

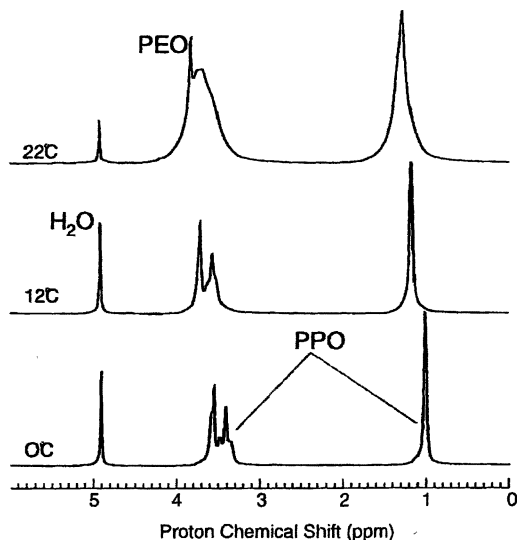


Figure 3. The effect of temperature on the proton NMR spectra of P103 in $^2\text{H}_2\text{O}$.

function of temperature. At low temperature the polymer adopts a random coil configuration and narrow linewidths are observed both for the methyl protons of propylene oxide and the main chain methylene and methine protons of the propylene oxide and ethylene oxide. As the temperature is increased, the linewidths also increase, particularly for the propylene oxide resonances. It is known from other studies (6) that the triblock copolymers form micelles, and these changes can be monitored from the proton linewidths. At ambient temperature the triblock copolymer forms micellar structures with a propylene oxide interior and a corona of ethylene oxide. Unfortunately the micelles (30-50 nm) are much larger than the pores required for the ultra low dielectric constant films.

The low- k films are prepared by solution casting the methyl silsesquioxane and the triblock copolymers mixtures from butanol. The size and distribution of polymer domains in the film will depend on the degree to which the polymer self-associates. Figure 4 shows the solution proton NMR spectra of the P103 triblock copolymer ($\text{EO}_{17}\text{-PO}_{60}\text{-EO}_{17}$) mixed with methyl silsesquioxane in butanol- d_{10} . The important feature to note is the narrow linewidths for the polymer methyl and main chain resonances. Both sets of peaks are narrower than the broad peaks shown in Figure 3 for the triblock

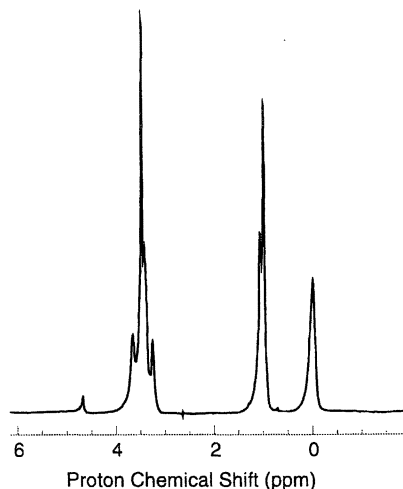


Figure 4. The solution proton NMR spectrum of the 50:50 methyl silsesquioxane: P013 mixture in butanol- d_{10} .

copolymer micelles. These experiments show that the casting solvent suppresses micelle formation.

The results for the butanol solution show that micelles are unlikely to form in the initial solvent mixture. As the film is cast and heated, the environment for the polymer changes substantially as solvent is driven off and the hydroxyl groups on the methyl silsesquioxane are condensed. To study the effect of the solvent loss we prepared a neat sample of the methyl silsesquioxane and the L101 triblock copolymer ($\text{EO}_4\text{-PO}_{59}\text{-EO}_4$). We were able to study the solution structure of the neat mixture because the L101 has a low ethylene oxide content and is liquid-like at ambient temperature. Figure 5 compares the solution spectra of the neat L101, the neat methyl silsesquioxane and the 50:50 mixture. Again we note the narrow lines for the polymer peaks, suggesting that micelle formation is also suppressed in the neat mixture with methyl silsesquioxane.

The ethylene oxide/propylene oxide triblock copolymers were chosen to maintain miscibility as the composite cures. To achieve this, it is necessary to have favorable interactions between the polymer and the matrix, even as the matrix becomes more hydrophobic. We have explored the intermolecular interactions between the matrix and the polymer using two-dimensional (2D) exchange NMR (7) on the neat mixture, and Figure 6 shows the 2D exchange

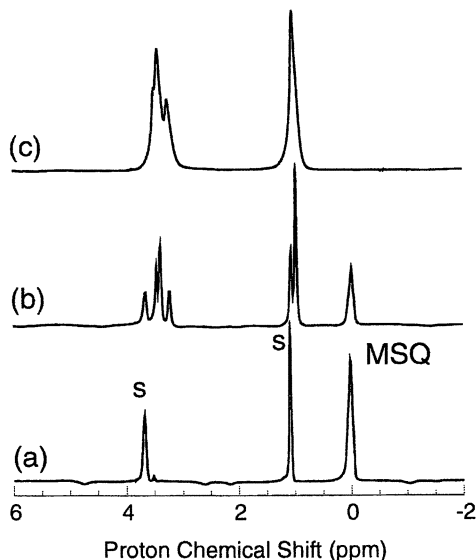


Figure 5. The 500 MHz proton NMR spectra of (a) neat methyl silsesquioxane, (b) the 50:50 methyl silsesquioxane:L101 mixture, and (c) neat L101. Residual solvent lines are marked (s).

spectrum recorded with a mixing time of 0.25 s. The peaks along the diagonal can be assigned to the peaks in the equilibrium spectra (Figure 5(b)). The off-diagonal peaks arise from magnetization exchange during the mixing time between pairs of protons in close ($> 5 \text{ \AA}$) proximity (12,13). Several intermolecular cross peaks are observed, including those between the methyl silsesquioxane methyl protons, the propylene oxide methyl protons, and the ethylene oxide and propylene oxide main-chain methine and methylene protons. The strength of the intermolecular interactions can be evaluated by comparing the relative intensities of the cross peaks in the 2D spectrum with the equilibrium spectrum. These data are compared in Figure 7 for the cross peak between the methyl silsesquioxane methyl protons and the main-chain ethylene oxide and propylene oxide protons enclosed in the box in Figure 6. The equilibrium spectrum (Figure 7(b)) for the mixture shows well-resolved peaks for the methine and methylene peaks for the propylene oxide and the methylene peaks for the ethylene oxide block. Since the L101 triblock copolymer has a low ethylene oxide fraction, the methylene peak for ethylene oxide is smaller than for the propylene oxide. The cross section through the 2D spectra (Figure 7(a)) shows cross peaks to both the propylene oxide and ethylene oxide protons, showing that the methyl silsesquioxane is favorably interacting with both the ethylene oxide and propylene oxide blocks in the triblock copolymer. However,

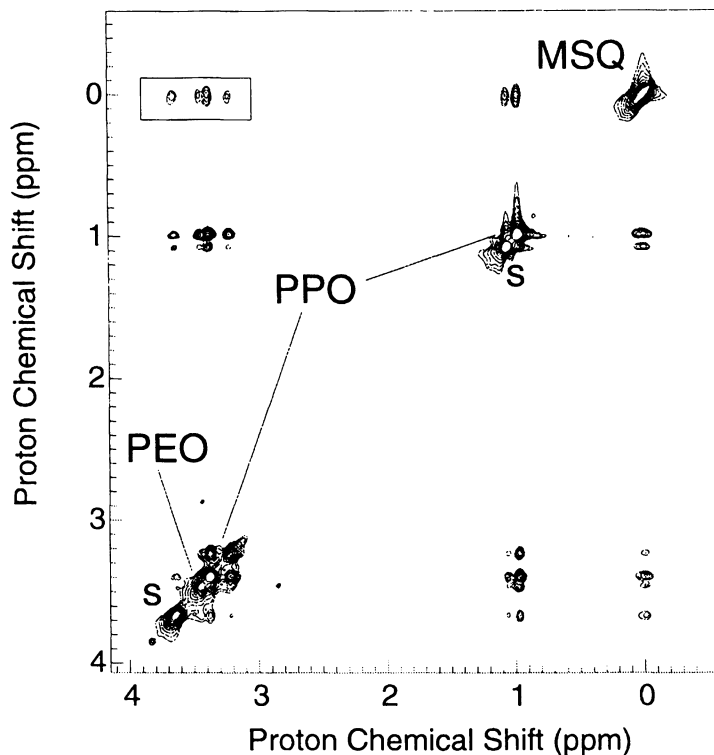


Figure 6. The 2D exchange spectrum of the 50:50 mixture of methyl silsesquioxane and L101 obtained with a 0.25 s mixing time. The solvent lines are marked (s).

the cross peaks to the propylene oxide block are enhanced relative to the ethylene oxide block when compared to the equilibrium spectrum. This shows that the propylene oxide block interacts more strongly with the methyl silsesquioxane than does the ethylene oxide.

Discussion

We have been designing films for low-k applications by using ethylene oxide/propylene oxide triblock copolymers as templates in porous films (5). The goal of this research is to discover polymers that phase separate from the matrix by forming small, isolated domains. The polymers are then removed in a high temperature step to generate the final porous material with a low dielectric

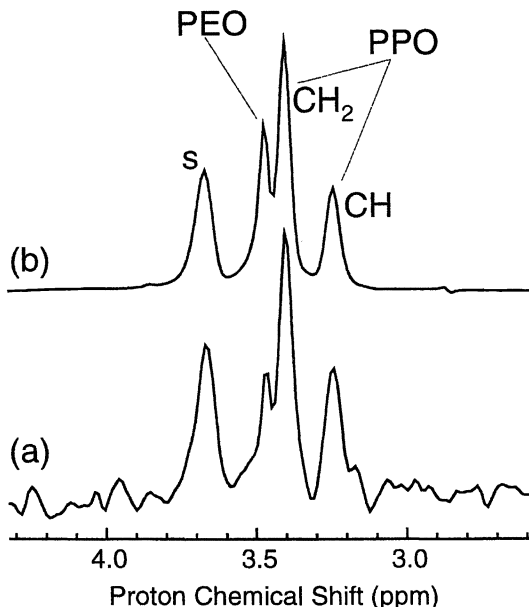


Figure 7. Comparison of (a) cross sections through the 2D exchange spectra of the methyl silsesquioxane cross peaks with the (b) equilibrium spectra. The solvent lines are marked (s).

constant. The size and distribution of the pores are determined by the polymer-matrix interactions as the composite is cured.

Ethylene oxide/propylene oxide triblock copolymers have been successfully used to template pore formation in ultra low- k films, and dielectric constants as low as 1.5 have been observed with polymer loading levels of 50 wt% (5). These films have good mechanical properties, a high breakdown voltage and a low moisture uptake. We have characterized the films with high-resolution solid-state proton NMR and found that the triblock copolymers form nm-sized core-shell structures with the propylene oxide block at the interface between the ethylene oxide block and the methyl silsesquioxane matrix (14).

In these studies we have used solution NMR to study structure formation and the intermolecular interactions between the polymer and the matrix during the cure that affect the miscibility. The triblock copolymers form micelles in aqueous solution with the propylene oxide block at the center and the ethylene oxide block at the exterior (6), and micelle formation can be monitored via the proton linewidths. The NMR studies show that the triblock copolymers do not form micelles in the butanol solutions used for solution casting films of the low- k dielectrics, or in neat mixtures of the triblock copolymers with the methyl silsesquioxane. The methyl silsesquioxane starting material contains a

high concentration of hydroxyl groups and become progressively more hydrophobic as the matrix cures. The 2D exchange NMR experiments on the neat mixture shows that both the ethylene oxide and propylene oxide blocks of the triblock copolymer interact with the methyl silsesquioxane starting material, but the interactions with the propylene oxide block are stronger. We believe that it is the favorable interactions between the methyl silsesquioxane and the triblock copolymer that promote miscibility as the system cures. The triblock copolymer remains miscible until late in the curing when the condensation of the matrix forms a rigid barrier that inhibits aggregation of the triblock copolymers into larger domains. The observation that the propylene oxide interacts more strongly with the matrix is consistent with the structure of the composite measured by solid-state NMR which shows that that propylene oxide block is at the interface in the cured composites (14).

References

1. Ryan, E. T.; Fox, R. J. *Future Fab Int.* **2000**, *8*, 169.
2. Miller, R. D. *Science* **1999**, *286*, 421.
3. Nguyen, C. V.; Carter, K. R.; Hawker, C. J.; Jaffe, R. L.; Miller, R. D.; Remenar, J. F.; Rhee, H. W.; Rice, P. M.; Toney, M. F.; Trollsas, M.; Yoon, D. *Chem. Mater.* **1999**, *11*, 3080.
4. Moyes, E. S.; Deis, T.; Lui, Y.; Chung, K.; Spaulding, M.; Saha, C.; Boisvery, R.; Chen, W.; Bremmer, J. *Chem. Mater.* **2000**, *12*, 2301.
5. Yang, S.; Mirau, P. A.; Pai, C.; Nalamasa, O.; Reichmanis, E.; Lin, E. K.; Lee, H.-J.; Gidley, D. W.; Sun, J. *Chem. Mater.* **2001**, *13*, 2762.
6. Alexandridis, P.; Holzwarth, J. F.; Hatton, T. A. *Macromolecules* **1994**, *27*, 2414.
7. Jeneer, J.; Meier, B.; Bachmann, P.; Ernst, R. *J. Chem. Phys.* **1979**, *71*, 4546.
8. States, D.; Haberkorn, R.; Ruben, D. *J. Magn. Reson.* **1982**, *48*, 286.
9. Coleman, M. M.; Serman, C. J.; Bhagwagar, D. E.; Painter, P. C. *Polymer* **1990**, *31*, 1187.
10. Holmqvist, P.; Alexandridis, P.; Lindman, B. *Macromolecules* **1997**, *30*, 6788.
11. Zhao, D.; Feng, J.; Huo, Q.; Melosh, N. A.; Fredrickson, G. H.; Chmelka, B. F.; Stucky, G. D. *Science* **1998**, *279*, 548.
12. Mirau, P.; Tanaka, H.; Bovey, F. *Macromolecules* **1988**, *21*, 2929.
13. Bovey, F. A.; Mirau, P. A. *NMR of Polymers*; Academic Press: New York, 1996.
14. Mirau, P. A.; Yang, S. *J. Am. Chem. Soc.* **2001**, *submitted*.

Chapter 3

High-Temperature Solid-State NMR of Cross-Linked, Insoluble, and Unswellable Polymers

Khalid Thakur

3M Corporate Analytical Technology Center, 3M Center, 201-BS-08,
St. Paul, MN 55144

The use of solid-state magic-angle spinning (MAS) and variable temperature (VT) NMR techniques as routine molecular structure characterization tools to analyze insoluble, high M.W., and/or cross-linked polymers is demonstrated. Increasing the mobility in the polymers by either swelling in a solvent and/or by elevation of temperature leads to narrow resonances with isotropic chemical shifts in MAS NMR spectra. Current instrumental capabilities of solid-state NMR spectrometers to acquire MAS spectra at temperatures up to 250 °C enable NMR measurements at temperatures wherein the mobility of the polymers is high and the material is viscous. In a viscous state, the T_1 time of a polymer is shorter than in a dilute solution or in an amorphous state. Combined with MAS, the viscous sample has long T_2 time (narrow resonances) and significantly reduced chemical shift anisotropy (CSA) such that spinning side bands are often not significant. Such line narrowing allows rapid acquisition of reasonably well-resolved proton, fluorine, carbon, phosphorous, or silicon NMR spectra of insoluble materials for their molecular structure characterization.

Chemical shifts of resonances obtained in solution NMR spectra have been routinely used for molecular structure identification and characterization of the organic solutes. In solution, the organic solutes undergo motion in all degrees of freedom including rotation and translation movement that is faster than the time scale of NMR measurement, *viz.* microseconds. As a result, the observed resonance is at the isotropic chemical shift, which is representative of the molecular structure and electronic environment averaged over all orientations with respect to the B_0 (static magnetic field) direction. The relative intensities of the various resonances are usually representative of the relative mole fractions of the respective nuclei in the solution.

During NMR measurements of rigid and semi-rigid materials, the rotation and translation motions are not rapid enough to average out the orientation dependent effects. In such cases, chemical shift anisotropy (CSA) and spin-spin dipolar coupling effects lead to a broad range of resonances and multiple overlap of resonances. Solid-state NMR spectrometers use magic-angle-spinning (MAS) to mechanically average over all orientations, which leads to reduction of CSA and spin-spin dipolar coupling effects. In rigid systems, the use of ^{13}C cross-polarization NMR from ^1H spin magnetization has been quite effective. However, if the material is not well ordered or highly crystalline, the CP-MAS spectral resonances are significantly broader than those observed in solution NMR spectra. Disorder in the rigid material under investigation often broadens the NMR resonances to a point where molecular structure identification can be a challenge. Here we discuss NMR techniques that can be used routinely and rapidly to identify and analyze rigid and semi-rigid materials by obtaining NMR spectra of $1/2$ spin nuclei with relatively narrow resonances at their isotropic chemical shifts.

Experimental

Solid-state NMR spectra were acquired by spinning the sample in Chemagnetics MAS probes at speeds of 6 kHz – 12 kHz in a 5 mm rotor or 15 kHz – 25 kHz in a 3.2 mm rotor. Varian INOVA wide bore 400 MHz spectrometer was used. Data were acquired at temperatures between 22 °C and 250 °C. Unless specifically mentioned, pulse sequences employing single pulse Bloch decay measurements were used. ^{13}C NMR spectra were acquired with less than 67° tip angle and proton cw decoupling during acquisition, while proton NMR spectra were acquired with less than 25° tip angle.

FT-NMR and Magic-Angle-Spinning

In order to discuss the effect of temperature on MAS-NMR spectra of polymers, it is necessary to develop a frame of reference. FT-NMR uses a radio frequency (RF) pulse to induce transitions between the two spin quantum states of $+1/2$ and $-1/2$. The induced transitions create a phase coherence of spins in the two states such that a net magnetization precesses coherently in the (XY) plane orthogonal to the direction (Z) of the static magnetic field B_0 . See Figure 1 below. It is this oscillating net magnetization orthogonal to B_0 direction that is detected as NMR signal by the receiver coil. The oscillation and eventual decay of the spin phase coherence magnetization in the XY plane is recorded as the Free Induction Decay (FID) in an NMR spectrometer. Fourier transform of the FID provides the distribution of Larmor frequencies, which are often reported in chemical shift (δ) values.

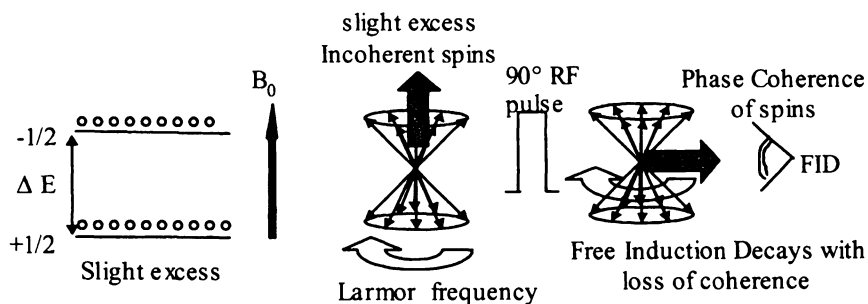


Figure 1. Process of generating FID in FT-NMR.

The phase coherence of spins can dissipate via various processes. One is by returning to the equilibrium Boltzmann distribution of spin states by exchanging energy with the lattice. The time constant for this process is referred to as the T_1 time. Alternatively, the spin phase coherence can also dissipate without exchange of energy. Such processes include (1) spin-exchange among the dipolar coupled spins and (2) the presence of multiple Larmor frequencies. The time constant for the loss of phase coherence of spins, and the resulting loss of NMR signal, is referred to as the T_2 time. In dilute solutions, due to the rapid motion of the molecules, the spin-exchange efficiency is low and often the loss of spin phase coherence is primarily by T_1 processes; i.e. $T_2 \approx T_1$. However in rigid and semi-rigid materials, the efficiency of spin-exchange processes is significantly higher and the resulting loss of spin phase coherence is more rapid than the rate of T_1 relaxation. The short T_2 time (i.e. $T_2 \ll T_1$), observed in rigid and semi-rigid materials, leads to broad resonances in the Fourier transformed spectrum.

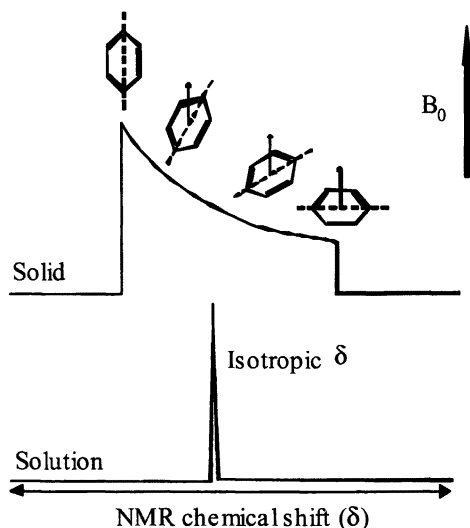


Figure 2. Lab frame orientation dependent Chemical Shift Anisotropy (CSA)



Spins maintain orientation with B_0 direction.

Hence, interaction between spins is dependent on orientation.

Figure 3. Lab frame orientation dependent dipolar couplings

In a homogenous static magnetic field B_0 , the net magnetic field observed by each nucleus, and hence its Larmor frequency, is dependent on the orientation of the molecule with respect to the B_0 direction (lab frame). Chemical shift anisotropy (CSA) is caused by orientation dependent shielding of nuclei by an asymmetric electronic environment, as shown pictorially in Figure 2 for the ring currents in benzene. Dipolar couplings are orientation dependent interactions between two or more nuclei, as shown pictorially in Figure 3 for a pair of nuclei whose spins must be aligned either with or against B_0 direction, irrespective of the orientation of the molecule. For the pair of nuclei shown, the two orientations with identical scalar distance between them have significantly different dipolar coupling. In dilute solutions, rapid molecular motions average over all possible orientations during the FID acquisition and only the isotropic chemical shifts are detected. In rigid and semi-rigid materials, molecular

motion is not rapid enough to average the orientations during the FID acquisition. In such cases, broad distributions of Larmor frequencies are observed. The resonances of rigid and semi-rigid materials can be narrowed if the various molecular orientations are averaged during the FID acquisition.

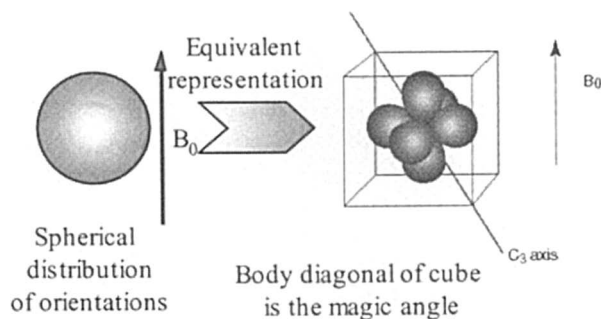


Figure 4. Magic Angle Spinning (MAS)

Magic angle of 54.74° is the body diagonal of a cube (C_3 symmetry axis) and solution to the equation $(3\cos^2\theta - 1) = 0$. In a powdered sample, all possible orientations have equal probability. An equivalent representation is presence of equal fractions of orientations along the three orthogonal axes, as shown in Figure 4, which is mathematically represented by the second order Legendre polynomial that contains the term $(3\cos^2\theta - 1)$. Constant rotation of a sample containing randomly oriented molecules along this magic-angle leads to mechanical averaging of all orientations. Acquisition of NMR FID while spinning the sample at this magic angle to the B_0 direction provides isotropic chemical shifts in the FT spectrum.

The broadening of the NMR spectral resonances by CSA effects and orientation dependent spin-spin interactions is “inhomogeneous” and normally averaged by MAS. However, the broadening of the FT NMR spectra caused by spin diffusion is “homogeneous” and in order to be reduced, usually higher than 15 kHz MAS speeds is required. Spin diffusion processes (i.e. spin-flip-flops) are a result of spin-spin dipolar couplings and require that the relative orientation of the interacting spins not change significantly for certain time duration. In a soft/flexible/viscous/visco-elastic state, the rapid fluctuations in relative position of all the surrounding nuclei lead to reduction in efficiency of spin diffusion. Higher the frequency of fluctuations, lower is the efficiency of spin diffusion, and narrower are the observed NMR resonances. The combination of MAS (to reduce magnetic susceptibility, CSA broadening, and static dipolar broadening), and temperature/plasticizing solvent (to reduce dipolar interactions) can lead to significantly narrow NMR resonances [1,2].

Discussion

Solution NMR is popular due to its ability to provide information about molecular structure. A primary criterion is that the material must be soluble. Insoluble materials, unless they form swollen gels, are usually not analyzed by NMR techniques for molecular structure characterization. Analysis of crystallinity and morphology of insoluble materials is normally carried out by mechanical averaging of all orientations by Magic-Angle-Spinning (MAS) and acquisition of NMR spectra of sparsely abundant nuclei such as ^{13}C and ^{29}Si while applying high power proton decoupling RF. The high power decoupling is used to reduce the NMR spectral broadening due to J-coupling between the sparse nuclei and abundant proton spins. Cross-polarization techniques, which employ transfer of magnetization from the abundant proton nuclei spins to the ^{13}C and ^{29}Si nuclei, are usually used to increase the signal strength. Unfortunately, the MAS NMR spectra of rigid materials are always broader than those observed in solution NMR spectra, partly due to disorder or defects, and partly due to spin diffusion processes. The disorder includes variations in bond lengths, angles, and environments, which lead to a distribution of isotropic chemical shifts.

Cross-linked polymers and high molecular weight polymers are commonly found in many products. Cross-linking can be used to impart many desirable properties in a polymer product, one of them being to hold shape. Finding analytical techniques to identify, analyze, and characterize cross-linked materials is often a challenge. Solution NMR techniques cannot be used since cross-linked polymers do not dissolve. However, some cross-linked polymers do swell and form gels in an appropriate solvent. If the mobility in the gel is high, conventional solution NMR techniques are adequate for the analytical analysis. If the polymeric material does not swell or if the mobility after swelling is insufficient to average out the CSA, the solution NMR spectral resonances are broad. MAS of such gels are known to provide narrower spectral resonances [3]. ^1H NMR spectra are especially sensitive to mobility. Due to the almost 100% natural isotopic abundance of protons, strong spin-spin dipolar couplings between various proton nuclei are always present. As mentioned earlier, the strong and abundant spin-spin dipolar couplings are responsible for rapid spin diffusion and loss of spin phase coherence during the ^1H NMR acquisition. Magic angle spinning can reduce the spectral broadening due to spin diffusion, but there is a limit to the MAS speeds that can be achieved. For elastomeric materials that are soft/viscous, MAS leads to spectral line narrowing [4-6]. For more rigid polymeric materials, an effective way of reducing the effects of spin diffusion is increase in mobility by either heating the sample, or addition of a plasticizing solvent, or a combination of the two (see Figure 5). In a viscous state, when various parts of the molecules are librating independently and

rapidly, nuclei do not stay fixed in relative 3-D space for long enough duration to interact and promote spin flips or spin exchange. An additional advantage of MAS measurement in viscous state is simultaneous partial averaging of the chemical shift anisotropy and reduction of the broadening caused by static dipolar couplings. The motion also reduces or eliminates broadening caused by variations in bond lengths, angles, and environments that is present in rigid materials.

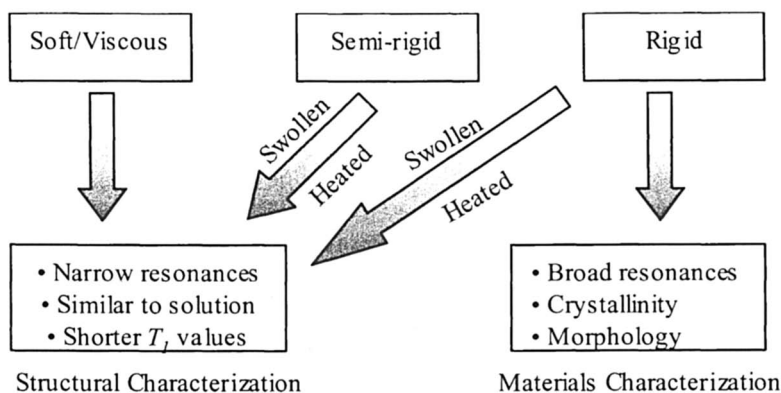


Figure 5. MAS NMR of Polymers in various physical states.

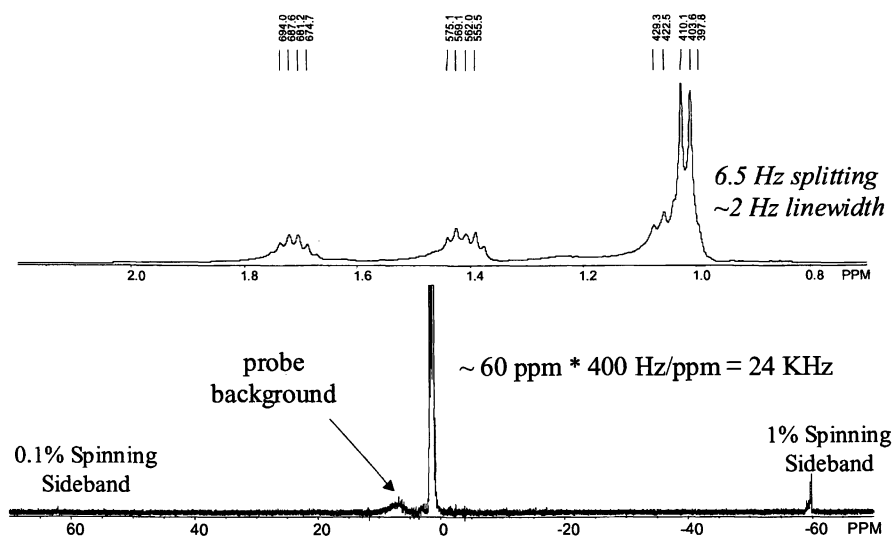


Figure 6. Proton MAS NMR of poly(propylene) at approx. 120 °C

The line narrowing under MAS and high temperature was first reported by Sterna and Smith for amorphous insoluble aromatic polymers in 1988 [1]. Additional papers on similar work on other non-aromatic systems have not been reported. Degradation of other polymeric systems at high temperatures is a valid concern. For analysis of fluoropolymers, Munson *et. al.* had shown that the combination of MAS and high temperature provides narrower ^{19}F NMR spectral resonances than only MAS or only temperature [2]. We have found that excellent resolution can be obtained in high temperature proton MAS NMR spectra of hydrocarbon polymers. See for example Figure 6 that shows a two Hz linewidth proton NMR spectrum of poly(propylene) acquired without addition of any solvent. The splitting of resonances from proton-proton couplings is easily observed in the spectrum – the methyl resonance has a 6.5 Hz splitting from coupling to methine group. The 24 kHz spinning sidebands with less than 1% integrated intensity are shown in lower part of the figure. These may be the MAS radial-field sidebands reported by Tekely and Goldman [7].

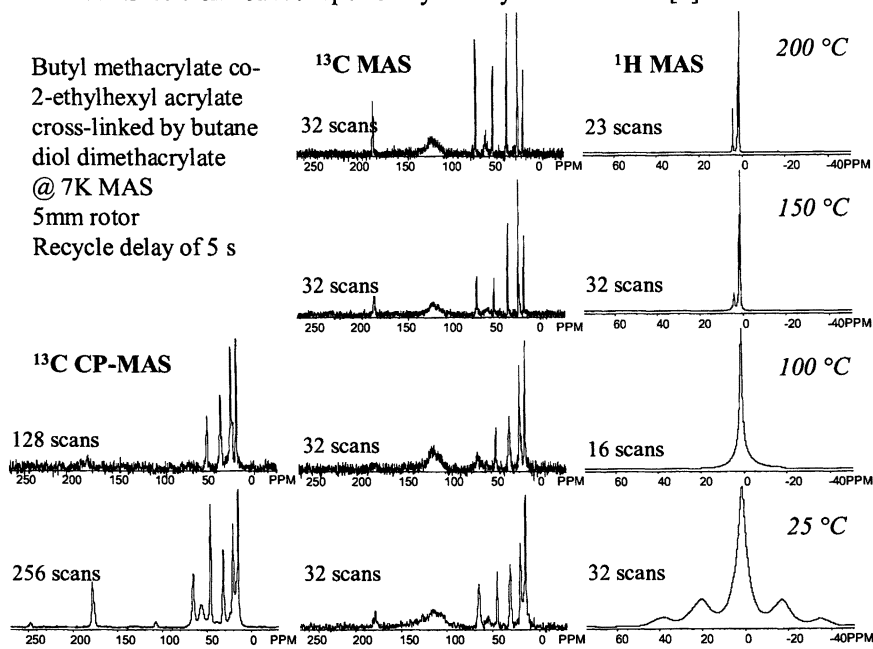


Figure 7. NMR spectra of an amorphous polymer at various temperatures.

MAS (7 kHz) NMR spectra acquired as a function of temperature for a representative cross-linked insoluble amorphous polymer are shown in Figure 7. The composition was determined from the NMR spectra to be 90% butyl methacrylate + 7% 2-ethyl hexyl acrylate + 3% butane diol dimethacrylate. At

room temperature the proton spectrum is broad and featureless, while the ^{13}C CP-MAS and one-pulse spectra are similar except for the carbonyl resonance that has a long T_1 time. Upon increasing the temperature to $100\text{ }^\circ\text{C}$, the proton spectrum gets significantly narrower while both the ^{13}C NMR spectra deteriorate. The deterioration of the ^{13}C NMR spectra may be due to interference between the molecular motion frequencies in the polymer and either proton decoupling frequency or magic angle spinning [1,8]. Increase of the temperature to $150\text{ }^\circ\text{C}$ further resolves the proton NMR spectrum and improves the ^{13}C one-pulse NMR spectra. The ^{13}C CP-MAS NMR on the other hand is extremely weak at this and higher temperatures, presumably due to significant reduction in spin-exchange (spin-diffusion) efficiency. Further increase in temperature to $200\text{ }^\circ\text{C}$ provides well-resolved proton and ^{13}C NMR spectra. From the NMR data acquisition perspective, the system in this state at $200\text{ }^\circ\text{C}$ is similar to that in solution. An evidence for this is the ease of acquisition of 2D NMR spectra using solution NMR pulse sequences. A COSY spectrum acquired under these conditions is shown in Figure 8. Gradients have also been used for 2D MAS NMR data acquisition of non-solid materials including gels and swollen resins [9]. However, commercial gradient MAS probes for operation at high temperatures are not yet available.

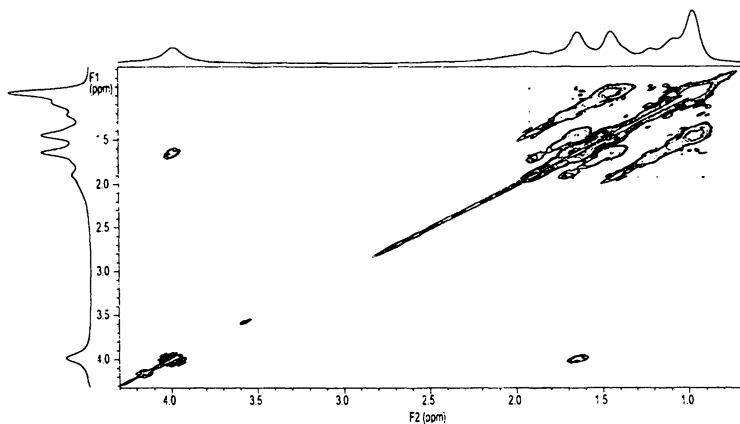


Figure 8. 7K MAS proton-proton COSY of poly(butyl methacrylate-co-2ethylhexyl acrylate) at $200\text{ }^\circ\text{C}$

In a semi-crystalline polymer or in a polymer that contains crystalline domains, it is necessary to break apart all the crystalline domains for a true representative high resolution NMR analysis. This can be achieved by either addition of solvent or acquisition of data at temperatures close to the melting temperature of the crystalline domains. At temperatures above the melting point

of a polymer, degradation and undesired reactions can occur. These can be minimized or made insignificant by using a low variable temperature (VT) gas flow rate. At a given VT gas temperature, the sample in the rotor will achieve the VT temperature at a rate that is inversely proportional to the VT gas flow rate, as long as all energy exchange processes available to the polymeric sample are reversible. However, since the degradation processes are irreversible, any excess energy available to the polymer will be sent along the degradation pathway. A low VT gas flow rate enables the sample in the rotor to maintain its temperature without providing significant excess energy that can be used for irreversible degradation processes. The presence of crystalline or rigid components can be determined by comparing the shape of the spinning side band in the proton NMR spectrum with that of the spectrum. For MAS speeds less than 10 kHz, presence of a broad side-band underneath the narrower side-band is an indication of the presence of crystalline domains. For higher MAS speeds, as attained in 3.2 mm probes, if the shape of the spinning side band is significantly different from that of the spectrum, most likely rigid domains are present at that given state/temperature.

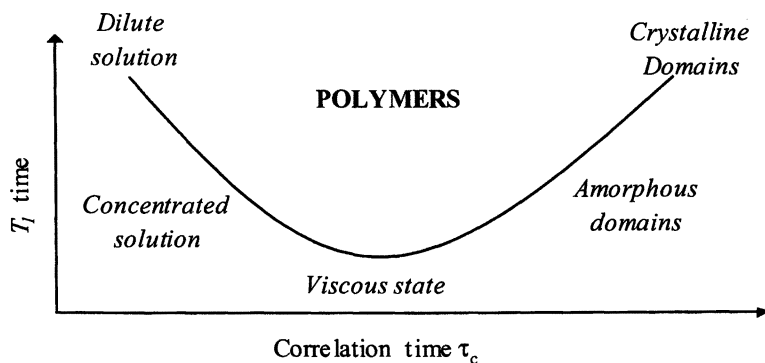


Figure 9. T_1 minima when in viscous or viscoelastic state

Another advantage of acquiring data in a viscous or viscoelastic state is presence of short T_1 times. On the chart of molecular correlation time versus T_1 time, depicted pictorially in Figure 9, dilute solutions and crystalline domains have long T_1 times at the two ends of the correlation spectrum. Concentrated solutions and amorphous domains have shorter T_1 times, but the viscous state is close to the T_1 minima and has the shortest T_1 time. This was reported a number of years ago by Farrar and Becker [10].

MAS NMR acquisition of polymeric materials at temperatures wherein the mobility is high provides multiple advantages:

- (1) The efficiency of spin diffusion processes is reduced, leading to increased T_2 and longer FID. This process also manifests as decreased cross-polarization efficiency with increasing temperature.
- (2) Fewer or no spinning side bands are observed because CSA is also averaged by the fluctuations.
- (3) The short T_1 time constant allows rapid acquisition of successive scans during signal averaging.
- (4) Isotropic chemical shifts (δ) are observed without interference from crystallization and morphological effects. These δ can be compared with values in databases of solution NMR spectra for identification and characterization.

Conclusions

The variable temperature capability of solid-state NMR spectrometers was exploited in order to obtain narrow NMR spectral resonances of rigid/semi-rigid polymeric materials. Acquisition of NMR spectra of polymeric materials in a soft/viscous state is possible by alteration of the physical state of the sample by any combination of temperature and plasticizing solvent.

Acknowledgement. *Thanks to Prof. Eric Munson at the University of Minnesota for numerous fruitful discussions. Support provided by Dr. Richard Newmark and the management at 3M CATC to these efforts for development of solid-state NMR techniques as molecular structure characterization tools is appreciated.*

Reference:

- [1] Sterna, L.L.; Smith, H.C. *J. Magn. Reson.* **1988**, *79*, 528-533.
- [2] Isbester, P.K.; Brandt, J.L.; Kestner, T.A.; Munson, E.J. *Macromolecules* **1998**, *31*, 8192-8200.
- [3] Stover, H.D.H.; Frechet, J.M.J. *Macromolecules* **1989**, *22*, 1574-1576.
- [4] English, A.D. *Macromolecules* **1985**, *18*, 178-181.
- [5] English, A.D.; Dybowski, C. *Macromolecules* **1984**, *17*, 446-449.
- [6] Fritzhanns, T.; Demco, D.E.; Spiess, H.W. *Mol. Phys.* **1999**, *97*, 931.
- [7] Tekely, P.; Goldman, M. *J. Magn. Reson.* **2001**, *148*, 135-141.
- [8] Rothwell, W.P.; Waugh, J.S. *J. Chem. Phys.* **1981**, *74*, 2721-2732.
- [9] Maas, W.E.; Laukien, F.H.; Cory, D.G. *J. Am. Chem. Soc.* **1996**, *118*, 13085-13086.
- [10] Farrar, T. C.; Becker, E.D. *Pulse and Fourier Transform NMR*; Academic Press: New York, 1971; Chapter 6, and Koenig, J. L. *Spectroscopy of Polymers*; ACS Professional Reference Book, American Chemical Society, Washington, DC, 1992, pp 260.

Chapter 4

NMR Studies of the Dynamics of Homo- and Block-Copolymer Poly(ϵ -caprolactone) Chains in Their Inclusion Compounds with α - and γ -CDs

J. Lu^{1,4}, P. A. Mirau², S. Nojima³, and A. E. Tonelli¹

¹Fiber and Polymer Science Program, North Carolina State University, Raleigh, NC 27695–8301

²Bell Labs-Lucent Technologies, 800 Mountain Avenue, Murray Hill, NJ 07974

³School of Material Science, Japan Advanced Institute of Science and Technology (JAIST), Tatsukonuchi, Ishikawa 923–12, Japan

⁴Current address: Department of Chemistry, University of Pennsylvania, Philadelphia, PA 19104

Solid-state NMR with magic-angle spinning has been used to study the structures and dynamics of semicrystalline homo- and copolymers of poly(ϵ -caprolactone) (PCL) and their inclusion complexes (ICs) formed with alpha and gamma-cyclodextrins (α - and γ -CDs), which are shown to have channel structures occupied by single and two parallel, side-by-side PCL homopolymer chains, respectively. In the PCL-polystyrene (PCL-PS) and PCL-poly(ethylene oxide)-PCL (PCL-PEO-PCL) di- and triblock copolymer-CD-ICs, only the PCL and both blocks are included in the CD channels, respectively. PCL (guest)-CD (host) magnetization exchange has been observed, but the results differ substantially from those usually evidenced by semicrystalline polymers and their blends. Conventional relaxation experiments [$T_1(^{13}\text{C})$, $T_{1\rho}(^{13}\text{C})$, and $T_{1\rho}(^1\text{H})$] and 2D wide line separation NMR with windowless isotropic mixing have been used to monitor the chain dynamics. The results show that the intermolecular interactions in the α -CD-IC channels restrict the dynamics of some PCL carbons more than others, but the PCL chains in both CD complexes are more mobile than in the

semicrystalline bulk samples. These results are also compared to the dynamics observed for valeric acid molecules when included in their IC with α -CD, which is also a channel complex structure.

It is well known that certain molecules such as urea, perhydrotriphenylene (PHTP) and cyclodextrins can form inclusion compounds (ICs) with polymers [1-2] during their cocrystallization, both from solution and the melt. An IC is formed when a small molecule “host” crystallizes into a matrix that encapsulates and squeezes individual polymer chains into separate, well-characterized channels. It is the well-defined geometrical environment (narrow cylindrical channels) that makes these complexes useful for studying the motions and conformations of segregated polymer chains. Cyclodextrins (CDs) are cyclic molecules. Since α -CD consists of six glucose units connected by α -1, 4-glucosidic linkages, the diameter of its cavity is only 4.9 Å, which is much less than that of γ -CD (7.9Å) consisting of eight glucose units. Because of size compatibility, only single PCL chains can be incorporated inside the α -CD channels, while two side-by-side, parallel PCL chains can be threaded inside the γ -CD channels. In this study, we investigated the length scale of mixing and molecular motions of PCL homo- and block copolymers in these two inclusion complexes by solid state NMR spectroscopy.

Experimental

Materials

PCL was purchased from Scientific Polymer Products, and CDs and valeric acid (VA) were obtained from Cerestar and Aldrich Chemical Co., respectively. PCL-poly(ethylene oxide) (PEO)-PCL triblock with $M_w = 14,140$ is characterized by PCL-PEO block lengths of 35, 140 repeat units. The PCL-polystyrene (PS) diblock has a $M_w = 16,470$ and PCL,PS block lengths of 35,120. The α -CD/PCL inclusion complex was prepared by a sonication method [3]. Both PCL (0.2 g in 50 mL acetone) and saturated α -CD solutions (7.25 g in 50 mL water) were heated to 70°C and the PCL solution was slowly added to the α -CD with sonication. The mixture was kept at 70°C for 17 minutes with sonication. A white precipitate was formed after 10 hours of quiescent storage. The γ -CD/PCL inclusion complex was prepared by a heating technique. Both PCL (0.2 g in 50 mL acetone) and saturated γ -CD solutions (11.6 g in 50 mL water) were heated to 70°C and the PCL solution was slowly added to the γ -CD with stirring and heating. A white precipitate was formed overnight. After filtration and washing with distilled water, the α -CD/PCL and γ -CD/PCL samples were dried in a vacuum oven. Valeric acid (VA)- α -CD/IC and the α - and γ -CD/ICs with the di- and triblock copolymers were similarly formed.

Solid State NMR Spectroscopy

Solid-state ^{13}C -NMR measurements were performed on a Varian Unity spectrometer at 100 MHz using a 7.5 mm magic-angle spinning probe. The spinning speed was regulated at 3500 Hz or 4500 Hz, and the carbon and proton pulse widths were set to 4.2 μs . The proton $T_{1\rho}$ relaxation times were measured using the cross polarization pulse sequence preceded by a variable proton spin-lock period [4]. The two-dimensional ^{13}C - ^1H HETCOR spectra were collected using the pulse sequence described previously [5]. BLEW-12/BB-12 decoupling was applied during the evolution period to suppress homonuclear proton and carbon-proton dipolar interactions, and the spectra were acquired with one WIM-24 mixing cycle [6]. Spin-lattice relaxation times (T_1) were measured by two pulse sequences, CP- T_1 and saturation-recovery- T_1 . The 2D wide line separation [7] spectra with windowless isotropic mixing [8] were measured [9,10] using a 300 kHz sweep width in the proton dimension and a 30 kHz sweep width in the carbon dimension

Results and Discussion

The inclusion complexes formed by α -CD and γ -CD with PCL have been characterized by DSC, FTIR and X-ray diffraction [3,11]. These studies showed that complexes are formed and adopt channel structures. PCL and PEO chains of the triblock copolymer are included in both α - and γ -CD/ICS, while the PS chains in the diblock copolymer are excluded from the channels of α - and γ -CD/ICS. In the bulk PCL-PS diblock the PCL blocks do not crystallize, and so rubbery, amorphous PCL blocks are bonded to glassy, amorphous PS blocks. Figure 1 shows the 100 MHz solid-state NMR spectra for α -CD, PCL and the α -CD/PCL inclusion complex. The signals from PCL are easily identified and are well resolved from the α -CD signals in the complex. The chemical shifts for PCL in the inclusion complex are similar to those observed in the semicrystalline sample, suggesting that the PCL in α -CD channels adopts an extended all-trans conformation [3]. We can observe similar characteristics in the complex between PCL and γ -CD. However, the cross polarization dynamics indicates that the maximum intensity for the PCL peaks was observed with a 4 ms cross polarization time, rather than the shorter 1 ms contact time used for the α -CD complex.

The length scale of phase separation is of interest in many polymeric systems, and several methods have been developed to measure domain sizes using proton spin diffusion. In the present study we have used the proton $T_{1\rho}$ relaxation rates to measure magnetization exchange between the guest polymer and the CDs. If there is efficient magnetization exchange on a length scale of 20 Å or less, then an average relaxation time will be observed between the polymer

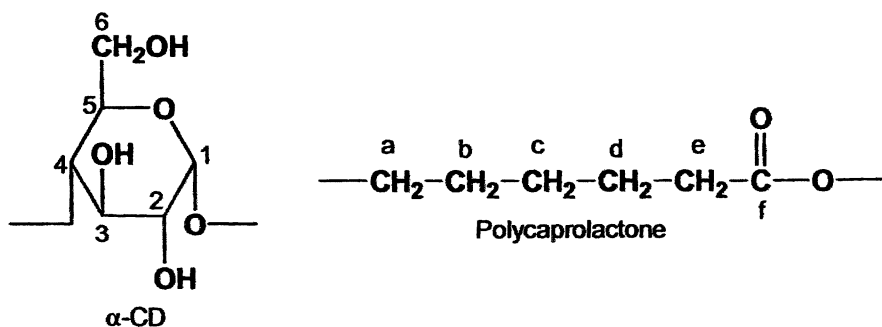
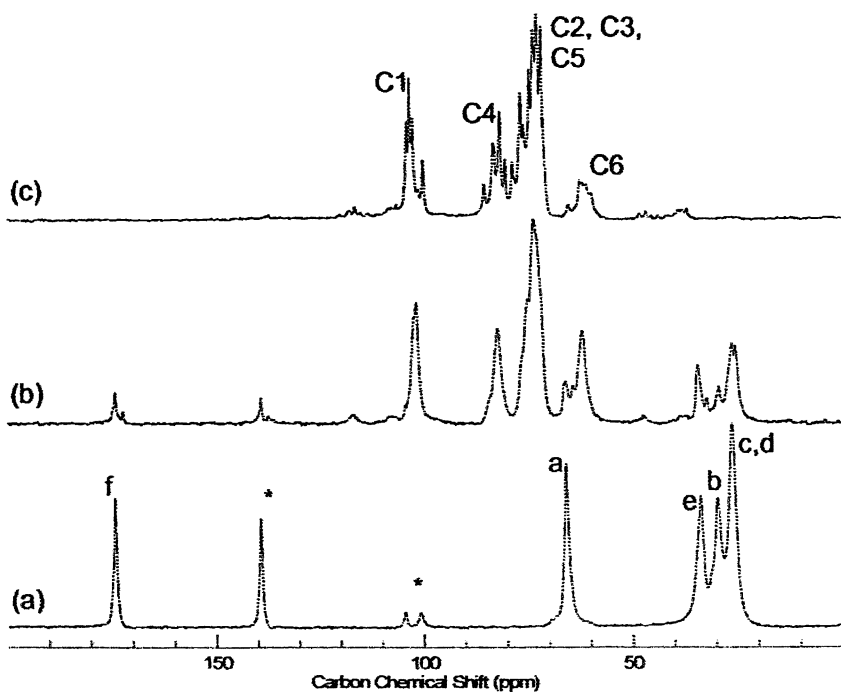


Figure 1. The CP/MAS spectra of (a) PCL, (b) PCL- α -CD-/C, and (c) α -CD. Spinning sidebands are marked with (*).

and the host matrix. Table 1 shows the results for the proton $T_{1\rho}$ relaxation measurements for α -CD, PCL and the α -CD/PCL complex. Semicrystalline PCL has a long relaxation time (54 ms) while the relaxation time for the pure α -CD is much shorter (4.9 ms). The values for α -CD and PCL in the complex are intermediate between these two values, showing that there is some spin diffusion between the host and the included polymer. However, the proton $T_{1\rho}$ relaxation times for PCL and α -CD are not identical, demonstrating that the spin diffusion is not complete. Such behavior is not expected, since the polymer in the α -CD channel is expected to be within the length scale of spin diffusion probed by proton $T_{1\rho}$ relaxation (20 Å). Proton spin diffusion over length scales as long as 200 Å is the result of many individual magnetization transfer steps. The rate of spin diffusion depends on polymer chain dynamics and the proton density. We believe that the fundamental difference between most materials and the polymer inclusion complexes is that the proton density is not uniform. There is a high density of protons along the polymer chain and in the α -CD that can promote efficient spin diffusion. In most solid polymers there are van der Waals contacts between chains that cause the protons from neighboring chains to be in close contact. The polymer in the inclusion complex is constrained by chain connectivity to occupy the center of the channel. It may be that this forces the PCL and the α -CD protons to be more distant than they would be in normal organic solids, and this greater separation is the reason that we do not see efficient spin diffusion between the polymer and the host. However, we observe that both the γ -CD and PCL carbons have the same relaxation times in the complex, showing that there is efficient spin diffusion between the crystal frame γ -CD and included PCL chains. This maybe because the guest is in closer contact with the host, since two PCL chains can be incorporated inside the γ -CD channels. In VA- α -CD-IC and the triblock copolymer α - and γ -CD/ICs, we observed efficient spin diffusion between the crystal frame CDs and the small molecule VA and triblock copolymer guest, while inefficient spin diffusion is observed between the PCL and CD protons in the diblock- α - and - γ -CD/ICs.

Table 1. Comparison of the $T_{1\rho}(^1\text{H})$ relaxation times for PCL- α CD/IC and PCL- γ CD/IC.

	$T_{1\rho}(^1\text{H})$ (ms)		Samples	$T_{1\rho}(^1\text{H})$ (ms)	
	α -CD	PCL		γ -CD	PCL
α -CD	4.9		γ -CD	2.7	
PCL- α CD-IC	11.9	15.4	PCL- γ CD-IC	9.3	9.1
PCL		54	PCL		54.0

In order to confirm this view, we performed the solid-state heteronuclear correlation experiment, which can measure spin diffusion more accurately. With

**American Chemical Society
Library**

1155 16th St., N.W.

In NMR Spectroscopy of Polymers in Solution and in the Solid State; Cheng, H., et al.; ACS Symposium Series, American Chemical Society: Washington, DC, 2003.

a short mixing time this experiment can give a correlation of the solid-state carbon and proton spectra. If there is efficient spin diffusion during the mixing time, the average proton chemical shifts for each resolved carbon resonance can be observed due to spin diffusion. Figure 2 shows the heteronuclear correlation spectrum of α -CD/PCL inclusion complex with two different mixing times: (1) 50 μ s and (2) 10 ms. A mixing time of 50 μ s is too short for significant spin diffusion and a normal heteronuclear correlation spectrum is observed. The proton chemical shifts of α -CD and the PCL are shifted toward each other due to spin diffusion during the 10 ms mixing time, however, the spin diffusion is not complete, with remaining proton chemical shift differences between the guest and the host. Comparing with the heteronuclear correlation spectrum of γ -CD/PCL complex (see Figure 3), we observed identical proton chemical shifts of the guest PCL and host γ -CD in the complex, indicating that there is efficient spin diffusion between them, as also observed in the VA- α -CD/IC, the di- and triblock- α -CD/ICs, and the triblock- γ -CD/IC, but not in the diblock- γ -CD/IC, where completely efficient spin diffusion is not observed during the 10 ms mixing time.

Figures 4 and 5 present the heteronuclear correlation spectra for the diblock PCL-PS ICs with α - and γ -CD, respectively, where it is apparent that the PS protons are not in close proximity to the host protons of α - or γ -CDs. This clearly confirms that the PS blocks are excluded from the CD channels. At the same time, however, the PCL and CD protons are proximal, and at $\tau_m = 10$ ms nearly identical proton resonance frequencies are observed for both guest PCL blocks and host CDs due to spin diffusion between their nearby protons. Also note that the aliphatic backbone carbons (g) at ~ 40 ppm show correlation to both the aliphatic and aromatic protons (h), which is possibly due to cross-polarization of the methine carbon by the ortho protons. There is clearly spin-diffusion between PS protons, but not between PS protons and the PCL or CD protons.

The dynamic behavior of the inclusion complexes can be studied by the measurement of the ^{13}C T_1 relaxation times and the application of specific pulse sequence. In this study we employed two pulse sequences to measure the ^{13}C T_1 relaxation rates: saturation-recovery T_1 and CP- T_1 , and obtained consistent results. The T_1 values for the carbon nuclei of the PCL, α -CD/PCL, α -CD, γ -CD/PCL and γ -CD are given in Table 2. Double exponential relaxation times are observed for the bulk PCL and the α -CD. Large changes in the $T_1(\text{C})$'s for bulk PCL are observed upon complex formation. Single exponential recovery is observed for both the polymer and α -CD in the complex. The relaxation rates of the PCL chains included inside the α -CD channels are fast: 0.24-0.31s for methylene carbons, which is only 0.1% to 0.2% of the relaxation times observed for bulk PCL. However, we did not observe much difference between α -CD/PCL and γ -CD/PCL complexes. Although the α -CD channel can only accommodate single PCL chains and the γ -CD channel is large enough to accommodate two side-by-side parallel chains, the PCL chains show

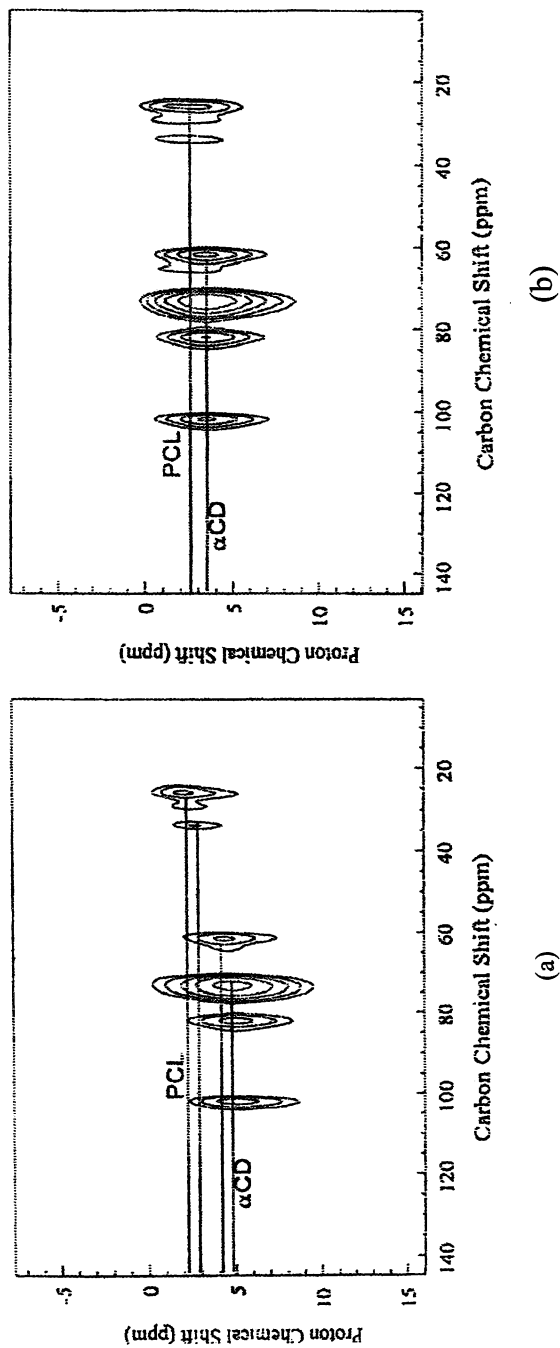


Figure 2. The heteronuclear correlation spectrum for the α -CD/polycaprolactone complex obtained with two different mixing times: (a) 50 μ s and (b) 10 ms.

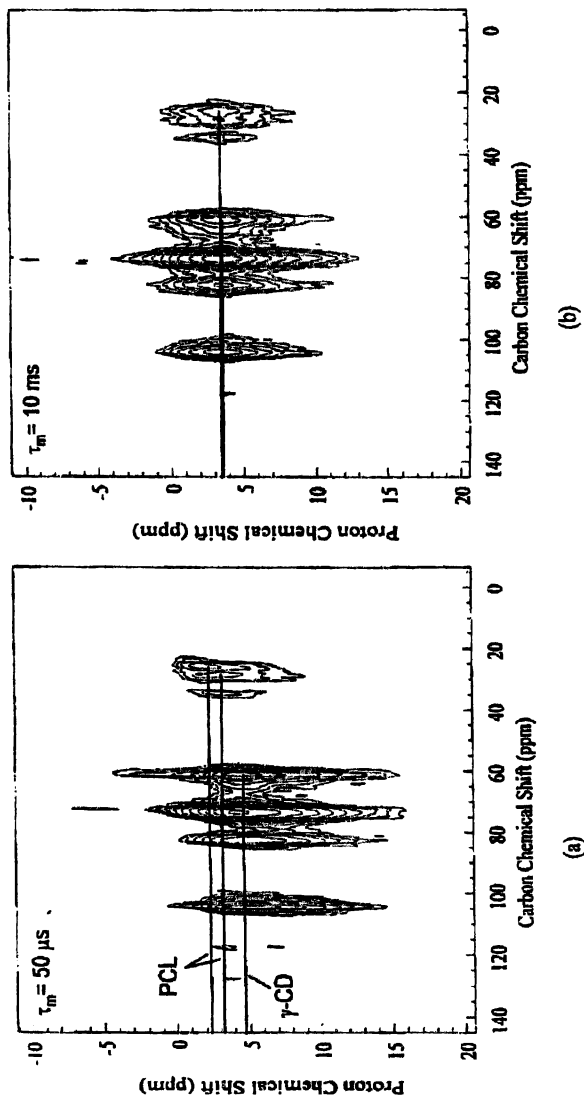


Figure 3. The heteronuclear correlation spectrum for the γ -CD/polycaprolactone complex obtained with two different mixing times: (a) 50 μ s and (b) 10 ms.

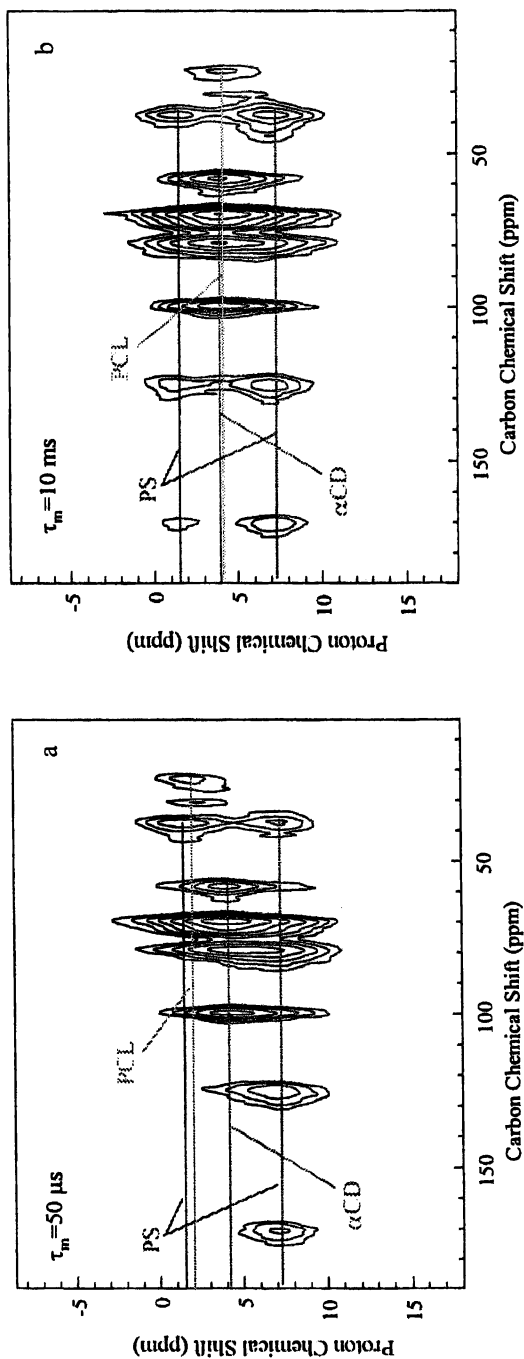


Figure 4. The heteronuclear correlation spectrum for the α -CD/PCL-PS complex obtained with two different mixing times: (a) $50 \mu\text{s}$ and (b) 10 ms .

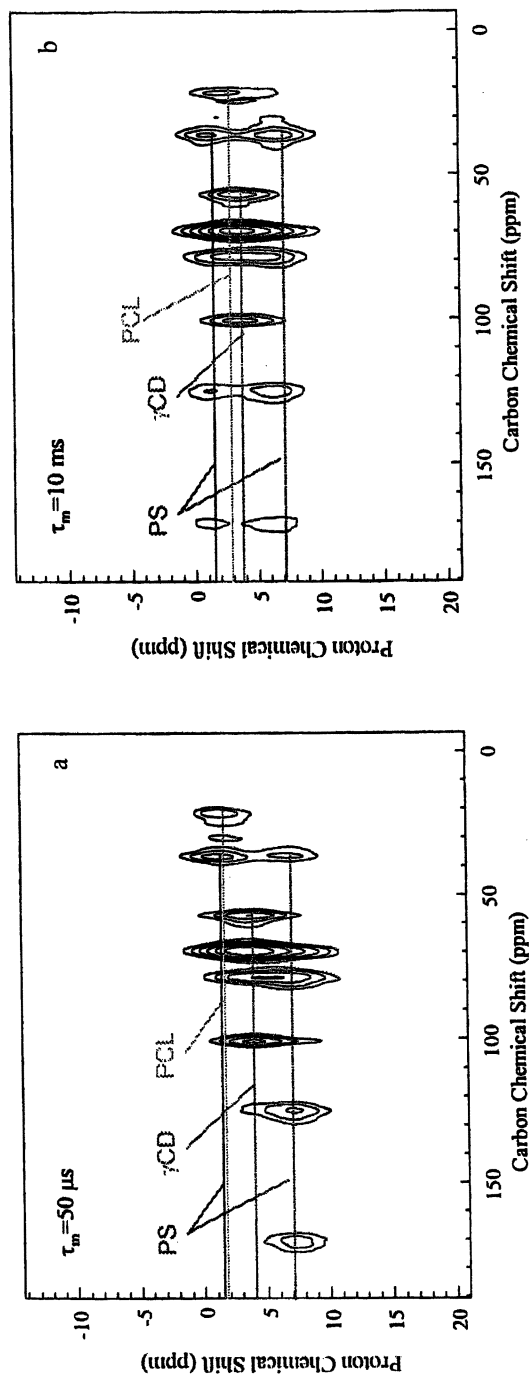


Figure 5. The heteronuclear correlation spectrum for the γ -CD/PCL-PS complex obtained with two different mixing times: (a) 50 μ s and (b) 10 ms.

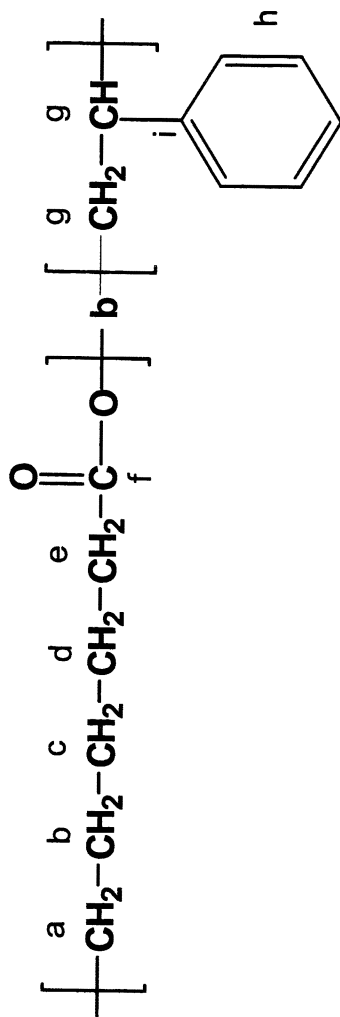


Table 2. $T_1(^{13}\text{C})$ values for the carbon nuclei of the α -CD, γ -CD, poly(ϵ -caprolactone) and their inclusion complexes.

Samples	Polycaprolactone				α, γ -CD			
	a	b	c, d	e	C1	C4	C2, C3, C5	C6
PCL	169.8 3.28	160.6 1.23	161.5 1.22	223.6 1.68				
α -CD/PCL	0.24	0.26	0.31	0.29	31.7	24.3	18.3	0.84
α -CD					147.4 1.32	169.4 8.64	161.5 3.34	110.5 6.65
γ -CD/PCL	0.22	0.19	0.28	0.17	31.3	22.2	18.0	0.85
γ -CD					78.1	35.9	36.4	16.2 1.04

similar mobility in the megahertz regime in these two different host environments. This would indicate that cooperative motion of side-by-side parallel PCL chains in the γ -CD/PCL inclusion complex, if they occur, are not influencing megahertz $T_1(\text{C})$ relaxation. Very similar $T_1(\text{C})$ s were observed for the PCL chains in the diblock and triblock α - and γ -CD-ICs, though in the bulk diblock the PCL are not crystalline and thus quite mobile with $T_1(\text{C})$ s ~ 1 s.

Interestingly the $T_1(\text{C})$ s observed for the PS block in the bulk PCL-PS diblock are shorter than those observed in the diblock α - and γ -CD/ICs. Connectivity of PS blocks to rubbery PCL in the bulk diblock copolymer, as opposed to included PCL blocks in the CD-ICs, apparently facilitates the high-frequency (MHz) motions of the glassy PS blocks.

We also employed 2D WIM/WISE experiments [9-11] to study the molecular dynamics of the complexes. The advantage here is that the WIM quenches spin diffusion during the cross polarization. This means that the proton line widths can be directly related to the dynamics of the individual protons rather than the average values for the entire chain that is measured using the original WISE experiment.[7] The line widths for PCL in the inclusion complex with α -CD are reduced relative to semicrystalline PCL, as seen in Table 3. The methylene nearest the carbonyl group (*e*) shows the largest reduction in line width, from 52 kHz in semicrystalline PCL to 26 kHz in the inclusion complex. The methylenes at the center of the PCL monomer (*c, d*) are reduced from 54 kHz in the crystal to 30 kHz in the complex. The methylene nearest the oxygen shows the smallest change in line width (51 to 41 kHz). This shows that the chain is not uniformly restricted in the channel, but that some methylene groups are more mobile than others, which may be due to hydrogen bonding between the guest and the host (see Figure 6). But we do not observe such a gradient in proton line widths for pairs of PCL chains included in γ -CD channels. Also the proton line-widths observed for the methylene groups in VA- α -CD/IC are very comparable to those observed in the PCL- α - and γ -CD/ICs, so over all rigid-body rotation or libration about the chain axis, which would be expected to

Table 3. The proton linewidths for α -CD, γ -CD, PCL, and their inclusion complexes measured by 2D WIM/WISE NMR.

Sample	Linewidth (kHz) ^a							
	α -CD				Polycaprolactone			
	C1	C4	C2,C 3,C5	C6	a	b	c,d	e
α -CD	45	46	45	59				
α - CD/PCL	44	47	40	45	41	33	30	26
γ -CD	45	46	45	59				
γ - CD/PCL	46	40	40			34	26	34
PCL					62	51	54	52

a - The reported line widths are the full width at half-maximum.

be more facile for VA, are likely not contributing to the mid-kHz motions of the included PCL chains.

Cooperative, long-chain motions in the mid-kilohertz regime for pairs of PCL-PEO-PCL chains in their γ -CD channels seem more restricted than for the single triblock chains in their α -CD/IC channels. For the PCL-PS diblock, where PS is excluded in the α -, γ -CD/ICs, the mid-kilohertz PCL chain motions are similar to those observed in the homopolymer PCL- α - and γ -CD/ICs. The PS proton line widths are broader in the PCL-PS- α and γ -CD/ICs than in the bulk PCL-PS diblock, where the glassy PS blocks are attached to rubbery PCL blocks. Thus the larger amplitude, lower frequency mid-kHz motions in glassy PS blocks are facilitated by attachment to rubbery PCL blocks, in comparison to PS chains attached to PCL blocks included in the CD-ICs. Thus, both the high-frequency (MHz), low-amplitude and lower-frequency (kHz), larger amplitude motions contributing to the $T_1(\text{C})$ relaxation and ^1H line-width narrowing, respectively, in phase-separated, glassy PS blocks are sensitive to the morphology and mobility of the PCL blocks to which they are attached.

Conclusions

In summary, we have used solid-state NMR to probe the structure and dynamics of the α - and γ - inclusion complexes with PCL homo- and block copolymers. The α -CD inclusion complex with PCL differs from other materials in that there is not an even distribution of protons, so that spin diffusion is inefficient when the PCL chains have to occupy the center of α -CD channels, but

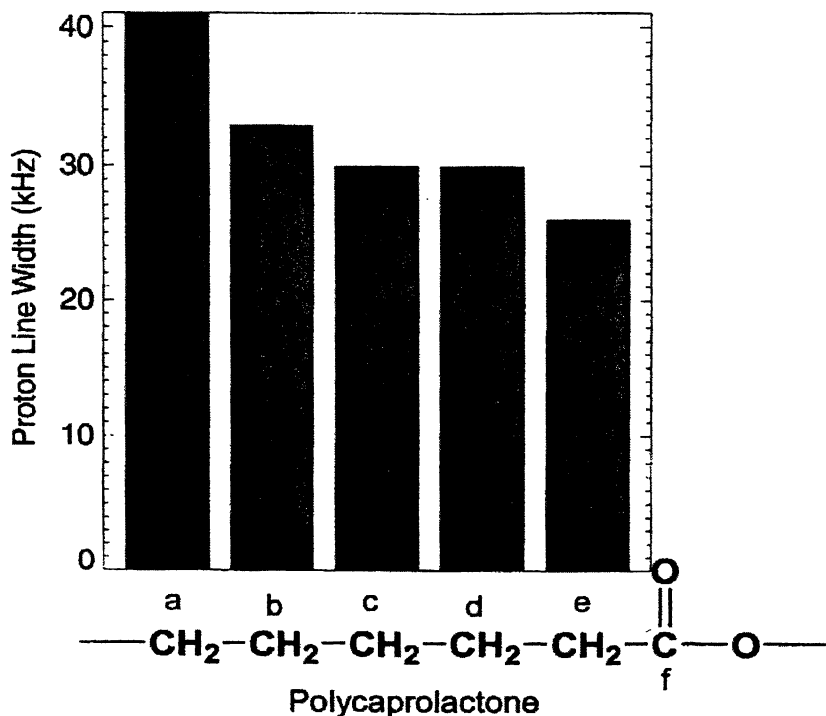


Figure 6. Plot of the proton line widths measured by 2D WIM/WISE NMR for each PCL methylene carbon in the PCL- α -CD-IC (See Table 3).

efficient for pairs of PCL chains in γ -CD channels due to the closer distance between the guest and the host. Complex formation is driven by intermolecular interactions, and these interactions exert an effect on the chain dynamics, with those portions of the chain nearest the main chain oxygen being the most restricted for the α -CD complex. However, we did not observe such a dynamic gradient for pairs of PCL chains in the γ -CD complex, which may be due to the increased cooperative nature of the motion of side-by-side, parallel PCL chains. Also we observe some difference between the motions of included block copolymer PCL chains depending on whether or not the non-PCL blocks are also included.

Solid-State NMR observations of polymer chains included and segregated in the narrow channels of the crystalline inclusion compounds formed with CD hosts reveal motions in the MHz and mid-kHz regimes which differ from those observed in their bulk samples. **What is not clear, as yet, is why?** However,

because of the well characterized structural environment experienced by polymer chains residing in the narrow cyclodextrin channels, and because their motions are necessarily unaffected by cooperative interchain interactions, except when pairs of narrow cross section polymer chains are included side-by-side in their γ -CD/ICs, we believe that further NMR observations and molecular modeling analyses of their motions may lead to a more complete description. By comparison to the motions observed in their bulk samples, we may then be able to better describe the solid-state dynamics of polymers.

Acknowledgements. The authors of this paper would like to thank the Army Research Office (MURI#DAAH04-96-1-0018-01), North Carolina State University and Bell Labs at Lucent Technologies for supporting this work.

References

1. Farina, M., *Inclusion Compounds*, eds J. Attwood, J. Davies and D. MacNicol, Academic press, London, **1984**, Vol. 2, Ch. 10.
2. Silvestro, G.; Sozzani, P. *Comprehensive Polymer Science*, eds G. Eastman *et al.*, Pergamon Press, Oxford, **1988**, Vol. 2, Ch. 18.
3. Huang, L.; Allen, E.; Tonelli A.E. *Polymer* **1997**, *39*, 4857.
4. Bovey, F. A.; Mirau, P. A. *NMR of Polymers*; Academic Press: New York, **1996**.
5. White, J. L.; Mirau, P. A. *Macromolecules* **1994**, *27*, 1648.
6. Caravatti, P.; Braunschweiler, L.; Ernst, R. R. *Chem. Phys. Lett.* **1983**, *100*, 305.
7. Schmidt-Rohr, K.; Clauss, J.; Spiess, H. *Macromolecules* **1992**, *25*, 3273.
8. Caravatti, P.; Bodenhausen, G.; Ernst, R. R. *Chem. Phys. Lett.* **1982**, *89*, 363.
9. Qiu, X.; Mirau, P. A. *J. Magn. Reson.* **2000**, *142*, 183.
10. Lu, J.; Mirau, P. A.; Tonelli, A. E. *Macromolecules* **2001**, *34*, 3276.
11. Lu, J.; Mirau, P. A.; Shin, I. D.; Nojima, S.; Tonelli, A. E. *Macromol. Chem. & Phys.*, **2001**, to appear.

Chapter 5

Structural Aspects of Low-Molecular-Weight Azocellulose Polymers: A Solid-State ^{13}C NMR Study[†]

Suizhou Yang, Monsey M. Jacob, Lian Li, Ashok L. Cholli, and Jayant Kumar

Center for Advanced Materials, Department of Chemistry and Physics,
University of Massachusetts at Lowell, Lowell, MA 01854

Azobenzene-modified cellulose (azocellulose) polymers were synthesized by covalently linking 4-cyanophenylazophenol to commercially available low molecular weight cellulose samples via Mitsunobu reaction. These azocellulose polymers were characterized by solid-state ^{13}C NMR and FTIR spectroscopic techniques. The analyses of data suggest that the coupling reaction occurs preferentially at the C6 carbon position and the primary alcohol is the most reactive group among the three-hydroxyl groups in the repeating β -D-glucopyranose units. These results are consistent with azocellulose polymers that were prepared with ultrahigh molecular weight natural cellulose. Surface relief gratings (SRGs) were also inscribed holographically on the thin films of azocellulose polymers.

[†]Dedicated in memory of Professor Sukant K. Tripathy

Since the discovery of the photoinduced surface relief gratings (SRGs) on the thin films of azobenzene-modified polymers (1,2) at temperatures below their glass-transition temperature (T_g), these azopolymers have received attention lately due to their potential use as optical storage materials (1-7). When irradiated with two interfering polarized laser beams, the azobenzene chromophores in the azopolymers will undergo trans-cis-trans isomerization and induce SRGs on the polymer thin films. This phenomenon has been observed on the films of various azobenzene polymers, such as epoxy polymers, polyacrylates, polyesters, conjugated polymers and polyazophenol (1-7). SRGs can also be inscribed on the films prepared from azobenzene-modified cellulose samples with ultrahigh molecular weights (8). It is interesting to know the role of molecular weight of cellulose on the formation of SRGs. The focus of this report is to investigate suitability of commercially available low molecular weight cellulose for the formation of SRGs.

Cellulose, a biomacromolecule composed of β -D-glucopyranose units linked together by (1-4)-glycosidic bonds, is the most abundant polymer in nature. The linked β -D-glucopyranose units alternate up and down and form a linear polymer backbone chain. Because of the bulky nature of β -D-glucopyranose rings and the strong intra- and inter-molecular hydrogen bonding, cellulose has a high T_g of ca. 230 °C (9). Every β -D-glucopyranose unit contains three hydroxyl groups, which can participate in the Mitsunobu reaction (10). One of the typical Mitsunobu reactions is the alkyl aryl ether formation from phenol and alcohol in the presence of diethylazodicarboxylate (DEAD) and triphenylphosphine (TPP) (10). Thus, azophenol can be covalently linked to the cellulose by Mitsunobu reaction to give azobenzene-modified cellulose for optical applications. In this paper, 4-cyanophenylazophenol was covalently linked to commercially available low molecular weight cellulose samples. The experimental results are also discussed on the formation of SRGs on these azopolymers. The solid state structural characterization using solid state ^{13}C NMR reveals (a) morphological changes as a result of azofunctionalization of cellulose, (b) preferential site for azocoupling on the cellulose, and (c) extent of coupling.

Experimental Section

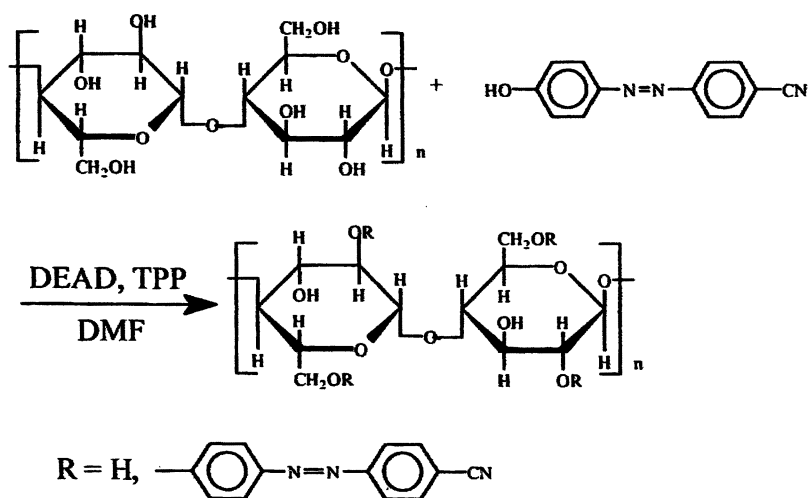
Materials

Two commercial cellulose samples were received from International Paper Company and are described as follows: (1) ESTERCELL; viscosity (CED) is 6.5 and DP (degree of polymerization) is ca. 1000, and (2) VISCOCELL; viscosity (CED) is 3.1 and DP is ca. 500. These samples were dried in vacuum

at 80 °C for overnight prior to their use in azocellulose synthesis by Mitsunobu reaction.

4-cyanophenylazophenol was synthesized by diazotation of 4-aminobenzonitrile with sodium nitrite and then coupling with phenol (11). The model compound 4-cyano-4'-methoxyazobenzene was also synthesized according to the procedure described in ref. (11).

Scheme 1. Synthesis of azocellulose polymers by Mitsunobu reaction



Scheme 1 shows the synthesis of azocellulose by Mitsunobu reaction. Cellulose was reacted with 4-cyanophenylazophenol in *N,N*-dimethylformamide in the presence of triphenylphosphine (TPP) and diethylazodicarboxylate (DEAD) (11). The azocellulose was obtained by precipitation with methanol and purified through repeated dissolution and precipitation with DMF and methanol. The Degree of substitution (DS) of polymers was determined on the basis of the molar extinction coefficient of the trans form of the model compound 4-cyano-4-methoxyazobenzene ($\lambda_{\text{max}} = 361$ nm, $\epsilon_{\text{max}} = 2.13 \times 10^4$) in DMF solution. Since there are three hydroxyl groups in the β -D-glucopyranose unit, the maximum DS would be 3 if all the hydroxyl groups were substituted by azobenzene chromophores in each glucose ring. Three azocellulose samples were prepared, AZOEST21, AZOEST49 and AZOVIS69, with varying composition that are listed in Table 1.

Characterization

The solid-state ^{13}C CP/MAS (cross polarization and magic angle spinning) NMR spectra were acquired on a Bruker DRX 300 MHz NMR spectrometer operating at a frequency 75.46 MHz. The magic angle-spinning (MAS) rate for the 4mm rotor was 10 KHz so that the solid-state NMR spectra were free from spinning side bands. The typical experimental parameters for collecting solid state NMR data were as follows: 2k data size, 2ms contact time, 31250 Hz spectral width, 32 ms acquisition time, and 15,000 FIDs were co-added. The data were weighed with an exponential function using a line broadening of 5 Hz prior to Fourier transformation (FT). The recycle time delay was 3 s. The proton $\pi/2$ pulse width was 3.6 μs . Infrared spectra were recorded on a Perkin-Elmer 1720 FT-IR spectrometer. The KBr pellets were prepared by using thermally treated KBr powder for cellulose and 4-cyanophenylazophenol samples. In the case of azocellulose polymer sample, a thin film was cast on KBr discs from the azocellulose sample solution in DMF.

Surface Relief Grating (SRGs) Fabrication

The polymer films were cast on a glass substrate from the polymer solution containing mixed solvents of hexafluoroisopropanol and trifluoroacetic acid (80:20 by volume). SRGs were fabricated on the azocellulose film of ca. 1 μ thick using a simple interferometric set-up (4) at 488 nm with an intensity of 200 mW/cm². The polarization of the two writing beams was set to $\pm 45^\circ$ with respect to the s-polarized beam. The SRGs were investigated by an atomic force microscopy (AFM) in the contact mode under ambient conditions. The surface topology and surface profiles from the AFM images provided the spacings and the surface modulation depths of the surface relief gratings.

Results and Discussion

Table 1 shows the experimental conditions for the synthesis of azocellulose polymers through alkyl aryl ether formation via Mitsunobu reaction (Scheme 1). Samples AZOEST21 and AZOEST49 were prepared from ESTERCELL cellulose, and Sample AZOVIS69 was prepared from VISCOCELL cellulose. The degrees of substitution (DS) for these samples are 0.21, 0.49 and 0.69, respectively.

Table 1. Azocellulose polymers obtained by modification of cellulose .

Sample (g)	Cellulose (g)	TPP (g)	DEAD (ml)	Dye (g)	DS
AZOEST21	1.00	6.00	3.30	5.00	0.21
AZOEST49	1.00	7.40	4.20	6.30	0.49
AZOVIS69	1.00	7.40	4.20	6.30	0.69

Figure 1 shows the ^{13}C CP/MAS NMR spectra of ESTERCELL cellulose (Spectrum a), AZOEST21 (Spectrum b), AZOEST49 (Spectrum c) and 4-cyanophenylazophenol (Spectrum d). The assignments of solid-state ^{13}C NMR resonance peaks for cellulose samples were based on the work of Atalla and VanderHart (12,13). For ESTERCELL cellulose in Spectrum a, C4 and C6 carbons show peaks due to crystalline and amorphous regions. Compared to the resonance peaks for crystalline regions, the amorphous resonance peaks are broad and appear up field. The narrow resonance peak at 64.4 ppm is assigned to the carbon C6, at which the primary alcohol groups is linked, in crystalline domains, whereas the amorphous region C6 carbons appear as a shoulder to this peak at 62.3 ppm. The C4 carbons in the crystalline domains appear at 88.4 ppm as a narrow resonance peak, whereas amorphous C4 carbons present at 83.4 ppm as a broad and up-field resonance peak. The resonances in the 70-80 ppm chemical shift range are associated with the ring carbons C2, C3, and C5. The most down field peaks in Spectrum a, at 105.1 and 103 ppm, are assigned to C1, the anomeric carbon. The multiplet peaks of C1 may be due to the occurrence of non-equivalent glycosidic linkages (12, 13).

The ^{13}C CP/MAS NMR spectrum of 4-cyanophenylazophenol is presented in Spectrum d (Figure 1). The assignments of these resonances have been reported before (11) and are shown in Figure 1. The resonance peak at 163.3 ppm is assigned to C1' carbon. Two carbons that are bonded to azo double bond $-\text{N}=\text{N}-$, C4' and C5' appear at 147.6 and 155.4 ppm, respectively. The carbon C8' is expected to be in the up-field of the aromatic region as result of its bonding to a cyano group ($-\text{C}\equiv\text{N}$) and it appears at 111.7 ppm. All the protonated aromatic carbon resonances (C2', C3', C6' and C7') appear in the 115-140 ppm region. The resonance for cyano carbon C9' is overlapped with the C2' resonance peak in the Spectrum d.

In the Spectrum b for azocellulose polymer, AZOEST21, a new broad peak in the up-field region appears at 53.8 ppm as a result of Mitsunobu reaction between ESTERCELL cellulose and 4-cyanophenylazophenol. This peak indicates the formation of alkyl aryl ether via linking azobenzene chromophores to the cellulose. It is interesting to compare the relative changes in the intensities of crystalline and amorphous peaks in the ^{13}C NMR spectra of cellulose and azocellulose polymers. The intensity of the broad resonance peak at 62.3 ppm

that is assigned to the amorphous domain of the cellulose in Spectrum a is decreased in Spectrum b and a new resonance appeared at 53.8 ppm. This suggests that the Mitsunobu type coupling is preferentially taking place in the amorphous region of the polymer. The position of this new peak also suggests that coupling is at the primary alcohol group. In addition, the slight changes in the peak intensities of resonances in the 70-80 ppm region indicate that there may be some coupling reactions which are taking place at the other hydroxyl groups on the ring. The appearance of downfield resonances in the aromatic region signifies the linkage of azochromophores to the cellulose polymer chains. As the DS is increased from 0.21 to 0.49, the prominent ^{13}C NMR spectral features were also changed. The peak at 53.8 ppm in Spectrum b becomes stronger in Spectrum c of AZOEST49, whereas the intensity of the C6 carbon resonance that appeared at 64.4 ppm decreased dramatically. The intensity of the resonance at 88.4 ppm, which is attributed to C4 carbons in the crystalline regions of the cellulose, also decreased significantly from a sharp and strong peak in Spectrum a to a weak and broad peak in Spectrum c. The strong and sharp resonance at 105.1 ppm in Spectrum a, the anomeric carbon C1, also decreased and a new broad up field shoulder appeared in the 90-102 ppm region. This broad peak may be assigned to carbon C1 in the amorphous region of azocellulose. Correspondingly, the intensity of downfield peaks associated with azobenzene chromophores in azocellulose is significantly increased with DS.

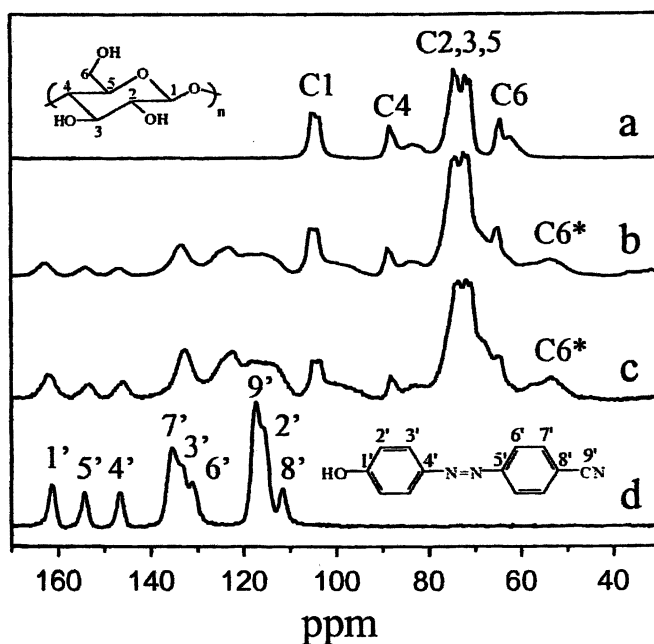


Figure 1. The ^{13}C CP/MAS spectra of ESTERCELL cellulose (a), AZOEST21 (b), AZOEST49 (c), and 4-cyanophenylazophenol (d).

Figure 2 shows the ^{13}C CP/MAS NMR spectra of VISCOCELL cellulose (molecular weight ca. 80,000) (Spectrum a), AZOVIS69 (Spectrum b) and 4-cyanophenylazophenol (Spectrum c). The assignments of solid-state ^{13}C NMR resonance peaks for VISCOCELL cellulose and 4-cyanophenylazophenol are the same as presented in Figure 1. In the ^{13}C CP/MAS NMR spectrum b, the C6 peak intensity decreased significantly and the new peak corresponding to C6* appear at 53.6 ppm, which indicates the formation of the alkyl aryl ether at C6 position. The peak at 88.3 ppm, which is associated with the crystalline region of polymer, decreased significantly in spectrum b compared with spectrum a. And at the same time, a broad peak up-field to C4 appeared and is overlapped with the resonances of C2, C3 and C5 carbons of azocellulose. The appearance of this broad peak also suggests that the polymer is transforming from crystalline to a highly amorphous polymer. This indicates that the long azobenzene chromophores attached at the C6 carbons may prevent polymer chains forming the crystalline domains in the azocellulose samples. The interchain spacings may be too large to form a packed crystalline order. The spectral changes for the resonance peak of anomeric carbon C1 in Figure 2 is similar to the changes that were observed for AZOEST in Figure 1.

The results of the solid-state NMR data on low molecular weight azocellulose (80,000-160,00) presented in Figures 1 and 2 and ultrahigh molecular weight azocellulose (ca. 5.8×10^8) (11) suggest that the coupling reaction takes place predominantly at the C6 carbon position. The Mitsunobu reaction is initiated preferentially in the amorphous region of cellulose and then through the crystalline region. As a result, the crystalline region decreases whereas the amorphous region increases.

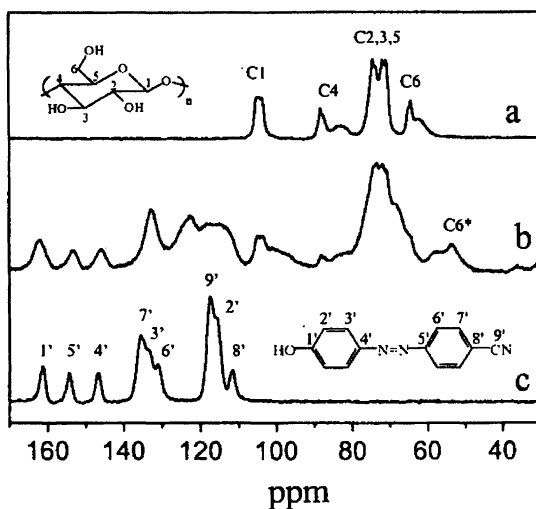


Figure 2. The ^{13}C CP/MAS spectra of VISCOCELL cellulose (a), AZOVIS69 (b), and 4-cyanophenylazophenol (c).

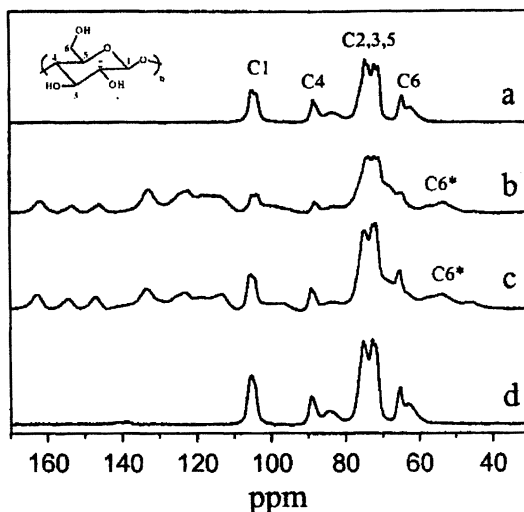


Figure 3. The ^{13}C CP/MAS spectra of ESTERCELL cellulose (a), AZOEST49 (b), high MW Azocellulose with a DS of 0.49 (c), and high MW cellulose (d).

In Figure 3, the solid-state ^{13}C NMR spectra of low molecular weight cellulose and corresponding azocellulose are compared with ultrahigh molecular weight cellulose and its azocellulose at the same level of DS (0.49). For ESTERCELL cellulose, the crystalline resonance peak at 64.4 ppm for the carbon C6 in Spectrum a decreases significantly in Spectrum b and appear as a small up-field shoulder to C2, C3 and C5 resonance peaks for the azocellulose polymer. In a similar way, the changes for C1 and C4 are also observed. For the cellulose with an ultrahigh molecular weight (5.8×10^8) (11) with the same DS of 0.49, the spectral changes for crystalline domain carbon resonances in Spectrum c are significantly smaller compared to the changes in Spectrum b for low molecular weight azocellulose. These results suggest that the crystalline regions of cellulose with low molecular weight are more susceptible to morphological changes than the cellulose with a high molecular weight as a result of functionalization with azobenzene chromophores.

The FTIR spectra of ESTERCELL cellulose (Spectrum a), AZOEST21 (Spectrum b) and AZOEST49 (Spectrum c) and 4-cyanophenylazophenol (Spectrum d) are shown in Figure 4. The absorption peaks of ESTERCELL cellulose are assigned according to the work of Ilharco et al. (14). In the Spectrum a of ESTERCELL cellulose, the band with maximum absorption at 3260 cm^{-1} is attributed to the O–H stretching. The presence of a broad O–H peak is probably due to distribution of peaks arising from different types of hydroxyl groups (one primary and two secondary alcohol groups), different kind of hydrogen bonding (intra- and intermolecular hydrogen bonding), and different chain order (amorphous and crystalline domains) in ESTERCELL cellulose. The bands at 2920 cm^{-1} and 2849 cm^{-1} are associated with the C–H

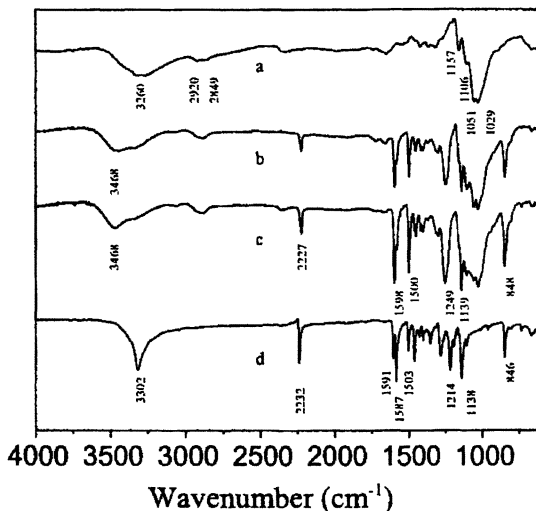


Figure 4. The FTIR spectra of ESTERCELLcellulose (a), AZOESTER21 (b), AZOESTER49 (c), and 4-cyanophenylazophenol (d).

stretching. The bands at 1157 and 1029 cm^{-1} are corresponding to the C–O stretching. The bands at 1051 and 1106 cm^{-1} are assigned to the C–O–C bending in the pyranose ring and the O–H in-phase bending or asymmetric stretching respectively (14).

Spectrum d in Figure 4 shows the FTIR spectrum of 4-cyanophenylazophenol. The band with maximum absorption at 3302 cm^{-1} is attributed to the O–H stretching of the phenol group. The band at 2232 cm^{-1} is associated the C \equiv N stretching. The bands at 1591, 1587, and 1503 cm^{-1} are corresponding to aromatic C=C stretching. The band at 846 cm^{-1} is attributed to the out-of- plane C–H bending of 1,4-disubstitued benzene rings. The bands at 1214 and 1138 cm^{-1} are assigned to C–O and C–N stretching respectively.

The characteristic peaks arising from the azocellulose polymers as a result of Mitsunobu reaction can be easily identified in Spectra b and c in Figure 4 if the spectra for azocellulose are compared with Spectra a and d. In the spectra of azocellulose polymers, the peak attributed to C–O stretching at 1214 cm^{-1} from 4-cynophenyazophenol does not appear, while a new sharp and strong vibration band appears in the region of asymmetrical C–O–C stretching for aryl alkyl ether at 1249 cm^{-1} . Also, the band of alkyl aryl ether C–O–C for AZOEST49 is much stronger than that for AZOEST21. These suggest the attachment of azophenol chromophores to the cellulose through the formation alkyl aryl ether. The C \equiv N stretching at 2227 cm^{-1} , the aromatic C=C stretching at ca. 1598 and 1500 cm^{-1} , the C–N stretching at 1139 cm^{-1} and the out-of-plane C–H bending of 1,4-disubstitued benzene rings at ca. 848 cm^{-1} are characteristic peaks of azophenol chromophores in the azocellulose polymer. The intensities of these vibration

peaks increase with the DS suggesting that azophenol chromophores are linked to ESTERCELL cellulose as a result of Mitsunobu reaction. The FTIR Spectra of low molecular weight cellulose VISCOCELL and its azopolymer show the similar spectral features of ESTERCELL.

The typical AFM three-dimensional images of the SRGs with grating spacing of 1 μm on the films of azocellulose polymers are shown in Figure 5. The SRGs on all samples were recorded at an intensity of 200 mW/cm^2 , and the writing beams were turned off after the diffraction efficiency saturated. The amplitudes of the surface modulation are 150nm, 200 nm for azocellulose AZOEST21, AZOEST49 respectively. This conforms to the increase trend in amplitude of SRGs with DS (δ). In the case of AZOVIS69, the amplitude of the surface modulation is over 300 nm. For the high molecular weight azocellulose polymer with a DS of 0.49, the amplitude is about 300 nm. The AFM data in Figure 5 indicate that the SRGs inscribed on the film of AZOEST49 are smoother than those of high molecular weight polymer.

Conclusions

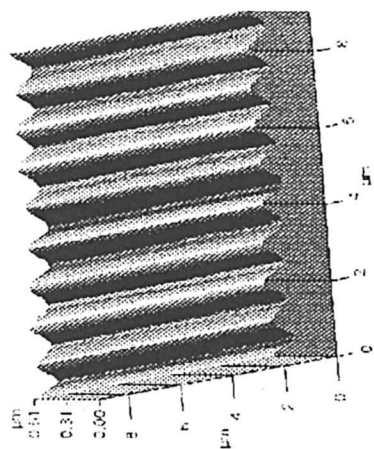
Azocellulose polymers have been synthesized by linking azobenzene chromophores to commercially available low molecular weight cellulose through Mitsunobu reaction. The solid-state ^{13}C CP/MAS NMR data suggest the coupling reaction take place preferentially at the C6 position. SRGs on the films of these azocellulose polymers were holographically induced in a single step process.

Acknowledgements

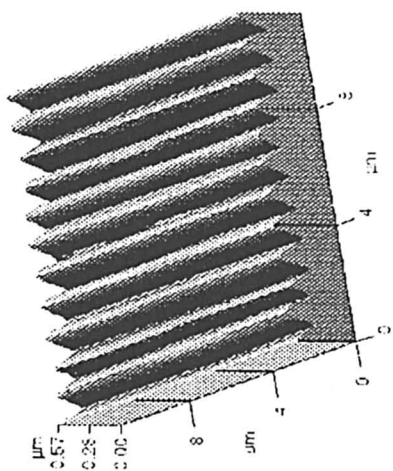
Financial support from NSF-DMR and ONR is gratefully acknowledged. The authors thank Dr. David VanderHart of NIST for helpful discussions.

References

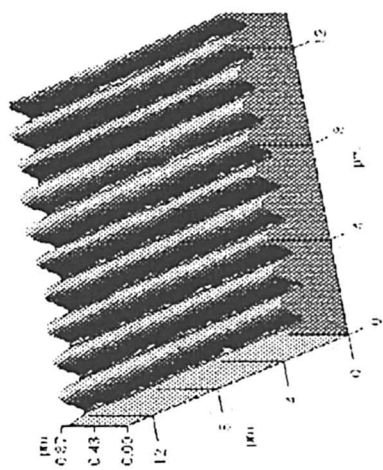
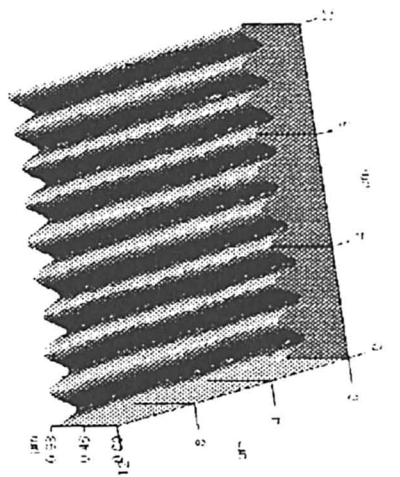
1. Kim, D.Y.; Tripathy, S.K.; Li, L.; Kumar, *J. Appl. Phys. Lett.* **1995**, *66*, 1166.
2. Rochon, P.; Batalla, E.; Natansohn, A. *Appl. Phys. Letter.* **1995**, *66*, 136.
3. Ramanujam, P.S.; Holme, N.C.R.; Hvilsted, S. *Appl. Phys. Lett.* **1996**, *68*, 1329.
4. Kim, D.Y.; Li, L.; Jiang, X.L.; Shivshankar, V.; Kumar, J.; Tripathy, S. *Macromolecules* **1995**, *28*, 8835.
5. Barrett, C.J.; Natansohn, A.L.; Rochon, P.L. *J. Phys. Chem.* **1996**, *100*, 8836.
6. Holme, N.C.R.; Nikolova, L.; Ramanujam, P.S.; Hvilsted, S. *Appl. Phys. Lett.* **1997**, *70*, 1518.



AZOEST49



AZOEST21



Azocellulose with High
MW and DS of 0.49

AZOVIS69

Figure 5. AFM images showing three-dimensional views of the SRGs with a grating spacing of 1 μm on the films of azocellulose polymers.

7. Bian, S.; Liu, W.; Williams, J.; Samuelson, L.; Kumar, J.; Tripathy, S. *Chem. Mater.* **2000**, *12*, 1585.
8. Yang, S.; Li, L.; Cholli, A.L.; Kumar, J.; Tripathy, S.K. *J. M.S.-PURE Appl. Chem.*, Submitted.
9. Gröbe, A. In *Polymer Handbook*. Brandrup, J. and Immergut, E.H., Eds.; 3rd Edition. John Wiley & Sons: New York, **1989**; V/126.
10. Mitsunobu, O.; Yamada, M.; Mukaiyama, T. *Bull. Chem. Soc. Japan* **1967**, *40*, 935.
11. Yang, S.; Monsey, M.J.; Li, L.; Cholli, A.L.; Kumar, J.; Tripathy, S.K. *Macromolecules*, submitted.
12. VanderHart, D.L.; Atalla, R.H. *Macromolecules* **1984**, *17*, 1465.
13. Atalla, R.H.; VanderHart, D.L. *Solid State Nuclear Resonance* **1999**, *15*, 1.
14. Ilharco, L.M.; Garcia, A.R.; Lopes da Silva, J.; Vieira Ferreira, L.F. *Langmuir* **1997**, *23(15)*, 4126.

Chapter 6

Structure of *Bombyx mori* Silk Fibroin before Spinning in Silkworm

Tetsuo Asakura, Jun Ashida, and Tsutomu Yamane

Department of Biotechnology, Tokyo University of Agriculture and Technology, Koganei, Tokyo 184-8588, Japan

The silk I structure (the structure of *Bombyx mori* silk fibroin before spinning in the solid state) was determined with ^{13}C two-dimensional (2D) spin-diffusion solid-state NMR, rotational echo double resonance (REDOR) and quantitative use of ^{13}C CP/MAS NMR chemical shifts. We used ^{13}C - ^{13}C double labeled and ^{13}C - ^{15}N double labeled model peptides, (AlaGly)₁₅ in silk I form for solid state NMR analyses. The structure was determined to a repeating type II β -turn. The solubility of *B. mori* silk fibroin in water was examined in the light of the presence of Tyr and Val residues in the repetitive domains of GAGAGYGAGAG and GAGVGYGAGAG sequences. The presence of amorphous domains, TGSSGFGPYVANGGYSGYEYAWSESDFGT was also considered as the origin of the solubility of silk fibroin in water. The solution structure of silk fibroin in *B. mori* silkworm is also discussed with previous circular dichroism (CD), optical rotatory dispersion (ORD) and solution NMR data.

The silkworms can produce strong and stiff fibers at room temperature and from an aqueous solution (1). Therefore, it is important to know the structure of the silk fibroin in silkworm in order to understand the mechanism of fiber formation at the molecular level. Two crystalline forms, silk I and silk II, have been reported as the dimorphs of silk fibroin from *B. mori* based on several spectroscopic investigations (2). The silk II structure (the structure of silk fiber after spinning) was first proposed by Marsh et al. (3) to be an anti-parallel β -sheet, which was subsequently supported by other researchers (1). However, the determination of the silk I structure was difficult because any attempts to induce orientation of the silk fibroin or the model polypeptides with silk I form for studies by X-ray and electron diffraction, causes the silk I form to readily convert to the more

stable silk II form (2). So it is necessary to use more appropriate analytical methods in order to determine the silk I structure at molecular level. Solid state NMR is reported to be one of the suitable techniques for the determination of silk I structure (4).

In this study, we attempt to investigate the silk I structure by employing a number of solid -state NMR (^{13}C - 2D spin-diffusion NMR, REDOR and quantitative use of ^{13}C CP/MAS NMR chemical shifts) methods (4). The primary structure of *B. mori* silk fibroin largely consists of repeat sequences of six residues (GlyAlaGlyAlaGlySer)_n (1). Therefore, we studied the (AlaGly)₁₅ sequence as the model for silk I structure. However, the model peptide, (AlaGly)₁₅, was found to be insoluble in water although the silk fibroin exists in the solution state in silkworm before spinning. Therefore, we also attempted to clarify the critical amino acids in silk fibroin which may be mainly responsible for its solubility. Recently, Zhou *et al.* reported its complete amino acid sequence of *B. mori* silk fibroin (5). The analysis showed that in addition to the repeating sequence of GAGAGS, the primary sequence of silk fibroin also contains GAGAGY and GAGAGVGY sequences. These repetitive sequences are flanked by the amorphous region: TGSSGFGPYVANGGYSGYEYAWSESDFGT, containing both polar and hydrophobic bulky residues. Therefore, the sequential model peptides selected from this primary sequence were also synthesized and the solubility of the peptides in water was examined. The structures of these peptides were characterized by solid-state NMR and compared with the (AlaGly)₁₅ model peptide. The solution structure of silk fibroin in *B. mori* silkworm will be discussed with reference to previous CD (6), ORD (7) and solution NMR data (8, 9).

Experimental

Peptide synthesis

All the peptides investigated here, were synthesized with the solid phase method by employ F-moc chemistry. The double labeled peptide: ^{13}C - ^{13}C and ^{13}C - ^{15}N of the (AlaGly)₁₅ sequence were synthesized for 2D spin-diffusion and REDOR experiments. To achieve purification the samples were dissolved in 9 M LiBr and then dialyzed thoroughly against distilled water for four days. The participated samples were collected and dried. The structures of all the samples were confirmed from the ^{13}C CP/MAS NMR and IR spectra (10). In order to examine the role of specific amino acids on the solubility, peptides with following sequences, 1-4, of silk fibroin were synthesized.

H-GAGAGSGAGAG-OH	1
H-GAGAGYGAGAG-OH	2
H-GAGVGYGAGAG-OH	3
H-TGSSGFGPYVANGGYSGYEYAWSESDFGT-OH	4

As described previously, the aqueous solution of silk fibroin was obtained directly from the silk gland of *B. mori*.

NMR

The 2D spin-diffusion NMR spectra were obtained with a Varian Unity/INOVA 400 NMR spectrometer and a 7mm ϕ Jakobsen-type double-tuned MAS probe at off magic angle condition ($\theta_m + 7^\circ$) and with the sample spinning of 6 kHz at room temperature. REDOR experiments were performed on a Chemagnetics CMX-400 spectrometer equipped with a solid-state accessory and a triple-channel magic-angle probe with a 5 mm coil, spinning at 5 kHz. The ^{13}C CP/MAS NMR measurements were performed on a Chemagnetics CMX-400 spectrometer as described previously (4).

Results and Discussion

Silk I structure in the solid state

Figure 1 (A) shows the ^{13}C CP/MAS spectrum of double labeled spectrum of (AlaGly)₁₅ after dissolving in 9 M LiBr and then dialyzing against water. The high field resonance region (10-70 ppm) was expanded. The observation of chemical shifts at 17.4 ppm for C β and 51.5 ppm for C α carbons of Ala residue, clearly indicate that the structure of the peptide is silk I (10). The ^{13}C solution NMR spectrum of *B. mori* silk fibroin obtained directly from the silk gland is also shown in Figure 1(B) for the sake of comparison. The observed ^{13}C chemical shifts of Ala C α , C β and Gly C α carbons are almost the same between the solid state and the solution state. It may be mentioned that the chemical shifts of Ala C α and C β carbons have been more quantitatively used for characterization of the Ala residue in silk I structure (11). The ϕ and ψ torsion angles satisfy the C α and C β chemical shifts, consistent with the values $\phi = -80^\circ$ to -20° , $\psi = 90^\circ$ to 180° .

ϕ and ψ angles of Ala and Gly residues in silk I form was determined by the 2D spin-diffusion solid-state NMR which is a powerful method to obtain the relative orientation of two chemical shift tensors of ^{13}C labeled sites in the local molecular framework (4). Under off magic angle condition, the 2D spin-diffusion NMR spectra of (AG)₆ A[1- ^{13}C]G₁₄[1- ^{13}C]A₁₅ G(AG)₇, along with the simulated spectrum for the torsion angles ($\phi = -60^\circ$ and $\psi = 130^\circ$) of Ala residue (only carbonyl regions), are shown in Figure 2A. The 2D spin-diffusion NMR spectrum of (AG)₇ [1- ^{13}C]A₁₅[1- ^{13}C]G₁₆ (AG)₇ is shown in Figure 2B along with the simulated spectrum for the torsion angles ($\phi = 70^\circ$ and $\psi = 30^\circ$) of the Gly residue. The simulation was performed for the regions in the Ramachandran map, which were selected from the chemical shift data of silk I obtained

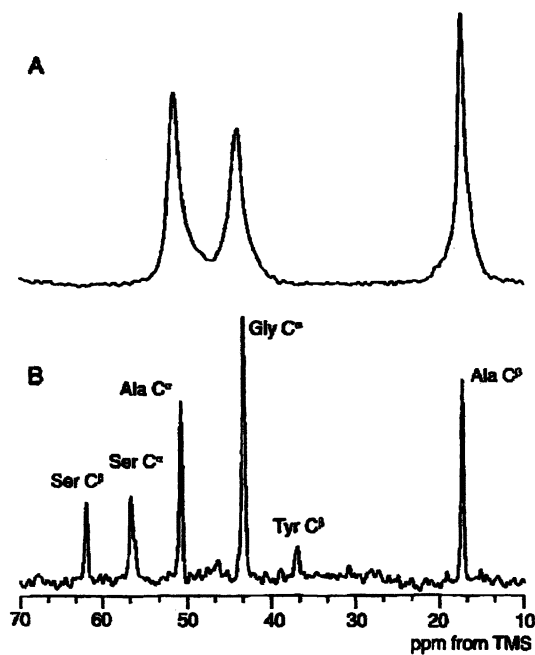


Figure 1. ^{13}C CP/MAS spectrum of $(\text{AlaGly})_{15}$ 30 mer (A) and ^{13}C solution NMR spectrum of *B. mori* silk fibroin in aqueous solution obtained directly from the silk gland (B). The resonance region, 10-70 ppm was expanded.

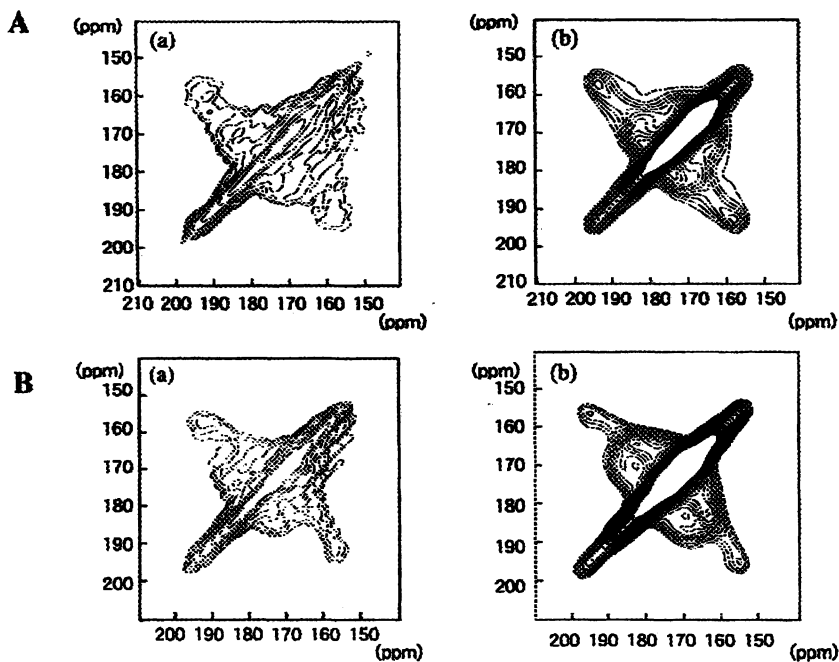


Figure 2. The experimental (a) and simulated (b) 2D spin-diffusion NMR spectra of $[1\text{-}^{13}\text{C Gly}_{14}, 1\text{-}^{13}\text{C Ala}_{15}]$ doubly-labeled $(\text{AlaGly})_{15}$ 30 mer (A) and $[1\text{-}^{13}\text{C Ala}_{15}, 1\text{-}^{13}\text{C Gly}_{16}]$ labeled $(\text{AlaGly})_{15}$ 30 mers (B). The torsion angles (ϕ and $\psi = -60^\circ$ and 130°) of Ala residue and (ϕ and $\psi = 70^\circ$ and 30°) of Gly residue were obtained from the simulation.

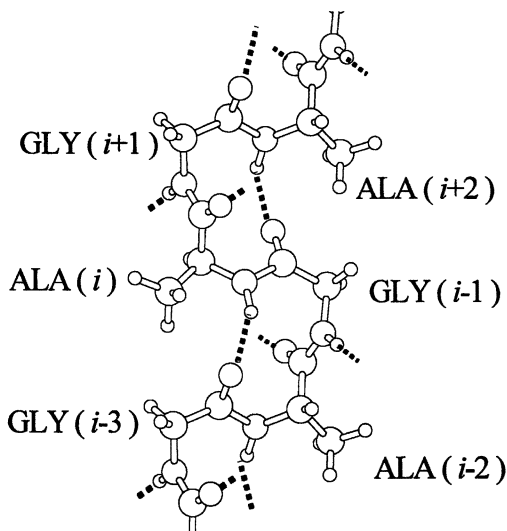


Figure 3. Repeated β -turn type II-like structure. For example, there is intra-molecular hydrogen bond between the carbonyl oxygen atom of the $(i-1)$ -th Gly residue and the amide hydrogen atom of the $(i+2)$ -th Ala residue

from solid-state NMR. To confirm the ϕ and ψ values of the Gly residues we also used the reported unit cell dimension along the c axis (8.88\AA) of the silk I structure (4). Figure 3 shows the model of silk I obtained with $\phi_{\text{Ala}} = -60^\circ$; $\psi_{\text{Ala}} = 130^\circ$ and $\phi_{\text{Gly}} = 70^\circ$; $\psi_{\text{Gly}} = 30^\circ$. In order to further confirm the proposed model the distance between the $^{13}\text{C}=\text{O}$ carbon of the 14th Gly residue and the ^{15}N nitrogen of the 17th Ala residue in the peptide $(\text{AG})_6\text{A}[1-^{13}\text{C}]\text{GAG}[^{15}\text{N}]\text{AG}(\text{AG})_6$ was determined by a REDOR experiment (4). The distance was determined to be $4.0 \pm 0.1\text{\AA}$ which agrees well with the distance of $3.9 \pm 0.1\text{\AA}$, calculated of intra-molecular hydrogen bonded structure of the silk I which accommodates repeated type II β -turn structure (the ideal backbone torsion angles of a type II β -turn are: $\phi_i \sim -60^\circ$, $\psi_i \sim 120^\circ$, $\phi_{i+1} \sim 80^\circ$ and $\psi_{i+1} \sim 0^\circ$).

Thus, there are intramolecular hydrogen bonds between the carbonyl oxygen atom of the $(i-1)^{\text{th}}$ Gly residue and the amide hydrogen atom of the $(i+2)^{\text{th}}$ Ala residue, between the amide hydrogen atom of the $(i)^{\text{th}}$ Ala residue and the carbonyl oxygen atom of the $(i-3)^{\text{th}}$ Gly residue, and between the carbonyl oxygen atom of the $(i+1)^{\text{th}}$ Gly residue and the amide hydrogen atom of the $(i+4)^{\text{th}}$ Ala residue. Moreover, the reported X-ray diffraction

data *i.e.* the WAXS pattern, of silk I further allowed us to confirm the formation of inter-molecular hydrogen bonds between the Ala C=O and Gly amide-NH of one strand and the Gly amide-NH and Ala C=O on the adjacent molecule, respectively (4). The direction of this inter-molecular hydrogen bonding is perpendicular to the fiber axis.

Origin of solubility of *B. mori* silk fibroin in water

The peptide (AG)₁₅ used for proposing the silk I solid state structure was found to be insoluble in water. Interestingly, the peptide 1, which incorporates Ser residues in the (AG)_n sequence, however, remains insoluble in water. As already noted earlier, the fraction of *B. mori* silk fibroin precipitated after cleavage by chymotrypsin (Cp fraction) is ~ 55% of total silk fibroin with the sequence (AGSGAG)₈. This is also insoluble in water indicating that the Ser OH group does not contribute the solubility of the peptide (1). It was of some interest to analyze the soluble fraction (Cs fraction) after chymotrypsin treatment. The comparison with the amino acid composition of Cp fraction showed the presence of Tyr and Val residues in Cs fraction (12). The gel filtration column chromatography (sephadex G-15) resulted in four fractions, S-I (32%), S-II(4%), S-III(46%) and S-IV(17%). The amino acid composition of the S-I fraction was similar to that of Cp fraction except that approximately half of the molecular weight of the Cp fraction. The amount of S-II fraction is small and the amino acid composition is similar to that of S-III fraction. The peptide sequences of the S-III fraction were reported to be GAGAGAGY and GAGVAGY. The S-IV fraction consists of a mixture of smaller sequences. From these results it can be safely speculated that the Tyr and Val residues may contribute to the solubility of the silk fibroin in water. In order to check the solubility of (AG)_n based sequences, we synthesized peptides GAGAGYGAGAG, 2 and GAGVGYGAGAG, 3 where the Tyr and both Val & Tyr residues were present, respectively in the center of the sequences. Surprisingly, both the peptides, 2 and 3, were easily soluble in water. The peptide 4 (TGSSGFGPYVANGGYSGYEWSSSEDFGT) of *B. mori* silk fibroin, called the amorphous sequence by Zhou et al., was also found soluble in water. So the presence of these sequences in silk fibroin may be the origin of its solubility in water. However, considering the relative fractions of each sequence in the whole silk fibroin, the role played by the Tyr and/or Val residues may be critical and appears to be important in controlling the solubility.

In order to characterize the structure of these peptides ¹³C CP/MAS NMR spectra of these model compounds were recorded (Figure 4). It is clear that the Ala residues in 1 take largely an anti-parallel β sheet, as judged from the ¹³C chemical shifts of Ala Cβ resonance at 20.3 ppm. However, there is a shoulder at ~ 16.5 ppm, indicating the presence of a small fraction of random coil structure. The observed chemical shifts at 48.9 ppm for Ala Cα and 172.0 ppm for Ala carbonyl carbons also support the anti-parallel β sheet structure of 1. The chemical shift values at 42.6 ppm and 169.1 ppm of the Cα and carbonyl carbons, respectively for Gly residues indicate that the residue also takes anti-parallel β-sheet structure. The small, but clearly resolved sharp peaks at 54.7

and 63.6 ppm are assigned to the C α and C β carbons, respectively of the Ser residue. These chemical shift values are also typical ones for anti-parallel β sheet structure *i.e.* silk II structure. The deuterium NMR dynamics study of the Ser residue in silk fibroin with silk II structure has also supported that the residue tends to stabilize the extended conformation via the formation of main-chain to side-chain hydrogen bonding interactions (13).

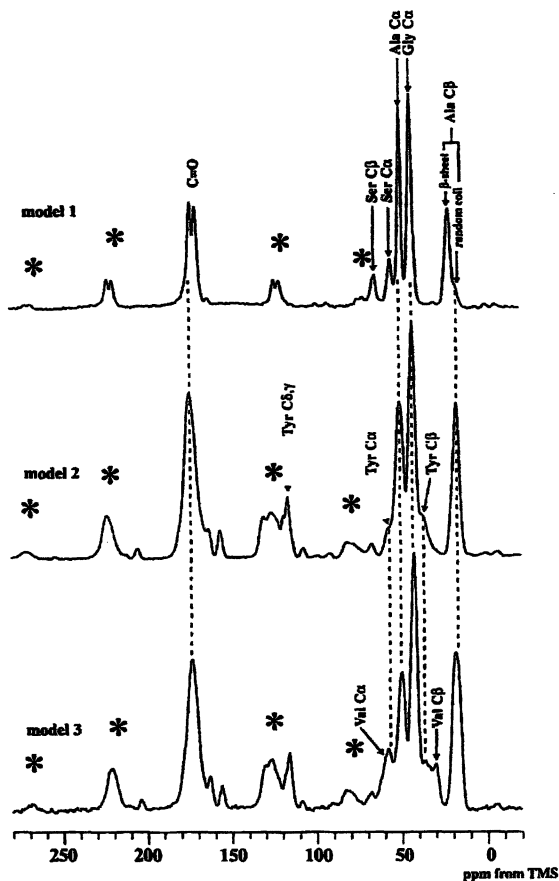


Figure 4 ^{13}C CP/MAS NMR spectra of the sequential model peptides, GAGAGSGAGAG (1), GAGAGYGAGAG (2) and GAGVGYGAGAG (3) selected from the repetitive domains of *B. mori* silk fibroin. * indicates spinning side bands.

Investigation the effect of the introduction of the Tyr residues in the (AlaGly) $_n$ sequence, could be of conformational interest. The observed C α and C β chemical shifts of the Ala residue in 2 at 49.5 ppm and 16.5 ppm, respectively, means that the conformation is either random coil or silk I. In this case, however, the line widths are considerably broader than that of silk I (10). Especially, a sharp peak of the Ala carbonyl

carbon should be observed at 176.8 ppm at the carbonyl carbon region if the structure is silk I (10), but this is not observed in Figure 4. The Gly carbonyl carbon peak of **2** resonates at lower field than the silk II peak (169.1 ppm), indicating that the Gly residue also takes a random coil. A similar tendency was also observed for the peptide, **3** and so the presence of Val residue is essentially no effect compared only the presence of the Tyr residue. The structure of Tyr and Val residues involved in the repeated GlyAla sequences can be discussed with the chemical shift values, although it is difficult to obtain the exact values because of small amounts of these residues in the chain and the peak overlapping. The chemical shifts; Tyr C α peak at \sim 55.5 ppm and Tyr C β peak at 36.3 ppm, are close to the random coil shift of Tyr residue (55.4 ppm and 36.1 ppm, respectively). Thus, Tyr residue in **2**, and both Tyr and Val residues (\sim 59 ppm) in **3** take random coil structure. Contrary to the case of Ser residues, Tyr and Val residues effectively destroy silk I *i.e.* β -turn structure, and make the silk fibroin stored in the middle silk glands soluble in water.

Solution structure of silk fibroin

Since the silk I structure appears when the silk fibroin stored in silk gland is dried gently, the evidence of the appearance of the ordered structure is expected with the previous solution NMR data reported by us (8,9) and other researchers (6,7) on silk fibroin extracted directly from the silk gland of silkworm. The CD spectra of *B. mori* silk fibroin obtained directly from middle silk gland, reported by Kataoka et al. (6), was studied at two widely different concentrations in water (Figure 5).

The observed CD pattern of silk fibroin at low concentration \sim 0.1%, may indicate that the predominant structure is random coil/unordered. However, there is residual negative ellipticity value at \sim 220 nm which may suggest contribution(s) from some ordered structure(s). It may be noted that the typical CD spectrum attributed to random coil/unordered structure has moderate positive ellipticity value at \sim 218 nm. Interestingly,

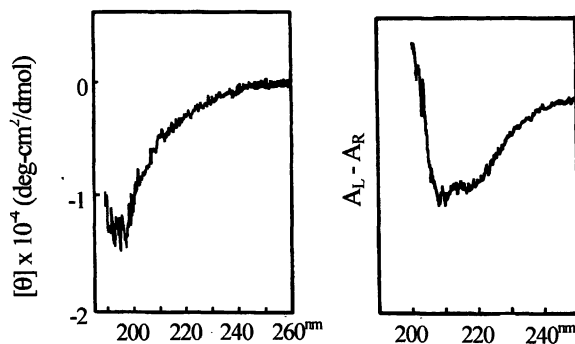


Figure 5. CD spectra of *B. mori* silk fibroin obtained directly from the silk gland at the concentrations, 0.1% (left) and 8.6% (right).

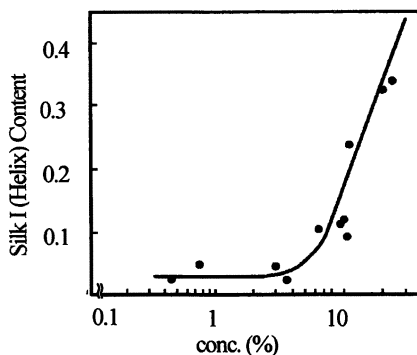


Figure 6. Helical (Silk I) content of *B. mori* silk fibroin obtained directly from the silk gland as a function of the concentration. These data were determined by ORD measurements

at significantly higher concentration $\sim 8.6\%$, a distinct CD pattern with poorly defined troughs, at ~ 218 nm and ~ 206 nm, was observed. The $[\theta]_m$ value could not be quantitated because of the high concentration of the sample. Latter CD pattern of silk fibroin does not appear to be the reminiscent of either helical or β -sheet structure. In fact ^{13}C solution NMR chemical shift data of silk fibroin clearly suggested the absence of helical structure (8). Thus, under experimental condition, the CD pattern presumably indicates the appearance of some ordered structure (8). Evidence for the induction of concentration-dependent ordered structure, as seen in the CD spectra, may suggest the existence of an equilibrium of different populations of silk structures. The ORD measurements were also performed by Kobayashi et al. (7) by changing the concentration of liquid silk from silkworm (Figure 6). The b_0 value, which reflects the fraction of helical structure, indicates that the helical contents start increasing from the 5% of silk concentration and reach 40% helical contents in the liquid silk obtained from middle silk gland (silk fibroin concentration $\sim 30\%$). This study also supports the generation of ordered structure(s).

The silk I in the solid state is repeated β -turn type II structure as mentioned above. Perczel et al. (14) reported typical CD pattern of type I and type II β -turn together with random coil. Actually, the random coil pattern is similar to the pattern of silk fibroin at 0.1%. Interestingly, the CD pattern at 8.6% is similar to type I β -turn and quite different from type II β -turn. The observed spin diffusion NMR spectra and REDOR data of Ala residue clearly show that the silk I structure is not type I β -turn ($\phi = -60^\circ, \psi = -30^\circ$). So both β -turns form intra-molecular hydrogen bonding, but the strong aggregation of silk

fibroin chains during drying process might promote the structural change from type I to type II.

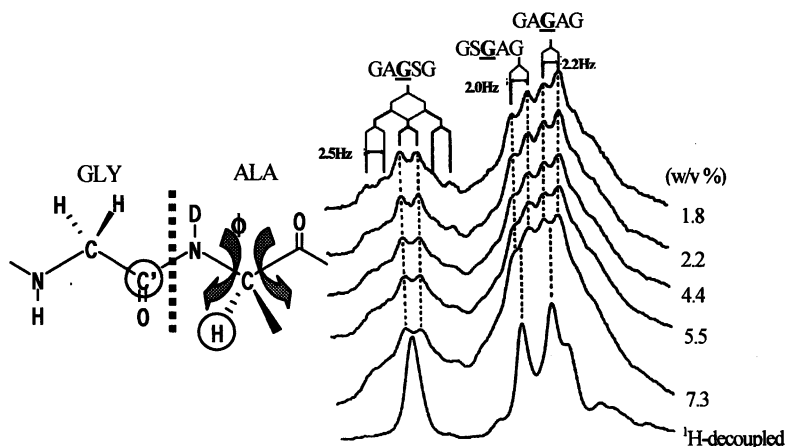


Figure 7. The ^1H -coupled and decoupled spectra of the carbonyl carbons for the Gly residue of $[1-^{13}\text{C}]$ Gly-labeled *B.mori* fibroin observed as a function of the concentration

Figure 7 shows the ^1H -coupled and decoupled ^{13}C solution NMR spectra of the carbonyl for the Gly residue of $[1-^{13}\text{C}]$ Gly-labeled silk fibroin in D_2O (8). The observations of the long-range coupling constant between ^{13}C and ^1H nuclei, $^3J_{\text{C-N-C}\alpha\text{H}}$ are expected to yield information concerning the local conformation. Splitting of the peaks in the carbonyl region of the ^1H -decoupling spectrum was assigned to specific sequences (15). The value of the $^3J_{\text{C-N-C}\alpha\text{H}}$ was readily determined from the spacing of the doublet for each Gly carbonyl carbon peak in the ^1H -coupled spectra. After correction by means of the peak-to-trough ratio of the doublet was applied to the determination of $^3J_{\text{C-N-C}\alpha\text{H}}$ values: 2.8Hz for G-A-G-S-G sequence, 2.4Hz for G-S-G-A-G, and 2.6Hz for the G-A-G-A-G sequence at 1.8 w/v%. These values decrease slightly with increasing concentration: 2.5Hz for the G-A-G-S-G, 2.0Hz for the G-S-G-A-G sequence and 2.2Hz for the G-A-G-A-G sequences at 7.3 w/v% (8). Since the ϕ value of the Ala residue is $\sim 60^\circ$, which is independent of whether type I or II β -turn structure, $^3J_{\text{C-N-C}\alpha\text{H}}$ can be calculated to be -0.75 Hz (8). Therefore, the decrease in the long range coupling constant might indicate the appearance of the silk I structure at increased in concentrations.

Acknowledgement

TA also acknowledges support from the Program for Promotion of Basic Research Activities for Innovative Biosciences, Japan.

References

1. *Encyclopedia of Agriculture Science*; Asakura, T.; Kaplan, D. L.; Arutzen, C. J., Eds, Academic Press: London, 1994; Vol. 4..
2. Lotz, B.; Cesari, F. C. *Biochimie* **1979**, *61*, 205.
3. Marsh, R.; Corey, R. B.; Pauling, L. *Biochem. Biophys. Acta* **1955**, *16*, 1,.
4. Asakura, T.; Ashida, J.; Yamane, T.; Kameda, T.; Nakazawa, Y.; Ohgo, K.; Komatsu, K. *J. Mol. Biol.* **2001**, *306*, 291.
5. Zhou, C-Z.; Confalonieri, F.; Medina, N.; Zivanovic, Y.; Esnault, C.; Yang, T.; Jacquet, M.; Janin, J.; Duguet, M.; Perasso, R.; Li, Z-G. *Nucleic Acids Research*, **2000**, *28*, 2413.
6. Kataoka, T.; Kobayashi, Y.; Fujiwara, T.; Kyogoku, Y. *Abstract in Symposium of study and utilization of non-mulberry silkworms*, **1981**, 71.
7. Kobayashi, Y.; Fujiwara, T.; Kyogoku, Y.; Kataoka, T. *Abstract in the 19th NMR meeting in Sapporo* **1980**, 149.
8. Asakura, T. *Markromol. Chem., Rapid Commun.*, **1986**, *7*, 755.
9. Asakura, T.; Watanabe, Y.; Uchida, A.; Minagawa, H. *Macromolecules*, **1984**, *17*, 1075.
10. Asakura, T.; Kuzuhara, A.; Tabeta, R.; Saito, H. *Macromolecules*, **1985**, *18*, 1841.
11. Asakura, T.; Iwadate, M.; Demura, M.; and Williamson, M. P. *Int. J. Biol. Macromolecules*, **1999**, *24*, 167.
12. *Zoku Kenshi no Kozo*; Shimura, K.; Hojo, N., Eds.; Shinshu University: Ueda, 1976.
13. Kameda, T.; Ohkawa, Y.; Yoshizawa, K.; Naito, J.; Ulrich A. S.; Asakura, T. *Macromolecules*, **1999**, *32*, 7166.
14. Perczei, A.; Hollosi, M.; Sandor, P.; Fasman, G.D. *Int. J. Peptide Protein Res.* **1993**, *41*, 223.
15. Asakura, T.; Watanabe, Y.; Itoh, T. *Macromolecules*, **1984**, *17*, 2421.

Chapter 7

Estimation of Physical Properties of Archeological Silk with NMR Relaxation Time and Fluctuation–Dissipation Theorem

Riichirô Chûjô, Kyoko Fukutani, and Yoshiko Magoshi

Department of Environmental and Material Engineering, Teikyo University
of Science and Technology, 2525 Yatsusawa, Uenohara-machi,
Yamanashi 409–0193, Japan

A detailed study of silk samples was carried out using both fresh and archeological samples. Good correlations were obtained between the NMR spin-lattice relaxation time and mechanical properties, such as initial compliance, initial tensile strength, and the ratio between these two parameters. These correlations were then used to estimate the physical properties of archeological silk samples from the T_1 data alone. The equivalence of the relaxation time and the mechanical properties was also suggested by the fluctuation-dissipation theorem. The effects of degradation and paramagnetic impurities were also addressed in this work. The results obtained herein have relevance to a cultural problem involving the definition of “left-and-right” in Japan.

The development of archaeology brings us lots of samples from ancient times. Polymeric samples, such as fibers, are included in the artifacts. These samples are very useful in an understanding of the prevailing culture at the time when the samples were produced. However, there are some limitations to such studies. A typical limitation pertains to physical properties of polymeric materials. The passage of time may induce degradation of the polymer. The

degradation may produce stress concentrations in the sample when a stress is applied. Thus, a measurement may not necessarily reflect the physical properties of the sample in its original state, but may instead reflect the degradation.

The measurements of physical properties can be categorized as "direct" or "indirect." In the former are included measurements of stress relaxation, creep compliance, and dielectric relaxation. In these experiments an excitation is applied which induces a direct change of mechanical parameters, and a response is observed as a result of this change. In these direct experiments the contribution from stress concentrations is inevitable. The indirect method may entail the measurement of fluctuations. For example, NMR spin-lattice relaxation time (T_1) is a fluctuation quantity. No change is induced in the mechanical properties during the indirect measurement; this analysis is therefore free from the stress concentrations. If the information from direct measurement is equivalent to that from indirect measurement, we can estimate the former through the measurement of the latter without the influence of the stress concentrations. The equivalence of these two measurements is guaranteed by the "fluctuation-dissipation theorem" (1,2). In the next section we will try an experimental verification of the theorem for fresh fiber samples.

It is well known that paramagnetic impurities affect the spin-lattice relaxation. The above theorem is valid only for samples without paramagnetic impurities. The third section is devoted to the effect of the impurities in the samples treated with dyestuff and mordant.

There is a beautiful and well-preserved hall named Konjikido (Gold Colored Hall) in Chusonji Temple in Hiraizumi, Iwate, Japan. In this hall three mummies from the twelfth century are still preserved. These mummies are Fujiwara chieftains: Kiyohira Fujiwara (the first chieftain, died in 1128), Motohira Fujiwara (the second, died in 1157), and Hidehira Fujiwara (the third, died in 1187). In the coffins of these mummies lots of silk fabrics have been preserved. These silk fabrics will be used for T_1 measurements. The results will be employed for the estimation of the physical properties in the fourth section.

Earlier, we had already analyzed the amino acid composition of these silk fibers with solid-state ^{13}C NMR (3). We had found the composition to be a function of silk cultivation temperature. Part of this finding had been presented at a symposium in the 211th ACS National Meeting (4) and also covered in the Chemical and Engineering News (5). This study has been extended to a cultural problem, namely, the definition of "left-and-right" (6). There are two different definitions in Japan: from lower hierarchy side, or from higher hierarchy side. The latter one is more popular in Japan. In a Japanese temple, the buddha image faces the prayers. The prayers, therefore, find the left hand of the buddha on their right side. Buddha is, of course, higher than the prayers in hierarchy. If this is the case, the definition for "left" and "right" in a buddhist temple would be opposite from the prayers. An old document states that the central, left, and

right mummies under the floor of Konjikido are Kiyohira, Motohira, and Hidehira, respectively. According to Japanese custom, this document should be read for prayers, and Motohira is therefore on the right and Hidehira is on the left. Actually, until 1950 this definition was adopted even in Chusonji Temple. However, the definition changed to the opposite one in 1950. The reason why the definition was changed is out of scope of this chapter. It will be valuable to reconsider which definition is more reasonable from the findings of NMR. Our previous paper (6) presented an opposition on the basis of physico-chemical data. More specifically, a comparison of the amino acid composition and the temperature estimated from dendrochronological data supported the original definition. In this paper this opposing view will be strengthened by the T_1 data. This will be another aim of the fourth section.

Experimental Verification of Fluctuation-Dissipation Theorem

As discussed in the Introduction, if equivalent information is obtained from both direct and indirect measurements of mechanical properties, then the fluctuation-dissipation theorem is applicable (1). The exact proof of the theorem has already been made. However, an experimental verification is still useful for experimental chemists in an understanding of this theorem. In order to carry out the verification, the spin-lattice relaxation times are compared with corresponding mechanical properties for fresh silk samples. A linear relationship between the two measurements would then constitute an experimental verification, at least for these samples. It may be noted that experimental verification does not imply a general proof because this is not a rigorous mathematical proof.

Fresh silk fabrics were used for the T_1 measurements as well as for the measurements of initial compliance (A), initial tensile strength (B), and the ratio (A/B) of these two quantities. For simplicity, the T_1 of alpha carbon in glycyl residue was chosen as representative of the T_1 values. T_1 values were measured on a JEOL Alpha 500 spectrometer operating in the solid-state high-resolution mode. The pulse sequence used was $180^\circ\text{-}\tau\text{-}90^\circ$. (A), (B), and (A/B) values reflect viscous, elastic, and viscoelastic quantities, respectively. These values were measured on a Tensilon/Utm-II instrument. In Figure 1 we show the correlation between (A) (top), (B) (middle), and (A/B) (bottom) and the reciprocal spin-lattice relaxation time. The three data points designated by K, M, and H will be explained in the fourth section. Least square analysis was done on each of the plots and the correlation coefficient determined. The coefficients were 0.919 (A), 0.747 (B), and 0.956 (A/B). As expected, the correlation was the best for A/B. This is because phenomenologically NMR

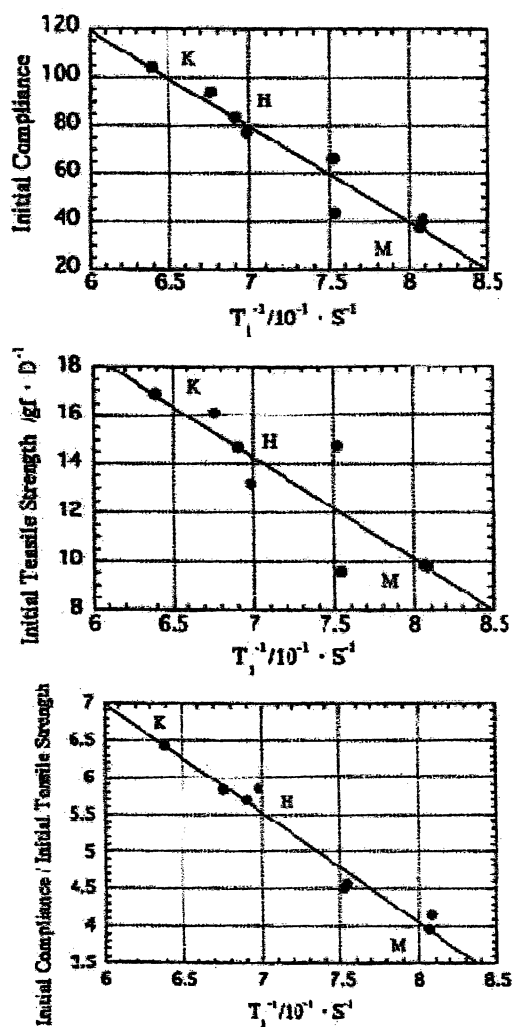


Figure 1. Correlation between initial compliance (A, top), initial tensile strength (B, middle), and the ratio (A/B) and the reciprocal spin-lattice relaxation time for fresh silk fabrics. K, M, and H are data points for the reciprocal spin-lattice relaxation times of the silk fabrics in Chusanji temple, placed on the least-square straight lines.

relaxation is closest to viscoelasticity. This good correlation between A/B and T_1 suggests the plausibility of the fluctuation-dissipation theorem.

Before moving to the next topic, we need to check whether the T_1 's are affected by degradation. If T_1 's are noticeably affected by degradation, then the T_1 's of archaeological samples do not reflect the mechanical properties in the sample in its original (non-degraded) state. The logarithmic free induction decay curves of one fresh sample (thin line) and of the corresponding degraded sample (thick line) are shown in Figure 2. The degradation was done by electron beam (230 Mrad) irradiation. The absolute intensity values are slightly different for the two lines, but the slopes of the two lines are almost equal. The slope corresponds to the reciprocal spin-lattice relaxation time. Thus, the data suggest that the T_1 is almost equal before and after degradation; the degradation does not induce serious change in NMR relaxation. In other words, the change in mechanical properties is primarily due to stress concentrations.

Effect of Paramagnetic Impurities on T_1

Silk fabrics are usually treated with dyestuff and mordant. In the latter there are several inorganic paramagnetic compounds, such as FeCl_3 . In addition, there are other paramagnetic compounds in archaeological samples, e.g., blood (which contains hemoglobin). The fluctuation-dissipation theorem states the correspondence and equivalence between the "direct" measurements and T_1 , which is modulated by molecular motion. If paramagnetic impurities are present, the data may also reflect the effect of these impurities. Thus, this effect needs to be checked. In this paper this paramagnetic contribution is considered to originate only from mordants.

Thirteen samples were used for the comparison between A/B and reciprocal T_1 . In Figure 3 are shown the correlation, in which \bullet , \blacksquare , and \blacktriangle stand for samples without dyestuff and mordant, with mordant, and with dyestuff and mordant, respectively. Only one point is an outlier. This is the data point from the sample that has been treated with commercial FeCl_2 . The exact recipe does not appear on the label of this mordant. We cannot judge whether this mordant is pure FeCl_2 . We surmise that part of FeCl_2 has changed into the paramagnetic FeCl_3 . Except for this isolated point, the remaining points are scattered, but the range of scattering is rather limited. This finding suggests that the effect of paramagnetic impurities is not very large. In the next section we will discuss the spin-lattice relaxation behavior of silk fabrics at Chusonji temple without taking consideration of paramagnetic impurities. Actually, the plot similar to that of Figure 3 is impossible for the samples taken from Chusonji temple due to the presence of stress concentrations.

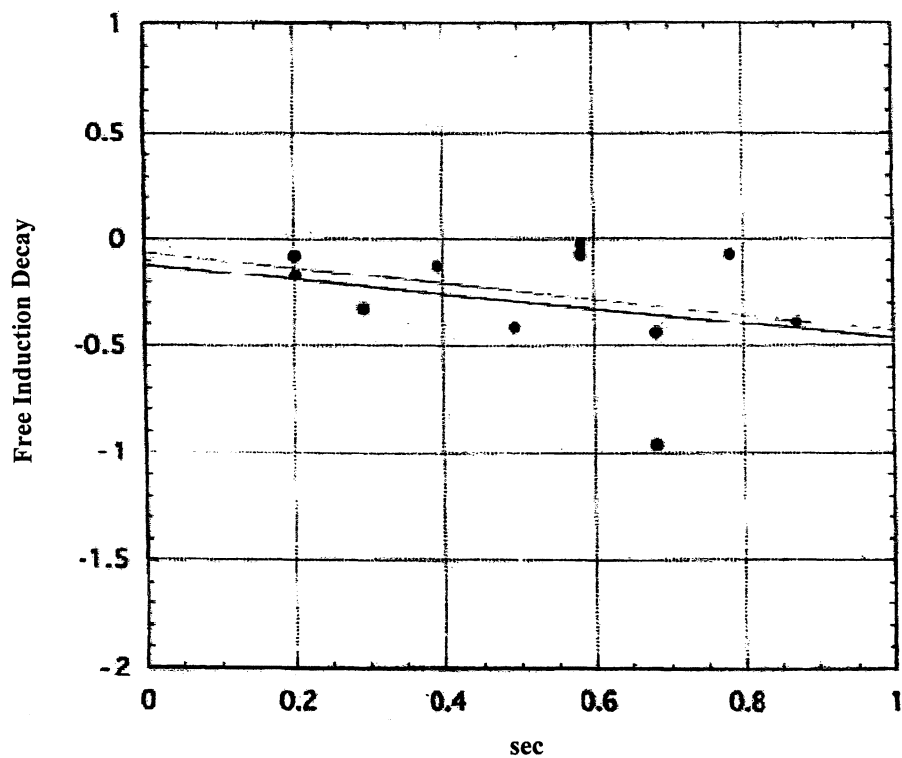


Figure 2. Logarithmic free induction decay curve of one fresh silk fabric sample (thin line) and the corresponding degraded sample (thick line)

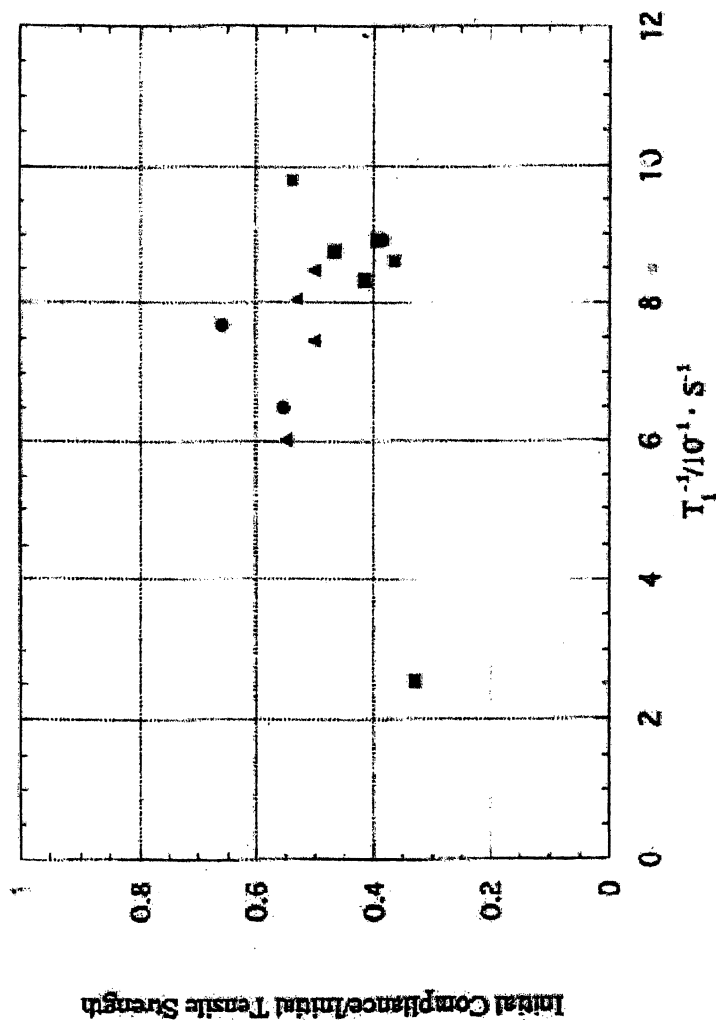


Figure 3. Correlation between the ratio of compliance and initial tensile strength with the reciprocal spin-lattice relaxation time for fresh silk fabrics without dyestuff and mordant (●), with mordant (■), and with dyestuff and mordant (▲).

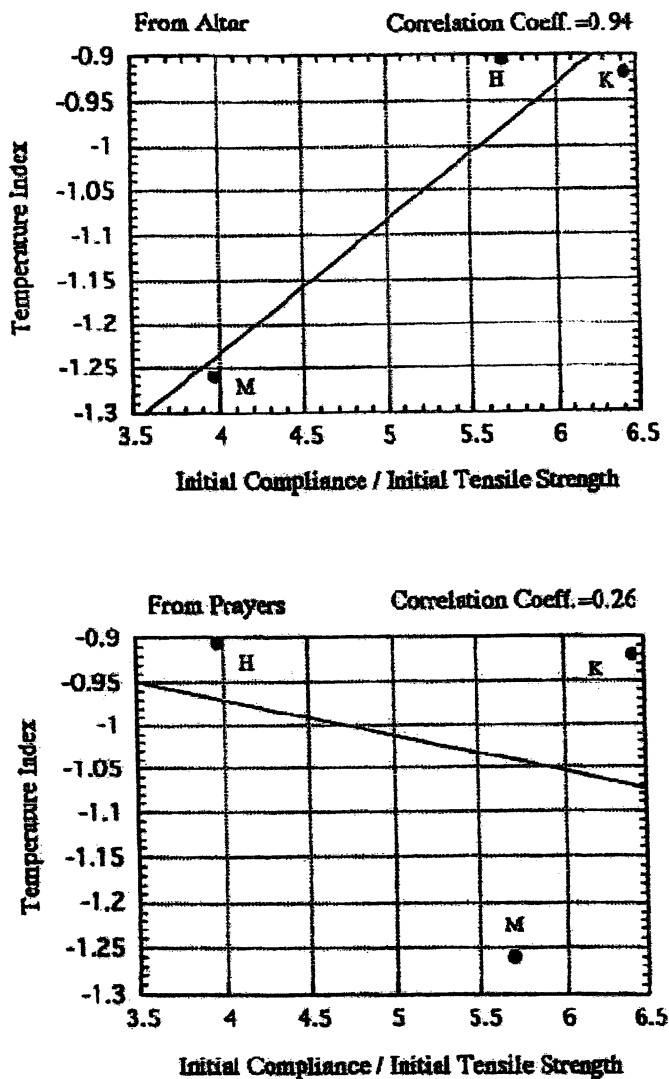


Figure 4. Relationship between temperature index and the ratio of initial compliance and initial tensile strength for the samples preserved in Chusanji temple. The top plot follows the old definition (before 1950) and the bottom plot follows the new definition.

Estimation of Physical Properties of Silk Fabrics Preserved in Chusonji Temple and the "Left-and-Right" Problem

Three data points (K, M, and H) in Figure 2 originate from silk fabrics in the coffins of Kiyohira, Motohira, and Hidehira, respectively. However, we have no data on the mechanical properties of these fabrics (i.e., (A), (B), and (A/B)). The consideration in the second section suggests possible correlations between these three quantities and the reciprocal T_1 . We can then use the observed reciprocal T_1 data and predict the (A), (B), and (A/B) values from the linear relationships obtained from the measurements of fresh samples. As described previously, only the values of (A/B) are reliable. From the data, we can say the viscoelastic parameters of silk fabrics preserved in Chusonji temple are almost similar to those of today.

We need to address the so-called "left-and-right" problem, which has already been mentioned in the Introduction. In Figure 4 are shown the relationship between the temperature index and (A/B). The index has been determined by Mitsutani (7) from dendrochronological data. For samples K, M, and H the old definition before 1950 is used in the top figure, and the new definition in the bottom figure. Correlation coefficients are 0.94 and 0.26 for the top and the bottom figures, respectively. The preference for the old definition is obvious. (Note that in Figure 1 we have already adopted this older definition.)

Sasaki (8), who is a priest in the Chusonji temple, is opposed to our previous paper (6). His opposition is based on the desire to maintain the dignity of the temple. We believe his position was not based on scientific facts. We have earlier indicated our opposing views (9). One of the rationales for carrying out this work is to verify our earlier results and to collect additional data. We believe we have done so and have vindicated our position through the current study.

References

1. Callen, H. B.; Welton, T. A. *Phys. Rev.* **1951**, *83*, 34-40
2. Kubo, R. *J. Phys. Soc. Jpn.* **1957**, *12*, 570-586
3. Chujo, R.; Shimaoka, A.; Nagaoka, K.; Kurata, A.; Inoue, M. *Polymer* **1996**, *37*, 3693-3696
4. Chujo, R. *ACS Polym. Prepr.* **1996**, *37*, 184-185
5. Stinton, S. C. *Chem. Eng. News* September 9, 1996, p. 34
6. Chujo, R.; Shimaoka, A.; Kusaka, T.; Fukuda, H.; Kasai, Y.; Seto, R.; Suzuki, M.; Okumura, I. *J. Archaeol. Pros. Soc. Jpn.* **1999**, *2*, 19-26
7. Mitsutani, T. unpublished data
8. Sasaki, H. *Kanzan* **1999**, No. 6, 46-48
9. Chujo, R. *J. Archaeol. Pros. Soc. Jpn.* **1999**, *2*, 57-62

Chapter 8

Polymer Characterization by 3D Solution NMR

Peter L. Rinaldi

Department of Chemistry, Knight Chemical Laboratory, The University
of Akron, Akron, OH 44325-3601

In this work the applications of three dimensional (3D) solution NMR techniques for characterizing the structures of synthetic polymers and dendrimers are illustrated, including: the characterization of polymer chain-end structure, monomer sequence, stereosequence, and branching. The utility of triple resonance and pulsed field gradient NMR techniques in these research endeavors are discussed.

Introduction

Since its discovery over half a century ago, NMR has been the most valuable tool in advancing our knowledge of organic structures in chemistry, biology and materials science. The development of multidimensional NMR methods, especially 3D-NMR techniques, in conjunction with isotopic labeling has been indispensable in developing our knowledge of protein structure and function in molecular biology.⁽¹⁾ Generally, 2D-NMR methods have been

sufficient in natural products chemistry, pharmaceutical science, and other fields involving the study of structures of relatively small molecules.⁽²⁾ The complex mixture of structures present in synthetic organic polymers makes this a fruitful area for applications of multidimensional NMR methods.

2D-NMR methods have been extensively exploited to tackle problems in polymer science, however, the use of 3D-NMR techniques in polymer science has been rare. Several factors have discouraged the exploitation of these techniques in polymer science, including the scarcity and expense of isotopically labeled monomers and the relatively small amount of funded research compared to that performed in the biological area. Nevertheless, 3D-NMR methods can be extremely useful for studying problems in polymer structure, mechanism and properties. In this review, we will summarize some of our work in this area in the hope that it will inspire others to use this methodology.

Polymer Structure.

Structure identification problems in polymer science generally entail identification of chain ends, main-chain repeat units and their sequences, and chain defects. All these factors influence the appearance of the polymer's NMR spectra, and are critical in determining the material's final physical and mechanical properties.

Chain-end Structure

Identification of chain-end resonances are useful since a comparison of these resonance intensities with those from the rest of the polymer provides a reliable means of determining number average molecular weight (M_n), a key factor in determining a polymer's physical and mechanical properties. Knowledge of the structures at the chain end is key in understanding the initiation, termination and chain-transfer reaction steps during polymer formation. All these factors are vital for altering reaction conditions to control a polymer's M_n . It is also thought that many polymer degradation processes begin with reactions at unique chain-end structures; if these structures and their degradation processes are known, it becomes possible to alter them to provide stable materials.

Main-chain Structure.

When polymerization of unsymmetrical monomers such as propylene occurs, addition can occur in a head-to-tail or a head-to-head fashion to provide a variety of different structures. If two or more monomers are copolymerized, a variety of monomer sequences (dyads, triads, tetrads, pentads, etc.) are possible as illustrated by the possible pentad monomer sequences for poly(1-chloro-1-fluoroethylene-co-isobutylene), (PCFEI), shown in Table 1. In general, it is possible to form copolymers having blocks of monomers, a statistically random distribution of two monomers, and all possible compositional variations between these two extremes. In the example of PCFEI, it is possible to form pentads with five sequential E's, five sequential I's, and all permutations of E's and I's between those extremes. The relative number of different monomer sequences provides information about the "blockiness" of the polymer, and is useful for determining the polymer's monomer composition.

Table 1. Most probable structures from polymerization of isobutylene (I) and 1-chloro-1-fluoroethylene (E)

E-EEE-E mm, mr, rr	E-EEI-E m, r	E-IEI-E	E-EIE-E m, r	E-EII-E	E-III-E
E-EEE-I mm, mr, rm, rr	E-EEI-E m, r	I-IEI-E	E-EIE-I m, r	E-EII-I	E-III-I
I-EEE-I mm, mr, rr	E-IEE-E m, r	I-IEI-I	I-EIE-I m, r	I-EII-E	I-III-I
	I-EEI-I m, r			I-EII-I	

If the vinyl monomer produces a stereogenic center upon incorporation into the polymer backbone, then additional structural permutations are possible. In the simplest case, we can consider the relative stereochemistry of adjoining monomer units in a polymer dyad. If these centers produce a mirror plane or a C_2 axis of symmetry, then the dyad is said to have meso (m) or racemic (r) relative stereochemistry, respectively, as shown in Figure 1. The relative stereochemistries of higher *n*-ad sequences are defined by the stereochemistries of the component dyad sequences as shown for the triad components of isotactic (mm), syndiotactic (rr), and heterotactic (mr) polymers.

The possible stereosequences of the middle triads of the PCFEI pentads are listed below each of the pentads in Table 1. Triads composed only of isobutylene units do not contain stereogenic centers, and therefore do not exhibit stereosequence effects in their NMR spectra. Even a relatively simple copolymer such as PCFEI is a mixture of over 30 microstructures, thus

explaining the complexity of the 1D-NMR spectra of this polymer, even at 600 MHz (Figures 2a-c).⁽³⁾

In this chapter, a small sample of the 3D NMR methods available to identify structures and obtain resonance assignments from synthetic polymers will be presented. Once assignments are obtained, they can be used together with standard quantitative 1D NMR to measure the compositions of structures present and to learn about the polymerization chemistry.

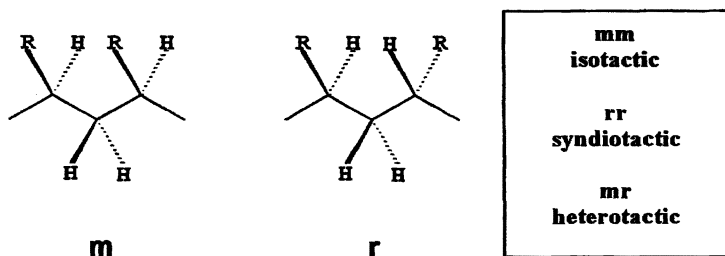


Figure 1. Relative stereochemistries in meso (m) and racemic (r) dyad and triad structures that constitute isotactic, syndiotactic and heterotactic polymers.

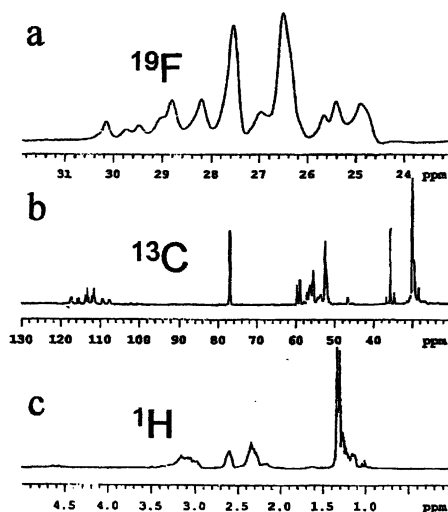


Figure 2. One dimensional NMR spectra of PCFEI: a) 586 MHz ^{19}F spectrum; b) 150 MHz ^{13}C spectrum; and c) 600 MHz ^1H spectrum. (Reproduced from reference 3. Copyright 1996 American Chemical Society.)

Multidimensional NMR

Two Dimensional NMR

Figure 3a shows the diagram of a one dimensional experiment, which consists of preparation and detection periods. In most instances, the preparation period is a relaxation delay, however, in special experiments, the preparation period can be some other special sequence such as a relaxation delay combined with an INEPT(4) polarization transfer delay. The resulting signal as a function of detection time (t_1), known as a free induction decay (FID), is Fourier transformed (FT) to provide the normal spectrum with peak intensity as a function of frequency (f_1).

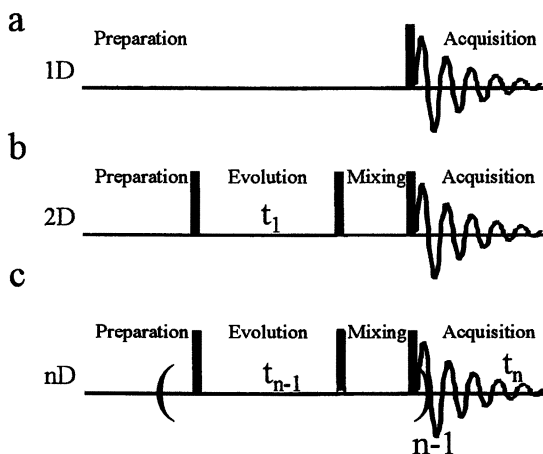


Figure 3. Schematic illustration of nD -NMR experiments: a) 1D, b) 2D, and c) nD .

In 2D-NMR experiments, an additional evolution delay, t_1 (and in some cases an optional mixing delay), is inserted between the end of the preparation period and the beginning of the detection period (t_2) (Figure 3b). A series of FID's are collected with the t_1 period incremented by an amount related to the inverse of the desired spectral window in the f_1 dimension (Figure 4a). In nD -NMR, the convention is to sequentially label the evolution delays $t_1, t_2, \dots, t_{(n-1)}$ in the order they are executed (Figure 3c), and the detection period is identified as t_n . Sequential FT with respect to t_2 (Figure 4b)

and then t_1 produces a 2D spectrum with the usual NMR characteristics of the detected nucleus plotted along f_2 (Figure 4d). The NMR parameters plotted along the f_1 axis depend upon the specific preparation period used, and the nature of the NMR coherence evolving during the t_1 period.

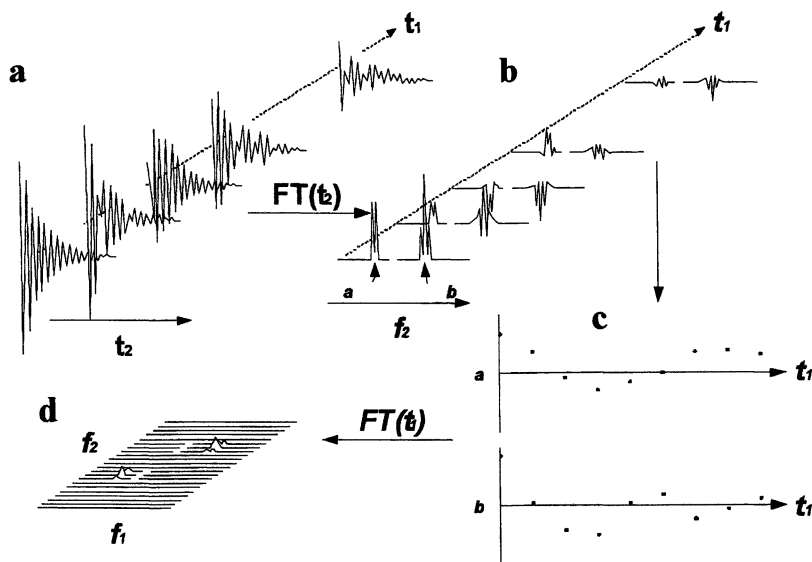


Figure 4. Schematic illustration of the steps in producing a 2D-NMR spectrum: a) raw t_1/t_2 data, b) after FT with respect to t_2 , c) t_1 modulation of the signal intensities at the shifts of peaks a and b in (b), and d) final spectrum after FT with respect to both t_1 and t_2 .

Thousands of 2D experiments have been reported in the literature. These experiments can be categorized into a few major classes based on the type of information obtained from the spectra. The experiments within a class contain different refinements of the same basic experiment, but they provide the same type of information. Different variations are most useful under different circumstances. Typically, information from two or more classes of experiments is used together to obtain a complete solution to a structure. In selecting appropriate experiments, one must first consider its feasibility in terms of sensitivity. Assuming availability of an instrument with a specific field strength and no limitations imposed by the amount of sample available (not unusual, especially when dealing with commercial polymers), the feasibility of an experiment is determined by the sensitivity for the nucleus to be detected,

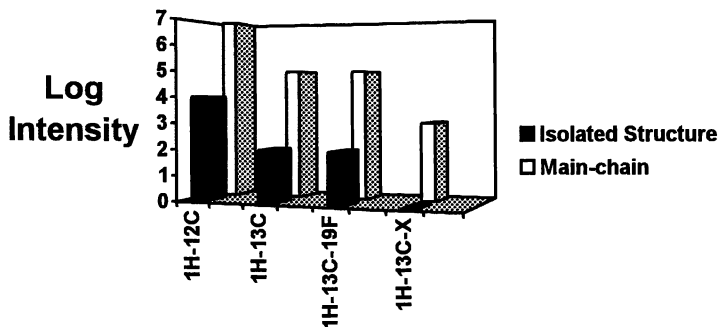


Figure 5. Diagram showing the relative intensities of different NMR signal components.

the abundance of the nuclear isotopes involved in the experiment, and the abundance of the structure fragment to be studied. This is illustrated in Figure 5.

Note that the intensity scale along the side is logarithmic. In the chart, the intensity of the main-chain resonances in the ^1H spectrum is assumed to be 10^7 . If one wants to detect resonances from a unique isolated structure such as the chain-end of a polymer with degree of polymerization (DP) of 100, and one assumes that there is a mixture of 10 different chain-end structures, then the intensity of the signals from each of these structures might be ca 10^4 . If an indirect detection experiment such as HMQC(5) is to be performed to detect chain end C-H correlations, then the natural abundance of ^{13}C (1.1%) must be factored into the equation. The intensities of the desired signals will be ca. 10^2 , or 100,000-fold weaker than the signals in a standard ^1H NMR spectrum. This creates a considerable sensitivity problem, equivalent to diluting the sample 100,000 fold. The enormous dynamic range of intensities for the signals present, creates some additional difficulties when it is necessary to detect weak signals in the presence of huge peaks from $^1\text{H}-^{12}\text{C}$ fragments in main chain repeat units. Furthermore, the intense signals must be completely and reliably removed from the spectrum while detecting the much weaker $^1\text{H}-^{13}\text{C}$ signals from 1.1% of the chain ends containing ^{13}C . Traditionally, phase cycling has been used for selective detection of the desired coherence, and cancellation (by difference spectroscopy) of the much more intense undesired signal components. These techniques work reasonably well for small molecules, however they are insufficient for collecting spectra of suitable quality to detect chain end correlations in the 2D-NMR spectrum. Typically, phase cycling provides up to 100-fold cancellation of undesired signals, however, this leaves

artifacts that are still 100-fold more intense than the desired chain-end resonances.

Coherence Selection Using Pulsed Field Gradients

To solve this problem, coherence selection using pulsed field gradients (PFG)(6) can be extremely useful. Pairs of magnetic field gradients are applied during pulse sequence delays, such that the effects of the inhomogeneous magnetic field cancel for the coherence components of interest. Consequently, the desired NMR signal component is refocused for detection. All other undesired coherence components suffer from the cumulative effects of the field gradients, are defocused, and thus the undesired signal components are not detected. Typically, more than 1000-fold suppression of undesired signal components can be achieved. When using this technique to perform multidimensional NMR studies of polymers, several advantages are realized. 1) Much better suppression of the undesired signals components is achieved, making it possible to detect signals that are orders of magnitude weaker than the main chain resonances. 2) Cancellation artifacts that produce *t*1 noise are eliminated. 3) If signal averaging is performed, phase cycling can be used in conjunction with PFG coherence selection, providing up to 10⁶-fold suppression of undesired signals; thus making it possible to detect weak chain-end signals of ¹H-¹³C fragments while suppressing the much larger main-chain ¹H-¹²C resonances. 4) Because the undesired signal components never pass through the instrument's receiver path (as they do in coherence selection via phase cycling alone), the receiver gain can be optimized for the detection of the weak signals of interest, greatly improving the dynamic range characteristics of the instrument. These factors make PFG coherence selection particularly valuable for polymer NMR spectroscopy.(7)

Figure 6 shows sections from the HMBC spectra of polyethylene. In Figure 6b, the spectrum is dominated by a huge *t*1 noise ridge at the shift of the

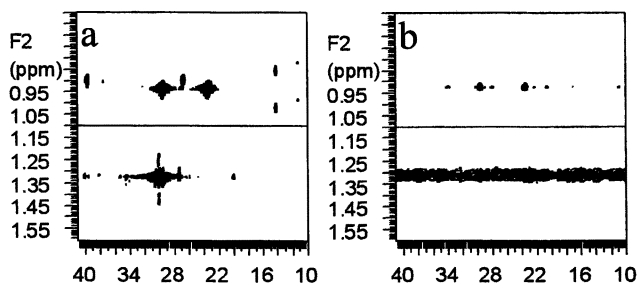


Figure 6. Sections from the 750 MHz HMBC spectra of polyethylene: a) with PFG coherence selection; and b) with coherence selection by standard phase cycling.

backbone methylene carbons, from incomplete cancellation of undesired signal components. Two small cross peaks, from a small number of branching structures, are barely detected. The spectrum in Figure 6a was obtained with combined use of PFG's and phase cycling for coherence selection. In the latter spectrum, the $t1$ noise ridge is completely eliminated revealing new correlations. The signals that were seen in the former spectrum are now very intense, a consequence of the fact that ca. 100-fold greater receiver gain could be used, reducing digital noise that restricted dynamic range.

3D-NMR Spectroscopy

If 2D NMR can be described as a series of 1D experiments repeated while incrementing a $t1$ evolution delay (Figure 3b), then 3D NMR can be described as a series of 2D experiments repeated while incrementing a $t2$ evolution period (Figure 3c). Due to sensitivity limitations, almost all solution 3D NMR experiments to date involve ^1H detection during the acquisition time. The NMR properties of the heteronucleus are indirectly detected (as in HMQC) through modulation of the signal by precession of coherence during one of the evolution delays.

3D NMR experiments can be constructed in two ways. In the first method, two 2D-NMR experiments can be combined to form a 3D experiment. For example, COSY and HSQC experiments can be combined to produce a HMQC-COSY experiment.⁽⁸⁾ The 3D spectrum from such an experiment would contain 2D-COSY planes at the shifts of each hydrogen-bearing carbon atom. The planes would only contain correlations between the shift of the proton bound to that carbon and those protons coupled to it. Dramatic simplification of the spectra are obtained by dispersing the components of the COSY spectrum into the ^{13}C chemical shift dimension. If two homonuclear experiments (such as COSY and NOESY) are combined, a homonuclear 3D experiment is obtained. These methods have the advantage of excellent sensitivity, since all the nuclei involved have essentially 100% abundance and high receptivity. Additionally, these experiments do not require special hardware and are easy to set up since they only require a single Rf channel. Unfortunately, the number of cross-peaks in such spectra is extremely large. For example, there are 64 peaks in the COSY-COSY spectrum of an AB spin system. This defeats the purpose of using multidimensional experiments. Nevertheless, experiments of this sort can be useful. Mirau et al. ⁽⁹⁾ have used a NOESY-J-resolved 3D-NMR experiment to study the conformation of poly(vinyl acetate-co-vinylidene cyanide).

Double resonance 3D NMR experiments are derived from the combination of a homonuclear 2D experiment and a heteronuclear 2D experiment such as HMQC. These experiments do not require special hardware, and are feasible

with essentially all modern instruments. Compared to homonuclear 3D experiments their sensitivity is reduced by the low abundance of the heteronucleus. However, they provide very good spectral dispersion since the heteronuclei generally are singlets dispersed over large chemical shift ranges. These experiments are feasible whenever a standard HMQC experiment is possible.

A second alternative for creating 3D experiments involves concatenating a series of coherence transfer sequences (such as INEPT), with evolution delays inserted when the coherence resides on the nuclei of interest. The resulting 3D spectrum will contain correlations at the intersection of the NMR parameters measured during the evolution time (usually chemical shift). Figure 7 shows a pulse sequence diagram for a general HXY 3D chemical shift correlation experiment. In this sequence, coherence is transferred from H to X (using J_{HX}); a second coherence transfer from X to Y is performed (using J_{XY}), while the coherence resides on Y, its chemical shift is encoded during the $t1$ evolution period; coherence is transferred back to X; the X chemical shift is encoded during the $t2$ evolution period; finally coherence is transferred back to ^1H for detection during $t3$.

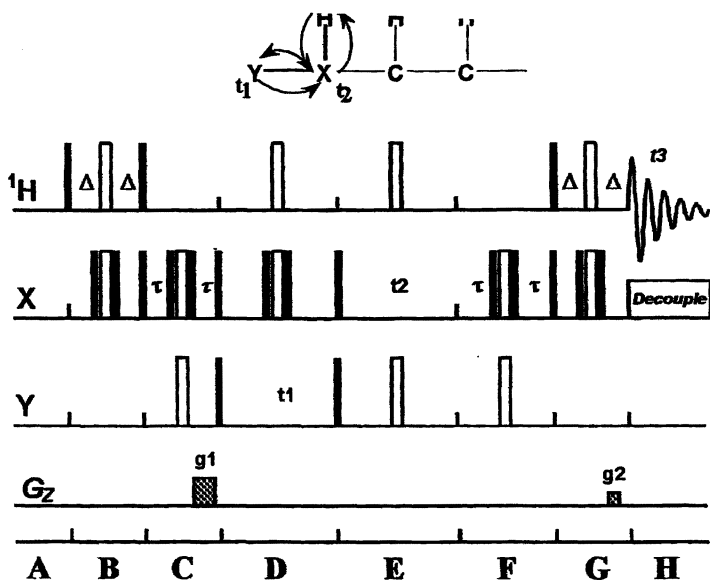


Figure 7. Pulse sequence diagram for an HXY triple resonance 3D-NMR, open rectangles represent 180° pulses and solid rectangles represent 90° pulses.

The sensitivity of this experiment compared to simple ^1H homonuclear experiments is governed entirely by the natural abundance of the X and Y

nuclei. Variations of this sequence, where $X = {}^{15}\text{N}$ and $Y = {}^{13}\text{C}$, are the basis for many of the 3D experiments used to study protein structures.⁽¹⁾ These experiments are usually performed on proteins with a high level of ${}^{13}\text{C}$ and ${}^{15}\text{N}$ incorporation so that the abundance of these isotopes is not a factor in determining sensitivity. However, experiments of this sort can be performed without the benefit of isotopic labeling. This is the subject of this review.

The primary factors in determining the feasibility of such experiments are the relative abundance of the fragment to be detected and the abundance of the NMR active isotopes of X and Y. In an HCX experiment, used to study polymer chain-end structures uniquely containing NMR active X nuclei, the diagram in Figure 5 illustrates the relative signal intensities of polymer structure fragments. We can define a parameter called degree of difficulty (DOD) by equation 1,

$$\text{DOD} = -\log[\text{abundance of } {}^{13}\text{C} \times \text{abundance of X} \times \text{abundance of structure}] \quad (1)$$

which provides an indication of the relative intensity of the desired signal component compared to the signals from abundant ${}^1\text{H}$ atoms of high occurrence main-chain repeat units. For a polymer with degree of polymerization (DP) of 1000 and X nucleus natural abundance of 1%, if we are to perform HCX experiments to detect ${}^1\text{H}$ - ${}^{13}\text{C}$ -X fragments of chain-ends, $\text{DOD} = -\log[0.001 \times 0.01 \times 0.01] = 7$. The signals of interest will be 10^7 less intense than those of protons from the polymer backbone structures. Use of experiments like this requires an instrument with three Rf channels, in order to simultaneously apply pulses at the H, X and Y frequencies, and to simultaneously decouple X and Y while acquiring the ${}^1\text{H}$ signal during t_3 .

Applications

Main-Chain Structure, Monomer Sequence and Stereosequence

Li et al. (10) used HCF triple resonance 3D NMR to assign the ${}^1\text{H}$, ${}^{13}\text{C}$ and ${}^{19}\text{F}$ resonances of poly(1-chloro-1-fluoroethylene) (PCFE). Figure 8 shows the 1D NMR spectra of this polymer. The ${}^1\text{H}$ spectrum contains very little useful information; and the ${}^{13}\text{C}$ spectrum shows essentially two clusters of resonances from C-F and CH_2 groups. The ${}^{19}\text{F}$ spectrum contains three groups of resonances in ca. 1:2:1 ratio, from mm, mr/rm and rr triad stereosequences. Application of HCF triple resonance 3D-NMR is particularly useful in this case, since ${}^{19}\text{F}$ has a natural abundance of 100% and an enormous chemical shift dispersion. The sensitivity of this experiment is comparable to that of a simple double resonance ${}^1\text{H}\{{}^{13}\text{C}\}$ -HMQC experiment.

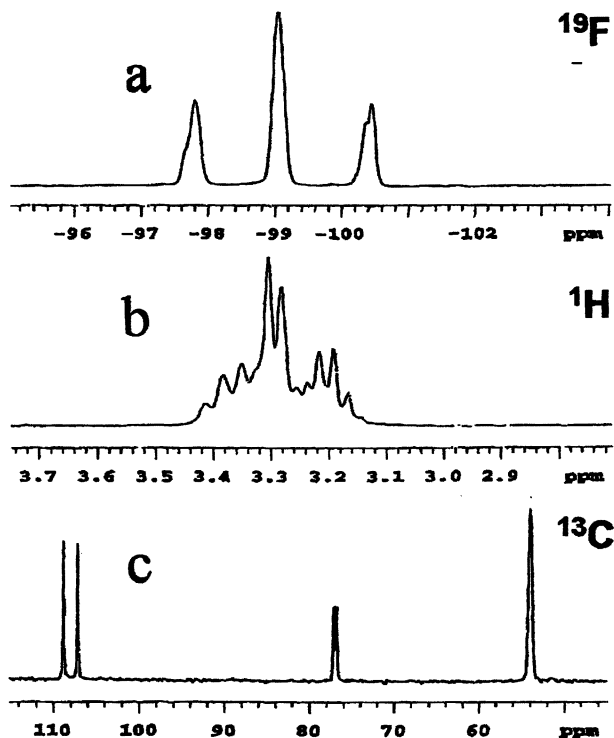


Figure 8. NMR spectra of poly(1-chloro-1-fluoroethylene) (PCFE): a) ^{19}F , b) ^1H , and c) ^{13}C with ^1H and ^{19}F decoupling spectrum. (Reproduced from reference 10. Copyright 1997 American Chemical Society.)

Figure 9 shows slices from the triple resonance HCF 3D-chemical shift correlation spectrum. In this experiment, coherence transfer occurs from ^1H to ^{13}C (using one-bond J_{CH} coupling); ^{13}C chemical shift is encoded during $t1$; coherence transfer is accomplished using two-bond J_{CF} ; ^{19}F chemical shifts are encoded during $t2$; and coherence transferred back to ^{13}C , then ^1H for detection. The $flf3$ slices (Figures 9a-c) at the three ^{19}F chemical shifts show C-H correlations for directly bound atoms of the CH_2 groups adjoining the ^{19}F atom with the chemical shift of that slice. At each ^{13}C chemical within a slice, correlations are observed to either one or two ^1H chemical shifts, depending upon whether the methylene exists in an r or m dyad, respectively. This makes it possible to determine that the slices in Figures 9a, 9b and 9c are from $\text{CH}_2\text{-CF}(\text{Cl})\text{-CH}_2$ fragments of mm, mr/rm and rr dyads, respectively. A more detailed analysis of a very high resolution 3D spectrum, by comparing the mutual existence of the same cross peaks in different slices, permitted the resolution and assignments of all 10 sets of resonances from pentad structures.

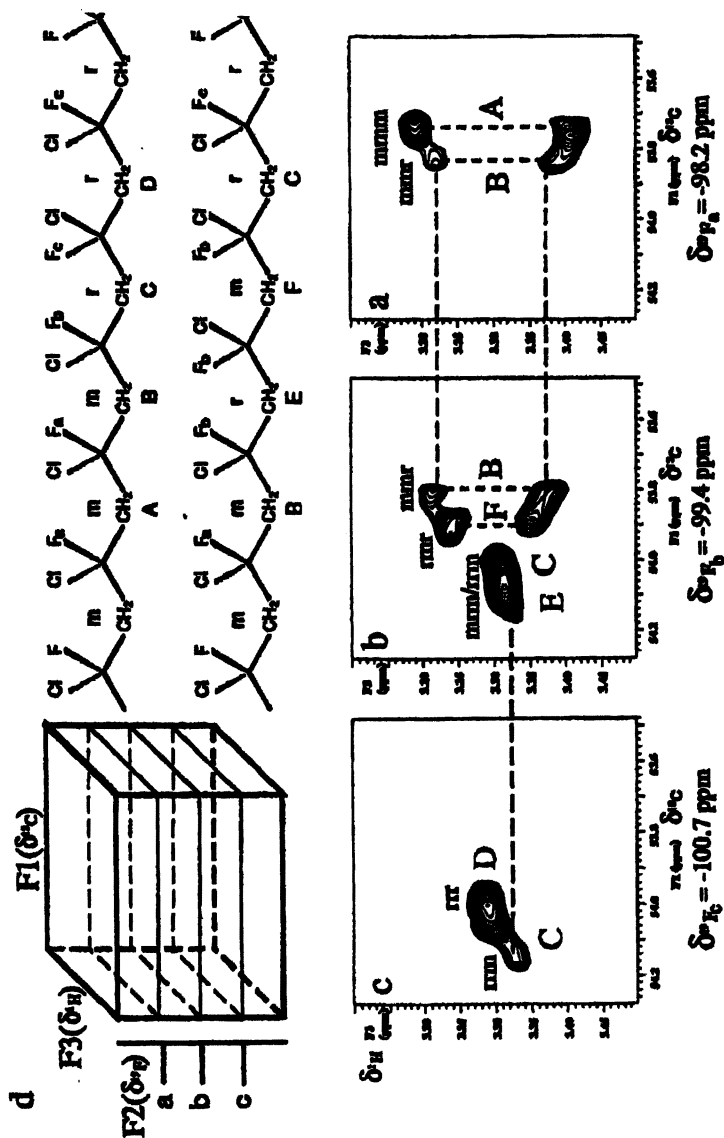


Figure 9. Slices corresponding to $f1f3$ planes (a-c) from the HCF triple resonance 3D-NMR spectrum (d) of poly(1-chloro-1-fluoroethylene) (PCFE) at the shifts of the three ^{19}F resonances. (Reproduced from reference 10. Copyright 1997 American Chemical Society.)

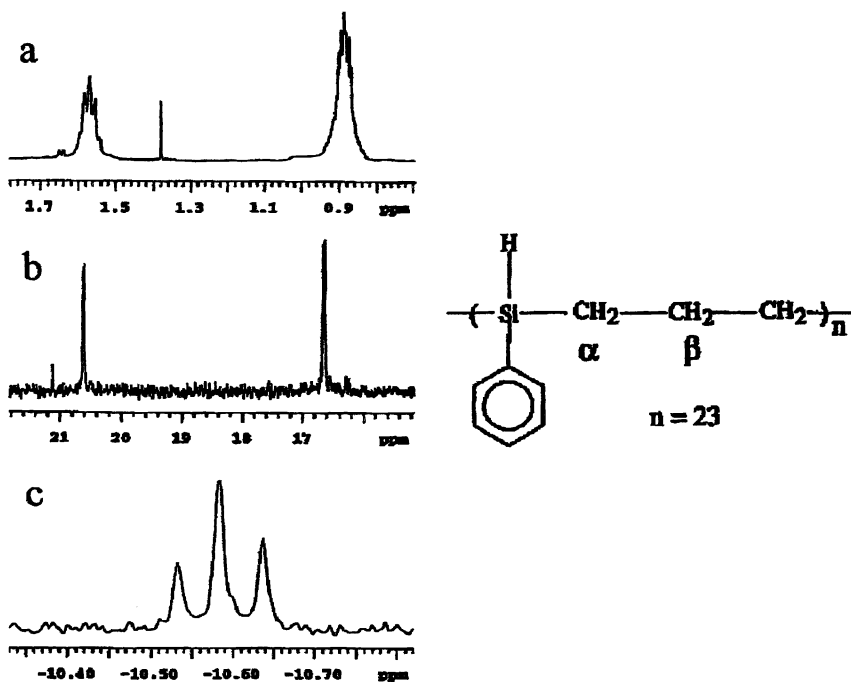
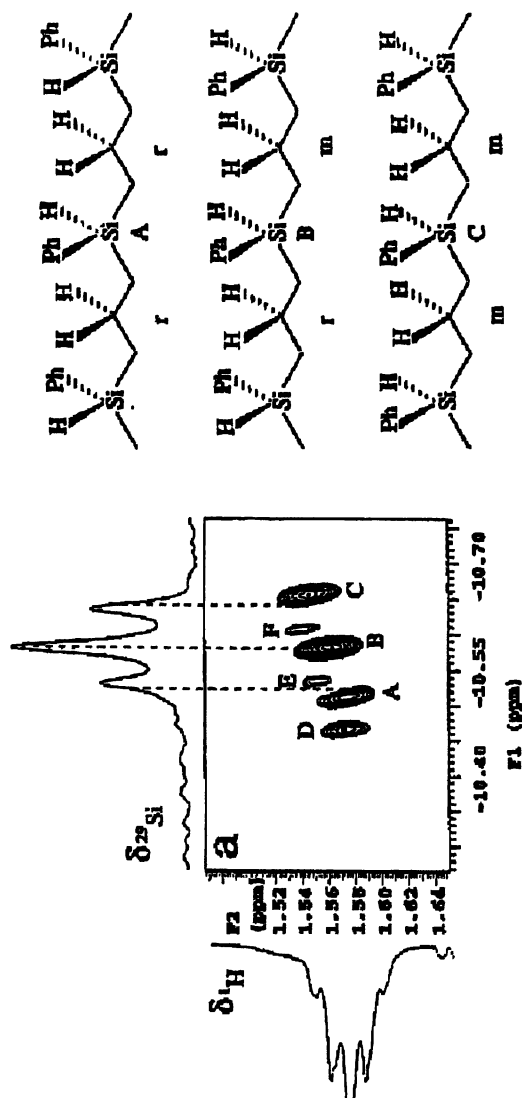


Figure 10. 1D NMR spectra of poly(1-phenyl-1-silabutane) (PPSB): a) ^1H , b) ^{13}C , and c) ^{29}Si . (Reproduced from reference 11. Copyright 1997 American Chemical Society.)

Similarly, $^1\text{H}/^{13}\text{C}/^{29}\text{Si}$ triple resonance 3D-NMR was used to study the structure of poly(1-phenyl-1-silabutane) (PPSB).⁽¹²⁾ In this polymer, stereogenic centers are present at the Si atoms. While the ^1H 1D NMR spectrum only revealed two sets of resonances from protons α and β to Si (Figure 10a), the 1D ^{29}Si NMR spectrum exhibited three peaks from mm, mr/rm and rr stereosequences (Figure 10c). As with PCFE, a $^1\text{H}-^{13}\text{C}-^{29}\text{Si}$ chemical shift correlated 3D-NMR spectrum (Figure 11) permitted assignment of the resonances from the three triad stereosequences.

Slices from the 3D NMR spectrum, at the shifts of each of the unique ^{29}Si atoms are shown in Figures 11b-d. As with PCFE discussed above, examination of the correlations from methylene groups β to Si reveals the same types of single and double correlations for r and m methylenes. It thus became possible to assign the sets of resonances (^1H , ^{13}C and ^{29}Si) to mm, mr/rm and rr triads structures. Similar techniques have also been used to study the structures of small oligomers of poly(dimethylsiloxane).⁽¹³⁾



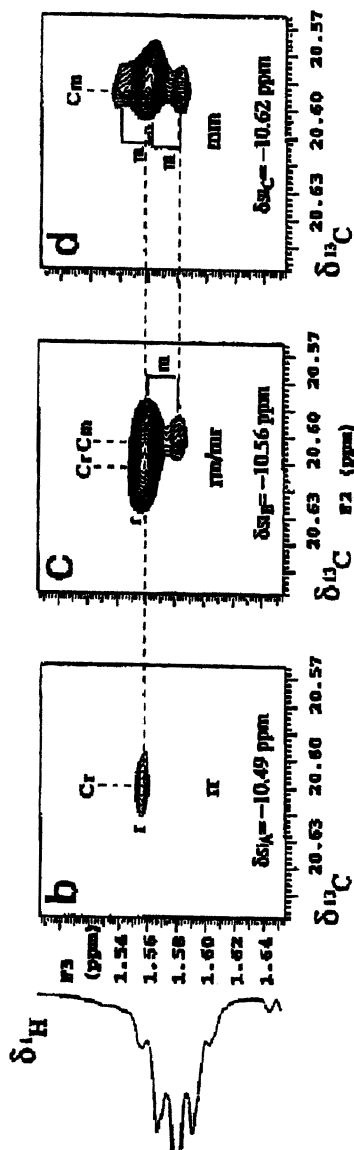


Figure 11. a) ^1H - ^{29}Si 2D HMQC spectrum, using $^2J_{\text{HSi}}$ for coherence transfer; and b-d) $f1f3$ slices from the HCSi triple resonance 3D-NMR spectrum of poly(1-phenyl-1-silabutane) (PPSB), at the $f2$ positions corresponding to the chemical shifts of the three ^{29}Si resonances. (Reproduced from reference 11. Copyright 1997 American Chemical Society.)

These experiments were used in a slightly different way to obtain complete characterization and resonance assignments for carbosilane-based dendrimers.(14) As an example, consider the second generation dendrimer shown in Figure 12. Two 3D-NMR spectra were obtained, both with ^1H to ^{13}C coherence transfer delays based on $^1\text{J}_{\text{CH}}$. In the first experiment (spectrum shown in Figures 13a-c), the ^{13}C to ^{29}Si coherence transfer delays were based on $^1\text{J}_{\text{CSi}}$, producing information about direct H-C-Si connectivities highlighted by the bold type bonds in the substructure in Figure 12a. From this spectrum, it is possible to identify three unique structure fragments.

In order to determine how the three fragments are connected, a second 3D-NMR experiment was performed with C to Si coherence transfer delays based on $^2\text{J}_{\text{CSi}}$ (spectrum shown in Figures 13d-f). This spectrum shows the same cross-peaks seen in the one-bond 3D spectrum (but without optimized intensities for these one-bond correlations) and a new set of cross peaks correlating the shifts of ^{29}Si with the shifts of ^1H and ^{13}C atoms of CH_n groups two bonds away. While there are methods to remove the one-bond correlations from the multiple-bond 3D NMR spectrum, this would have lengthened the pulse sequence, potentially resulting in loss of signal intensity through relaxation processes. The spectra are well dispersed, and the presence of these extra peaks does not hinder the resolution and assignment of important peaks.

These HCSi 3D NMR experiments had a DOD of 4 to 5. In order to compensate for the loss of signal intensity, ca. 20-30 mg of material was used in a 5 mm sample tube. 3D-NMR experiments typically required 4-8 hours, however, the experiment times were not governed by sensitivity requirements. All spectra contained more than adequate signal-to-noise, and were it for this factor alone, could probably have been completed in just a few minutes. The longer experiments times were required to collect a 3D data matrix having a sufficient number of increments in the t_1 and t_2 dimensions.

Three-dimensional NMR techniques at 750 MHz have been used to study the structures, resolve and assign the resonances, and study the interactions between DAB-type dendrimers.(15) If HCN triple resonance techniques had been applied without the benefit of isotopic labeling, the DOD for these experiments would have been on the order of 6-7, about an order of magnitude too difficult to perform on even the best of modern NMR instruments. This difficulty is largely due to the very low (0.37%) natural abundance of ^{15}N . At the very high field, all of the ^{13}C resonances from third and fourth generation DAB-16 and DAB-32 were resolved. This fact was exploited by using HMQC-TOCSY(16) double resonance 3D NMR to resolve and assign all of the ^1H resonances of DAB-16. It was possible to resolve all of the ^1H resonances in the 3D-NMR spectrum from this experiment (based on dispersion of the ^1H resonances in the ^{13}C chemical shift dimension), despite the fact that many of the ^1H atoms have essentially the same chemical shift. Once the resonances were assigned, a NOESY-HSQC experiment(17) was used to study the inter- and intramolecular interactions of these molecules in a variety of solvents.

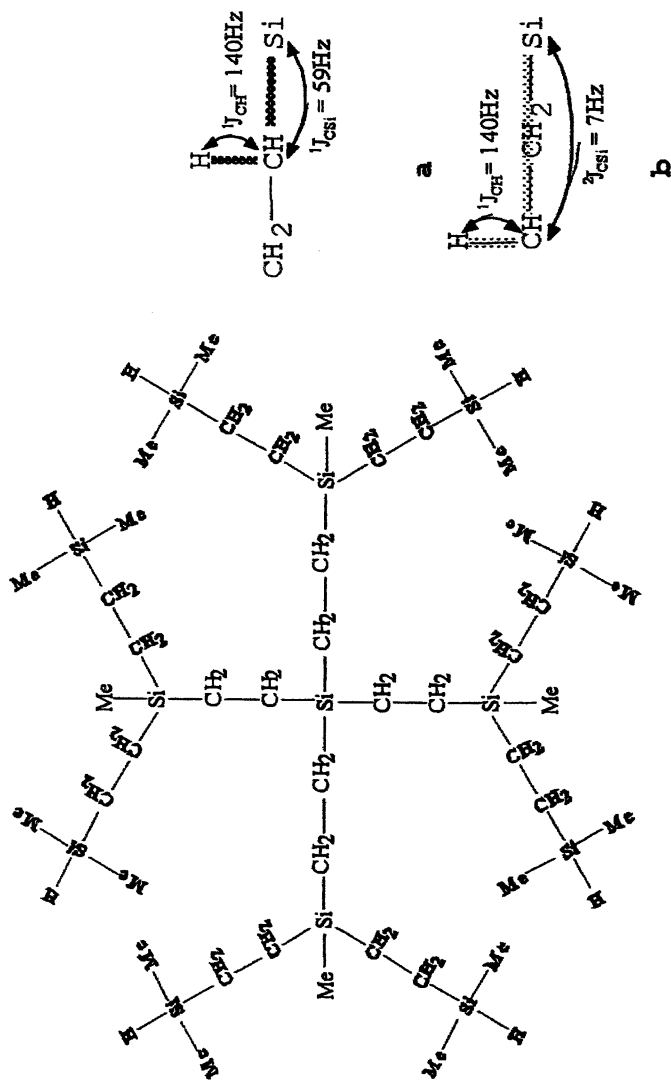


Figure 12. Structure of second generation carborane based dendrimer with illustration of coherence transfer pathway for two 3D NMR experiments using pulse sequence delays based on: a) $^1J_{\text{CSi}}$, and b) $^2J_{\text{CSi}}$. (Reproduced from reference 13. Copyright 2001.)

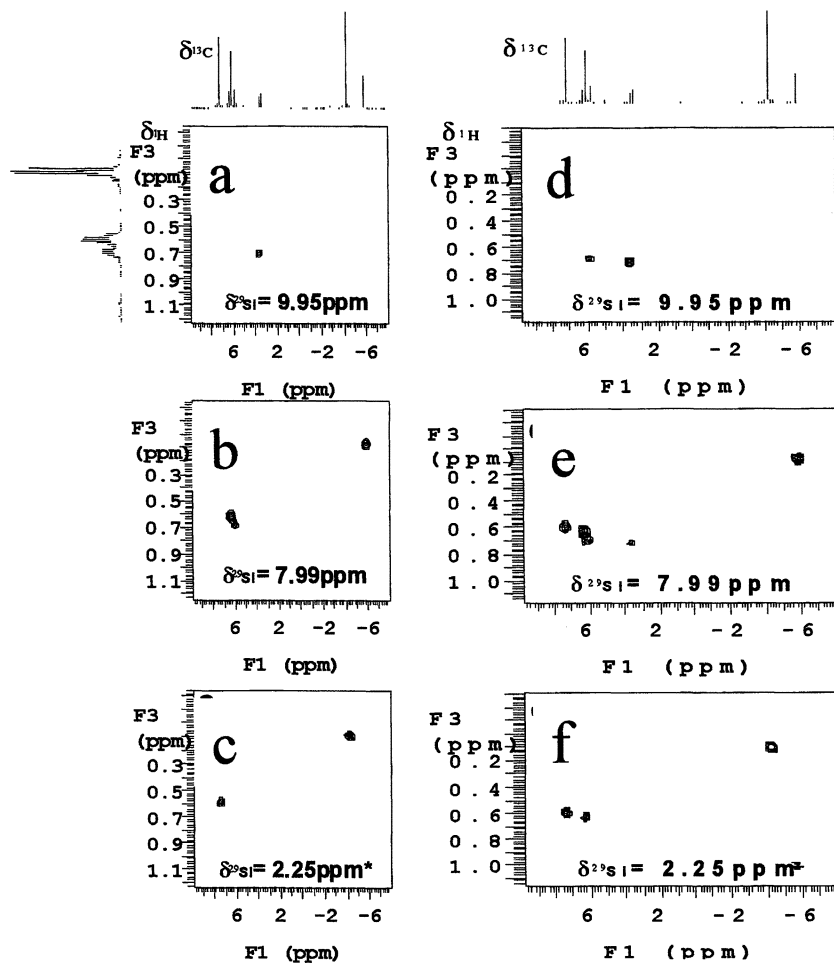


Figure 13. Slices from the HCSi 3D NMR spectrum of carbosilane dendrimer using coherence transfer delays based on: (a-c) $^1J_{CH}$ and $^1J_{CSi}$; and (d-f) $^1J_{CH}$ and $^2J_{CSi}$. (Reproduced from reference 14. Copyright 1999 American Chemical Society.)

Chain-End Structure

In a manner similar to that used for the carbosilane dendrimer discussed above, $^1\text{H}/^{13}\text{C}/^{119}\text{Sn}$ triple resonance 3D-NMR was used to study the chain-end structures of tri-*n*-butyltin-capped polybutadiene.⁽¹⁸⁾ If only the last monomer unit on the chain is considered, there are at least 3 possible chain end structures, depending upon whether 1,3-butadiene is enchainned by 1,2 addition, cis-1,4-addition or trans-1,4 addition, as shown by the structures in Figure 14. If the penultimate monomer unit is also considered, there are at least 9 possible chain-end structures. Long-range couplings between ^{13}C and metal atoms in organometallic structures are usually quite large. For organotin species similar to those present in the structures of interest here: $^1J_{\text{CSn}} \approx 300$ Hz, $^2J_{\text{CSn}} \approx 20$ Hz, and $^3J_{\text{CSn}} \approx 50$ Hz. Three separate HCSn chemical shift correlated 3D-NMR experiments were performed with delays optimized for one-, two- and three-bond ^{13}C - ^{119}Sn couplings. These experiments were used to identify the CH_n groups one-, two- and three-bonds from Sn in the chain-end. Slices ($f1/f3$) correlating ^1H and ^{13}C at four separate ^{119}Sn chemical shifts in the $f2$ dimension are shown in Figure 14. Applications involving organometallic species are most promising since even three- and four-bond long range couplings are often large enough to produce 3D correlations.

In a study to learn about the polymerization chemistry of a new class of phosphorus-centered radical initiators, a combination of 3D-NMR techniques was used to study the ^{31}P -containing chain-end structures of polystyrene.⁽¹⁹⁾ Several of the possible chain-end structures are shown in Figure 15, along with the 1D ^1H , ^{13}C and ^{31}P NMR spectra. In the ^1H and ^{13}C NMR spectra, the weak signals from chain-end structures are buried under the much larger signals of the polymer backbone.

A simple HCP chemical shift correlated 3D-NMR spectrum provided information about the CH_n groups directly bound to ^{31}P at the chain ends. Since ^{31}P is present in 100% natural abundance, this experiment has sensitivity comparable to that of a standard HMQC double resonance experiment. Additionally, because only the chain-end structures contain ^{31}P , the experiment selectively detects chain-end resonances, and filters all other signals from the spectrum. Figure 16 shows the standard HMQC spectrum along with the truncated 3D spectrum. In the HMQC spectrum (Figure 16a), all the resonances from the polymer are observed. It is difficult to discern resonances from the chain-end because they are buried by the much larger signals from the polymer backbone. Figure 16b contains the truncated HCP 3D-NMR spectrum showing $f2/f3$ correlations (^{13}C - ^1H). It is equivalent to an HMQC spectrum except for the fact that coherence must pass through ^{31}P in order to be detected during the acquisition time. It therefore behaves as an HMQC spectrum selective for CH_n groups bound for ^{31}P .

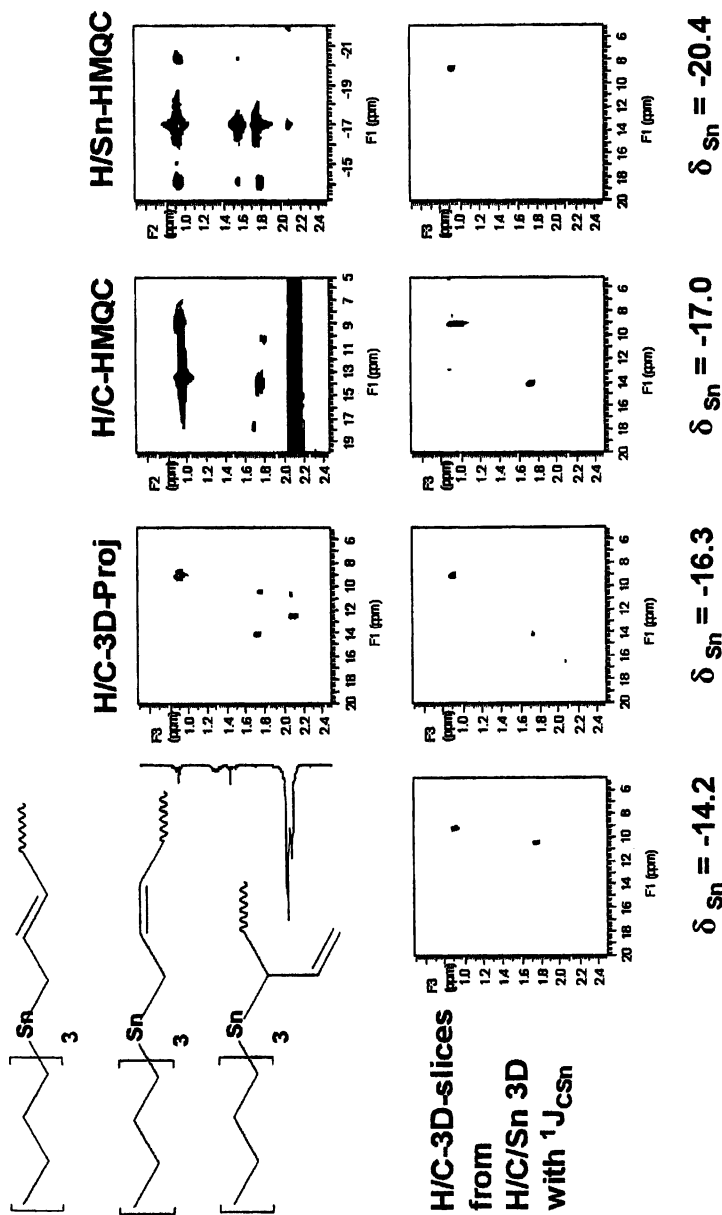


Figure 14. Slices from the 1H CSn 3D NMR spectrum of *n*-butyl₃Sn-terminated polybutadiene using coherence transfer delays based on $^1J_{CH}$ and $^1J_{CSn}$. (Reproduced from reference 18. Copyright 2000 American Chemical Society.)

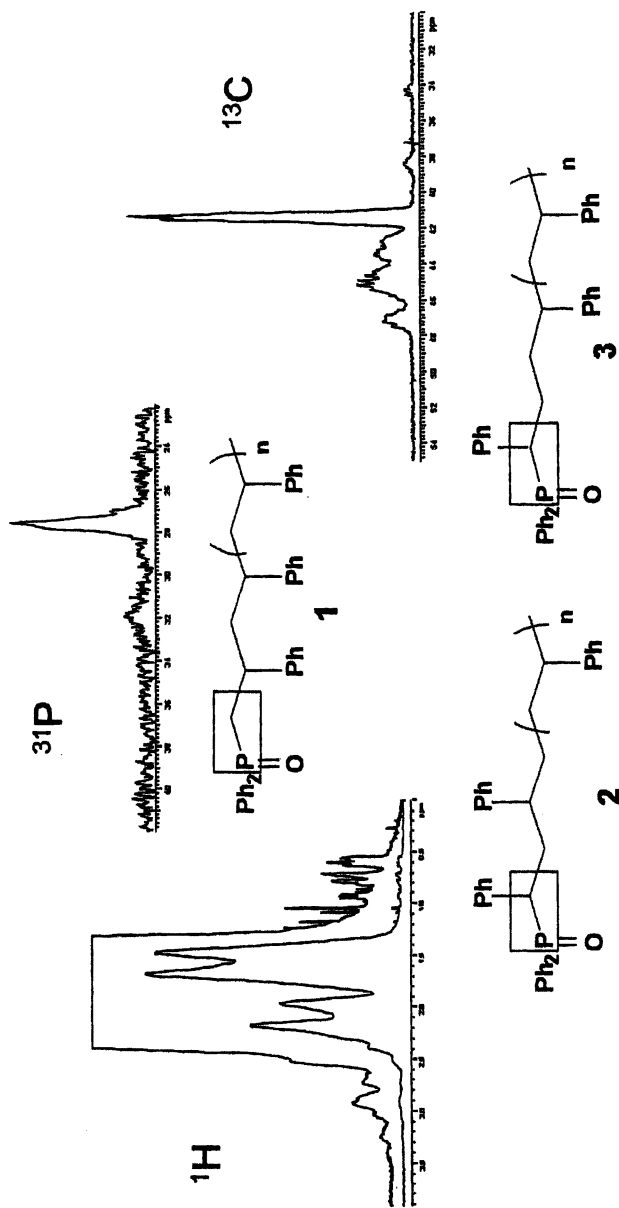


Figure 15. One-dimensional ¹H, ¹³C and ³¹P NMR spectra, and possible phosphorus-containing chain-end structures formed by styrene polymerization, initiated by diphenylphosphinyl radical.
(Reproduced from reference 19. Copyright 2001 American Chemical Society.)

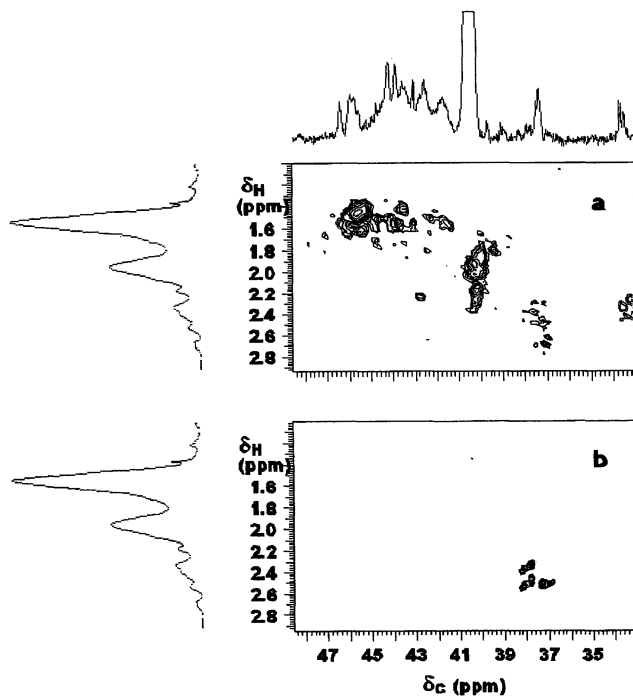


Figure 16. Two-dimensional NMR spectra of polystyrene with phosphorus-containing chain ends: a) standard HMQC spectrum; and b) truncated HCP-3D (2D) spectrum. (Reproduced from reference 19. Copyright 2001 American Chemical Society.)

The full 3D version of the experiment is shown schematically in Figure 17. It is possible to identify the CH_n ^1H and ^{13}C resonances of eight types of chain-end structures, without interference from signals from the rest of the polymer structure. Unfortunately, unlike the organotin structures discussed above, long-range ^{13}C - ^{31}P couplings are relatively small (ca. 5 Hz). The short relaxation times of this polymer, together with the long coherence transfer delays required to produce correlations between ^{31}P resonances and the resonances of CH_n groups more than one bond away, preclude the use of the HCP 3D-NMR experiment for obtaining additional structure information. Fortunately, there is a solution to the problem.

A nearly identical polystyrene sample was prepared, but with uniform ^{13}C labeling of all the polymer backbone carbons. This permitted the use of the pulse sequences shown in Figure 18. The naming of these sequences follows the convention used by those working in the protein structure area. Listing the atoms in the coherence transfer pathway forms the acronym. Those atoms in the coherence transfer pathway whose chemical shifts are not encoded during

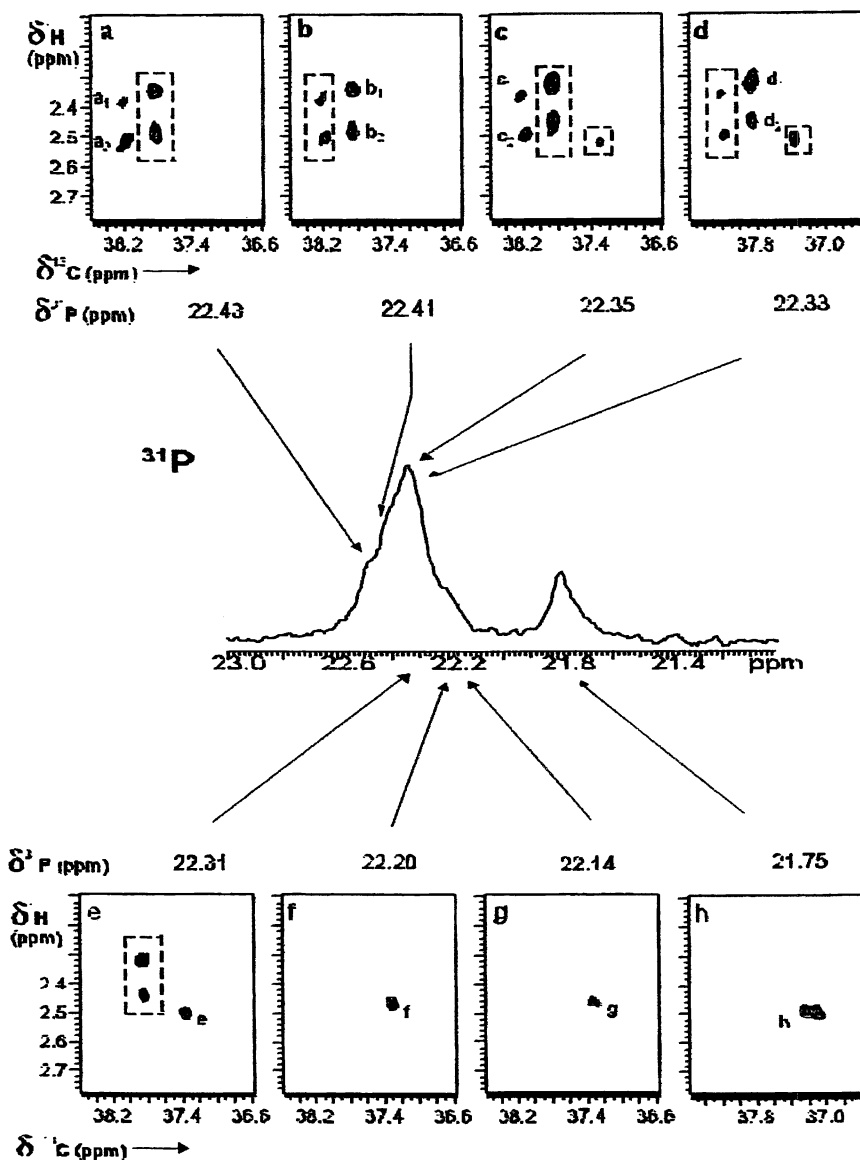


Figure 17. Illustration of the HCP 3D-NMR spectrum of phosphorus-containing chain-end structures formed through styrene polymerization initiated by diphenylphosphinyl radical. (Reproduced from reference 19. Copyright 2001 American Chemical Society.)

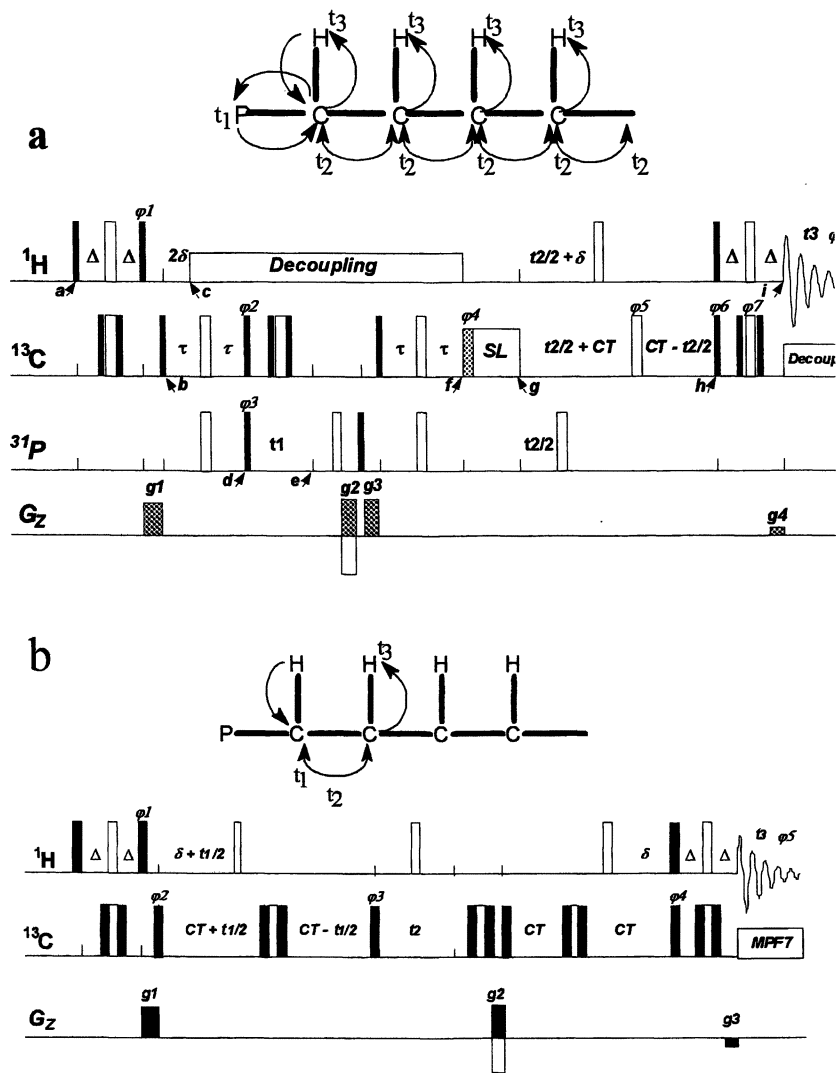


Figure 18. Pulse sequence diagrams for 3D H(CA)P-CC-TOCSY (a) and HCCCH (b) experiments. (Reproduced from reference 19. Copyright 2001 American Chemical Society.)

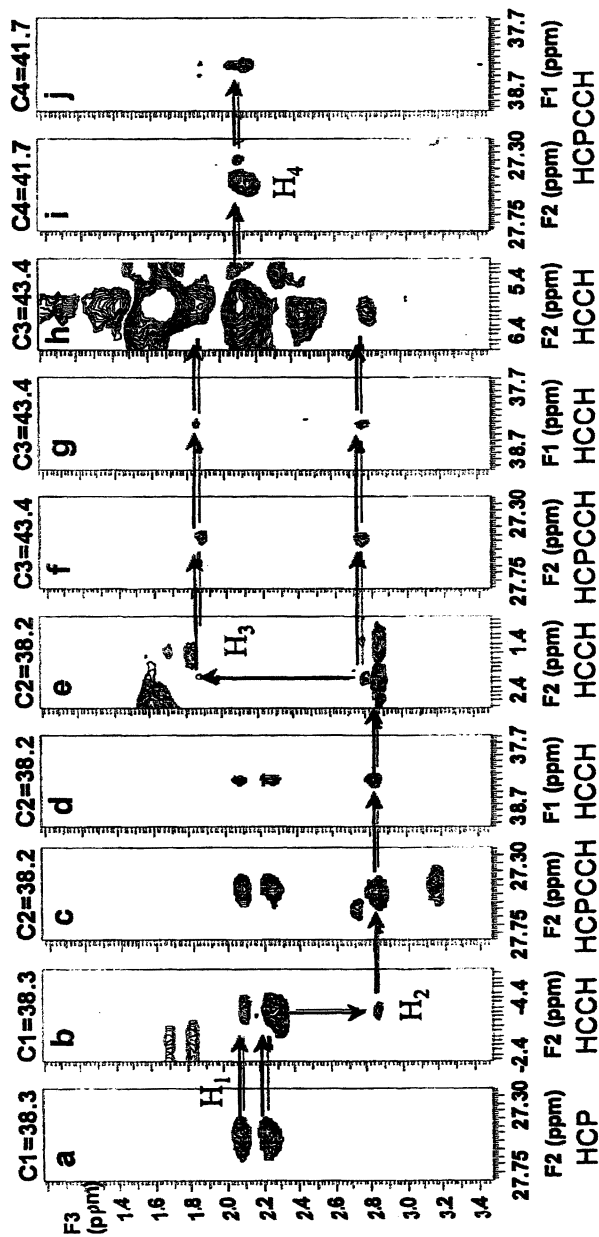


Figure 19. Selected regions from the HCP, H(CA)P-CC-TOCSY and HCCH experiments, showing the resonance assignments for one of the ^{31}P -containing chain-ends of the polymer formed of diphenylphosphinyl radical initiated polymerization of styrene. (Reproduced from reference 19.)

Copyright 2001 American Chemical Society.

an evolution delay, are included in parentheses. The H(CA)P-CC-TOCSY experiment (Figure 18a) starts with coherence on protons; transfers coherence to phosphorus through the carbon α to phosphorus using $^1J_{\text{CH}}$, then using $^1J_{\text{CP}}$; the ^{31}P chemical shift is encoded during $t1$; coherence is transferred back to the carbon α to phosphorus, then a TOCSY spin lock pulse is used to distribute coherence among the first few carbons along the polymer backbone; the ^{13}C chemical shifts of these carbons are encoded during $t2$; and coherence is transferred back from each of the ^{13}C atoms to their directly bound ^1H atoms for detection. Slices at each ^{31}P chemical shift exhibit C-H correlations for the first few CH_n groups at the polymer chain end containing that phosphorus atom. The length of the TOCSY spin lock sequence governs the extent of coherence transfer down the chain from phosphorus. Typically, the upper limit is about 4 carbons due to dephasing of the magnetization in the spin lock field, relaxation, and attenuation of the signal from distribution of the coherence over many carbons. This experiment requires a high level of ^{13}C labeling to succeed.

The second pulse sequence (HCCH) provides detection of 2D-INADEQUATE spectra in the $f1f2$ planes with detection of ^1H in $f\beta$. If a particular ^1H chemical shift is selected, the $f1f2$ plane will contain the INADEQUATE spectrum of the directly bound ^{13}C and adjoining ^{13}C atoms. Because the experiments were performed on ^{13}C labeled polymers, the sensitivity was fairly high, however, this experiment does not filter resonances of the polymer backbone from the spectrum. Practical aspects of using these pulse sequences are described by Saito et al. (20)

These last two experiments were used together with the HCP spectrum to provide assignments of the backbone CH and CH_2 carbons of the first two monomer units along the polymer chain. Selected regions of slices from the HCP, H(CA)P-CC-TOCSY and HCCH spectra, containing resonances from one of the chain-end structures, are shown in Figure 19 to illustrate the methodology. In Figure 19a, a pair of correlations are seen in one slice from the HCP spectrum at one of the ^{31}P chemical shifts; these are C-H correlations from one of the CH_2 groups bound to phosphorous. The next step is to search for these correlations in the HCCH (Figure 19b) and H(CA)P-CC-TOCSY spectra (Figure 19c). At the ^{13}C chemical shift of this correlations in the H(CA)P-CC-TOCSY spectrum, two other CH correlations can be identified and attributed to the second and third carbons from the chain end. It is not possible to identify the order of the carbons from this single 3D spectrum, however, there are several ways to accomplish this. Among them are to order them based on the INADEQUATE-type data present in the HCCH spectrum. At their common double quantum frequency, the slice from the HCCH spectrum shown in Figure 19b contains the initial correlation from the methylene group bound to phosphorus, and a second correlation from the next methine group in the polymer backbone. Alternately working from the HCCH and the H(CA)P-CC-TOCSY in the slices shown in Figures 19d-h, it is possible to identify for the third and fourth CH_n groups along the polymer chain.

Conclusions

Three dimensional NMR experiments can be enormously useful for studying the structures of synthetic polymers. Although these experiments are much easier when isotopic labeling is performed, they are clearly feasible and useful, even when labeling is not possible. When performing HCX experiments where X is a low abundance NMR active isotope or when trying to detect resonances from low occurrence structures such as polymer chain ends, PFG coherence selection is essential. If the low occurrence structure uniquely contains structural features such as an NMR active X nucleus (or if a label such as ^{13}C can be selectively incorporated into the structure of interest) these experiments can be useful for selective detection of interesting resonances while removing much more intense interfering signals from other parts of the molecule. One of the main obstacles to general application of these methods is the short T_2 of most polymer resonances, however, recently developed probes for performing high temperature PFG experiments should be helpful in circumventing this problem.

Acknowledgements

The Kresge Foundation and donors to the Kresge Challenge at The University of Akron are acknowledged for funds used to purchase the 600 and 750 MHz NMR instruments used in this work. The National Science Foundation (DMR-9617477 and DMR-0073346) is acknowledged for much of the research support for the work described here. The hard work of the many students, postdoctoral research associates and staff affiliated with the Molecular Spectroscopy Laboratory at The University of Akron who performed the NMR work, and the many collaborators who provided the polymer samples and the many interesting research problems is also appreciated. This list of workers is too extensive to name here, however, contributors are listed as coauthors in the references cited in this review.

References

1. (a) Bax, A.; Grzesiek, S. *Acc. Chem. Res.*, **1993**, 26, 131. (b) Clore, G. M.; Gronenborn, A. M. *Progress in NMR Spectroscopy*, **1991**, 23, 43. (c) J. Cavanagh, J.; Fairbrother, W. J.; Palmer III, A. G.; Skelton, N. J. *Protein NMR Spectroscopy Principles and Practice*, Academic Press, 1996. (d) Wagner, G. *Progress in NMR Spectroscopy*, **1990**, 22, 101. (e) Clore, G. M.; Gronenborn, A. M. *Prog. Biophys. Mol. Biol.*, **1994**, 62, 153 (1994). (f) Griesinger, C.; Sorensen, O. W.; Ernst, R. R. *J. Magn. Resonance*, **1989**, 84, 14.

2. (a) Croasmun, W. R.; Carlson, R. M. K. *Two-Dimensional Nuclear Magnetic Resonance Spectroscopy: Applications for Chemists and Biochemists*, VCH Publishers, N. Y., 1994. (b) Braun, S; Kalinowski, H.-O.; Berger, S. *150 and More Basic NMR Experiments*, Wiley-VCH, New York, 1998.
3. Li, L.; Ray III, D. G.; Rinaldi, P. L.; Wang, H. T.; Harwood, H. J. *Macromolecules*, 1996, 29, 4706.
4. Morris, G. A.; Freeman, R. J. *J. Am. Chem. Soc.*, 1979, 101, 760.
5. (a) Muller, L. *J. Am. Chem. Soc.*, 1979, 101, 4481. (b) Bax, A.; Griffey, R. H.; Hawkins, B. L. *J. Magn. Resonance*, 1983, 55, 301.
6. (a) Rinaldi, P. L.; Keifer, P. A. *J. Magn. Resonance, Ser. A*, 1994, 108, 259. (b) Rinaldi, P. L.; Ray III, D. G.; Litman, V. E.; Keifer, P. A. *Poly. Int.*, 1995, 36, 177.
7. Liu, W.; Ray III, D. G.; Rinaldi, P. L.; Zens, T. *J. Magn. Resonance*, 1999, 140, 482.
8. Fesik, S. W.; Zuiderweg, E. R. P. *J. Magn. Resonance*, 1988, 78, 588.
9. (a) Mirau, P. A.; Heffner, S. A.; Bovey, F. A. *Macromolecules*, 1990, 23, 4482. (b) Mirau, P. A.; Heffner, S. A.; Koegler, G. K.; Bovey, F. A. *Polymer International*, 1991, 26, 29. (c) Mirau, P. A.; Heffner, S. A. *Polymer*, 1992, 33, 1156.
10. Li, L; Rinaldi, P. L. *Macromolecules*, 1997, 30, 520.
11. Chai, M.; Saito, T.; Pi, Z.; Tessier, C.; Rinaldi, P. L. *Macromolecules*, 1997, 30, 1240.
12. Chai, M.; Saito, T.; Pi, Z.; Tessier, C.; Rinaldi, P. L. *Macromolecules*, 1997, 30, 1240.
13. Chai, M.; Hu, S.; Rinaldi, P. L. *Polymer Preprints*, 2001, 42(1), 15.
14. Chai, M.; Saito, T.; Pi, Z.; Tessier, C.; Rinaldi, P. L. *J. Am. Chem. Soc.*, 1999, 121, 273.
15. Chai, M.; Niu, Y.; Youngs, W. J.; Rinaldi, P. L. *J. Am. Chem. Soc.*, 2001, 123, 4670.
16. (a) Bax, A. and Lerner, L. *J. Magn. Resonance*, 1986, 69, 375-380. (b) Domke, T. *J. Magn. Resonance*, 1991, 95, 174-177. (c) John, B. K.; Plant, D.; Heald, S. L.; and Hurd, R. E. *J. Magn. Resonance*, 1991, 94, 664. (d) Willker, W.; Leibfritz, D.; Kerssebaum, R.; and Bermel, W. *J. Magn. Resonance*, 1993, 31, 287.
17. (a) Talluri, S.; Wagner, G. *J. Magn. Resonance, Ser. B* 1996, 112, 200. (b) Jahnke, W.; Baur, M.; Gemmecker, G.; Kessler, H. *J. Magn. Resonance, Ser., B* 1995, 106, 86. (c) Ikura, M.; Kay, L. E.; Tschudin, R.; Bax, A. *J. Magn. Resonance*, 1990, 86, 204.
18. Liu, W.; Saito, T.; Li, L.; Rinaldi, P. L.; Hirst, R.; Halasa, A. F.; Visintainer, J. *Macromolecules*, 2000, 33, 2364.
19. Meng, H.; Saito, T.; Rinaldi, P. L.; Wyzgoski, F.; Helfer, C. A.; Mattice, W. L.; Harwood, H. J. *Macromolecules*, 2001, 34, 801.
20. Saito, T.; Rinaldi, P. L. *J. Magn. Resonance*, 1998, 132, 41.

Chapter 9

Triple Resonance $^1\text{H}/^{13}\text{C}/^{19}\text{F}$ Multidimensional Solution NMR of Fluoropolymers: Experimental Aspects

Olivier Assemat and Peter L. Rinaldi

Department of Chemistry, Knight Chemical Laboratory, The University
of Akron, Akron, OH 44325-3601

In this work the use of 1D and multidimensional $^1\text{H} / ^{13}\text{C} / ^{19}\text{F}$ triple resonance 750 MHz NMR techniques for characterizing fluoropolymers are illustrated. When characterizing fluoropolymers, it is possible to take advantage of the large spectral dispersion, the high natural abundance, and the large gyromagnetic ratios of the ^1H and ^{19}F nuclei. However, the enormous ^{19}F chemical shift range creates some practical difficulties. The indirect detection pulse sequences had to be modified to introduce composite pulses on the transmitter channel to reduce offset problems, and WURST adiabatic decoupling was used to reduce problems associated with decoupling over the large frequency range. Vinylidene fluoride – hexafluoropropene copolymer was studied. High field, $^1\text{H}/^{13}\text{C}/^{19}\text{F}$ triple resonance, and multidimensional NMR provides enormous spectral simplification, permitting the extraction of structural information. Experimental conditions for collecting high quality spectra are outlined and complete resonance assignments for the most abundant structures in the polymer are given.

Introduction

Fluoropolymers have many applications because of their unique properties. They exhibit very good stability when exposed to high temperatures, organic solvents, reactive chemicals, and oxidative environments. Fluoroelastomers are a significant part of this family; they are widely used for sealing applications in hostile environments. In using ^{19}F NMR to study fluoropolymers, it is possible to take advantage of the large chemical shift range (over ten times that of ^1H), the high natural abundance, and the high resonance frequency of the fluorine nucleus. Consequently, ^{19}F NMR is an extremely useful and sensitive technique for characterizing these materials. When combined with high field, triple resonance, and multidimensional methods, enormous spectral dispersion is achieved, permitting the extraction of detailed structural information. But these factors also entail complications, especially at very high field. Here we describe some of the complications associated with the performance of $^1\text{H}/^{13}\text{C}/^{19}\text{F}$ triple resonance, multidimensional NMR of fluoropolymers on a 750 MHz spectrometer. Experimental methods are illustrated to circumvent problems with uniform excitation, multiple quantum interferences, and decoupling over wide spectral windows. Results from the characterization of poly(1,1,2,3,3,3-hexafluoropropylene-co-1,1-difluoroethylene) (PVH) microstructure with $^1\text{H}/^{13}\text{C}/^{19}\text{F}$ triple resonance, multidimensional NMR are used to illustrate the applications of these techniques.

Experimental

Materials.

Poly(1,1-difluoroethylene-co-1,1,2,2,3,3,3-hexafluoropropylene), a commercially available material, was supplied by Atofina and was used as received. For ^1H and ^{19}F detected experiments, 20-30 mg of material was dissolved in 1 mL acetone- d_6 contained in a 5mm NMR tube. For ^{13}C detected experiments 80-100mg of polymer was dissolved in 1mL acetone- d_6 contained in a 5mm NMR tube.

NMR Measurements.

All the NMR spectra were obtained with a Varian UnityPlus-750 MHz spectrometer equipped with a pulsed field gradient accessory (PFG); four RF channels, two of them full band (^1H to ^{15}N); and a 5 mm $^1\text{H}/^{13}\text{C}/^{19}\text{F}/^2\text{H}$ four-channel PFG probe (optimized for ^{19}F detection). The temperature was regulated at 25.0°C. All data processing was performed on a Sun Ultrasparc-10 using Varian's Vnmr software. Acetone was used as an external reference for the ^1H and ^{13}C chemical shifts, and CFCl_3 was used as an external reference for the ^{19}F chemical shifts.

1D-NMR.

The ^{19}F spectrum was acquired at 705 MHz with ^1H decoupling using a 0.7s acquisition time, $3\mu\text{s}$ (20°) pulse width, 16 transients, and a 3s relaxation delay. The $^{13}\text{C}\{^1\text{H}\}$ spectrum was acquired at 188.6 MHz with WALTZ-16 modulated ^1H decoupling, a 0.5s acquisition time, $5\mu\text{s}$ (45°) pulse width, 34000 transients, and a 1.5s relaxation delay. The $^{13}\text{C}\{^1\text{H}, ^{19}\text{F}\}$ spectrum was acquired at 188.6 MHz with WALTZ-16 modulated ^1H decoupling and WURST modulated ^{19}F decoupling, using a 0.2s acquisition time, $14\mu\text{s}$ pulse width (45°), 42000 transients, and a 1s delay.

^{19}F Detected 2D-PFG-HSQC Spectra.

The $^{19}\text{F}/^{13}\text{C}$ 2D spectra were obtained using a modified version of a pulsed field gradient heteronuclear single quantum coherence (PFG-HSQC) sequence (1). This sequence was modified to include 180° composite pulses on the ^{19}F channel and 180° ^1H decoupling pulses centered in the evolution and polarization transfer delays. These spectra were obtained using the States (2) method of phase-sensitive detection in the evolution time dimensions, using 90° pulses for ^{19}F and ^{13}C of $16.5\mu\text{s}$ and $27\mu\text{s}$, respectively, and a 2s relaxation delay. The Δ delays for one-bond experiments were 0.89ms, 1ms, and 1.25ms for the CF_3 , CF_2 , and CF regions, respectively (based on $^1J_{\text{CF}_3} = 280$ Hz, $^1J_{\text{CF}_2} = 250$ Hz, and $^1J_{\text{CF}} = 200$ Hz). The Δ delays for 2 bond correlation experiments were 6.25 ms, based on $^2J_{\text{CF}} = 40\text{Hz}$. A 0.5s acquisition time was used with WALTZ-16 modulated ^1H decoupling and GARP modulated ^{13}C decoupling; 64 transients were averaged for each of 512 increments during t_1 . The two PFG pulses were 2.0 ms and 0.5ms in duration and had amplitudes of 0.1 and 0.106

T/m, respectively. Data were zero filled to an 8k x 2k matrix and weighted with a sine bell function before Fourier transformation.

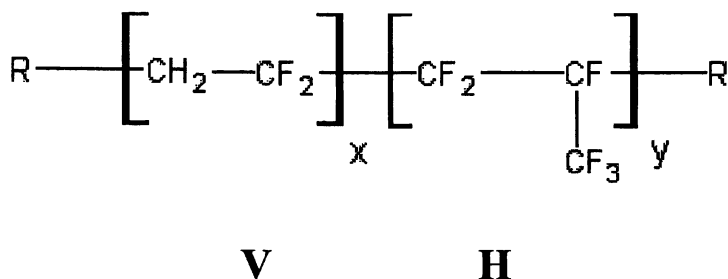
Decoupling.

The WURST decoupling sequence was implemented with the Pbox in Varian's VNMR software, using a constant adiabaticity modulated frequency, a 0.92 ms pulsewidth, and a 1.2 adiabaticity factor (Q). The constant radiofrequency level $\gamma B_2(\text{rms})$ was 4.3 kHz. In order to compensate for residual imperfections in spin inversion, the five-step phase cycle (0°, 60°, 150°, 60°, 0°) of Tycko et al (3) was used.

Results and Discussion

Polymer Structure.

The PVH used in this work is typically prepared by radical emulsion polymerization of 1,1-difluoroethylene (V) and 1,1,2,2,3,3,3-hexafluoropropylene (H),



and therefore a statistical distribution of monomer units might be expected. Under the reaction conditions, both monomers can add in either a head-to-tail or a head-to-head fashion. Since the units resulting from H monomer produce an unsymmetrical structure in the polymer chain, a variety of stereosequences are also formed. The most straightforward way to represent monomer units from reverse addition is to treat these as if they are derived from separate monomer units (V' and H') for the purpose of describing microstructure. The number of possible triads from co-polymerization of 4 monomer units is $4^3 =$

64. In reality, reverse addition occurs in less than 5% of the additions of V and H units, so that the probability of a triad containing two monomer units derived from reverse addition is very small. Furthermore, H units do not add to H units (4,5) at the end of a growing radical chain-end. These factors greatly reduce the number of possible triad structures in the polymer; however, there are still 20 possible triad sequences to be considered. Some of the most prevalent structures are summarized in Figure 1. The number of possible structures is increased if we consider that with the HVH type of structures (HVH, HV'H, H'VH, HVH'....), it is possible to have several stereosequences.

The one-dimensional (1D) ^{19}F NMR spectrum of PVH is shown in Figure 2. In this spectrum, three main regions can be distinguished; from CF_3 , CF_2 and CF groups. One easy way to test for uniform excitation is to integrate both CF_3 and CF regions and to make sure that the $I_{\text{CF}_3}:I_{\text{CF}}$ ratio is 3:1, since these two groups of signals come from the same monomer. Despite the enormous chemical shift range (over 90 kHz) there is still considerable signal overlap within each region, even on a 750 MHz spectrometer. The complicated spectrum results from the large number of structures present, and the large number of ^{19}F - ^{19}F homonuclear couplings present. Triple resonance and multidimensional NMR techniques offer solutions to these problems; however, the use of these experiments is complicated by the large spectral windows involved.

Decoupling.

In ^{13}C detected NMR experiments, simultaneous ^1H and ^{19}F decoupling provides enormous spectral simplification, however, at high field, the spectral window is enormous (90 kHz in this work). To solve this problem, ^{19}F WURST (6,7,8) decoupler modulation was used. The main advantage of adiabatic decoupling such as WURST is that the effective bandwidth is proportional to the square of decoupler field strength, γB_2 ; while in WALTZ and GARP decoupling the bandwidth has a linear dependence on γB_2 . The decoupler profile in WURST also has a relatively flat top and very sharp edges. Additionally, adiabatic decoupling is not very sensitive to RF field strength and inhomogeneity as long as the adiabatic condition is satisfied (9). Unfortunately, adiabatic decoupling suffers from the introduction of significant decoupler modulation sidebands (10,11), especially at very high field where wide effective decoupling bandwidths are needed. Modern high field spectrometers provide very good dynamic range and permit the achievement of tremendous signal to noise ratios so that very weak peaks ($1:10^6$) can be easily observed. In such cases, sidebands can produce severe problems. Different solutions to the sidebands problems have been proposed, such as: bilevel decoupling (12), ECHO-WURST (13), adiabatic defocusing (14), and recently an analytical

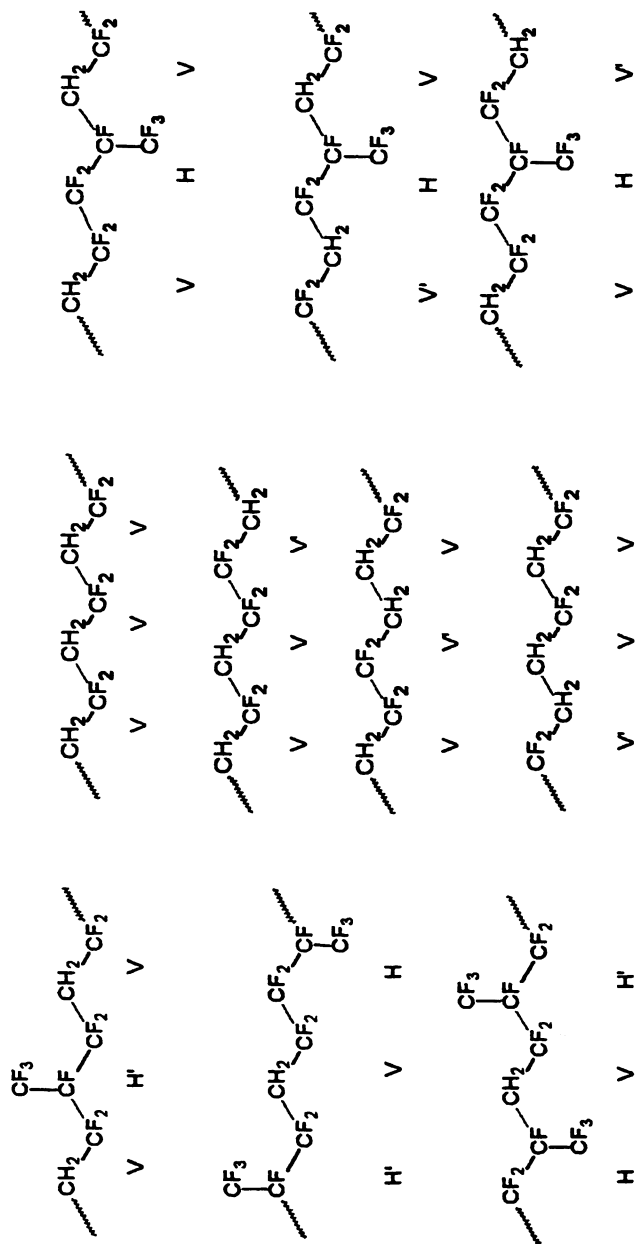


Figure 1. Most probable structures from polymerization of V and H..

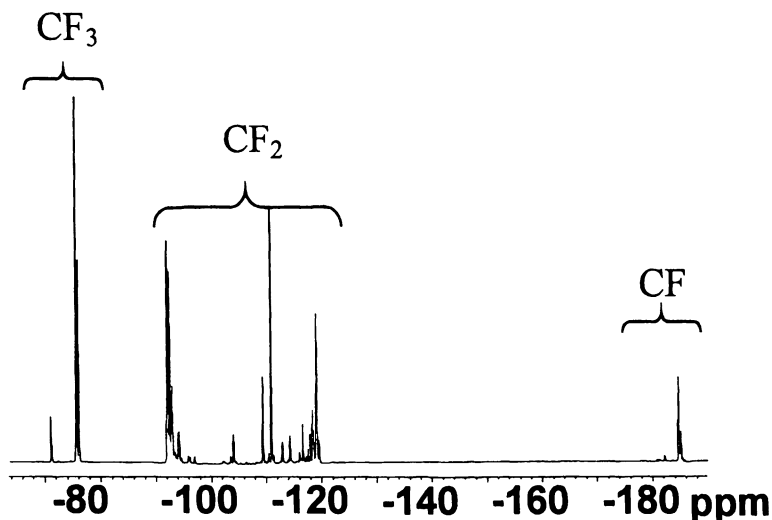


Figure 2. 705.5 MHz 1D ^{19}F NMR spectrum of PVH.

solution for amplitudes and phases of decoupling sidebands as a function of inversion time (15). Since the purpose of this work is the identification of the most abundant structures in the fluoropolymers, the complete elimination of the sidebands is not so critical. However, discrimination of decoupler modulation sidebands from weak signals of low-occurrence (ca. 1 mole%) structure components can be problematical.

The illustration in Figure 3 can be used to compare the relative effectiveness of various decoupler modulation schemes, including the recently reported WURST modulation; it shows the results from decoupling a C-F doublet (from $\text{CH}_2\text{F-CHOH-CH}_2\text{F}$ in acetone- d_6) in a series of spectra obtained with various decoupler offsets, using a decoupler field strength $\gamma B_2 = 4.4\text{kHz}$. The most commonly used WALTZ-16 decoupling technique provided effective decoupling over a 15 kHz window, whereas WURST provided efficient decoupling over a 90 kHz window, as required for $^{13}\text{C}\{^{19}\text{F}\}$ experiments.

Figure 4 shows the CF_n containing regions of the normal ^{13}C 1D NMR spectrum from PVH obtained with WALTZ-16 ^1H decoupling (Figure 4a), and with both WALTZ-16 ^1H and WURST ^{19}F decoupling (Figure 4b). Triple resonance (i.e. dual broad band decoupling) provides considerable spectral simplification in ^{13}C detected experiments by eliminating both ^1H and ^{19}F couplings. Unresolved C-F couplings were also eliminated in the CH_2 region, resulting in considerable narrowing of the peaks in that region. Figure 5 shows the CH_2 region from the ^{13}C 1D NMR spectrum from PVH obtained with WALTZ-16 ^1H decoupling (Figure 5a), and with both WALTZ-16 ^1H and WURST ^{19}F decoupling (Figure 5b).

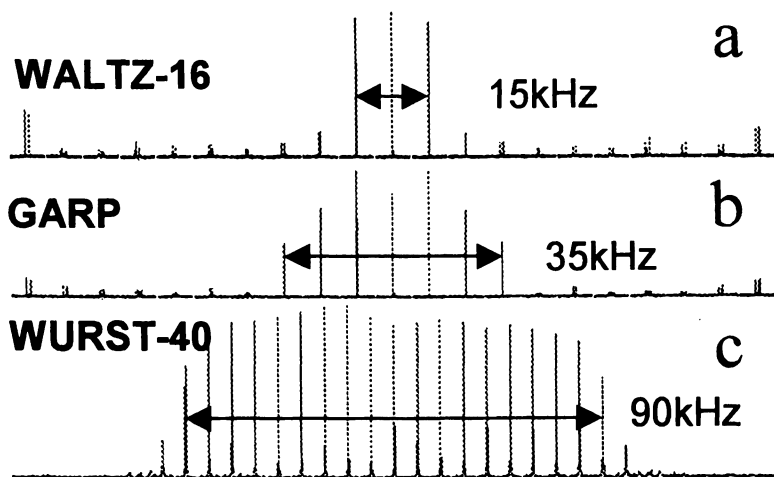


Figure 3. Three series of ^{13}C spectra from a C-F doublet with different ^{19}F decoupler modulation schemes. In each series, the decoupler offset was incremented in 5kHz step: (a) WALTZ-16, (b) GARP, and (c) WURST-40.

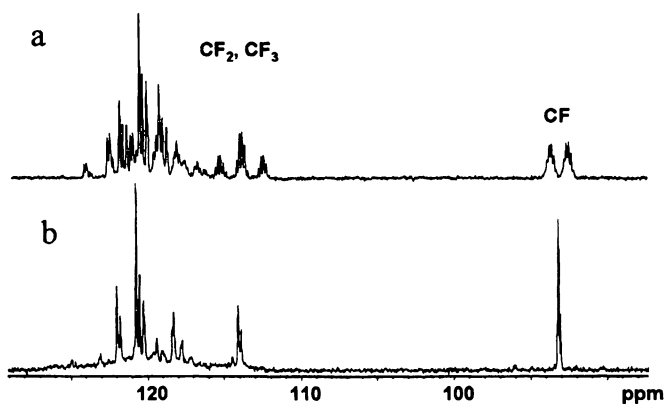


Figure 4. 188.6 MHz ^{13}C NMR spectrum of PVH, CF_n region: (a) with ^1H decoupling, and (b) with both ^1H and ^{19}F decoupling.

Multidimensional NMR.

Multidimensional NMR combined with ^{19}F detection provides enormous chemical shift dispersion, and considerable improvement in sensitivity. When used with ^1H and ^{13}C decoupling, simple, well-resolved and easily interpreted cross peak patterns should result. However, attempts to apply pulsed field gradient (PFG) heteronuclear multiple quantum coherence (HMQC) (16) methods produced enormously complex spectra when cross peaks were observed. PFG heteronuclear single quantum correlation (HSQC) (17) experiments were used instead. During the evolution period in the HMQC experiment, only the chemical shifts and the heteronuclear couplings are refocused. Homonuclear couplings evolve and are not refocused, creating antiphase dispersive components in the phase sensitive 2D spectrum (18). If a heteronuclear I-S spin system is considered, the magnetization transfer process can be summarized by :

$$\text{(HMQC)} : I_z \rightarrow -I_y \cos(\Omega_s t_1) \quad [1]$$

$$\text{(HSQC)} : I_z \rightarrow I_x \cos(\Omega_s t_1) \quad [2]$$

Expression [2] shows that pure absorptive lines can be obtained with the HSQC experiment. Homonuclear ^{19}F - ^{19}F couplings do not affect the f_1 dimension.

However considering another fluorine nucleus K coupled to I or S, [1] becomes:

$$I_z \rightarrow -I_y \cos(\pi J_{IK} t_1) \cos(\Omega_s t_1) + 2I_x K_z \sin(\pi J_{IK} t_1) \cos(\Omega_s t_1) \quad [3]$$

The expression in [3] shows that the signal contains four-multiplet components, composed of in phase absorptive and antiphase dispersive contributions. In the case of the fluoropolymers of interest in this work, numerous fluorine homonuclear couplings exist. Since these couplings can be very large ($^2J_{\text{FF}} = 50$ Hz and $^3J_{\text{FF}} = 10\text{-}20$ Hz), they contribute to the production of spectra with extremely complex coupling patterns leading to loss of signal intensity and uninterpretable cross-peak patterns.

The HSQC pulse sequence is normally used with simple pulses on the transmitter (observe) channel because this sequence is normally used with ^1H detection, and requires relatively narrow f_2 spectral windows. Reasonably uniform excitation of the large ^{19}F chemical shift window, especially at high field, requires the use of composite 180° pulses on the ^{19}F (transmitter) channel. In this work, $^{19}\text{F}\{^{13}\text{C}\}$ -HSQC spectra were collected with gated ^1H decoupling (using WALTZ-16 modulation only during the acquisition time); and 180° refocusing pulses on the ^1H channel are used to remove C-H couplings during the evolution period (180°_θ pulses were replaced with 180°_θ - $180^\circ_{\theta+90}$ - 180°_θ composite pulses). The modified HSQC sequence of Keeler and Laue (1) shown in Figure 6 was used to accomplish these objectives. Representative results from this experiment are shown in Figure 7.

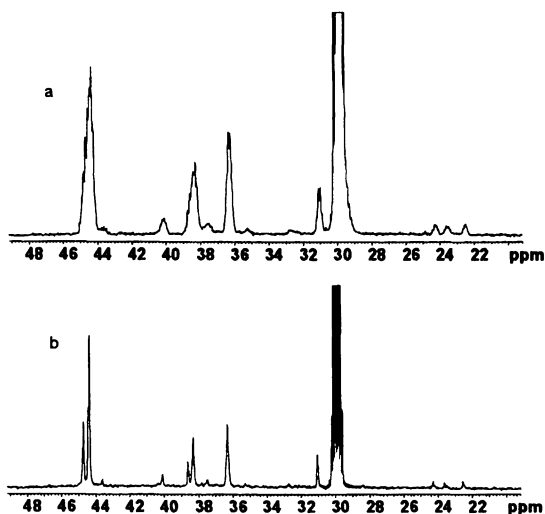


Figure 5. 188.6 MHz ^{13}C NMR spectrum of PVH, CH_2 regio.: (a) with ^1H decoupling, and (b) with both ^1H and ^{19}F decoupling.

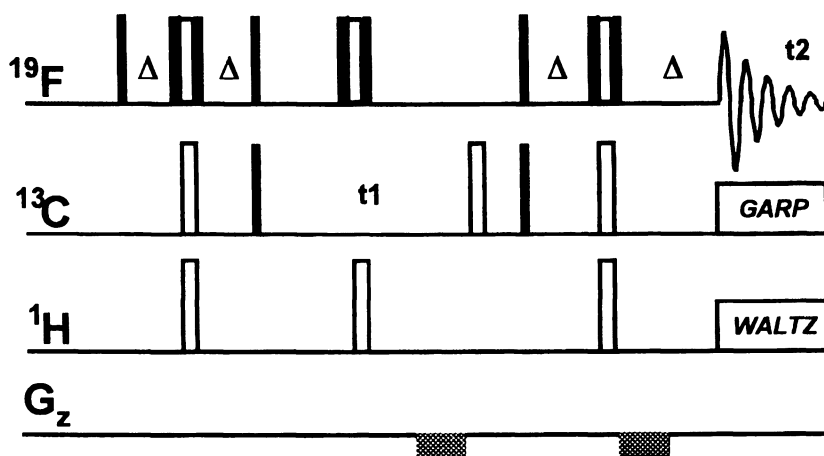


Figure 6. Pulse sequence diagram for the $^{19}\text{F}\{^{13}\text{C}\}$ -PFG-HSQC experiment. Solid and open pulses are 90° and 180° respectively. Phase cycling is that used by the standard HSQC sequence provided by Varian.

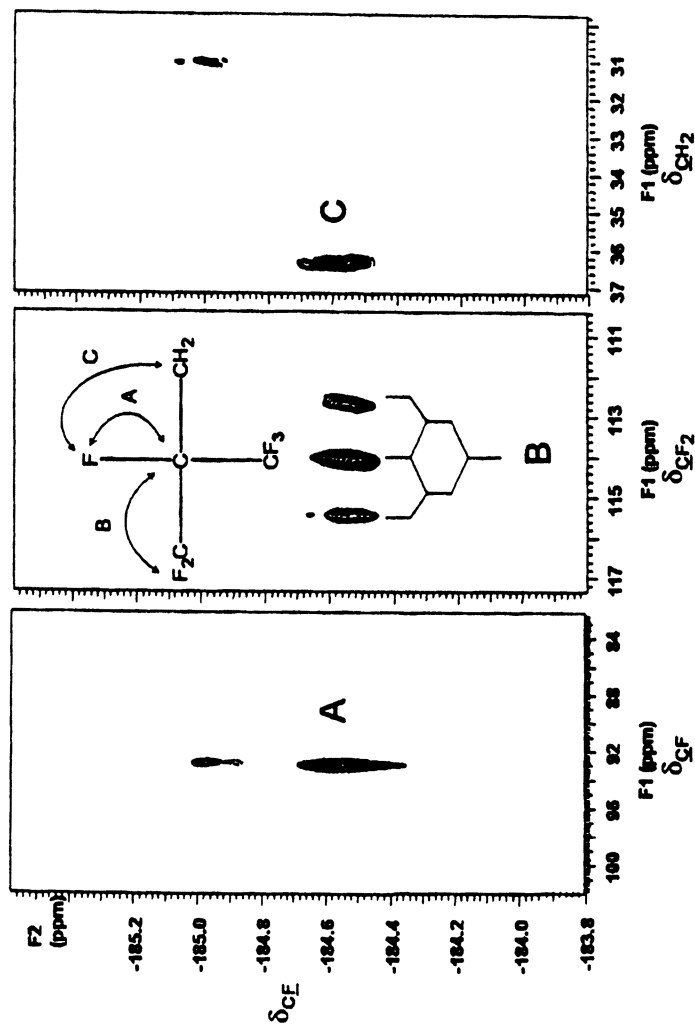


Figure 7. Expansions from the $^{19}\text{F}\{^{13}\text{C}\}$ -PFG-HSQC spectra of PVH obtained with ^1H WALTZ-16 decoupling: a) one bond PFG-HSQC, C-F correlations; b) two bond PFG-HSQC, $\text{CF}-\text{CF}_2$ correlations; and c) two bond PFG-HSQC, $\text{CF}-\text{CH}_2$ correlations.

The HSQC experiment can be performed in the usual manner (using delays $\Delta = 1/2^1J_{CF}$) to provide information regarding two directly attached C-F atoms. Figure 7a shows a section from the CF region of the spectrum from such an experiment performed on PVH. Two one-bond C-F correlations are observed. Rather than using HMBC, which suffers from the same problems encountered with HMQC, better results were obtained using HSQC with Δ delays set to $1/(2 \times {}^nJ_{CF})$ based on the desired n-bond correlations. Typical coupling values are 20-50 Hz for ${}^2J_{CF}$, 5-15 Hz for ${}^3J_{CF}$, and 0-5 Hz for ${}^4J_{CF}$. A series of HSQC spectra were collected with Δ delays optimized to produce 2-bond correlations from cross peaks. In these spectra, residual 1-bond correlations are usually observed. It is possible to introduce a J-filter (19) in the pulse sequence to selectively remove cross peaks from one-bond correlation, which might appear in presence of correlations from smaller couplings, but the spectral dispersion is large enough so that this simplification is not required. Furthermore, the added complexity of the pulse sequence with J-filters is not advantageous for producing good quality spectra, and provides the opportunity for relaxation processes to diminish peak intensities. Figures 7b and 7c show expansions from the \underline{CF}_2 and \underline{CH}_2 carbon regions, respectively, of the ${}^{19}F\{^{13}C\}$ HSQC spectrum of PVH obtained with $\Delta = 10\text{ms}$ (${}^2J_{CF-CF_2} = 50\text{ Hz}$) and $\Delta = 14\text{ms}$ (${}^2J_{CF-CH_2} = 35\text{ Hz}$). The correlations in Figure 7b is a triplet from the coupling between the carbon and the two directly attached fluorines of the CF_2 group. The presence of this coupling is explained by the fact that the transmitter on the fluorine channel is centered on the CF region, approximately 50 kHz from the CF_2 region, so the 180° decoupling pulse ($33\mu\text{s}$) on the ${}^{19}F$ channel during the ${}^{13}C$ evolution time is ineffective for inverting the CF_2 fluorines. In Figure 7c, two cross-peaks are observed, resulting from two bonds correlations between \underline{CF} and ${}^{13}\underline{CH}_2$ resonances. The combination of A, B, and C correlations permits identification of the resonances from a CF_2 -CF(CF_3)- CH_2 structure fragment.

When performing multidimensional NMR on fluoropolymers, it is usually more efficient to detect ${}^{19}F$ during the acquisition time because the ${}^{19}F$ chemical shift range is so large. In this way, a two-fold improvement in the ${}^{19}F$ chemical shift dimension digital resolution can be obtained with minimal effect on the total experiment time. If ${}^{19}F$ chemical shifts were encoded during an evolution time (for example in a 1H -detected ${}^1H/{}^{13}C/{}^{19}F$ triple resonance chemical shift correlated 3D-NMR experiment), a two-fold improvement in the ${}^{19}F$ chemical shift dimension digital resolution would require twice the experiment time.

Conclusions

Combined use of high field, ${}^1H/{}^{13}C/{}^{19}F$ triple resonance and multidimensional NMR methods provides enormous spectral dispersion and

simplification, permitting the extraction of detailed structural information about fluoropolymers. It is possible to use new experimental techniques to surmount the difficulties encountered, especially when the work is performed on spectrometers with resonance frequencies above 500 MHz. Complete resonance assignments for the most abundant structures of many fluoropolymers can be obtained. We also have outlined here the experimental conditions required for the collection of high quality spectra.

Acknowledgements

We wish to thank the Kresge Foundation and donors to the Kresge Challenge at The University of Akron for funds used to acquire the 750 MHz NMR instrument used in this work, The National Science Foundation (DMR-9617477 and DMR-0073346) for research support, and the Ministère Français des Affaires Etrangères for a fellowship (to OA).

References

1. Davis, A. L.; Keeler, J.; Laue, E. D.; Moskau, D. *J. Magn. Reson.* **1992**, *98*, 207.
2. States, D. J.; Haberkorn, R.; Ruben, D. J. *J. Magn. Reson.* **1982**, *48*, 286.
3. Tycko, R.; Pines, A.; Gluckenheimer, R. *J. Chem. Phys.* **1985**, *83*, 2775.
4. Dixon, S.; Redford, D. R.; Ruggs, J. S. *Ind. Eng. Chem.* **1957**, *49*, 1687.
5. Adam, R. M.; Bovey, F. A. *J. Polym. Sci.* **1952**, *9*, 481.
6. Kupce, E.; Freeman, R. *J. Magn. Reson.* **1997**, *36*, 127.
7. Kupce, E.; Freeman, R. *J. Magn. Reson. A* **1996**, *115*, 299.
8. Kupce, E.; Freeman, R. *Chem. Phys. Lett.* **1996**, *250*, 523.
9. Freeman, R.; Kupce, E. *NMR in Biomedicine* **1997**, *10*, 372.
10. Kupce, E.; Freeman, R. *J. Magn. Reson. A* **1995**, *117*, 273.
11. Zhang, S.; Gorenstein, D. G. *J. Magn. Reson.* **1999**, *138*, 281.
12. Kupce, E.; Freeman, R. Wider, G.; Wuthrich, K. *J. Magn. Reson. A* **1996**, *122*, 81.
13. Kupce, E.; Freeman, R. *J. Magn. Reson.* **1997**, *127*, 36.
14. Kupce, E. *J. Magn. Reson.* **1997**, *129*, 219.
15. Zhang, S.; Gorenstein, D. G. *J. Magn. Reson.* **2000**, *144*, 316.
16. Rinaldi, P. L.; Keifer, P. A. *J. Magn. Reson.* **1994**, *108*, 259.
17. Kay, L.; Keifer, P.; Saarinen, T. J. *J. Am. Chem. Soc.* **1992**, *114*, 10663.

18. Bax, A.; Ikura, M.; Kay, L. E.; Torchia, D. A.; Tschudin, R. *J. Magn. Reson.* **1990**, *86*, 304.
19. Salazar, M.; Zektzer, A. S.; Martin, G. E. *Magn. Reson. Chem.* **1988**, *26*, 28.

Chapter 10

$^1\text{H}/^{13}\text{C}/^{29}\text{Si}$ Triple Resonance 3D NMR Study of Poly(dimethylsiloxane) $\text{MD}_3\text{M}^{\text{H}}$

Minghui Chai¹, Peter L. Rinaldi^{2,*}, and Sanlin Hu³

¹Department of Chemistry, Marshall University,
Huntington, WV 25755–2520

²Department of Chemistry, Knight Chemical Laboratory, The University
of Akron, Akron, OH 44325–3601

³DowCorning Corporation, Midland, MI 48686

$^1\text{H}/^{13}\text{C}/^{29}\text{Si}$ triple resonance 3D NMR combined with pulse field gradient (PFG) techniques has been utilized for characterizing poly(dimethylsiloxane) (PDMS), $\text{MD}_3\text{M}^{\text{H}}$. The signals from $^1\text{H}-^{13}\text{C}-^{29}\text{Si}$ connectivities among ^1H atoms coupled to both ^{13}C and ^{29}Si at natural abundance have been selectively detected, which provide information for complete resonance assignments of $\text{MD}_3\text{M}^{\text{H}}$. The study showed that the considerable spectral dispersion in ^{29}Si NMR of siloxanes compared with the narrow ^1H and ^{13}C spectral ranges allows detailed examination of the structure of PDMS by the 3D $^1\text{H}/^{13}\text{C}/^{29}\text{Si}$ NMR correlation experiment.

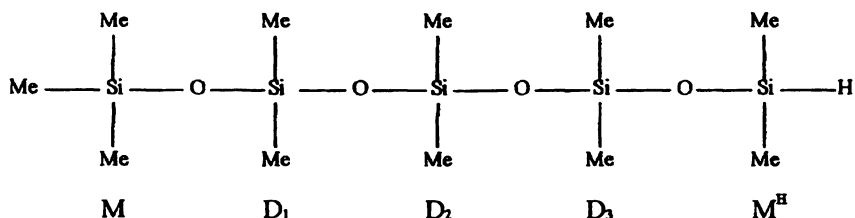
Introduction

Poly(dimethylsiloxane) (PDMS) is the simplest of organosilicone elastomers. PDMS was commercially developed by Dow Corning in the 1960's. It possesses inertness and useful mechanical properties, and can also be readily made into various desired shapes for medical items including prostheses of different bone and soft tissue elements (in surgery), and ancillary components such as tubes, catheters, shunts and drug carriers. In addition, PDMS has shown good compatibility in clinical research.⁽¹⁾ So it has been a very useful synthetic polymer in medicine. In fact, silicone polymers are often employed in checking the biocompatibility of new polymers. Furthermore, organosilicones comprise an important class of compounds used in resins, and room temperature and heat-cured rubber industrial and consumer products.

NMR has been a powerful technique for structural analyses of macromolecules. However, 1D NMR spectra of PDMS are usually complicated due to signal overlap. Their complete characterization often requires combinations of several techniques. Multidimensional NMR techniques, especially inversely detected 3D heteronuclear shift correlation experiments, offer the opportunity to obtain the complete structural characterization by using NMR experiments alone. Biological 3D-NMR experiments are usually performed in conjunction with uniform ^{13}C and ^{15}N isotopic labeling. In polymer chemistry, when isotopic labeling is possible, it is often very difficult and expensive. By modifying the 3D-pulse sequence used for biopolymers, triple resonance 3D-NMR techniques have been adapted for studying the structures of polymers, which involve ^1H - ^{13}C - ^{19}F , ^1H - ^{13}C - ^{31}P , ^1H - ^{13}C - ^{29}Si spin systems.⁽²⁾ These results have shown that 3D-NMR spectroscopy can be tremendously useful for characterizing polymer structures, even without isotopic labeling. Performance of $^1\text{H}/^{13}\text{C}/^{29}\text{Si}$ triple resonance NMR (natural abundance of $^{29}\text{Si} = 4.7\%$) is extremely challenging because it requires selective detection of the ^1H - ^{13}C - ^{29}Si spin systems which are present in only 0.05% of the molecules, while suppressing the signals from the remaining 99.95% of the molecules. Nevertheless, with modern instrumentation and a stable instrument environment, such experiments are possible and can produce very useful data.^(2c, 2d)

The nomenclature used to define siloxane compounds combines the use of the letters M, D, T and Q, which represent $\text{R}_3\text{Si}-\text{O}-$, $\text{R}_2\text{Si}(\text{O}-)_2$, $\text{RSi}(\text{O}-)_3$ and $\text{Si}(\text{O}-)_4$ units respectively, where R stands for aliphatic and/or aromatic substituents or H. In this study, substituents other than methyl groups are indicated as superscripts; for example, $\text{M}^{\text{H}} = (\text{Me}_2\text{HSi}-\text{O}-)$. Scheme 1 shows the structure of $\text{MD}_3\text{M}^{\text{H}}$. We use $\text{MD}_3\text{M}^{\text{H}}$, which is a simple but important oligomer of PDMS, to show the use of 3D $^1\text{H}/^{13}\text{C}/^{29}\text{Si}$ triple resonance NMR for the characterization of PDMS structures.

Scheme 1



Experimental

MD₃M^H was obtained from Dow Corning Corporation. 200 mg of this colorless oil was dissolved in 0.7 ml CDCl₃ solvent and put into a 5-mm NMR tube for the following NMR measurements. All NMR spectra were collected at 25 °C on a Varian Unityplus 750 MHz NMR spectrometer equipped with four RF channels, a Performa II z axial pulse field gradient (PFG) accessory, a 5 mm Varian ¹H/¹³C/X (where X is tunable over the range of the resonance frequencies from ¹⁵N to ¹¹³Cd) triple resonance four channel probe with a PFG coil (for 1D ¹H, 2D and 3D NMR experiments), and a 5 mm Varian ¹H/ X (X = ³¹P-¹⁵N) switchable probe with a PFG coil (for 1D ¹³C and ²⁹Si NMR experiments). The solvent was also used as the internal reference for ¹H and ¹³C chemical shifts. TMS was used as an external reference for ²⁹Si chemical shifts. All data were processed with Varian's VNMR software on a SUN Ultra-10 workstation.

1D NMR

The ¹H spectrum was acquired at 750 MHz using a 3.5 s acquisition time, 4.2 μs (30°) pulse width and 16 transients. The ¹³C spectrum was acquired at 188.6 MHz with WALTZ-16 modulated ¹H decoupling using a 1.2 s acquisition time, 4.2 μs (45°) pulse width and 256 transients. The ²⁹Si spectrum was acquired at 149 MHz with WALTZ-16 modulated ¹H decoupling using a 1.4 s acquisition time, 13.4 μs (90°) pulse width, 5 s delay and 256 transients.

2D NMR

The ¹H²⁹Si long range PFG-HMQC(3) 2D NMR spectrum was collected with ¹H and ²⁹Si 90° pulses of 12.7 and 22.0 μs, respectively, a relaxation delay

of 1 s, $\Delta = (2 \times {}^n J_{HSi})^{-1} = 73.5$ ms (optimized for 2 bond ${}^1\text{H}$ - ${}^{29}\text{Si}$ correlations), 5000 Hz and 6000 Hz spectral windows in the ${}^1\text{H}(f_2)$ and ${}^{29}\text{Si}(f_1)$ dimensions and a 0.045 s acquisition time with ${}^{29}\text{Si}$ GARP(4) decoupling; 8 transients were averaged for each of 512 real t_1 increments. The gradient strengths of three 2.0 ms PFGs were 0.325, 0.325, and -0.129 Tm^{-1} , respectively.

The ${}^1\text{H}$ ${}^{13}\text{C}$ PFG-HMQC3 2D NMR spectrum was collected with ${}^1\text{H}$ and ${}^{13}\text{C}$ 90° pulses of 12.9 and 25.0 μs , respectively, a relaxation delay of 3 s, $\Delta = (2 \times {}^1 J_{HC})^{-1} = 3.57$ ms (optimized for 1 bond ${}^1\text{H}$ - ${}^{13}\text{C}$ correlations), 5000 Hz and 600 Hz spectral windows in the ${}^1\text{H}(f_2)$ and ${}^{13}\text{C}(f_1)$ dimensions and a 0.05 s acquisition time with ${}^{13}\text{C}$ GARP decoupling. 8 transients were averaged for each of 256 real t_1 increments. The gradient strengths of three 2.0 ms PFGs were 0.216, 0.216, and -0.109 Tm^{-1} , respectively.

The 2D-NMR data were processed with sinebell weighting; spectra were displayed in the magnitude-mode in both dimensions; 2D FT was performed on a 1024 x 1024 matrix.

3D NMR

The 3D-NMR spectrum was obtained with 90° pulses for ${}^1\text{H}$, ${}^{13}\text{C}$ and ${}^{29}\text{Si}$ of 13.8 μs , 28.0 μs and 23.0 μs , respectively, relaxation delay 1 s, $\Delta = 2.08$ ms ($1/(4 \times {}^1 J_{CH})$, ${}^1 J_{HC} = 120$ Hz), $\tau = 10$ ms ($1/(4 \times {}^1 J_{CSi})$, ${}^1 J_{CSi} = 59$ Hz), acquisition time = 0.05 s (with simultaneous ${}^{13}\text{C}$ and ${}^{29}\text{Si}$ GARP decoupling); 4 transients were averaged for each of 2×18 increments during t_1 and 2×18 increments during t_2 . Evolution times were incremented to provide a 5000 Hz spectral window in f_3 (${}^1\text{H}$), a 2800 Hz spectral window in f_1 (${}^{29}\text{Si}$), and a 600 Hz spectral window in f_2 (${}^{13}\text{C}$) dimensions in the 3D-NMR experiment. The durations and amplitudes of the gradient pulses were 3, 1 and 1 ms; and 0.541, 0.325, and 0.0645 T/m, respectively. The first gradient pulse serves as a homospoil pulse, so its value relative to the other two is not critical. The total experiment time was 5.3 hours. The data were zero filled to $512 \times 512 \times 512$ and weighted with a shifted sinebell function before Fourier transformation.

Results and Discussion

1D-NMR Spectra

The 750 MHz ${}^1\text{H}$ spectrum (Figure 1a) exhibits six groups of resonances: the silicon hydride proton at 4.74 ppm, and five different methyl protons between 0.06 - 0.23 ppm. From the relative intensities of the methyl resonances (see integration values in the spectrum), it is possible to assign the M-CH₃ proton resonances to the signals at 0.116 ppm. Also the doublet at 0.21 ppm

can be assigned to the protons of M^H-CH_3 because of the adjoining silicon hydride proton coupling. At this very high magnetic field (750 MHz), five methyl protons can be resolved, the three peaks at 0.07 - 0.1 ppm can't be directly assigned from the 1D spectrum. However, the 188.6 MHz ^{13}C NMR spectrum (Figure 1b) shows five peaks within 0.8 - 2.2 ppm region corresponding to five different methyl groups of MD_3M^H . Also, based on the relative intensities of these signals, the peak at 2.02 ppm can be assigned to the carbons of $M-CH_3$. The other resonances can't be determined just from the 1D spectrum. In the ^{29}Si NMR spectra of siloxanes, the resonances from, M-Si, D-Si, T-Si and Q-Si are distinctive because ^{29}Si resonance frequencies strongly depend on the number of directly bonded oxygen atoms. For instance, the resonance from M type silicon (R_3SiO-) is normally found around +10 ppm; and the resonance from D type silicon ($R_2Si(O-)_2$, R = alkyl, not H) is normally found around -20 ppm. So, according to these empirical rules,⁽⁵⁾ in ^{29}Si NMR spectrum (Figure 1c), the peak at 7.06 ppm can be attributed to the M silicon of MD_3M^H , three resonances at -20.13, -21.59 and -22.17 ppm are from D-type silicons of MD_3M^H . The silicon of M^H is a silicon hydride, which normally appears around -10 ppm in the ^{29}Si NMR spectrum. Thus the resonance at -7.14 ppm is from the silicon of M^H . For D-type silicons, the detailed assignment can be made based on the comparison with the ^{29}Si NMR spectrum of MD_3M . Based on the reported ^{29}Si chemical shift assignments of D-type silicon atoms in MD_3M ,^(5c) it is possible to assign the resonance at -21.59 ppm in Figure 1c to the D_1 silicon and the resonance at -22.17 ppm to the D_2 silicon. The resonance at -20.13 ppm belongs to the silicon of D_3 . Now based on the assigned silicon resonances, multidimensional NMR techniques can be employed to disperse 1H and ^{13}C signals, that fall in narrow frequency ranges of the 1D spectra, into more dimensions, and to correlate these signals with the reliably assigned silicon resonances in the multidimensional NMR spectra. Thus additional structural information can be obtained for siloxane compounds via nD NMR spectroscopy.

2D NMR Spectra

The 2D 1H - ^{13}C PFG-HMQC NMR spectrum (Figure 2a) of MD_3M^H exhibits crosspeaks from directly bonded 1H - ^{13}C atoms. Some of the assignments for 1H and ^{13}C resonances made in 1D NMR spectra can be confirmed from the 2D spectrum. For example the 1H - ^{13}C correlations of the $M-CH_3$ and M^H-CH_3 groups can be identified. The 1H - ^{13}C correlations for three D-type methyl groups can also be observed clearly in the spectrum. However, the detailed assignments for individual D- CH_3 groups cannot be obtained.

The 2D 1H - ^{29}Si long-range PFG-HMQC NMR spectrum (Figure 2b) of MD_3M^H provides information about 2-bond 1H - ^{29}Si correlations. Because

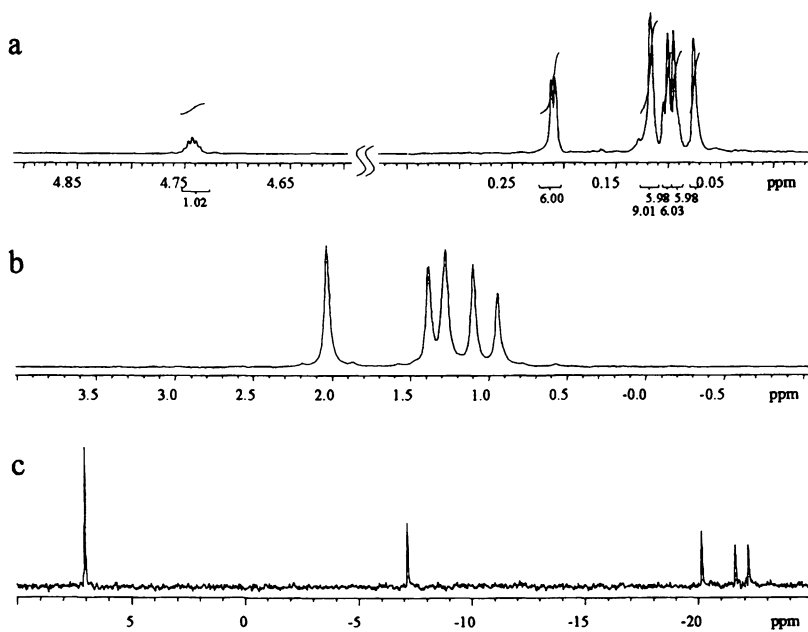


Figure 1. One-dimensional NMR spectra of $\text{MD}_3\text{M}^{\text{H}}$: (a) 750 MHz ^1H spectrum; (b) 188.6 MHz ^{13}C spectrum; (c) 149 MHz ^{29}Si spectrum.

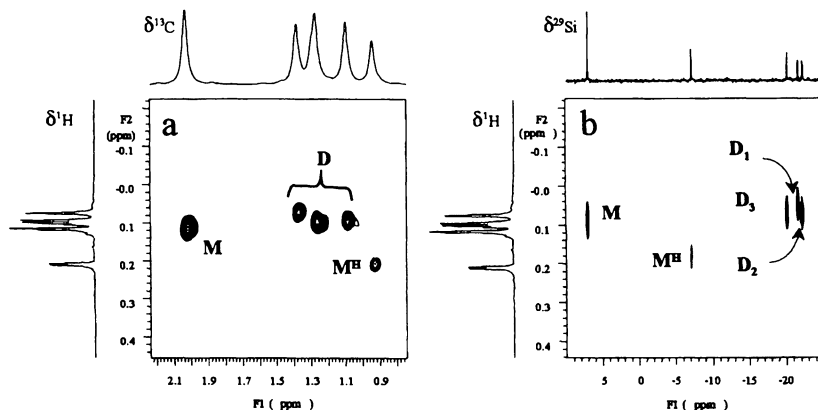


Figure 2. The 2D PFG-HMQC NMR spectra of MD_3M^H : (a) 1H - ^{13}C PFG-HMQC spectrum acquired with delays based on $^1J_{HC} = 140$ Hz; and (b) 1H - ^{29}Si long-range PFG-HMQC spectrum acquired with delays based on $^1J_{HSi} = 6.8$ Hz.

resonances in the 1D ^{29}Si spectrum can be reliably assigned, the 1H resonance assignments can be clearly made from this 2D 1H - ^{29}Si long-range correlation spectrum, as labeled in Figure 2b.

3D NMR Spectrum

Figure 3 shows the selected 2D f_2f_3 slices, which were taken at each of the ^{29}Si chemical shifts (f_i) from the 3D $^1H/^{13}C/^{29}Si$ spectrum of MD_3M^H . In order to narrow the relatively wide spectral window of ^{29}Si for better resolution in the 3D spectrum, a narrow ^{29}Si spectral window was carefully selected so that the ^{29}Si resonance at 7.06 ppm would fold into a non-interfering region near -11.6 ppm. Later, the chemical shift was corrected according to the value obtained from the 1D ^{29}Si spectrum. This triple resonance $^1H/^{13}C/^{29}Si$ heteronuclear correlation 3D experiment was set to selectively detect the 1-bond 1H - ^{13}C and 1-bond ^{13}C - ^{29}Si correlations in the structure of MD_3M^H . Therefore, the connectivity between each type of methyl group and its attached silicon atom can be proven from the 3D spectrum. Assignments are labeled in each f_2f_3 slice related to the chemical shifts of the directly bound ^{29}Si atoms in the f_1 dimension. The chemical shift assignments from this 3D experiment are summarized in Table 1.

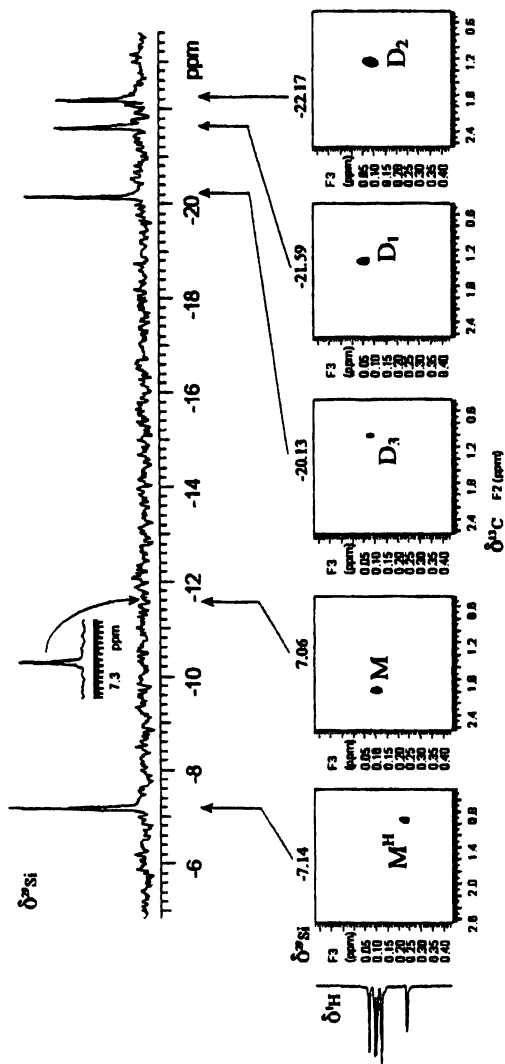


Figure 3. Selected 2D f_1f_3 slices from 3D $^1\text{H}/^{13}\text{C}/^{29}\text{Si}$ spectrum of MD_3M^1

Table 1. Chemical Shift Assignments for MD₃M^H

MD ₃ M ^H	Chemical Shifts (ppm)		
	$\delta^1\text{H}$	$\delta^{13}\text{C}$	$\delta^{29}\text{Si}$
M	0.116	2.02	7.06
D ₁	0.075	1.37	-21.59
D ₂	0.100	1.26	-22.17
D ₃	0.095	1.09	-20.13
M ^H	0.210 4.743 (Si-H)	0.94 ---	-7.14

Conclusion

Triple resonance 3D-NMR experiments can be useful for studying polymeric structures without resorting to isotopic labeling, even when the nuclei involved are present in low natural abundance. This study of MD₃M^H shows that the considerable spectral dispersion obtained in the ²⁹Si NMR spectra of siloxanes, compared with the narrow ¹H and ¹³C chemical shift ranges, permits detailed examination of the structure of PDMS by the 3D ¹H/¹³C/²⁹Si NMR correlation experiment. These techniques can also be useful for characterizing star-branched polymers which contain NMR active nuclei, polymers with low concentrations of heteroatoms (e.g. at the chain end or at low occurrence branch points) and many organometallic compounds.

Acknowledgement

We would like to acknowledge the NSF (DMR-9617477 and DMR-0073346) for support of this research and the Kresge Foundation and donors to the Kresge Challenge program at the University of Akron for funds used to purchase the 750 MHz NMR instrument.

References

1. Gumargalieva, K. Z.; Zaikov, G. E.; Moiseev, Yu. V. In *Polymer in Medicine*; Zaikov, G. E., Ed; Nova Science Publisher, Inc.: Commack, NY, 1998; Ch. 1.

2. (a) Li, L.; Rinaldi, P. L. *Macromolecules*, **1997**, *30*, 520. (b) Saito, T.; Medsker, R. E.; Harwood, H. J.; Rinaldi, P. L. *J. Magn. Reson. Ser. A* **1996**, *120*, 125. (c) Chai, M.; Saito, T.; Pi, Z.; Tessier, C.; Rinaldi, P. L. *Macromolecules* **1997**, *30*, 1240. (d) Chai, M.; Pi, Z.; Tessier, C.; Rinaldi, P. L. *J. Am. Chem. Soc.* **1999**, *121*, 273.
3. Vuister, G. W.; Boelens, R.; Kaptein, R.; Hurd, R. E.; John, B.; van Zijl, P. C. M. *J. Am. Chem. Soc.* **1991**, *113*, 9688.
4. Shaka, A. J.; Barker, P. B.; and Freeman, R. *J. Magn. Reson.* **1986**, *64*, 547-552.
5. (a) Takayama, Y. In *The Chemistry of Organic Silicon compounds*; Zappoport, Z.; Apeloig, Y., Eds.; Vol. 2, Part 1; John Wiley & Sons, Inc.: New York, NY, 1998, Ch. 6. (b) Smith, A. L. *The Analytical Chemistry of Silicones*; John Wiley & Sons, Inc.: New York, NY, 1992; Vol. 112. (c) Williams, E. A. *Annual Report on NMR Spectroscopy*; 1983, 15, pp 235-289. (d) Marsmann, H. In *NMR Basic Principles and Progress*; Diehl, P.; Fluck, E.; Kosfeld, R., Eds.; Springer-Verlag: New York, NY, 1981, Vol. 17, pp 97.

Chapter 11

Multidimensional NMR Studies on Polyurethane-Based Dendritic Wedges

Minghui Chai¹, Peter L. Rinaldi^{2,*}, Uraiwan Puapaiboon³, and Richard T. Taylor³

¹Department of Chemistry, Marshall University,
Huntington, WV 25755–2520

²Department of Chemistry, Knight Chemical Laboratory, The University
of Akron, Akron, OH 44325–3601

³Departments of Chemistry and Biochemistry, Miami University,
Oxford, OH 45056

Multidimensional NMR techniques with pulse field gradient (PFG) enhancement have been applied to study 1st, 2nd and 3rd generation polyurethane dendritic wedges, which are a novel type of linking element in the convergent approach to dendrimer synthesis. By using PFG- HMQC and HMBC 2D NMR experiments, ¹H and ¹³C resonance assignments have been obtained for these compounds, and structure proofs have been accomplished.

Introduction

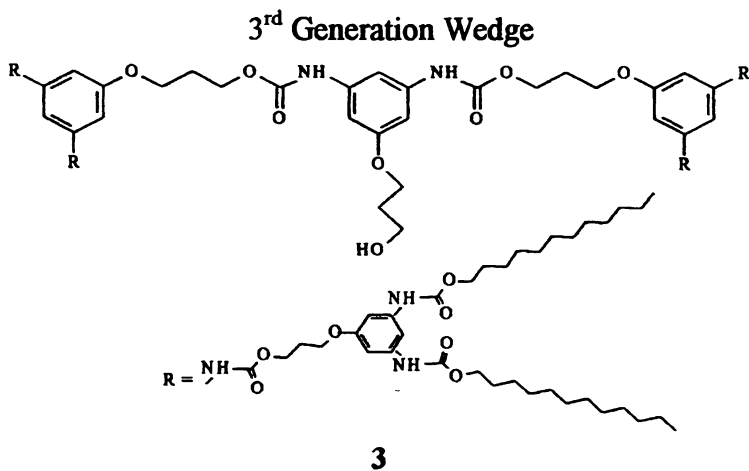
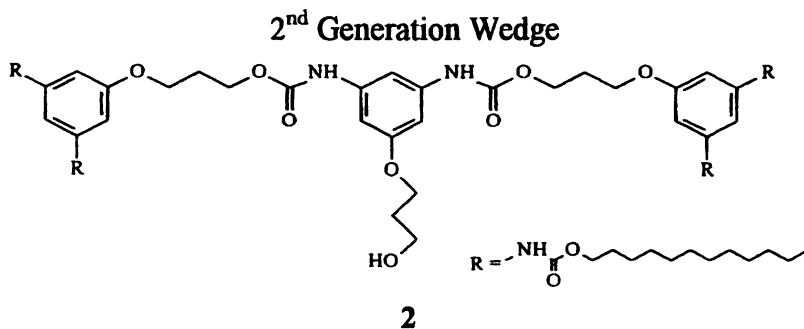
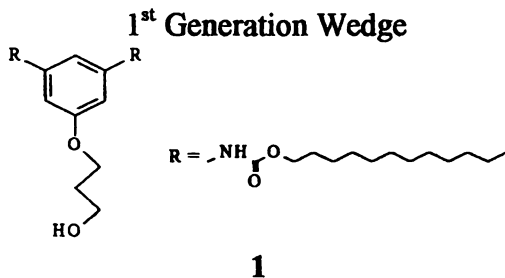
Dendrimers, which are highly symmetrical cascade polymers, have drawn a lot of attention because of their unique physical and chemical properties such as low intrinsic viscosity, high solubility, high miscibility, and high reactivity. The co-existing features, extensive branching and high surface functionality, have distinguished dendrimers from the classic linear and cross-linked polymers. So it is very important to know detailed information about the structure of dendrimers in order to understand their special properties and to devise new applications for these compounds. NMR has been a very powerful tool for structural characterization. However, until now, NMR has not been the preferred method for studying dendrimers, despite the wealth of information available from measurable NMR parameters. This is largely a result of the limited ability to resolve the resonances from the many unique, but very similar groups in these molecules. Because of the high cost and the difficulty of preparing isotopically labeled polymer and dendrimer samples, multidimensional NMR methods used in biomolecular structure determination have not been used to study dendrimers. To date, 1D NMR has been used as a routine method for characterization of dendrimers. Only a few multidimensional NMR studies on dendrimers have been reported.^(1,2,3) Polyurethane dendritic wedges (Scheme 1) are a novel type of linking element in the convergent approach to dendrimer synthesis. By using multidimensional PFG-HMQC and HMBC experiments, confirmation of the ^1H and ^{13}C resonance assignments have been obtained for these compounds, and structure proofs have been accomplished.

Experimental

NMR Measurements

About 150 mg of each sample (1st, 2nd and 3rd generation wedges⁽⁴⁾) was dissolved in 0.7 mL deuterated acetone in a 5 mm NMR tube for NMR studies. NMR spectra were obtained on a Varian Unityplus 750 MHz NMR spectrometer equipped with four *RF* channels, a Performa II z axis pulse field gradient (PFG) accessory, and a Varian $^1\text{H}/^{13}\text{C}/^{31}\text{P}/^2\text{H}$ four channel triple resonance probe with a PFG coil. Acetone- d_6 was also used as internal references for both ^1H (2.05 ppm) and ^{13}C (29.92 ppm) chemical shifts. All experiments were performed at $25.0 \pm 0.1^\circ\text{C}$. All data were processed with Varian's VNMR software on a SUN Ultra-10 workstation.

Scheme 1



1D NMR Experiments

The ^1H spectra of all generation wedges were acquired at 750 MHz using a 3.5 s acquisition time, 8 kHz spectral width, 2.8 μs (30°) pulse width and 16 transients. All ^{13}C spectra were acquired at 188.6 MHz using a 0.8 s acquisition time, a 20 kHz spectral width, an 8.0 μs (45°) pulse width and averaging of 4800 transients with WALTZ-16 modulated ^1H decoupling.

2D-NMR Experiments

$^1\text{H}^{13}\text{C}$ gradient HMQC(5) spectra of all generation wedges were collected with a relaxation delay of 1 s, $\Delta = (2 \times {}^1J_{\text{HC}})^{-1} = 3.57$ ms (optimized for 1 bond ^1H - ^{13}C correlations), and a 0.05 s acquisition time. The gradient strengths of three 2.0 ms PFGs were 0.462, 0.462, and -0.235 Tm^{-1} , respectively. $^1\text{H}^{13}\text{C}$ gradient HMBC(6) spectra of all generation wedges were collected with a relaxation delay of 1 s, a 0.256 s acquisition time, a delay, $\Delta = (2 \times {}^1J_{\text{HC}})^{-1} = 3.57$ ms for suppressing coherences from 1-bond correlations and a delay, $\tau = (2 \times {}^nJ_{\text{HC}})^{-1} = 0.05$ ms for optimizing crosspeak intensities from long-range correlations. The gradient strengths of two 2.0 ms pulse field gradients (PFGs) were 0.462 and 0.342 Tm^{-1} , respectively.

For both 2D experiments, ^1H and ^{13}C 90° pulses of 8.8 and 13.0 μs respectively, were used; 8000 Hz and 32000 Hz spectral windows were used for the ^1H (f_2) and ^{13}C (f_1) chemical shift dimensions, respectively; 16 transients were averaged for each of 1024 real t_1 increments. 2D data were processed with sinebell weighting; zero filling was used so that 2D FT was performed on an 8192×8192 matrix; and the spectra were displayed in the magnitude-mode in both dimensions.

Results and Discussion

The ^1H NMR spectrum of **1** (Figure 1) shows resolved resonances for all the protons in the structure except for some of the aliphatic methylene protons in the long aliphatic chain. However, the ^{13}C NMR spectrum (Figure 2) displays nicely resolved resonances for each carbon in the structure, including those in the long aliphatic chain. Therefore by using PFG HMQC and HMBC 2D NMR experiments, the proton resonances can be dispersed based on the resolved carbon resonances.

In Figure 1c, the singlet at 8.51 ppm is attributed to the amide proton. The singlets at 7.27 and 6.97 ppm are from H_4 and H_2/H_6 of the benzene ring, respectively. The singlet around 2.82 ppm is the resonance from the water in

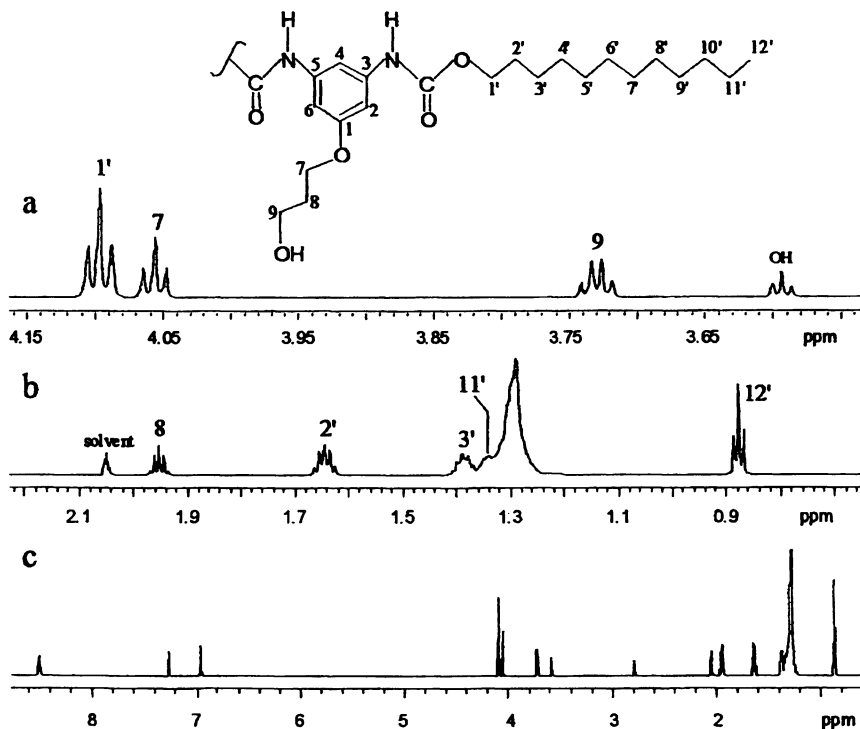


Figure 1. 750 MHz ¹H 1D NMR spectrum and the partial structure 1: (a) the expansion of alkoxy region, (b) the expansion of the aliphatic region, and (c) the full ¹H NMR spectrum.

the sample. Assignments of some of the resonances in the expansion shown in Figure 1a can be made based on the relative peak intensities, multiplicities and their chemical shifts; the triplet at 4.10 ppm is attributed to H₁. This triplet splitting is from coupling with two neighboring H₂ atoms. The triplet at 4.06 ppm is from the H₇ atoms, which are coupled with two H₈ atoms; and the doublet of triplet at 3.73 ppm is from the H₉ atoms, which are coupled to the –OH proton and two H₈ protons. Here $J_{H,H_{OH}}$ is 5.25 Hz and J_{H,H_1} is 6.00 Hz. The small triplet at 3.59 ppm is from the –OH proton, which is coupled with two H₉ protons. The positions of the resonances from both –OH and >NH protons are concentration dependent. In Figure 1b, the quintet near 2.05 ppm is from the residual protons of deuterated acetone solvent. The quintet around 1.95 ppm is attributed to the H₈ protons, which are coupled with two H₇ protons and two H₉

protons. A second quintet near 1.64 ppm is from the H₂ protons, which are split by two H₁ protons and two H₃ protons. Because the two coupling constants in each multiplet are very similar (ca. 7.5 Hz), they each look like a quintet instead of triplet of triplets. The resonances in the 1.30 - 1.50 ppm region are attributed to the H₃ - H₉ protons in the dodecyl chains. Among them, two quintets near 1.39 ppm and 1.34 ppm are resolvable. However, based on the 1D ¹H spectrum it is not possible to assign them. The triplet at 0.88 ppm is from the methyl groups (H₁₂) in the dodecyl chains, which are coupled to two nearby H₁₁ methylene protons.

Figure 2 shows the 188.6 MHz ¹³C 1D NMR spectrum of **1**. In addition to the septet from the solvent that is marked with *s, nearly all twenty carbon resonances can be resolved. However, without the aid of 2D-NMR, only partial assignments can be made. For example, in the downfield region, the signal at 141.63 ppm can be assigned to C₃ and C₅ of the benzene ring based on the chemical shifts and relative peak intensities. But for the peaks at 154.52 ppm and 161.01 ppm, it is not possible to determine which is from C₁ of the benzene ring and which is from the >C=O carbons. The peaks at 101.75 and 100.10 ppm can be assigned to C₄ and C₂/C₆ of the phenyl ring, respectively based on their relative intensities. In the alkoxy region (Figure 2a), Three resonances at 65.60 ppm, 59.17 ppm and 65.32 ppm are well resolved, however it is hard to make specific assignment. In Figures 2b and 2c, the highest field resonances at 14.44, 23.41, and 32.72 ppm can be attributed to C₁₂, C₁₁ and C₁₀, respectively, based on the known chemical shifts of similar carbons in long-chain hydrocarbons. However it is not possible to assign the remaining methylene carbon resonances based on the 1D spectrum alone. Thus 2D HMQC and HMBC NMR experiments were performed to complete the resonance assignments.

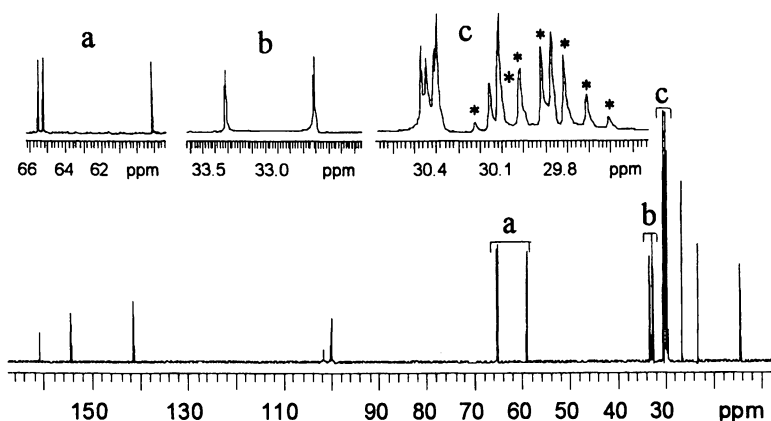


Figure 2. 188.6 MHz ¹³C 1D NMR spectrum of **1** with expansions of alkoxy (a) and aliphatic (b and c) regions; the solvent (acetone-*d*₆) resonances are marked with *.

The 2D HMQC and 2D HMBC spectra of **1** are shown in Figures 3 and 4, respectively. The resonance assignments of the crosspeaks have been marked in both spectra according to the numbering in the partial structure shown in Figure 1. The ^1H - ^{13}C HMQC crosspeaks from atoms 4 and 2/6 of the benzene ring are shown in Figure 3a. Figure 3b displays clear ^1H - ^{13}C 1-bond correlations from the $-\text{OCH}_2-$ groups. The ^1H - ^{13}C HMQC correlations from aliphatic region are shown in Figure 3c. All the ^1H - ^{13}C HMQC crosspeaks are well resolved except methylenes 4' through 9'. Based on the ^1H resonance assignments (discussed above) and the correlations observed in Figure 3b, it is possible to assign the $-\text{OCH}_2-$ ^{13}C resonances as labeled in the figure. Similarly the ^{13}C resonance assignments of C_2 , C_8 and C_3' can be made, and the assignments of $\text{C}_{10'}$, $\text{C}_{11'}$ and $\text{C}_{12'}$ can be confirmed based on the crosspeaks observed in Figure 3c.

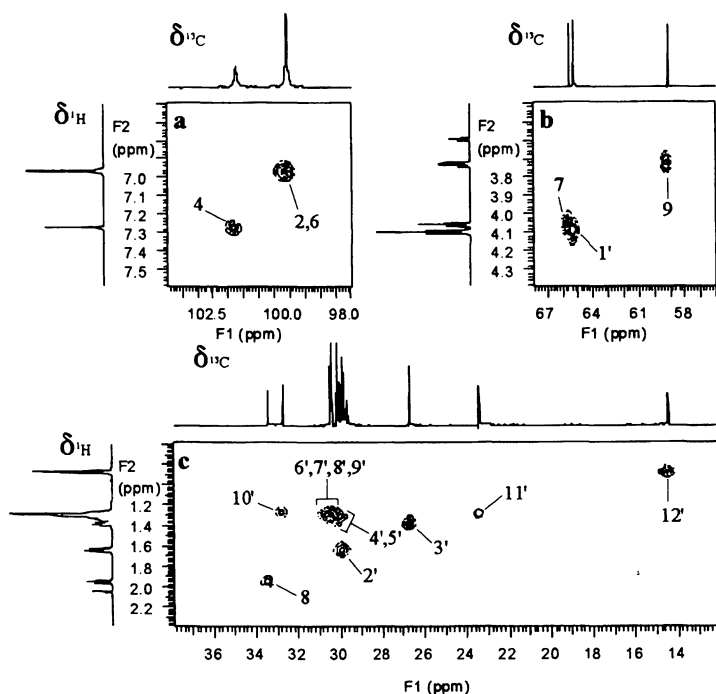


Figure 3. PFG-HMQC 2D NMR spectrum of **1**: expansions of the (a) aromatic region, (b) $-\text{OCH}_2-$ region, and (c) aliphatic region except $-\text{OCH}_2-$ types.

The 2D HMBC experiment can provide further information needed to make many of the remaining assignments. This experiment is essential to

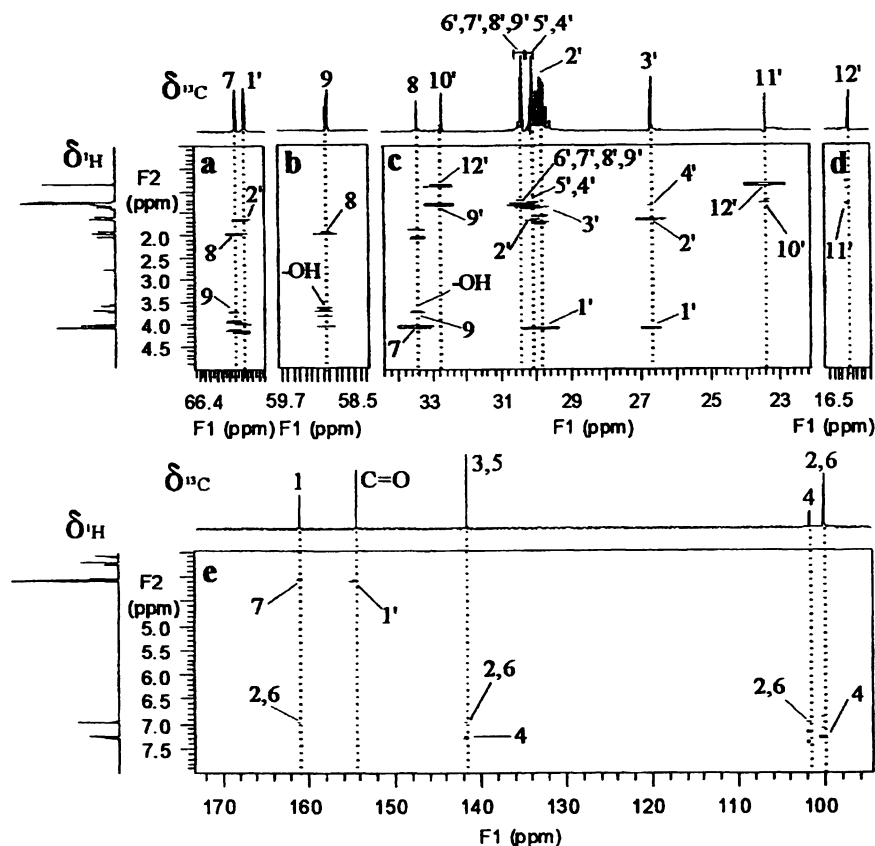


Figure 4. $^1\text{H}^{13}\text{C}$ PFG-HMBC 2D NMR spectrum of **1**: (a) and (b) the expansions of alkoxy regions, (c) and (d) the expansions of aliphatic regions, and (e) the downfield (aromatic and carbonyl) regions.

obtain many of the assignments labeled in Figure 3. It can also be used to verify the assignments of ^1H and ^{13}C resonances obtained from the 1D ^1H , ^{13}C and 2D HMQC experiments discussed above. Figures 4a-d show the long-range ^1H - ^{13}C (HMBC) correlations of **1** in the upfield (aliphatic and alkoxy) regions. The crosspeaks from $-\text{OCH}_2-$ groups can be clearly assigned based on the additional long-range ^1H - ^{13}C correlations. For instance, C_7 is correlated with both H_8 (2-bond) and H_9 (3-bond); C_1 is only correlated with H_2 (2-bond). Thus

these resonances can be distinguished. In Figure 4b, C₉ exhibits correlations with the OH, H₈ and H₇ protons. Thus it is easy to differentiate H₇/C₇, C₁/C₁' and H₉/C₉ from the HMBC experiment. In a similar way the H₈/C₈, H₃/C₃, H₁₀/C₁₀, H₁₁/C₁₁' and H₁₂/C₁₂' resonance assignments can be confirmed. In Figure 4c, the 2' and 4' methylene carbon resonances both exhibit long-range correlations with the H₁' and H₃' resonances, enabling their resolution and confirming the H₂/C₂' and H₄/C₄' resonance assignments. Furthermore, based on the H₄/C₄' assignments, H₅/C₅' resonances can be assigned. The H₉ resonance can be assigned based on its HMBC crosspeak with C₁₀'.

Figure 5 shows the expansions of the methylene (4'-9') regions from the HMBC spectrum plotted with different thresholds. In Figure 5a, the crosspeak between C₂' and H₃' confirms the assignment of 2' methylene group. Similarly the crosspeaks between C₃' and H₄' and between C₄' and H₅', which are labeled in Figure 5b, provide information for the assignments of 4' and 5' methylene groups. However, due to the limited resolution in the HMBC spectrum, the resonances from the 6', 7' and 8' methylene groups are not resolved.

Figure 4e shows the ¹H-¹³C correlations of **1** in the downfield region of the HMBC spectrum. The resonance from C₁ exhibits correlations with the H₇ and H₂/H₆ resonances; the resonances from C₃/C₅ are correlated with the resonances from H₄ and H₂/H₆; and the carbonyl resonance is correlated with H₁', providing a proof of the carbonyl resonance assignment. The C₄ resonance has a correlation with the H₂/H₆ resonance while the C₂/C₆ resonance is correlated with the H₄ resonance. These correlations, which are clearly shown in the HMBC spectrum, prove the assignments discussed previously. The ¹H and ¹³C resonance assignments of **1** are summarized in the Table 1.

Figures 6, 7, 8 and 9 illustrate the 1D ¹H NMR, 1D ¹³C NMR, 2D HMQC and 2D HMBC spectra of **2**. Figures 10, 11, 12 and 13 illustrate the 1D ¹³C NMR, 1D ¹H NMR, 2D HMQC and 2D HMBC spectra of **3**. For both **2** and **3**, the resonances from dodecyl chains are very similar to the ones in the spectra of **1**. Therefore the assignments for these resonances can be concluded based on the assignments of **1**. The major differences between the spectra of **1**, **2** and **3** are exhibited in the resonances of amide, aromatic and alkoxy groups. With increasing generation, the NMR spectra become more complicated in these regions. However, it is still possible to distinguish most of the resonances of higher generation structures in the 1D and 2D NMR spectra.

Here, the 1st generation dendritic wedge (**1**) has been used to demonstrate the NMR characterization of these compounds. In the same manner, the 2nd and 3rd generation dendritic wedges (**2** and **3**) have been characterized; chemical shift assignments for these compounds are summarized in Table 1.

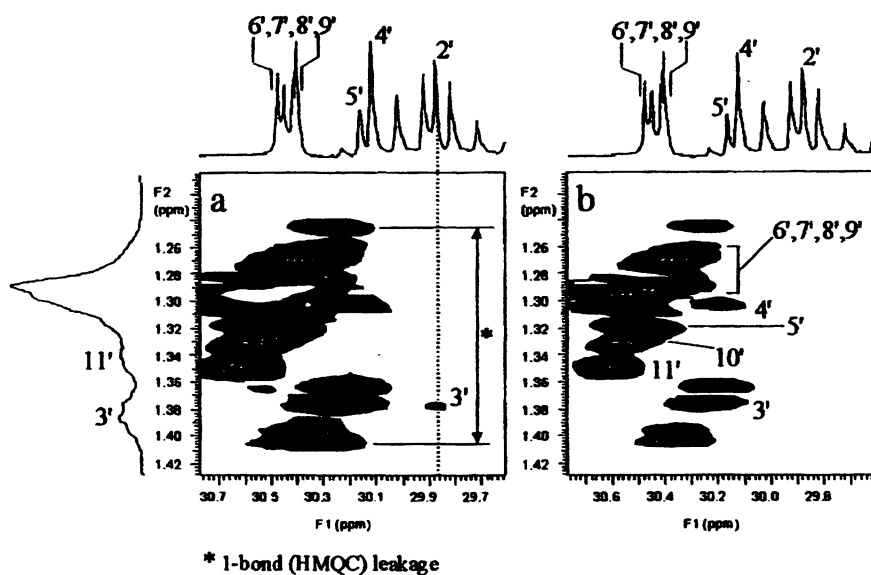


Figure 5. The expansions of aliphatic regions from the $^1\text{H}^{13}\text{C}$ PFG-HMBC 2D NMR spectrum of **1**: (a) the 2D plot with lower threshold (2), and (b) the 2D plot with higher threshold (3); both plots are at the same vertical scales.

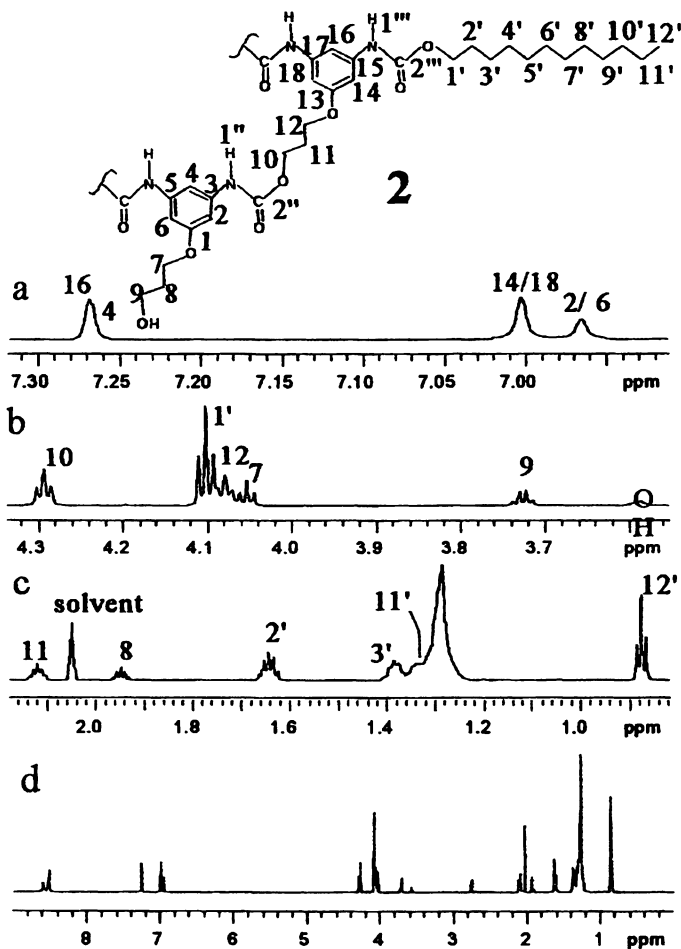


Figure 6. 750 MHz ^1H 1D NMR spectrum and the partial 2nd structure of 2: (a) the expansion of the aromatic region, (b) the expansion of the alkoxy region, (c) the expansion of the aliphatic region, and (d) the full ^1H NMR spectrum.

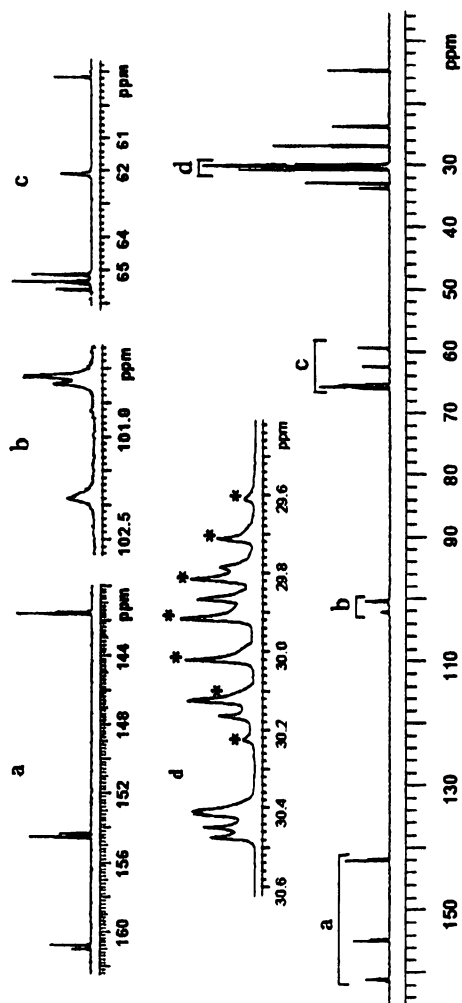


Figure 7. 188.6 MHz ^{13}C ID NMR spectrum of 2 with expansions of crowded regions: a through d shown in the insets; the solvent (acetone- d_6) resonances are marked with *.

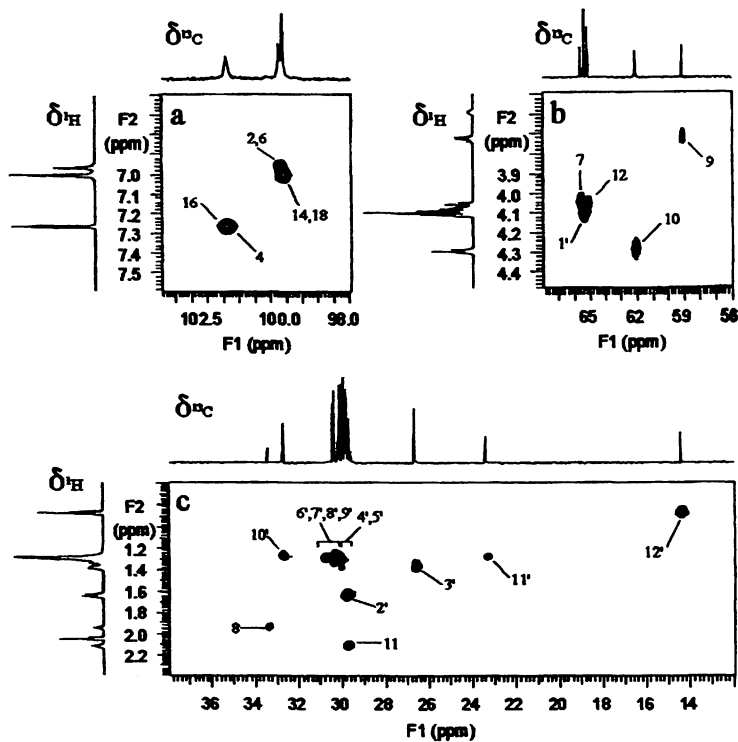


Figure 8. $^1\text{H}/^{13}\text{C}$ PFG-HMQC 2D NMR spectrum of 2: (a) the expansion of the aromatic region, (b) the expansion of the $-\text{OCH}_2-$ region, and (c) the expansion of the aliphatic region.

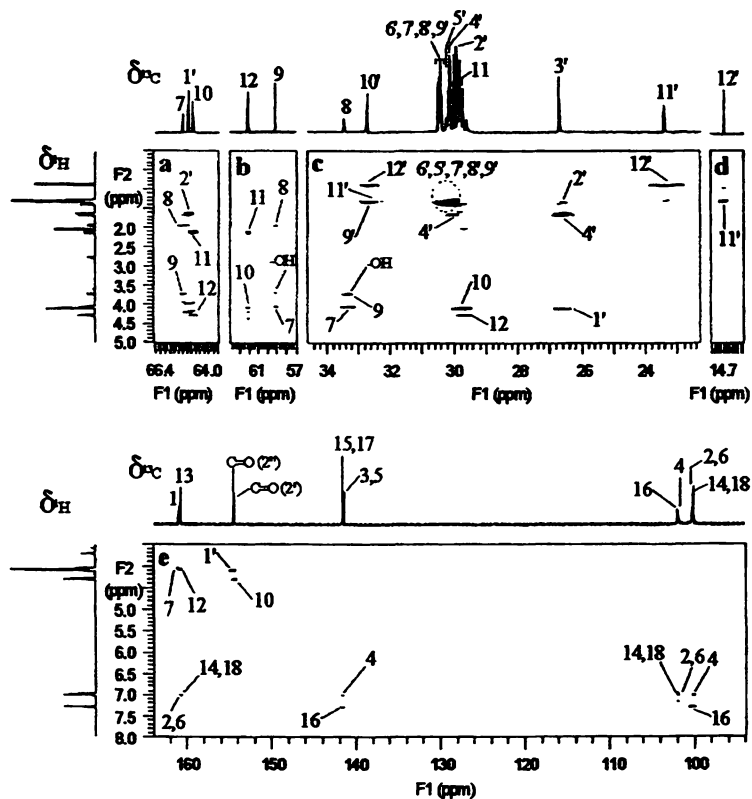


Figure 9. $^1\text{H}^{13}\text{C}$ PFG-HMBC 2D NMR spectrum of 2: (a and b) expansions of the alkoxy regions, (c and d) expansions of the aliphatic regions, and (e) the expansion of the downfield (aromatic and carbonyl) regions.

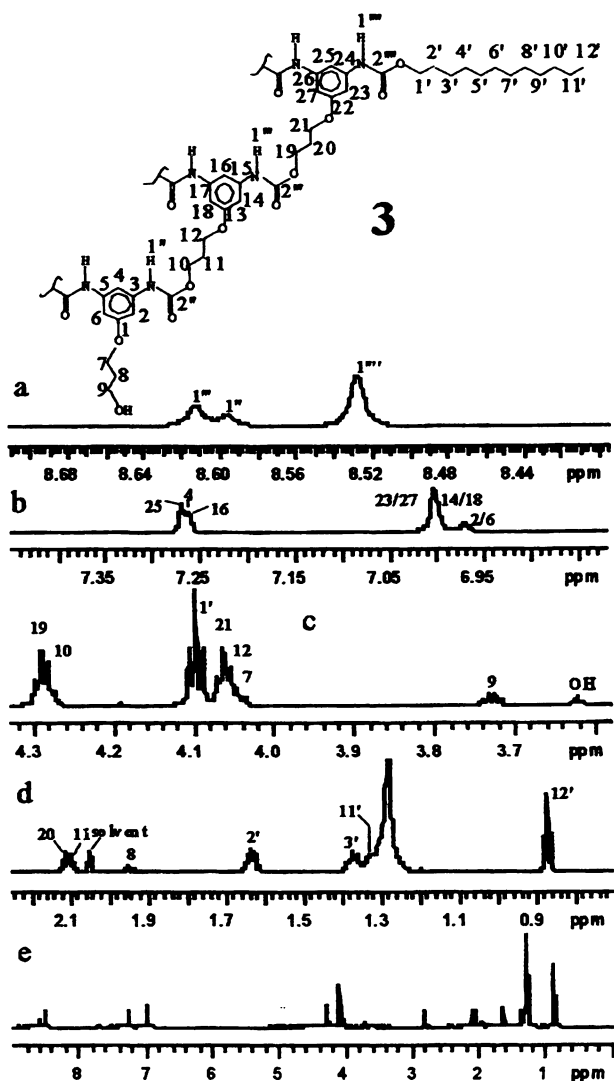


Figure 10. 750 MHz ^1H NMR spectrum of **3**: (a) expansion of the amide region, (b) expansion of the aromatic region, (c) expansion of the alkoxy region, (d) expansion of the aliphatic region, and (e) the full ^1H NMR spectrum.

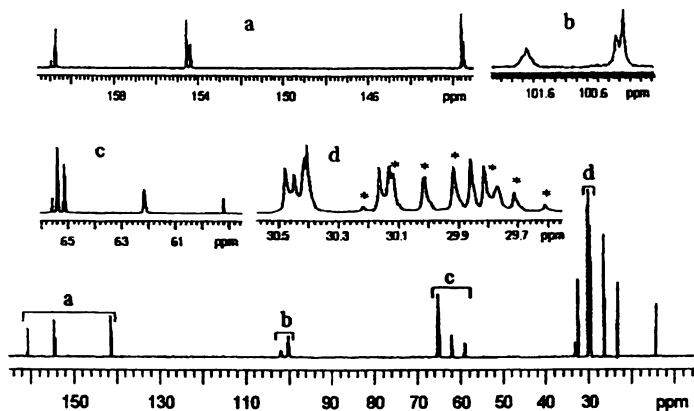


Figure 11. 188.6 MHz ^{13}C 1D NMR spectrum of **3** with expansions of crowded regions: a through d shown in the insets; the solvent (acetone- d_6) resonances are marked with *.

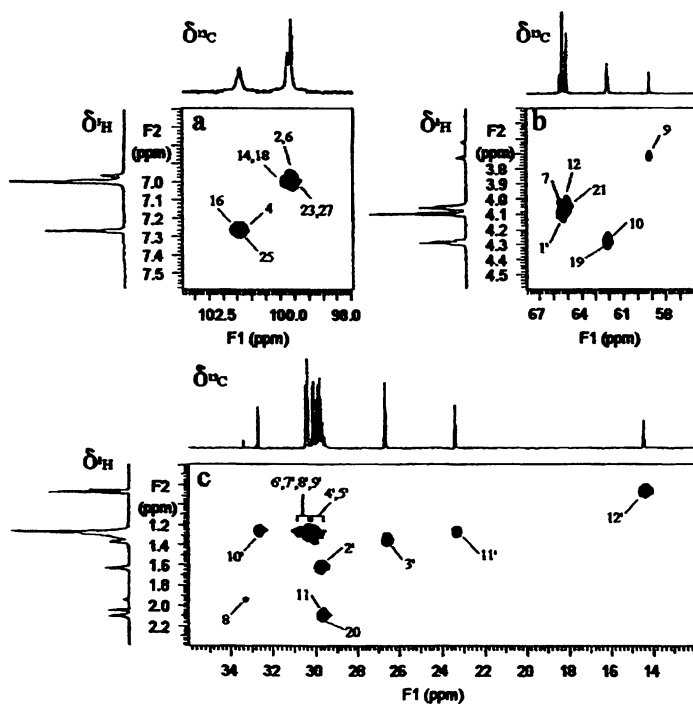


Figure 12. $^1\text{H}^{13}\text{C}$ PFG-HMQC 2D NMR spectrum of **3** expansions of the: (a) aromatic, (b) $-\text{OCH}_2-$, and (c) aliphatic regions.

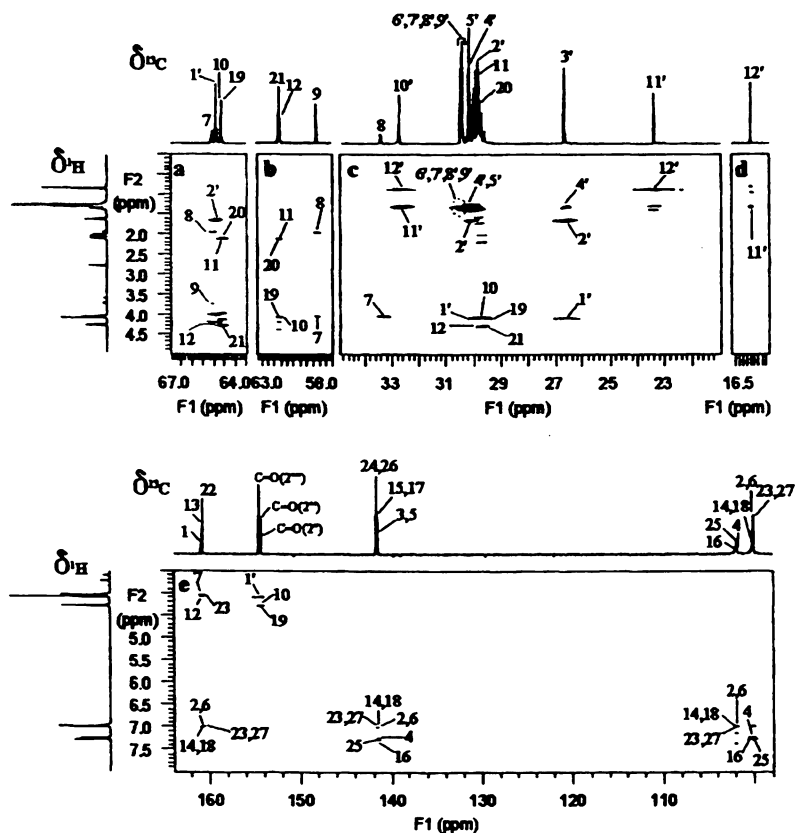


Figure 13. $^1\text{H}/^{13}\text{C}$ PFG-HMBC 2D NMR spectrum of **3**: (a and b) expansions of the alkoxy regions, (c and d) expansions of the aliphatic regions, and (e) the expansion of the downfield (aromatic and carbonyl) regions.

Table 1. The Chemical Shift Assignments of 1, 2 and 3

Partial Structure of Wedges		Chemical Shifts (ppm)					
		1		2		3	
		^1H	^{13}C	^1H	^{13}C	^1H	^{13}C
	1	---	161.01	---	161.03	---	161.00
	2.6	6.97	100.10	6.97	100.24	6.97	100.24
	3.5	---	141.63	---	141.53	---	141.49
	4	7.27	101.75	7.27	101.83	7.26	101.84
	7	4.06	65.60	4.06	65.62	4.05	65.61
	8	1.95	33.42	1.95	33.43	1.95	33.40
	9	3.73	59.17	3.73	59.17	3.73	59.20
	OH	3.59	---	3.59	---	3.62	---
	NH (1 ^m)	8.51	---	8.61	---	8.60	---
	C=O (2 ^m)	---	154.52	---	154.36	---	154.37
	10			4.29	62.12	4.28	62.11
	11			2.12	29.79	2.10	29.80
	12			4.08	65.17	4.06	65.17
	13			---	160.80	---	160.80
	14,18			7.00	100.13	7.00	100.27
	15,17			---	141.68	---	141.52
	16			7.26	101.91	7.26	102.03
	NH (1 ^m)			8.52	---	8.61	---
	C=O (2 ^m)			---	154.56	---	154.40
		19					4.29
20						2.11	29.77
21						4.06	65.14
22						---	160.78
23,27						7.00	100.14
24,26						---	141.63
25						7.27	101.94
NH (1 ^m)						8.53	---
C=O (2 ^m)						---	154.59
		1'	4.10	65.32	4.10	65.38	4.10
	2'	1.64	29.88	1.64	29.87	1.64	29.86
	3'	1.39	26.70	1.39	26.70	1.38	26.70
	4'	1.29	30.12	1.28	30.13	1.28	30.13
	5'	1.31	30.16	1.30	30.17	1.29	30.17
	6'	1.29	30.40~30.47	1.28	30.41~30.48	1.27	30.41~30.49
	7'	1.29	30.40~30.47	1.28	30.41~30.48	1.27	30.41~30.49
	8'	1.29	30.40~30.47	1.28	30.41~30.48	1.27	30.41~30.49
	9'	1.30	30.40~30.47	1.28	30.41~30.48	1.28	30.41~30.49
	10'	1.32	32.72	1.30	32.73	1.29	32.73
	11'	1.33	23.41	1.34	23.41	1.33	23.41
	12'	0.88	14.44	0.88	14.45	0.88	14.47

Conclusions

The structures of precursors to Fréchet-type dendrimers have been proven by high field 2D-NMR at 750 MHz. These techniques can be very useful for the characterization of dendrimers, and to obtain the unambiguous chemical shift assignments of their NMR resonances.

Acknowledgement

We would like to acknowledge the NSF (DMR-9617477 and DMR-0073346) for support of this research, and the Kresge Foundation and donors to the Kresge Challenge program at the University of Akron for funds used to purchase the 750 MHz NMR instrument used in this work.

References

1. (a) Lambert, B.; Basso, E.; Qing, N.; Lim, S. H.; Pflug, J. L. *J. Organomet. Chem.* **1998**, *554*(2), 113. (b) Chai, M.; Pi, Z.; Tessier, C.; Rinaldi, P. L. *J. Am. Chem. Soc.* **1999**, *121*(2), 273.
2. Chai, M.; Pi, Z.; Tessier, C.; Rinaldi, P. L. *J. Am. Chem. Soc.* **1999**, *121*(2), 273.
3. (a) Chai, M.; Niu, Y.; Youngs, W. J.; Rinaldi, P. L. *Macromolecules*, **2000**, *33*, 5395. (b) Chai, M.; Niu, Y.; Youngs, W. J.; Rinaldi, P. L. *J. Am. Chem. Soc.* **2001**, *123*(20), 4670.
4. Preparations of the materials studied here have been described in: Taylor, R. T.; Puapaboon, U., *Tetrahedron Lett.*, **1998**, *39*, 8005.
5. (a) Müller, L. *J. Am. Chem. Soc.* **1979**, *101*, 4481. (b) Bax, A.; Griffey, R. G.; Hawkins, B. L. *J. Am. Chem. Soc.* **1983**, *105*, 7188.
6. Bax, A.; Summers, M. F. *J. Am. Chem. Soc.* **1986**, *108*, 2093.

Chapter 12

Compositional and Configurational Assignments of Acrylonitrile Copolymers by 2D NMR Spectroscopy

A. S. Brar

Department of Chemistry, Indian Institute of Technology,
Delhi 110016, India

The copolymers of acrylonitrile with methyl methacrylate (A/M), Glycidyl methacrylate (A/G) and acrylic acid (A/B) of different monomer concentrations were prepared. The carbon-13 and proton spectra of these copolymers are overlapping and complex. The complete spectral assignment of ^{13}C - and ^1H -NMR spectra were done with the help of Distortionless Enhancement by Polarisation transfer (DEPT) and two dimensional ^{13}C - ^1H Heteronuclear Single Quantum Correlation (HSQC) and Total Correlated spectroscopy (TOCSY) experiments. The methylene, methine and methyl (A/M and A/G) carbon resonances show both stereochemical (triad level) and compositional (dyad, triad, tetrad, pentad and hexad level) sensitivity. 2D Double Quantum Filtered Correlated Spectroscopy (DQFCOSY) experiment was used in A/B copolymers to assign the complex ^1H NMR spectrum to different compositional sequences.

Introduction

It is well known that NMR spectroscopy is a powerful technique for structure determination of macromolecules. In case of macromolecules, ^{13}C and ^1H NMR spectra are quite complex and overlapped, hence microstructure determination of such molecules is carried using usual 1D NMR techniques coupled with 2D-NMR techniques such as HETCOR and TOCSY¹⁻³. DEPT is used extensively for analysis of the overlapping carbon resonances in ^{13}C -NMR spectra^{4,5}. HETCOR gives information not only on direct carbon to proton linkages, but also on compositional⁶ and configurational^{7,8} sequences in polymers. TOCSY, both low and high mixing time is further used to resolve broad and overlapping proton spectra of polymers and also to determine intramolecular chain structure of polymers. Acrylonitrile copolymers are used in textile industry and as precursor of carbon fibers.

In this chapter, we will discuss the applications of various 1D and 2D- NMR techniques on the microstructure characterization in terms of compositional and configurational sequences of different acrylonitrile copolymers.

Acrylonitrile/Methyl methacrylate (A/M) copolymers

The complex and overlapped $^{13}\text{C}\{^1\text{H}\}$ NMR spectrum of A/M copolymer is resolved using DEPT-135 and HETCOR spectra. The overlapping methine and methyl carbon region are further resolved and assigned to pentad compositional and configurational level, using DEPT-90 and DEPT-135 subspectra.

Using ^{13}C - ^1H inverse HETCOR, the methylene carbon region is first assigned to AA (δ 30.0-38.0 ppm), AM (δ 38.0-45.0 ppm) and MM (δ 45.0-55.0 ppm) centered dyads as shown in fig.1. Further splitting within these dyads is assigned to tetrad level on the basis of change in intensity of signals with copolymer composition. The three signals in AA dyad are assigned to AAAA (δ 34.0-35.5 ppm), AAAM (δ 34.0-35.5 ppm) and MAAM (δ 35.5-38.0 ppm). The splitting within these tetrad sequences can be assigned to hexad compositional sequences, on the basis of change in intensity with change in copolymer composition using ^1H - ^{13}C inverse HETCOR spectra. In fig.1, the cross peaks in HETCOR spectrum at δ 33.19/2.16, δ 33.40/2.04, δ 34.88/2.14, δ 35.37/1.97, δ 36.65/2.10, δ 37.14/1.89, and δ 38.25/1.72 ppm can be assigned to AAAAAM (MAAAAA), MAAAAM, AAAAMA, MAAAMM, AMAAMA, AMAAMM and MMAAMM, respectively.

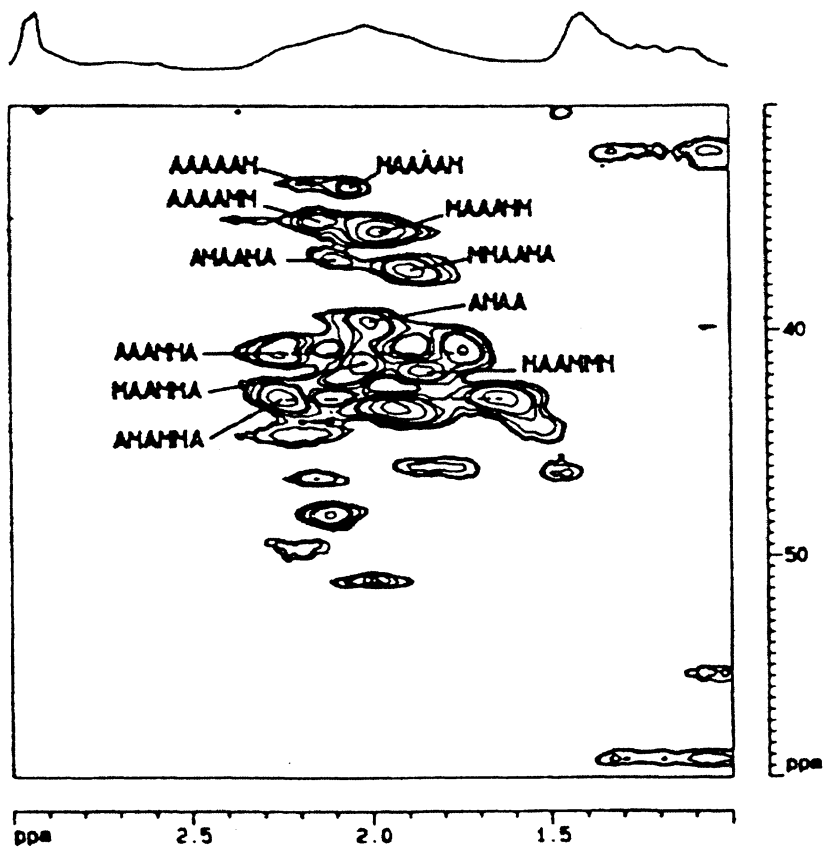


Figure 1. The methylene region of the inverse-HETCOR spectrum of A/M copolymer.

The AM(MA) dyad can also be divided into three tetrads ,AAMA (δ 38.0-39.9 ppm), AAMM +AMAM (δ 39.9-42.0 ppm) and MAMM(δ 42.0-45.0 ppm). These tetrads further show hexad compositional sensitivity.

The three MM centered tetrads AMMA, AMMM(MMMA) and MMMM are assigned around δ 45.0-47.5, δ 47.5-51.5 and δ 50.5-55.5 ppm, respectively. The further splitting in the MMMM and MMMA tetrads can be assigned to hexad sequences , on the basis of variation in the intensities of the peaks with the composition . The methylene carbon signals at δ 54.34, δ 52.87, δ 51.40, δ 49.78 and δ 48.03 ppm can be assigned to MMMMMM, MMMMMA(AMMMMM), AMMMMM + MMMMAM, MMMMAA and AMMMAA, respectively.

Once $^{13}\text{C}\{^1\text{H}\}$ NMR spectrum is assigned completely, it is easy to assign complex and overlapping ^1H - NMR spectrum with the help of inverse HETCOR experiment. All the methine proton signals are assigned to various pentad sequences.

Acrylonitrile/Glycidylmethacrylate (A/G) copolymers

The $^{13}\text{C}\{^1\text{H}\}$ NMR spectrum of A/G copolymer is quiet complex and overlapping. The overlapping methine and methylene carbon signals are resolved with the help of DEPT-135. The methine carbon signals are first assigned to three broad triad compositional sequences AAA, AAG and GAG. Further splitting in these are assigned to pentad compositional and configurational sequences using DEPT-90 spectra of A/G copolymer of different compositions. The methylene carbon resonances are assigned to tetrad compositional sequence, using DEPT- 135 NMR spectra. Using 2D- inverse HETCOR NMR spectra the methylene group carbon region is first assigned to AA(δ 32.0-38.0 ppm), AG(δ 38.5-44.6 ppm) and GG(δ 44.6-55.0 ppm) centered dyads. Further splitting within these dyads is assigned first to tetrad level and then to hexad compositional sequences, on the basis of change in intensity with change in copolymer composition. The methyl carbon signals overlap with the methine carbon signals, which can be resolved by DEPT experiments. However, the non overlapping methyl proton signals could be clearly assigned around δ 0.60-1.5 ppm and show both compositional and configurational sensitivity. The methyl proton region can be split into three broad envelopes that vary with copolymer composition and are assigned to AGA (δ 1.19-1.5 ppm), GGA(AGG) (δ 0.98-1.19 ppm) and GGG (δ 0.80-0.98 ppm). These triad fractions further show signals that can be assigned to configurational or compositional sequences. In the GGG triad region, the signals at δ 1.06, 0.88 and 0.83 ppm are assigned to AGGGA, GGGGA (AGGGG) and GGGGG pentad sequences on the basis of the change in intensity with the copolymer composition. These assignments can also be confirmed by the inverse-HETCOR spectrum as shown in fig.2, where

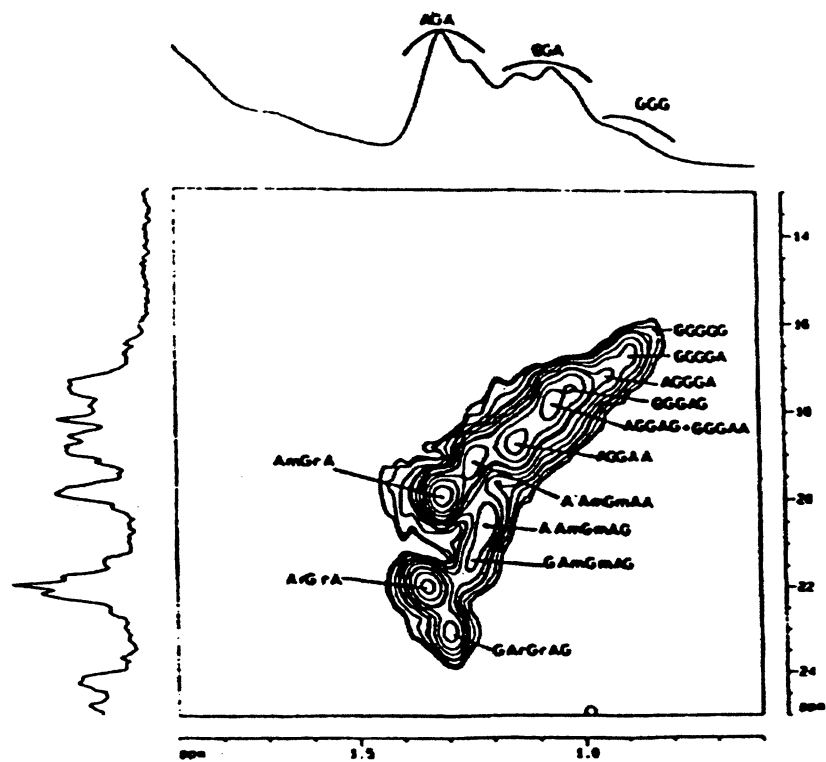


Figure 2. Methyl region of the inverse-HETCOR spectrum of A/G copolymer ($F_A = 0.48$).

the cross peaks at δ 17.00/1.06, 16.51/0.88 and 16.06/0.83 ppm are assigned to these three GGG-centered pentads, respectively. Similarly, in the AGG (GGA) triad region, the three GGA-centered pentads are assigned at δ 18.61/1.14 (AGGAA), 17.79/1.06 (AGGAG + GGGAA) and 17.36/1.02 (GGGAG) ppm (fig.2). The signals in the AGA triad region, which do not change with the copolymer composition, are assigned to A_mG_mA (δ 1.24 ppm), A_mG_rA (A_rG_mA) (δ 1.31 ppm) and A_rG_rA (δ 1.35 ppm). Further compositional sequences within these triads are assigned with the help of the inverse-HETCOR spectrum. Thus with the help of the inverse-HETCOR experiment, overlapping methyl carbon signals can be assigned without ambiguity.

Acrylonitrile/ Acrylic Acid (A/B) copolymers

The methine carbon signals of A- unit shows configurational and compositional sensitivity. The multiplets can be assigned to rr, rm(mr) and mm triad respectively, on the basis of signal assigned in homopolymer spectra. Further splittings within these can be assigned to compositional sequences. Similarly, the methine carbon signals of B- unit shows triad compositional sensitivity.

The DQFCOSY spectrum of A/B copolymer recorded in DMSO- d_6 is shown in fig. 3. In the DQFCOSY spectrum, the multiplets in the methine proton region of A- unit can be assigned to triad compositional sequences. The cross peaks at δ 3.14/2.07, 3.02/2.05, 3.02/1.90 and 2.92/1.78 ppm can be assigned to AAA, AAB(BAA) and BAB. In the AAB triad fraction, two cross peaks are seen as the methine proton is coupled to two different types of methylene protons. The AAA triad further shows configurational sensitivity. The cross peaks at δ 3.22/2.17, 3.14/2.07 and 3.12/2.03 ppm are assigned to $AmAmA$, $AmArA$ and $ArArA$ respectively. The methine protons at δ 3.22, 3.14 and 3.12 ppm show three bond coupling with the methylene proton at δ 2.17, 2.07 and 2.03 ppm which further shows three bond coupling with the methylene proton at δ 1.94, 1.86 and 1.80 ppm. Thus accounting for the head to head linkages. The absence of any methine cross peaks indicates that there are no CH/CH coupling in the polymers. Similarly, in AAB and BAB triad fractions the methine protons at δ 2.94 and 2.98 ppm shows three bond coupling with the methylene proton at δ 1.88 and 1.81 ppm which further shows three bond coupling with the methylene proton at δ 1.39 and 1.52 ppm, respectively, accounting for the head to head linkages in these triad fractions (AAB and BAB). In the methine proton region of B- unit, the multiplets can be assigned to triad compositional sequences. The cross peaks at δ 2.32/1.59, 2.55/1.78 and 2.70/1.94 ppm can be assigned to BBB,

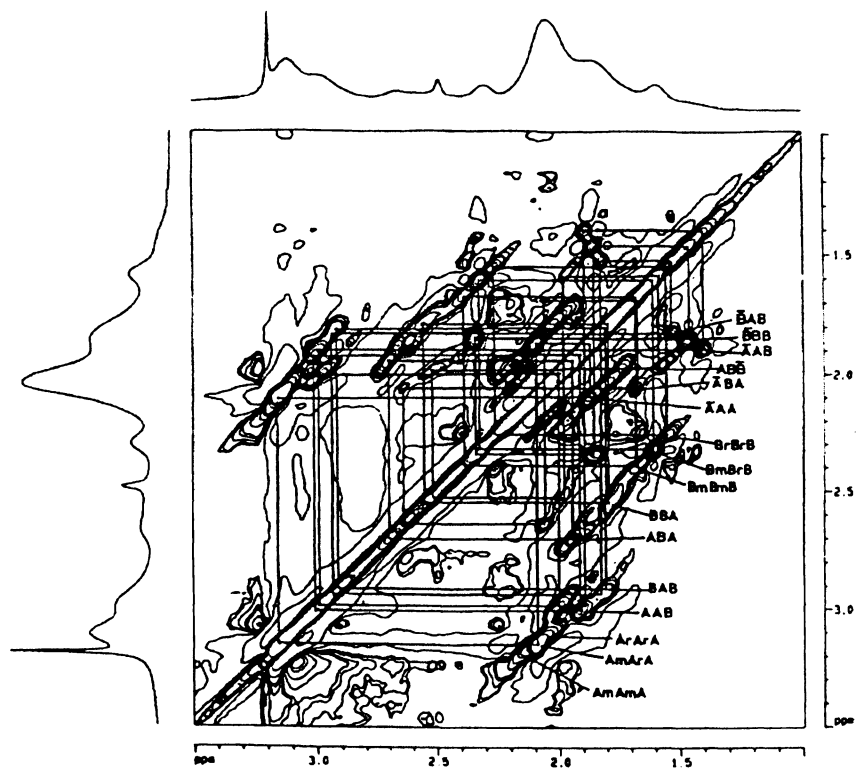


Figure 3. The 2D-DQF-COSY spectrum of the acrylonitrile/acrylic acid copolymer in DMSO-d_6 .

BBA and ABA triads sequences respectively. The BBB triads further shows configurational sensitivity. The cross peaks at δ 2.26/1.55, 2.32/1.59 and 2.38/1.66 ppm are assigned to BmBmB, BmBrB and BrBrB triad fractions respectively on the basis of assignment done in the homopolymer. The methine protons at δ 2.34, 2.53 and 2.64 ppm show three bond coupling with the methylene protons at δ 1.84, 1.98 and 2.06 ppm respectively, which further shows three bond coupling with the methylene proton at δ 1.46, 1.56 and 1.67 ppm. Thus accounting for the head to head linkages in triad fractions BBB, BBA and ABA, respectively.

Conclusions

The overlapping and broad signals in the carbon and proton spectra was assigned completely to various compositional and configurational sequences with the help of inverse HETCOR and TOCSY / DQFCOSY experiments.

References

1. Brar, A. S.; Dutta, K.; Hekmatyar, S. K. *J. Polymer Sci.* **1998**, 36,1081
2. Brar, A. S.; Dutta, K. *Macromolecules* **1998**, 31,4695
3. Brar, A. S.; Dutta, K. *Eur. Polym. J.* **1998**, 34, 1585
4. Grobelny, J.; Kotas, A. *Polymer* **1995**, 36, 1363 .
5. Brar, A. S.; Shiv charan *Polymer* **1996**, 37,2451.
6. Brar, A. S.; Malhotra, M. *Macromolecules* **1996**, 29. 7470
7. Suchoparek, M.; Spevacek, J. *Macromolecules* **1993**, 26, 102
8. Mijangoes, C.; Lopez, D. *Macromolecules* **1995**, 28, 1364.

Chapter 13

Structure Determination of Poly(vinyl alcohol) by 2D NMR Spectroscopy

A. S. Brar, R. Kumar, A. Yadav, and M. Kaur

Department of Chemistry, Indian Institute of Technology,
Delhi 110016, India

The spectral assignment of poly(vinyl alcohol) (PVA) prepared by the basic hydrolysis of poly(vinyl acetate) was studied using a combination of one and two-dimensional NMR spectroscopy. The $^{13}\text{C}\{^1\text{H}\}$ and ^1H NMR spectra of the homopolymer (PVA) were assigned to the configurational pentads (CH region) and tetrads (CH_2 region). These assignments were substantiated by the use of two dimensional heteronuclear single quantum correlation (HSQC), heteronuclear single quantum correlation - total correlation spectroscopy (HSQC-TOCSY) and total correlated spectroscopy (TOCSY) experiments.

Introduction

The use of 2D NMR spectroscopy for characterizing the stereochemical structures of the polymers has got tremendous importance¹⁻⁴. The two dimensional techniques that couples single-bond carbon-proton and proton-proton correlation spectroscopy (2D HSQC-TOCSY) can help in unambiguous stereochemical and compositional assignments of the polymers⁵⁻⁶. Levy et al.⁷ have assigned the methylene region upto tetrad and methine region upto penrad levels in the poly(vinyl chloride) spectrum by the application of spin lock relay experiment. This is achieved by elucidating the conductivity of the carbons belonging to even and odd ad sequences along the polymer chain. Although poly(vinyl alcohol) has been studied extensively by many coworkers Ovenall⁸, Terao et al⁹ and Matsuzaki et al¹⁰, a complete and unambiguous signal assignment of the $^{13}\text{C}\{^1\text{H}\}$ NMR spectrum has not been reported so far. In this

paper, we assign the methylene and methine carbons upto tetrad and pentad levels respectively with the help of HSQC-TOCSY spectrum. In the 2D HSQC-TOCSY experiment the assignments of the proton and the carbon signals correspond to each other to arrive at unambiguous assignments.

Experimental

Poly(vinyl alcohol) was prepared by the basic hydrolysis of Poly(vinyl acetate). The homopolymer was precipitated in Hexane and purified in H₂O-Hexane solvent system. All the 2D NMR spectrum was recorded in DMSO-d₆ at 100°C on a Bruker DPX-300 NMR spectrometer operating at 300.13 and 75.5 MHz for ¹H and ¹³C nuclei respectively. 2D (HSQC-TOCSY, TOCSY) NMR experiments were performed using standard pulse sequences as described in our previous papers^{5,11}.

Results and Discussion

In the HSQC-TOCSY spectrum (Figure 1) of poly(vinyl alcohol) (PVA) in DMSO-d₆ at 100°C, the signals around δ68.2-63.7 and δ46.0 - 44.0 ppm are assigned to methine (-CH) and methylene (-CH₂) carbons respectively. All these carbon signals show various levels of configurational sensitivity. The signals at δ64.07, δ65.95 and δ67.73 ppm are assigned to rr, mr and mm triads respectively. These triads further shows splitting and assigned upto pentad level. In rr the signals at δ63.89, δ64.07 and δ64.25 ppm are assigned to mrrm, mrrr and rrrr respectively. The four mr centered pentads are assigned at δ65.79 (mmrm), δ65.95 (mmrr + rrrm) and δ66.13 ppm (rmrr), whereas the mm centered pentads at δ67.55, δ67.73 and δ67.94 ppm are assigned as mmmm, mmmr and rmmr respectively. These assignments can be confirmed by 2D HSQC-TOCSY experiment. Since both heteronuclear (C-H) and homonuclear (H-H) correlations are established in a single 2D experiment, the resulting spectrum has the high resolution of ¹³C spectrum and high sensitivity of proton nuclei. The methine is more sensitive than methylene. In the spectrum apart from the direct (C-H) correlation crosspeaks (Figure 1 a and c), relayed coupling by magnetization transfer through the spin system (H-H) are also observed (Figure 1 b and d). The methine proton signals were assigned from the one to one correlations with the corresponding methine carbons (Figure 1a).

The corresponding relay peaks, arising from the magnetization transfer from CH protons to the neighboring CH₂ protons confirm the methine carbon assignments (Figure 1 b).

The CH proton in the rrrr pentad gives relay peak to the CH₂ protons in rr tetrad at δ64.25/1.43 ppm whereas the mrrr pentad will give relay peaks to rrr

($\delta 64.07/1.45$ ppm) and mrr ($\delta 64.07/1.43$ ppm). The third r centered pentad mrrm shows one relay crosspeak at $\delta 63.89/1.45$ ppm. The CH proton in mrrm pentad show relay peaks to the CH₂ protons in mmr ($\delta 65.79/1.51$ ppm) and mrm ($\delta 65.79/1.46$ ppm) tetrads, whereas the mrrr and rrrm pentads show relay peaks to the CH₂ protons in mmr ($\delta 65.95/1.51$ ppm), mrr ($\delta 65.95/1.45$ ppm), and rmr ($\delta 65.95/1.49$ ppm), mrm ($\delta 65.95/1.45$ ppm) tetrads respectively. The other mr centered pentad (rmrr) show relay peak to rmr ($\delta 66.13/1.49$ ppm) and mrr ($\delta 66.13/1.45$ ppm) tetrads. Similarly the CH protons in the mm centered (mrrm, mrrr and rrrm) pentads will show CH/CH₂ three bond coupling with mmm ($\delta 67.55/1.48$ ppm), mmm ($\delta 67.73/1.48$ ppm), mmr ($\delta 67.73/1.51$ ppm), rmm ($\delta 67.94/1.51$ ppm) tetrads. All these assignments are summarized in the Table 1.

Table 1. The methine Carbon Crosspeaks and Their Corresponding Pentads

<i>Peak No.</i>	<i>Pentads</i>	<i>Corresponding Tetrads crosspeaks (ppm)</i>
1	mrrm	mrr ($63.89/1.45$) + rrm ($63.89/1.45$)
2	mrrr	mrr ($64.07/1.45$) + rrr ($64.07/1.43$)
3	rrrr	rrr ($64.25/1.43$) + rrr ($64.25/1.43$)
4	mmrm	mmr ($65.79/1.51$) + mrm ($65.79/1.46$)
5	mmrr + rrrm	mmr ($65.95/1.51$) + mrr ($65.95/1.45$) rmr ($65.95/1.49$) + mrm ($65.95/1.46$)
6	rmrr	rmr ($66.13/1.49$) + mrr ($66.13/1.45$)
7	mrrm	mmm ($67.55/1.48$) + mmm ($67.55/1.48$)
8	mrrr	mmm ($67.73/1.48$) + mmr ($67.73/1.51$)
9	rrmr	rmm ($67.94/1.51$) + mmr ($67.94/1.51$)

Thus in the CH₂ protons region the r centered tetrads are assigned around $\delta 1.15$ - 1.47 ppm whereas the m centered tetrads are assigned around $\delta 1.43$ - 1.60 ppm. After assigning the CH₂ protons, one can assign the methylene carbon of PVA. The methylene carbon assignments of PVA given by us are similar to those given by Matsuzaki et al¹⁰. The methylene carbon in rrr ($\delta 45.39$ ppm) tetrad shows one cross peak at $\delta 1.43$ ppm. The rmr ($\delta 45.03$ ppm) tetrad shows two crosspeaks to the two non-equivalent protons at $\delta 1.49$ and $\delta 1.45$ ppm (Figure 1c). The crosspeaks at $\delta 44.53/1.51$ and $\delta 44.53/1.46$ ppm are assigned to mmr and mrm tetrads respectively. Similarly the CH₂ protons in the mmm tetrad is assigned at the crosspeak $\delta 44.16/1.48$ ppm. These assignments of the methylene carbons can also be confirmed by analyzing the corresponding relay peaks to the methine protons.

Conclusions

Poly(vinyl alcohol) prepared by the basic hydrolysis of poly(vinyl acetate) was characterized by two-dimensional NMR spectroscopy. The methylene and methine carbon resonances were assigned to tetrad and pentad configurational sequences. These assignments were justified with the help of 2D HSQC-TOCSY NMR experiment.

Acknowledgements

The authors wish to thank the Department of chemistry, Indian Institute of Technology, Delhi and Council of Scientific and Industrial Research (CSIR), India, for providing the funding and NMR facility for this work.

References

1. Dong, L.; Hill, D.J.T.; O'Donnell, J.H.; Whittakar, A.K. *Macromolecules* **1994**, *27*, 1830.
2. Bulai, A.; Jimeno, M.L.; Roman, J.S. *Macromolecules* **1995**, *28*, 7363.
3. Suchoparek, M.; Spevacek, J. *Macromolecules* **1993**, *26*, 102.
4. Asakura, T.; Nakayama, N.; Demura, M.; Asano, A. *Macromolecules* **1992**, *25*, 4876.
5. Dutta, K.; Mukherjee, M.; Brar, A.S. *J Polym Sci, Part A, Polym Chem* **1999**, *37*, 551.
6. McCord, E.F.; Shaw, Jr. W.H.; Hutchinson, R.A. *Macromolecules* **1997**, *30*, 246.
7. Crowther, M. W.; Szeverenyi, N. M.; Levy, G. C. *Macromolecules* **1986**, *19*, 1333.
8. Ovenall, D.W. *Macromolecules* **1984**, *17*, 1458.
9. Terao, T.; Maeda, S.; Saika, A. *Macromolecules* **1983**, *16*, 1535.
10. Matsuzaki, K.; Uryu, T.; Asakura, T. "NMR Spectroscopy and Stereoregularity of Polymers", Japan Scientific Societies Press, Tokyo **1996**.
11. Dutta, K.; Brar, A.S. *J Polym Sci, Part A, Polym Chem* **1999**, *37*, 3922.

Chapter 14

2D NMR of Polymers: Comparison of Some of the Standard Pulse Sequences

Richard A. Newmark, John L. Battiste, and Michael N. Koivula

**3M Corporate Analytical Technical Center, 3M Center Building,
201-BS-05, St. Paul, MN 55144**

Good 2D NMR spectra can usually be obtained on the backbone protons and carbons of polymers despite their short transverse relaxation times. Off-diagonal correlations found in proton-proton (TOCSY) 2D spectra show better signal/noise than analogous gCOSY 2D spectra because of cancellation of anti-phase multiplets. Long range $^{\text{J}}\text{CH}$ correlations are best observed using gHMBC spectra optimized for 8 or 10 Hz correlations instead of 5 Hz even though the long range couplings are probably closer to 5 Hz. Although accordion pulse sequences are excellent for observing correlations in small molecules, they do not work well for backbone or ring carbons with short transverse relaxation times (T_2).

Two dimensional and multi-pulse NMR experiments are an invaluable tool in an industrial analytical laboratory in order to determine the chemical structures of commercial polymers used in new products, impurities in production lots, or to analyze for differences between lots of samples which may be the source of production problems. Although numerous text books are available which describe the experiments, (1,2,3) there is little information comparing the pulse sequences for spectra of unknown polymers in which short spin-spin relaxation times (T_2) of the backbone protons and carbons can dramatically impact the signal/noise in the 2D experiments. We have compared gCOSY (gradient CORrelation SpectroscopY) and TOCSY (TOtal CORrelation SpectroscopY) spectra for proton-proton correlations, gHMBC (gradient Heteronuclear Multiple Quantum Correlation), gHSQC (gradient Heteronuclear Single Quantum Correlation), and HETCOR spectra for one bond ^1H , ^{13}C heteronuclear correlations, and gHMBC (gradient Heteronuclear Multiple Bond Correlation) and accordion enhanced gHMBC spectra for long range heteronuclear correlations in three commercially available polymers, cellulose acetate butyrate (CAB, **I**), poly(2-ethylhexyl acrylate) (**II**), and a 50:50 copolymer (**III**) of n-butyl (**IIIa**) and i-butyl (**IIIb**) methacrylate.

Assignments

The ^1H and ^{13}C chemical shifts and assignments (based on the 2D NMR analyses) are given in Table I. The assignments of the acrylates and methacrylates have been published; a recent review with spectra is by Brandolini and Hills (but note the backbone assignments in the acrylates and methacrylates are reversed and the OCH_2 protons misassigned in **III** in this reference) (4). The ^1H and ^{13}C assignments for cellulose esters has been described in a recent review by Lowman (5). We obtained spectra of CAB in acetone; the chemical shifts and degeneracy observed in the ^1H spectrum in this solvent are different than those in reference 5, but the order of shifts is the same.

Relaxation Times: Included in Table I are most of the T_1 (spin-lattice) and T_2 (spin-spin) relaxation times; the proton T_2 's are estimated for multiplets in which cross correlation occurs since coupling between protons results in a modulation of the peak intensity (3). The only accurate ^1H T_2 values are from the methyl on the backbone in the methacrylates since all other protons are unresolved multiplets. The relaxation times are included in Table I since they have a significant and often unappreciated impact on the signal/noise of 2D NMR experiments. Derome (1) has shown that optimal recycle times for 2D experiments are 1.3 times T_1 for the best signal/noise. Further, numerous arti-

Table I. ^1H and ^{13}C Chemical Shifts, Assignments, and T_1 and T_2 relaxation times (sec) for cellulosic CH in I and all carbons in II - IV. Chemical shifts are given for the centers of the multiplets

Assignment	^1H	^{13}C	^{13}C	^{13}C	^1H	^1H
	δ	δ	T_1	T_2	T_1	T_2
I, CAB, 1-CH	4.70	101.01	0.37	0.028	1.6	0.026
I, CAB, 2-CH	4.70	72.31	0.34	0.023	1.6	0.026
I, CAB, 3-CH	5.08	72.96	0.36	0.020	1.6	0.014
I, CAB, 4-CH	3.79	77.08	0.36	0.018	1.5	0.023
I, CAB, 5-CH	3.79	73.58	0.35	0.023	1.5	0.023
I, CAB, 6-CH ₂	4.15, 4.43	63.27	0.26	0.020	1.4	0.012
II, 2EH CH ₃ -6	0.85	13.86	2.13	0.22	1.1	0.30
II, 2EH CH ₂ -5	1.20	22.78	1.20	0.25		
II, 2EH CH ₂ -4	1.28	28.68	0.69	0.22		
II, 2EH, CH ₂ -3	1.30	29.96	0.40	0.19		
II, 2EH, CH-2	1.50	38.31	0.46	0.21	0.61	
II, 2EH, CH ₂ OH	3.90	66.70	0.29	0.09	0.60	0.08
II, 2EH, CHCH ₂ CH ₃	1.20	23.41	0.39	0.15		
II, 2EH, CHCH ₂ CH ₃	0.86	10.52	1.53	0.15	1.1	0.30
II, 2EH CO		174.20				
II, backbone CH ₂	1.9, 1.5	35.14	0.17	0.025	0.73	0.05
II, backbone CH	2.20	41.32	0.33	0.048	0.83	0.05
IIIa, Bu Me	0.99	13.60	2.00	0.16		
IIIa, Bu CH ₂ Me	1.28	19.20			0.90	
IIIa, Bu CH ₂ CH ₂ O	1.42	30.30	0.56	0.15	0.72	
IIIa, Bu CH ₂ O	3.96	63.10	0.42	0.08	0.92	0.04
IIIb, iBu CH ₃	0.99	19.20	0.79		0.72	
IIIb, iBu CH	1.95	27.40	0.55	0.15		
IIIb, iBu CH ₂ O	3.73	70.90	0.37	0.06	0.88	
III backbone CH ₂	1.84, 1.95	54.20	0.20	0.024	0.60	0.04
III backbone C		44.90	2.31	0.13		
III backbone CH ₃	0.90, .99	18.1, 16.4	0.10	0.03	0.42	0.04
IIIa, CO		176.60	1.21	0.20		
IIIb, CO		177.40	1.28	0.25		

facts can occur and lead to incorrect assignments when recycle times are less than T_1 (1,6). Finally, exponential T_2 relaxation occurs during the evolution time of 2D array experiments and irreversibly reduces the signal intensity which can be observed during the acquisition. The observed intensity is reduced by 63% in time T_2 .

Experimental: Spectra were obtained on a Varian INOVA spectrometer operating at 500 MHz (^1H) on commercially available polymers using the vendor supplied pulse sequences on a dual broadband probe with a ^{13}C inner coil. Typical absolute value gCOSY and phase sensitive TOCSY spectra were obtained in 9 minutes and 18 minutes, respectively, using 1 transient/increment with 256 increments for the absolute value gCOSY and 2 transients with 128 increments for the phase sensitive TOCSY or DQCOSY spectra. More transients (4 or 16) doubles or quadruples the signal/noise, but does not change the qualitative appearance of the homonuclear correlation spectra. gHMBC and accordion (7) spectra were time averaged for 3.5 hours with 256 increments, a 0.19 sec acquisition time, and a relaxation delay of 0.75 sec for poly-2-ethylhexyl acrylate and 1.12 sec for the copolymer of iso-butyl and n-butyl methacrylate. Standard weighting (sinebell for gCOSY and gaussian for the other experiments) based on the inverse acquisition time of each experiment was employed in order to simulate the conditions that would be typical in a high throughput industrial laboratory. The accordion and gHMBC spectra were also obtained at 32 and 64 increments on the copolymer III. Relaxation times were measured using the inversion recovery and Carr-Purcell Meiboom-Gill pulse sequences (3). The values in Table I were determined using the vendor supplied 3 parameter least squares fit to the peak intensities, except for the ^1H T_2 which was estimated from peak heights after correcting for some of the signal modulation due to cross relaxation (3).

Results and Discussion

Numerous multipulse and two dimensional experiments are used to identify unknown (co)polymers and these experiments are most useful in analyzing differences between copolymers or impurities in production problems. The Distortionless Enhancement via Polarization Transfer (DEPT) pulse sequence is frequently used to determine the carbon multiplicity (CH vs. CH_2 vs. CH_3) of a carbon spectrum. Newmark showed excellent DEPT spectra could be obtained on sidechain groups in vinyl polymers or in typical polyesters and polyurethanes, but that it was difficult to observe good DEPT spectra (at 200 MHz) on backbone carbons, such as the ring carbons in cellulose acetate butyrate (CAB) with very short carbon spin-spin relaxation times (T_2) (8).

Homonuclear Correlations: The gCOSY two dimensional (2D) NMR experiment is a very rapid technique to determine if protons are mutually

coupled. The gCOSY spectrum of the cellulose ring protons of **I** is shown in Figure 1. The off-diagonal elements indicate correlations between mutually coupled protons, but the spectrum shows very poor signal/noise (s/n) in the region of the ring protons. However, excellent TOCSY spectra are observed for the cellulose ring protons in CAB (Figure 2) with 3-fold stronger off-diagonal elements (relative to the noise). TOCSY (total correlation spectroscopy) is similar to gCOSY but also displays relayed gCOSY correlations from all coupled protons within a spin system. For short mix times (such as 20 msec, Figure 2), only gCOSY type correlations should be observed whereas all the relayed correlations (up to about six bonds) are observed with longer mix times (80 msec, Figure 3) (2). Although the H-2/H-3 (4.70/5.08 ppm) and H-3/H-4 (5.08/3.79 ppm) correlations are observed in both the gCOSY and TOCSY 20 msec spectra (Figs. 1-2), the improved signal/noise makes the assignment unambiguous in the TOCSY spectrum. In less concentrated solutions it is often impossible to observe critical gCOSY correlations. But note some of the gCOSY type correlations can be lost in TOCSY spectra with long mix times as the magnetization is transferred along the chain. Thus in CAB the two geminally inequivalent protons in the CH₂O, at 4.15 and 4.43 ppm, show correlations in the gCOSY and TOCSY 20 msec spectra (Figs. 1-2), but not in the 80 msec TOCSY spectrum (Figure 3). Double quantum gCOSY (DQCOSY or gDQCOSY) 2D spectra also showed very weak correlations. In summary, while one might expect TOCSY experiments to be relatively insensitive because of potential relaxation in the rotating frame during the spin-lock mixing time, TOCSY is quite robust for observing correlations of even the backbone protons of polymers. The TOCSY spectra show improved s/n since the TOCSY mixing step avoids signal cancellation due to overlap of broadened antiphase multiplets in a gCOSY spectrum (2); TOCSY has been recommended for 3D diffusion-ordered spectra in preference to the analogous COSY type experiments (9).

Heteronuclear Correlation Experiments: A comparison of HMQC, HSQC, and the analogous gradient experiments used to correlate one bond proton and carbon chemical shifts (¹J_{CH}) showed little differences. In all cases the signal/noise for the backbone CH₂ of a methacrylate copolymer was identical within experimental error. As expected, the ¹³C detected heteronuclear detection experiment (HETCOR) showed significantly (~ 4 fold) lower s/n.

Space does not permit including a description of the gHMBC or accordion pulse sequences used to obtain long range ⁿJ_{CH} coupling constants; they are described in detail in the literature (1,2,7). It is well known that the multiple bond correlations observed in long range indirect detection experiments are very sensitive to the choice of the delay corresponding to ⁿJ_{CH}. The major part of the evolution time in the gHMBC type experiments is proportional to 1/(ⁿJ_{CH}) to allow correlations to build up, or 100 to 36 msec for the 5 to 14 Hz range in ⁿJ_{CH}

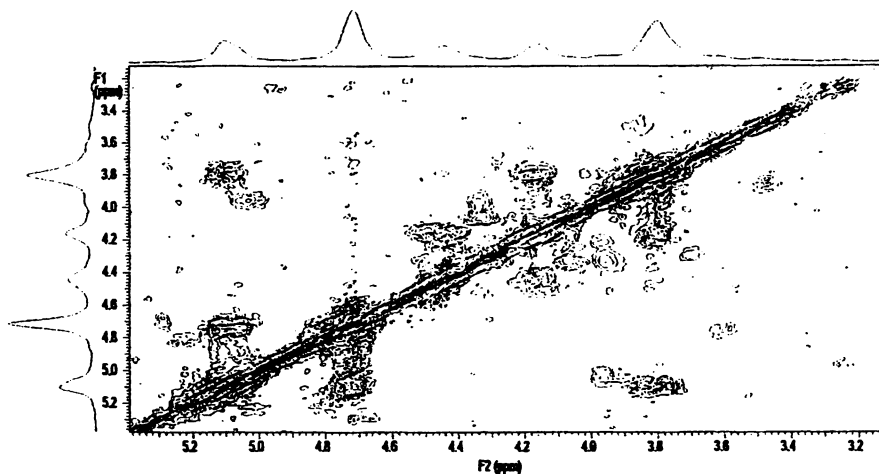


Figure 1. 2D gCOSY spectrum of cellulose acetate butyrate (CAB), 1 transient & 256 increments (9 minutes). Contour spacing in all figures is a factor of 1.7.

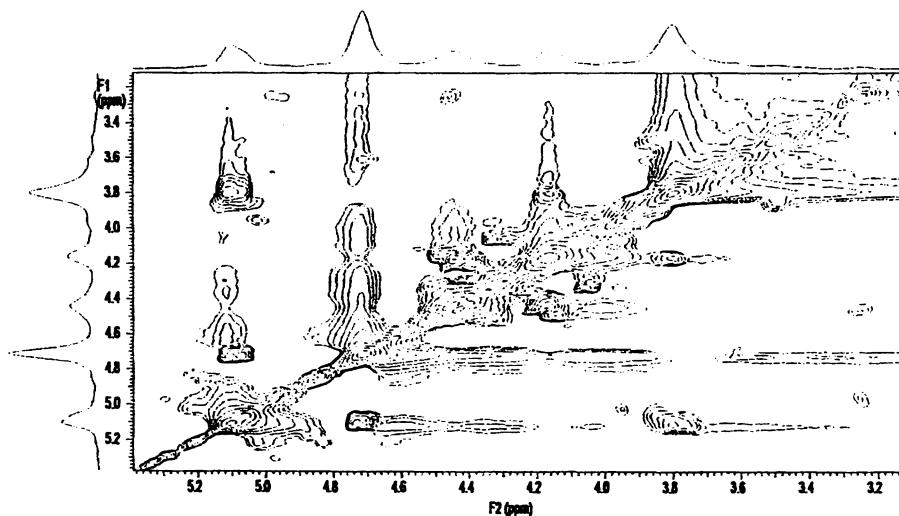


Figure 2. 2D TOCSY spectrum of (CAB) with a 20 msec mix time; 2 transients (phase sensitive) and 128 increments. Contour spacing is a factor of 1.7.

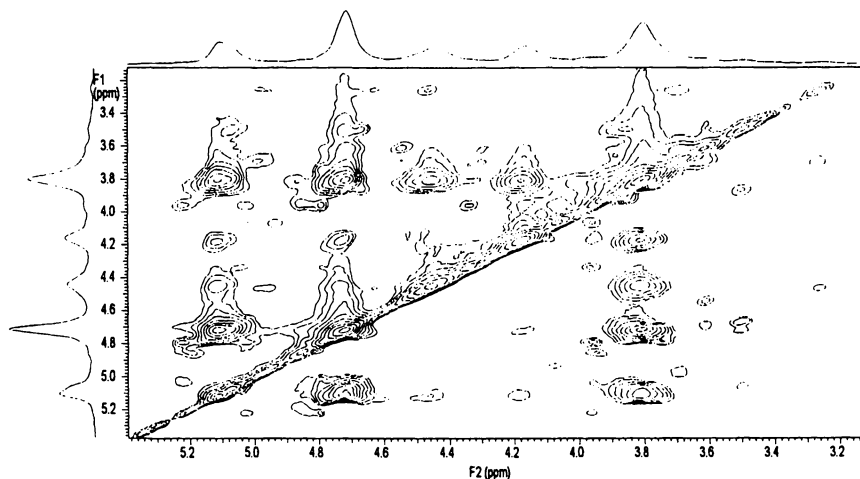


Figure 3. 2D TOCSY spectrum of (CAB) with a 80 msec mix time.

used in Table I. Additional delays are incorporated into the pulse sequence to allow for gradient recovery and the 2D array. The total time between the excitation pulse of the 2D sequence and the acquisition is included in Tables II and III. This time is variable in the gHMBC experiment, but the same for all increments in the constant time accordion pulse sequence. The variation due to the number of increments is minor compared to the delay required for the evolution of the long range spin coupling, although some signal/noise loss will still occur if too many increments are used in the gHMBC experiment. Table II gives the signal/noise for a few typical long range correlations to the backbone carbons of copolymer III in a gHMBC experiment and in a recently described accordion pulse sequence experiment (7). The latter has been shown to give excellent long range correlations (especially ${}^4J_{\text{CH}}$) in strychnine (7) including correlations which are not observed in a regular gHMBC experiment; the accordion sequence is much less sensitive to the value of ${}^nJ_{\text{CH}}$. However, the opposite is observed with the methacrylate copolymer and CAB such that many long range correlations to the backbone carbons are much weaker or not observed (Table II). Similar results are observed for a polymer of 2-ethylhexyl acrylate (Table III).

Examples of accordion and normal gHMBC spectra of poly(2-ethylhexyl acrylate) are shown in Figs. 4 and 5, respectively. The accordion correlations to the backbone CH_2 resonances centered at 1.86 ppm are very weak, but readily observed in the gHMBC spectrum with 3-fold greater intensity than the accordion spectrum. The intensities of the gHMBC correlations are a sensitive

Table II. Signal/noise of Long Range gHMBC or Accordion type Intensities vs. $^nJ_{CH}$ from the CO to the OCH_2 of the n-Bu or to the backbone CH_2 in a 50:50 Copolymer of iso-Butyl and n-Butyl Methacrylate (III). The total evolution time is approximately the sum of the $1/2J$ and 2D array delays.

<i>experiment</i>	$^nJ_{CH}$	<i>C=O to</i> <i>1.83</i> <i>backbone</i>	<i>C=O to</i> <i>3.93</i> <i>OCH₂</i>	<i>1/2J</i> <i>delay</i> <i>(msec)</i>	<i>2D array</i> <i>delay</i> <i>(msec)</i>
gHMBC	5	6	43	100.0	0-10
gHMBC	8	72	132	62.5	0-10
gHMBC	11	94	74	45.5	0-11
gHMBC	14	100	57	35.7	0-11
accordion	2-10	0	1	250.0	15
accordion	3-8	3	8	166.7	15
accordion	5-10	0	16	100.0	15

Table III. Signal/noise of Long Range gHMBC or Accordion type Intensities vs. $^nJ_{CH}$ from the CO to the OCH_2 , and to the $CHCH_2$ backbone protons in poly(2-ethylhexylacrylate)

<i>experiment</i>	$^nJ_{CH}$	<i>polymer</i> <i>C=O to</i> <i>1.86 CH₂</i>	<i>polymer</i> <i>C=O to</i> <i>2.25 CH</i>	<i>polymer</i> <i>C=O to</i> <i>4.00</i>	<i>monomer</i> <i>C=O to</i> <i>4.02</i>	<i>evolution</i> <i>time</i> <i>(msec)</i>
accordion	5-11	3.4	4.5	26	41	115
accordion	8-14	6	171	170	45	78
gHMBC	5	8	9	78	71	105-115
gHMBC	6.5	10	83	153	27	81-92
gHMBC	8	30	245	90	20	67-78
gHMBC	9.5	22	105	102	30	57-68
gHMBC	11	19	42	96	20	50-61
gHMBC	14	8	12	94	10	40-51
gHMBC	17	8	6	34	4	34-45

function of the delay corresponding to the long range coupling constant. Table III gives the relative s/n for the correlations from the carbonyl to the backbone CH_2 at 1.86 ppm, backbone CH at 2.25 ppm, and OCH_2 at 4.00 ppm. This sample also contained 4% residual monomer and the s/n for the correlations of the monomer CO to the monomer OCH_2 at 4.02 ppm are also included in the table. Although the monomer is only at the 4% level, it has a much longer T_2 and the correlations to the monomer OCH_2 are comparable to those observed in the polymer for spectra run with long delays even though the monomer concentration is 25 fold lower. The strongest correlations for the monomer are observed for the spectrum when the delay corresponds to a coupling of 5 Hz,

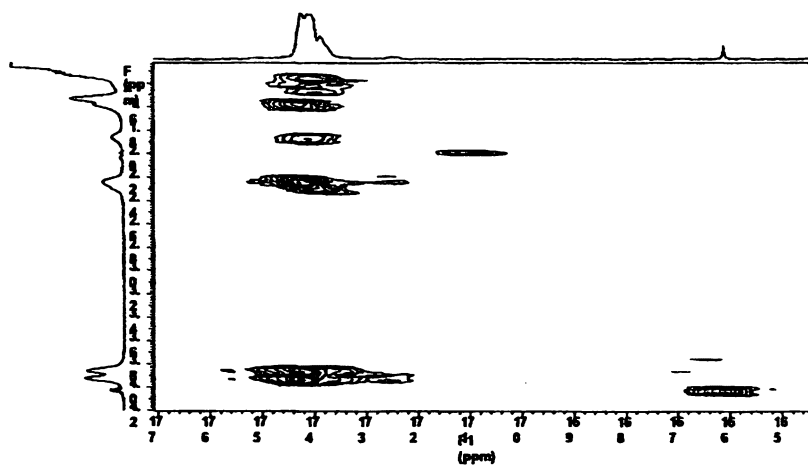


Figure 4. 2D gHMQC spectrum of poly-2-ethylhexyl acrylate optimized for ${}^nJ_{CH} = 8$ Hz. Contour spacing in all figures is a factor of 1.7.

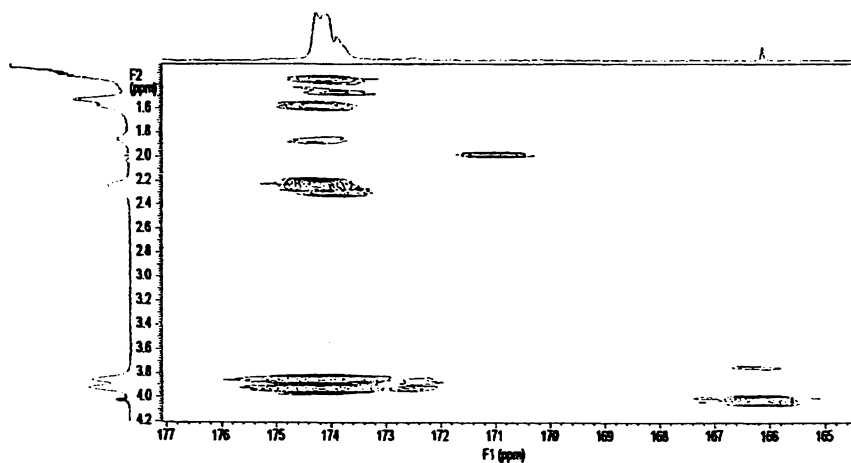


Figure 5. Accordion⁴ 2D spectrum of poly-2-ethylhexyl acrylate optimized for ${}^nJ_{CH} = 8$ to 14 Hz.

whereas the strongest correlations in the polymer occur at 8 or 11 Hz. The backbone relaxation times are approximately 20 to 40 msec and a 63% reduction in the intensity of the correlations is thus expected if the duration of the gHMBC pulse sequence is lengthened by 20 to 40 msec. The intensities in Tables II - III thus reflect a competition between the optimum value of ${}^nJ_{\text{CH}}$ (probably under 5 Hz) and T_2 . The dramatic decreases in intensity for the sequence optimized to ${}^nJ_{\text{CH}}$ suggests the backbone T_2 may be even less than 40 msec.

The diminished intensity in this particular accordion gHMBC is probably due to the constant time interval used to remove unwanted J-coupling modulation in the indirectly detected dimension. In the constant time mode, the total time for heteronuclear transfer is inversely proportional to the smallest J-coupling value of the accordion array (typically 5 Hz), such that magnetization loss from T_2 relaxation becomes even more significant for polymers. Hence, for polymers, caution must be taken when using pulse sequences designed for small organic molecules. The results obtained in this study suggest the best 2D spectra can be obtained with the standard gHMBC pulse sequence with a large J-coupling value (8-10 Hz), which keeps the delay short and is a good compromise for sensitivity of small J-coupling values by minimizing relaxation losses. Alternatively, Rinaldi et al have pointed out that increasing the temperature will increase T_2 and give better gHMBC NMR spectra (10).

Although the results reported in the tables were from spectra obtained with 256 increments, corresponding to 93 Hz resolution in the ${}^{13}\text{C}$ spectrum, better signal/noise is achieved (at minimal cost in resolution if linear prediction is used) for the backbone protons with 32 or 64 increments. We find a typical increase in signal/noise of about 3 using 64 increments instead of 256 increments, but with a loss in resolution which makes assignments of closely spaced ${}^{13}\text{C}$ multiplets more difficult.

Conclusion

Excellent 2D NMR spectra can be obtained on the backbone protons and carbons of polymers despite their short transverse relaxation times, but TOCSY spectra with short mix times are recommended in place of gCOSY spectra to avoid anti phase cancellation of the correlations. Long range ${}^nJ_{\text{CH}}$ correlations are best observed using gHMBC spectra optimized for 8 or 10 Hz correlations instead of 5 Hz even though the long range couplings are probably closer to 5 Hz. Although accordion (7) pulse sequences are excellent for observing correlations in small molecules, they do not work well for backbone or ring carbons with short transverse relaxation times (T_2).

Acknowledgements

The authors thank James Hill for his help in running the spectra and Gary Martin (Pharmacia) for helpful discussions.

References

1. Derome, A. E. *Modern NMR Techniques for Chemistry Research*; Pergamon Press: New York, NY, 1987, p. 212.
2. Claridge, T. D. W.. *High-Resolution NMR Techniques in Organic Chemistry*; Pergamon Press: New York, NY, 1999.
3. Atta-ur-Rahman, *Nuclear Magnetic Resonance: Basic Principles*; Springer-Verlag: New York, NY, 1986, pp 123-128.
4. Brandolini, A. J.; Hills, D. D. *NMR Spectra of Polymers and Polymer Additives*; Marcel Dekker: New York, NY, 2000, pp 200, 216-219
5. Lowman, D. W. ACS Symp. Ser. **1998**, 688 (Cellulose Derivatives), 131.
6. Newmark, R. A.; Boardman, L. D.; Siedle, A. R. *Inorg. Chem.* **1991**, *30*, 853-6.
7. Hadden, C. E.; Martin, G. E.; Krishnamurthy, V. V., *Magn. Reson. Chem.* **2000**, *38*, 143.
8. R. A. Newmark, *Appl. Spectroscopy* **1985**, *39*, 507.
9. Jerschow, A.; Muller, N. *J. Magn. Reson. Series A*, **1996**, *123*, 222.
10. Liu, W.; Ray, D. G. I; Rinaldi, P. L.; Zens, T., *J. Magn. Reson. Series A.* **1999**, *140*, 482.

Chapter 15

Recent Advances in the NMR Description of Polypropylene

V. Busico¹, L. Mannina², A. L. Segre^{3,*}, and V. Van Axel Castelli¹

¹Dipartimento di Chimica, Università di Napoli “Federico II”, via Cintia, 80126 Napoli, Italy

²Dipartimento di Scienze MM.FF.NN., Università del Molise, via Mazzini 8, 86170 Isernia, Italy

³Istituto di Metodologie Chimiche, Consiglio Nazionale delle Ricerche, C.P. 10, 00016 Monterotondo stazione, Roma, Italy

The significance of a monomer sequence distribution is higher, the longer is the sequence length that can be attained. The complete assignment of ¹³C spectrum of regio-regular polypropylene at 150 MHz was recently accomplished in our laboratory. From ad hoc synthesized polymers through a simple set of semi-empirical rules we obtained the full assignment of methyl and methylene resonances of the ¹³C 150 MHz spectrum. Moving from the initial assignment of the well-resolved methyl region, through a cumbersome INADEQUATE experiment it was possible to achieve also that of the much more “crowded” methine regions.

A very interesting 1D INADEQUATE experiment allowed us to further improve the assignment of resonances in the methine region. On the other hand a ¹³C 200 MHz experiment gave us the opportunity to unambiguously detect the methyl resonance of the typical junction stereosequence *rrrrrrmmmm*.

Another advantage of high-field ¹³C NMR is that the resonances arising from “anomalous” stereosequences close to the chain ends can be recognized and explicitly evaluated also for relatively short chains.

Introduction

The mechanistic study of Ziegler-Natta and related catalysts represents a very interesting field of study (1). Despite of this, several considerations limit the direct analysis. In most cases only a (very) small fraction of the transition metal atoms are catalytically active. This holds not only for heterogeneous catalysts, but for homogeneous catalysts as well. In the case of heterogeneous catalysts, several classes of active species with different productivities and/or selectivities are invariably present. Our understanding of the surface structure, mainly relying on crystallochemical considerations, is limited and made difficult by the known occurrence of reconstruction phenomena. Another limitation is the fact that the coordination of the monomer to the active metal is weak (back-donation missing or unimportant for early transition metals), and the activation barrier for its insertion into the metal-carbon bond is usually low. This implies that it is virtually impossible to intercept reaction intermediates, even at very low temperatures, with only a few "special" exceptions. In the view of the above, a "direct" investigation of the catalytic species is practically unfeasible.

The most useful approach is the "indirect" mechanistic study in which the polymer microstructure represents the fingerprint of the catalyst (2). A polymer chain is a permanent record of the statistical chain of events which constituted the polymerization process. With appropriate tools the information can be decoded so as to reveal not only the various monomer reaction modes and to measure their relative rates, but also to infer their interdependence. This represents an extraordinary advantage in the study of reaction selectivities, compared with the case of low-molecular-mass products; the longer is the chain segment that can be considered, the richer is its message. Besides this the microstructural approach provides by definition, information exclusively on the active species. In particular, even in the case of extensive catalyst deactivation, the polymer remains a faithful and highly reproducible fingerprint, very few selective deactivation processes -if any- being known.

The statistical analysis of polypropylene stereostructure in the "routine" ^{13}C NMR is usually performed at pentad level (3). This analysis is not adequate only in the following cases: *i*) polymers from multisite catalysts (at least 5 adjustable parameters for "only" 3 different active species); *ii*) polymers from "fluctuating" catalysts (at least 4 adjustable parameters); *iii*) weakly tactic polymers (all models degenerate into the Bernoullian statistics). In most such cases, however, unambiguous conclusions can be reached from the analysis of high-field ^{13}C NMR data at heptad/nonad level.

Experimental

Inversion-recovery experiments devoted to determine the relaxation times T_1 of $\{^1\text{H}\}^{13}\text{C}$ nuclei in an undegassed polypropylene sample have been

performed at 150 MHz (4). Results are summarized in Table I. Experimental data show that each ^{13}C nucleus is characterized not only by a different T_1 value depending on the number of directly bond hydrogen nuclei (dipolar relaxation mechanism) but that stereochemical environment plays also a role (5). As a consequence, for any quantitative analysis, the choice of the proper delay time is fundamental ($>5 T_1$). Methyl groups are characterized, as expected, by the longer T_1 . On the other hand, on methyl resonances, the observed differences are well within the experimental error. Thus even if methyl resonances are not completely relaxed during the recycling time, the observed internal distribution of stereosequences is not affected. In the case of methylene and methine resonances, despite of a relatively fast recycling time, larger differences -up to 25% for CH_2 and 22% for CH - are observed in T_1 times for different stereosequences. On the basis of this observations, at 150 MHz, typical ^{13}C NMR experiments are performed as follows: $T = 343 \text{ K}$, 12-14 mg/mL solution in 1,1,2,2-tetrachloroethane- d_2 , pulse length $\approx \pi/2$, recycling time $\approx 5 \text{ s}$.

Each experimental spectrum was subjected to a thorough mathematical analysis, based on its full simulation, by means of the program Shape 2000 (6). As an example of simulation, see Figure 1.

The quantitative stereosequence distribution was then reproduced by making use of matrix multiplication methods in the framework of appropriate stochastic models (7).

Table I. Relaxation times T_1 in undegassed polypropylene at 150 MHz

	δ (ppm)	Stereosequence	T_1 (msec)
CH_2	47.2	m r r r r	370 ± 30
CH_2	46.2	m m m m m	470 ± 30
CH	28.4	m m m m	810 ± 40
CH	28.2-28.0	r r + m r	650 ± 40
CH_3	21.9	m m m m	1190 ± 50
CH_3	20.3	r r r r	1140 ± 80

Choice of Model Polymers

The analysis of polypropylene at heptad and nonad level requires the attribution of different resonances to particular stereosequences (8). "Single-site" metallocenes represent very useful catalytic systems in order to obtain relatively

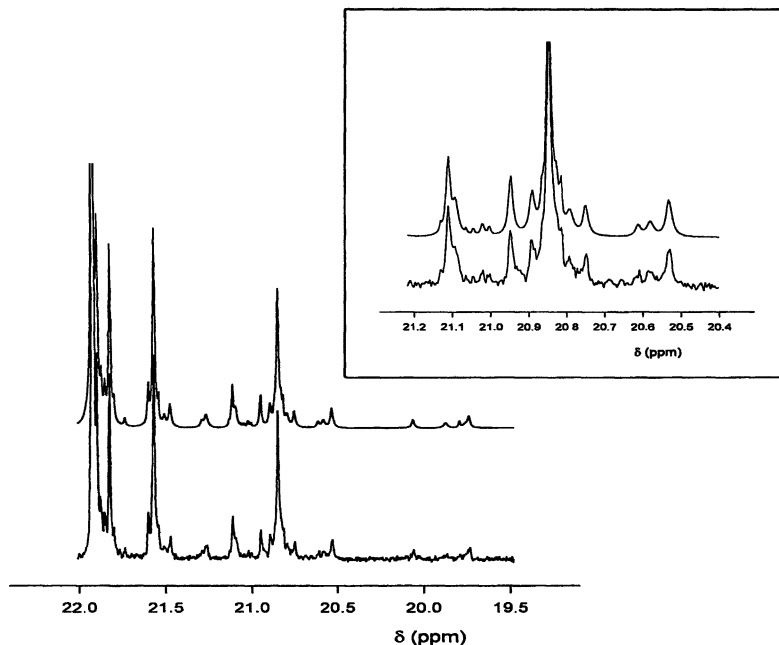


Figure 1. Methyl region of ^{13}C NMR spectrum of a polypropylene sample. Bottom: experimental spectrum. Top: full simulation. In the insert an expansion of the *mr* triad region.

simple polypropylene samples useful for the assignment. Polymers obtained with four different catalysts produce a really wide set of stereosequences such as those outlined in Chart I.

Bis(cyclopentadienyl) TiCl_2 (1) in the presence of MAO (MAO = methylalumoxane) reacts according to a chain-end mechanism to yield an isotactic polypropylene in which stereodefects with a single *r* (a) are present.

Rac-ethylenebis(4,5,6,7-tetrahydro-1-indenyl)- ZrCl_2 (2) with MAO gives rise to isotactic polymer in which stereodefects with double *r* (b) are present, according to the enantiomeric-site statistics.

$\text{Me}_2\text{C}(\text{cyclopentadienyl})(9\text{-fluorenyl})\text{ZrCl}_2$ (3) and MAO result in a predominantly syndiotactic polypropylene, characterized by the chain-migratory statistics that show both single and double *m* as defects (c).

Finally a hemiisotactic polymer (d) is obtained with the system $\text{Me}_2\text{C}(3\text{-Me-cyclopentadienyl})(9\text{-fluorenyl})\text{ZrCl}_2$ (4) / MAO.

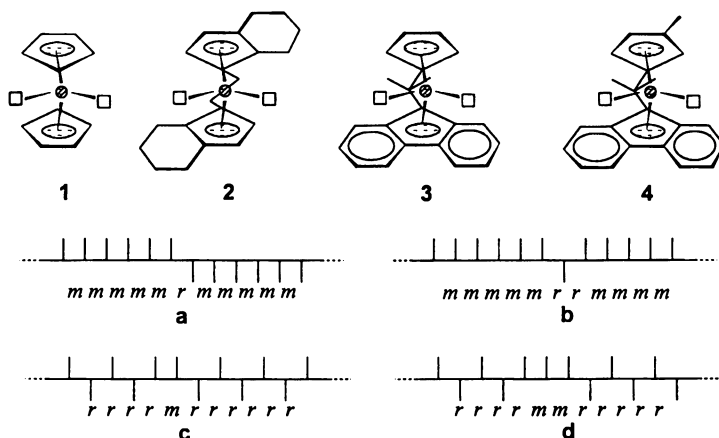


Chart I

Rules of Assignments of CH₃ and CH₂

A common way for calculating the chemical shift of different stereosequences is based on the Rotational Isomeric State (RIS) approximation (δ). In this case the effect of the conformation on the chemical shift δ of the magnetic carbon \bar{C} is ascribed to changes in populations of rotamers differing only for the $\bar{C}-C(\alpha)-C(\beta)-C(\gamma)$ dihedral angle. It can be translated into the following equation,

$$\delta = \delta_0 + \sum_i \gamma_i p_i \quad (1)$$

in which δ_0 is the conformation independent part of δ , p_i is the sum of the probabilities that each of the C(α)-C(β) bonds flanking \bar{C} be in the i -th rotational isomeric state, and γ_i is the contribution to δ of such state. The RIS model, improved by Suter on an original Flory model, was firstly introduced by Tonelli. A further common approximation is to assume that in equation (1), $\gamma_i \neq 0$ only when \bar{C} and C(γ) are in a *gauche* arrangement (γ -*gauche* effect).

Empirical rules can also be considered:

Rule 1 (methyl). The four steric n -ads (n even) centered on a given $(n-2)$ -ad can be divided in two hemistereosequences. The n -ad with both hemistereosequences containing an even number of r diads will be the one occurring at lower field. The n -ad with both hemistereosequences containing an odd number of r diads will be the one occurring at higher field. Nothing can be

said on the relative ordering of the remaining two *n*-ads, apart from a tendency to show close values of chemical shift.

Rule 2 (methylene). Let us consider the four *n*-ads (*n* odd) centered on a given (*n*-2)-ad. The four (*n*-1)-ads obtained by dropping the central diad can be divided in two hemistereosequences for which a rule opposite to *Rule 1* holds.

Rule 3 (methylene). Of two *n*-ads (*n* odd) differing *only* for the central diad, the one centered on an *m* diad will occur at lower field.

It should be noted that methylene chemical shifts can be considered the result of a "side effect" (*Rule 2*) and of a "central effect" (*Rule 3*). Their delicate balance makes the methylene region of the spectrum by far richer in peak overlaps than the methyl region.

On the basis of the previous considerations a semiempirical assignment of the observed chemical shifts was performed. Subsequently a least square multiple regression was applied to equation (1) and the following values for δ_0 and γ were obtained (8): $\delta_0(\text{CH}_3) = 27.07 \pm 0.06$ ppm, $\gamma(\text{CH}_3) = -5.24 \pm 0.06$ ppm, $\delta_0(\text{CH}_2) = 49.18 \pm 0.04$ ppm, $\gamma(\text{CH}_2) = -3.97 \pm 0.05$ ppm.

These values resulted to be very close to Tonelli's numbers ($\gamma(\text{CH}_3) = -5.3$ ppm; $\gamma(\text{CH}_2) = -3.7$ ppm) (9).

Assignment of CH

The previous method for the assignments of the observed polypropylene resonances holds for methyl and methylene regions only. In the case of methine, besides the lack of simple semiempirical rules, a relatively low resolution in the ^{13}C NMR spectrum is observed. In the case of those polypropylene samples already used for CH_3 and CH_2 , the assignment of chemical shift was performed even in the case of methine resonances (10), essentially thanks to a ^{13}C - ^{13}C correlated (INADEQUATE) 2D NMR map (11). Figure 2 shows the INADEQUATE 2D map in the region CH - CH_3 . On the basis of semiempirical calculations of methine chemical shift, it has been found that a CH group undergoes one γ -*gauche* effect in states *t* and *g* and two γ -*gauche* effects in state \bar{g} (Chart II).

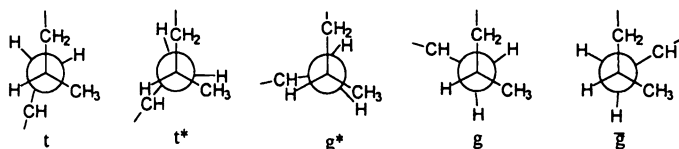


Chart II

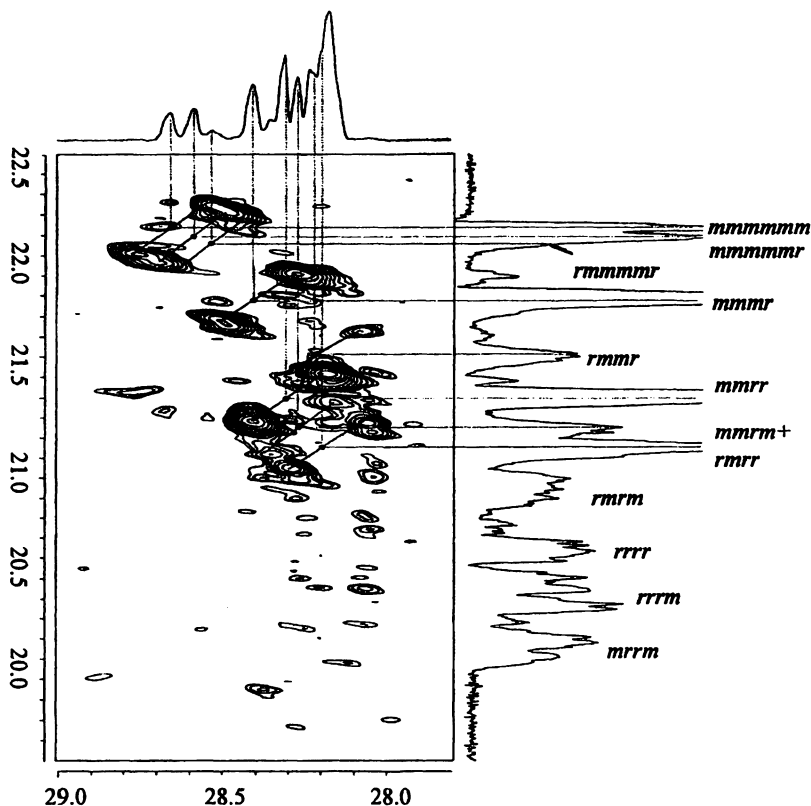


Figure 2. CH-CH₃ region of INADEQUATE 2D NMR map of polypropylene recorded at 150 MHz, $T = 343$ K, in CDCl₃-CDCl₂. (Adapted from reference 10. Copyright 1998 American Chemical Society.)

At variance with previous results the full assignment of methine resonances implies the following parameters (10): $\delta_0(\text{CH}) = 38.7 \pm 0.1$ ppm; $\gamma_t(\text{CH}) = -5.8 \pm 0.1$ ppm; $\gamma_r(\text{CH}) = -6.4 \pm 0.1$ ppm.

A significant further improvement of the above assignment was obtained in the case of syndiotactic polypropylene samples. The weak, high field peak shown in the expanded area of the syndiotactic sample in Figure 3, and previously unassigned, was selectively irradiated in a 1D selective INADEQUATE experiment. The standard BRUKER SELINA sequence (12) was used, in which the signal at 27.89 ppm was excited by means of a 90° selective gauss-shaped pulse. The following parameters were chosen: time

domain, 128 K; ^{13}C - ^{13}C coupling constant, 35 Hz; acquisition time, 4.3 s; and relaxation delay, 2 s. The expanded methyl and methylene regions of the resulting spectrum are reported in Figure 4 (top and bottom respectively).

While the methyl spectral region does not offer any further clue to the interpretation, see Figure 4-top, the CH_2 spectral region presents a small but significant splitting of the resonance due to the *rrrrrrr* octad. Thus we can assess that the small resonance centered at 27.89 ppm can be attributed to a sequence centered on *rrrrrr* heptad. On the basis of statistical data the peak is tentatively assigned to the *rrrrrrrmm* undecad.

High Field ^{13}C Spectra

For a further improvement of the above assignment, ^{13}C spectra were run at 200 MHz (a large toll is paid by the longer recycle time!). A polypropylene sample obtained with $\text{MgCl}_2/\text{TiCl}_4$ in the presence of $\text{AlEt}_3/2,6$ -dimethylpyridine was analyzed at 343 K, both at 150 MHz and 200 MHz. Expanded regions of such spectra are reported in Figures 5-8 for comparison. In the methine region (Figure 5) only a slight improvement in the resolution of the syndiotactic zone is observed. In the case of methylene (Figure 6) besides a substantial equivalence of the spectra in the low field region, some differences are observed in the *rrmmrrm* octad (Figure 6, top) as well as in the *mmmmrrm* octad and in *mmmm* region (Figure 6, middle). A better resolution is also observed in the case of the *rrmmrrr* and *mmmmrrm* octads (Figure 6, bottom). In the case of methyl resonances a fine structure emerges in the *rrmmr* pentad (Figure 7, top) and in the *mmmmrrm+mmmmrrr* region (Figure 7, middle). Minor improvements are observed in *mmrm+rmrr* pentads region (Figure 7, bottom), whereas syndiotactic region shows some interesting deconvolution (Figure 8, top). Finally a significant improvement of the resolution is evident in the case of *rrrm* and *mrrm* (Figure 8, bottom).

The splitting of peaks observed in the spectrum run at 200 MHz needs a further work for the assignment. In some cases the assignment is straightforward. In other cases an accurate analysis is required using different polypropylene samples. Note that the obtained results do not seem to add any significant and determinant data for the subsequent statistical analysis. By taking also into account the longer recycling time, ^{13}C spectral analysis of polypropylene at 200 MHz does not seem significantly advantageous on respect to the data obtained at 150 MHz. However at 200 MHz in one particular spectral region a very interesting result was observed. A picture of the expanded *rrrrmm + mrrrrm* region, where the junctions between isotactic and syndiotactic parts resonate, is reported in Figure 9. By comparing the spectra of all our model polypropylene samples (data not shown) it is possible to unambiguously recognize the *rrrrrrmmmm* resonance which is the typical junction sequence whose presence was previously supposed but never observed (2).

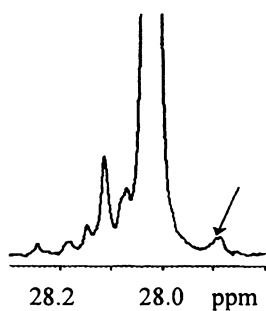


Figure 3. Methine region of a 150 MHz ^{13}C NMR spectrum ($T = 343\text{ K}$) of regioregular syndiotactic polypropylene.

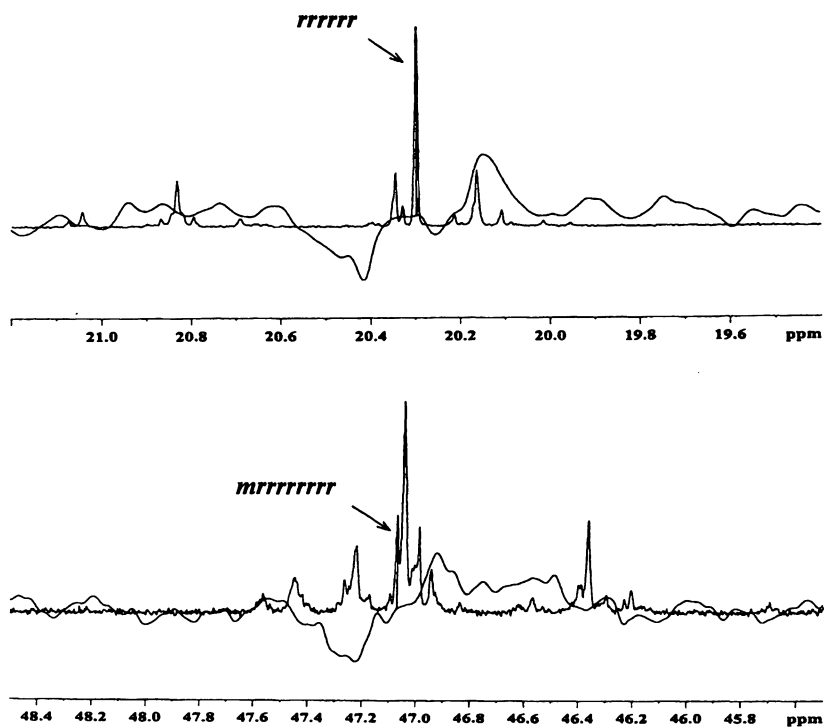


Figure 4. 1D Selective INADEQUATE spectra obtained by selective irradiation at 27.89 ppm, overlapped to ^{13}C spectra of a syndiotactic polypropylene sample. Top: methyl region. Bottom: methylene region.

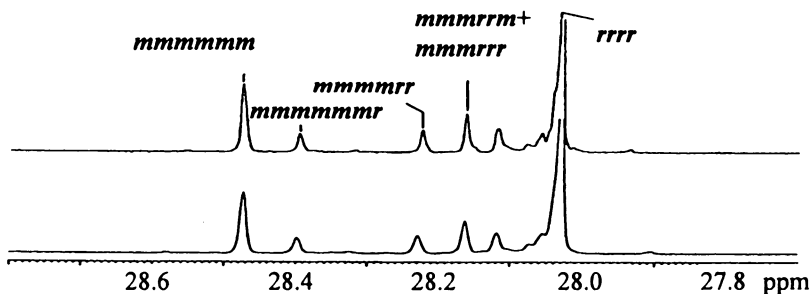


Figure 5. Methine region of ^{13}C NMR spectra of polypropylene sample recorded at 343K at different fields. Top: 200 MHz. Bottom: 150 MHz.

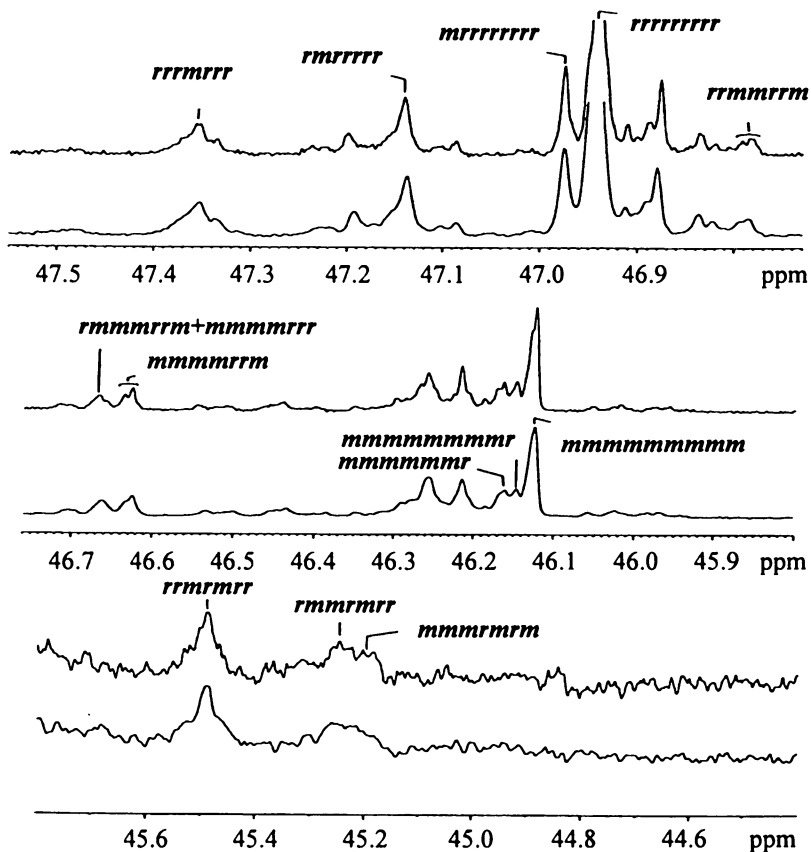


Figure 6. Portions of the methylene region of ^{13}C NMR spectra of a polypropylene sample recorded at 343 K at different fields. Top: 200 MHz. Bottom: 150 MHz.

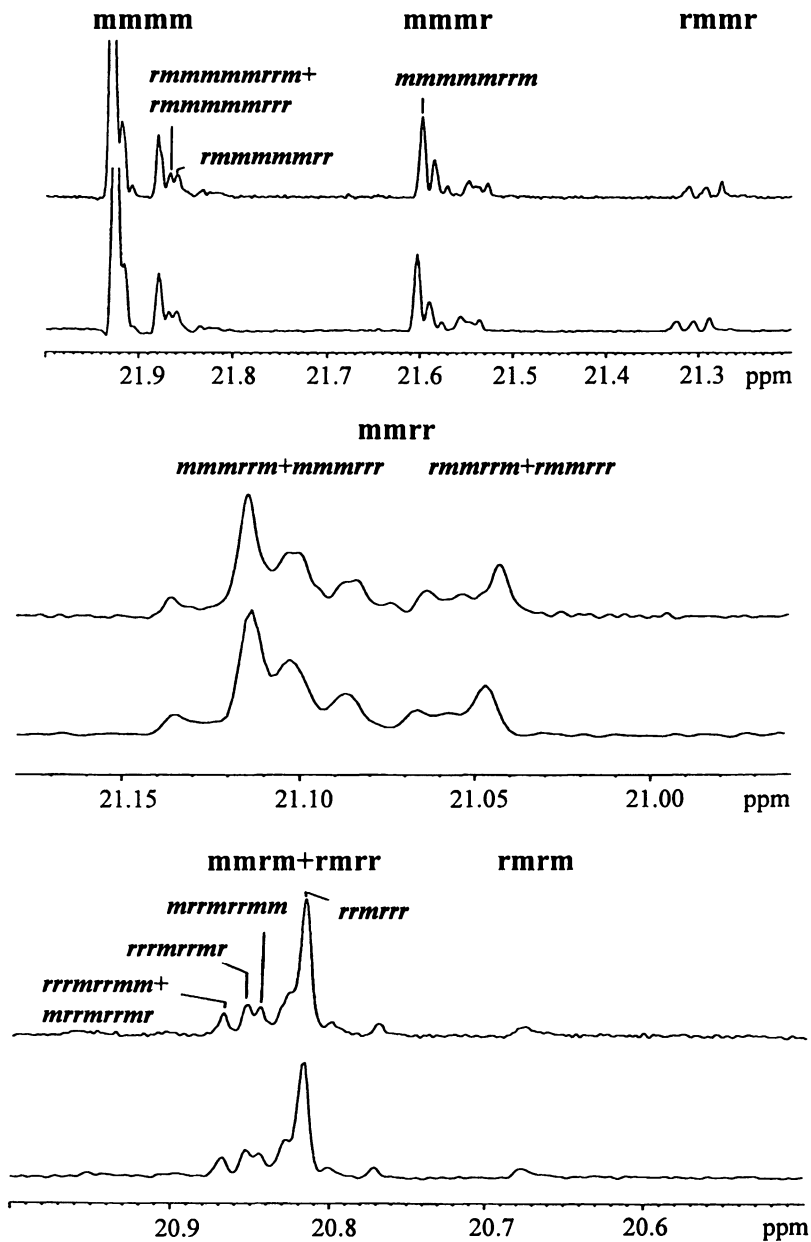


Figure 7. Portions of the methyl region of ^{13}C NMR spectra of a polypropylene sample recorded at 343 K at different fields. Top: 200 MHz. Bottom: 150 MHz.

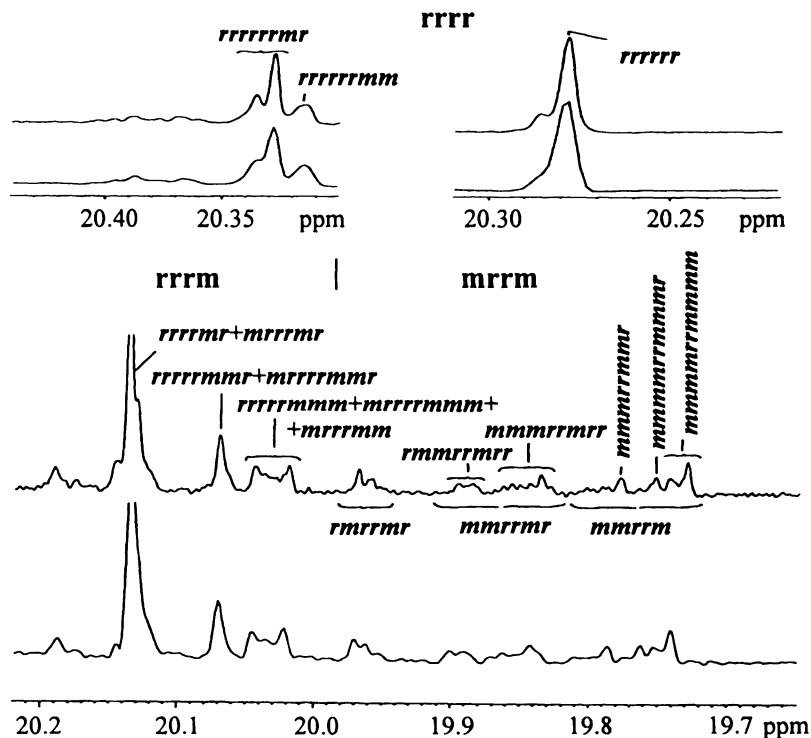


Figure 8. Portions of the methyl region of ^{13}C NMR spectra of a polypropylene sample recorded at 343 K at different fields. Top: 200 MHz. Bottom: 150 MHz.

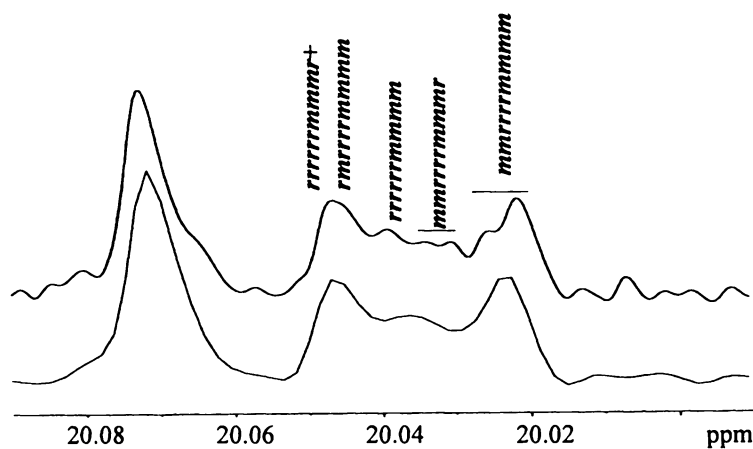
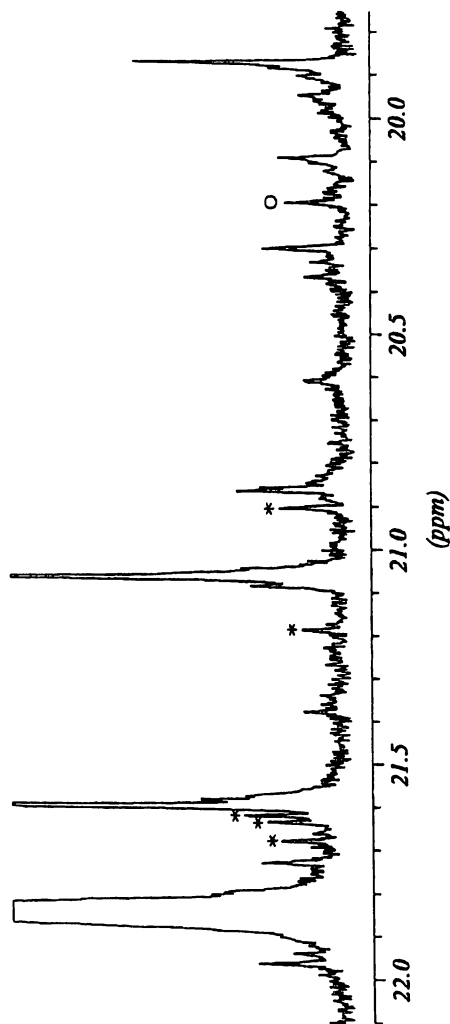


Figure 9. Portions of the methyl region of ^{13}C NMR spectra of a polypropylene sample recorded at 343 K at different fields. Top: 200 MHz. Bottom: 150 MHz.



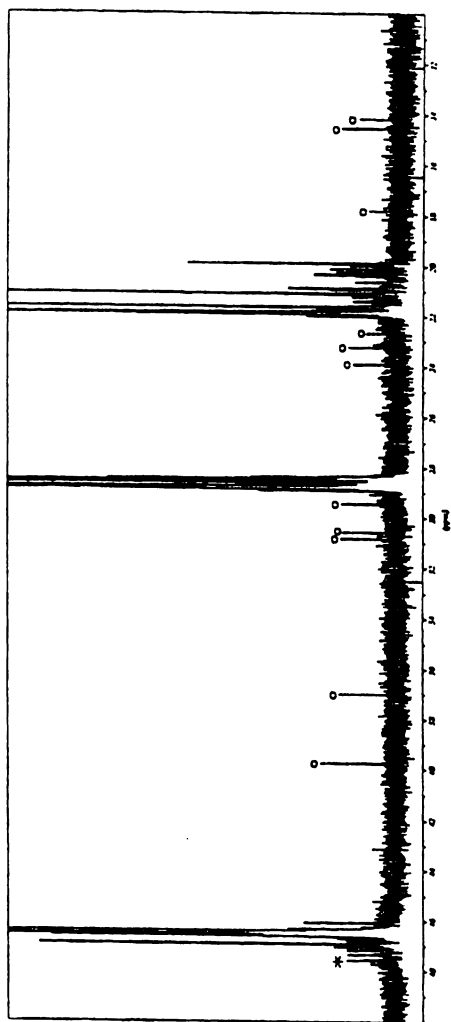


Figure 10. ^{13}C NMR spectrum at 150 MHz of a low molecular weight ($M_n = 10000$) polypropylene. O refer to terminal units. * refer to units next to terminal units. See also Table II.

Chain Ends and Terminations

Special techniques of selective ^{13}C enrichment and/or labeling can be devised to reveal the structure of chain ends even in the case of high molecular weight polymers (13). In this case only terminal units can be observed and assigned.

In the case of low molecular weight however it was possible to observe both terminal units and units next to terminal units. The ^{13}C NMR spectrum of a polypropylene ($M_n = 10000$) sample obtained by a heterogeneous catalyst is reported in Figure 10 as an example. In this case different chain ends can be recognized. The assignments of terminal units are reported in Table II, in which P is propyl chain, nB is *n*-butyl chain, and iB is isobutyl chain, as given in Chart III.

Table II. Chemical shift values (ppm) of ^{13}C resonances of terminal units of the polypropylene sample of Figure 10. Assignment of different terminal units is shown in Chart III.

	C1	C2	C3	C4	C5	C1'
P	14.54	20.19	39.73	30.55		
nB	14.16	23.22	29.42	36.97	30.80	
iB	23.88	25.85				22.66

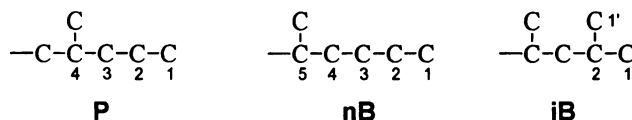


Chart III

Conclusions

It has been shown that a synergic matching between the application of general concepts and new techniques allowed us a deeper insight in polypropylene microstructure. In particular it was possible to exploit the assignment of stereosequences as long as heptads/nonads. More recently this approach has been successfully extended to even longer sequences, some of which of high mechanistic significance. Indeed NMR data, integrated with other more usual characterization methods, constitute the fundamental basis for a mechanistic analysis of polymerization processes. It is now possible to get a

deeper insight into complex catalytic systems such as multisite or fluctuating catalysts. Moreover we can tackle those catalysts which give weakly tactic polymers.

It is well known that in Ziegler-Natta and related polymerizations it is virtually impossible to intercept reactions intermediates. High field techniques represent a promising tool also in the "direct" investigation of catalytic species. Along this line we were able to count active and "dormant" sites in metallocene-catalyzed polymerization (14). We hope to extend these studies in the next future.

Acknowledgements. This work was partly supported by Italian Ministry for the University (PRIN2000). Thanks are due to Lucci M., and Morelli E. for their help in running the ^{13}C 200 MHz spectra, and to the CIRMMMP (Consorzio Interuniversitario Risonanze Magnetiche di Metalloporfirine Paramagnetiche) of Florence. The Broad band ^{13}C probe used at 200MHz for ^{13}C was kindly given by Bruker AG.

References

1. Moore, E.P. *Polypropylene Handbook*; Hanser Publisher: Munich, 1996.
2. Busico, V.; Cipullo, R. *Progr. Polym. Sci.*, **2001**, *26*, 443-533.
3. Tonelli A.E. *NMR Spectroscopy and Polymer Microstructure*; VCH: Deers Field, FL, 1989.
4. Braun, S.; Kalinowski, H.-O.; Berger, S. *150 and More Basic NMR Experiments*; 2nd edition; Wiley-VCH: Weiheim, 1998; pp 155-158.
5. Segre, A.L.; Andruzzi, F.; Lupinacci, D.; Magagnino, P.L. *Macromolecules* **1983**, *16*, 1207-1212.
6. Program "Shape 2000", Vacatello, M. University of Naples "Federico II".
7. Program "Confstat", Vacatello, M. University of Naples "Federico II".
8. Busico, V.; Cipullo, R.; Monaco, G.; Vacatello, M.; Segre, A.L. *Macromolecules*, **1997**, *30*, 6251-6263, and literature cited therein.
9. Schilling, F.C.; Tonelli, A.E. *Macromolecules* **1980**, *13*, 270-275.
10. Busico, V.; Cipullo, R.; Monaco, G.; Vacatello, M.; Bella J.; Segre, A.L. *Macromolecules* **1998**, *31*, 8713-8719.
11. Bax, A.; Freeman, R.; Kempell, S.P. *J. Am. Chem. Soc.* **1980**, *102*, 4849-4851.
12. Berger, S. *Angew. Chem., Int. Ed. Engl.* **1988**, *27*, 1196-1197.
13. Zambelli, A.; Locatelli, P.; Rigamonti, E. *Macromolecules* **1979**, *12*, 156-159.
14. Busico, V.; Guardasole, M.; Margonelli, A.; Segre, A.L. *J. Am. Chem. Soc.* **2000**, *122*, 5226-5227.

Chapter 16

Effect of Internal Donors in Propylene Polymerization Analyzed with NMR and the Internet

Kenichi Shimozawa¹, Masayoshi Saito¹, and Riichirô Chûjô²

¹Toho Catalyst Company, Ltd., 3-5, Chigasaki 3-Chome, Chigasaki-City, Kanagawa, 253-0041 Japan

²Department of Environmental and Material Engineering, Teikyo University of Science and Technology, 2525, Yatsusawa, Uenohara-machi, Kitatsuru-gun, Yamanashi 409-0193, Japan

The two-site model was applied to obtain stochastic parameters for MgCl₂/internal donor/TiCl₄ solid catalyst component used in combination with Al(C₂H₅)₃ and external donor for propylene polymerization. The type and the amount of internal donor were varied. With respect to the fraction for asymmetric site, the two-site model enabled us to conclude that new kinds of active centers are generated in specific cases where external donor is believed to be replacing weaker internal donor during polymerization.

Since the discovery of Ziegler-Natta catalyst, isotactic polypropylene has been widely used as a commodity material due to its low cost and excellent physical properties. As the modulus of the resin is closely related to isotacticity, an understanding in polymerization mechanism is important in the chemistry of propylene polymerization as well as in the industry.

Since 1962 (1), NMR has been one of the most powerful analytical tools for the determination of the microstructure of polypropylene. Many attempts have been made to describe statistical formation of isotactic polymer chains (2), and the two-site model is widely accepted as a desirable stochastic model for olefin polymerization(3). This model has been proven to be valid for not only polyolefins but also vinyl-type polymers such as polystyrene. The model is especially useful to describe the polymerization mechanism by using pentad fractions of ^{13}C -NMR spectra of polyolefins. Indeed, this model is effective toward a better understanding of the nature of the polymerization centers for propylene.

In the area of isotactic polypropylene, there have been several publications (4-6) where the two-site model stochastic parameters are successfully utilized to explain the effect of external donors that are used in combination with solid catalyst component. However, few studies employing the two-site model have been made of the effect of internal donor on catalyst components.

In this study, the authors focused on the effect of internal donors on stereoregularity of Ziegler-Natta catalyst systems with the aid of the two-site model analysis system now available through the Internet (7).

The Two-Site Model

The theory and the parameters of the two-site model have been presented elsewhere in detail (3), but is briefly reviewed here for convenience. The model is composed of three parameters; these are stochastic parameters describing the role of the first and the second sites, and the fraction of the polymers obtained from the first site. More precisely, the first parameter α is the probability of the selection of *d* (or *l*) monad in an asymmetric site; the second parameter σ is that of *m* diad in a symmetric site; and the last parameter ω is the fraction of the polymers obtained from the asymmetric site.

Experimental

Catalyst Preparation

MgCl_2 (30g, S.A. 11 m^2/g) and internal donor were placed in a 1 L stainless steel vibration mill pot with 50 balls (25 mm ϕ) under nitrogen and vibrated at room temperature for 30 h. The ground product (10 g as MgCl_2) was reacted with TiCl_4 (200 mL) in a 500 mL flask two times for two hours each at 110°C, followed by washing with n-heptane. The types of internal donor as well as the amount were varied to obtain a series of solid catalyst components. The Ti and donor contents analyzed are summarized in Table 1.

Propylene Polymerization

The propylene polymerization was carried out in a 2.0-L stainless steel autoclave. In the presence of a small amount of n-heptane, $\text{Al}(\text{C}_2\text{H}_5)_3$ (1.32 mmol) and an external donor, cyclohexylmethyldimethoxysilane were placed in the autoclave, and then the catalyst (2.6 $\mu\text{mol-Ti}$) was introduced at room temperature. After hydrogen (2.0 L) was charged, liquid propylene (740 g) was introduced and prepolymerization was conducted at 20 °C for 5 min. The temperature was then raised to 70 °C, and polymerization was conducted at 70 °C for 60 min. Typically, about 300 g of polypropylene powder were obtained. The results were summarized in Table 2.

$^{13}\text{C-NMR}$ Measurements

$^{13}\text{C-NMR}$ measurements were done only for p-xylene insoluble fractions. $^{13}\text{C-NMR}$ spectra of the polymers were obtained on a JEOL GSX-270 spectrometer using 10 mm o.d. tubes. Sample concentration was about 5 wt% in 1,2,4-trichlorobenzene/ C_6D_6 . The chemical shifts were referenced to TMS.

The results were analyzed using an Internet system for two-site model analysis (7).

Results and Discussion

The Effects of Internal and External Donors on α

Figure 1 shows the relationship between α and the molar ratio of internal donor to Ti (iD/Ti) in the solid catalyst, while Figures 2 and 3 show the relationship between ω and iD/Ti in the solid catalyst. In both cases the results are included where the polymerization was conducted with and without the external donor. Regardless of the presence of external donor, the value of α became larger along with the increase in the iD/Ti . α also increased as the Si/Ti in polymerization increases. This means that α , the probability of the selection of *d* (*l*) monad in the asymmetric Bernoullian site, is attributed to both the amount of internal donor of catalyst component and the amount of external donor during polymerization relative of active centers (Ti).

Table 1. The Catalysts and the Internal Donors

Catalyst	Internal Donor*	Donor Content (mmol/g)	Ti Content (mmol/g)	iD/Ti (molar ratio)
1a	DEP	0.06	0.25	0.24
1b	DEP	0.22	0.34	0.65
1c	DEP	0.36	0.41	0.88
2a	DBP	0.03	0.31	0.10
2b	DBP	0.10	0.37	0.27
2c	DBP	0.18	0.37	0.49

*DEP, diethylphthalate; DBP, di-n-buthylphthalate.

Table 2. Polymerization Results

Catalyst	Si/Ti (mol/mol)	Activity (g-PP/g-cat.)	<i>p</i> -XI* (wt%)	XI fraction		
				m m m m (mol%)	α	ω
1a	0	14,100	43.0	81.8	0.968	0.965
	10	14,500	76.9	89.3	0.981	0.983
	50	12,700	87.3	92.8	0.987	0.989
1b	0	18,800	61.8			
	10	23,600	92.1	92.9	0.989	0.983
	50	21,600	94.7	93.7	0.989	0.989
1c	0	30,500	61.0	85.6	0.976	0.966
	10	37,900	92.4	94.3	0.990	0.992
	50	36,600	95.9	95.9	0.992	0.997
2a	0	19,700	37.0	80.7	0.967	0.959
	10	15,600	79.6	89.9	0.983	0.981
	50	14,100	87.9	91.9	0.986	0.985
2b	0	25,700	44.5			
	10	29,200	88.1	91.9	0.986	0.987
	50	24,800	92.4	93.1	0.988	0.990
2c	0	44,700	56.5	85.9	0.976	0.968
	10	41,100	92.0	93.7	0.989	0.991
	50	36,500	94.4	95.4	0.992	0.994

**p*-xylene insoluble.

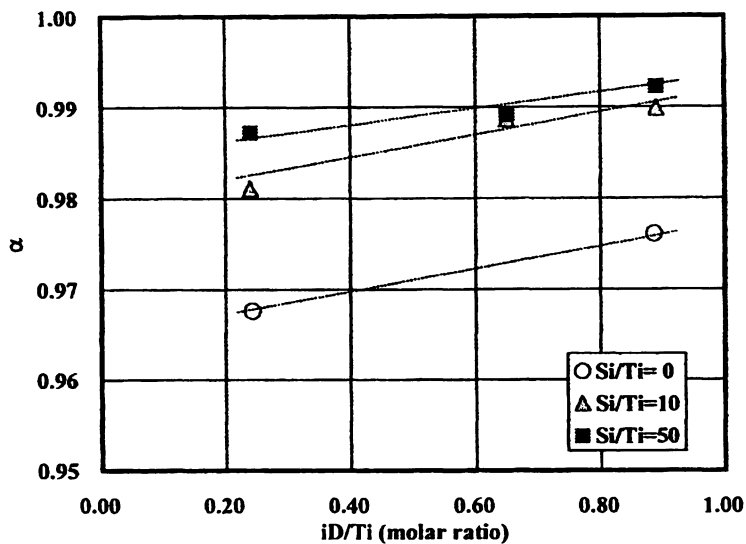


Figure 1. The relationship between iD/Ti and α (internal donor = DEP).

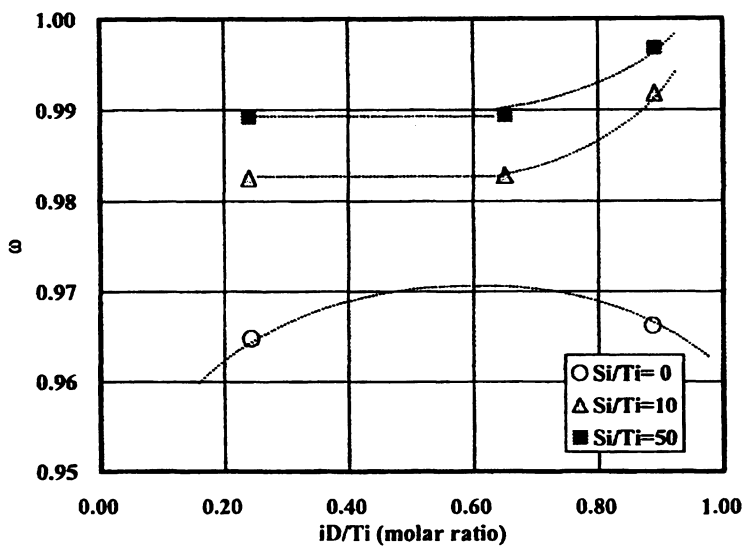


Figure 2. The relationship between iD/Ti and ω (internal donor = DEP).

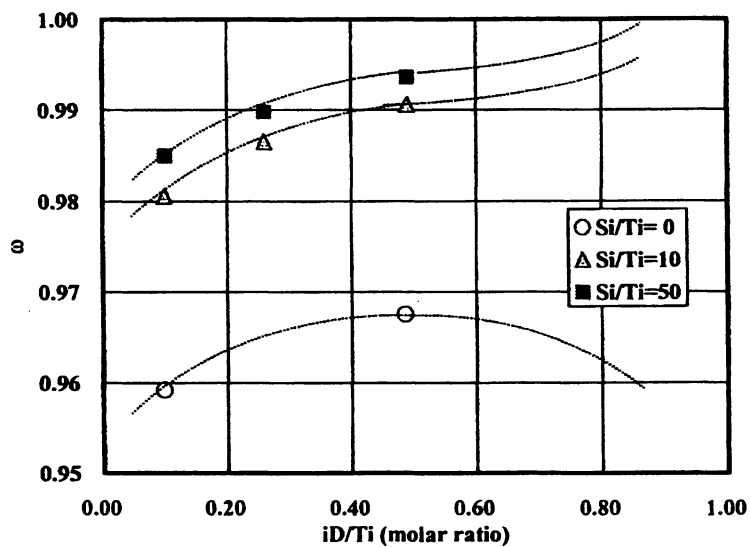


Figure 3. The relationship between iD/Ti and ω (internal donor = DBP).

The Effects of Internal and External Donors on ω

ω shows an interesting profile for the range of this study where iD/Ti was varied using DEP as an internal donor. In the absence of external donor ($Si/Ti = 0$), ω becomes greater along with an increase in iD/Ti to reach its maximum at around $iD/Ti = 0.5$. However, it appears to drop gradually with further increase in iD/Ti . In contrast, in the case where external donor is incorporated, ω increases with an increase in iD/Ti , and drastically goes up at a point where iD/Ti exceeds ca. 0.6.

These results may well imply complementary function of external donor on the formation of active isotactic polymerization centers for a specific region of iD/Ti in the catalyst component. We deduced the following hypothesis to account for such differences in the change of ω . In the region of $iD/Ti < 0.6$, the internal donor may be low enough in concentration to adsorb preferentially on strong acid sites. In this way, the internal donor resulted in increase in asymmetric sites (ω) as well as increase in the probability of selection of d (or l) monad (α). The presence of external donor favored this trend probably by substituting the internal donor which was partly extracted by $Al(C_2H_5)_3$ during the course of polymerization. In the region of higher internal donor concentrations, some of asymmetric sites may lose its asymmetric configuration or just may become inactive by accepting coordination of excess internal donor molecules in their vicinity, with the effect of decreasing ω . However, if the external donor is present, it may readily replace such weak internal donor after extraction by $Al(C_2H_5)_3$ and the active centers of new kind are regenerated as the asymmetry of the site is restored. This will lead to an increase in ω as well as an increase in the probability of selection of d (l) (α).

Conclusions

The two-site model was applied to obtain stochastic parameters for $MgCl_2/iD/TiCl_4$ solid catalyst component used in combination with $Al(C_2H_5)_3$ and external donor for propylene polymerization. Both the concentration of internal donor of catalyst component and that of external donor contributed to the higher probability in the selection of d (or l) monad in the asymmetric site. With respect to the fraction for asymmetric site, the two-site model enabled us to conclude that the new kinds of active centers are generated in specific cases where external donor is believed to be replacing weaker internal donor during polymerization.

Appendix

The internet <http://d-rep.sric.co.jp/twosite> is available for free access and use except for a telecommunication fee.

References

1. Satoh, S.; Chûjô, R.; Ozeki, T.; Nagai, E. *J. Polym. Sci.* **1962**, *62*, S101.
2. For example, (a) Soga, K.; Shiono, T.; Doi, Y. *Makromol. Chem.* **1988**, *189*, 1531; (b) Kakugo, M.; Miyatake, T.; Naito, Y.; Mizunuma, K. *Makromolekules* **1988**, *21*, 314 etc.
3. Chûjô, R. *Kagaku* **1981**, *36*, 420.
4. Chûjô, R.; Kogure Y.; Väänänen T. *Polymer* **1994**, *35*, 339.
5. Härkönen, M.; Seppälä, J. V.; Chûjô, R.; Kogure Y. *Polymer* **1995**, *36*, 1499.
6. Busico, V.; Corradini, P.; Martino, L. D.; Graziano, F.; Iadicicco, A. *Makromol. Chem.* **1991**, *192*, 49.
7. Internet site: <http://d-rep.sric.co.jp/twosite>

Chapter 17

Branching Polyester Oligomers and Fractals

Gavin P. Andrews¹, Allan H. Fawcett^{1,*}, and Majid I. M. Hania^{1,2}

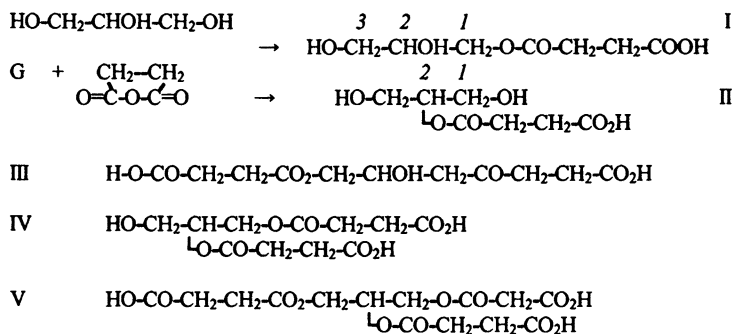
¹Chemistry Department, The Queen's University, Belfast, North Ireland,
United Kingdom

²Current address: The Islamic University, Gaza, Egypt

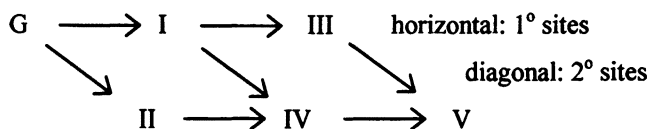
We examine how the ¹³C shifts of oligomers of branching polyesters made from glycerol or erythritol and the difunctional carboxylic acids malonic acid, succinic acid or glutaric acid reflect the location of the ester links on the alcohols, and whether these are influenced by a reaction of the acids at their second site. Assignments were made by observing the new shifts that appeared as the oligomers formed in reactions whose initial conditions were chosen to simplify the products; symmetry of structure was also used. Substitution parameters for each acid were obtained for each carbon in the alcohols, and found to be sensitive to whether the second function of the malonic and succinic acids had participated in ester formation. Cyclic products were discovered early in transesterification reactions of dimethyl malonate. For a fractal polyester a nomenclature is provided, an example prepared and characterized, and then shown to be modified by reactions: Fractal(G,S[-O-H]), fringed with hydroxyl groups, gave an acid-fringed fractal: Fractal(G,S[-CO-O-H]) (a hyperbranch of glycerol and succinate residues).

How the constituents of a polymer link together is a fundamental characteristic. It determines whether the polymer is linear or branched, records the chemistry of its formation, and controls the properties, both physical and chemical. The main method for characterizing polymer microstructure is ^{13}C NMR spectroscopy (1,2), and the details are better detected the higher the resolution of the instrument, the factor that drove developments such as superconducting magnets for spectrometers (3). For hydrocarbon polymers such as polyethylene, the Grant and Paul parameters (1-6) were shown to provide consistent connectivity information by Bovey and by Randal, the first taking the values of the α , β and γ shift effects from small molecules (1), and the second by analyzing the shifts of linear low density polyethylenes with known side chains, so that the analysis of low density polyethylenes might better be performed (6). Here we adopt an approach suitable for step growth polymerization, by performing the synthesis as the spectrum is observed, and using the composition of the feed to govern which oligomers form initially. We illustrate this approach with polyesters made from the difunctional acids, malonic acid, succinic acid and glutaric acid, each of which we linked by ester functions to glycerol or erythritol. The oligomers of such tri- and tetra-functional alcohols are branched and are precursors to fractals and networks. Standard network theories neglect cycles, but a recent theoretical treatment predicts them in the present $\text{A}_2 + \text{B}_3$ and $\text{A}_2 + \text{B}_4$ systems (7). We seek to identify such species by NMR spectroscopy, noting that success has been obtained in similar AB_f reactions by MALDI-TOFF (8), by detecting a fall in mass on ring closure.

The methodology depends upon the chemistry for obtaining ester links. The anhydride of succinic acid or glutaric acid are convenient, for when added to the glycerol or the erythritol, a single ester link forms most readily, to give a simple series of oligomers such as that shown in Scheme I (9). The acid function that also forms reacts less readily to give extra links, and the use of an excess of the anhydride prevents fewer other structures by removing alcohol functions more quickly. Since there are primary and secondary alcohol sites, glycerol may react in two ways, and after that, other routes again may be taken, as Scheme II shows: oligomers III and IV appear only after their precursors. The symmetry of the molecules is also helpful. Eventually the trisuccinate, V, is obtained, with two shifts in an intensity ratio of 2:1. The same sequence of oligomeric products forms if the reaction is done with an ester, such as dimethyl malonate, $\text{Me-O-CO-CH}_2\text{-CO}_2\text{-Me}$, but other products are then possible, especially if the diester is in a minor proportion, so that the second ester site undergoes an ester exchange too. Some such oligomers are shown for glycerol in Scheme III, after the products with once-reacted dimethyl malonate have formed in an ester exchange.



Scheme I: five oligomers of glycerol and succinic acid.



Scheme II: the succession of the glycerol oligomers in a reaction with an excess of succinic anhydride.

The glycerol shifts conveniently sense the pattern of substitution (9), though the reaction site is one bond further, beyond the oxygen atom, than is the case for hydrocarbons:

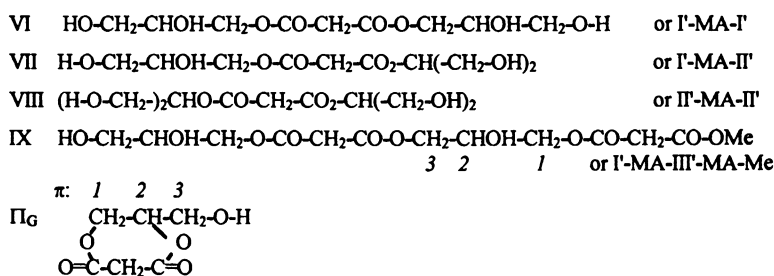
Hydrocarbons: $\sim \text{CH}_2\text{-CH}_2\text{-CH}_2\text{-CH}_2\text{-H}$
 Substituted: $\sim \text{CH}_2\text{-CH}_2\text{-CH}_2\text{-CH}_2\text{-CH}_3$
 Grant and Paul (4) - $\delta \quad \gamma \quad \beta \quad \alpha$ Me substitution parameters

Ester shift changes: $\text{HO-CH}_2\text{-CHOH-CH}_2\text{-OH}$ (G)
 Substituted: $\text{HO-CH}_2\text{-CHOH-CH}_2\text{-O-CO-CH}_2\text{-COOMe}$ (I)
 Primary alcohol - $\gamma_1 \quad \beta_1 \quad \alpha_1$ shift parameters

Substituted: $\text{HO-CH}_2\text{-CH-CH}_2\text{-OH}$ (II)
 $\quad \quad \quad \text{O-CO-CH}_2\text{-CO}_2\text{Me}$
 $\quad \quad \quad \alpha_2 \quad \beta_2$ shift parameters

The substitutions at the primary and secondary alcohol sites by methyl malonate cause different shift changes, as we allow above, just as the sites within a hydrocarbon modify slightly the parameter values (1,11). As an extension, we shall seek to determine whether the identity of the group on the second site of the dicarboxylic acid modifies the shift effects such as α_1 , β_1 and α_2 . For microstructure features such as tacticity and residue form of linear polymers, it is the ^{13}C fine structure that is sensitive (1,2); now we

wish to find whether the shifts of the carbons of one node can provide information on the structure at the neighbouring sites. Since the origin of features such as *meso* (*m*) diads, lies in the manner in which the γ -*gauche* effect (*1,10*) operates: its magnitude is determined by the statistical weight of the *gauche* conformations, a weight controlled by the neighbouring structures. Such a mechanism depends upon the distance between the centers that vary, so that we expect that in the series of, malonic acid, succinic acid and glutaric acid ($\text{HO-CO-(CH}_2)_n\text{-CO-OH}$, with $n = 1, 2, 3$ respectively) the former will provide a greater chance of the required sensitivity of chemical shift fine structure to branching. In Scheme III we have distinguished the glyceryl residues in acid centred trimers from those in dimers, by marking them with a prime, '. The three carbon shifts of the oligomers VI and VII may differ from those of oligomer I, since the second maleic acid function has reacted. Thus we may describe the oligomers VI and VII in terms of the component structures, as I'-MA-I' and I'-MA-II'. Should I dimerise, the oligomer I'-MA-III'-MA-Me or IX would be obtained.



Scheme III: higher glycerol methyl-malonate oligomers – three trimers, a tetramer and a cyclic dimer.

Experimental

Esterification Reactions. Reactions of the alcohols with succinic acid and glutaric acid anhydrides were performed, as in an earlier study (9), by placing quantities of the anhydride and either glycerol or *meso* erythritol in hot dioxane. To encourage the formation of the oligomers I to V of Scheme I a five-fold molar excess of the anhydride was used. Samples were taken and the volatile solvent evaporated off before the NMR spectrum was recorded. Another experiment used an excess of dicyclohexylcarbodiimide to link the second acid functions of succinate residues to the alcohols left in a set of oligomers. The reactions of dimethyl malonate with the alcohols took place at 100°C over an acidified Amberlite ion exchange resin, methyl alcohol being distilled off.

NMR spectra. These were recorded with a General Electric GNQ instrument at 126 MHz (1). The shift of DMSO-d₆ was a secondary standard, 39.80 ppm.

Results and Discussion

The Glycerol – Dimethyl Malonate System

A typical ^{13}C NMR spectrum of a sample from the reaction of glycerol with dimethylmalonate is shown in Figure 1. In the region between 60 and 80 ppm, where the glyceryl residue carbon shifts are found, the two prominent peaks are from the glycerol itself, and as time lapsed the second set of three shifts from the initially formed monoglyceryl ester, I, developed, and were joined by two other shifts, with intensities in the ratio of 2:1. Subsequently, the I shifts fell away, as in each of these dimers the second methyl ester exchanged, and closeby each new shifts appeared. Afterwards the shifts of the oligomer II also vanished. At the end were shifts of I' and II' residues from trimers centered on the malonic residue, oligomers VI, VII and VIII of Scheme III above, but there were also the three shifts we have labelled π . From the ratio of the I and II shifts present after 1 hour we found that each primary alcohol site was $3.4(\pm 0.1)$ times as reactive as the secondary alcohol site. The I' and II' shifts are clearly sensitive to whether the second site of the malonic ester exchanges methyl for glyceryl, but not sensitive to whether the second glyceryl residue reacted at a primary or secondary site.

The shifts labelled π in Figure 1 were found in the several spectra, their intensities rose as time lapsed, and so they were not from impurities. A DEPT experiment found π_1 , π_2 , and π_3 were respectively methylene, methine and methylene carbons. We rejected trimers of the type (I' or II')-Malonate-(I' or II') as in oligomer VII, for the intensities of the π shifts were always identical; we concluded that they came from a single molecule, a cyclic species in which primary and secondary alcohol sites had both participated to form a 7-membered ring: Π_G in Scheme III. The shifts of the glyceryl residue in Π_G differ from those of IV by up to 14 ppm, which has the same pattern of substitution, because of ring strain. Under the conditions that prevailed in the experiment, the second methyl ester group was able to react intramolecularly.

We found the shifts of Table I after reacting a mixture of 2 moles of glycerol and 3 moles of dimethyl malonate kept for 1 hour at 100°C , when other oligomers formed in the sample. The values of the parameters, Δ , show that a reaction at the second ester site caused a large (1 ppm) effect at glycerol carbons 6, 7 and even 8 bonds away. In the tetramer IX: I'-MA-III'-MA-Me the III' carbon, C_1 , moved upfield (again by 0.7 ppm of that in III) and the C_2 carbons moved downfield (by 0.2 ppm), according to a spectrum of a sample got after 24 hours. Shift effects are associative. No chirality effects in IX were detected.

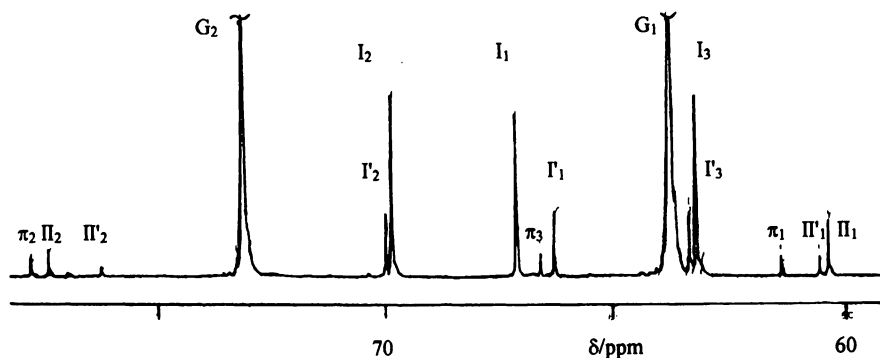


Figure 1. The ^{13}C NMR spectrum of a sample in DMSO-d_6 at 25°C of a mixture of 0.15 moles of glycerol and 0.03 mole of dimethyl malonate after ester exchange for 10 hours in 100 ml dioxane at 100°C over 0.35 g of resin. The glycerol shifts predominate, and are left off-scale, but the three shifts of the monoglyceryl methyl ester of malonic acid, I, have been joined by three shifts of the diglyceryl ester, I'. Shifts of the II residues are similarly joined by those of II', and a third set of shifts also is present, labeled π . After further heating, the shifts of I and II vanished, when the second methyl ester exchanged.

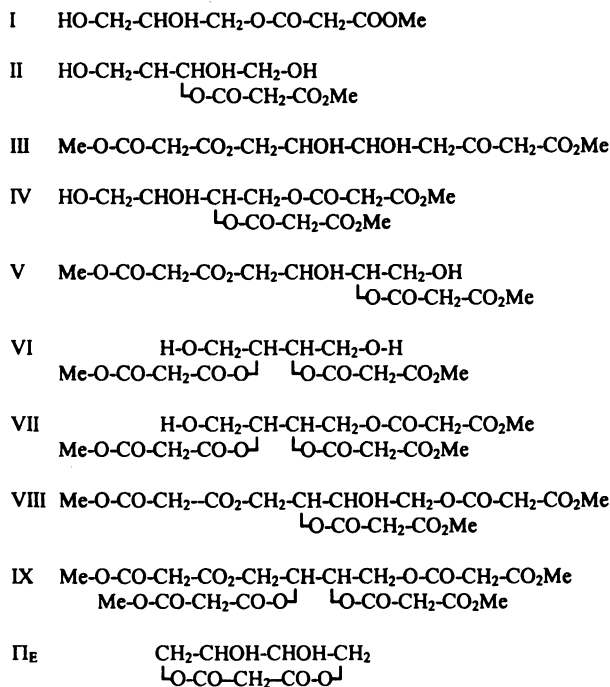
Table I. The ^{13}C NMR Shifts of Glyceryl Residues of Malonate Oligomers at 25°C in DMSO-d_6^a

Residue\C	1	2	3	Δ_1^b	Δ_2	Δ_3
I	67.10	69.84	63.18			
I'	66.28	69.99	63.32	-0.82	0.15	0.14
II	60.35	77.73				
II'	60.55	76.23		0.20	-1.50	
III	66.12	66.42				
IV	73.47	63.50	59.77			
V	63.51	69.60				
II _G	67.15	78.19	62.12			

a Shifts in ppm from TMS are given to 2 decimal places, but varied by 0.05 ppm in other spectra. In the spectrum used, G_1 and G_2 were at 63.63 and 69.60 ppm respectively. The structures are shown in Schemes I and III above.

b Shift in the diglyceryl ester - shift in the monoglyceryl monomethyl ester.

SOURCE: Reproduced with permission from *Polym. Prepr.* 2001, 42, 1, 37.



Scheme IV: some oligomeric malonic esters of erythritol.

The Erythritol - Malonic Ester System

These oligomers were obtained in a reaction over Amberlite ion exchange resin. A typical ^{13}C NMR spectrum is shown in Figure 2, where may be seen the four shifts of oligomer I, the primary mono ester shown in Scheme IV above, are joined by a second set, a development we attribute to the reaction of the second site of the malonic ester with the excess of erythritol present. The shifts of I'_4 are barely distinguished from those of I_4 . The four shifts of residues of type II are joined by a second set, each down field except for II'_2 – the site of attachment. Besides the shifts from the trimers there are near 72 ppm two prominent peaks of equal intensity that we have labelled π , the low-field peak at 71.1 ppm being methylene, according to a DEPT experiment, and the other methine. We attribute these two peaks to a 1,4-cyclised oligomer, two peaks to a 1,4-cyclised oligomer, Π_E , a molecule that contains a nine-bond ring. It is probably the *meso* structure of the erythritol together with the higher reactivity of the primary

site that causes the symmetrical 9-membered ring rather than a second, unsymmetrical, 7-membered ring to form. In this reaction primary sites initially again react faster ($\times 4.1(\pm 0.3)$) than the secondary sites.

The Erythritol Succinate System

We show in Figure 3 one of the the ^{13}C NMR spectra of the oligomers obtained in a reaction of erythritol with an excess of succinic anhydride. The four shifts of the initially formed species, I, have diminished much in intensity, but the shifts of oligomers III still remain, for the unreacted 2° alcohol sites are less reactive. The four shifts of the trisuccinate, VIII may be seen, as the next most prominent set, together with the two shifts of the final product, the tetra succinate, IX, whose intensities grew after further time. Some shifts of other oligomers are also seen (V and VI), identified by observing which group of peaks succeeded each other in time. In Scheme IV we show the structures of a related series of oligomers.

Other Series of Oligomers.

In the manner described above, reactions between succinic acid and erythritol, glutaric acid and erythritol, glutaric acid and glycerol, and dimethyl malonate and adonitol were conducted, and the shifts of the alcohol residues within the oligomers assigned. From these and observations made during a reaction of glycerol with acetic anhydride we used the shifts of the single primary and secondary dimeric esters to calculate the set of shift parameters presented in Table II. α parameters are about 3 ppm, β parameters are about -3 ppm, the negative value being reminiscent of the hydrocarbon γ parameter (4). Here γ and δ parameters are smaller than 1 ppm, and negative. The α parameters for methyl malonate are about 1 ppm greater than for the others, from the proximity of the second ester group, and the parameter for the glutarate is a little less in each case than for the succinate. Differences at the β and γ - sites are ~ 0.1 ppm. The adonitol $\text{H}-(\text{CH}_2)_5\text{-H}$ results demonstrate a similar pattern. If other values of α_1 and α_2 are obtained, eg. by comparing the shifts of III with those of I within a set of oligomers, variations of about 0.5 ppm are found, so there are neighbouring group effects, as with hydrocarbons (11). When the shifts of I and III, of II and IV, and IV and V are compared, values of α_1 are respectively 3.8₈, 3.3₄ and 3.7₅ ppm. For the erythritol systems the β_2 effects have fairly different values, eg. for glutaric anhydride the β_2 parameter at C_1 was -3.7₃ ppm, and at C_2 was -2.1₄ ppm. Despite these variations, on the basis of the parameters of Table II the shifts of oligomers above I and II could be reliably forecast.

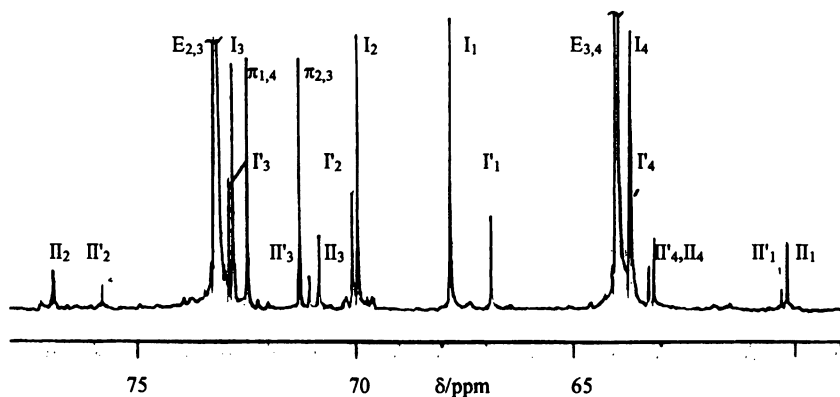


Figure 2. The ^{13}C NMR spectrum of the oligomers of erythritol and dimethyl malonate (5:1 moles) after reacting at 100°C for 25 hours. A proportion of the second sites of the malonic ester have exchanged, and a pair of peaks from a symmetrical cyclic form are present: π . (Structures are in Scheme IV).

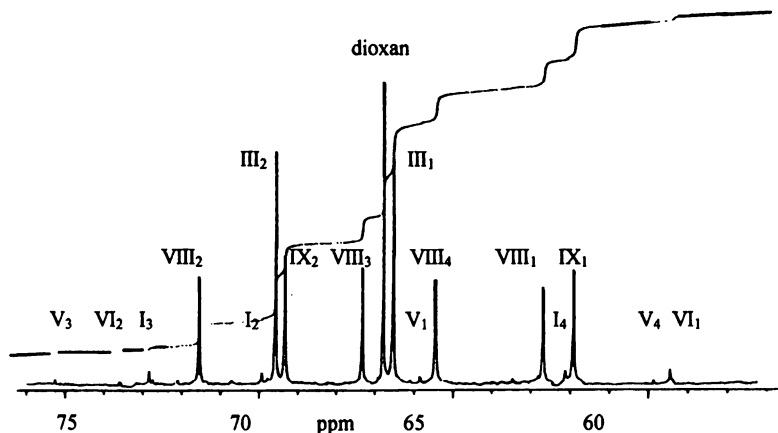


Figure 3. The ^{13}C NMR spectrum of the oligomers of succinic anhydride and meso-erythritol (3:1 mole ratio) formed after 7 hours in refluxing dioxane. Structures in Scheme IV are similar to these.

Table II. Chemical Shift Parameters for Substitutions at the Sites of Glycerol, of Erythritol and of Adonitol*

Alcohol	Acid/ester	α_1	β_1	γ_1	δ_1	α_2	β_2	γ_2
Glycerol	Acetic	2.6 ₁	-3.2 ₂	-0.4 ₆		3.1 ₄	-3.3 ₁	
	Malonate	3.4 ₀	-3.3 ₄	-0.6 ₁		4.2 ₆	-3.5 ₈	
	Succinic (I)	2.6 ₂	-3.1 ₀	-0.4 ₁		3.3 ₃	-3.2 ₅	
	Glutaric	2.5 ₂	-3.3 ₁	-0.4 ₆		3.0 ₇	-3.2 ₇	
Erythritol	Malonate	3.8 ₃	-3.2 ₆	-0.3 ₇	-0.3 ₅	3.7 ₈	-3.1 ²	-0.8 ₆
	Succinic (I)	3.1 ₃	-3.1 ₆	-0.2 ₅	-0.2 ₈	2.8 ₆	-2.9 ²	-0.6 ₉
	Glutaric	2.8 ₇	-3.1 ₈	-0.2 ₅	-0.2 ₇	2.6 ₅	-3.0 ²	-0.7 ₂
Adonitol	Malonate	3.8 ₉	-3.0 ₅	-0.2 ₇	-0.2 ₈	4.1 ₂	-4.0 ²	-0.8 ₁

* following reactions with acetic anhydride, dimethyl malonate, succinic anhydride and glutaric anhydride. The shifts were measured in DMSO-d₆.

□ the mean of two values: C₁ value was greater by ~0.8 ppm, C₃ was less by ~0.8 ppm.

SOURCE: Reproduced with permission from *Polym. Prepr.* 2001, 42.1, 37.

Fractal Forms of the Polyesters

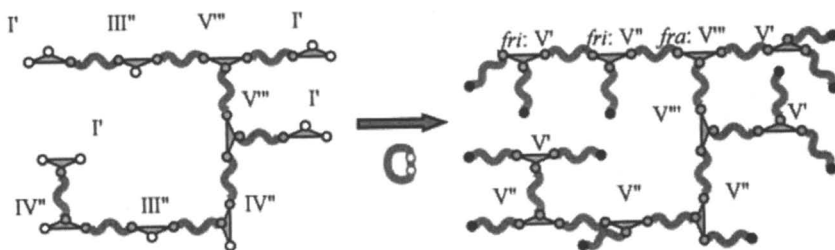
Mixtures of the oligomers have been converted to polymeric forms by linking carboxylic acid groups with free alcohol groups with the aid of the dehydrating agent, dicyclohexylcarbodiimide, DCCDI. A nomenclature is introduced for these hyperbranched structures that explicitly recognizes the fractal form - made from glycerol and succinic acid and fringed with hydroxyl groups: Fractal(Glycerol, Succinate[-O-H]), or Fractal(G,S[-O-H]).

To examine the manner in which the architecture of hyperbranched structures may be monitored we refluxed a 1:1 mixture of succinic anhydride and glycerol for 1 hour in dioxane. The ¹³C NMR spectrum showed that the proportions of the mono-glycerol structures then present were G : I : II : III : IV : V = 0.24 : 0.48 : 0.06 : 0.15 : 0.07 : 0.01; the main component was I. Dehydration with dicyclohexyl-carbodiimide for 9 days gave a polymer, Fractal(G,S[-O-H]). The absence of carbonyl groups from the spectrum between 173.5 and 174.5 ppm confirmed the success of the preparation, and the presence of shifts from I', II', III'', IV'' residues demonstrated the presence of hydroxyl-fringed glyceryl residues. They were then in the proportions of G : I : II : III : IV : V = 0.02 : 0.23 : 0.02 : 0.34 : 0.17 : 0.22, that is, branch points : chain extenders : tips = 22 : 51 : 25, proportions surprisingly close to 1 : 2 : 1, considering the unequal reactivity of the two types of hydroxyl function.

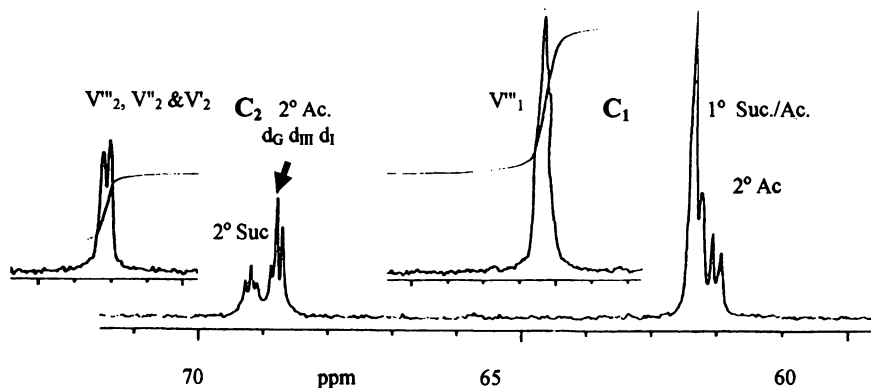
When the Fractal(G,S[-O-H]) was treated with acetic anhydride, the product had the ¹³C NMR spectrum of Figure 4, whose simplicity indicates that every alcohol has become esterified. The fine structure near 62 ppm derives from the primary ester carbons, and that near 69 ppm from the

secondary ester carbons, groups sensing the type of substituent as labeled. From the intensities of the lines we have concluded that the major peak is from the III'' whose C₂ has been acetylated, an assignment consistent with the smaller value of α_2 for the acetyl group than for the succinyl group (Table 2). On each side of this are the shifts of acetylated glycerol and I' residues, as indicated; the other shifts were assigned in increasing order to IV'', V''' and II' groups after the acetylation of the primary sites (if any). Not all possible 1° carbon sites are distinguished, but the two shifts at 62.0 ppm probably derive from carbons of I' and IV'' groups after acetylation.

A reaction of Fractal(G,S[-O-H]) with succinic anhydride gave an acid-fringed fractal, Fractal(G,S[-CO-O-H]) whose even simpler spectrum we show as an insert in Figure 4. All the glyceryl residues are of the form of V, but the fine structure we saw in a previous study [9] is now missing, for these species have a higher molecular weight. The two shifts from the methine carbon measure the framework (*fra*: V''') and fringing residues (upfield: *fri*: V' and V'' - Scheme V), the order corresponding to that found as oligomers V were polymerized by heating [3,9]. A shoulder is just seen upfield of the 1° carbon signal. A second route to this fractal was taken by reacting glycerol with two moles of succinic anhydride for three hours, to yield an oligomer mixture of composition: G : I : II : III : IV : V = 0.01 : 0.19 : 0.02 : 0.42 : 0.19 : 0.18; when this was treated with DCCDI for 1 day in THF and then for 5 days in CHCl₃ the product was shown to be again Fractal(G,S[-CO-O-H]), for no residues with hydroxyl groups remained, but the ¹³C spectrum differed. Then the upfield C₂ shift was only half the intensity of the downfield peak, so that a greater proportion of these sites are involved in the framework; and the C₁ region had three resolved components, the downfield part being less dominating, for the C₁ carbons are less frequently part of the framework. It appears that the form of the fractal framework depends upon the manner in which it is assembled: when the oligomers are mainly like I it differs from that formed from a mixture in which III is the most common component.



Scheme V: reacting a fractal(G,S[-O-H]) with succinic anhydride, to make framework and fringing 2° C residues of type V (shown as triangles).



Figures 4. The ^{13}C NMR spectrum of the acetate-fringed Fractal(G,S[-O-Ac]), and, insert, the spectrum of the succinic acid fringed fractal, Fractal(G,S[-CO-O-H]).

REFERENCES

1. Bovey, F., *High Resolution NMR of Macromolecules*, Academic Press, London, 1972.
2. Koenig, J.L., *Chemical Microstructure of Polymer Chains*, Wiley, Chichester, UK, 1980.
3. Fawcett, A.H.; Hamilton, J.; Rooney, J.J., in *Polymer Spectroscopy*, Ed. Fawcett, A.H., John Wiley & Sons, Chichester, 1996.
4. Grant, D.M.; Paul, R.D., *J. Amer. Chem. Soc.*, **1964**, *86*, 2984.
5. Wehrli, F.W.; Werthlin, T., *Interpretation of NMR Spectra*, Heyden, London, 1976.
6. Randal, J.C., *Polymer Sequence Determination: Carbon-13 Method*, Academic Press, London, 1977.
7. Armitage, D.; Cameron, C.; Fawcett, A.H.; Hetherington, C.R.; Mee, R.A.W.; McBride, F.C., *Macromolecules*, **2000**, *33*, 6569.
8. Gooden, J.K.; Gross, M.L.; Muller, Stephanecu, A.D.; Wooley, K., *J. Amer. Chem. Soc.*, **1998**, *120*, 10180.
9. Fawcett, A.H.; Hania, M.; Lo, K-W.; Patty, A. *J. Polym. Sci.: Part A: Polym. Chem.* **1994**, *33*, 815.
10. Tonelli, A., Chapter 2, p. 55, in ref. 3.
11. Lindeman, L.P.; Adams, J.Q., *Anal. Chem.*, **1971**, *43*, 1245.

Chapter 18

An NMR Study on the Bulk Cationic Copolymerization of Trioxane with 1,3-Dioxepane

Min-Hui Cui¹, Yuli Zhang¹, Mark Werner¹, Nan-Loh Yang^{1,*},
Steven P. Fenelli², and John A. Grates²

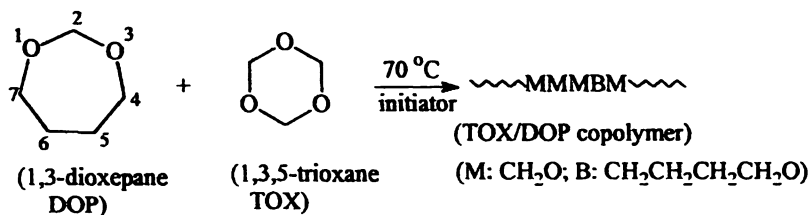
¹Department of Chemistry, City University of New York, College of Staten
Island, 2800 Victory Boulevard, Staten Island, NY 10314

²Celanese AG, 90 Morris Avenue, Summit, NJ 07901

The mechanism of cationic copolymerization of trioxane with 1,3-dioxepane was investigated using *in situ* ¹³C NMR based on microsequence data established *via* PFG-HMQC and PFG-HMBC two-dimensional NMR. Kinetic profiles of pentad sequences and butylene oxide (CH₂CH₂CH₂CH₂O) *counit* placement were obtained. The incorporation of 1,3-dioxepane into the copolymer sequences was found to involve its initial homopolymerization followed by redistribution of *counits* through chain transfers, e.g. transacetalization. Unlike the copolymerization of trioxane with dioxolane, the insertion of formaldehyde into 1,3-dioxepane to form a larger acetal ring prior to substantial copolymerization does not play a significant role. For the first time nonad sequences were observed directly by NMR analysis of the copolymer.

Introduction

The cyclic acetal 1,3-dioxepane (DOP) can be copolymerized with TOX to form copolymers having properties comparable to other acetal resins:



Only limited information on the TOX/DOP copolymer is available from the literature (1,2). Commercial products from TOX and DOP copolymerization, such as Ultraform, have been described in patents. The initiation mechanism of bulk cationic copolymerization of TOX with DOP has not been reported, although homopolymerization of DOP was first described in 1935 (3). The polymerization of DOP can be initiated with various types of initiators. NMR spectra show that the polymer of DOP consists of regular sequences of $-\text{O}-\text{CH}_2-\text{O}-(\text{CH}_2)_4-$ units derived from DOP.

For TOX copolymerization with ethylene oxide (EO), EO was first converted to low molecular weight copolymer and cyclic oligomers such as dioxolane (DOL) and 1,3,5-trioxepane (TOP) (4). For either EO and DOL as comonomer with TOX, they were found to be preferentially incorporated during the induction period (5).

We report here an investigation on the copolymerization of TOX with DOP using *in situ* ¹³C NMR based on data obtained from two-dimensional NMR. The microstructure of TOX/DOP copolymer, including pentad, heptad, and nonad sequences, is developed. The kinetic profiles of comonomer DOP, counit butylene oxide (B; CH₂CH₂CH₂CH₂O), and microsequences of the counit distribution in copolymer are also obtained. The initiation mechanism and the process of the incorporation of butylene oxide ('B') counits originating from DOP are discussed through analyzing kinetic data obtained from ¹³C NMR. Nonad copolymer sequences are also observed and monitored for the first time.

Experimental

Materials

Trioxane, 1,3-dioxepane, and boron trifluoride diethyl etherate were obtained from Aldrich Chemical Co. TOX was refluxed continuously in the presence of sodium for at least 48 hours to remove trace amounts of water in a Fuchs style reflux apparatus under dry argon at 120 °C. Dioxepane was purified using a similar procedure. Initiator $\text{BF}_3\cdot\text{OEt}_2$ was added with dried 1,4-dioxane as carrier.

Copolymerization of TOX with DOP

Copolymer samples for NMR structural analysis were prepared as follows. TOX and DOP were charged into dry polymerization tubes in the required molar ratio through a septum stopper. To initiate the polymerization, $\text{BF}_3\cdot\text{OEt}_2$ solution was added to the monomer solution at 70 °C in an oil bath with constant stirring. The reaction was allowed to proceed for 20 hrs. The resulting copolymers were pulverized, the powder neutralized by stirring in methanol containing 1% triethanolamine for 1 h to destroy remaining initiator, and were then collected by filtration. Unstable end groups were removed by base hydrolysis using dimethylformamide, benzyl alcohol and triethanolamine mixture (volume ratio: 50:49:1) (6).

NMR Measurements

A Varian Instruments UNITY*plus* 600 NMR spectrometer operating at a ^1H resonance frequency of 599.939 MHz and a ^{13}C resonance frequency of 150.866 MHz was used for copolymer structural analysis. ^1H NMR spectra for base hydrolyzed copolymers in DMSO-d_6 were obtained at 140 °C using a 5mm Indirect Detection Probe (ID600-5, Nalorac Cryogenics Corporation). Parameters used were: delay time, 3 s; pulse angle, 24.3°; acquisition time, 3.506 s; and 128 transients for each spectrum. For 2D NMR experiments, PFG-HMQC and PFG-HMBC, a 5mm Quad Resonance Gradient Probe (IDQG600-5, Nalorac Corporation) was used. Pulse field gradient experiments were carried out at 50 °C on 0.7 mL polymer solutions in a mixed solvent of ca. 20% v/v 1,1,1,3,3,3-hexafluoro-2-propanol in CDCl_3 . The 2D spectra were obtained by

collecting 32 transients of 2048 points each for each of 640 increments. Spectral analyses were performed using Varian VNMR software.

Kinetic Experiments

A Varian UNITY*plus* 300 NMR spectrometer operating at a ^{13}C frequency of 75.435 MHz was used for obtaining the *in situ* ^{13}C NMR spectra of the bulk copolymerization of TOX with DOP at 70 °C. Parameters used were: delay time of 4 s, pulse angle of 37.4 degree, and an acquisition time of 1.19 s, with 128 transients for each spectrum. Since gated decoupling was not used, the results obtained can be considered only semi-quantitative. The comonomers TOX and DOP at a 9:1 molar ratio of methylene oxide unit (M) to butylene oxide unit (B) were injected into a dried 10 mm NMR tube. The acquisition of the first spectrum was followed by the addition of the initiator $\text{BF}_3\cdot\text{OEt}_2$ at a molar ratio of 30 ppm to M. The process of acquisition was begun immediately after the initiation of the sample. Chemical shifts were as referenced on the TOX resonance at 93.23 ppm calibrated on the chloroform triplet at 77.00 ppm.

Results and Discussion

Assignment of Pentad Sequences of TOX/DOP Copolymer

For the TOX/DOP copolymers butylene oxide units, 'B', are not expected to be adjacent to each other because a highly unstable carbonium ion on butylene unit would have to be the propagating center. A positive charge on the methylene carbon stabilized by α oxygen is greatly preferred, giving rise to what is perhaps best thought of as an oxycarbonium ion. Therefore, the number of pentad sequences observed is limited to nine: six 'M'-centered pentad sequences (MMMM, BMMM, BMMB, MBMM, MBMB, and MBMB) and three 'B'-centered pentad sequences (MMBM, BMBM, and BMBM), where 'M' is a methylene oxide unit and 'B' is a butylene oxide unit.

The assignment of proton chemical shift of the pentad sequences was first established by comparison with pentad sequences of TOX/DOL copolymers (7). The count $\text{CH}_2\text{CH}_2\text{CH}_2\text{CH}_2\text{O}$ ('B') in TOX/DOP copolymer is expected to show higher shielding effect than $\text{CH}_2\text{CH}_2\text{O}$ ('E') in TOX/DOL copolymer. The chemical shifts of the pentad sequences of TOX/DOP copolymers are therefore usually upfield from the corresponding pentad sequences of TOX/DOL copolymers (Table I). Six 'M'-centered pentad sequences from TOX/DOP were

assigned based on the data from TOX/DOL copolymer system. For each 'B' unit, two different protons in 'B'-centered region were observed: $\text{MMCH}_2\text{CH}_2\text{CH}_2\text{CH}_2\text{O}$ and $\text{BMCH}_2\text{CH}_2\text{CH}_2\text{CH}_2\text{O}$. The resonance at 1.59 ppm was assigned to the two central methylene units of $-\text{OCH}_2\text{CH}_2\text{CH}_2\text{CH}_2\text{O}-$, B_2 .

Table I. Proton (^1H) and Carbon (^{13}C) Chemical Shift* of Pentad Sequences from TOX/DOP and TOX/DOL Copolymers

<i>Pentad Sequence</i>	^1H (ppm)	^{13}C (ppm)	<i>Pentad Sequence</i>	^1H (ppm)	^{13}C (ppm)
MMMMM	4.84	90.04	MMMMM	4.84	90.04
BMMMM	4.82	89.60	EMMMMM	4.83	90.74
BMMMB	4.80	89.18	EMMME	4.82	89.34
MBMMM	4.72	92.74	MEMMMM	4.75	92.92
MBMMB	4.70	92.24	MEMME	4.74	92.62
MBMBM	4.59	95.14	MEMEM	4.66	95.56
MMB ₁ **	3.54	68.70	MMEMM	3.67	67.72
BMB ₁ **	3.50	68.04	EMEMM	3.66	67.14
B ₂ **	1.59	26.13, 26.07	EMEME	3.64	67.22

*The proton chemical shift (^1H) data were obtained at 140 °C with DMSO- d_6 as solvent and referenced at 2.49 ppm of DMSO- d_5 ; the carbon chemical shift (^{13}C) data were obtained at 50 °C with solution of ca. 20% v/v 1,1,1,3,3,3-hexafluoro-2-propanol in CDCl_3 as solvent and referenced on chloroform triplet 77.00 ppm.

** 'B₁' and 'B₂' denote ' $\text{OCH}_2\text{CH}_2\text{CH}_2\text{CH}_2$ ' and ' $\text{OCH}_2\text{CH}_2\text{CH}_2\text{CH}_2$ ', respectively

The chemical shifts of pentad sequences in ^{13}C NMR spectra (Table I) were then assigned through PFG-HMQC experiments following the assignment of proton chemical shifts. The assigned pentad sequences both in ^1H and ^{13}C NMR spectra were further ascertained with PFG-HMBC experiments. In PFG-HMBC experiments, the pentad sequences should have multiple-bond correlation to two flanking pentads. For example, pentad MMBMB sequence should show correlation to two 'M'-centered sequences MMMMB and BMMMB and to two 'B'-centered sequences MMBMM and MMBMB.

Kinetic Study on Initiating Mechanism

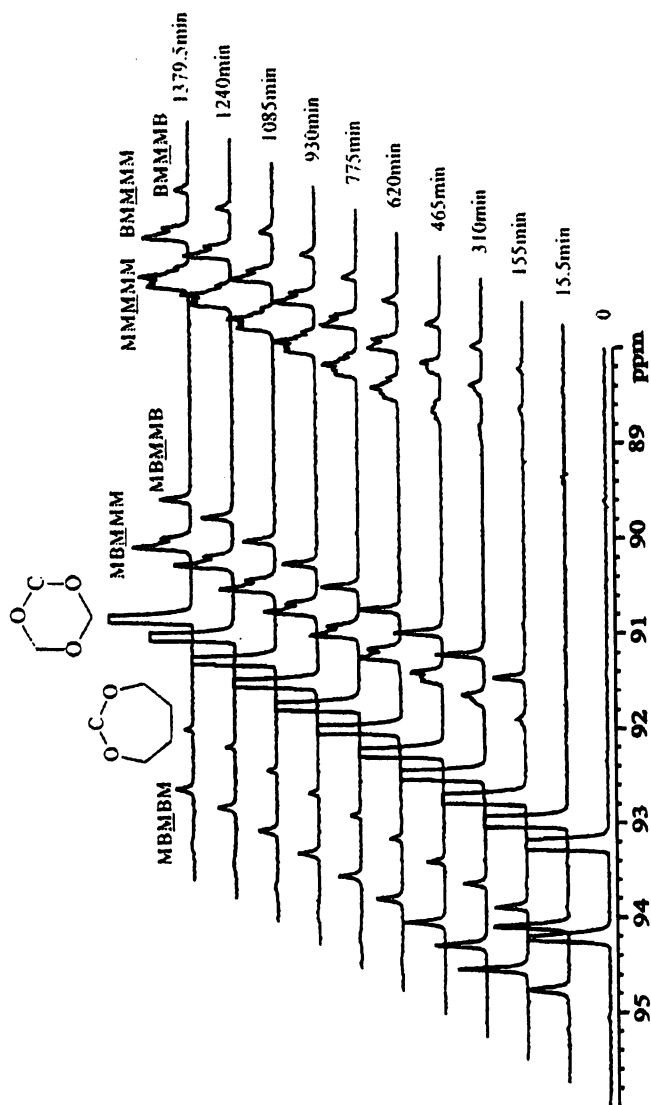
Under selected conditions of comonomer ratio and initiator concentration, the polymerization reaction is sufficiently slow to allow *in situ* monitoring of

monomer and polymer species using ^{13}C NMR. Bulk copolymerizations of TOX with DOP initiated by $\text{BF}_3\cdot\text{OEt}_2$ were carried out at a 9:1 molar ratio of methylene oxide unit to butylene oxide unit. Figure 1 shows the ^{13}C NMR spectra accompanying the process of copolymerization of TOX with DOP. Figure 2 displays the kinetic profiles derived from Figure 1.

After injection of initiator, the resonance at 95.02 ppm arose quickly in the first spectrum (15.5 min.). According to the 2D NMR assignment, this resonance was from the MBMBM pentad sequence. This assignment of MBMBM sequence was also established by an *in situ* ^{13}C NMR experiment of DOP homopolymerization under comparable conditions for TOX/DOP copolymerization. At 15.5 minutes, about 50% DOP had been consumed and almost all had been incorporated as MBMBM sequence. No other pentad sequences were observed in the first spectrum. It follows in the copolymerization of TOX with DOP that initially DOP homopolymerization dominated. Then, accompanying the continuing increase of MBMBM sequence, the pentad sequences with 'B' separated by more 'M', i.e., MBMMB and BMMMB, emerged. At 93 minutes, all of the pentad sequences appeared with the exception of the pentad without 'B', MMMMM. At this time, 80% DOP and 20% TOX were consumed and TOX had been contributing to 'M' incorporated with 'B' into the pentad sequences.

Associated with the MBMBM pentad, $\text{BMCH}_2\text{CH}_2\text{CH}_2\text{CH}_2\text{O}$ should also appear in the 'B'-centered region. A peak at 67.24 ppm was assigned to $\text{BMCH}_2\text{CH}_2\text{CH}_2\text{CH}_2\text{O}$ overlapping with the resonance of the carbon adjacent to oxygen in 'B' unit of DOP (67.28 ppm). This resonance was not resolved until 80% DOP consumption reached. Although the integral value of this peak could not be accurately determined due to its overlap with DOP, its rapid increase was clearly parallel to MBMBM. On the other hand, the central carbon in 'B' units ($\text{OCH}_2\text{CH}_2\text{CH}_2\text{CH}_2\text{O}$) of MBM sequences showed a well-resolved resonance at 26.43 ppm, over 3 ppm upfield from the central CH_2 in 'B' units of the DOP ring (29.11 ppm). This peak emerged in the first acquired spectrum after initiation. Similar to MBMBM sequence, the resonance of the central CH_2 in 'B' units originating from DOP increased rapidly within the first 62 minutes (Figure 2), followed by a much slower growth to a plateau at about 140 minutes. At the same time, MBMBM declined at a significant rate due to its conversion into pentads with 'B' separated by more than one 'M' unit through processes including transacetalization. In addition to the contribution from transacetalization involving already formed sequences, a significant portion of the growth of the pentads MBMMB, MBMMM, BMMMB and BMMMM, was due to copolymerization of TOX with DOP. At this time, MMMMM pentad sequence was not observed.

For the first acquired spectrum after the injection of initiator, the resonances of C-2 (acetal carbon) and C-4 of comonomer DOP shifted downfield by ca. 0.2



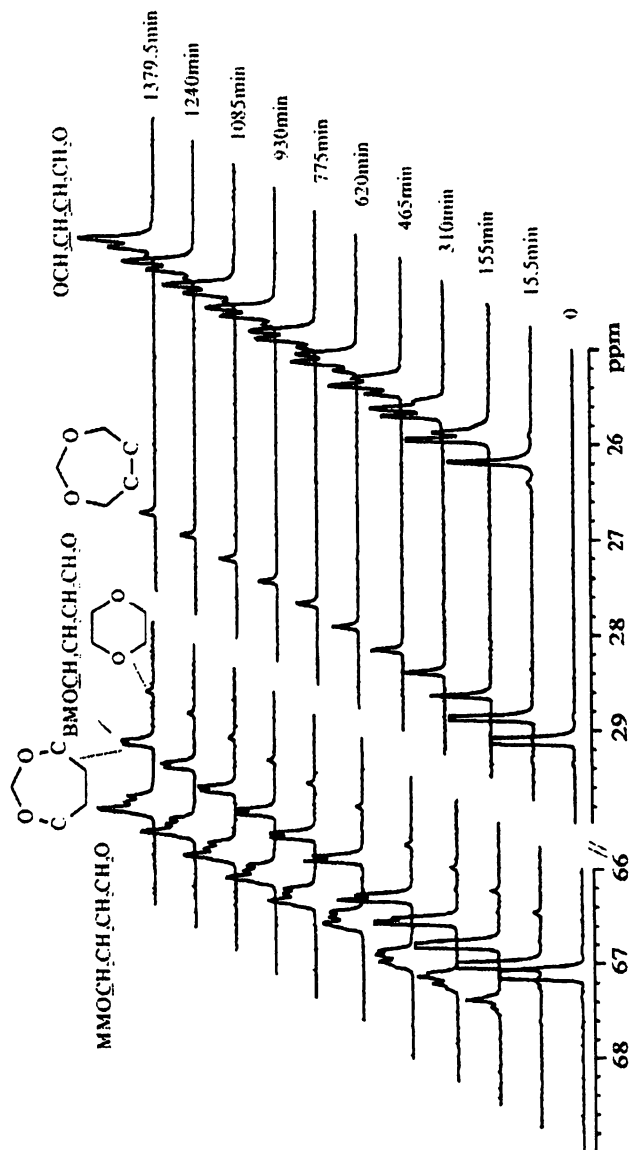


Figure 1. ^{13}C NMR spectra as a function of time for the bulk copolymerization of TOX with DOP at 70 °C. Molar ratio: $M/B = 9$; $\text{BF}_3 \cdot \text{OEt}_2/M = 30$ ppm; upper Figure, 'M'-centered region; lower Figure, 'B'-centered region.

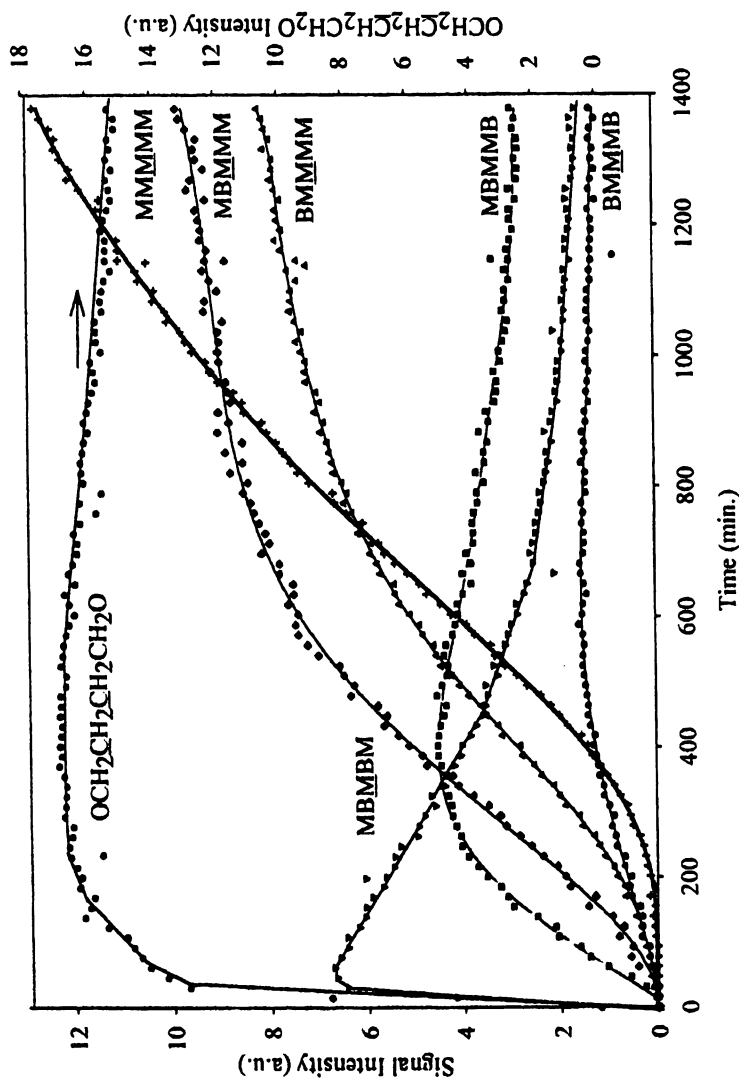


Figure 2. TOX/DOP copolymerization: kinetic profiles of pentad sequences and central carbon of $\text{CH}_2\text{CH}_2\text{CH}_2\text{O}$ count, B_2 . Molar ratio: $M/B=9$; $\text{BF}_3\cdot\text{OEt}_2/M=30$ ppm

ppm (Figure 1, 15.5 min. curve). This is likely caused by the protonation of the DOP, leading to an equilibrium between protonated and unprotonated DOP with exchange at a rate faster than the NMR time scale. The process of initiation of polymerization by protonated DOP was supported by the immediate observation of the end group $\text{HOCH}_2\text{CH}_2\text{CH}_2\text{CH}_2\text{OCH}_2^-$ ($\text{HOCH}_2\text{CH}_2\text{CH}_2\text{CH}_2\text{OCH}_2^-$, 61.59 ppm and $\text{HOCH}_2\text{CH}_2\text{CH}_2\text{CH}_2\text{OCH}_2^-$, 29.55 ppm). These two resonances, with chemical shifts in agreement with literature values (8), were also observed in our control experiment of DOP homopolymerization. The resonance at 61.59 ppm was well resolved whereas the resonance at 29.55 ppm partially overlapped with the corresponding carbon of comonomer DOP. The resonance at 61.59 ppm was clearly observed to increase first and then decline at the time the MBMBM sequence started to decline.

After the initial growth of the pentad sequences with at least one 'B', the MMMMM pentad corresponding to 'B' separated by at least five 'M' emerged and was accompanied by the continued decline of MBMBM sequence. Then, the sequence MMMMM showed a sustained increase together with the rate leveling off for MBMMM and BMMMM at a later stage. At the same time, TOX resonance decreased rapidly, followed by the growth of MMMMM pentad at the highest rate. Unlike the MMMMM pentad, the rate of growth for pentads MBMMM and BMMMM eventually slowed down. Eventually, all three curves became less steep. The two pentads with two 'B' (BMMMMB and MBMMMM) first increased and then decreased in a manner similar to MBMBM but with their maxima occurring much later. The decline of MBMBM and MBMMMM reflected the randomization of the counit 'B', resulting in a TOX/DOP copolymer having thermal stability.

Nonad Sequences

It is noteworthy that in the *in situ* ^{13}C NMR experiment, not only pentads but also heptads and even nonads were observed for some sequences. Heptad sequences have been reported previously for TOX/DOL copolymer (9). In the present study, a number of nonads were identified for 'M'-centered sequences.

For the pentad MMMMM , i.e. $(\text{M})_5$, six nonads are possible through adding 'M' or 'B' to both sides of the pentad: $\text{MM}(\text{M})_5\text{MM}$, $\text{BM}(\text{M})_5\text{MB}$, $\text{MM}(\text{M})_5\text{MB}$, $\text{MB}(\text{M})_5\text{MM}$, $\text{MB}(\text{M})_5\text{MB}$ and $\text{MB}(\text{M})_5\text{BM}$. Only five distinct resonances were observed (Figure 3). It is reasonable to assume that the pentad with nine 'M', $\text{MM}(\text{M})_5\text{MM}$, was not detected due to its very low concentration. Even at the end of the period of our observation, the consumption ratio of 'M'-to-'B' was only 5 to 1. Similarly for the pentad BMMMM , i.e. $\text{B}(\text{M})_3\text{M}$, six nonads are possible: $\text{MMB}(\text{M})_3\text{MMM}$, $\text{BMB}(\text{M})_3\text{MMM}$, $\text{BMB}(\text{M})_3\text{MMB}$, $\text{MMB}(\text{M})_3\text{MMB}$, $\text{MMB}(\text{M})_3\text{MBM}$, and $\text{BMB}(\text{M})_3\text{MBM}$. However, only three

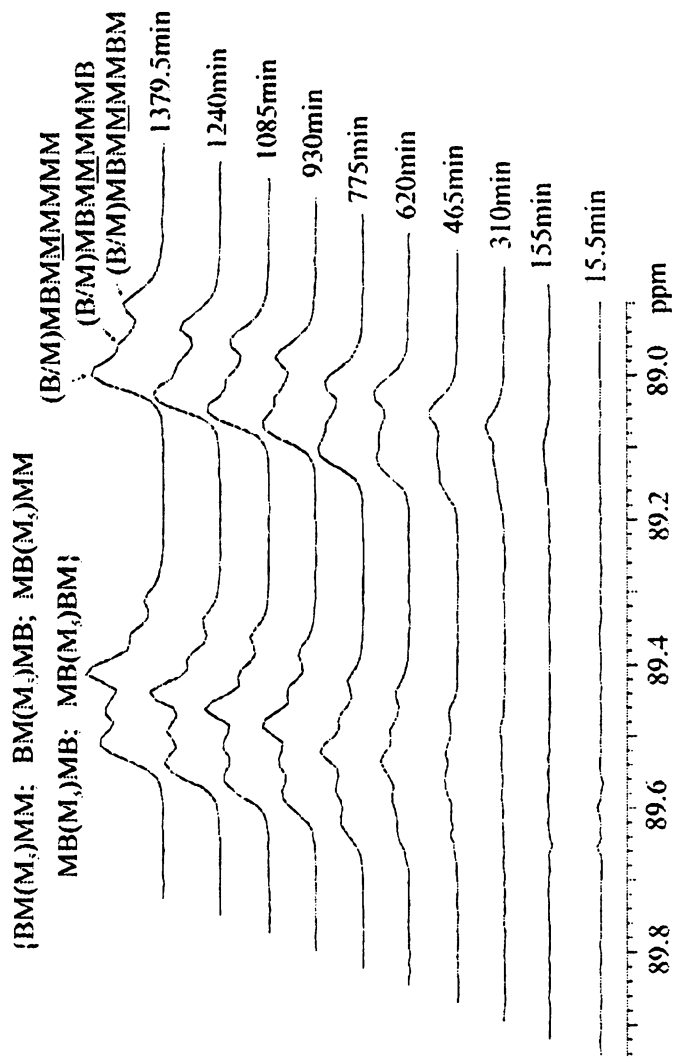


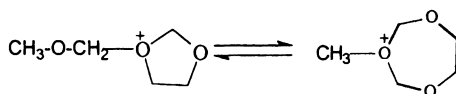
Figure 3. Nonad sequences as a function of time for the bulk copolymerization of TOX/DOP, From Figure 1.

separate resonances were observed. We conclude that the two nonads in each of the three pairs have the same chemical shift: $\text{MMB}(\text{M})_3\text{MMM}$ and $\text{BMB}(\text{M})_3\text{MMM}$; $\text{BMB}(\text{M})_3\text{MMB}$ and $\text{MMB}(\text{M})_3\text{MMB}$; $\text{MMB}(\text{M})_3\text{MBM}$ and $\text{BMB}(\text{M})_3\text{MBM}$. A reasonable generalization is that without the interruption of 'B', which contributes five bonds to the backbone, chemical shift of the center-'M' can be influenced by a *counit* separated by three 'M' units. Within the BMMMM pentad manifold, three separate peaks were assigned as the nonads (Figure 3): $(\text{B}/\text{M})\text{MBMMMMMM}$ at 89.22 ppm, $(\text{B}/\text{M})\text{MBMMMMMB}$, 89.18 ppm and $(\text{B}/\text{M})\text{MBMMMMBM}$, 89.12 ppm.

The above nonad assignments are also consistent with the growth pattern of sequences with separation of 'B' by more 'M' as polymerization proceeds. The nonads $(\text{B}/\text{M})\text{MBMMMMBM}$ contained and therefore contributed to the pentads MMMMB and MMMMB ; all three showed similar growth pattern of emerging at early stage with significant increase followed by a slow leveling off. The nonads $(\text{B}/\text{M})\text{MBMMMMMM}$ contain the pentads MMMMM and MBMMM . The nonads $(\text{B}/\text{M})\text{MBMMMMMM}$ and the pentad MMMMM showed continued significant growth. The nonads $(\text{B}/\text{M})\text{MBMMMMMB}$, containing the pentads MMMMB and MMMMM , slowed down in growth at later periods and contributed to a portion of the MMMMM growth. Detailed separate assignments are not available at present for the five nonads associated with the pentad MMMMM . The *counit* 'B' assumes a range of conformations different from those of 'E' and 'M', thus leading to a different manifestation in chemical shift of microsequences. Replacing the two B_2 carbons of the pentad MBMMM (92.74 ppm) with a 'M' *counit* gives MMMMM (90.04 ppm), leading to an upfield shift of 2.70 ppm. Substituting the edge-'M' of the MMMMM pentad by a 'B' or a 'E' *counit* gives BMMMM (89.60 ppm) and EMMMM (90.74 ppm), resulting in an upfield shift of 0.44 ppm and a downfield shift of 0.70 ppm respectively. Chemical shift assignments are also complicated by the possible involvement of δ -effecton carbon chemical shift for TOX/DOP copolymers. For 'B'-centered sequences, the following sequences were observed: $(\text{M})_4\text{B}_1\text{M}(\text{M}/\text{B})_3$, $\text{B}(\text{M})_3\text{B}_1\text{M}(\text{M}/\text{B})_3$, $\text{BMMB}_1\text{M}(\text{M}/\text{B})_3$, $\text{MBMB}_1\text{M}(\text{M}/\text{B})_2$, $(\text{M})_3\text{B}_2\text{M}(\text{M}/\text{B})_2$, $\text{BMMB}_2\text{M}(\text{M}/\text{B})_2$, and $\text{MBMB}_2\text{M}(\text{M}/\text{B})_2$.

Unlike TOX/DOL copolymerization, where the insertion of formaldehyde into DOL forming trioxepane plays an important role, the insertion of formaldehyde into DOP to form the 9-membered ring, 1,3,5-trioxacyclononane (TOCN), is not observed during the copolymerization of TOX with DOP in our experiments. Two plausible contributing factors can be considered: one is the difficulty of forming 9-membered ring TOCN based on thermodynamics. The second factor is the higher basicity of DOP than DOL. The *comonomer* DOP was found (10) to be more basic and more reactive than DOL. For example, the polymerization of DOP initiated by anhydrous perchloric acid in CH_2Cl_2 was reported (11) to be a thermodynamically more favored process than that of DOL

under comparable conditions. The higher basicity of DOP leads to its much stronger preference to protonation over TOX. The protonation of DOP starts the initial polymerization, hence the immediate appearance of the end group $\text{HOCH}_2\text{CH}_2\text{CH}_2\text{CH}_2\text{OCH}_2^-$. The 5-membered ring DOL was also shown by NMR to behave differently from the 7-membered ring DOP under the influence of cationic species. For methoxycarbenium hexafluoroantimonate as the cationic initiator, the initiation steps for cationic homopolymerization DOL and DOP were shown to be different (12). For DOL, based on NMR data the following species are proposed to coexist at -70°C , with the equilibrium strongly shifted to the right:



In contrast, for the DOP the reaction of the methoxymethyl cation at low temperature was considered to give mostly cationated DOP instead of ring expansion. These observations support our finding of initial DOP homopolymerization without formaldehyde insertion in TOX/DOP copolymerization.

Conclusion

The initial process of copolymerization of TOX with DOP is markedly different from the TOX/DOL system. For the TOX/DOP system, insertion of formaldehyde into DOP to form a larger acetal ring before substantial copolymerization does not play a significant role. The initiation of the homopolymerization of DOP to give a burst of MBMBM sequence dominates the early events. Then a steady decline of MBMBM after its initial burst is accompanied by the emergence of MBMBB , a pentad with 'B' separated by one more 'M' and the growth of pentad sequences with 'B' separated by additional 'M'. Finally, the growth of MMMMM pentad shows the highest rate. The randomization of 'B' units is manifested in the decline of pentad sequences with two 'B' units. The difference in the initiation mechanism between TOX/DOP system and TOX/DOL system is explained in terms of the higher ring strain of TOCN than TOP and the basicity difference between DOP and DOL. The kinetic profiles obtained are based on chemical shift assignment for TOX/DOP copolymers through PFG-HMQC and PFG-HMBC NMR experiments. Sequence nonads have been observed for the first time in copolymer microstructure NMR analysis.

References

1. Fejgin, J.; Tomaszewicz, M.; Cieslak, J. *Polimery (Warsaw)* **1976**, *21*(7), 298; *Chem. Abstr.* **1976**, *85*, 160567.
2. Xu, Y.-M.; He, J.-P.; Huang, X.-Y.; Yang, S.-Y.; Hu, Q.-Z. *Fudan Xuebao, Ziran Kexueban* **1999**, *38*(6), 696; *Chem. Abstr.* **2000**, *133*, 120767.
3. Hill, J. W.; Carothers, W. H. *J. Am. Chem. Soc.* **1935**, *57*, 925.
4. Weissemel, K.; Fisher, E.; Gutweiler, K. *Kunststoffe* **1964**, *54*, 410.
5. Price, M.B.; McAndrew, F.B. *J. Macromol. Sci. A-I*, **1967**, *2*, 231.
6. Pesce-Rodriguez, R. A.; Wang, S.; Yang, N.-L. *Makromol. Chem.* **1990**, *191*, 99.
7. Werner, M. D. Copolymerization Studies of Trioxane and Dioxolane. Ph.D. Thesis, The City University of New York, Staten Island, NY, 1996
8. Liu, Y.; Wang, H.; Pan, C. *Makromol. Chem. Phys.* **1997**, *198*, 2613.
9. Fleischer, D.; Schulz, R. C. *Makromol. Chem.*, **1975**, *176*, 677.
10. Okada, M.; Yamashita, Y. *Makromol. Chem.* **1969**, *126*, 266.
11. Plesch, P. H.; Westermann, P. H. *Polymer* **1969**, *10*, 105.
12. Penczek, S., Kubisa, P., Matyjaszewski, K. *Adv. Poly. Sci.*, **1980**, *37*, 1.

Chapter 19

^1H and ^{13}C Solution NMR of Polyimides Based on 4,4'-Diaminotriphenylmethane: Conformational Analysis Using NOE and Molecular Modeling

Antonio Martínez-Richa¹, Ricardo Vera-Graziano², and Dmitri Likhatchev²

¹Facultad de Química, Universidad de Guanajuato. Noria alta s/n. C.P. 36050. Guanajuato, Gto. México

²Instituto de Investigaciones en Materiales, UNAM, Apdo. Postal 70-360, Coyoacán, 04510, México, D.F.

^1H and ^{13}C -NMR spectra of a model compound and polyimides based on 4,4'-diaminotriphenylmethane were analyzed and assigned. NOE measurements in DMF for a representative polymer were recorded and interpreted with the aid of conformational analysis. Results indicate that conformational forces in the polymer lead to the formation of a round-shape geometry along the polymer chain that comprises five repeating units. This finding is supported by the measured NOE's, which indicates proximity between nuclei that look far apart in the repeating unit. From molecular modeling and NOE's, internuclear distances were evaluated. Limitations of this approach are also discussed.

Aromatic Polyimides find widespread technological applications due to their unique combination of low dielectric constant, chemical resistance and high

thermal and thermooxidative stability. (1-4) Polyimides (PIs) can be conveniently prepared by the condensation polymerization of dianhydrides with diamines. In general, polyimides are synthesized by a multistep method through a polyamic acid or a polyamic ester intermediate. Direct one-step high temperature polycondensation is an alternative route to the preparation of PI when they are soluble in organic solvents.

We have previously reported that polyimides obtained by one-step high-temperature polycondensation of diaminotriphenylmethane (DA-TPM) and aromatic dianhydrides yield flexible and tough films with good mechanical properties. (5-7) Properties of these polyimides, named PI-TPMs, are mainly due to the homogeneity of the repeating units in the polymer backbone, which was demonstrated by UV-visible spectroscopy, CP-MAS ^{13}C -NMR and WAXD analysis. (7,8)

PI-TPMs are soluble in dimethyl formamide (DMF), so they are amenable to be studied by solution NMR in that solvent. In this paper we report a study of the solution NMR spectra of a model compound and PI-TPMs obtained by the one-step route, in DMF- d_7 . NOE measurements aided by molecular modeling proved to be a very valuable tool to understand the conformational details of this class of polymers in solution. It was found that a pentamer model satisfactorily explains the NOE values measured experimentally. The structure of the model compound and the polymers studied are shown in Figure 1.

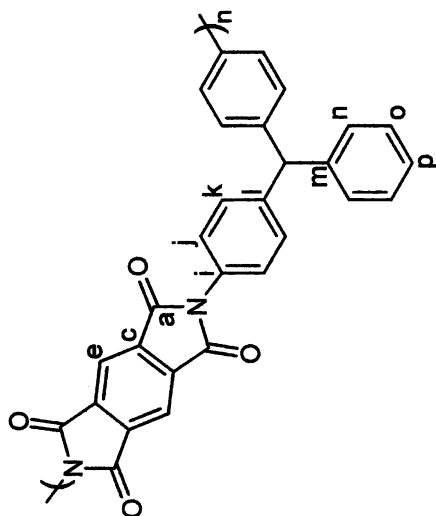
Experimental.

Synthesis of Model Compound.

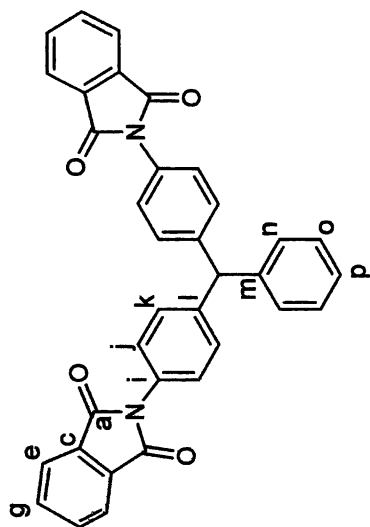
Model compound were obtained by condensation of phthalic anhydrides with DA-TPM, as described elsewhere. (7)

Synthesis of Polyimides.

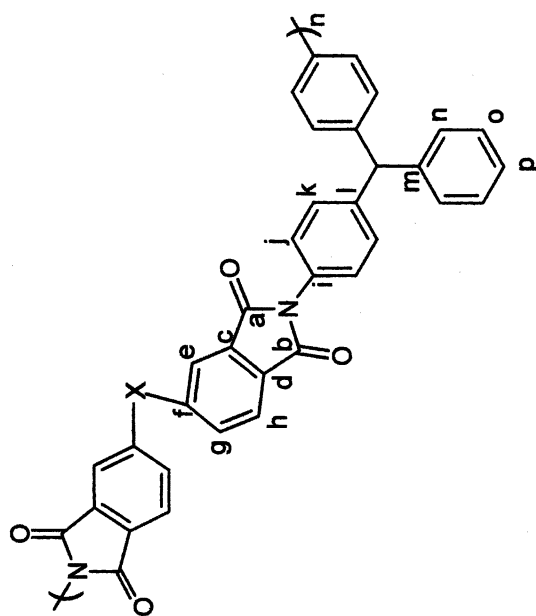
The polyimide films of PI-TPMs were prepared via polycondensation of DA-TPM with the aromatic dianhydrides by one step high temperature procedure in nitrobenzene. (5-7) Structures of PI-TPMs are shown in Figure 1, and the used nomenclature is based on the dianhydride moiety as PM-TPM, BSA-TPM, ODP-TPM and BZP-TPM.



Parent Polymer, PM-TPM



Model Compound



X = SO₂ BSA-TPM
X = O ODP-TPM
X = C=O BZP-TPM

Figure 1. Structures of the Model compound, Parent Polymer (PM-TPM) and the other PI-TPMs studied in this work.

NMR Measurements.

All the solution NMR measurements were performed at ambient probe temperature using 5 mm o.d. sample tubes. Solution ^1H and ^{13}C NMR spectra in $\text{DMF-}d_7$ (PI-TPM's) and CDCl_3 (Model Compound 1) were recorded using Varian Gemini 200 and Varian Unity *Plus* 300 spectrometers. Oxygen was removed from samples by freeze-pump thaw cycles. The chemical shifts are reported taking as a reference the chemical shift positions of the solvent with respect to TMS.

For APT, COSY and $^{13}\text{C}/^1\text{H}$ HETCOR experiments, standard pulses sequence were used. (9-11) For the long-range HETCOR experiment, $J(\text{C,C,H})$ was assumed to be 8 Hz. NOE Difference spectra (homonuclear $^1\text{H}\{^1\text{H}\}$ decoupling experiments) were recorded using the *cyclenoe* sequence. 1024 scans were recorded for each spectrum.

Theoretical calculations.

Energy minimization, conformational searching and molecular mechanics were performed using Alchemy 2000 program system from Tripos loaded on a PC Pentium Computer. For molecular mechanics optimization, the MM3 Molecular Mechanics subroutine with a value of 4.7 for dimethyl formamide dielectric constant, a RMS gradient of 0.05 kcal/Å mol and a delta of energy of 0.001 kcal/Å was used.

Results and Discussion

^1H and ^{13}C NMR spectroscopy.

To assign ^1H and ^{13}C spectra of model compound and PI's, tentative chemical shifts were determined using substituent additivity rules. The APT spectrum allows to determine the number of protons attached to each carbon. $^{13}\text{C}/^1\text{H}$ chemical shift correlation experiment permits the assignment of the protonated carbons, while the non-protonated carbons connectivity is obtained from the long-range HETCOR diagram.

The ^1H NMR spectrum for BZP-TPM is presented in Figure 2. A discussion on the main features of this spectrum is given elsewhere. (12) This spectrum is the base for NOE measurements described below.

In Tables I and II, the proton and carbon-13 chemical shifts for model compound and polyimides are tabulated.

Table I. ^1H NMR chemical shifts in solution (δ_{H} from TMS)*

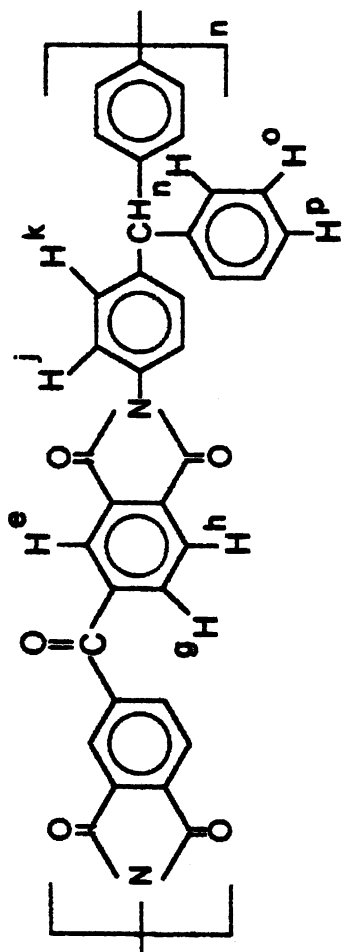
	<i>Model I</i>	<i>PI-TPM</i>	<i>ODP-TPM</i>	<i>BZP-TPM</i>	<i>BSA-TPM</i>
H-e	7.95 ($J_{\text{eg}} = 6.0$ Hz, $J_{\text{eg}} = 3.0\text{Hz}$)	8.48	7.68	8.31	8.69
H-g	7.78		n.d.	8.38 ($J_{\text{gh}} =$ 7.5 Hz)	8.75 ($J_{\text{gh}} =$ 8.5 Hz)
H-h			8.08 ($J_{\text{gh}} =$ 8.0 Hz)	8.22	8.25
H-j	7.4 ($J_{\text{jk}} = 8.5$ Hz)	7.62 ($J_{\text{jk}} =$ 8.1 Hz)	7.56 ($J_{\text{hj}} =$ 8.0 Hz)	7.62 ($J_{\text{jk}} =$ 7.8 Hz)	7.53 ($J_{\text{jk}} =$ 8.5 Hz)
H-k	7.29	7.46	7.43	7.49	7.40
H-n	7.17	n.d.	7.40	7.46	7.30
H-o	7.31	n.d.	7.30	7.35	7.34
H-p	7.21	n.d.	7.24	7.30	7.25
CH	5.64	5.92	5.88	5.92	5.86

* In some cases, chemical shifts for protons n, o and p were resolved by 2-D NMR. n.d. = non determined

Conformational Analysis.

Conformation of model compound and polymers can be described using four or six torsion angles. Conformational search was made by a combinatorial process on 2,985,984 conformers for six torsion angles and 20,796 for four torsion angles. 30 degrees increments were used, and the van der Waals scaling factor was 0.7. The method of conformational analysis searches the global minimum based on the value of total steric energy (which in turn is computed from the sum of compression, van der Waals and torsional energy). So, the final outcome is a family of conformations having populations according to a Boltzmann distribution.

In order to detect structural differences among the computed geometries, 20 conformers with the lowest steric energies were analyzed in terms of internuclear distances and torsion angles. The main variation observed is in the value of torsion angle τ_5 , which indicates that the phenyl ring conformational mobility of the triphenylmethane moiety is the less restrained. This also implies that



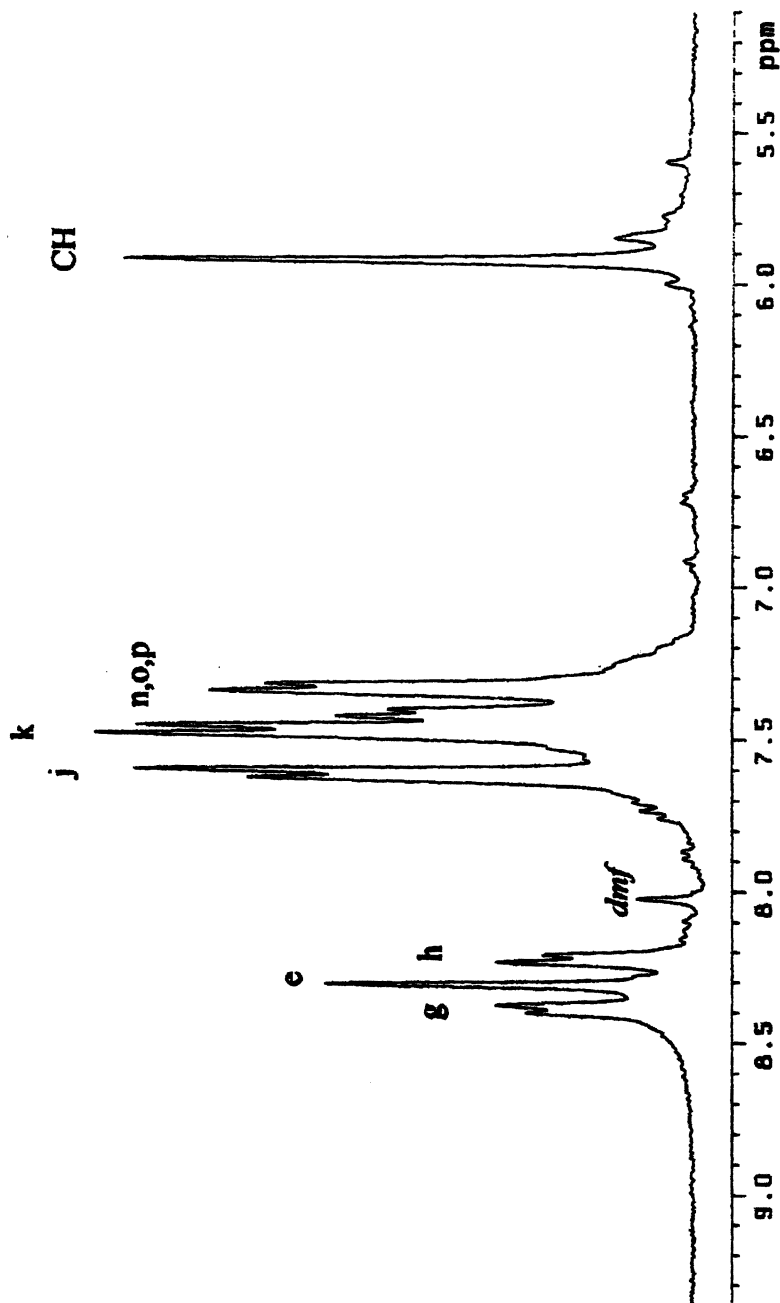


Figure 2. 300.1 MHz High-resolution ^1H NMR spectrum (5.1–9.4 ppm region) of BZP-TPM in dmf-d_7

Table II. ^{13}C NMR chemical shifts in solution (δ_{C} from TMS)

	<i>Model I</i>	<i>PI-TPM</i>	<i>ODP-TPM</i>	<i>BZP-TPM</i>	<i>BSA-TPM</i>
C-a	167.3	167.5	167.1	166.0	166.4
C-b			166.9	167.9	166.2
C-c	131.7	133.7	135.4	132.9	133.8
C-d			128.1	135.7	135.2
C-e	123.8	123.0	114.4	124.6	125.5
C-f	134.4		161.8	142.7	146.4
C-g			125.6	136.7	136.9
C-h			126.6	123.4	123.3
C-i	130.0	131.4	131.2	131.1	130.8
C-j	126.3	128.0	127.8	127.8	127.8
C-k	130.2	130.4	130.8	130.4	130.3
C-l	143.3	145.7	144.4	144.6	144.6
C-m	142.9	144.5	144.2	144.1	143.9
C-n	129.5	130.0	129.9	129.9	129.8
C-o	128.5	129.3	129.2	129.2	129.2
C-p	126.7	124.8	123.8	124.4	127.2
CH	56.2	57.5	56.2	56.4	56.2
C=O				194.1	

internuclear distances calculated between carbons and protons *m*, *n*, *o* and *p* and other atom(s) in the molecule have more variation (up to $\pm 1\text{\AA}$). The other measured torsion angles and internuclear distances in the conformers showed a very small variation (for internuclear distances, the error is lesser than $\pm 0.2\text{\AA}$.)

The molecular structure for the lowest energy conformer of the PM-TPM and BZP-TPM repeating units obtained by this method is depicted in Figure 3. The torsion angles defining the chain conformation are also shown. The energy minima for repeating units and model compounds are close to the torsion angles reported in Table III.

Energy calculations revealed some different characteristics for the two Ar-X torsion angles (see Table III). Analysis of the torsion angles τ_1 and τ_2 indicates that a deviation from coplanar geometry is present, and for X = SO₂ the orientation of sulfone group in the lowest energy conformer is almost perpendicular to the aromatic rings. As a consequence, there is a lack of conjugation between the phenyl ring and the X groups in all repeating units.

Dihedral angles between rings and N-Ar bond of the triphenylmethane moiety are also non-planar, but values do not differ significantly from 0°. Deviation from planarity are more pronounced for torsion angles τ_5 , which

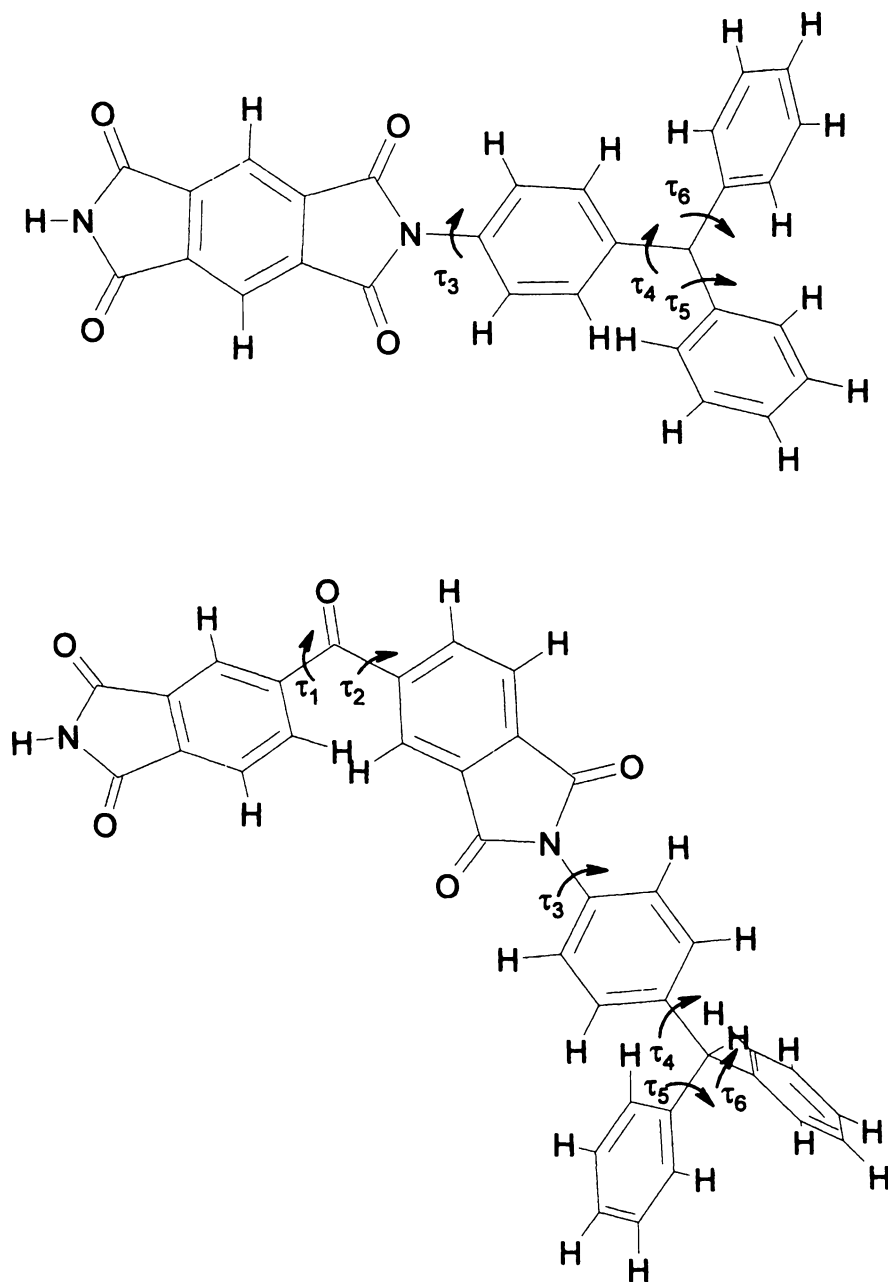
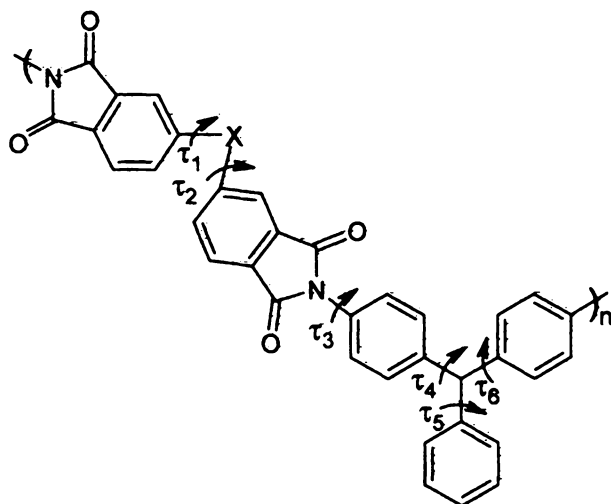


Figure 3. Molecular structure of the minimum-energy conformers for the PM-TPM and BZP-TPM repeating units.

Table III. Torsion angles for model compound and repeating units

Torsion angle	Model compound	PM-TPM	X = O	X = CO	X = SO ₂
τ_1			40.3°	15.9°	82.2°
τ_2			31.0°	38.3°	83.1°
τ_3	8.5°	9.8°	9.2°	-9.5°	15.2°
τ_4	-6.3°	-10.1°	29.4°	5.2°	-11.0°
τ_5	-59.7°	-58.3°	35.7°	59.5°	-60.4°
τ_6	33.6°	-9.2°	35.1°	5.9°	-8.8°

correspond to the phenyl ring that do not bear a substituent in the *para* position. The non-planarity of the aromatic rings in TPM is due to steric hindrance (13)

NOE Difference Spectrum of BZP-TPM.

Nuclear Overhauser Enhancements (NOEs) are useful to understand the conformation and steric configuration of substituents along the polymer backbone. (14,15) NOEs depend in a complex way upon the distances from the observed nucleus to the nearest neighbor protons.

In Figure 4, NOE Difference spectra for BZP-TPM upon irradiation of the different protons are shown. Large homonuclear NOEs are observed in the difference spectra, and these are reported in Table III. As expected, NOE between neighbors atoms are present, but negative peaks near irradiated protons are due to partial saturation by the used irradiation. Spectra obtained upon irradiation of protons *e*, *g* and *h* show a positive NOE with protons *j* and *k*. There is a very small NOE interaction between protons *e*, *g* and *h* and proton *n*. When CH is irradiated, a positive NOE can be distinguished for protons *j*, *k* and a small negative NOE with proton *n*. Interatomic distances derived from the molecule shown in Figure 1 (see Table IV) are longer than expected based on the observed NOEs. So, distances from protons *e*, *g* and *h* to proton *n* indicates that these atoms are very far from each other, so peaks are not expected in the NOE difference spectra. (16) In other words, the measured experimental NOEs can not be explained based on the interatomic distances found in the minimum energy conformer of the repeating unit. This means that the real conformation of the overall polymer in *dmf* can not be properly represented by the repeating unit, and a more realistic representation for PI-TPMs must be obtained.

Refinement of the molecular model for the polyimides.

One approach to understand the molecular geometry of PI-TPMs in solution is to determine the preferred conformation of a short-chain segment of the polymeric chain. With this in mind, the number of repeating units was increased up to five monomeric units and geometry optimization by Molecular Mechanics was undertaken. In Plate 1 we present the molecular geometry of a BZP-TPM pentamer obtained after energy minimization. It is clear that polymer chain shows a strong preference to coil up and adopt a round-shape geometry that is mainly a consequence of the TPM stereochemical influence. The pendant phenyl ring which is only attached to the CH carbon points outward and produce kinks in the polymeric backbone with the resulting round-shape form. Such a close packing molecular arrangement allows a close proximity between some groups that look far apart in the monomeric unit. Internuclear distances observed for this structure are reported in Table IV. It is clear that internuclear distances between interacting protons predicted by this model are shorter than those measured in the repeating unit.

Measured NOEs depends upon many experimental parameters, such as decoupler power, duration of decoupler irradiation, presence of relaxation mechanisms other than dipolar, correlation times of the molecules and the effects of other nearby nuclei through cross-relaxation. (17,18) In that regard, NMR- distance geometry calculations are always approximate. In order to facilitate

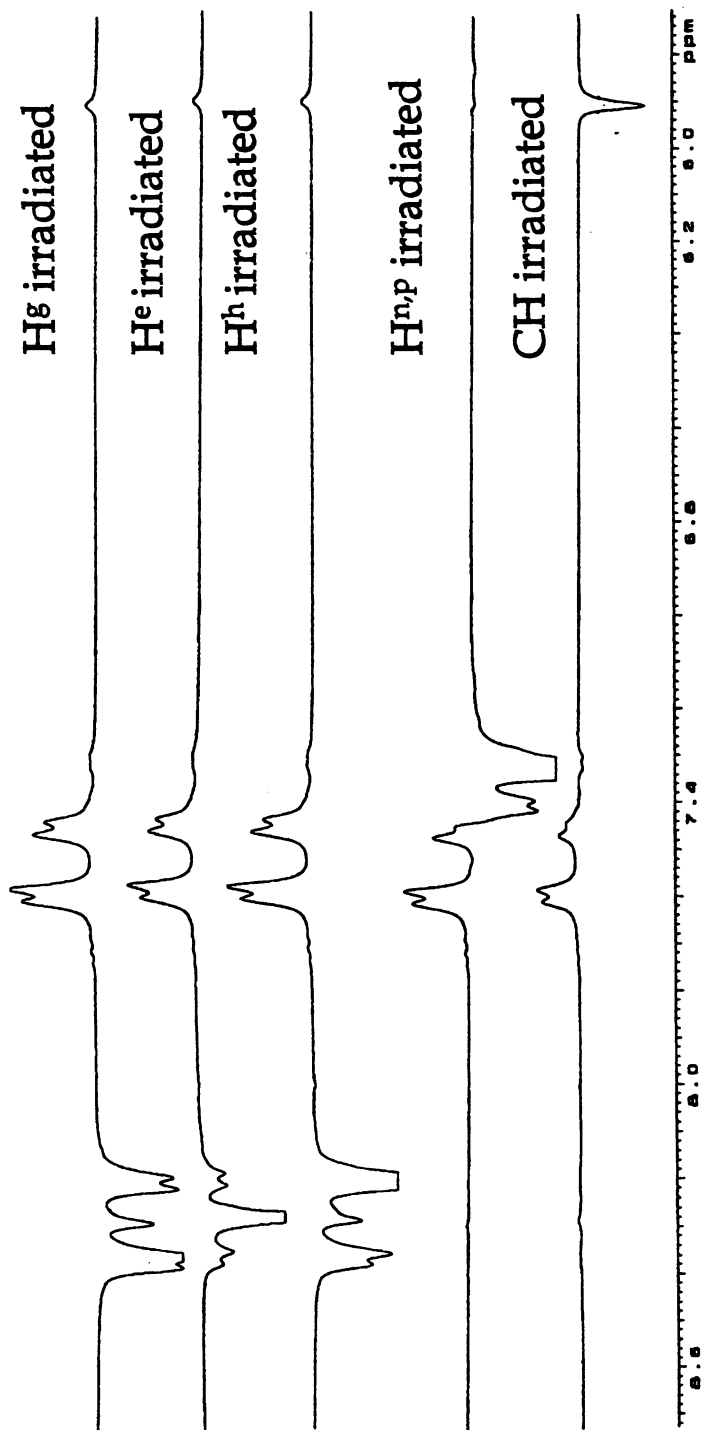
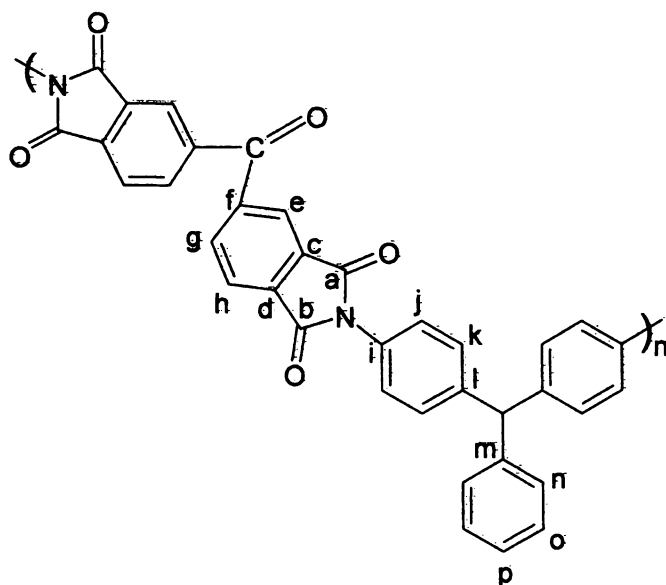


Figure 4. NOE difference spectra of BZP-TPM.

Table IV. Atomic bond distances for the structure obtained after geometry optimization for BZP-TPM repeating unit and for a pentamer



Atomic bond distance (Å)	$n=1$	$n=5$	Observed NOE (%)	Bond distances from NOE
H^e-H^n	8.9, 11.1	5.3, 8.7	w	w
H^e-H^j	5.0, 6.9	3.2, 7.4	55	3.4
H^e-H^k	7.5, 8.8	4.6, 8.1	27	3.8
H^h-H^n	9.8, 11.7	7.9, 10.2	w	w
H^h-H^j	7.2, 9.4	4.5, 7.0	75	3.2
H^g-H^j	7.2, 7.9	5.0, 7.9	75	3.2
H^g-H^k	9.6, 10.2	7.1, 9.4	38	3.6
H^h-H^k	7.4, 8.8	6.1, 8.2	35	3.6
$H^{np}-H^j$	4.3, 6.1	3.5, 6.4	60	3.3
$CH-H^j$	4.8, 5.3	3.5, 4.3	45	3.5*
$CH-H^k$	2.7, 3.5	2.9, 3.9	40	3.6

w = a weak signal was observed in the NOE difference spectrum

* Taken as $r_0 = 3.5 \text{ \AA}$

comparison for data obtained from molecular modeling, internuclear distance calculations were obtained based on the general equation: (16)

$$\text{NOE}({}^1\text{H}) = k r_{\text{AB}}^{-6}$$

where k is an empirically determined constant and r_{AB} is the internuclear distance between protons A and B. Using a value of 3.5\AA for the distance between methine and H^{I} as a standard (r_0), a value of 827\AA^6 is recorded for k . In Table III, the calculated distances from the experimental NOEs for the other interacting protons are tabulated. The computed distances compare better with the values obtained for the pentamer.

Conclusions

Based on one- and two-dimensional NMR experiments, the chemical shifts observed in the proton and carbon-13 NMR spectra of PI-TPMs and model compound were assigned. Conformational energy calculations were used to explain the large experimental NOEs for BZP-TPM in DMF- d_7 . It was found that a model with five repeating units is more appropriate to explain the interaction through NOE present in the polymer chain.

Acknowledgment.

The authors would like to thank Dr. Guillermo Mendoza-Díaz (Universidad de Guanajuato) for recording NOE Difference spectra and insightful comments.

References

1. *Advances in Polyimides and low Dielectric Polymers*; Sachdev, H.S.; Khojasteh; M.M.; Feger, C., Eds.; Proceedings of the 6th International Conference on Polyimides; Society of Plastics Engineers: Hopewell, NY 1997.
2. *Polyimides: Synthesis, Characterization and Applications*; K.L. Mittal, Ed.; Plenum: New York, 1984; Vol. 1 and 2,
3. Sroog, C.É. *Prog. Polym. Sci.*, **1991**, *16*, 561

4. *Materials Science of High Temperature Polymers for Microelectronics*; Grubbs, D.T.; Mita, I.; Yoon, D.Y., Eds.; Materials Research Society Symposium Proceedings; **1991**; Vol. 227
5. Likhatchev, D.; Alexandrova, L.; Tlekopatchev, M.; Vilar, R.; Vera-Graziano, R. *J. Appl. Polym. Sci.*, **1995**, *57*, 37-44
6. Likhatchev, D.; Alexandrova, L.; Tlekopatchev, M.; Martínez-Richa, A.; Vera-Graziano, R. *J. Appl. Polym. Sci.*, **1996**, *61*, 815-818
7. Martínez-Richa, A.; Vera-Graziano, R. *J. Appl. Polym. Sci.*, **1998**, *70*, 1053-1064
8. Likhatchev, D.; Chvalun, S. in ref. 1, pp 167-178
9. Bax, A.; Freeman R.; Morris, G. *J. Magn. Reson.*, **1981**, *42*, 164
10. Bax, A.; Morris, G. A. *J. Magn. Reson.*, **1981**, *42*, 501
11. Bax, A. *J. Magn. Reson.*, **1983**, *53*, 517
12. Martínez-Richa, A.; Vera-Graziano, R.; Alexandrova, L.; Likhatchev, D. in ref. 1, pp 191-219
13. March, J. *Advanced Organic Chemistry*, Wiley: New York, 3rd edition, 1985; pp 149
14. Bovey, F.A.; Mirau, P. *NMR of Polymers*, Academic Press: New York, 1996
15. *NMR Spectroscopy of Polymers*; Ibbett, R.N., Ed.; Chapman and Hall: London, 1993.
16. Farrar, T.C. *Introduction to Pulse NMR Spectroscopy*, Farragut: Madison, 1989; pp 133-140
17. Neuhaus, D.; Williamson, M.P. *The Nuclear Overhauser Effect*, Wiley-VCH: New York, 2nd edition, 2000
18. Dudgeon, H.; Dietrich, W.; Tóth, G. *Structure Elucidation by Modern NMR*, Spinger: New York, 1998

Chapter 20

In-Situ NMR Spectroscopy to Understand the Mechanism of Enzymatic Polymerization of Engineering Polymeric Materials: Poly(phenols)[†]

Sangrama K. Sahoo¹, Wei Liu¹, Lynne Samuelson²,
Jayant Kumar¹, and Ashok L. Cholli^{1,*}

¹Center for Advanced Materials, Departments of Chemistry and Physics,
University of Massachusetts at Lowell, Lowell, MA 01854

²Natick Soldier Center, U.S. Army Soldier and Biological Chemical
Command, Development and Engineering Center, Natick, MA 01760

Coupling mechanism at the early stage of enzymatic polymerization of phenol and substituted phenol such as *p*-sulfonated phenol and *p*-cresol was investigated by in-situ ¹H NMR spectroscopy. The progress of the reaction was monitored in-situ with incremental addition of H₂O₂. At the beginning, the reaction mixture contains mainly monomers along with low molecular weight oligomeric species such as dimers, trimers, etc. Except in the case of *p*-cresol, the consumption of monomers and dimers appeared to be a competing process at the later stage of polymerization. NMR data analysis allows structural identification of various dimers that are formed at the early stage of the reaction. In case of phenol, mixture of C-C and C-O-C coupled products are dominant from the beginning of the polymerization. In contrast, the enzymatic polymerization of *p*-sulfonated phenol shows the predominance of C-O-C coupling while C-C coupling is favored in the case of *p*-cresol.

[†]Dedicated in memory of Professor Sukant Tripathy

Phenolic polymers and phenol-formaldehyde resins are of great commercial interest for a number of electronic and industrial applications (1). However, there have been serious concerns regarding their use due to various toxic effects of formaldehyde and harsh synthesis environments (2). Peroxidase-catalyzed oxidative polymerization of phenol and substituted phenols provides an alternate route for the synthesis of phenolic polymers (3,4). The increased interest in this type of enzyme-based polymerization is mostly due to its environmental compatibility and potential for producing industrial polymers in high yield (5).

Typically, peroxidase-catalyzed polymerization of phenol is carried out in the presence of H_2O_2 , which acts as an oxidizing agent. The free radicals of monomers (substrates) formed initially undergo coupling to produce dimers, and successive oxidation and coupling eventually results in the formation of polymers. The peroxidase-catalyzed polymerization of phenols and substituted phenols usually produce the polymer with complicated structures. The main structure was estimated to be of phenylene units or a mixture of phenylene and oxyphenylene units (5).

Although the structural characterization of the polymers obtained from various phenolic monomers are widely studied, there are limited reports of the nature of coupling at the early stage of the reaction and the nature and position of the substituents on the polymerization mechanism. Till date, very limited nuclear magnetic resonance (NMR) spectroscopy research on the study of mechanism of enzyme-catalyzed polymerization of phenolic monomers was reported (6-8). Recent NMR work on understanding the coupling mechanism of 8-hydroxyquinoline-5-sulfonate and *p*-sulfonated phenol shows that NMR is a sensitive technique to elucidate the molecular mechanism of enzymatic coupling of monomers to form polymers. In this approach it is possible to know the coupling position on the phenol ring and the progress of the reaction with incremental addition of H_2O_2 . Thus, in the present work, we report a detailed structural characterization of enzymatic oxidative polymerization of phenol and two of its substituted derivatives (*p*-sulfonated phenol and *p*-cresol) by in-situ 1H NMR spectroscopy. The emphasis in this report is on the study of coupling mechanism of monomers during the early stage of the enzymatic polymerization.

Experimental

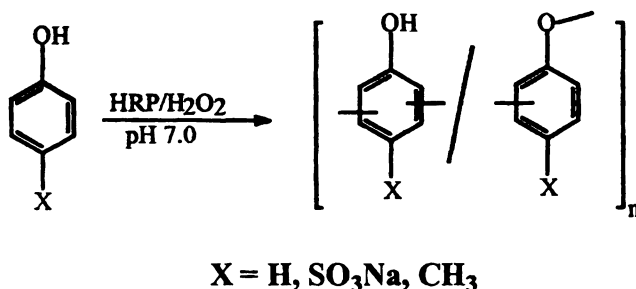
In-situ 1H NMR spectra were recorded on a Bruker ARX-500 MHz NMR Spectrometer at ambient temperature. The polymerization reaction was carried out in the 5 mm NMR tube. The polymerization of phenol and *p*-cresol was carried out in an aqueous-organic medium (0.4 mL of acetone- d_6 and 0.1 mL of pH 7.0, 0.01M phosphate buffer (prepared in D_2O)) to avoid the inhibition of polymerization due to insolubility of the monomers and the resulting dimers and oligomers in aqueous medium. However, polymerization of

p-sulfonated phenol was carried out in purely aqueous medium (0.5 ml, 0.01 M, pH 6.0 phosphate buffer solution) since both the monomers and the resulting dimers and oligomers are readily soluble in water and no precipitate was formed.

To a NMR tube containing 0.5 mL of solvent mixtures, 2 mM of monomer, 0.3 mg of HRP and 0.5 mg of pyrazine were added. Pyrazine was used as an internal standard for monitoring the reaction and its products. The spectrum was calibrated by assigning the singlet for pyrazine to 8.7 ppm with respect to tetramethylsilane (TMS). ^1H NMR data were collected before and soon after each addition of 5 μL of H_2O_2 (0.5 M in D_2O) to the NMR tube containing the reaction mixture. A total 40 μL of H_2O_2 was added in eight increments. A series of spectra were recorded after each incremental addition of H_2O_2 , till there were no changes in the spectral pattern.

Results and Discussion

A generalized oxidative coupling reaction of phenolic monomers is shown in Scheme 1. Two kinds of couplings are possible, (a) C-C coupling to form phenylene units, and (b) C-O-C coupling to form oxyphenylene units.



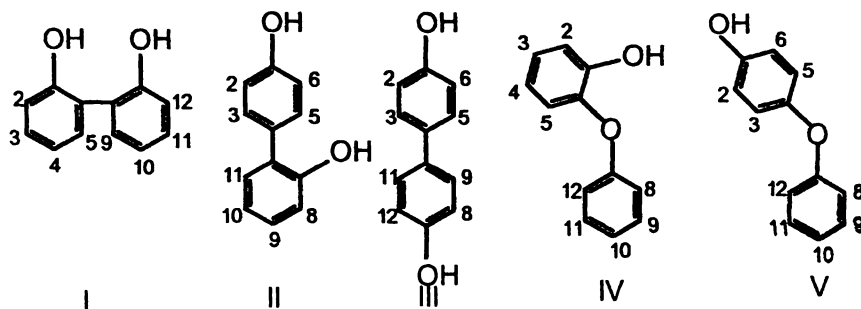
Scheme 1. Schematic of enzymatic polymerization of phenolic monomers.

Polymerization of Phenol

The stack plots of vertically expanded ^1H NMR spectra of the reaction mixture containing phenol and HRP before (a) and after each incremental addition of H_2O_2 (b-h) are shown in Figure 1. The ^1H NMR spectrum of phenol shows two peaks, one triplet (7.21 ppm, meta (*m*-)) and the other one is overlapping multiplet of a triplet and a doublet (6.85 ppm, para (*p*-) and ortho (*o*-)). Each spectrum in Figure 1 is normalized with the height of the internal standard peak at 8.7 ppm. The ^1H NMR spectra shows the decrease in the intensity of the monomer resonances (insert in Figure 1), indicating the

consumption of monomers and simultaneous appearance of new resonance peaks in the same aromatic region. As expected, the intensities of these new peaks are weak compared to the monomer resonances at the early stage of the reaction due to their low concentrations in the reaction mixture.

It is interesting to note that the peak intensities of the two doublets (marked as *) at 6.70 and 8.35 ppm (Figure 2a) that were formed soon after the addition of H_2O_2 , decrease with time and eventually undetectable in the ^1H NMR spectrum (Figure 2a-d). However, subsequent addition of H_2O_2 resulted in the reappearance of these doublets and may be assigned to the formation of an intermediate species, which is subsequently consumed during the reaction. In contrast, the intensities of the other resonances continue to increase with incremental addition of H_2O_2 . A broad overlapped resonance peaks (6.5-8.0 ppm) begin to appear in the ^1H NMR spectrum after few successive addition of H_2O_2 suggesting the formation of high molecular weight products.



Scheme 2. Possible dimers from oxidative coupling of phenol.

The possible dimers from the radical coupling of phenols is shown in Scheme 2. Among the five possibilities, three dimers are as a result of C-C coupling (I-III) while the other two are from C-O-C coupling (IV-V). To get a detailed analysis of the weak resonances, a vertically expanded ^1H NMR spectrum recorded at the intermediate stage of the reaction is shown in Figure 3.

Our emphasis in the analysis of these spectra is to focus on the predominant resonances by comparing the spectra of model compounds along with the use of software for NMR spectral simulation. The peaks at 6.9, 7.1 and 7.35 ppm are assigned to dimer formed by the *p*-C-O-C coupling. The spectrum of the model compound, *p*-phenoxy phenol is shown as an inset in Figure 3. This spectrum was recorded with the same solvent mixture (acetone- $\text{D}_6/\text{D}_2\text{O}$) and shows a strong peak at 6.9 ppm for four protons of the phenol ring (2, 3, 5 and 6) and two *o*-protons of the phenoxy ring (8 and 12) [see Scheme 2(V)]. The other resonances appear at 7.1 (10) and 7.35 (9 and 11) ppm for *p*- and *m*-protons of the phenoxy ring, respectively. All these resonances for the dimers formed by *p*-C-O-C coupling (Structure V, Scheme 2) are identified during the

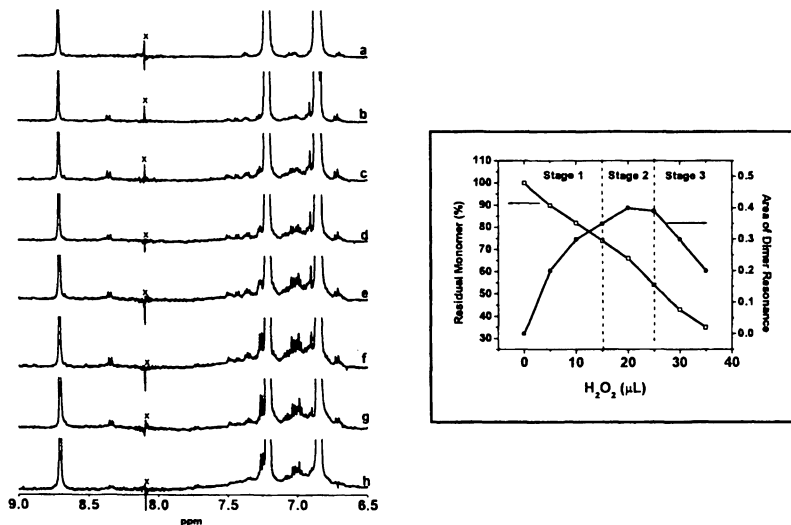


Figure 1. Stack plots of ¹H NMR spectra of the reaction mixture of phenol before (a) and after (b-h) incremental addition of H₂O₂: (b) 5 μL H₂O₂; (c) 10 μL H₂O₂; (d) 15 μL H₂O₂; (e) 20 μL H₂O₂; (f) 25 μL H₂O₂; (g) 30 μL H₂O₂; (h) 35 μL H₂O₂. (X marked for instrumental artifact.)

[Insert: Variation in concentration of residual monomer (open circles) and dimers (filled circles) as function of H₂O₂.]

early stage of the reaction and are marked by * in Figure 3. This observation shows that the formation of C-O-C dimers is a predominant product at very early stage of the reaction. The concentration of these dimers increases rapidly at the initial stage of the reaction but after few incremental additions of H₂O₂, the concentration almost remains the same. At the later stage of the reaction, the concentration of the C-O-C dimer starts decreasing with incremental addition of H₂O₂. The decrease of C-O-C dimer concentration during the later stage of reaction is also accompanied by the appearance of additional resonances, in particular, a doublet at 7.25 ppm. Even though this resonance is not yet assigned but may be related to the formation of oligomers.

The two doublets at 6.70 and 8.35 may be assigned to the *o*- and *m*-protons of the quinone intermediate (e.g. 4,4'-diphenoquinone) formed by the *p-p* C-C coupling of phenol. The NMR spectral analysis of these doublets that were formed soon after the addition of H₂O₂ and subsequently decreased as a function of time (Figure 2a-d), suggests that they are related to the intermediate quinone species formed during the polymerization. This is based on the observation that the quinone intermediate formed by *p-p* coupling of monomers gives only two doublets with larger chemical shift difference than parent phenol and is consistent with the experimental data. There are several other species that are formed during the reaction resulting many weak resonances that are

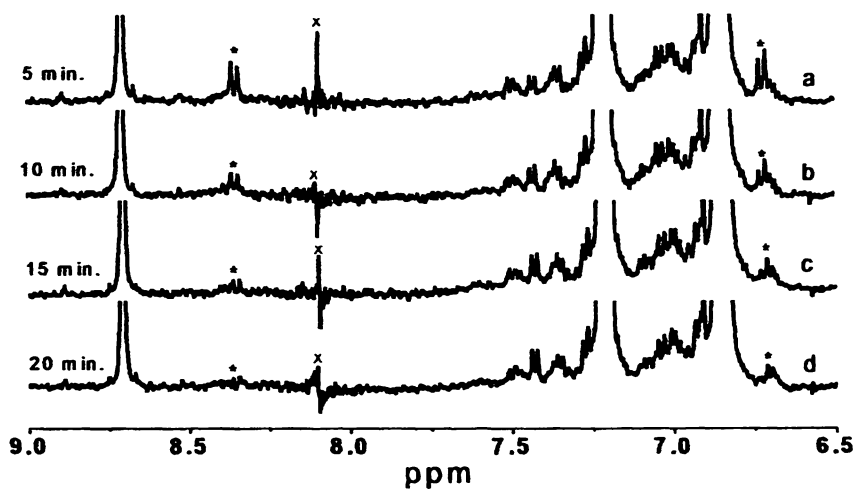


Figure 2. Stacked Plot showing vertically expanded ^1H NMR spectra recorded at different interval of time after addition of fixed amount of H_2O_2 : (a) 5 min., (b) 10 min., (c) 15 min., (d) 20 min. (X marked for instrumental artifact.)

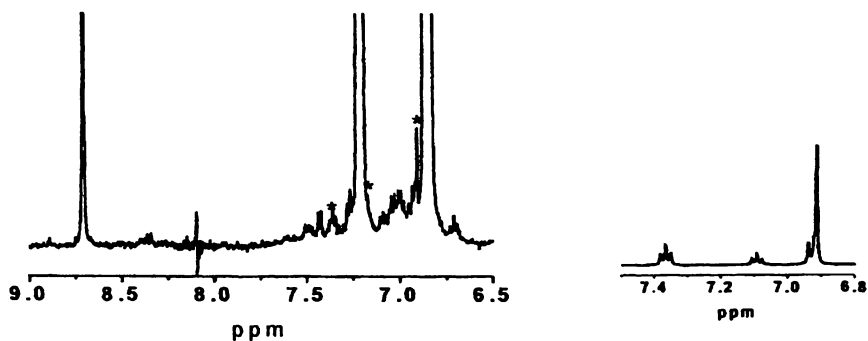


Figure 3. Vertically expanded ^1H NMR spectrum of the reaction mixture after addition of $25\ \mu\text{L}$ of H_2O_2 (Insert: ^1H NMR spectrum of *p*-phenoxy phenol).

overlapped in Figure 1 and may not be easy to assign these resonances. NMR spectral simulation software is useful in predicting the chemical shift ranges for the *o-o* and *o-p* coupled species. This approach allowed us to identify the weak resonances in the 6.9–7.1 ppm and 7.4–7.5 ppm ranges to these *o-o* and *o-p* couplings.

Polymerization of *p*-Sulfonated Phenol

In the case of enzymatic polymerization of *p*-sulfonated phenol, a stack plot of vertically expanded ^1H NMR spectra that were recorded after incremental addition of H_2O_2 is shown in Figure 4. Two doublets at 7.6 and 6.8 ppm are assigned to *m*- and *o*-protons of the monomer (Figure 4a), respectively. With the addition of H_2O_2 , the intensity of these two resonance peaks decreases (Figure 5). New resonance peaks from the polymerized products are also observed (Figure 4(b-i)). The major difference of the reaction mechanism of *p*-sulfonated phenol in comparison to phenol is the absence of intermediate quinone like species. One possible explanation for the absence of quinone like intermediate may be the presence of bulky sulfonated group at the para position with respect to phenolic $-\text{OH}$ groups, restricting the coupling at para position.

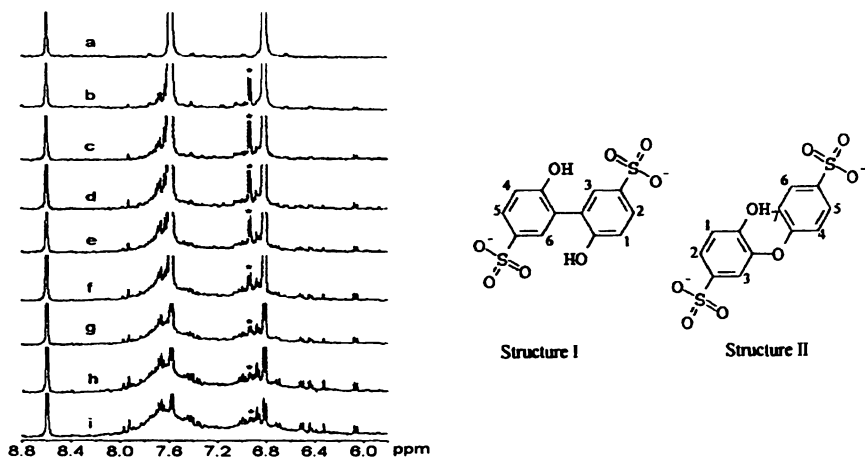


Figure 4. Stack plots of ^1H NMR spectra of the reaction mixture of *p*-sulfonated phenol before (a) and after each 5 μL addition of H_2O_2 (b-i) (Reproduced from reference 7. Copyright 2001 American Chemical Society.)

A strong doublet appears at 6.9 ppm (labeled with *) in the ^1H NMR spectrum of the early stage reactions and it is believed that this peak is from one of the predominant dimer products formed during the polymerization. Among the four possible monomer coupling reactions for the formation of dimers, two likely occurring dimers are shown in Figure 4: 1) *o-o* C-C coupling (Structure I);

2) *o*-C-O-C coupling (Structure II). The observed experimental results suggest that the formation of the dimer with Structure I is not predominant in the reaction. On the other hand, the spectral pattern of the observed resonance peaks matches well with Structure II that results from the C-O-C coupling. The *o*-protons (4 and 7) are assigned to the resonance peaks at 6.90 ppm, while the *m*-protons (5 and 6) to the resonance peaks at 7.60 ppm. The *m*-protons 2 and 3 of the other phenyl ring are assigned to the singlet resonance peak at 7.40 ppm and to the doublet resonance peak at 7.70 ppm, respectively. The resonance peak of the proton 1 is expected to be slightly upfield compared to the protons 4 and 7, and may be overlapped with the monomer peak at 6.80 ppm.

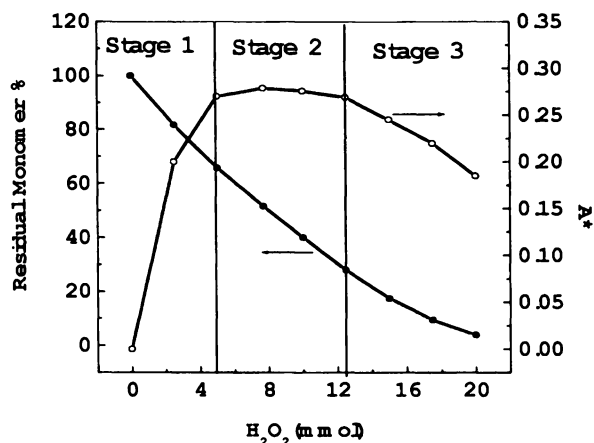


Figure 5. Plots of residual monomer (% in filled circles) and the peak integrals (A^* , in open circles) at 6.9 ppm from the formed dimer product in Figure 4 as a function of H_2O_2
(Reproduced from reference 7. Copyright 2001 American Chemical Society.)

The concentration variation of the predominant dimer (the area under the doublet at 6.90 ppm) is plotted as a function of the concentration of H_2O_2 (Figure 5). The process of this peroxidase-catalyzed polymerization reaction may be divided into three different stages based on the variation of the dimer concentration in the system (separated with lines). Stage 1 is the proliferation of the dimer products. A rapid population growth of dimers is observed at early stage of the reaction. Stage 2 is the dynamic equilibrium of the dimer products. The concentration of dimer products is almost kept at the same concentration level in the system at stage 2, though the monomer is continuously being converted. This is an indication that the dimers are also consumed in the reaction to form higher molecular weight products such as trimer and tetramer etc. The last stage is the reduction of the dimer products (Stage 3). After the conversion

of the monomer is over 70%, the dimer concentration in the system decreases gradually.

Polymerization of *p*-Cresol

The ^1H NMR spectrum of *p*-cresol show two doublets due to *o*- and *m*-protons at 6.75 and 7.0 ppm respectively (spectrum not shown). In addition new resonance peaks appeared in the 6.0 to 7.60 ppm range after first incremental addition of H_2O_2 . In the subsequent spectra recorded after successive incremental addition of H_2O_2 , the intensity of these new peaks increased resulting a complex spectral pattern in the 6.60 to 7.30 ppm region. The nature of dimers and oligomers are identified with a similar approach that was adopted for phenol and *p*-sulfonated phenol polymerization.

The vertically expanded ^1H NMR spectrum after addition of 20 μL of H_2O_2 is presented in Figure 6 to show all the new peaks arising from the enzymatic polymerization of *p*-cresol. Because of the complex spectral pattern arising from various products, again, only the prominent peaks that appear at early stage of the reaction are assigned. Similar to what we observe in *p*-sulfonated phenol, both the C-C and C-O-C couplings are possible in the present case. However, unlike sulfonated group, the methyl group is less bulky to hinder sterically the *p*-position from the coupling reaction. But the coupling at *p*-position leads to the formation of quinone type species as observed in the polymerization of phenol. Two doublets at 6.30 and 7.50 ppm are appeared after each incremental addition of H_2O_2 (Figure 6) and clear distinct from the rest of the resonances. The up- and down-field shifts of these two resonances compared to monomer resonances are assigned to the formation of quinone type species (8). However, the detail analysis of this doublets by 2D NMR and NMR spectral simulation showed that unlike in phenol, the coupling in *p*-cresol to form quinone is not by *p-p* but by *o-p* coupling. However, during the each step, quinone rearranges to form a ketonic type species, known as Pummerer's ketone (8,9). Unlike in phenol, the majority of the ketones formed remains as an isolated side product, and only a few take part in the polymerization. The presence of ketonic moieties in the final polymer product is also reported by Premachandran et al. (9) for poly(*p*-ethyl phenol).

However, the main chain growth during the polymerization is expected to involve the *o*-position of the ring and two possible dimer structures are shown in Figure 6. The NMR spectrum of Structure I (Figure 6) should contain two doublets and one singlet. A doublet at 6.93 ppm (*o*-protons; 2,12) and singlet 7.04 ppm (*m*-protons; 5,9) are intense at the early stage of the reaction. A partially overlapped doublet (which is resolved in the COSY plot, not shown) also present adjacent to 7.04 ppm (*m*-protons; 3,11) resonance. These three

resonances are tentatively assigned to the formation of *o-o* C-C dimers. Structure II shows the other possible C-O-C dimer structure. The two doublets in the region 6.8 (*o*-protons; 8,12) and 7.1 (*m*-protons; 9,11) ppm are assigned to the four protons of the Structure II (Figure 6). The resonances for protons at 2 and 3 position of Structure II appear in the 6.85-6.9 ppm range while the peak of proton 5 may be overlapped with the monomer peak at 6.75 ppm. The ^1H NMR data analysis suggests that, *o-o* C-C coupling takes place preferentially compared to the *o-C-O-C* coupling.

The integral area of protons of residual monomer is shown in Figure 7. The monomer concentration decreases with each incremental addition of H_2O_2 . However, unlike phenol and *p*-sulfonated phenol, in this case, the dimer concentration increases and gradually decreases. There is no equilibrium stage in which both the formation and consumption of dimer takes place. This suggests that the reactivity of monomer may be higher compared to dimers and the rate of consumption of dimers accelerates only when the monomer concentration is depleted to a very low level.

Conclusion

Monitoring the enzymatic polymerization during the early stage by NMR shows the formation of predominant dimeric species. The higher concentration of C-C coupling during the early stage of the enzymatic polymerization of *p*-cresol is an interesting observation simply because, in the case of *p*-sulfonated phenol, the predominant coupling is through C-O-C coupling where as both type of couplings are equally probable in case of phenol. The variation may be due to the nature of substituents in the para-position of the monomer with respect to phenolic -OH group. In case of *p*-sulfonated phenol, the para substituents are electron withdrawing while $-\text{CH}_3$ is electron-donating group and may have a role in the radical coupling mechanism.

Acknowledgement

The support of this research by the National Science Foundation (NSF Grant No. DMR-9986644) is gratefully acknowledged.

Literature Cited

1. Brode, G.L. Kirk-Othmer Encyclopedia of Chemical Technology, 3rd Ed., Wiley, New York, 1982, 17, p 384.

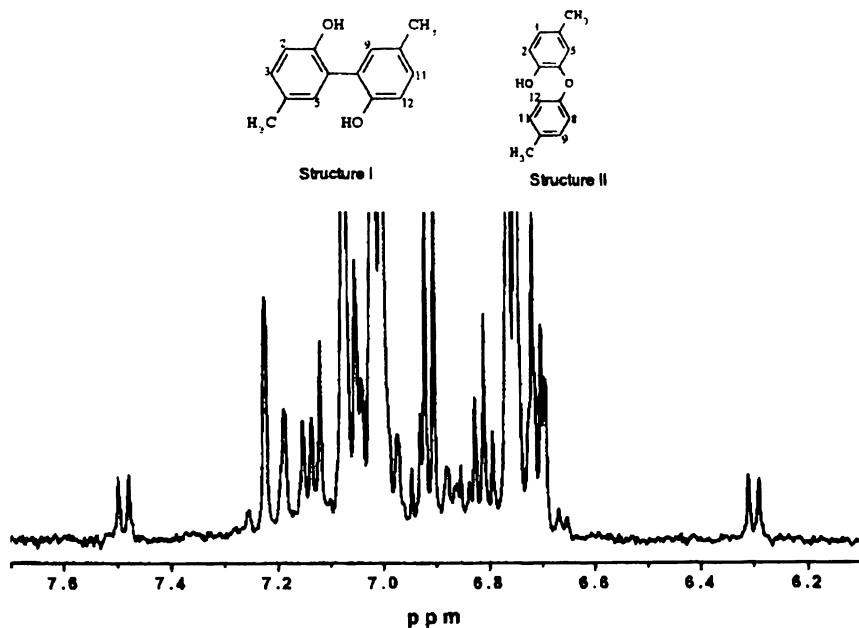


Figure 6. Vertically expanded ^1H NMR spectrum of the reaction mixture after addition of $20\ \mu\text{L}$ of H_2O_2 .

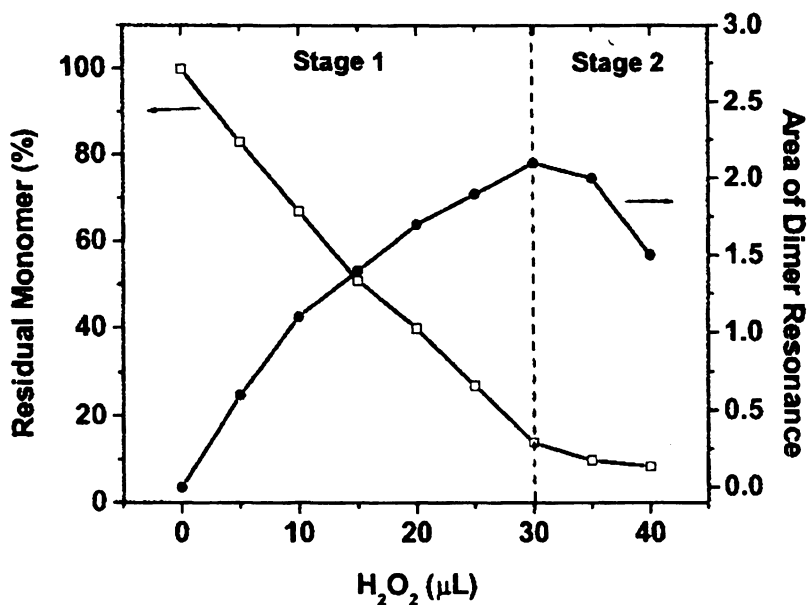


Figure 7. Plot showing the variation in concentration of residual monomer (in open squares) and dimers (Structure I, in filled circles) as a function of H_2O_2 concentration.

2. Dordick, J. S.; Marletta, M. A.; Klibanov, A. M. *Biotechnol. Bioeng.* **1987**, *30*, 31-36.
3. Akkara, J. A.; Senecal, K. J.; Kaplan, D. L. *J. Polym. Sci., Part A: Polym. Chem.* **1991**, *29*, 1561-1574.
4. Ayyagar, M.S.; Marx, K.A.; Tripathy, S.K.; Akkara, J.A.; Kaplan, D. L. *Macromolecules*, **1995**, *28*, 5192-5197.
5. Uyama, H.; Kurioka, H.; Kaneko, I.; Kobayashi, S. *Chem. Lett.* **1994**, 423-426.
6. Alva, K. S.; Samuelson, L.; Kumar, J. Tripathy, S. K. Cholli, A. L. *J. Apl. Polym. Sci.* **1998**, *70*, 1257-1264.
7. Liu, W.; Cholli, A.L.; Kumar, J.; Tripathy, S.; Samuelson, L. *Macromolecules* **2001**, *34*, 3522-3526.
8. Sahoo, S.K.; Liu, W.; Samuelson, L.; Kumar, J.; Cholli, A.L. *Polym. Mat. Sci. Engg.* **2001**, *42*, 569-570.
9. Premachandran, R. S.; Banerjee, S.; Wu, X.-K.; John, V. T.; McPherson, G. L.; Akkara, J. A.; Ayyagari, M.; Kaplan, D. L.; *Macromolecules* **1996**, *29*, 6452-6460.

Chapter 21

Origins of Flexibility in Complex Polysaccharides

C. Allen Bush

Department of Chemistry and Biochemistry, University of Maryland
Baltimore County, Baltimore, MD 21250

Abstract

Flexibility in complex bacterial polysaccharides and glycosaminoglycans is important both for their interactions with proteins and for such physical properties as gel formation and viscosity. Although the existence of high resolution NMR spectra for some polysaccharides with molecular weights over 100 kD implies some elements of flexibility, in fact molecular modeling shows the individual disaccharide linkages to be less flexible than those of peptides. Some small oligosaccharide epitopes adopt compact and rigid folded conformations as can be shown by NOE studies, molecular modeling and measurements of residual dipolar coupling in liquid crystal solutions. In polysaccharides, the rigid epitopes are connected by flexible hinges characterized by conformational exchange among a few local energy minima. ^{13}C scalar coupling measurements are an effective tool for characterizing the hinge residues.

The nature of polysaccharide flexibility

The complex polysaccharides of bacterial capsules and of glycosaminoglycans typically have high molecular weights, generally over 100 kD and some can be millions. Yet many of them give NMR spectra that are well resolved with line widths of a few Hz. In contrast, globular proteins with molecular weights over 100 kD give generally poorly resolved spectra due to broad lines caused by slow tumbling. The short T_2 prevents coherence transfer so that many NMR experiments commonly used for assignment of spectra are ineffective. This is a serious limitation of the use of NMR spectroscopy for larger proteins. Clearly there are some very fundamental differences in the dynamic behavior of polysaccharides and globular proteins.

If all the glycosidic linkages were completely rigid, the polysaccharide would tumble as a single extended unit and the polysaccharide would be expected to have very short T_2 and extensive line broadening. The existence of NMR spectra for polysaccharides argues that at least some of the glycosidic linkages must be partially flexible.

A possible conclusion from these observations is that the linkages of polysaccharides are more flexible than are those of polypeptides. But in fact, molecular modeling of the glycosidic linkages in disaccharides shows that, while the conformational space available is variable depending on details of the stereochemistry, disaccharides are generally somewhat less flexible than are dipeptides. When calculated with similar methods, the latter have a greater low energy area on the dipeptide map than is available in disaccharide maps. The conformational space available for linkages to the secondary hydroxyl groups for a typical disaccharide linkage is more restricted than that for a dipeptide map. This is illustrated in Figure 1 which compares the energy contour map for a typical β -linked (1 \rightarrow 3)-disaccharide with that for the alanine dipeptide calculated with the same algorithm and force field and plotted with the same energy range and contour interval. The greater restrictions on the disaccharide map result from stereochemical clashes between the bulky rings of the sugars. These restrictions are even more pronounced in the case of branched oligosaccharides or (1 \rightarrow 2)-linkages in which sugar substituents occur on adjacent positions, (1).

An important result of the flexibility of the peptide linkage is that if polar or nonpolar attractive interactions occur among the residues of a peptide, the flexibility of the chain allows it to fold into a compact globular form. While a polypeptide of random amino acid composition and sequence might not fold, the globular proteins which are generally studied by NMR spectroscopy are those which do express their inter residue interactions by adopting a folded conformation. In contrast, the less flexible linkages of a polysaccharide do not allow the polymer to fold into a globular conformation.

Since polysaccharides have polar groups as well as some hydrophobic features, there can be inter residue interactions in a polysaccharide as well, but these attractions are expressed as interactions between different chains giving rise to such phenomena as crystallization which is prominently expressed in chitin and in cellulose. Other types of polysaccharides exhibit multistrand helix formation as in the case of scleroglucan whose tendency for triple helix formation leads to unusual physical properties. Still other types of polysaccharides can form cross links in a more random way leading to gel formation as in the case of pectin, agarose and alginates. Chain interactions in other polysaccharides such as hyaluronan, chondroitin or

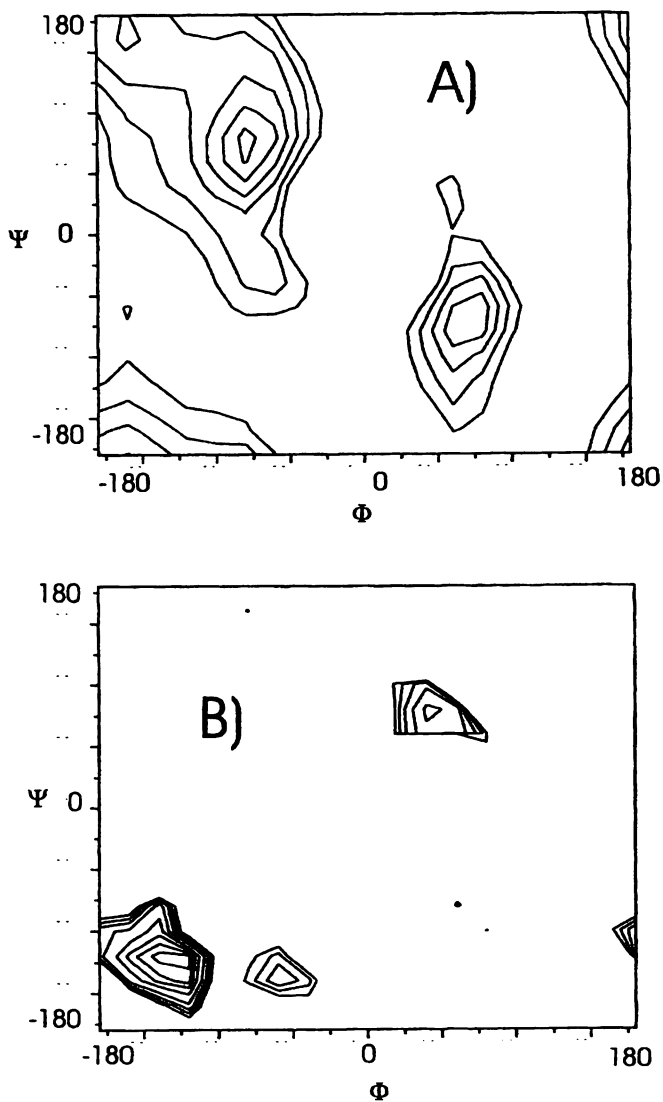


Figure 1 Comparison of relaxed maps made with Charmm software and plotted at contour intervals of 1 kcal/mole. A) Alanine dipeptide. B) Disaccharide, Gal β -(1 \rightarrow 3)-Gal β -

xanthan produce highly viscous solutions. These inter chain interactions give rise to some important biological properties which are characteristic of high molecular weight polysaccharides.

The highly varied physical properties of polysaccharides are of considerable interest both in technology and in biology. Likewise the NMR spectroscopic properties of different polysaccharides are highly varied. On the one hand, some polysaccharides, such as the antigenic cell wall polysaccharide of the common oral bacterium *Streptococcus mitis* J22 give very well resolved spectra with line widths of 1-2 Hz even in spectra recorded at room temperature (Figure 2). Heteronuclear relaxation experiments on this polysaccharide show that this is a typical dipolar relaxation phenomenon, (2). Oligosaccharides made from the polysaccharide show spectra which are not too widely different and detailed measurements of the relaxation data show the dynamics differ but only modestly (3).

Other high molecular weight polysaccharides, such as the capsule of *V. cholerae* O139, have modest line broadening and the line widths in room temperature spectra are quite large. But as shown in Figure 2, at temperatures of 60° C the line widths are reduced to approximately 5 Hz and the standard NMR coherence transfer experiments work reasonably well, (4). Since heteronuclear ¹³C NMR spectroscopy has become the predominant tool for obtaining information on the covalent structure of complex bacterial polysaccharides, the improvements in spectral line widths at elevated temperatures are important with NMR methods replacing many of the chemical techniques greatly simplifying complete structure determinations, (5).

But there are some serious complications in complete structure determination of polysaccharides by NMR. As illustrated in Figure 2C, some polysaccharides such as pneumococcal type 1 capsule give line widths so broad that they cannot be readily assigned by standard coherence transfer methods, (6). Even at elevated temperature the standard COSY and TOCSY methods for coherence transfer fail and modern NMR methods for structure determination become useless. In the most extreme situation, there are certain polysaccharides which apparently dissolve well giving clear non-viscous solutions free from light scattering but which give NMR spectra so broad as to be essentially non-observable. Examples of this behavior are not generally discussed in the primary literature.

Both the wide variations in hydrodynamic properties and in the NMR spectroscopic properties of polysaccharides having different chemical structures must depend on details of the composition and linkages. Unlike polypeptides, the stereochemical possibilities for saccharide linkages are highly varied. The bond between the glycosidic carbon and oxygen atoms of a pyranoside residue can be either axial or equatorial as can be

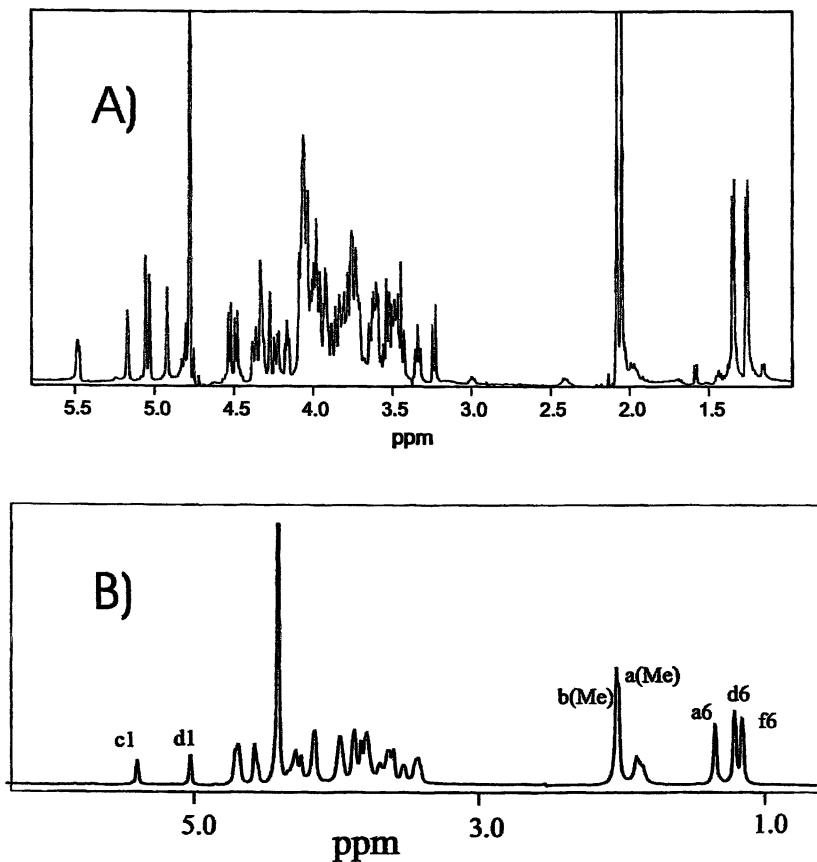


Figure 2. Comparison of ^1H NMR spectra recorded at 500 MHz for three high molecular weight bacterial polysaccharides. A) Cell wall polysaccharide from *Streptococcus mitis* J22 at 23°C . B) Capsular polysaccharide of *Vibrio cholerae* O139 at 60°C . C) Capsular polysaccharide from *Streptococcus pneumoniae* type 1 at 50°C .

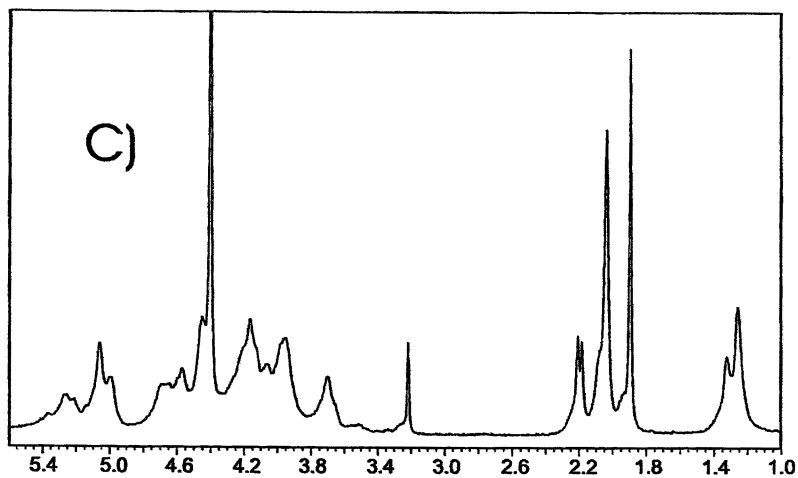


Figure 2. *Continued.*

the configuration of the aglycone carbon atom providing four fundamentally different stereochemical schemes. An additional influence is the chemical functionality of substituents at positions adjacent to the linkage atoms. Commonly found in polysaccharides are amides and acetates, as well as additional glycosidic linkages and charged groups such as sulfate or phosphate. It is just such substituents which limit the conformational freedom of an individual glycosidic linkage.

Rigid linkages and internal motion of the first kind

At the extreme limiting case of the least flexibility are certain glycosidic linkages with very crowded stereochemistry and very little internal motion. The most well known of these relatively rigid oligosaccharide epitopes composed of three or four residues are the blood group oligosaccharides, especially the Lewis epitopes. They have been studied by workers in a number of different laboratories using different techniques over a span of many years. The results of NOE studies (7,8), molecular dynamics simulations (9,10) scalar coupling (11,12) x-ray crystallography (13,14) and most recently residual dipolar coupling measurements (15) generally agree on well defined single conformations for such oligosaccharides. Rather than considering such epitopes as completely rigid, we characterize them as having internal motion of the first kind. The pyranoside rings adopt well defined chair conformations which are readily characterized by ^1H - ^1H scalar coupling constants. The chair puckering motions are of a small amplitude and on a picosecond time scale. The glycosidic dihedral angles exhibit rapid fluctuations on the time scale of a few picoseconds and amplitudes on the order of 10 to 15°.

Flexibility and internal motion of the second kind

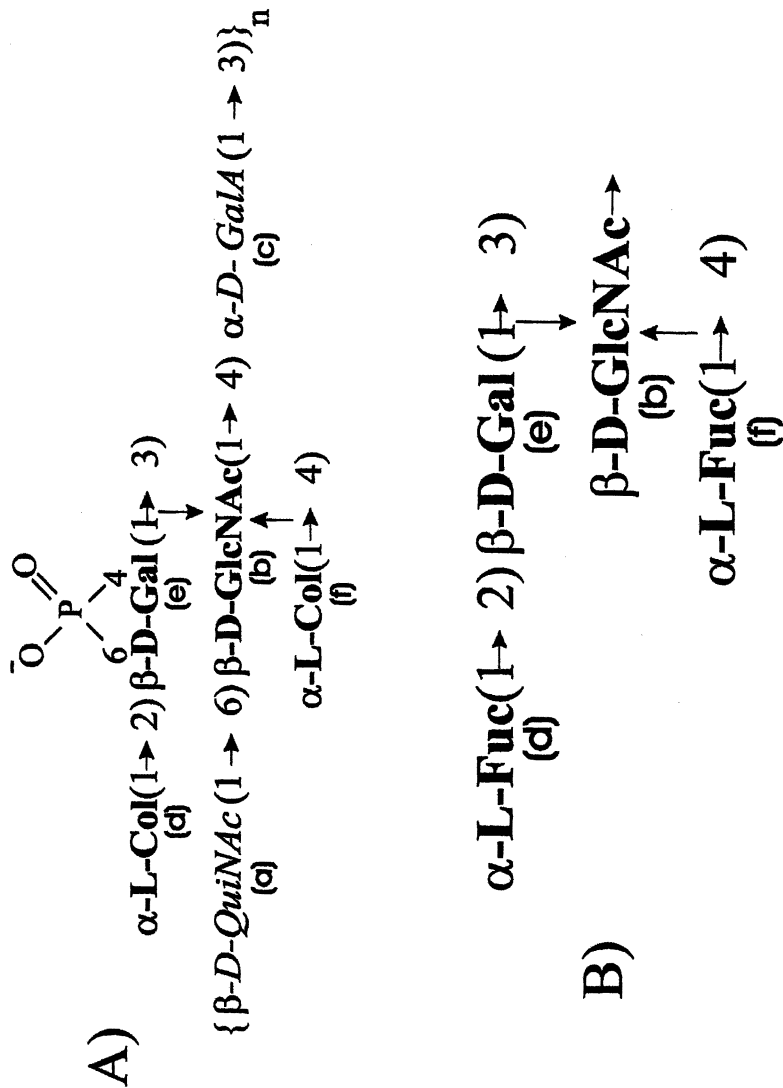
Obviously not all glycosidic linkages are so restricted and they may have much larger amplitude fluctuations which we will characterize as internal motions of the second kind. We will further describe this motion as being conformational exchange between local energy minima on the map of the Φ vs. Ψ surface such as Figure 1B. The energy minima differ by more than 30 to 50° and they are separated by an energy barrier. The height of such barriers is not generally well known but its magnitude clearly determines the kinetics of the conformational exchange involved in this type of internal motion. The detailed kinetics of this conformation exchange is also not known very well but NMR relaxation rates imply that the time scales must be more than a few nanoseconds and in some cases could be much longer (2,16,17).

The time scale is probably not longer than a few microseconds for if it were, the motions could be detected by well known methods for characterizing slow "chemical exchange" motions which range between 100 microsec

and a few millisecond. Although such motions have been detected in a number of cases for proteins, they have not generally been seen in either polysaccharides or oligosaccharides. The fact that the broad NMR lines seen for some polysaccharides (Figure 2) are never seen in oligosaccharides argues against the wide occurrence of such slow chemical exchange broadening. Small oligosaccharides containing a few repeating units have been prepared from both the type 1 pneumococcal polysaccharide (6) and from the *V. cholerae* O139 polysaccharide (Stroop, Adeyeye and Bush, unpublished results) and in both cases these oligosaccharides show line widths of 1-2 Hz in room temperature spectra in contrast to the data of Figure 2. There remains considerable uncertainty about the kinetics of internal motion of the second kind in complex polysaccharides. The time range between 50 ns and 50 microseconds spans three orders of magnitude of unknown territory and unfortunately most NMR measurements are not very sensitive to motions in that time range.

Flexibility of high molecular weight polysaccharides

This classification of flexibility into distinct categories suggests that flexibility in complex polysaccharides can be described in terms of rigid units of several sugar residues exhibiting internal motion of the first kind which are connected by relatively more flexible hinges having internal motion of the second kind. Such a model has been shown to be applicable for the antigenic cell wall polysaccharide of *Streptococcus mitis* J22. (See Figure 3.) This polysaccharide, with seven sugar residues in the repeating subunit, is important in the coaggregation of oral bacteria in the early stages of formation of dental plaque. It has, in addition to an antigenic epitope composed of four sugar residues, a lectin receptor epitope of two residues and has been studied by NMR techniques such as nuclear Overhauser effects and long-range C-H and C-C scalar coupling measurements on ^{13}C enriched samples of the polysaccharide (18). The isolated repeating subunit, a heptasaccharide, has been studied by similar methods and also by residual dipolar coupling data partially oriented in liquid crystalline media, (19). The data are interpreted with molecular modeling studies which show that the heptasaccharide contains a relatively rigid unit of four sugar residues which make up the antigenic site of the polysaccharide. A distinct disaccharide which serves as the lectin binding site in coaggregation with certain species of actinomyces is also shown to adopt a well defined conformation. Flexibility in this heptasaccharide occurs in the linkages of the β -galactofuranoside residue which joins these two more rigid structures by (1 \rightarrow 6)-linkages (Figure 3). In the polysaccharide, the heptasaccharide units are joined by phosphodiester linkages which confer additional flexibility to the high molecular weight polysaccharide. While the models for the rigid epitopes of this polysaccharide are reasonably well defined, the



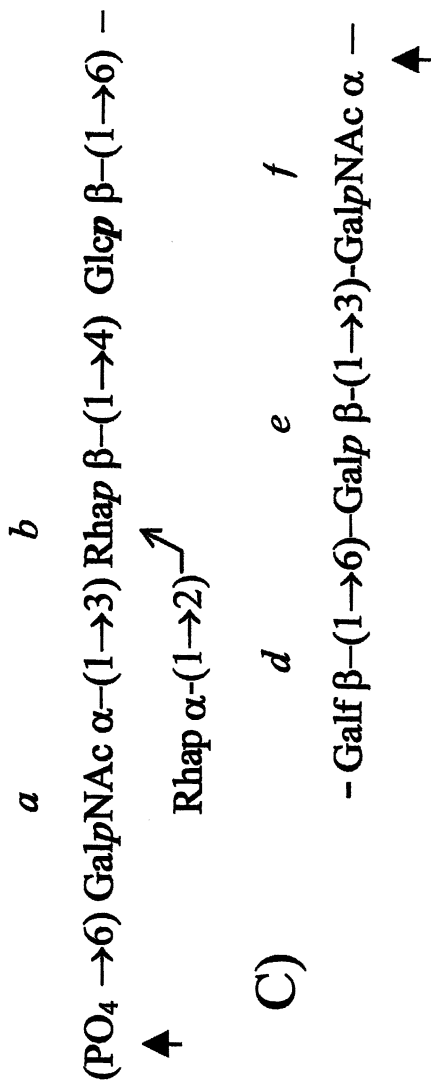


Figure 3 A) Repeating hexasaccharide subunit of the capsular polysaccharide of *V. cholerae* O139. Colitose is 3,6 di-deoxy-L-galactose. QuiNAc, N-Acetyl quinovosamine is 6-deoxy N-Acetyl glucosamine. B) The Lewis^b tetrasaccharide epitope. C) The repeating heptasaccharide subunit of the cell wall polysaccharide of *S. mitis* J22

motions of the flexible hinge region are known with much less precision (18). Clearly some new experimental approaches will be needed to more fully characterize internal motions of the second kind.

In contrast to the polysaccharide of *S. mitis* J22, which has rather narrow ^1H NMR lines of just a few Hz when measured at room temperature (Figure 2A), the spectra of a number of polysaccharides of similar molecular weight exhibit greater line widths such as the capsular polysaccharide of *V. cholerae* O139 (Figure 2B). This high molecular weight polysaccharide has six residues in the repeating subunit with four residues in a tightly folded epitope which is a structural homologue of the Lewis^b blood group tetrasaccharide (Figure 3A, 3B). It has been shown by NOE and molecular modeling studies that this tetrasaccharide indeed adopts a conformation similar to the Lewis epitope (4). Presumably the remaining two residues, which have α -(1 \rightarrow 3)- and a β -(1 \rightarrow 6)-linkages provide the flexible hinge which confers some flexibility to this polysaccharide. At this point, no details on the internal motions of this hypothetical hinge region are available.

Methods for determining detailed models for polysaccharides

The remainder of this review will be devoted to some details of the NMR methods which could be useful for testing and refining the model which we have proposed above for a flexible complex polysaccharide. Of the two components of this model, it is the more rigid parts that are most easily treated and many studies using simple molecular modeling and NOE experiments have been reported. Since these topics have been extensively reviewed, (20), we will focus our attention on a more recently introduced method involving residual dipolar coupling in weakly oriented solutions of oligosaccharides.

Residual dipolar coupling

Dipolar coupling, which occurs directly through space rather than through chemical bonds, should not be confused with scalar coupling which is generally more familiar to most chemists. Two structural parameters affect the strength of the dipolar coupling interaction between two nuclei. One is the distance r^3 separating the two nuclei in the molecule and the other is the angle Θ which defines the direction of the vector joining the two interacting magnetic dipoles with respect to the static magnetic field. The dipolar interaction is most commonly associated with solid state NMR where the fixed orientation of the internuclear vectors leads to the maximum dipolar interaction and causes it to dominate over the effect of chemical shift. In solution NMR the molecular motions result in a random and isotropic variation in time of the orientation of the dipole with respect to the mag-

netic field. In this situation the term, $\langle 3\cos^2\Theta - 1 \rangle$, which describes the angular dependence of the dipolar coupling averages to zero and no static contribution to the dipolar coupling interaction remains. Only the distance dependence can be indirectly observed by measuring NOE which depends on fluctuations in the dipolar coupling interaction. In the presence of certain mixtures that form liquid crystals which can be oriented in the magnetic field, a small degree of orientation of the oligosaccharide can occur since such an anisotropic medium imposes a preferred orientation to the molecule under study and the dipolar interaction does not average to zero.

Recently, it has been shown that orientation of molecules can be conveniently achieved in phospholipid bilayers known as bicelles (21) when the molecule under study is oriented by hydrodynamic interactions with the bicelles (22). The degree of orientation achieved by these weak hydrodynamic interactions is small, typically of the order of 1 molecule in 1000 being oriented. A scaled or reduced dipolar interaction occurs resulting in measurable dipolar couplings while the spectrum retains high resolution and the spectral simplicity of the regular isotropic phase. Using this technique several groups have reported residual dipolar couplings in oligosaccharides (23,24,25) which can readily provide, at least for the case of relatively rigid models, highly accurate structural information which includes long range structural information not available from either NOE or scalar coupling data.

While several different liquid crystal orienting media have appeared in the literature for the measurement of residual dipolar couplings with carbohydrates, the first used was a binary mixture of long and short-chain phosphatidylcholines. It forms a well-oriented discotic nematic phase over a reasonably wide range of phospholipid composition and has been well characterized by NMR studies (21,26). The total lipid concentration affects the degree of alignment obtained and hence the magnitude of the residual dipolar couplings to be measured. This concentration can be adjusted in the range 5-40% (w/w) and the temperature can be used to modulate a phase transition (21, 26, 27) so that the system remains isotropic near 20° C while at about 35° C, the liquid crystal is formed and oriented in the NMR magnetic field.

Among the residual dipolar couplings that can be easily measured in carbohydrates, it is the one-bond ^{13}C - ^1H values which are most often used since natural abundance gives good results. The dipolar coupling, which is the difference between the total coupling in the oriented and in the isotropic phase, can be measured for CH and CH₃ groups in carbohydrates using a t_1 -coupled ^{13}C - ^1H HSQC experiment in which the proton 180° refocusing pulse in the middle of t_1 evolution is removed. Multiple bond $^nD_{HH}$ and $^nJ_{HH}$ can be determined using a homonuclear CT-COSY experiment in

which the magnitude of ${}^nD_{HH}$ is determined quantitatively by the trigonometric dependence of the intensities in a series of experiments with different constant time delays (28,29). For complex carbohydrates for which ${}^{13}\text{C}$ chemical shift resolution is critical to avoid overlap, a heteronuclear ${}^1\text{H}$ - ${}^{13}\text{C}$, ${}^1\text{H}$ - ${}^1\text{H}$ TOCSY experiment (30) can be applied. This experiment provides E.COSY type signals resolved in the ${}^1\text{H}$ and ${}^{13}\text{C}$ dimensions from which the splitting in the proton dimension can be used to determine the sign and magnitude of ${}^nD_{HH}$ (19).

Since orientation is essential for the observation of dipolar coupling, the precise orientation of the molecular model must be known for interpretation of the experimental data. The direction as well as the degree of orientation can be determined from the experimental data if at least five dipolar coupling values, each corresponding to a distinct direction in space, can be measured for an oligosaccharide fragment exhibiting internal motion of the first kind (25). Of the five parameters which must be determined, three correspond to the Euler angles needed to orient the molecular model, one is the overall degree of order and one describes the departure from axial symmetry of the molecular model.

For rigid epitopes, measurement of the C-H bond vectors provides adequate data for calculation of the orientation and very accurate models of these epitopes can be constructed (31). For more flexible oligosaccharides having internal motion of the second kind, interpretation of dipolar coupling values is more difficult. One must treat the orientation of individual pyranoside rings which tumble as a rigid unit. Since in pyranosides all axial C-H bonds are essentially parallel, other types of dipolar coupling must be measured in order to gather five independent values (29). In this case, ${}^1\text{H}$ - ${}^1\text{H}$ couplings and long range ${}^{13}\text{C}$ - ${}^1\text{H}$ couplings must be acquired. A detailed interpretation of dipolar coupling for flexible oligosaccharides is difficult and no established method is available.

Methods for more flexible polysaccharides

The characterization of the motion of the flexible hinges in oligosaccharides and polysaccharides is a major challenge and requires some sort of simplifying framework. For this purpose, we propose a model in which motion is characterized by exchange among a small number of well defined energy minima. In support of this hypothesis, we argue that the bulky stereochemistry of the saccharides restricts the conformational space available to the linkage so that the allowed conformations are limited to a very small number of well defined energy minima, separated by significant energy barriers (Figure 1). Thus each minimum exhibits very restricted internal motion but there can be conformational exchange among them. Characterization requires we locate the energy minima and determine their statistical weights. If the number of significant minima is only two or perhaps three,

we will propose schemes for determining the parameters describing such a conformational model for flexible polysaccharide hinges. The concept may be less useful for peptides, proteins or RNA for which motion may occur within much broader energy minima.

Molecular modeling

Although molecular dynamics simulations ought to be a suitable method for describing the internal motion in polysaccharides, this approach has some serious limitations. First, it has been shown that explicit inclusion of solvent in the simulation is necessary for quantitative accurate results for oligosaccharides which are very polar with hydroxyl groups that bind water strongly. If water is left out of simulations, the polar hydroxyl groups interact with each other in an unrealistic way. In practice, solvent water breaks up these interactions with the formation of new hydrogen bonding patterns between the water and the sugar. Only by explicitly including water can the hydrogen bonding effects of these specific bridging water molecules be adequately described. (32, 33). MD simulations with an adjustment of the treatment of electrostatic effects or with an approximate bulk water treatment such as the GB-SA model minimizes the formation of artifactual intraresidue hydrogen bonds but accurate calculation of the contribution of specific hydrogen bonding to the energy minima is sacrificed. Thus it is possible to calculate the locations of most of the energy minima but without explicit water and a description of effect of solvent, the breaking of hydrogen bonds and competition with intra molecular hydrogen bonding is not accurately described. Therefore in vacuum MD simulations, the accuracy of relative energies of the minima is limited to a few kcal per mole which is the typical energy of a hydrogen bond. Without solvent, approximately correct location of the minima can be found but energies are not sufficiently accurate to get good statistical weights for them.

While explicit inclusion of water in the MD simulations considerably increases the size of the calculation, very accurate simulations have been reported for disaccharides which accurately reflect the specific effects of bridging waters, (33, 34). The disaccharides treated in these calculations have been generally flexible. But extensions of such rigorous calculations to larger complex oligosaccharides have not been reported. Simulations of the more flexible oligosaccharides having internal motion of the second kind have serious limitations on practical length of solvent MD trajectory. When explicit solvent water is included, it is difficult to simulate for times longer than about 10 ns. Since the time scale for conformation exchange between minima is at least 10 ns and might be considerably longer, it may not be possible to describe the kinetics of conformational transitions without resorting to more difficult techniques such as umbrella sampling or adiabatic mapping.

Scalar coupling

Given simple molecular modeling to locate positions of minimum energy wells, experimental data can be used to derive statistical weights. While NOE data are not a very satisfactory experimental method for this purpose because of difficulties in interpretation for flexible structures, scalar coupling has been very successful for these purposes (3, 18). Scalar coupling has the advantage of giving local information on the value of a single dihedral angle not complicated with other conformational parameters. This greatly simplifies early stages of the molecular modeling search by allowing individual glycosidic linkages to be treated independently (18). Moreover, averaging the scalar coupling for two different conformers is a simple linear problem independent of the rates of conformational exchange. The main problem with interpretation of scalar coupling is in the details of the Karplus curve correlating the data with dihedral angles. Recent advances in *ab initio* methods for calculation of scalar coupling give us growing confidence in the reliability of these correlations (35, 36). Measurements of $^3J_{CH}$, $^3J_{CC}$ and $^2J_{CC}$ for the glycosidic linkages yields multiple coupling constants for a single glycosidic bond and provides an over determined system avoiding difficulties arising from the multivalued nature of the trigonometric correlation function. The data can also be used to determine whether a single value of a dihedral angle can fit all the data implying internal motion of the first kind. If multiple values of the dihedral angle are implied, statistical weights can be calculated for individual conformers.

For calculating the statistical weights of the low energy conformers, a procedure has been described by Martin-Pastor and Bush (18). Allowed regions of the dihedral angle space for the linkages are determined by molecular modeling and singular value decomposition is used to determine which combinations of those minima can be combined to reproduce the experimental $^3J_{CH}$, $^3J_{CC}$ and $^3J_{HH}$ coupling data.

The method described using ^{13}C scalar coupling measurements in complex oligosaccharides and polysaccharides has not been applied in many polysaccharide systems. While the principle of the method is sound and attractive, the experimental application is complicated by the requirement for isotope enrichment. While it is possible to measure $^3J_{CH}$ in natural abundance samples, more extensive and accurate data are available with ^{13}C enrichment and isotope enrichment is essential for $^3J_{CC}$ measurements. The scalar coupling values are small and the experiments are difficult. Dipolar coupling would be a very attractive alternative for studying the distribution of conformations in flexible oligosaccharides and a few reports have appeared in the literature (19, 29). But at this point there is no well established procedure for evaluating the data.

Conclusions

Some complex oligosaccharides contain rigid domains composed of three or four sugar residues which tumble together with a well defined 3-dimensional conformation. The existence of such rigid epitopes is strongly dependent on a particular stereochemical arrangement and other types of linkages may be more flexible. While experimental techniques exist for accurate determination of the conformation of the rigid domains, more flexible domains having internal motion of the second kind remain difficult to reliably characterize. The combination of these two types of domains in a complex polysaccharide produces a model which can be viewed as rigid domains connected by hinges. A detailed model of the flexible polysaccharide remains difficult and will require new experimental and computational methods for characterization of the flexible hinges.

Acknowledgements: This research was supported by NIH grant GM-5721

References

1. Yan, Z.Y.; Bush, C.A. *Biopolymers* **1990**, *29*, 799-812.
2. Xu, Q.; Bush, C.A. *Biochemistry* **1996**, *35*, 14512-14520.
3. Martin-Pastor, M.; Bush, C.A. *Biopolymers*, **2000**, *54*, 235-248.
4. Gunawardena, S.; Fiore, C.R.; Johnson, J.A.; Bush, C.A. *Biochemistry* **1999**, *38*, 12062-12071.
5. Abeygunawardana, C.; Bush, C.A. In *Advances in Biophysical Chemistry* Bush, C.A.; Ed; JAI Press: Greenwich, CT, 1993; Vol. 3, pp. 199-249.
6. Stroop, C.J.M.; Xu, Q.; Ratzlaff, M.; Abeygunawardana, C.; Bush, C.A. (2001) (submitted)
7. Lemieux, R.U.; Bock, K.; Delbaere, L.T.J.; Koto, S.; Rao, V.S. *Canad. J. Chem.* **1980**, *58*, 631-653.
8. Bush, C.A.; Yan, Z.-Y.; Rao, B.N.N. *J. Amer. Chem. Soc.*, **1986**, *108*, 6168-6173.
9. Miller, K.E.; Mukhopadhyay, C.; Cagas, P.; Bush, C.A. *Biochemistry* **1992**, *31*, 6703-6709.
10. Mukhopadhyay, C.; Bush, C.A. *Biopolymers*, **1991**, *31*, 1737-1746.
11. Kogelberg, H.; Frenkiel, T.A.; Homans, S.W.; Lubineau, A.; Feizi, T. *Biochemistry*. **1996**, *35*, 1954-1964.
12. Xu, Q.; Gitti, R.; Bush, C.A. *Glycobiology*, **1996**, *6*, 281-288.
13. Perez, S.; Mouhous-Riou, N.; Nifantev, N.E.; Tsvetkov, Y.E.; Bachet, B.; Imberty, A. *Glycobiology* **1996**, *6*, 537-542.

14. Delbaere, L.T.J.; Vandonselaar, M.; Prasad, L.; Quail, J.W.; Wilson, K.S.; Dauter, Z. *J. Molec. Biol.* **1993**, *230*, 950-965.
15. Martin-Pastor, M.; Bush, C.A. *Biochemistry* **2000**, *39*, 4674-4683.
16. Hricovini, M.; Guerrini, M.; Torri, G.; Casu, B. *Carbohydr. Res.* **1997**, *300*, 69-76.
17. Catoire, L.; Braccini, I.; Bouchemal-Chibani, N.; Jullien, L.; Herve du Penhoat, C.; Perez, S. *Glycoconjugate. J.* **1997**, *14*, 935-943.
18. Martin-Pastor, M.; Bush, C.A. *Biochemistry* **1999**, *38*, 8045-8055.
19. Martin-Pastor, M.; Bush, C.A. *J. Biomolec. NMR* **2001**, *19*, 125-139.
20. C. A. Bush, C.A.; Martin-Pastor, M.; Imberty, A. *Annu. Rev. Biophys. and Struct. Biol.* **1999**, *28*, 269-293.
21. Vold, R. R.; Prosser, R. S. *J. Magn. Reson., Ser. B* **1996**, *113*, 267-271.
22. Tjandra, N.; Bax, A. (1997) *Science.* **1997**, *278*, 1111-1114.
23. Bolon, P.J.; Prestegard, J.H. *J. Am. Chem. Soc.* **1998**, *120*, 9366-9367.
24. Kiddle, G.R.; Homans, S.W. *FEBS. Lett.* **1998**, *436*, 128-130.
25. Martin-Pastor, M.; Bush, C.A. *Carbohydr. Res.* **2000**, *323*, 147-155.
26. Ottiger, M.; Bax, A. *J. Biomolec. NMR* **1998**, *12*, 361-372.
27. Sanders, C.R.; Schwonek, J.P. *Biochemistry.* **1992**, *31*, 8898-8905.
28. Tian, F.; Bolon, P. J.; Prestegard, J.H. *J. Amer. Chem. Soc.* **1999**, *121*, 7712-7713.
29. Tian, F.; Al-Hashimi, H.M.; Craighead, J.L.; Prestegard, J.H. *J. Amer. Chem. Soc.* **2001**, *123*, 485-492.
30. Willker, W.; Leibfritz, D. *J. Magn. Reson.* **1992**, *99*, 421-425.
31. Azurmendi, H.F.; Martin-Pastor, M.; Bush, C.A. *Biopolymers*, **2001** (in press).
32. Liu, Q.; Brady, J.W. *J. Amer. Chem. Soc.* **1997**, *118*, 12276-12286.
33. Liu, Q.; Schmidt, R.K.; Teo, B.; Karplus, P.A.; Brady, J.W. *J. Amer. Chem. Soc.* **1997**, *119*, 7851-7862.
34. Naidoo, K.J.; Brady, J.W. *J. Amer. Chem. Soc.* **1999**, *121*, 2244-2252.
35. Bose, B.; Zhao, S.; Stenutz, R.; Cloran, F.; Bondo, F.; Bondo, G.; Hertz, B.; Carmichael, I.; Serianni, A. *J. Amer. Chem. Soc.*, **1998**, *120*, 11158-111173.
36. Cloran, F.; Carmichael, I.; Serianni, A. S. *J. Am. Chem. Soc.* **1999**, *121*, 9843-9851.

Chapter 22

Keratan Sulfates: Structural Investigations Using NMR Spectroscopy

Thomas N. Huckerby, Gavin M. Brown, Robert M. Lauder, and
Ian A. Nieduszynski

Department of Biological Sciences, IENS, Lancaster University, Bailrigg,
Lancaster LA1 4YA, United Kingdom

The application of NMR spectroscopy in the structural study of the families of keratan sulfate glycosaminoglycans is briefly reviewed. Parallel approaches via examinations of intact polymer chains and by isolation and characterization of oligomeric fragments are described.

Introduction

Almost fifty years ago, Meyer (*1*) recognised the polymeric species now named keratan sulfate (KS) as a significant component of cornea. It is an atypical member of the glycosaminoglycan (GAG) family in which there is no acidic residue alternating in the repeat sequence structure with an *N*-acetylated amino-sugar. The basic motif of the KS polymer is a repeating *N*-acetylated lactosamine sequence, namely $-\text{[Gal}(\beta 1\text{-4)GlcNAc}(\beta 1\text{-3)}\text{-]}_n$ partially substituted with *O*-ester sulfate groups located on the pendant methylenes (carbon 6) of the monosaccharide residues. The extent of Gal sulfation is quite varied and relates to the provenance of the KS; at the GlcNAc site, esterification often appears to be complete.

Three distinct KS families are now recognised, classified according to the nature of the 'linkage region' attachment to a protein core. That of type-I, which includes corneal KS, is *N*-linked to asparagine through an *N*-acetylglucosamine extending from the central residue of a triple mannose unit. In the type-II linkage typical of skeletal KS found, e.g., in articular and non-articular cartilage, nasal septa, and tracheal rings, the connection is through an *N*-acetylgalactosamine *O*-linked to protein through either serine or threonine. Proton NMR reporter group examinations revealed that there were two related types of cartilage KS. That from load-bearing (articular) sites, KS-II-A, was more complex (2), containing (α 1-3)-linked fucose and (α 2-6)-linked *N*-acetyl-neuraminic (or sialic) acid as well as the (α 2-3)-linked sialic acid present also in non-articular KS-II-B. A third class of KS exists in brain tissue; an *O*-glycosidic linkage connects a -GlcNAc(β 1-3)Man- sequence to either serine or threonine. Recently, with the aid of a range of nano-scale assaying procedures, it has been shown that the distribution of keratan sulfates in nature is very widespread. Currently, the details of molecular composition for these species remain almost unknown. Members of the KS families have been identified in such diverse tissue sites as prostate secretory cells, human endometrium, nerve cells and on a variety of cell surfaces as well as in bone, tendon, growing antlers and avian eggshells. So far, only the structural diversity of types-I and -II KS has been examined in detail and much of the evidence has been derived through high-resolution NMR studies.

Structural Studies

For KS, in common with many other carbohydrate polymers of the GAG family (e.g. the heparan sulphate/heparin systems) and elsewhere, the anticipated molecular structures are not unique. They are present as distributions, both in terms of molecular size and in the nature of substituents and their placements. Thus they differ greatly from the ordered world of peptides and proteins and are more akin to synthetic polymers in their nature, their chromatographic and spectroscopic behaviour and in the resultant analytical problems. It is apt to consider substituent placements along the repeat unit backbone as exhibiting microstructural patterns within diad, triad or larger groups of monomer units, for which statistical data can be elicited, e.g. in terms of sulfation and its distribution. The spectroscopic route to KS structure can also be similar to that used for synthetic macromolecules.

Various NMR approaches may be considered. ^1H is the obvious choice because of its relative sensitivity but, as for many carbohydrate-based systems, spectra prove exceedingly complex since many resonances from CH / CH₂ environments fall within a narrow bandwidth of chemical shifts. 2D-NMR

methodologies can provide maps for the negotiation of these mazes. For ^{13}C data, the much greater chemical shift range and signal dispersion offers potential advantages, offset by poor inherent receptivity and the tricky problem of unambiguous signal assignment. Potentially, ^{15}N experiments could also be considered; these currently appear non-viable since KS systems are necessarily isolated from natural tissue sources not compatible with isotopic labelling strategies using ^{15}N (and/or ^{13}C) such as those commonly used to good effect, for example, in the study of peptides.

Non-destructive examination of intact KS is valuable, but this is still not a fully practicable approach for the complete analysis of either ^1H or ^{13}C data. It is essential to learn first the detailed grammar concerning the behaviour of signals reporting in all relevant microenvironments. This is the equivalent of examining families of stereochemically or structurally related oligomers prior to assigning spectral features for synthetic polymers. The isolation and complete characterisation of appropriate fragments is thus required and involves consideration of three separate regions within the polymer chains, viz. the nature of the capping units at the non-reducing termini, features which rise to microstructural variations within the main poly(*N*-acetylglucosamine) repeat unit sequence, and the characteristics of the linkage region segment through which KS molecules are attached to a protein core. There are two specific keratan sulphate degrading enzymes. The first, keratanase, is known to cleave keratan sulfate chains at the reducing terminus of an unsulfated galactose. Unlike the alternative endo- β -galactosidase, which can also cleave within unsulfated regions of the chain, this enzyme requires at least one 6-*O*-sulfated *N*-acetylglucosamine residue (GlcNAc6S), located at the reducing terminus of the galactosidic linkage to be attacked. As a result of its action on skeletal KS a large number of oligosaccharides are produced, many of which represent homologous series of fragments either from the main repeat-sequence or from non-reducing terminal chain capping segments. These have proved useful for exploring the relationships within families of polymer chains (3) but are not adequate for describing microstructural detail and provide little information about the variability of sulfation within repeat unit sequences nor do they yield sufficient data concerning the microenvironments of minor components such as the fucose substituents found in articular cartilage KS.

An alternate enzyme, keratanase-II, catalyses the cleavage of the glucosaminidic linkages in KS and requires the presence of a 6-*O*-sulfate ester at that site. The fragmented products do not show homologous series patterns and most are hexasaccharide or smaller in size. These oligosaccharides can readily be parsed into separate families (chain caps, repeat region, linkage region and fucosylated fragments) through ^1H -NMR examination of their specific sugar contents (4, 5) and have important consequences for keratan sulphate structural

fingerprinting. Chemical degradations, such as hydrazinolysis / nitrous acid treatment, are also of use (6). The full characterisation of these fragments is vital. This process has relied heavily on the use of both one- and two-dimensional NMR approaches including the use of TOCSY methods, in order to unravel the complex and intereaved spin systems for total signal assignment.

Fingerprints from Fragments

These collated structural data may be put to use in various ways. They inform us about the ground rules; what are the modes of action of the enzymes; how do substituents dictate fragmentation; what are the salient features which they reveal; what potential molecular recognition sites may be present in KS polymer chains?

A Choice of Weapons

The hydrazinolysis approach permits chain scission at the anomeric carbon of each GlcNAc site *except* when this residue is fucosylated. Fragments are few and rather small. They reveal nothing about KS polymer block structure and, importantly, require the preparation to be uncontaminated by other GAGs since these would also become fragmented, confusing the analysis.

The enzyme routes are chemically less hazardous and keratanases would leave other GAG components unaltered. Keratanase has the potential for providing data about homologous series of cleavage resistant blocks. It is not, however, suited to the calculation of gross chemical composition; a large number of fragments, diverse in size, are formed. For keratanase-II the pattern is simple; it can cleave at any sulfated *N*-acetylglucosamine and limit digest fragments contain 2–7 residues. The limited range of molecular sizes combined with differing charge densities leads to a fortunate compromise permitting calibration and use of chromatographic methods for the identification and subsequent quantification of fragments and enabling structural profiling on a small scale for keratan sulphates of novel origin.

Geographical Features; Sites of Interest

There is evidence for a considerable diversity in the detailed constitution of articular cartilage KS chain capping structures. It is reasonable to assume that,

because of their peripheral locations, these regions of the polymer chains may have some role in molecular recognition processes. Indeed, there are monoclonal antibodies which recognise the sialylated caps of KS chains and that are capable of responding to extended repeat unit segments built from disulfated *N*-acetyllactosamine disaccharides. In articular cartilage KS there is the additional possibility of repeat unit fucosylation. Chain segments bearing this substituent are of interest because their environments represent variants of known antigenic sequences. There is still much more to be learned about these epitope structures. In particular, the detailed chain architecture for corneal keratan sulfate, the first member of the KS family to be recognised, is still incompletely characterised; a significant number of structural fragments are as yet still unclassified.

The Sum of the Parts; Spectra from Intact Polymers

The various sets of fragment data may be used in turn to analyse spectra derived from intact polymers. By using 2D as well as 1D data it is possible to elicit a great deal of information from undegraded KS polymers. There are some unresolved problems. For ^1H data, even at 600 MHz the resonances are strongly overlapped and, in particular, those from GlcNAc6S are strongly second-order, causing difficulties with correlation assignments since protons H(2) – H(5) may all fall within a chemical shift range of less than 0.05 ppm. There are still many gaps in the assignments for ^{13}C analysis; some model data are still to be determined. It has been possible to examine the polymer structure of bovine tracheal cartilage KS in some detail using a combined $^1\text{H}/^{13}\text{C}$ approach (7) and to assess the changes which occur in human articular cartilage during the developmental process (8, 9).

To illustrate the types of information accessible using 2D NMR, Figure 1 shows details of a small spectral region containing H(1) / H(2) cross peaks from a human fetal cartilage KS sample. This is similar to that previously described (9) but the use of Linear Prediction in the f_1 axis has yielded superior resolution and sensitivity. In both, response **A** comprises a cluster of cross peaks connecting H(1) and H(2) in repeat unit GlcNAc6S residues. Typically, these are poorly resolved and their precise microstructural assignments are not obvious. In principle, at least four sets of signals must be anticipated, but the necessary model penta- or hexa-saccharide systems containing various combinations of flanking Gal or Gal6S units are not available. Within cluster **B** are galactose cross peaks, also inadequately separated. The signals at **C** and **D** both report on unique locations within the polymer structure. The former indicates the H(1) / H(2) coordinate for the branching Gal in the asialo form of the linkage region,

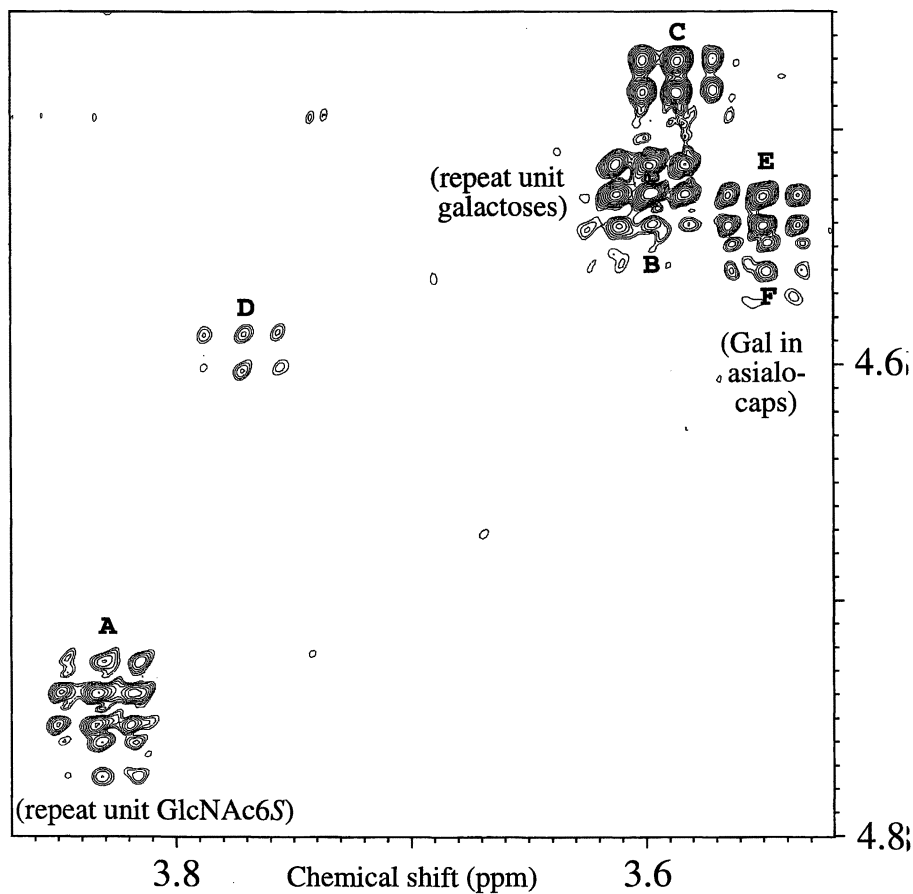
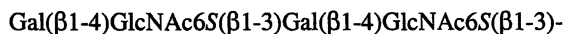


Figure 1. Partial 600 MHz COSY spectrum for the H(1)/H(2) region of human fetal cartilage KS. The t_1 dimension was processed using forward Linear Prediction.

while the latter correlates protons within that GlcNAc6S residue which is, uniquely, attached to the linkage region GalNAc-ol. At locations **E** and **F**, two separate components have now been resolved. The major contributor (**E**) had been assigned (9) to the Gal residue terminating an asialo capping sequence with the structure



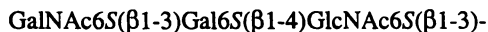
which forms the dominant non-reducing terminal structure for foetal KS. The minor component (**F**), with H(1) at 4.555 and H(2) at 3.542 ppm, not previously visualised or reported, is now seen, *via* comparison with keratanase-II oligosaccharide data (4, 5), to represent the more sulphated variant,



These two terminating structures are not present in KS at later stages of development where capping by sialyl groups is essentially complete. Information about such asialo structures, clearly visible on the 2D spectrum, is not available from keratanase-II profiling, since the fragments formed are, of course, identical with the di- or tetra-saccharides afforded by the poly(*N*-acetylglucosamine) repeat sequence. The assignments for many of these cross peaks are made possible because of the availability of extensive ¹H NMR signal assignments for oligosaccharides which have been obtained from KS through chemical or enzymic cleavage procedures. The parameters thus obtained are exquisitely sensitive to the specific microenvironments of individual protons and can therefore be reliably employed for the identification of 'reporter group' cross peaks on 2D NMR spectra which indicate the presence of a range of specific chain-capping structural units.

Continuing Studies

Why are these structural investigations important? It is now apparent that the keratan sulfates have an important role in the regulation of three-dimensional order within tissue matrices. A group of KS proteoglycans is present in cornea, and have specific functions in the maintenance of corneal transparency through interactions which uphold the regular spacing of collagen fibrils. NMR has shown the chain capping structures of these polymers to be highly complex (10) and work currently in progress has implicated the interaction of specific epitopes such as



with one or more small proteins within the tissue.

The functions of the various KS-containing species within cartilage are still unclear. It has been shown that the main cartilage proteoglycan, aggrecan, contains a repeating hexapeptide motif within its 'KS-rich' region that is capable of interacting with collagen (11). The KS chains pendant from this and from other cartilage proteins such as fibromodulin (12) contain sialylated epitopes for which there may be binding sites among the non-collagenous, non-proteoglycan macromolecules now known (13) to be present in cartilage. Undoubtedly these afford specific recognition sites. KS chains have been proved present in varied tissue locations; notably, one such manifests fleetingly in the endometrium at ovulation (14, 15).

Detailed knowledge of the architecture of KS chains will continue to be an important factor in eliciting the modes of action and biological roles for these species. The structural and NMR assignment data currently available for these systems now provide a base for the assessment of KS epitope molecular shapes. This is a difficult process because of the inherent spectral complexity, but is being aided by the application of a modified transverse-ROESY method. However, the structural features present within the recently discovered members of this diversely distributed KS family, which would be anticipated to contribute specific behavioural properties or to permit selective interactions with other, non-carbohydrate, molecular sites, are still largely unexplored. Recent KS structural studies are reviewed in depth in a forthcoming article (16).

Acknowledgements

We thank the Arthritis and Rheumatism Council, the Wellcome Trust and BBSRC for their financial support of this work.

References

1. K. Meyer, A. Linker, E. A. Davidson and B. Weissman, *J. Biol. Chem.* **205**, 611 (1953)
2. I. A. Nieduszynski, T. N. Huckerby, J. M. Dickenson, G. M. Brown, G.-H. Tai, H. G. Morris and S. Eady, *Biochem. J.* **271**, 243 (1990)

3. T. N. Huckerby, J. M. Dickenson, G. M. Brown and I. A. Nieduszynski, *Biochim. Biophys. Acta* **1244**, 17 (1993)
4. G. M. Brown, T. N. Huckerby, H. G. Morris, B. L. Abram and I. A. Nieduszynski, *Biochemistry* **33**, 4836 (1994)
5. G. M. Brown, T. N. Huckerby and I. A. Nieduszynski, *Eur. J. Biochem.* **224**, 281 (1994)
6. G. M. Brown, T. N. Huckerby and I. A. Nieduszynski, *Biochem. J.* **286**, 235 (1992)
7. T. N. Huckerby and R. M. Lauder, *Eur. J. Biochem.* **267**, 3360 (2000)
8. G. M. Brown, T. N. Huckerby, M. T. Bayliss and I. A. Nieduszynski, *J. Biol. Chem.* **273**, 26408 (1998)
9. T. N. Huckerby, G. M. Brown, I. A. Nieduszynski and M. T. Bayliss, *Eur. J. Biochem.* **266**, 1174 (1999)
10. G.-H. Tai, T. N. Huckerby and I. A. Nieduszynski, *J. Biol. Chem.* **271**, 23535 (1996)
11. H. Hedlund, E. Hedbom, D. Heinegård, S. Mengarelli-Widholm, F. P. Reinhold and O. Svensson, *J. Biol. Chem.* **274**, 5777 (1999)
12. R. M. Lauder, T. N. Huckerby and I. A. Nieduszynski, *Eur. J. Biochem.* **242**, 402 (1996)
13. P. J. Neame, H. Tapp and A. Azizan, *Cell. Mol. Life Sci.* **55**, 1327 (1999)
14. M. E. Hoadley, M. W. Seif and J. D. Aplin, *Biochem. J.* **266**, 757 (1990)
15. J. D. Aplin, N. A. Hay and R. A. Graham, *Glycobiology* **8**, 269 (1998)
16. T. N. Huckerby, *Prog. NMR Spectrosc.* to be published

Chapter 23

Gelling Mechanisms of Glucomannan Polysaccharides and Their Interactions with Proteins

I. C. Baianu¹ and E. M. Ozu²

¹College of ACES, FSHN Department and ²AFC-NMR Facility, University of Illinois at Urbana, 101 Bevier Hall, 908 South Goodwin Avenue, Urbana, IL 61801

Gelling properties of glucomannan polysaccharides (GP) are important in good science and technology. The functional properties of GP gels and related polysaccharides were recently reviewed in relation to gelling mechanisms that are likely to operate both in gels made from purified GP or konnyaku flour (1). We are now presenting a more detailed account of the most likely gelling mechanism in glucomannans mixed with water and in the presence of added wheat gluten proteins than it has been previously reported. Our results suggest a model of glucomannan gels in which divalent cations, such as Ca⁺⁺, act as a crosslinker, both in the presence or absence of wheat gluten proteins.

Konnyaku flour obtained from plant cultivars of *Amorphophallus konjac* K. Koch is an important food material because of its remarkable gelling properties at very low solids concentrations in water (less than ~0.5%). It has been employed in certain regions of Asia, such as Japan, to make a variety of foods that were claimed to have significant health benefits. Glucomannan polysaccharides (GP) are the main active component of Konnyaku flour, and can

be readily extracted and purified from konnyaku flour. Gelling properties of glucomannan polysaccharides are therefore important in food science and technology. The functional properties of GP gels and related polysaccharides were recently reviewed in relation to gelling mechanisms that are likely to operate both in gels made from purified GP or konnyaku flour (1). New experimental results are here presented together with a detailed model of the gelling mechanisms of glucomannans in water with, or without, added wheat gluten proteins.

Materials and Methods

Konnyaku flour was obtained from tubers of plant cultivars of *Amorphophallus konjac* K. Koch that were kindly provided by Ajinomoto Co. Glucomannan polysaccharides were extracted from konnyaku flour and further purified from precipitates in ethanolic mixtures. The range of glucomannan oligosaccharides that are obtained by partial hydrolysis of GP is illustrated in Table I.

NMR Spectroscopy and Relaxation

Pulsed Nuclear Magnetic Resonance (NMR) instrumentation and methodology that we employed to study GP and/or wheat gluten protein hydration in gels are as described in our previous report (1). An approach and analysis that combines low-field NMR relaxation data with high-field NMR spectroscopic data obtained on the same samples was recently reported (2) that is also applicable to structural and hydration studies of GP gels with/without added wheat gluten proteins in water. High-resolution NMR spectra of solutions were obtained with a Varian Unity 400 spectrometer operating at 400 MHz ^1H resonance frequency.

IR Spectroscopy

Transmission, mid-IR cw-spectra of GP were obtained by employing KBr pellets with GP powder homogeneously embedded in the pellets. Reflectance NIR spectra of GP were obtained from purified powders (without KBr) on a Perkin-Elmer Spectrum ONE NTS spectrometer equipped with an integrating sphere and an extended-range InGaAs detector.

Table I. Glucomannan Oligosaccharides Formed by Partial Hydrolysis

<i>Oligosaccharide</i>	^a <i>Man</i>	<i>Composition and Ratio of the Monomers</i>	<i>Terminal Residue</i>
A	0.83	G, M (1:1)	M ^b
B	0.67	G	G ^c
C	0.53	M	M
D	0.46	G, M (1:1)	G
E	0.36	G, M (1:2)	M
F	0.29	G, M (1:3)	M
G	0.20	G, M (2:3)	M
H	0.16	G, M (1:4)	M
I	0.07	G, M (3:4)	M

<i>Oligosaccharide</i>	<i>DP</i>	<i>Type and Configuration of the Bond</i>	<i>Structure</i>
A	2	β -(1 \rightarrow 4)	G \rightarrow M
B	2	β -(1 \rightarrow 4)	G \rightarrow G
C	2	β -(1 \rightarrow 4)	M \rightarrow M
D	2	β -(1 \rightarrow 4)	M \rightarrow G
E	3	β -(1 \rightarrow 4)	G \rightarrow M \rightarrow M
F	4	β -(1 \rightarrow 4)	G \rightarrow M \rightarrow M \rightarrow M
G	5	β -(1 \rightarrow 4)	M \rightarrow G \rightarrow G \rightarrow M \rightarrow M
H	5	β -(1 \rightarrow 4)	M \rightarrow G \rightarrow M \rightarrow M \rightarrow M
I	7	β -(1 \rightarrow 4)	G \rightarrow M \rightarrow G \rightarrow G \rightarrow M \rightarrow M \rightarrow M

^aMannose fraction^bMannopyranose^cGlucopyranose

Results and Discussion

Broadband, proton decoupled, ^{13}C HR-NMR of GP oligosaccharides were assigned by comparison with spectra of individual oligosaccharides and disaccharides. Such chemical shift assignments are summarized in Table II.

Pulsed NMR measurements of transverse water relaxation (T_2) at 10 MHz ^1H resonance frequency were carried out for GP gels and GP-wheat gluten mixtures in water. Whereas the transverse relaxation curve of water in GP gels was found to be a single exponential for the concentration range from 0 to 6% GP solids by weight, that of wheat gluten protein mixtures with GP in varying proportion was found to be non-exponential. The transverse relaxation curve of water protons in fully hydrated GP-wheat gluten mixtures was best fitted by a model with three different relaxation components that was previously introduced for suspensions of homogenized muscle in water (2). Although GP hydration in gels exhibits a constant slope in the range from 0.1 to 5% GP gels in water, GP micro-rheological properties change markedly above 1% GP in water. However, in the presence of hydrated wheat gluten proteins, the GP gels and wheat gluten protein hydration properties change dramatically above 1% GP concentration. Such changes are also observed in the apparent viscosities of GP-wheat gluten mixtures in water.

The addition of EDTA to the GP-wheat gluten protein mixture in water (followed by extensive dialysis at 4°C) reduces only by approximately 15% the hydration of the protein-polysaccharide mixture. These results strongly suggest a model of hydrated glucomannan gels in which divalent cations, such as Ca^{++} , act as a *cross-linker* (Figure 1), both in the presence and the absence of wheat gluten proteins. (The divalent Ca-ions are represented as open circles in Figure 1). Although fewer peaks are resolved for GP in the NIR spectra in comparison with NMR, such NIR spectra (Figure 2) are strongly indicative of a complex, macromolecular structure in GP powders similar to that of starches from other plants, without any evidence of smaller oligosaccharides being present in the purified GP employed in our studies. On the other hand, X-ray diffraction patterns of dried GP films in which GP fibers were oriented in the plane of the film seem to indicate a structure with H-bonds between adjacent GP fibers that is significantly different from that of fully hydrated GP gels. Further NIR experiments with GP gels in D_2O are in progress and have the potential to identify specific divalent cation cross-linking groups in GP gels.

Conclusions

Gelling mechanisms of glucomannan polysaccharides (GP) extracted from konnyaku flour obtained from plant cultivars of *Amorphophallus konjac* K. Koch

Table II. ^{13}C Chemical Shift Assignments of Glucomannan Oligosaccharides Obtained by Hydrolysis

^{13}C Chemical Shifts	Assignments
103.8-104.2	C 1 Glcp ^a β
101.45-101.6	C 1 Manp ^b α, β
95.1-95.3	C 1 Manp
75.95-80.15	C 4 Glcp β
78.1-78.3	C 5 Manp β
77.4-78.0	C 4,5 Manp β
	C 4 Manp α
76.4-76.9	C 3 Glcp β
76.15-76.3	C 5 Glcp β
75.4-75.5	C 5 Glcp β
74.3-74.7	C 2 Glcp β
72.9-73.1	C 3 Manp β
72.5-72.6	C 5 Manp α
71.4-72.0	C 2 Manp β and Manp α
71.0-71.1	C 3 Manp α
70.4-70.5	C 4 Glcp β
68.0-68.1	C 4 Manp β
62.4-62.5	C 6 Manp β
61.7-62.1	C 6 Manp α, β
	C 6 Glcp β

^aGlucopyranose^bMannopyranose

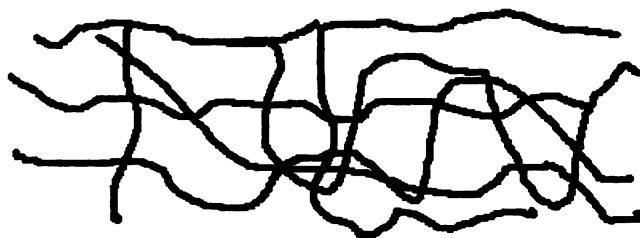
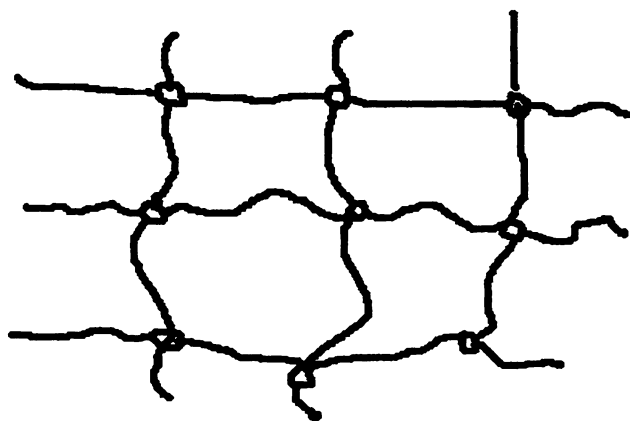
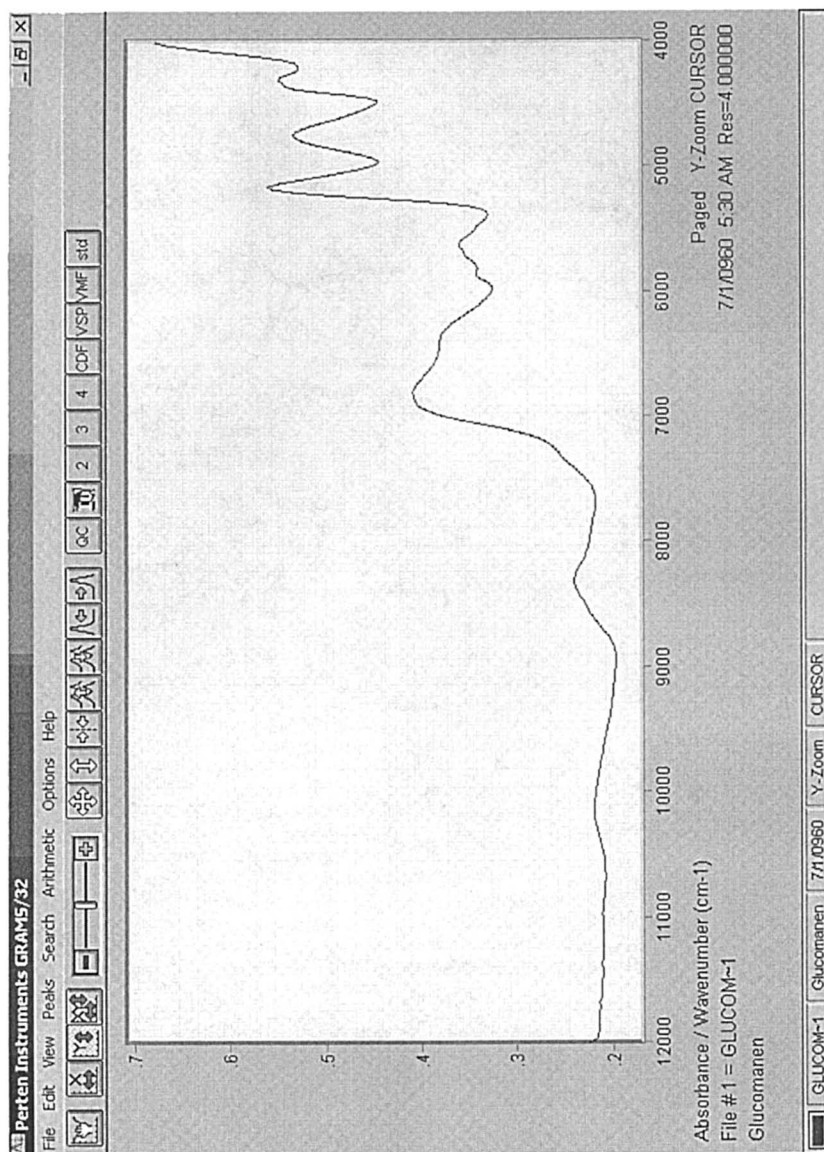
A. Entangled polymer chains in a gel that is not cross-linked**B. Cross-linked polymers in a gel**

Figure 1. Schematic diagram of gel networks:

- A. Gels without cross-links;
- B. Cross-linked Gels, such as GP gels, with the open circles representing cross-linkers, such as Ca^{++} ions in GP gels.

**Figure 2. Near Infrared (NIR) spectrum of glucomannan polysaccharide**

were investigated by Nuclear Magnetic Resonance (NMR) techniques. Detailed mechanisms of glucomannan gel formation and GP hydration were obtained by combining data from pulsed NMR transverse relaxation with high-resolution ^1H and ^{13}C NMR spectra of glucomannan gels in water. Our results suggest a model of glucomannan gels in which divalent cations, such as Ca^{++} , act as a *crosslinker*, both in the presence, or absence, of wheat gluten proteins. Such a mechanism may also have technological significance for developing novel, functional foods based on both konnyaku and wheat flours that must also contain calcium ions in order to form a homogenous GP-wheat protein matrix.

References

1. Ozu, E., Baianu, I.C., and Wei, L-S. Ch.14 in *Physical Chemistry of Food Processes*, vol.2; Baianu, I.C., Pessen, H., and Kumosinski, T.F. , Eds., New York, London, S. Melbourne, and Ontario: Intl. Thomson Pubs.1992. (ISBN 0-422-00582-2).
2. Lee, J.R.; Baianu, I.C.; Bechtel, P. *Macromol. Symp.* **1999**,*140*, 243.

Chapter 24

Synthesis, Physical, and NMR Characteristics of Di- and Tri-Substituted Cellulose Ethers

Navzer (Nozar) D. Sachinvala^{1,*}, David L. Winsor²,
Walter P. Niemczura³, Karol Maskos⁴, Tyrone L. Vigo¹,
and Noelle R. Bertoniere¹

¹Cotton Textile Chemistry Research Unit, Southern Regional Research Center (SRRC), Agricultural Research Service, U.S. Department of Agriculture, 1100 Robert E. Lee Boulevard, New Orleans, LA 70124

²Hawaii Agricultural Research Center, New Orleans Office, SRRC, New Orleans, LA 70124

³Department of Chemistry, University of Hawaii at Manoa, 2545 The Mall, Honolulu, HI 96822

⁴Coordinated Instrumentation Facility, 604 Lindy Boggs Building, Tulane University, New Orleans, LA 70118

*Corresponding author: nozar@srrc.ars.usda.gov

Introduction

In June 1998, at USDA-ARS's Southern Regional Research Center we were asked to design new materials from cotton and bagasse-derived cellulose **1** that could serve emerging needs in the textile, composites, and chiral materials markets. At that time, we had synthesized and characterized sucrose-based epoxies (1) and we wanted to extend our work to cellulose-derived epoxies and take advantage of existing cellulose epoxy literature (2). We chose to work with cellulose ethers, because unlike its esters, ethers are kinetically and thermodynamically more stable, and they appeared easy to prepare and characterize. However, after a few early experiments with cellulose ether derived epoxies, my collaborators and I soon found our efforts hampered. This is because we were unable to use existing information to:

- Make well defined cellulose ethers and their epoxies on 10 to 50g scales;
- Explain the complete ¹H and ¹³C chemical shift characteristics of cellulose ethers; and

[†]Dedicated to Professor Roger E. Cramer, Department of Chemistry, University of Hawaii at Manoa, Honolulu, HI 96818

(c) Correlate cellulose polymer structure with the thermal and the dynamic mechanical properties of final materials.

Consequently, we chose to focus on learning efficient methods for the synthesis of cellulose ethers, understanding their structural and physical characteristics, and generating guidelines for new materials designing with them (Figure 1). We prepared and studied tri-*O*-methylcellulose, **2** (**3**), then tri-*O*-allyl and tri-*O*-crotyl celluloses, **3**, **4** (**4**), and then 6-phenyl-6-deoxy-2,3-di-*O*-methylcellulose, **9** (**5**). Our work with tri-*O*-methyl, tri-*O*-allyl, and tri-*O*-crotyl celluloses taught us (a) innovative large-scale preparation techniques, (b) NMR methods that employ coupling interactions (^1H - ^1H and ^1H - ^{13}C) to correlate chemical shifts, and (c) polymer film behavior. Our work with 6-phenyl-6-deoxy-2,3-di-*O*-methylcellulose, for the first time, laid the ground work for the synthesis of carbon-carbon bonded deoxy cellulose derivatives, and extended our work on making unequivocal chemical shift assignments. In this review we will:

- Highlight the synthesis of these polymers (Figure 1);
- Summarize their physical characteristics (Table 1);
- Describe the nomenclature system for making chemical shift assignments of the anhydroglucose repeating units and the ether pendants (Figure 2);
- Use methylcellulose as an example to show the strategies for making unambiguous C and H assignments; and
- Provide all ^1H and ^{13}C chemical shifts of polymers **2**, **3**, **4**, and **9**.

Experimental details for all works are in the original papers (3-5).

Reagents and Yields: (a) Cellulose (**1**), DMAc, LiCl, NaOH, alkylating agent, 30 to 91%; (b) **1** (25 g), DMAc, LiCl, Et₃N, CPh₃Cl, 96%; (c) Sodium hydride, dry DMSO, **5**, CH₃I, 95%; (d) **6**, formic acid (88% in water), 79%; (e) Bromomethylene dimethylammonium bromide (freshly prepared), DMF, **7**, 83%; (f) **8**, THF, CuCN, LiPh, 51%

Results and Discussion

Polymer Synthesis Highlights

Tri-*O*-methylcellulose, **2:** This polymer was prepared in 83 % yield from commercial partially *O*-methylated cellulose (DS ~ 1.6, average DP ~ 90) by use of sodium hydride in DMSO and dimethyl sulfate (DS = 3, average DP ~ 83). It was also prepared in 30 % yield from **1** (average DPw 361) by the method described below for the synthesis of tri-*O*-allyl and crotyl celluloses, **3** and **4**. The average DPw of polymer **2** obtained by this method was ~160.

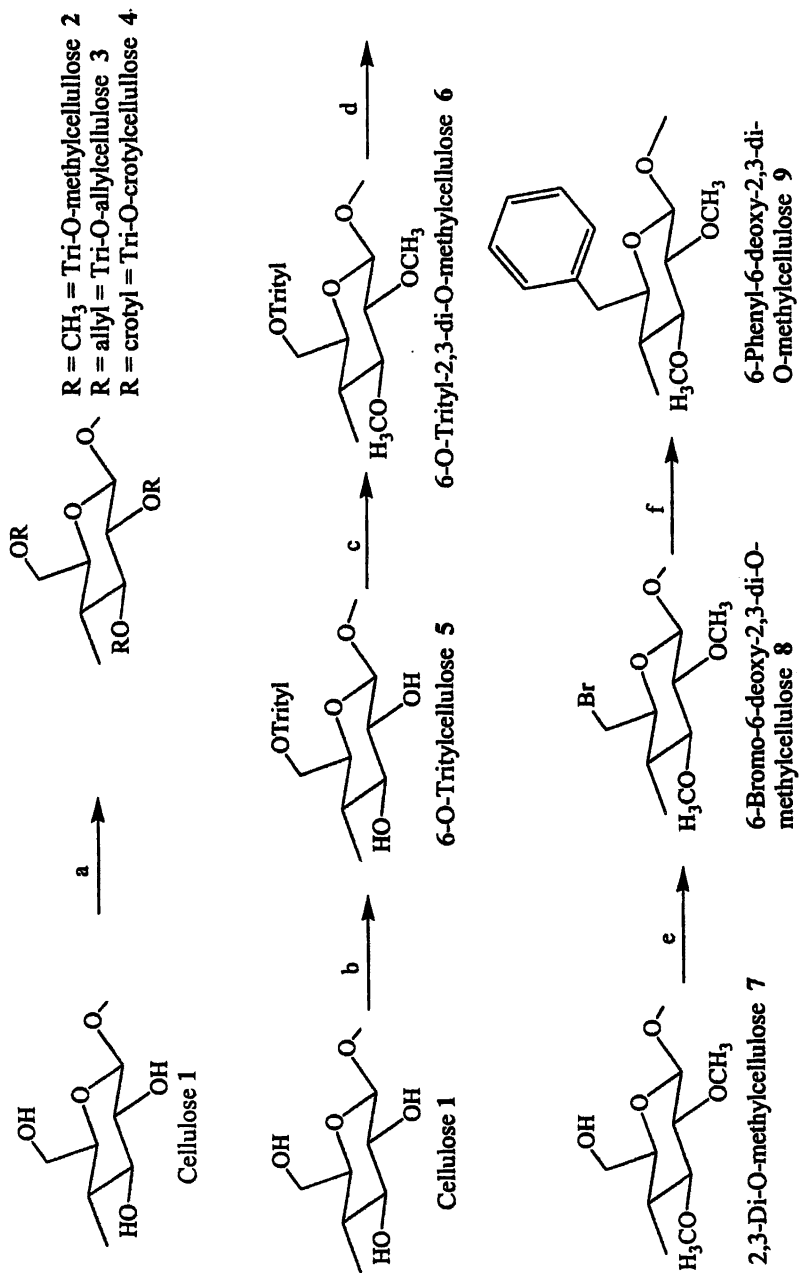


Figure 1: Synthesis of Cellulose Ethers

Tri-O-allylcellulose and Tri-O-crotylcellulose, 3, 4: These polymers were prepared on 20 to 50 g scales by treating well mixed, degassed, anhydrous solutions of microcrystalline cellulose, **1** in LiCl/DMAc, followed by addition of powdered sodium hydroxide, and then the alkylating agents. However, unlike previous protocols (**6**) the following precautions were taken to generate trisubstituted ethers in one step: (a) In all preparations nitrogen gas was purged through the reaction mixture to remove dissolved air, which was found to darken cellulose products (**7**). (b) Because excess LiCl was present in the reaction mixture, Teflon needles and cannulae, instead of stainless steel needles and cannulae, were used to deliver nitrogen and reagents. (c) To further prevent the introduction of air, a Gutche tube was used to introduce LiCl and cellulose, and an addition funnel for solids was used to introduce powdered sodium hydroxide. (d) Liquid reagents were transferred via cannulae under nitrogen pressure. (e) A high torque (1/15hp) overhead stirrer was used to prevent the solids from caking on walls of flasks and becoming nucleating sites for exotherms (explosions). (f) We used vacuum (0.1 mm Hg, 50-60 °C), instead of chloroform extraction to remove DMAc, allyl and crotyl alcohols, and diallyl and dicrotyl ethers. (g) The polymers were washed with bicarbonate and then water to remove inorganic salts and residual solvents. (h) Further removal of low molecular weight oligo sugars, solvents, alcohols, and ethers was effected by Soxhlet extraction with methanol. (i) Finally, small samples for NMR analysis were purified by flash column chromatography on silica gel (60 to 200 mesh, using ethyl acetate in hexane, 1:1). For all practical purposes, the cellulose ethers after Soxhlet extraction were pure by elemental analysis and NMR but they appeared yellow. Polymers that were flash chromatographed were very pale yellow to white. Yields of the fully O-alkylated methyl, allyl, and crotyl celluloses were 30, 91, and 56%, respectively.

6-Phenyl-6-deoxy-2,3-di-O-methylcellulose, 9: This polymer was prepared in 33% overall yield from **1** in five steps (Figure 1) involving the intermediacy of 6-O-tritylcellulose, **5**, 6-O-trityl-2,3-di-O-methylcellulose, **6**, 2,3-di-O-methylcellulose, **7**, and 6-bromo-6-deoxy-2,3-di-O-methylcellulose, **8**. Tritylation of **1** was effected in 96% yield using a solution of microcrystalline cellulose ($DP_w \sim 361$) in DMAc containing LiCl followed by the addition of triethylamine, and then trityl chloride. Triethylamine instead of pyridine (**8**) was used because it was easier to work with, is less toxic than pyridine, and was easily removed from product mixtures to furnish good elemental analysis data.

While 6-O-trityl-2,3-di-O-methylcellulose, **6** is known in the literature (**9**), it was prepared *de novo* using **5**, sodium hydride in DMSO (instead of DMF, **10**), followed by addition of dimethyl sulfate or methyl iodide. With sodium hydride

and methyl iodide (or dimethyl sulfate) in DMF (11) we isolated tetramethylammonium salts and partially O-alkylated celluloses. We explained the presence of tetramethylammonium salts as arising from the decomposition of DMF to carbon monoxide and sodium dimethylamide, which consumed the alkylating agent. With sodium or potassium hydroxide (9), methyl iodide (or dimethyl sulfate), in wet DMSO, 2,3-di-O-methylation was incomplete after three attempts, and partial removal of the trityl-protecting group was also observed.

Trityl protection at O6 was removed in 79% yield, by treating a methylene chloride solution of **6** with 88% aqueous formic acid (11). After 30 minutes at room temperature, the volatile contents were removed *in vacuo*, and the O6 formate esters were hydrolyzed with methanolic ammonia to afford **7**.

From this beginning, tens of reactions were explored to determine conditions that would effect the conversion of **7** to **9** in good yields. While details of methods and results are in the original paper (5), review herein is restricted to the transformations that worked. Reaction of polymer **7** with bromomethylenedimethyliminium bromide (freshly prepared, **13**) in DMF afforded bromide **8** in 90 % yield after flash column chromatography, and the extent of bromination was quantitative (determined by ^{13}C NMR integration and elemental analysis). Coupling of the phenyl ring to the C6 carbon was effected by reaction of bromide **8** with phenyl lithium in the presence of copper (1) cyanide in THF (14), and **9** was purified by flash column chromatography. The extent of phenylation in **9** was 81 % and the yield of the reaction was 51%. Unfortunately, to date, the last two reactions can only be performed in good yields on 0.5 to 2g scales. We have yet to discover conditions under which we can perform all reactions with cellulose on much larger scales without substantial loss in yields and DP.

Physical Characteristics

Table 1 summarizes the physical properties of polymers **2** to **9**.

Tri-O-methylcellulose, 2: Polymer **2** was prepared for the purpose of discovering a strategy to completely assign all shifts of the closed spin network of seven protons and six carbons of the anhydroglucose portion, and the 3 carbons and nine hydrogens of 3-methyl appendages in the repeating unit (Figure 2). It was readily soluble in most organic solvents and no other physical properties were determined.

Tri-O-allylcellulose, 3: This polymer was prepared from cellulose of average $\text{DP}_w = 361$. Its average DP_w was found to be 691, which suggested that chain branching may have occurred by hydrogen atom chain transfer and coupling of allyl radicals (10b). Polymer **3** appears to change color (darken) when left open

Table 1: Physical Properties of Polymers 2 to 9

Polym #	2	3	4	5	6	7	8	9
MW/Rep.Unit	204.25	282.37	324.46	404.47	432.52	190.20	253.09	250.29
% Yield	83	91	56	96	95	79	90	51
Anal.								
C:H(calc.)	52.9:7.9	63.8:7.9	66.6:8.7	74.2:5.8	74.9:6.5	50.5:7.4	37.9:5.1	68.1:7.2
C:H(Observed)	52.0:8.0	63.2:7.8	66.6:8.5	75.3:5.9	74.3:6.3	50.2:6.7	37.9:5.1	55.6:6.5
Substitution.	~3 Me	~3 allyl	~3 crotyl	Ph ₃ C~1	Ph ₃ C~1	Me~2	Br~1	Ph~0.8
					Me~2		Me~2	Me~2
GPC								
M _n	17,000	31,600	45,100	54,700	47,700	24,200	25,900	17,600
M _w		191,800	118,200	143,100	108,800	32,000	29,600	18,400
DP _w		679.25	364.29	353.79	251.55	168.20	102.37	73.51
DSC ^c								
T _g °C	a	-3 to +2	-5 to +3	a	a	a	a	a
Deg. °C		295	>310	296.0	225.0	294.6	201.6	198.1
MP °C		a	185.8	a	a	a	a	a
C ₁ st. °C		a	168.9	a	a	a	a	a
TGA								
Deg. °C	327.17	296.8	343.6	308.6	227.6	273.9	200.4	207.2
% Char		7.0	11.1	6.3	9.7	30.2	25.6	27.0
DMA								
(E') at 20°C ^b		0.58GPa	c	3.26GPa	c	c	c	c
T _g °C ^{a,d}		-29	c	126.7	c	c	c	c

a = not observed by differential scanning calorimetry (DSC, deg = degradation temperature °C); b = thin film solution cast; c = were unable to obtain thin films by solution casting or pressing for dynamic mechanical analysis (DMA) d = observed by DMA

to air at ambient light and temperature. The material was cast into film from methylene chloride ($T_g = -3$ to $+2$ by DSC and -29 by DMA), and its elastic modulus (E') at $20\text{ }^\circ\text{C}$ was 0.59 GPa . Polymer **3** was converted to epoxy allyl celluloses upon treatment with 32% peracetic acid in acetic acid in methylene chloride (**2b**). However, verifiable characterization of the number of epoxy groups per repeating unit by titration, DSC, and quantitative ^{13}C and ^1H NMR became difficult; this was due to polymer instability. Thus, further work with this polymer was not possible.

Tri-O-crotylcellulose, 4: Cellulose (average DPw = 361) was easily converted to the title polymer (DPw = 264) which showed melting (MP = $185.8\text{ }^\circ\text{C}$, peak) and recrystallization ($168.9\text{ }^\circ\text{C}$) behaviors by DSC (Table 1). This shows liquid crystal behavior, as is true for many cellulose polymers. Normal polymers recrystallize 50 to 100 degrees below their melting points. Polymer **4** degraded at $343.6\text{ }^\circ\text{C}$ by TGA. The material did not form films suitable for DMA analysis. Epoxidation of **4** with peracetic acid proceeded satisfactorily to afford epoxy crotyl celluloses and addition of acetate to the epoxy groups was not observed. The reaction was controlled and provided epoxy crotyl celluloses with different degrees of epoxidation. We were able to determine the extent of epoxidation (number of epoxy groups per repeating unit) by ^{13}C NMR integration by: (a) the disappearance of the olefin methine signals (at δ 127-130 ppm) and the cis and trans crotyl methyl signals at [δ 13.43ppm (cis), and 17.88ppm (trans)]; and (b) the appearance of the epoxy methine signals (at δ 50-58 ppm, mixture of cis and trans) and the epoxy methyl signals [at δ 13.1ppm (cis), and 17.6 ppm (trans)]. Epoxy crotyl celluloses formed excellent films when cast from THF or methylene chloride solutions (8% by weight). At 33 and 66% epoxidation, elemental analysis, titration, DSC data, and quantitative ^{13}C NMR indicated an average of one and two epoxy groups per repeating unit, respectively. For epoxy crotyl celluloses (66%), the modulus at $20\text{ }^\circ\text{C}$ and T_g by DMA were 0.17 GPa and $-9.5\text{ }^\circ\text{C}$, respectively. In addition, its melting and recrystallization temperatures by DSC were 204.5 and 179.3°C , respectively. A manuscript discussing the synthesis, physical and dynamic mechanical characteristics of epoxy crotyl celluloses is forthcoming.

6-O-Tritylcellulose, 5: This polymer gave satisfactory elemental analyses, and showed no apparent loss in DPw upon formation (Table 1). When doped with 5% by weight triphenylmethyl compounds (triphenylmethane and triphenylmethanol) or left unpurified from the reaction mixture, it formed films from methylene chloride. These exhibited T_g at $126.7\text{ }^\circ\text{C}$ (by DMA) and modulus (E') of 3.26 GPa at $20\text{ }^\circ\text{C}$. The material degraded at $308\text{ }^\circ\text{C}$ by TGA. Polymer **5**, when pure, did not provide useful films for DMA analysis.

6-O-Trityl-2,3-di-O-methylcellulose, 6: Polymer 6 gave satisfactory elemental analysis (Table 1), however, the conversion of polymer 4 to 5 resulted in a drop in the average DPw from 353 to 251 anhydroglucose units. While many mechanisms can be postulated to explain DP loss upon reactions with base, acids, organometals, and the like, none are satisfactory. Therefore, in this article we report DP loss upon reaction, but do not attempt to explain it. The polymer thermally degraded above 224 °C, and we were unable to generate films for DMA analysis.

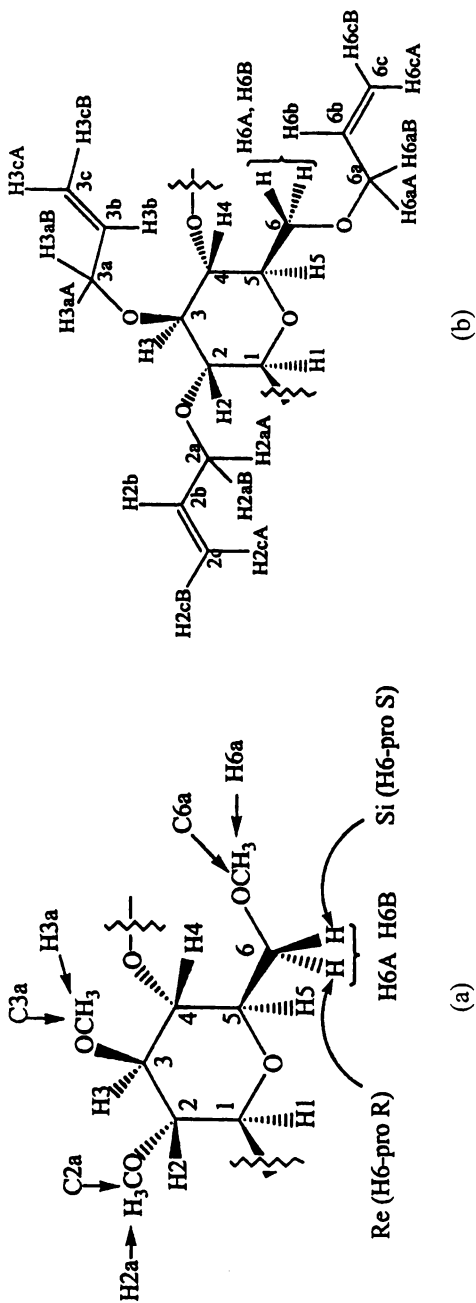
2,3-Di-O-methylcellulose, 7: Polymer 7 was formed by removal of the trityl group from 6, and the conversion reduced DPw from 251 to 168. The material decomposed at 273 °C by TGA and left a 30 % by weight char residue. This suggests that methylated celluloses may be useful in the design of flame resistant materials. We could not generate coherent films of this polymer for DMA work by solution casting. However, it is interesting to note that when the methyl groups are randomly placed on anhydroglucose, as in DS 1.6 (commercial) methylcellulose, solution casting can generate useful thin films.

6-Bromo-6-deoxy-2,3-di-O-methylcellulose, 8: Polymer 7 was converted to its bromo adduct 8, and the conversion lowered average DPw from 168 to 102. The polymer degraded at 200 °C by TGA, and the extent of residue was 25 %. The bromo polymer afforded very brittle films when cast from methylene chloride that crumbled upon further handling.

6-Phenyl-6-deoxy-2,3-di-O-methylcellulose, 9: The conversion of polymer 8 to 9 reduced DPw from 102 to about 73 repeating units, and elemental analysis showed that the extent of phenylation was 80 %. The compound average reduction in DPw in the 5-step conversion of 1 to 9 was $[(73/361)^{1/5} - 1 \times 100 =]$ 27 % per step, and the overall yield for the conversion of 1 to 9 was 33%. Polymer 9 decomposed at 207 °C and left a 27 % char residue. We were unable to solution cast coherent films of polymer 9.

Nomenclature System for Chemical Shift Assignments

Figure 2 shows the nomenclature system we used for making chemical shift assignments of the repeating units of polymers 2, 3, 4, and 9. The pyran ring carbons are sequentially numbered 1 to 6 starting with the anomeric carbon as C1 and ending the exocyclic equatorial methylene carbon as C6. Hydrogens and oxygens attached to the anhydroglucose carbons bear the same numbers. In situations with diastereotopic methylene hydrogens, the down field hydrogen is arbitrarily designated H#A, and the upfield hydrogen H#B (where # = anhydroglucose carbon number). The methyl ether carbons are called C#a, because they represent the first ether appendage carbons. And, the methyl ether hydrogens are called H#a. Continuing with the lowercase alphabet system to assign ether carbons, then, the second allyl ether carbon is called C#b, and the



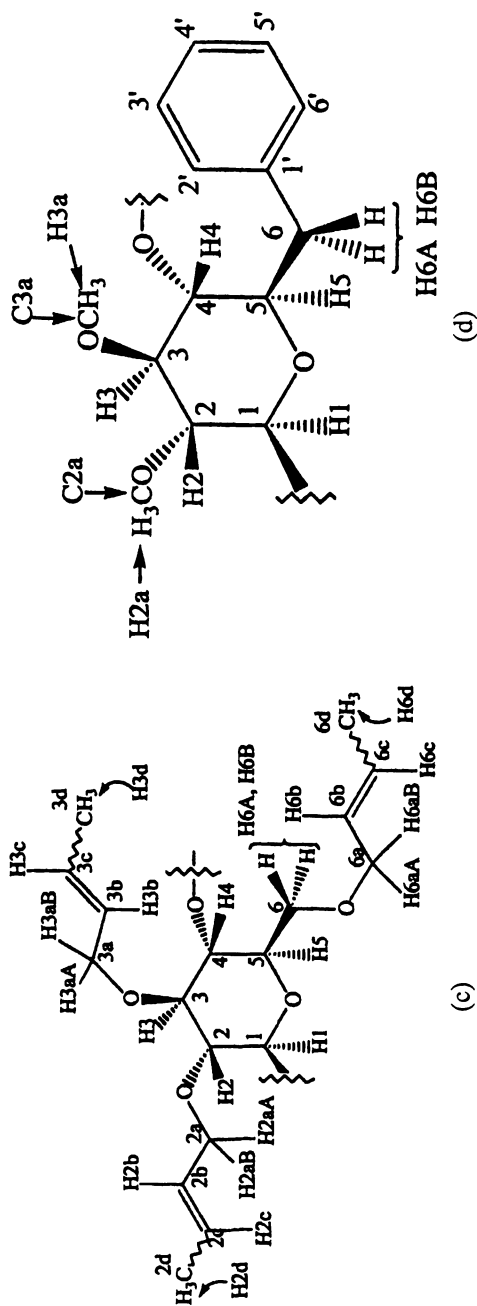


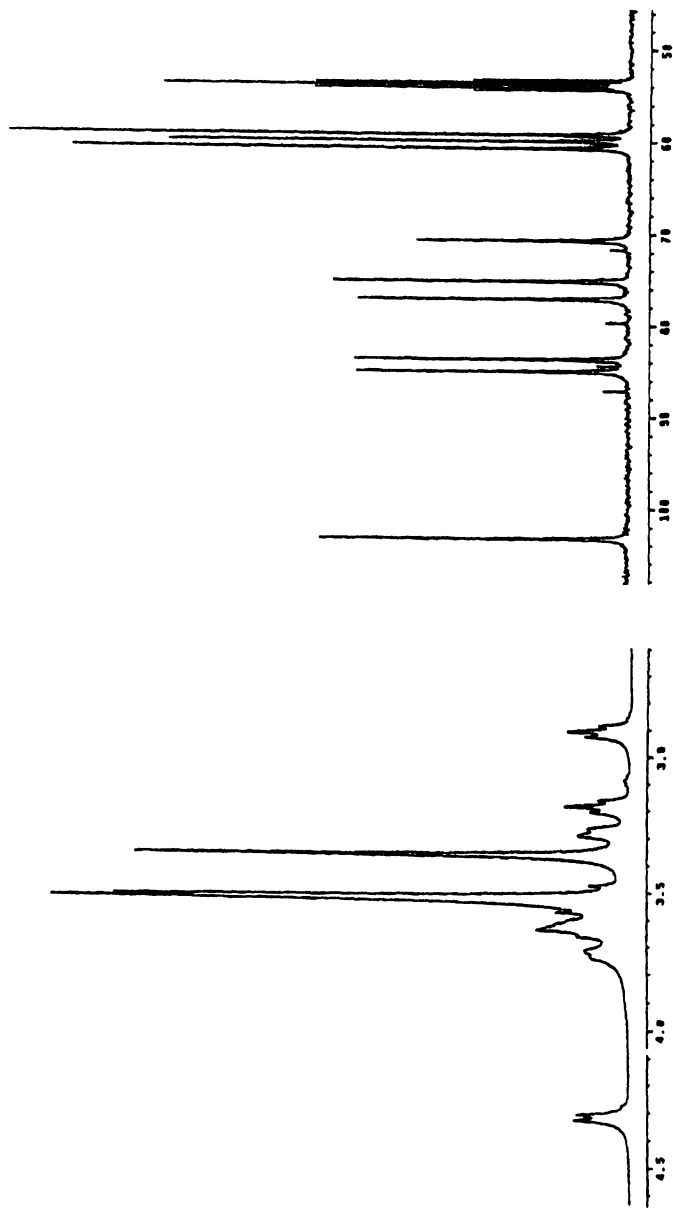
Figure 2: Carbohydrate and Ether Appendage Numbering System
(a) 2,3,6-Tri-O-methylcellulose Repeat Unit, 2; (b) 2,3,6-Tri-O-allylcellulose Repeat Unit, 3; (c) 2,3,6-Tri-O-crotylcellulose Repeat Unit, 4; (d) 6-Phenyl-6-deoxy-2,3-di-O-methyl-cellulose Repeat Unit, 9

third allyl ether carbon is C#c. And the fourth crotyl methyl carbon in **4** is called C#d. Since commercial crotyl chloride is a mixture of cis and trans isomers, cis and trans crotyl ethers were obtained. For these signals, the down field methyl resonances of C#d are trans, and the upfield (shielded) signals of C#d are cis. Finally, the prime (#') system was used to identify atoms of attached ring structures. E.g., the first and fourth carbons of the phenyl ring attached to C6 of anhydro-6-deoxyglucose in polymer **9** are C1' and C4', respectively.

Methods for Making Unambiguous Chemical Shift assignments: 2,3,6-Tri-O-methylcellulose:

One dimensional ^1H and ^{13}C spectra (Figures 3a and 3b) of the title compound were used to assign functional groups and to compare with literature data (6, 9). To transcend previous work regarding chemical shift assignments of tri-O-methylcellulose, double quantum filtered proton-proton correlation spectroscopy (15) was used to assign the proton shifts to the closed network of seven protons in the anhydroglucose portion of the repeat unit (Figure 4a). Thereafter, the heteronuclear multiple quantum coherence (HMQC, 16) spectrum was used to establish connectivities between the bonded protons and carbons (Figure 4b). Having generated the chemical shift assignments of the protons and carbons in the anhydroglucose portion of the repeat unit, we turned our attention to the methyl ether appendages and used the heteronuclear multiple bond correlation (HMBC, 17) spectrum to connect the hydrogens of the methyl ethers to their respective sugar carbons (Figure 4c). Then, a combination of HSQC and HMBC spectra was used to assign the ^{13}C shifts of the methyl ethers (Table 2), and complete all chemical shift assignments. First order proton coupling constants data ($J_{\text{H,H}}$ in Hz) were obtained from the resolution enhanced proton spectra (18). Comparative examination of the proton coupling constants about the C5-C6 bond ($J_{5,6\text{A}}$ and $J_{5,6\text{B}}$, Table 3) in the nOe difference spectra with published spectra of methyl- d_3 2,3,4,6,-tetra-O-methyl- d_3 α - and β -D-glucopyranosides (19) cellulose triacetate (20), and 1,2,3-tri-O-acetyl-4,6-O-isopropylidene- β -D-glucopyranose (21) revealed that the C6 O-methyl group is predominantly in the gauche-gauche (gg) conformation about the C5-C6 bond for the polymer in solution.

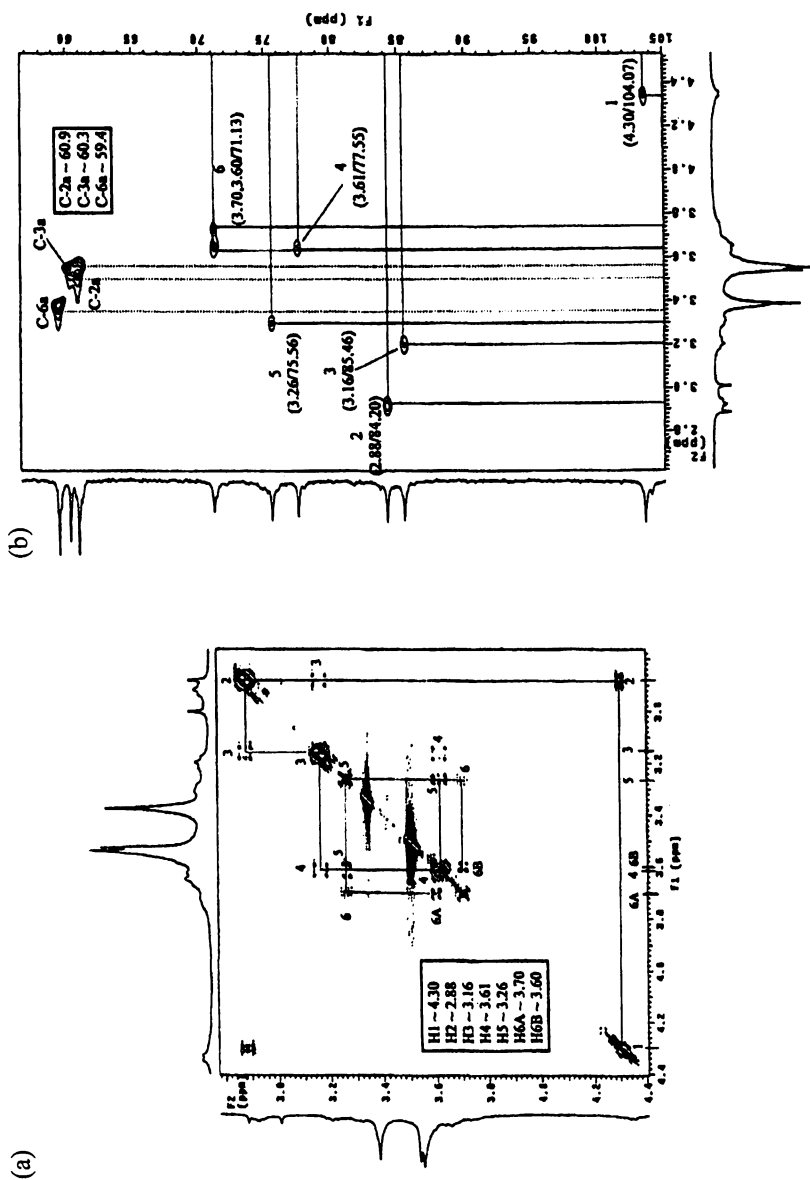
Likewise, the proton and carbon-13 chemical shifts of tri-O-allyl- and tri-O-crotyl- celluloses and 6-phenyl-6-deoxy-2,3-di-O-methylcellulose were obtained (Tables 4, 5).

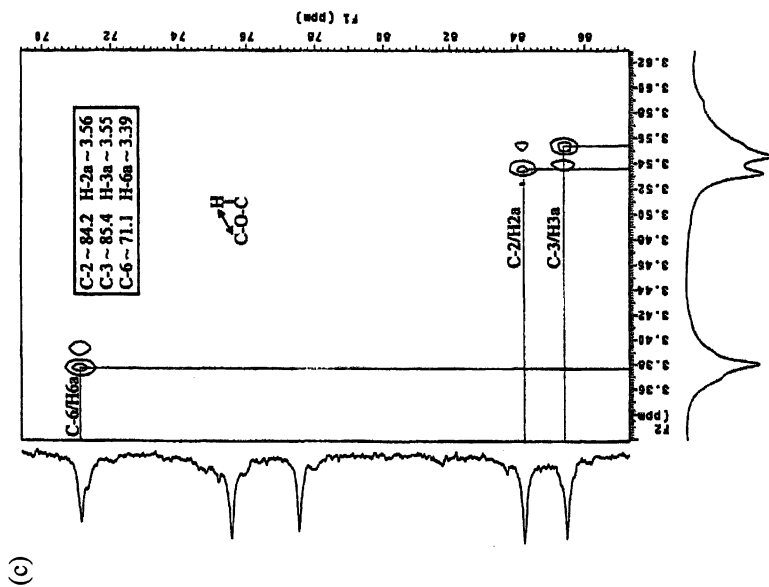


(a)

(b)

(a) ^1H NMR of 2,3,6-Tri-O-methylcellulose, **2**; (b) ^{13}C NMR of 2,3,6-Tri-O-methylcellulose, **2**





(a) COSY Spectrum of Polymer 2; (b) HMQC Spectrum of Polymer 2; (c) HMBC Spectrum of Polymer 2

Table 2: ^1H & ^{13}C Chemical Shifts of 2,3,6-Tri-O-methylcellulose

Assignment	^1H δ (ppm)	^{13}C δ (ppm)
1	4.30	104.07
2	2.88	84.20
3	3.16	85.46
4	3.64	77.55
5	3.26	75.56
6a	3.70	71.13
6b	3.62	
OCH ₃ (2a)	3.50	60.93
OCH ₃ (3a)	3.56	60.31
OCH ₃ (6a)	3.36	59.40

Table 3: Comparing the Coupling Constant ($J_{\text{H,H}}$ in Hz) of Polymer **2** with Other Cellulose and Glucose Derivatives

$^3J_{1,2}$	$^3J_{2,3}$	$^3J_{3,4}$	$^3J_{4,5}$	$^3J_{5,6A}$	$^3J_{5,6B}$	$^2J_{6A,6B}$
2,3,6-Tri-O-methylcellulose, 2						
7.6	8.2	8.8	9.3	4.2	3.3	-11.0
Methyl-d₃ tetra-O-methyl-d₃-β-D-glucoside, 10 (19)						
7.8	8.9	9.0	9.6	2.1	4.9	-10.8
Cellulose triacetate, 11 (20a)						
7.9	7.3	9.2	9.2	--	--	-10
Cellulose triacetate, 11 (20b)						
7.6	9.0	9.0	9.5	1	5.0	--
1,2,3-Tri-O-acetyl-4,6-O-isopropylidene-β-D-glucopyranose, 12, (21)						
8	9	9	9.5	6	9.5	-10.5

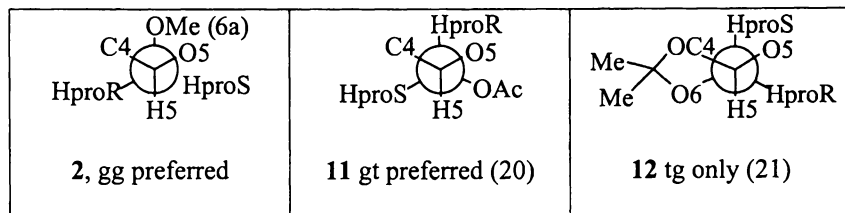


Table 4: ^1H and ^{13}C NMR Assignments for 2,3,6-Tri-O-allyl- and 2,3,6-Tri-O-crotyl Celluloses.

Tri-O-Allylcellulose, 3			Tri-O-Crotylcellulose (4)				
H1	4.42	C1	102.97	H1	4.85	C1	103.19
H2	3.09	C2	81.71	H2	3.50	C2	81.42
H3	3.32	C3	83.19	H3	3.73	C3	83.01
H4	3.80	C4	77.16	H4	4.18	C4	77.33
H5	3.24	C5	75.37	H5	3.67	C5	75.51
H6A; B	3.83; 3.67	C6	68.35	H6A; B	4.27; 4.12	C6	68.11
H2aA; B	4.24; 4.24	C2a	74.05	H2aA; B	4.61; 4.57	C2a	73.77
H3aA; B	4.44; 4.18	C3a	74.16	H3aA; B	4.80; 4.53	C3a	73.49
H6aA; B	4.07; 4.01	C6a	72.31	H6aA; B	4.46; 4.38	C6a	71.90
H2b	5.93	C2b	135.84	H2b	6.04	C2b	127.53
H3b	5.99	C3b	136.74	H3b	6.09	C3b	127.87
H6b	5.94	C6b	135.49	H6b	6.06	C6b	128.21
H2cA; B	5.28; 5.14	C2c	116.19	H2c	6.10	C2c	128.77
H3cA; B	5.24; 5.08	C3c	115.65	H3c	6.15	C3c	129.76
H6cA; B	5.30; 5.16	C6c	116.40	H6c	6.19	C6c	129.14
				H2d <i>cis</i>	2.11	C2d <i>cis</i>	13.43
				H3d <i>cis</i>	2.11	C3d <i>cis</i>	13.43
				H6d <i>cis</i>	2.11	C6d <i>cis</i>	13.43
				H2d <i>trans</i>	2.16	C2d <i>trans</i>	17.88
				H3d <i>trans</i>	2.16	C3d <i>trans</i>	17.88
				H6d <i>trans</i>	2.16	C6d <i>trans</i>	17.88

Table 5: Complete Proton and Carbon-13 NMR Assignments of the 6-Phenyl-6-deoxy-2,3-di-O-methyl-1,4-anhydroglucose Repeating Unit

Assignment	^1H δ (ppm) ¹	^{13}C δ (ppm) ¹
1	4.54	102.56
2	2.99	84.09
3	3.62	81.25
4	3.32	84.11
5	3.48	73.79
6a	3.38	37.75
6b	2.71	
OMe 2	3.63	60.87
OMe 3	3.53	60.35
1'		138.67
2',6' (ortho)	7.28	130.02
3', 5' (meta)	7.31	128.63
4' (para)	7.23	126.76

¹Relative to CD_2Cl_2 (δ proton = 5.32; δ ^{13}C = 53.1) at 40 °C (sealed tube).

Conclusions:

Since 1923 the synthesis of allyl cellulose has been discussed many times (6), however, typical successful fully substituted preparations employ one-gram of cellulose. For our work, we needed larger quantities; attempting scale-ups by keeping the reported molar ratios unchanged did not work. This was because the reported conditions for making and isolating the products were no longer relevant. By trial and error, we discovered that we could reproducibly and safely start with 50 to 60 g of cellulose, and generate uncontaminated products by employing the above-discussed procedural modifications. In addition, our desire to make well-defined cellulose epoxies for powder coatings and film adhesive applications opened the door to a wealth of unique opportunities:

- (a) For the first time we completely characterized all the ^1H and ^{13}C chemical shifts of cellulose ethers by a combination of one- and two-dimensional NMR methods;
- (b) Prepared and characterized carbon-carbon bonded celluloses; and
- (c) Found cellulose derivatives and their epoxies that exhibited melting and recrystallization hysteresis behavior for adhesives and coatings applications.

These discoveries should open the door for many new commercial uses for cotton and other celluloses.

Acknowledgment: We are thankful to Professors Marcus A Tius, and Roger E. Cramer, University of Hawaii at Manoa, and Professor Morton H. Litt, Case Western Reserve University of many helpful discussions and review of this manuscript. The United States Department of Agriculture, Agriculture Research Service, through a CRIS in the Cotton Textile Chemistry Research Unit (No. 6435-41000-064-00D) provided funding for this work.

References and Notes:

1. (a) Sachinvala, N. D., and Litt, M. H. US Patent 5,571,907, November 5, 1996. (b) Sachinvala, N. D. and Litt, M. H., US Patent 5,646,226, July 8, 1997. (c) Sachinvala, N. D., Winsor, D.L., Menescal, R.K., Niemczura, W. P., Litt, M. H., and Ganjian, I. *J. of Polym. Sci., Part A Polym Chem. Ed.*, **1998**, *36*, 2397-2413.
2. (a) Hiatt, G. D., and Rowley, M. E. US Patent 3,349,080, October 24, 1967. (b) Lin, M-S., and Huang, C-S. *J. of Polym. Sci., Part A Polym Chem. Ed.*, **1992**, *30*, 2303-2312.
3. Sachinvala, N.D., Hamed, O.A., Winsor, D.L., Niemczura, W.P., Maskos, K., Parikh, D.V., Glasser, W., Becker, U., Blanchard, E.J., and Bertoniere, N.R. *J. Poly. Sci.: Part A: Poly. Chem. Ed.*, **1999**, *37*, 4019-4032.
4. Sachinvala, N. D., Winsor, D. L., Hamed, O. A., Niemczura, Maskos, K., Glasser, W., Bertoniere, N. R. *J. of Poly. Sci.: Part A: Poly. Chem. Ed.*, **2000**, *38*, 1889-1902.

5. (a) Sachinvala, N. D., Winsor, D. L., Hamed, O. A., Niemczura, Maskos, K., Bertoniere, N. R., 219th ACS Natl. Meeting, Abs. No. CELL071, San Francisco, CA. March 27, 2000. (b) Sachinvala, N.D., Winsor, D. L., Hamed, O. A., Niemczura, W. P., Maskos, K., *Polymers for Advanced Technologies*. 2001. Accepted.
6. (a) Tomecko, C. G. and Adams, R. *J. Am. Chem. Soc.*, **1923**, *45*, 2698-2701. (b) Sakurada, I. *Zeitschr. Fur Angew. Chemie*, **1929**, *42*, 549-550. (c) Timell, T. *Svensk Papperstidn.*, **1949**, *7*, 165-167. (d) Wilson, W. O. Masters Thesis, Institute of Textile Technology, Charlottesville, VA, **1951**. (e) Yoshiura, S. *Sen-I Gakkaishi*, **1965**, *21(6)*, 317-326. (f) Hoiness, D. E., Wade, C. P., and Rowland, S. P., *Can. J. Chem.*, **1968**, *46*, 667-672. (g) Isogai, A., Ishizu, A., and Nakano, J. *J. Appl. Poly. Sci.*, **1984**, *29*, 2097-2109. (h) Isogai, A., Ishizu, A., and Nakano, J., *J. Appl. Poly. Sci.*, **1984**, *29*, 3873-3882. (i) Isogai, A., Ishizu, A., and Nakano, J. *Carbohydr. Res.*, **1985**, *138*, 99-108. (j) Kondo, T., Isogai, A., Ishizu, A., and Nakano, J. *J. Appl. Poly. Sci.*, **1987**, *34*, 55-63. (k) Kondo, T., Ishizu, A. and Nakano, J. *J. Appl. Poly. Sci.*, **1988**, *35*, 885-893. (l) Sawatari C. and Yagi, T. *Sen-I Gakkaishi*, **1991**, *47(9)*, 467-475. (m) Ishikuro, T., Inoue, S., Meshitsuka, G., Ishizu, A., Murakami, K., and Watanabe. K. *Sen-I Gakkaishi*, **1995**, *51(12)* 571-579; (n) Blasutto, M., Delben, F., Milost, R., and Painter, T.J., *Carbohydr. Polym.*, **1995**, *27*, 53-62.
7. Dawsey, T. R., McCormic, C. L. *J. Macromolecular Sci. Reviews, Macromolecular Chem.* **1990**, *30*, 405-440.
8. (a) Harkness, B. R., Gray, D. G., *Macromol.*, **1990**, *23*, 1452-1457. (b) Klemm, D., Philipp, B., Heinze, T., Heinze, U., Wagenknecht, W; *Comprehensive Cellulose Chemistry*, Wiley-VCH: New York, **1997**, Vol. 2, pp. 359-360.
9. (a) Kondo, T., Gray, D. G., *Carbohydr. Res.*, **1991**, *220*, 173-183. (b) Kondo, T., Gray, D. G., *J. Appl. Polym. Sci.*, **1992**, *45*, 417-423. (c) Kondo, T. *Carbohydr. Res.*, **1993**, *238*, 231-240.
10. (a) Sachinvala, N.D., Niemczura, W.P., and Litt, M.H. *Carbohydr. Res.*, **1991**, *218*, 237-245. (b) Sachinvala, N.D., Ju, R.F., and Litt, M.H., and Niemczura, W. P. *J. Poly. Sci. Part A. Polym. Chem. Ed.*, **1995**, *33*, 15-29.
11. Descotes, G., Praly, J. P., Bouchu, A. *Carbohydr. Res.*, **1986**, *148*, 137-142
12. (a) Bessodes, M., Komiotis, D., Antonakis, K., *Tetrahedron Lett.*, **1986**, *27*: 579-580. (b) Kocienski, P. J., *Protecting Groups*, Thieme: New York, **1994**, pp. 54-59.
13. (a) Hanessian, S., and Plessas, N., *J. Org. Chem.*, **1969**, *34*, 2163-2170. (b) Hepburn, D. R., Hudson, H. R. *J.C.S. Perkin I*, **1976**, 754-757.
14. (a) Lipshutz, B. H., Parker, D., Kozlowski, J. A., and Miller, R. D. *J. Org. Chem.*, **1983**, *48*, 3334-3336. (b) Mirviss, S. B., *J. Org. Chem.* **1989**, *54*, 1948-1951. (c) Taylor, R. J. K. in *Organocopper Reagents*, L. M. Harwood

- and C. J. Moody, Eds., Oxford University Press: Oxford, UK, **1994**, pp.1-26.
15. DQF-COSY: (a) Croasmum, W. R. and Carlson, M. K. Two-dimensional NMR Spectroscopy, VCH Press: New York, **1994**, pp. 42-45 and 304-308. (b) Rahman A. and Choudhary, M. I., *Solving Problems with NMR Spectroscopy*, Academic Press: New York, **1996**, pp. 249-251; (c) Braun, S., Kalinowski, H. A., and Berger, S. 100 and More Basic NMR Experiments: A Practical Course, VCH: New York, **1996**, pp. 356-359.
 16. HMQC: (a) *idem, ibid*, pp. 61-63. (b) *idem, ibid*, pp.271-273. (c) *idem, ibid*, pp. 360-363.
 17. HMBC: (a) *idem, ibid*, pp. 61-64. (b) (a) *idem, ibid*, pp. 273-274. (c) *idem, ibid*, pp. 315-317
 18. Hall L. D. and Sanders, J. K. M. *J. Amer. Chem. Soc.*, **1980**, *102*, 5703-5711.
 19. (a) Haverkamp, J., vanDongen, J. P. C., and Vliegenthart, J. F. G. *Tetrahedron*, **1973**, *29*, 3431-3439. (b) Haverkamp, J., DeBie, M. J. A., and Vliegenthart, J. F. G, *Carbohydr. Res.*, **1975**, *39*, 201-211. (c) Streefkerk, D. G. and Stephen, A. M. *Carbohydr. Res.*, **1977**, *57*, 25-37.
 20. (a) Rao, V. S.; Sauriol, F.; Perlin, A. S.; and Phanviet, M. T. *Can. J. Chem.*, **1985**, *63*, 2507-2511; (b) Buchanan, C. M.; Hyatt, J. A.; and Lowman, D. W.; *Macromolecules*, **1987**, *29*, 2750-2754.
 21. Wolfrom, M. L.; Diwadkar, A. B.; Gelas, J.; and Horton, D. *Carbohydr. Res.*, **1974**, *35*, 87-96.

Chapter 25

2D NMR Analysis of Ethylcellulose

Qiuwei Xu¹, Mark Brickhouse², and Huiming Wang²

¹Merck Research Laboratory, P.O. Box 4, WP78-107,
West Point, PA 19486

²Hercules Incorporated, Research Center, 500 Hercules Road,
Wilmington, DE 19808

2-D NMR was used to characterize native and acid hydrolyzed ethylcellulose (EC), a Hercules product widely used as a film-former in ink and coatings applications and as a binder and filler in pharmaceutical applications. An important parameter in controlling the properties of ethylcellulose is the degree of substitution (DS) of ethyl functionalities on the cellulose backbone. NMR is one technique that was used to determine both the total and positional DS (ethylation at the 2,3 and 6 positions of the anhydroglucose unit (AGU)). This analysis requires complete hydrolysis of the sample, and an improved acid hydrolysis technique was developed for this application. Two-dimensional (2-D) NMR techniques were used to confirm peak assignments related to positional DS determinations that were previously made by comparison with standards. In addition, 2-D NMR methods were used to evaluate positional DS of native ethylcellulose prior to acid hydrolysis. A comparison of the analytical results for the acid hydrolysate and native polymer will be discussed.

Ethylcellulose is cellulose ethyl ether. It is a widely added ingredient to formulations of varnishes, inks, lacquers and adhesives. Its elasticity enables it to form films, foils and plastics (1). Owing to its inert chemical properties, it can be used for food-contacting packaging, drug tablet coating and binding. Microencapsulating drugs with ethylcellulose can control drug release *in vivo* (2,3,4).

In β 1 \rightarrow 4 linked D-glucose, there are three accessible hydroxyl groups for substitutions, the C2, C3 and C6 positions (Figure 1). Ethyl substitutions at these positions are measured as degree of substitution (DS) and positional degree of substitution (PDS). The former indicates the averaged number of ethoxy groups on each glucose residue. The latter shows the distribution of substitution over the C2, C3 and C6 positions. The physical properties of ethylcellulose are determined by these structural parameters.

NMR has played an important role in determining the chemical structures of industrial and bacterial polysaccharides (5,6,7,8). Typical polysaccharides show fingerprint region on 1D proton and carbon spectra. Anomeric protons or carbons usually appear in the downfield region; however, ring protons tend to be crowded in a narrow region of chemical shift (\sim 1ppm). Despite the better chemical shift dispersion of ^{13}C NMR, its low sensitivity and low natural abundance makes it undesirable to acquire direct carbon spectra, especially of rigid or associated polysaccharides. The extension of 1D proton NMR into proton-proton 2D NMR has shown an improvement in resolving overlapping proton peaks in the upperfield region while maintaining a proper sensitivity. Inverse-detected ^1H - ^{13}C spectra were acquired and used to investigate the structural differences of ethylcellulose polymers and their acid hydrolysates.

Experimental

Preparation of acid hydrolyzed EC was performed exclusively with disposable glassware. \sim 500 mg of EC is dispersed in 4-5 ml of a trifluoroacetic acid (TFA)/water solution (prepared gravimetrically, 74.47 grams TFA in 32.52 grams deionized water). The dispersion was prepared in a loosely capped 17 ml vial and heated on a Thermolyne Type 16500 DriBath @ 75-80C for 24-45 hours. The samples were heated sufficiently long to minimize the glycosidic C-1 carbon peak @ 102 ppm (from intact polymer and oligomer). However, care was taken to prevent caramelization of the samples. It was typical for the samples to turn light brown under these conditions; overheating caused the samples to turn black. After heating, the samples were allowed to air-dry in a disposable evaporating dish for at least two hours with mild heating. The resulting solids were dissolved, with mild heating, in \sim 4ml d_6 -DMSO, which contains 0.04M $\text{Cr}(\text{acac})_3$ as a relaxation agent. The native EC polymer was dissolved in CDCl_3 at \sim 40mg/ml.

Most NMR measurements were made on a Bruker Avance 500MHz instrument with a 5mm pulse field gradient (PFG)-Broadband Inverse(BBI)

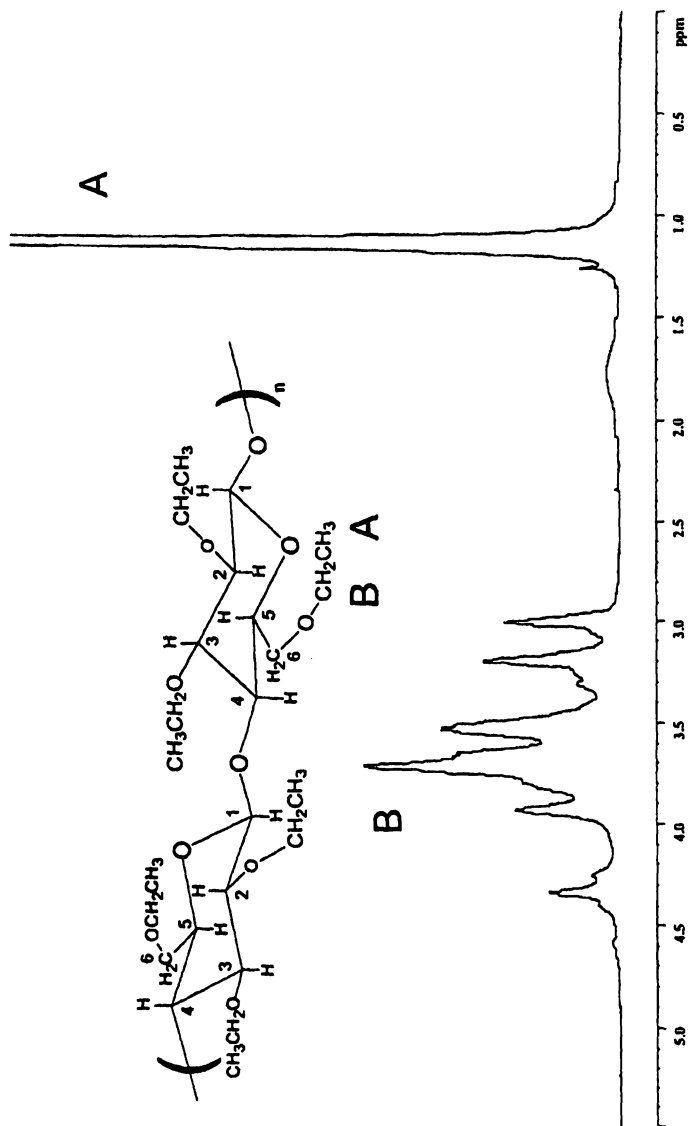


Figure 1. Annotated Proton NMR Spectrum of Ethylcellulose in CDCl_3 with Generic Structure of Ethylcellulose of $\text{DS}=3$

probe. The data were acquired without sample spinning at 40°C for the polymer sample, and at 25°C for the hydrolysate. The phase sensitive spectra were acquired using the TPPI-States or TPPI scheme. The Hartmann-Hahn transfer in the Homonuclear Hartmann-Hahn (HOHAHA) experiments were realized with the composite pulses of MLEV17 at 4.16kHz. The mixing time was set to 40ms. The 90 degree pulse of carbon high power was 10.5 μ sec. During proton acquisition in the Heteronuclear Multiple Quantum Coherence (HMQC) experiments, the carbon decoupling was applied with a field strength of 3.88 kHz. The duration of magnetization transfer from proton to carbon in HMQC was set at 3.22ms (155Hz). The duration of developing long range proton-carbon correlation in the Heteronuclear Multiple Bond Correlation (HMBC) experiments was set at 70ms. For the polymer sample, the proton and carbon carrier frequencies were set at 500.1316568 and 125.7684284 MHz, respectively. The spectral widths of proton and carbon dimension were 5122.951 Hz (~10ppm) and 18865.393 Hz (150ppm) respectively. The 90 degree pulse of proton was 7.60 μ sec @ 5.0 dB power level. For the hydrolysate sample, the proton and carbon carrier frequencies were set at 500.132 and 125.768 MHz respectively. The spectral widths of proton and carbon dimension were 3501.40 Hz (~7ppm) and 18865.393 Hz (150ppm) respectively. Double Quantum Filtered Correlated Spectroscopy (DQF-COSY, 9,10,11) HOHAHA (12,13), HMQC (14,15) and HMBC (16) spectra were acquired sequentially on each sample using multiple experiment automation on the Bruker 500 spectrometer. Between runs, lock was reset to 90% and Z1 was re-shimmed without any sample spinning.

The NMR spectrum shown in Figure 3 was acquired on a 600 MHz Bruker Avance NMR with a 5 mm PFG-TXI probe. The proton and carbon carrier frequencies were set at 600.1336081 and 150.9177568 MHz, respectively. The spectral widths of proton and carbon dimension were 8012.82 Hz (~13 ppm) and 33557.015 Hz (222 ppm) respectively. The 90 degree pulse of proton was 6.90 μ sec @ -2.0 dB power level.

2-D NMR Analysis of Intact Ethylcellulose

Two structural features that affect the physical properties of EC are degree of substitution (DS) and positional substitution of ethyl groups. DS indicates the averaged number of ethoxy groups on each anhydroglucose repeating unit (AGU). Positional substitution is the distribution of ethyl groups at the three potential substitution sites, the hydroxyl groups C2, C3 and C6 (Figure 1). Historically, Hercules has used 1-D 13 C NMR of acid-hydrolyzed EC to determine positional DS (17). One of the goals of this work was to

determine if 2-D NMR could be used to determine positional DS and positional DS of intact EC.

The proton spectrum (Figure 1) of the polymer shows broad peaks, typical for a rigid polymer. The peaks on the left side of the spectrum ($\delta \sim 4.3$ ppm) are anomeric protons, the large peak on the right side are from the methyl protons of the ethyl groups ($\delta \sim 1.2$ ppm). The middle region contains the pyran ring and methylene protons of the ethoxy groups.

The identification of proton correlation was assisted by DQF-COSY, which identified adjacent protons by off-diagonal cross peaks. The assignments of the three pendant methylene proton substituents at 2,3 or 6 of the AGU ring were made through long range proton-carbon correlation (HMBC) as discussed below. The HMQC and HMBC proton-carbon correlation experiments were used in combination to make the assignments of the ring protons as shown in Figure 2.

The HMQC and HMBC spectra are overlaid in Figure 2. HMQC correlated proton with one-bond-linked carbon, and HMBC correlated protons and carbons that are typically 2-3 bonds apart. The contours in black were generated by HMQC, and the ones in gray by the HMBC techniques, respectively. The ethyl linkages to the glucose and glucose-glucose linkages were revealed by the three-bond proton-carbon correlation. With the help of chemical shift dispersion along the carbon dimension, we could see that H4 overlaps with H6, so does H3 with H5. The cross peaks (H1-C4 and C1-H4) on HMBC arose through glycosidic linkages rather than through intra-ring coupling interactions. These cross peaks reflected the $\beta 1 \rightarrow 4$ linkage for cellulose backbone.

The substitution position of ethoxyl groups was located based on the correlation peaks of methylene proton on ethoxyl groups and ring carbons. For example, the gray HMBC peaks labeled $S3CH_2-C3$ indicates the three bond coupling between the sidechain methylene protons and the glycosidic carbon at position C3.

The degree of substitution (DS) of the ethylcellulose sample described above was determined to be 2.7 by the Sealed-Tube Zeisel (STZ) technique. However, STZ DS determinations require the exhaustive acid degradation of polymer samples such as ethylcellulose. DS determinations of ethylcellulose were not usually performed on intact polymer samples. The peak separation from two-dimensional NMR spectra could conceivably help obtain DS values directly from intact polymer.

Relative positional DS at C2, C3 and C6 could be obtained from the integration of cross peaks on HOHAHA (Figure 3). The adjacent proton coupling constants for the three ethoxyl groups were found to be similar (~ 15 Hz) as measured from DQF-COSY. The three HOHAHA cross peak

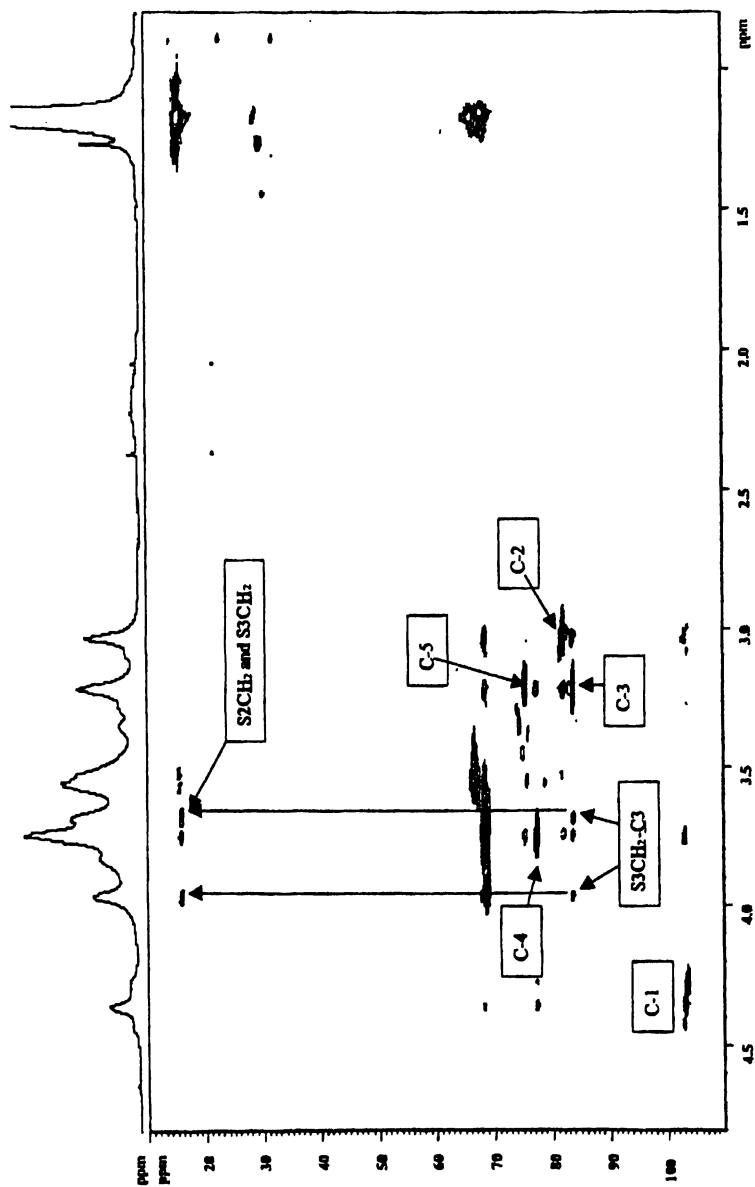


Figure 2. ^1H - ^{13}C 2-D Short Range HMQC (black) and Long Range HMBC (gray) Correlation Spectra of Ethylcellulose in CDCl_3

intensities were estimated to reflect the relative substitution percentages on these three positions. The overlapping methyl protons of the 1-D ^1H spectrum were resolved thanks to the chemical shift dispersion of the methylene protons. The relative positional DS values were determined by integrating the peaks labeled as C3, C2 and C6 on both sides of the diagonal line, and taking the average of these two sets of data.

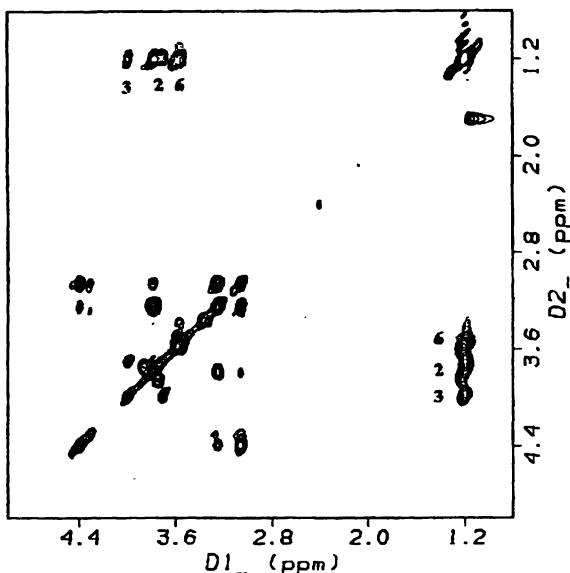


Figure 3. HOHAHA of ethylcellulose polymer, 40ms mixing

The calculated amounts of relative ethyl substitution at C2, C3 and C6 are tabulated in Table 1 together with the results of the analyses from GC-MS and ^{13}C NMR analysis of acid-hydrolyzed EC monomers. While the general trend of lesser substitution at the 3-position is correct, the relative amount of 3-substitution for an EC with a DS value of 2.7 (as determined by the STZ technique), as is the case with this EC, cannot drop below 26%. This is because if ethylation of C2 and C6 is complete, positional DS at C2 (PDS_2) = 1, PDS_6 = 1 and then $\text{PDS}_3 = 0.7$. Since $0.7/2.7 = 26\%$, the minimum relative substitution at C3 is 26%.

Table 1. Relative Positional DS of intact ethylcellulose polymer.

Position	3	2	6
Percentage	10% (29% ^a , 31% ^b)	40% (36% ^a , 33% ^b)	50% (34% ^a , 35% ^b)

- calculated from GC-MS data on an acid hydrolysate
- calculated from 1D carbon data on an acid hydrolysate

A review of the ^1H - ^{13}C HMQC (black) and HMBC (gray) spectra shown in Figure 3 shows the S3- CH_2 ^1H signal is split in the proton dimension into two peaks centered at 3.7 and 4.0 ppm. The former peak overlaps the S2- CH_2 peak in the lower resolution HOHAHA spectrum shown in Figure 4. As a result, relative positional DS values calculated from the HOHAHA spectrum would be low for C3 and high for C2. This work shows that 2-D NMR analysis of *intact* EC can provide structural information on polymer substitution, but not quantitative data on positional DS without substantially more effort to resolve peak overlaps spectroscopically or by deconvolution of overlapping 2-D peak volumes.

2-D NMR Analysis of Acid Hydrolysed Ethylcellulose

Previous positional DS determination of ethylcelluloses were performed on samples subjected to exhaustive acidic methanolysis and analyzed by 1-D ^{13}C NMR (17). This method required four days for the digestion of each sample, and assignments of the side chain methylene carbons bonded to C2, C3 and C6 were made by comparison with synthetically prepared reference materials. Recently, a faster digestion method was developed (as described in the Experimental section), and it was necessary to confirm that ^{13}C assignments (Figure 4) used to determine positional DS after acidic methanolysis method were still valid for samples digested in TFA solutions.

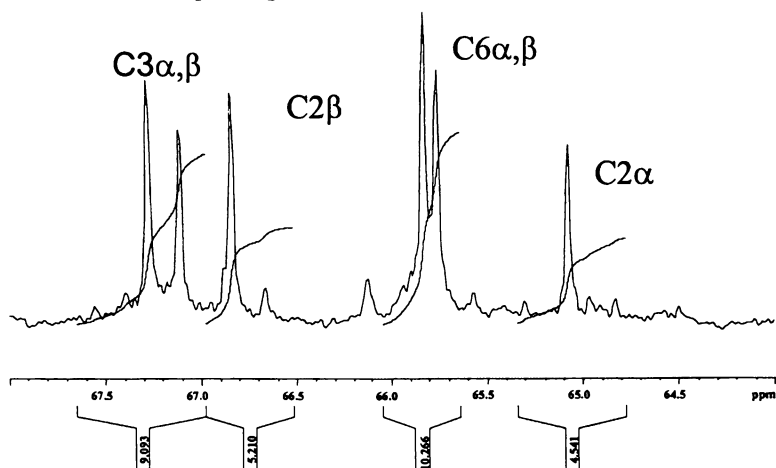


Figure 4: ^{13}C NMR Spectrum of TFA-Hydrolyzed Ethylcellulose Side Chain Methylene Carbons Assigned According to Reference Spectra from Acidic Methanolysis Method (α and β are anomers of ethylated glucose)

A combination of HMQC and HMBC spectra, as described above, allowed for confirmation of the ^{13}C chemical shifts without the need of re-acquiring external reference standards. Figure 5 shows how scalar coupling interactions were tracked from βC1 to the sidechain methylene carbons substituted at the C2 position (Since the EC has been hydrolytically digested, the hydrolysate contains a mixture α and β anomers of glucose ethoxylated at C2, C3 and C6).

The same “spin-walk” analysis was also performed for the C3 and C6 side chain methylenes, on both α and β anomers. The ^{13}C chemical shifts of the sidechain methylene carbons determined in this fashion confirmed the assignments used to determine positional DS by 1-D NMR, as shown in the assigned spectrum in Figure 5.

Like the calculation of the relative DS made for the intact polymer, the relative positional DS of the TFA-hydrolyzed EC can also be calculated from the cross peaks on HOHAHA spectrum (Figure 6). The relative positional DS values are listed in Table 2. Because of the improved spectral resolution of the hydrolyzed EC relative to the intact EC, there are no signal overlaps for the sidechain methylene protons and the calculated values are almost the same as those determined by GC-mass spectrometry and 1D ^{13}C NMR analyses on the acid hydrolysate. However, since the ^{13}C NMR method provides an absolute rather than relative positional DS value, it is still the method of choice for EC characterization.

Table 2. Relative Positional DS of TFA-hydrolyzed ethylcellulose polymer

Position	3	2	6
Percentage	30% (29% ^a , 31% ^b)	36% (36% ^a , 33% ^b)	34% (34% ^a , 35% ^b)

- a. calculated from GC-mass data
b. calculated from 1D carbon data

Conclusions

This study shows that 2-D NMR analysis of *intact* EC can provide structural information, such as confirming the presence of cellulose ethoxylated at the C3 position, but does not readily yield quantitative information such as positional DS. 2-D NMR analysis of TFA-hydrolyzed EC confirms formation of a complex mixture of ethoxylated α and β - glucose anomers. A combination of HMQC and HMBC analyses was used to confirm the assignments used for quantitative 1-D ^{13}C NMR analysis without reference to external standards. Because of improved spectral resolution, HOHAHA analysis of hydrolyzed EC afforded relative positional DS that agreed well with values determined by GC-

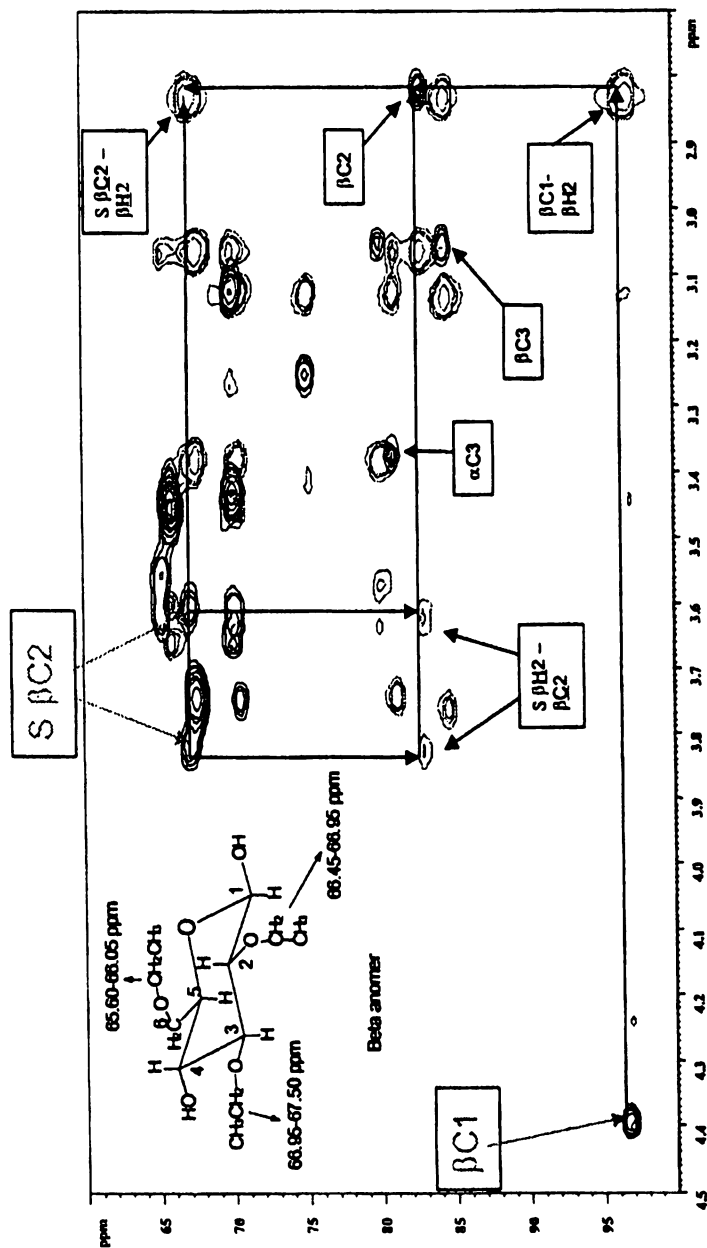


Figure 5: ^1H - ^{13}C 2-D Short Range HMQC (black) and Long Range HMBC (gray) Correlation Spectra of TFA-Hydrolyzed Ethylcellulose in d_6 -DMSO

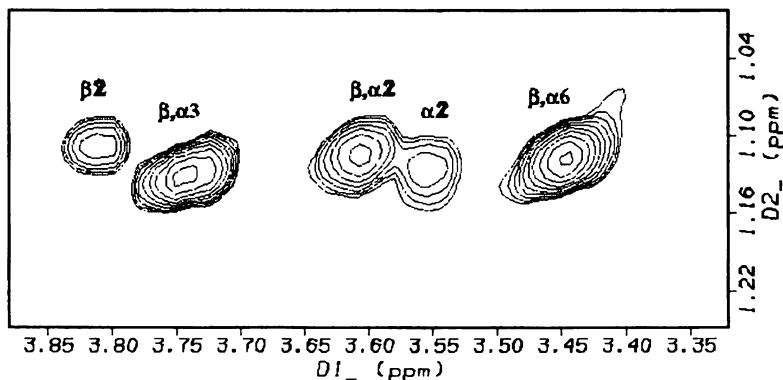


Figure 6: A section of cross peaks in the HOHAHA spectrum of the ethyl cellulose hydrolysate

MS and 1-D ^{13}C NMR. In general, it was found that while 2-D NMR techniques were superior for absolute structure determination, 1-D NMR analyses were preferable for quantitative analysis.

References

1. "Aqualon Ethylcellulose (EC) Physical and Chemical Properties" Hercules Inc.
2. PB Deasy, MR Brophy, B. Ecanow, MM Joy J. Pharm Pharmacol 32, 15-20 (1980)
3. M. Ito, M Nakano, Chem. Pharm. Bull (Tokyo) 28, 2816-2819 (1980)
4. J. R. Nixon, M. R. Meleka J. Microencapsul 1, 53-64 (1984)
5. Abeygunawadana C., and C. A. Bush Adv. Biophys. Chem. 3, 199-249 (1993)
6. B. Molly, Mol Biotechnol 6, 241-265 (1996)
7. L. Lerner, Basic Life Sci. 56, 255-271 (1990)
8. TA Koerner, RK Yu, JN Scarsdale, PC Demou, JH Prestegard Adv. Exp. Med. Biol. 228, 759-784 (1988)
9. U. Piantini, O. W. Sorenson, R. R. Ernst, J. Am. Chem. Soc. 104, 6800-6801 (1982)
10. M. Rance, O. W. Sorenson, G. Bodenhausen, G. Wagner, R. R. Ernst, K. Wuthrich Biochem. Biophys. Res. Commun. 117, 479-485 (1983)
11. A. E. Derome, M. P. Williams, J. Magn. Reson. 88, 177-185 (1990)
12. L. Braunschweiler, R. R. Ernst, J. Magn. Reson. 53, 521-528(1983)
13. A. Bax, D. G. Davis, J. Magn. Reson. 65, 355-360 (1985)
14. L. Muller, J. Am. Chem. Soc. 101, 4481-4484 (1979)
15. A. Bax, R. H. Griffey, B. L. Hawkins, J. Magn. Reson. 55, 301-315 (1983)
16. A. Bax, M. F. Summers, J. Am. Chem. Soc. 108, 2093-2094 (1986)
17. J. Reuben and H.T. Conner, Hercules DDR 28-096-1, December 21, 1982

Chapter 26

On-Line HPLC-NMR of Polymers

Wolf Hiller¹ and Harald Pasch²

¹Varian Deutschland GmbH, Alsfelder Strasse 3, 64289 Darmstadt,
Germany

²Deutsches Kunststoff-Institut, Schlossgartenstrasse 6, 64289 Darmstadt,
Germany

We have used on-line HPLC-NMR to analyze complex polymer systems. This combined technique takes advantage of the separation power of HPLC and the structure elucidation ability of NMR. It is also relatively easy to do and provide very valuable information. The utility of the HPLC-NMR has been shown for three polymeric systems: a) determination of chemical structure and degree of polymerization of technical-grade poly(ethylene oxide); b) analysis of end-group structure, degree of polymerization, and tacticity of oligostyrene; c) determination of chemical composition and chemical heterogeneity at high conversions of random poly(styrene-co-ethyl acrylate).

On-line HPLC-NMR offers unique opportunities for analyzing complex polymer systems. Using a selective chromatographic technique, the sample can be separated according to the chemical structure. The structural analysis of the polymer can then be conducted by on-line ¹H-NMR. Because of sensitivity enhancements and improved solvent suppression techniques of the NMR, it is possible to work under experimental conditions which are common in liquid chromatography of polymers, i.e. sufficiently high flow rate, moderate sample concentration, protonated solvents, and on-flow detection.

Experimental

Samples. The following polymer systems were investigated:

1. Technical-grade poly(ethylene oxide) from BASF, Ludwigshafen, Germany;
2. Oligostyrene used as GPC standards prepared by anionic polymerization and provided by Polymer Standards Service, Mainz, Germany;
3. Poly(styrene-co-ethyl acrylate) samples prepared by bulk polymerization. Styrene was provided by Fluka and ethyl acrylate by BASF.

HPLC. The experiments were carried out on a Varian HPLC system consisting of a Varian 9012 pump, a Varian 9050 UV detector and a Valco injection valve.

NMR. The NMR measurements were done on a Varian 500 MHz UNITY *INOVA* spectrometer. The probe used for the flow experiments was a 60 μ l flow probe with PFG.

Results and Discussion

The power of the HPLC-NMR has been shown for three polymeric systems:

1) The analysis of technical-grade poly(ethylene oxide) was performed via LC-NMR with respect to chemical structure and degree of polymerization. The separation was observed according to the functional end groups (1). Through the use of an octadecyl-modified silica gel as the stationary phase and an eluent composition of 50:50 (by volume) acetonitrile-deuterium oxide, the mixture was separated into fractions. The first elution peak appeared between 1.2 and 1.7min. Further elution peaks were obtained at retention times of 5.14 and 7.80 min. The main component which eluted between 14 and 25 min showed even a partial oligomer separation. Since most of the fractions showed strong UV absorptions at 280 nm, perhaps some aromatic moieties were present. The chemical structure, however, could not be derived from UV. Therefore, the NMR spectrometer was coupled on-line to the HPLC to help in the structural identification of the fractions. The data from the NMR on-flow run were processed as a contour plot, similar to the first Fourier transformation of a two-dimensional plot. All four fractions show well-separated NMR spectra. These spectra could be used for the assignments of the polymer structures. The first fraction was identified as poly(ethylene glycol). The other fractions were found to be alkyloxy-terminated PEO, tert-butylphenoxy-PEO and isooctylphenoxy-PEO, respectively. For the two latter materials the degree of polymerization could be determined as well.

2) Oligostyrene can be effectively analyzed with respect to chemical structure and tacticity. Information on the end-group structure, the degree of

polymerization and the tacticity were obtained (2). An isocratic elution with 100% acetonitrile on a reversed phase column RP-18 was used for the separation into tactic isomers. A flow rate gradient was applied (starting with 1ml/min, then linearly from 8 to 20min to 2ml/min, and staying at 2ml/min for further 5min). In this case, separation into oligomers of different chain lengths was obtained. The first peak belonged to the dimer (degree of polymerization $n=2$), the second to the trimer ($n=3$), and so on, up to $n=7$. The peak of the dimer appeared uniform, whereas the peaks for the higher oligomers were split. These splittings were due to the presence of different tactic isomers. For structural determination, coupled HPLC-NMR was employed. These experiments were carried out with normal protonated acetonitrile without deuterium lock. With the aid of on-flow NMR and WET solvent suppression, the chemical structures of the oligomers, their chain lengths, and microstructure could be determined. Figure 1 shows the NMR on-flow results processed as a contour plot (retention time vs. chemical shift). It demonstrates the separation of the different chain lengths of the oligostyrene (from dimer up to heptamer).

The detailed structures of the different cross sections can be analyzed by scanning through the traces of the contour plot. Figure 2 shows these traces. It is evident that the separation not only shows the different chain lengths but also the microstructure.

The dimer spectrum (bottom spectrum of Figure 2) belongs to not just one structure but two isomeric structures. The trimer shows two different patterns (basically four isomers). Finally, the tetramer shows four different spectral patterns representing eight isomeric structures. The assignments of the end group $\text{CH}_3\text{-CH}_2\text{-CH}(\text{CH}_3)\text{-}$ and the isomeric structures can also be confirmed by off-line 2D-NMR of individual components.

3) Random styrene-ethyl acrylate copolymers can be effectively analyzed regarding chemical composition distribution by using LC-NMR. In this case the information on the chemical composition and the chemical heterogeneity of copolymers with high conversion has been obtained (3). A series of copolymers of different comonomer concentrations and conversions were prepared. The styrene content varied from 10 to 90 mol-%. The mobile phase composition consisted of HPLC grade tetrahydrofuran (THF) and acetonitrile (ACN). The mobile phase composition was changed linearly from a THF/ACN ratio of 10:90 to 100:0 in 25min. In this case on-flow NMR experiments were carried out to determine the chemical composition at different retention times continuously. These results were compared with the chemical composition calibration curve obtained from narrow-disperse copolymer standards. A perfect agreement of the two methods was found (Figure 3).

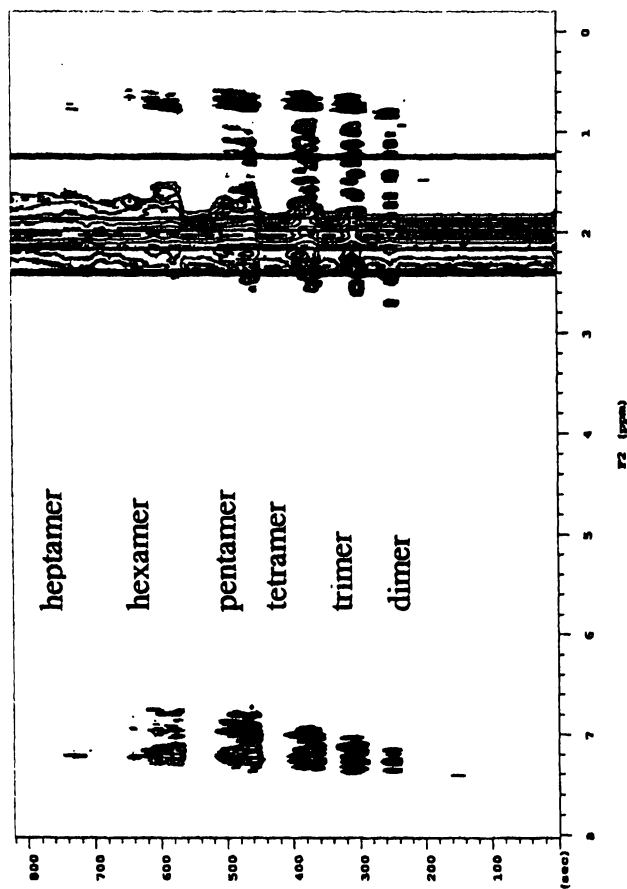


Figure 1. NMR on-flow run of oligostyrene in 100% protonated acetonitrile (with no deuterium lock). Retention time vs. ^1H chemical shift. The separation into different chain lengths is apparent. (Reprinted from *Polymer*, Vol.39, H.Pasch, W.Hiller, R.Haner "Investigation of the tacticity of oligostyrenes by on-line hplc/ ^1H nmr", 1515-1523, 1998, with permission from Elsevier Science)

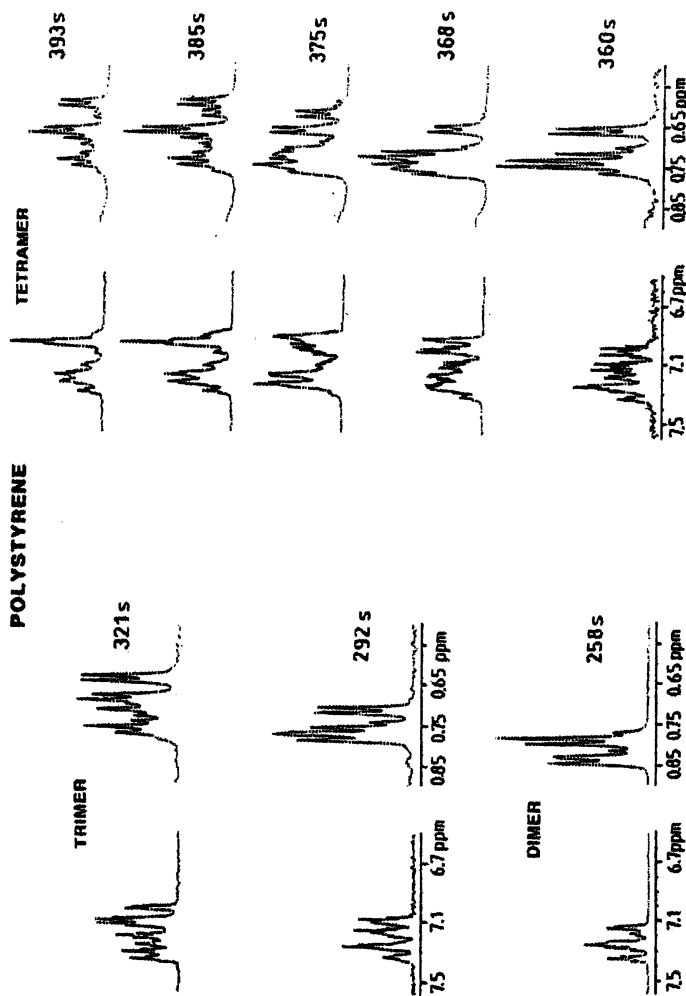


Figure 2. NMR spectra taken from the cross-sections of Figure 1 at different retention times. The aliphatic and the aromatic regions are shown for the dimer, trimer and tetramer, respectively. (Reprinted from *Polymer*, Vol.39, H.Pasch, W.Hiller, R.Haner "Investigation of the tacticity of oligostyrenes by on-line hplc/¹H nmr", 1515-1523, 1998, with permission from Elsevier Science)

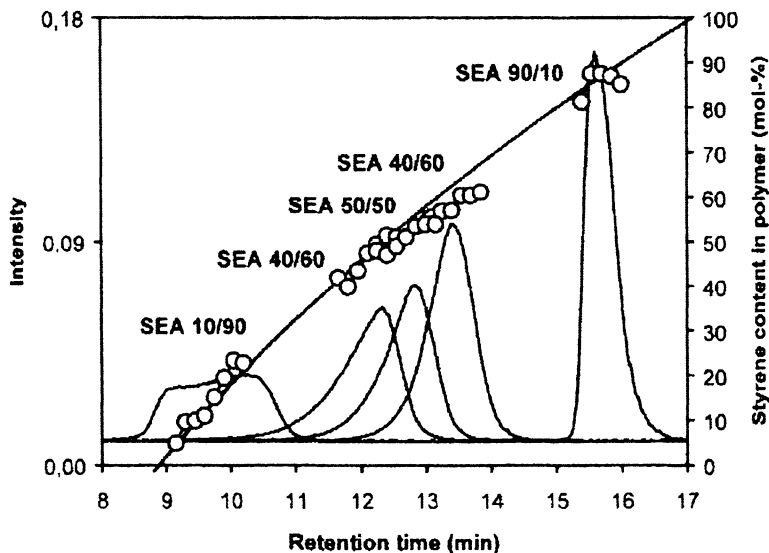


Figure 3. HPLC-chromatogram of styrene-ethyl acrylate copolymers at different compositions and high conversion. Also shown is the styrene content obtained by HPLC calibration(-) and on-line HPLC- ^1H NMR experiments (o). (Reprinted from *Macromol. Chem. Phys.*, Vol.201, I.Krämer, W.Hiller, H. "On-line coupling of gradient-HPLC and ^1H NMR for the analysis of random poly[(styrene)-co-(ethyl acrylate)]s", 1662-1666, 2001, with permission from Wiley-VCH)

Conclusion

HPLC-NMR is a powerful tool for the analysis of complex polymer systems. Using this coupled technique, an analyst can determine the end-group structure, chain length, as well as the composition and the microstructure of the polymers. It has been shown that on-flow experiments, in particular, can be used for the structural analysis of the polymer systems. The analysis can be done with conventional HPLC-grade solvents. Quantitation of the NMR data has been facilitated through the use of multiple solvent suppression experiments (the WET pulse sequence).

References

- (1) Pasch, H.; Hiller, W. *Macromolecules* **1996**, *29*, 6556.
- (2) Pasch, H.; Hiller, W.; Haner, R. *Polymer* **1998**, *39*, 1515
- (3) Krämer, I.; Hiller, W.; Pasch, H. *Makromol. Chem. Phys.* **2000**, *201*, 1662

Chapter 27

Complex Polymer Mixture Analysis by On-Line LC(GPC)-NMR

Jian Wu¹ and Kebede Beshah¹

¹Analytical and Computational Technology Center, Rohm and Haas Company, Route 413 and Old Route 13, P.O. Box 219, Bristol, PA 19007

²Rohm and Haas Company, 727 Norristown Road, Spring House, PA 19477

We have recently explored the application of on-line LC-NMR and GPC-NMR methods to quantitatively determine polymer compositions in a mixture or as a function of molecular weight distribution. Such a powerful tool has not been fully exploited for polymer characterization due to strong solvent (eluent) signals in NMR. In this study, we have successfully applied the bipolar gradient pulses stimulated echo sequence (BPPSTE) to suppress solvent and small molecule impurity signals, based on the different diffusion property between polymers and small eluent molecules. The lower the molecular weight of the species, the higher the diffusion coefficient, hence the faster the signal decays with BPPSTE NMR. Using a reverse-phase C-18 column and acetonitrile/THF solvent gradient, we have examined poly(methyl methacrylate) (pMMA), polystyrene, poly(butyl acrylate) (pBA) and polybutadiene polymer mixtures and have completely determined the structure and blockiness (monomer sequences) of various copolymers in the mixture. With on-line GPC-NMR, we were able to determine the complete composition and blockiness of pMMA, pBA and polystyrene mixtures at various molecular weights. The GPC-NMR method proved to be an excellent approach to examine the chemical composition and microstructure of polymers as a function of the distribution of molecular weight.

Introduction

LC-NMR, the coupling of HPLC separation with NMR detection, is rapidly becoming a powerful tool for the separation and structural characterization of complex mixtures (1). The major hurdle to realizing the tremendous potential of this technique has been the overwhelming signals from the solvents (eluent). A number of solvent suppression methods in LC-NMR have been proposed in the past few years, for example, the WET method developed by Smallcombe et. al. (2) is an excellent method for aqueous acetonitrile (ACN) mobile phase. Pasch and Hiller have applied the WET solvent suppression method in LC-NMR to analyze poly(ethylene oxide) and the tacticity of oligostyrenes (3,4). In polymer separation, tetrahydrofuran (THF) and acetonitrile are commonly used in reverse-phase HPLC. Unfortunately, THF is not very stable and tends to generate peroxide impurities and a variety of oligomers. In order to stabilize THF, a small quantity of inhibitor, such as 2,6-di-*tert*-butyl-4-methylphenol (BHT), is frequently added to the solvent. Due to the severe interference of the peroxide impurities and inhibitor signals in THF, the mobile phase of acetonitrile/THF in LC-NMR has been difficult to handle, and hence hinders the extensive application of LC-NMR in polymer mixtures. Even if the solvent suppression techniques such as WET can suppress the major solvent peaks, it is difficult to get rid of the many low intensity signals that arise from THF degradation, unreacted residual monomers and reaction byproducts.

The bipolar gradient pulses stimulated echo sequence (BPPSTE) was first proposed by Johnson's group (5) in 2D diffusion-ordered NMR spectroscopy (DOSY) to reduce the eddy-current effect and offset the inhomogeneous background gradients. In this study, we have successfully optimized and applied the one-dimensional BPPSTE sequence in LC-NMR to suppress THF, CH₃CN and impurity peaks, and selectively detect the 'clean' polymer signals. The experiment utilizes the pulse-field gradient (PFG) technique and relies on the orders of magnitude difference of diffusion constants between small solvent molecules and polymers. The BPPSTE suppression method was compared to the conventional WET sequence and showed much better results for solvent suppression in acetonitrile/THF mobile phase. The suppression method, based on the diffusion property of the solvent molecules, also permits us to use normal HPLC-grade organic solvents and eliminates the need for any expensive deuterated solvents. In addition, the BPPSTE technique is not affected by constantly moving ¹H chemical shifts of the eluents as a result of solvent gradient. Using a reverse-phase C-18 column and acetonitrile/THF solvent

gradient, we have examined poly(methyl methacrylate) (pMMA), polystyrene (pSty), poly(butyl acrylate) (pBA) and polybutadiene polymer mixtures and have completely determined the structure and blockiness (monomer sequences) of various copolymers in the mixtures. We further explored the BPPSTE method in Gel Permeation Chromatography-NMR (GPC-NMR) to examine the polymer compositions as a function of molecular weight distribution.

Experimental

Material

PMMA ($M_n=5.3k$, $M_w/M_n=1.06$), p(Styrene-*b*-MMA) (M_n of pSty=13k, M_n of pMMA=13k, $M_w/M_n=1.05$), p(MMA/BA) (random copolymer, $M_n=138k$, $M_w/M_n=1.5$), pBA ($M_n=193k$, $M_w/M_n=1.08$), p(Butadiene), p(BA-*b*-MMA) (M_n of pBA= 40k, M_n of pMMA=46k, $M_w/M_n=1.11$) were purchased from Polymer Source, Inc. The pStyrene ($M_n=630k$) was obtained from Polymer Laboratories, Inc. The THF (ultra low H₂O grade) and acetonitrile (spectroscopic grade) were purchased from JT Baker and EM Science, respectively.

Instrumentation

The on-line stop-flow ¹H NMR spectra were acquired on a Varian UNITY-INOVA 600 MHz NMR spectrometer with a 60 μl ¹H{¹³C, ¹⁵N} triple resonance flow probe. The polymer solution (~1.0 wt-%) in THF was filtered through a 0.2 μm filter and ~20-80 μl sample was injected into the HPLC/GPC system. In LC-NMR, the separation was carried out on a SUPLECOSIL reverse-phase C-18 column (25cm x 4.6mm), with a solvent gradient of acetonitrile/THF from 90/10 to 10/90 in 40 minutes, maintain at 10/90 ACN/THF for 5 minutes, bring back to 90/10 ACN/THF in 5 minutes and equilibrate at 90/10 ACN/THF for another 5 minutes before the next injection. For GPC-NMR, two Ultra Styragel linear columns (30cm x 7.8mm ID) in serial connection were employed with THF as the eluent in an isocratic run. A flow rate of 1 ml/min was used in both LC and GPC separations. A needle valve splitter was installed immediately after the column to split the mobile phase between UV (wavelength 220 nm) and Evaporative Light Scattering (ELS, Polymer Laboratories, Inc.) detectors. Typically, about 85-95 % of the eluent was carried to the UV detector and subsequently to the NMR flow probe. The remaining 5-15 % of the eluent was split into the ELS detector. The evaporator and nebulizer temperatures were set at 105 °C and 65 °C, respectively for the ELS detector.

The bipolar gradient pulse stimulated echo sequence (BPPSTE) (Figure 1) was employed to selectively suppress the THF and ACN solvent peaks, as well as the small molecule impurities. A diffusion time (Δ) of 24 ms and a gradient of 30 G/cm with 2 ms duration time (δ) were employed. The NMR spectrum for each polymer component was acquired with 256 scans, a spectral width of 8080 Hz, and a relaxation delay of 2 s. For the on-flow GPC-NMR, the WET sequence was employed to suppress THF solvent peaks, and each ^1H spectrum was acquired with an acquisition time of 0.45s, 32 scans and no relaxation delay. This condition was used for qualitative detection of the various components at a given elution time of the GPC separation.

Results and Discussions

BPPSTE Diffusion

The pulse sequence for the bipolar gradient pulses with stimulated echo is illustrated in Figure 1. After the first 90° RF pulse, the magnetization is rotated to the x-y plane, then a pair of gradient pulses is applied to dephase the signals. The second pair of gradient pulses is used to rephase the magnetization. The large molecules diffuse slowly and thus remain in approximately the same B_0 magnetic field throughout the diffusion period. In contrast, the small molecules, such as solvent, diffuse rapidly and thus are not refocused later, resulting in diminished net magnetization. In general, polymers possess a short transverse relaxation time, T_2 . For example, the T_2 values of 175, 74 and 55 ms were determined (CPMG T_2 experiment) for MMA methoxy, MMA heterotactic α -methyl and styrene aromatic protons, respectively in a p(Styrene-*b*-MMA) ($M_n = 84$ k) di-block copolymer solution. To minimize the loss of magnetization of polymer signals due to the short T_2 relaxation, the diffusion time (Δ) was optimized to 20-25 ms in the BPPSTE sequence (Figure 1). A relatively high gradient strength (25-35 G/cm) was used to suppress the signals of small molecules. With the optimized parameters, the polymer and oligomer compositions obtained from the BPPSTE sequence were comparable to the conventional one pulse ^1H experiment in a variety of acrylic and styrene copolymers we have examined. For example, in the ^1H NMR spectra of the polymer mixture of pMMA, pBA and p(BA-*b*-MMA) in THF (Figure 2), without solvent suppression (Figure 2A), the methoxy proton of MMA was buried under the huge $-\text{OCH}_2-$ signal of THF and was hard to identify. After the BPPSTE gradient suppression (Figure 2B), the excellent signal-to-noise ratio for

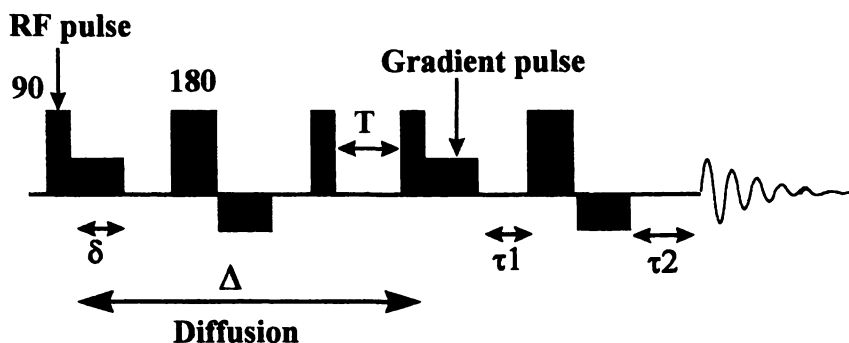


Figure 1. Bipolar stimulated echo pulse sequence (BPPSTE). The gradient time δ , T , τ_1 and τ_2 delays were set to 2 ms, 20 ms, 68 μ s and 78 μ s, respectively. (Reproduced with permission from *Polym. Prepr.* 2001, 42.1, 23–24.

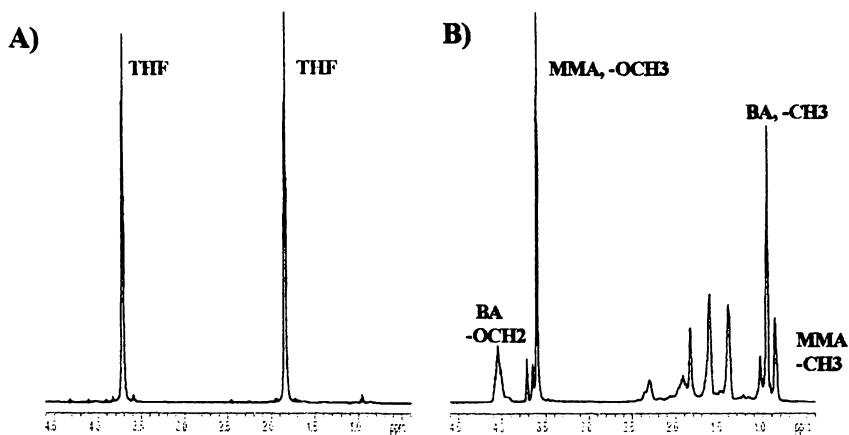


Figure 2. The proton NMR spectra of the mixture of pMMA, pBA, and p(BA-*b*-MMA) diblock copolymer in THF, before (A) and after (B) the BPPSTE solvent suppression, showing the excellent suppression of THF solvent peaks.

the polymer was achieved, which allow us to quantitatively determine the polymer composition. We also compared the WET method with BPPSTE sequence for the suppression of THF and CH₃CN, with the latter showing much superior results, especially in the suppression of numerous peroxide impurity signals.

LC-NMR

A mixture of pMMA, p(Sty-b-MMA) and pSty was chosen to test the BPPSTE solvent suppression. As illustrated in Figure 3, the three polymers were separated very nicely on the reverse-phase HPLC (C-18 column), with retention times of 3.34, 19.38 and 25.48 min. for pMMA, p(Sty-b-MMA) and pSty, respectively. The separation is based on the hydrophobic interaction of the polymers with the C-18 stationary phase. The more hydrophobic the polymer, the stronger the interaction between the polymer and the stationary phase, and the longer the elution time.

Using the BPPSTE diffusion sequence, the stop-flow ¹H LC-NMR for each polymer component was acquired and is shown in Figure 4. An excellent suppression of solvent and impurity signals was achieved. In the ¹H spectrum of p(Sty-b-MMA), the aromatic protons of styrene and the α-CH₃ protons of MMA were integrated to calculate the molar percentage of each monomer component. The blockiness of the random p(MMA/Styrene) was determined by examining the methoxy (-OCH₃) protons of MMA in the samples. For the MMA/Sty random copolymer (data not shown), the methoxy protons of MMA appear as several broad peaks, with the signal up-field at ~2.95 ppm representing the MMA component neighboring styrene and the signal at ~3.60 ppm corresponding to the MMA component next to MMA. In contrast, in the p(MMA-b-Styrene) block copolymer (Figure 4), the methoxy protons (-OCH₃) of MMA appear as a symmetrical single peak at ~3.60 ppm, similar to pMMA homopolymer. Alternatively, the α-CH₃ protons of MMA could be used to examine the stereochemistry of p(MMA/Sty). In the block copolymer, the alpha-methyl protons of MMA appear as two sharp peaks at 1.02, and 0.85 ppm, corresponding to *hetero-* (H) and *syndio-* (S) tactic components (The isotactic signal at 1.22 ppm was too small and partially overlapped with the polymer backbone signal and thus was not included). In contrast, for the random copolymer of p(MMA/Sty), multiple broadened peaks were observed for the α-CH₃ resonance of MMA apparently due to its interaction with the aromatic ring of styrene resulting from the comonomer sequence. It is interesting to note that there is a difference in ratios between heterotactic and syndiotactic MMA for pMMA homopolymer and p(Sty-b-MMA). This reflects the difference in polymerization mechanism of homopolymer (free-radical) that has a significant amount of the heterotactic component, while the block copolymer synthesized by anionic polymerization favors the syndiotactic stereochemistry.

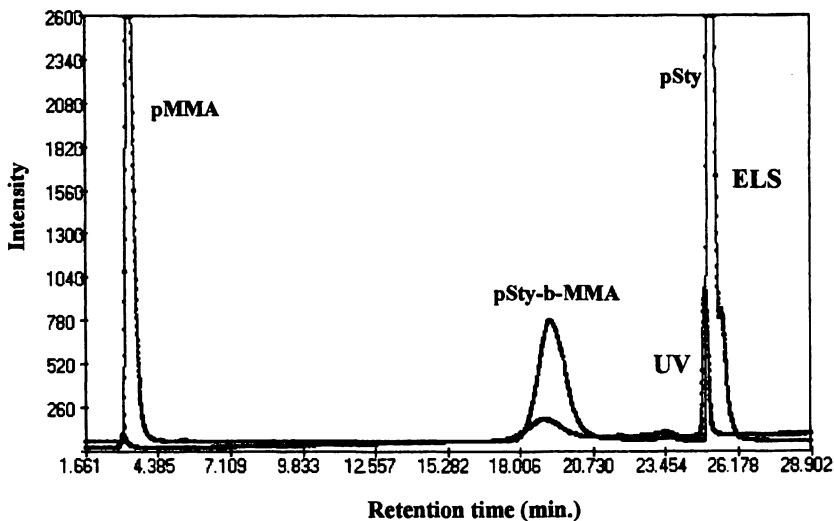


Figure 3. The reverse phase HPLC chromatograms of the pMMA, polystyrene, p(Sty-b-MMA) mixture with ELS and UV detection.

(Reproduced with permission from *Polym. Prepr.* 2001, 42.1, 23–24.

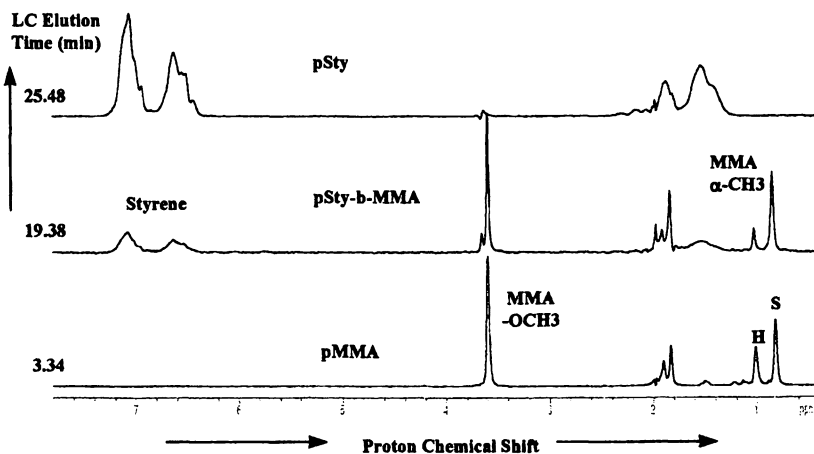


Figure 4. The stop-flow LC-NMR on the mixture of pMMA, polystyrene, and p(Sty-b-MMA), showing the proton signals for polystyrene and pMMA segments.

(Reproduced with permission from *Polym. Prepr.* 2001, 42.1, 23–24.

To extend the applications of LC-NMR, we have further examined the compositions and blockiness of various polymer mixtures, including pBA and polybutadiene, where 1,4-butadiene, 1,2-butadiene and BA were identified by their unique ^1H chemical shifts at approximately 5.35, 4.95 and 3.98 ppm, respectively. In reverse-phase HPLC with the same solvent gradient conditions as above, homopolymer pBA and polybutadiene eluted at 21.76 and 34.20 min., respectively. The random copolymers of p(MMA/BA) and p(MMA/Sty) both eluted between 8 and 18 minutes. Owing to their hydrophobicity, the higher the percentage of BA and styrene in the copolymer, the longer the retention time. Figure 5 illustrates the LC separation of pMMA, pBA, p(MMA/BA) and p(BA-b-MMA) by a reverse-phase column. A comparison of p(MMA/BA) random copolymer (retention time \sim 13.9 min.) to p(BA-b-MMA) block copolymer (retention time \sim 18.3 min.) with similar composition shows that the block copolymer interacted more with the C-18 stationary phase and eluted at a later time. This result demonstrated that the retention of p(MMA/BA) copolymer by reverse-phase LC is predominately influenced by the pBA portion of the copolymer. The block copolymer, which mimics the homopolymer pBA, is more hydrophobic and retained more on the C18 column than the random copolymer. The excellent LC separation permits us to quantitatively determine

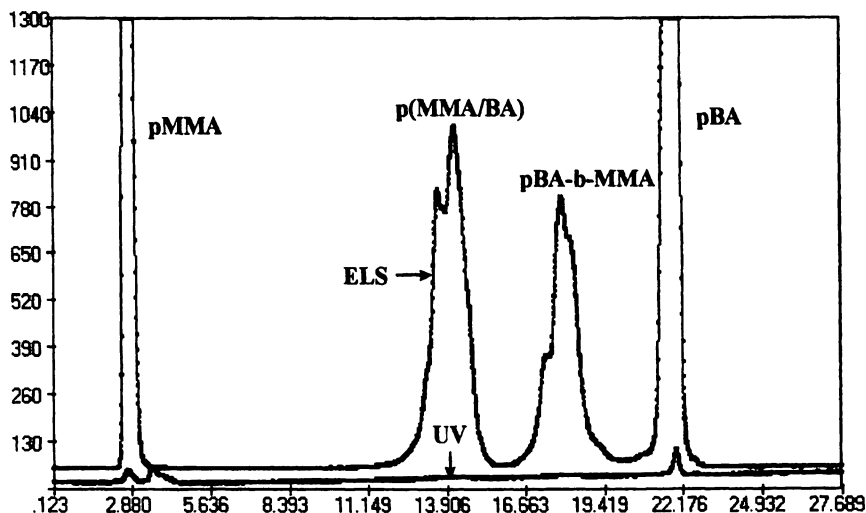


Figure 5. The reverse phase HPLC chromatograms of the mixture of pMMA, pBA, p(MMA/BA) and p(BA-b-MMA) with ELS and UV detections. The SUPELCOSIL Octadecyl column (25cm x 4.6mm ID) was used with acetonitrile/THF solvent gradient (flow rate: 1ml/min).

the composition of each copolymer in these complicated polymer mixtures using BPPSTE gradient method (Figure 6). For the p(MMA/BA) random copolymer, the α -methyl protons of MMA appear as multiple broad peaks. In contrast, the α -CH₃ signals for the p(BA-b-MMA) block copolymer show three distinct peaks at 1.22, 1.02, and 0.85 ppm, corresponding to *iso*-, *hetero*- and *syndio*- tactic MMA components, a unique feature of the atactic homopolymer p(MMA). This allow us to differentiate the random p(MMA/BA) from its block copolymer. A difference in the methoxy proton of MMA was also observed between random and block MMA/BA copolymer, where a sharp single and a broad peak were identified for block and random copolymer, respectively. But, the partial overlapping of the MMA -OCH₃ signals with the THF solvent peak hinders the clear differentiation here. It should be pointed out that LC-NMR generates a snap shot of the detailed polymer structure at any LC retention time and therefore could be extremely powerful for examining unresolved or overlapping LC peaks, as well as shoulder and minor component peaks in LC chromatograms.

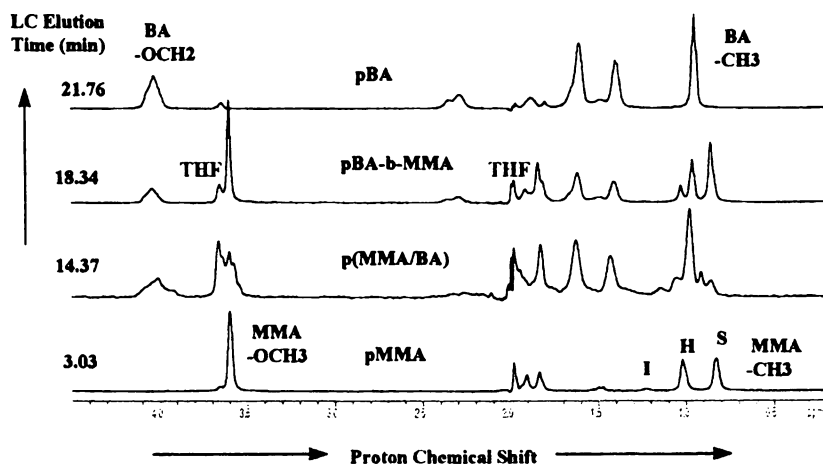


Figure 6. The stop-flow LC-NMR on the mixture of pMMA, pBA, p(MMA/BA) and p(BA-b-MMA), showing the proton spectra for the four separated polymer components.

GPC-NMR

The chemical composition and microstructure of copolymers as a function of molecular weight (MW) distribution is one of the most challenging aspects of polymer characterization. Depending on the polymerization process and reaction mechanism, the molar mass (GPC curve) may not have uniform chemical composition of the different monomer components. In addition, the mixing process can further complicate the MW distribution of the formulated polymer mixtures. The on-line GPC-NMR allows us to determine polymer composition at various molecular weights and thus help to understand the polymerization reaction process. Hatada and his coworkers have recently used GPC-NMR to directly determine the molecular weight distribution of isotactic pMMA (δ) using the relative NMR intensity for polymer repeating units and the t -C₄H₉ end group.

In our study, a mixture of pMMA (Mn = 5.3k), polystyrene (Mn = 629.5k) and p(Sty-b-MMA) (Mn = 25.7k) was loaded onto a GPC column (mobile phase: THF) and the polymers were well separated according to their molecular weights, with the highest MW polystyrene eluting first and the lowest MW pMMA eluting last (Figure 7). The stop-flow BPPSTE ¹H NMR spectrum was then collected for each polymer component and the composition of

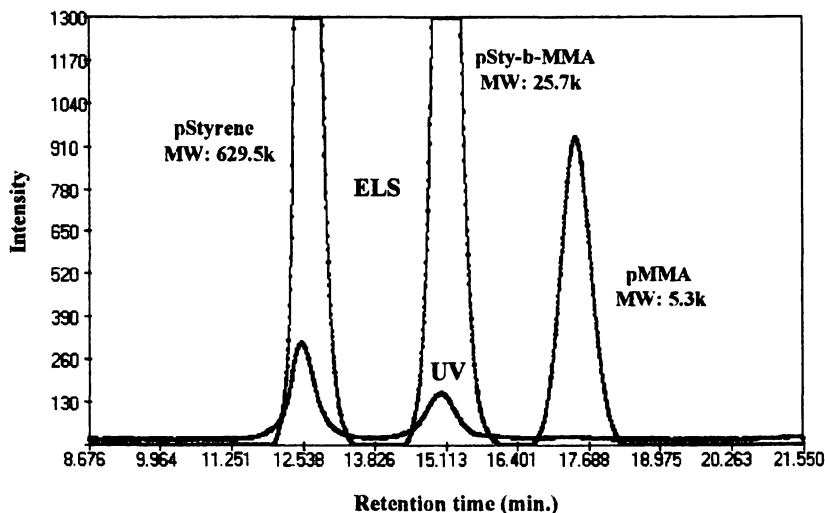


Figure 7. The GPC chromatograms of the pMMA, pStyrene and pSty-b-MMA mixture with ELS and UV detections. The Waters UltraStyragel Linear column (30cm x 7.8mm ID) was used with THF as eluent (flow rate: 1ml/min).

p(Sty-b-MMA) was calculated. To facilitate the analysis, we further examined on-flow GPC-NMR of the same mixture sample, with WET solvent suppression.

The α -methyl protons of pMMA and the aromatic protons of styrene as a function of GPC retention time (MW distribution) are displayed in Figure 8. Clearly, both the styrene and MMA signals were detected in the second GPC peak of p(Sty-b-MMA) (retention time: 15.2 min.), and polystyrene and pMMA were identified in the first and third elution peaks, respectively. Noticeably, a difference in the heterotactic and syndiotactic ratio of MMA was reflected in the 2D NMR cross peak intensities for GPC elution peaks of pMMA and p(Sty-b-MMA).

Conclusions

As illustrated in the examples above, LC-NMR and GPC-NMR are indispensable tools to characterize polymer mixtures and/or study the composition, blockiness and tacticity of (co)polymers as a function of molecular weight distribution.

The PFG NMR solvent suppression approach as discussed in this work removes all solvent peaks, impurities from the solvents, residual monomers, and small molecules reaction byproducts. As a result, the PFG NMR method permits the acquisition of a 'clean' spectrum of polymers by LC-NMR and GPC-NMR. One can detect a signal such as the methoxy signal of pMMA (3.6 ppm) in THF which also resonates at about the same frequency. This is not possible with other well established techniques such as WET since the suppression is applied at selected solvent frequencies and all signals, solvent and polymer, in the vicinity of those frequencies will be eliminated.

One short coming of the PFG NMR method is that there could be a small loss in signal to noise of the polymer signal if one desires to completely remove the solvent peaks. Polymers with short T_2 could suffer the most and care should be taken to understand the T_2 of the different polymer components before drawing quantitative information from the data. Most random copolymers are not affected as much from this T_2 effect since the components have similar T_2 while block copolymers tend to exhibit properties of the respective homopolymers and suffer from variable loss in intensity due to possible variations in T_2 . Hence, more caution is required in optimization of the PFG NMR method for quantitative analysis of LC-NMR or GPC-NMR of block copolymers. This may involve increasing PFG pulses ($\delta > 35$ G/cm) together with shortening diffusion times ($\Delta < 20$ ms).

In situations where there is no interference from the solvent, impurity and byproduct signals on the polymer signals of interest, the WET approach gives better signal to noise than the PFG NMR approach. This may dictate a choice of

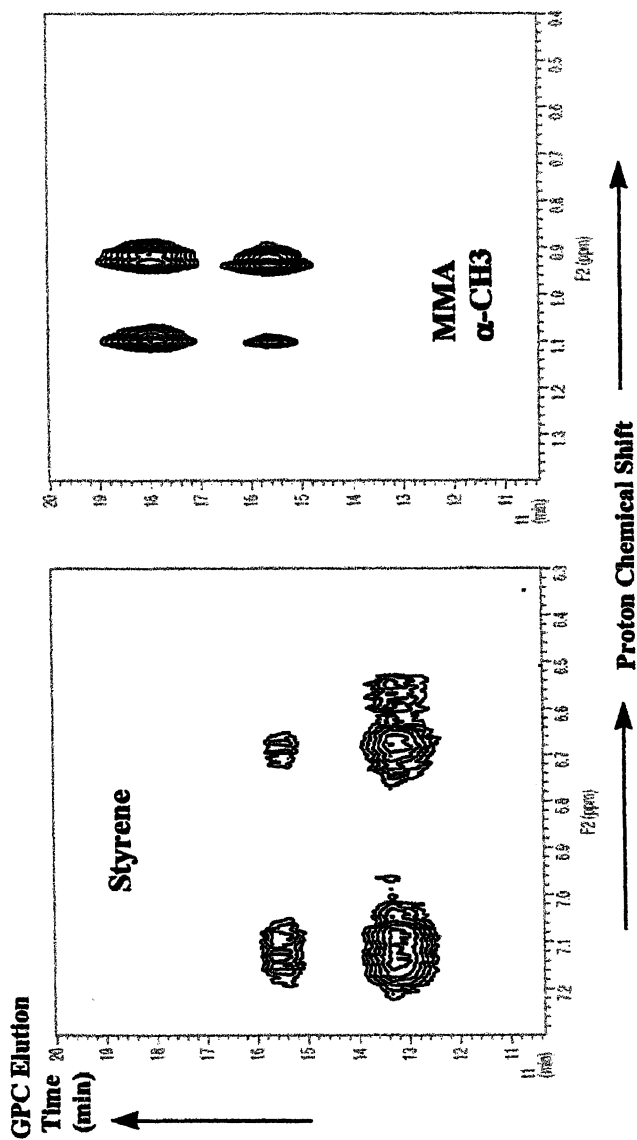


Figure 8. The on-flow GPC-NMR on the mixture of *pMMA*, *pStyrene*, and *pSty-b-MMA*, showing the α -methyl protons of *pMMA* and the aromatic protons of *styrene* as a function of GPC retention time.

(Reproduced with permission from *Polym. Prepr.* 2001, 42.1, 23–24.

solvent (eluent) relevant for the NMR experiment that may not be optimal for the separation of the various components; such as not using THF in polymers that contain MMA. Thus, we believe the PFG NMR solvent suppression method for LC-NMR and GPC-NMR as demonstrated in this work is a broadly applicable and robust technique and one need only optimize the solvent condition for the best separation condition which in turn will determine the quality of the NMR data. The advantage of the PFG NMR method becomes more critical in cases where separations are made at critical adsorption points (LC CAP) (7,8) where the choice of solvents and relative ratios are strictly defined by the adsorption/exclusion property of the polymer(s) and the eluent solvents.

Acknowledgments

The authors thank Dr. Igor Goljer of Varian, Inc. for his excellent technical support and helpful discussion on LC-NMR. We are grateful to Drs. Dan Dohmeier and Haojie Yuan of Rohm and Haas Co. for their assistance on polymer separation. We thank Drs. David Streelman and Larry Mink, Rohm and Haas Co. for their support and helpful discussions.

References

1. Albert, K. *J. Chromatogr. A* **1995**, *703*, 123-147.
2. Smallcombe, S.; Patt, S.; Keifer, P. *J. Magn. Reson. A* **1995**, *117*, 295-303.
3. Pasch, H.; Hiller, W. *Macromolecules* **1996**, *29*, 6556-6559.
4. Pasch, H.; Hiller, W.; Haner, R. *Polymer* **1998**, *39*, 1515-1523.
5. Wu, D.; Chen, A.; Johnson, C. *J. Magn. Reson. A* **1995**, *115*, 260-264.
6. Ute, K.; Niimi, R.; Hongo, S.; Hatada, K. *Polymer. J.* **1998**, *30*, 439-443.
7. Belenkii, B. G.; Valchikhina, M. D.; Vakhtina, I. A.; Gankina, E.; Tarakanov, O. G. *J. Chromatogr.* **1976**, *129*, 115
8. Skvortsov, A. M.; Gorbunov A. A.; Berek D.; Trathnig B. , *Polymer*, **1998**, *39*, 423

Chapter 28

Copolymer Characterization by SEC-NMR and SEC-MALDI

Maurizio S. Montaudo

Istituto per la Chimica e la Tecnologia dei Materiali Polimerici, Consiglio Nazionale delle Ricerche. Viale A. Doria, 6-95125 Catania, Italy

Off-line SEC-NMR and SEC-MALDI measurements are performed on a series of random copolymers of methyl methacrylate, butyl acrylate, styrene and maleic anhydride. First, a method is used, consisting of fractionating the copolymer by SEC and recording both the NMR and MALDI spectra of the fractions. In a successive step, the bivariate distribution of chain sizes and composition maps are derived from a knowledge of the molar mass, weight and composition of the copolymer fractions. The compositional distribution is obtained by summation of the sections of the bivariate distribution which belong to a narrow compositional range. Secondly, a model for SEC fractionation of copolymers is developed. It permits the prediction of the composition and dispersity of each SEC fraction. Thirdly, offline SEC-MALDI measurements are performed, in order to measure dispersity experimentally for the random copolymer. The agreement between theoretical and experimental values for dispersity and for the composition of the SEC fraction (as derived from SEC-NMR measurements) is good. The predictions of the model also compare favorably with literature SEC fractionation data of a copolyester of butylene adipate and butylene sebacate.

Size Exclusion Chromatography (SEC) is widely used technique polymer characterization. The standard configuration of a SEC apparatus consists of three parts (1-5), viz., a solvent-delivery system (equipped with an injection port), the columns, and a differential refractive index (RI) detector. This basic configuration can be modified by adding an additional detector, either in series or in parallel to the RI detector (1-5). The second detector can be a viscometer (2), a concentration detector (3), an UV detector (4) or a Light Scattering (LS) device (5).

NMR can be used as a detector for SEC of polymers. SEC and NMR can be connected on-line, using a commercial probe which was initially developed for other purposes (6,7) and this technique (8-10) has been applied to copolymers (11-14). The on-line SEC-NMR technique has one disadvantage. The NMR probe for on-line coupling is quite sophisticated and increases the cost of the set-up. Moreover, experiments on copolymers are usually performed on high-field magnets (mostly 600 MHz or more, as far as I know) and the cost of the SEC set-up increases substantially (at least by tenfold) with respect other SEC assemblies. The reason for using high fields is that the signal-to-noise ratio (S/N) of the NMR spectrum is related to the strength of the magnetic field (B) by a nonlinear relationship ($S/N \propto B^{1.5}$). Thus, when an NMR with a low-field magnet is used, the signal-to-noise ratio of the NMR spectrum may be poor.

Off-line SEC-NMR (which consists of collecting the SEC fractions, evaporating the solvent and then adding a deuterated solvent) does not suffer the above drawbacks. The signal-to-noise ratio is good when medium-field magnets (200 MHz up to 500 MHz) are employed; thus, the cost of such experimental set-up is attractive, i.e., on the same order of magnitude of double-detector SEC assemblies.

Although NMR can determine the composition of a copolymer fraction (independent of its molar mass), it provides reliable molar mass (MM) estimates only up to 10,000-20,000 Daltons. One may try to estimate the molar mass from SEC retention times. Specifically, a mixture of five or more polymer samples, each possessing a narrow MM distribution and known mass (the so-called SEC primary standards), is prepared. The mixture is injected in the SEC apparatus and the resulting chromatogram is recorded. By measuring the elution volumes and plotting them against the logarithm of the mass, a calibration line is obtained. However, calibration standards with narrow distribution, known composition and known molar mass are often not available. For this reason, approximate calibration lines are often used. In the latter case, surprises may show up (especially for high conversion samples), since the calibration is logarithmic (i.e. $\log(\text{MM})$) and the law of propagation of errors in indirect measurement predicts that the M_n and M_w estimates performed with the use of an inaccurate calibration line are useless and even misleading.

In order to cope with the difficulty of the conversion from elution volume to molar mass, one can use a MALDI mass spectrometer and record the MALDI mass spectra of the SEC fractions of homopolymers and copolymers(14-23). The MALDI technique possesses extraordinary sensitivity and can measure molar mass up to 10^6 daltons. Moreover, a complete picture can be obtained by recording both the NMR and the MALDI spectrum of each SEC fraction (22-23).

Off-line SEC-NMR is certainly more labour-intensive and time-consuming than on-line SEC-NMR. Nevertheless, this difference can be minimized by reducing the number of fractions. Clearly, the reduction cannot go beyond a certain limit, otherwise it will cause a loss of accuracy in the measurement of copolymer properties. The hypothesis that it is possible to reduce the time for copolymer analysis without the cited loss of accuracy was put forward by Murphy et al. (24) in another context (2D-chromatography). It would be interesting to check whether the hypothesis is valid also in SEC-NMR and to develop a methodology which allows the determination of the optimal conditions, viz., those where the cited loss of accuracy is still negligible.

In this paper, off-line SEC-NMR measurements are performed (along with SEC-MALDI) on random copolymers of methyl methacrylate (MMA), butyl acrylate, styrene and maleic anhydride reacted at high conversions. In the first series of measurements, each copolymer is fractionated by SEC, the fractions are collected, and the NMR and the MALDI spectra are recorded. The results are employed to derive some copolymer properties, such as the composition distribution histogram, which provides the weight fraction of the polymer with a given composition. In the second series of measurements, the fractionation conditions are varied, and the sampling rate (which is proportional to the total number of fractions) is reduced by increasing the volume of the fraction. The goal of these experiments is to find the optimal conditions such as to maximize the fraction volume and to minimize the loss of accuracy.

In order to interpret the resulting data, a model is developed for copolymers obtained by SEC fractionation, taking into account the fractionation conditions and specifically the number of fractions. The model predicts the composition and the ratio $D(x)$ of the SEC fraction. $D(x)$ is the ratio between the number-average and the weight-average molar mass, and x is the fraction number. The predictions of the model are compared with SEC-NMR and SEC-MALDI data for the random copolymer of styrene and MMA reacted at high conversion.

In SEC of copolymers a very subtle "mass coelution" effect shows up (1,22,23). The calibration establishes a correspondence between mass and elution volume. In the case of homopolymers the calibration process is straightforward, since the cited correspondence is unequivocal. For compositionally homogeneous copolymer samples, the correspondence is still unequivocal because the polymer chains have similar compositions. In the case

of compositionally heterogeneous copolymers, the calibration process is more complex. The above correspondence is not unique, and chains at different masses are co-eluted in the same SEC fraction. The predictions are made based on the model for the "mass coelution" effect. Theoretical estimates are compared with literature data for SEC fractionation of a copolyester of butylene adipate and butylene sebacate.

Theory

In a typical experiment, a certain amount of copolymer sample is injected in the SEC apparatus. The sample is a copolymer in which two repeat units A and B are found along the chain. The macromolecular chains are of the type $A_m B_n$, the size of the chain being $s = m + n$, the mass of the chain being $(m\mu_A + n\mu_B)$ where μ_A and μ_B are the masses of A and B. The mass is approximately $(s\mu)$ where μ is the average mass of the repeat unit, namely $\mu = (\mu_A + \mu_B)/2$.

The chromatographic columns separate the copolymer chains, the detector records the trace, $f(V)$, where V is the elution volume, various fractions are collected, and the spectrum of each fraction is recorded. Fraction 1 contains the copolymer solution eluted between $(V_0 + V_1)$ and $(V_0 + 2V_1)$, fraction 2 contains the copolymer solution eluted between $(V_0 + 2V_1)$ and $(V_0 + 3V_1)$, fraction x contains the copolymer solution eluted between $V_{ini} = (V_0 + x V_1)$ and $V_{fin} = (V_0 + (x+1)V_1)$.

For chains of the type A_s , one has $V = [\log(s\mu) - a_0] / b_1$, whereas for chains of the type B_s , one has $V = [\log(s\mu) - b_0] / b_1$, where a_0, b_0, b_1 are calibration constants.

The quantity of interest is $c(x, q)$, the molar fraction of A units for chains of size q in SEC fraction x , which turns out to be:

$$c(x, q) = c(x, s - s_{mid}) \quad (\text{eq. 1})$$

where s_{mid} is the size of chains which possess middle dimensions and it is given by $s_{mid} = (s_{fin} - s_{ini})/2$. Here s_{fin} , s_{ini} denote the average sizes of chains eluted at volumes V_{fin} and V_{ini} , and where the molar fraction of A units for chains of size s in SEC fraction x . The quantity $c(x, s)$ is given by:

$$c(x, s) = \left(\int_m I(x) \delta_s dm \right) / \left(\int_s I(x) \delta_s dm \right) \quad (\text{eq. 2})$$

where the integration goes from $m=0$ to s , and δ_s indicates that the integration is extended to chains $A_m B_n$ for which $m + n = s$. (See the paper on copolymer and blends (25) by Ogawa.) The quantity $I(x)$ which appears both in the numerator and the denominator is the molar fraction of chains $A_m B_n$ in SEC fraction x .

When the coupling between size and sequence is weak, $I(x)$ splits in two parts, namely the size distribution and the composition distribution (see the quantitative description of polymers by Kuchanov (26) and calculations by Tobita (27) for random St-MMA copolymers). In our case, $I(x)$ is given by:

$$I(x) = g_1 \exp(y + J) Q \quad (\text{eq. 3})$$

where g_1 is a suitable normalization factor, J (the sequence distribution) is given by $J=[m/s-d]/h$, with $d=d_0+d_1s+d_2s^2$, where d_0, d_1, d_2 are parameters which describe the sample's compositional heterogeneity, where h is the width of the compositional distribution, $y = y_1 \log(s) - s/y_2$ where y_1 and y_2 are given by $y_1 = (2\bar{M}_n - \bar{M}_w) / (\bar{M}_w - \bar{M}_n)$, $y_2 = \mu / (\bar{M}_w - \bar{M}_n)$ and \bar{M}_n, \bar{M}_w are the number- and weight- average molar masses of the unfractionated copolymer, Q is a function which describes the fact that SEC fraction x contains chains $A_m B_n$ of a given size and it does not contain chains $A_m B_n$ of other sizes. Clearly, Q is always equal to zero, except in a small range of elution volumes between V_{ini} and V_{fin} . When the separation process is extremely efficient, one has:

$$Q = H(V - V_{ini}) H(V_{fin} - V) \quad (\text{eq. 4})$$

where the function H is equal to zero when its argument is negative and it is equal to 1 when its argument is positive.

The quantity $c(x, q)$ in eq. 1 can be expanded in a MacLaurin series around $z=0$, yielding

$$c(x, q) = c(x) + z \rho_1 \rho_2 \quad (\text{eq. 5})$$

where $\rho_1 = a_0 - b_0$, where ρ_2 is a parameter related to \bar{M}_n, \bar{M}_w , and to the chromatographic conditions, namely b_1, V_0, V_1 , and where $c(x)$ is the average molar fraction of A units in the fraction.

It is useful to introduce a quantity which measures the difference between the compositional properties of the unfractionated copolymer and those of the SEC fraction. This can be done as follows:

$$\phi = \log | c(x) - c_{AVE} | \quad (\text{eq. 6})$$

where c_{AVE} is the average molar fraction of A units in the unfractionated copolymer. It follows from eq. 1 that

$$\phi = \log(c_3) - \lambda \quad (\text{eq. 7})$$

where c_3 is a parameter (of the order of 0.01-0.03 mL) and $\lambda = \log(V_1)$.

Let's denote with $D(x)$ the ratio between the weight-average and the number-average molar mass in fraction x . Using the definitions, $D(x)$ becomes:

$$D(x) = \sum (\mu)^2 I(x) / \sum (\mu) I(x) \quad (\text{eq. 8})$$

When SEC fraction x is mixed together with SEC fraction y , the value of the molar fraction of A units in the resulting fraction $c(z)$, will depend on weight of copolymer in the two fractions, $w_{\text{copo}}(x)$ and $w_{\text{copo}}(y)$ and the value will be intermediate between $c(x)$ and $c(y)$, namely:

$$c(z) = k [v(x) c(x) + v(y) c(y)] \quad (\text{eq. 9})$$

where $v(x) = w_{\text{copo}}(x) (\mu_{\text{mid}})$, $v(y) = w_{\text{copo}}(y) (\mu_{\text{mid}})$ and $k = 1 / [v(x) + v(y)]$.

The Bivariate Distribution reports the weight, $W(s, c_A)$, of chains which possess a given size (s) and a given composition (c_A). It is related to $I(x)$ in a simple manner, viz.,

$$W(s, c_A) = g_2 s \mu I(x) \quad (\text{eq. 10})$$

where g_2 is a suitable normalization factor. The compositional distribution histogram reports, instead, the weight $W(c_A)$ of chains which possess given composition (c_A) and it is therefore obtained by summation over all chain sizes:

$$W(c_A) = \sum W(s, c_A) \quad (\text{eq. 11})$$

where the summation is over s and it goes from one to infinity.

Equations 1-11 were implemented in a computer program called COPOFRAC which is written in QuickBasic and runs on PC. COPOFRAC accepts as input the fractionation conditions, namely a_0, b_0, b_1, V_0, V_1 , the parameters which describe the heterogeneity of the copolymer sample, $\overline{M}_n, \overline{M}_w, d_0, d_1, d_2$ and it gives as output the mass spectrum and the $^1\text{H-NMR}$ spectrum of each fraction. COPOFRAC also gives as output the Bivariate Distribution (see eq. 10) and the compositional distribution histogram (see eq. 11). Furthermore, it allows us to predict what happens when two (or more) SEC fractions obtained from a random copolymer are mixed together (see eq. 9).

Experimental Section

Materials

Copolymer samples MB25 and MB41 were purchased from Rohm and Haas (Frankfurt, Germany). They are random copolymer samples of methyl methacrylate (MMA) and butyl acrylate (BA). Sample MB25 was polymerized in ethyl acetate using azobisdiethylisobutyrate as initiator. The monomers conversion amounts to about 4% and the average molar fraction of MMA in the copolymer is 0.25, as measured by NMR. Sample MB41 was polymerized in ethyl acetate using tert-butylperpivalate as initiator. The monomer conversion amounts to about 100% and the average molar fraction of MMA in the copolymer is 0.41, as measured by NMR.

Copolymer samples SH91 and SH78 were purchased from MP-DAJAC (Feasterville, PA). They are random copolymer samples of styrene (St) and maleic-anhydride (MAH) obtained at high conversion from solution polymerization using AIBN (N, N' -azobisisobutyronitrile) as the initiator. The average molar fraction of St in the copolymer is 0.78 for sample SH78 and 0.91 for sample SH91.

Copolymer sample M30 was purchased from Polyscience (Feasterville, PA). It is a random copolymer sample containing units of styrene (St) and of methyl methacrylate (MMA) obtained at high conversion. The average molar fraction of MMA in the copolymer is 0.30

SEC Fractionation

The analyses were performed on a Polymer Lab apparatus, equipped with five ultraStyragel Waters columns (in the order 1000, 500, 10000, 100, and 100000 Å pore size) attached in series, using a Polymer Lab differential refractometer. The solvent was THF or CHCl_3 , the flow rate was 1 mL/min, and 60 microliters of polymeric solution (15 mg/ml) were injected. Normally 50 fractions of 0.2 mL were collected. In the case of sample M30, four different fractionation experiments were performed, and 50 fractions of 0.2 mL, 25 fractions of 0.4 mL, 15 fractions of 0.8 mL, 15 fractions of 1 mL were collected. The chromatogram was calibrated using the result of the analysis of MÅLDI-TOF spectra of selected fractions (see Tables 1 and 2). The average molar masses (M_n and M_w) of the copolymer were measured using the Caliber software distributed by Polymer Lab. The type of calibration selected by us was a "narrow standards"; the calibration function was "polynomial of order 1" and the calculation method was "area based."

NMR Measurements

The ^1H -NMR spectra of the SEC fractions 34, 37, 40, 43, 45, 50 and 53 of sample M30 were recorded on a Bruker A-CF 200 spectrometer. All the other NMR analyses were performed on a Varian Unity Inova 500 spectrometer at room temperature using CDCl_3 as a solvent and tetramethylsilane as internal standard. The ^1H -NMR spectra were acquired with the following acquisition parameters: spectral width 4722.3 Hz, 131072 data points, 700 accumulations and an acquisition time of 3.47 sec.

DEPT subspectra of SH91 and SH78 were generated using a combination of the $\pi/4$ and $3\pi/4$ experiments: $\text{CH}_2 = (\pi/4) + 1.15 (3\pi/4)$. Experiments were performed using a recycle time of 2 sec and a J-modulation time of 3.7 millisecc. ^1H and ^{13}C $\pi/2$ pulse times were 22 and 15 microsec respectively.

NMR Calculations

The ^1H -NMR spectra for random MMA-BA copolymer MB41 yielded an estimate of the copolymer composition (28). The molar fraction of MMA in the copolymer, F_{MMA} is given by:

$$F_{\text{MMA}}(x) = 1/[1 + 1.5 A_{\text{MMA}}/A_{\text{BA}}] \quad (\text{eq. 12})$$

where A_{MMA} is the area of the region 4.16-3.92 ppm, corresponding to MMA units, and A_{BA} the area in the region 3.66-3.51 ppm, corresponding to butyl acrylate units. The variance of compositional distribution for MMA, σ^2 , was

computed from the frequencies, I_{MMM} , $I_{MMB+BMM}$, I_{BMB} , of the M-centered triads using the formula:

$$\sigma^2 = \{(3 I_{MMM} - k)^2 + (2 I_{MMB+BMM} - k)^2 + (I_{BMB} - k)^2\} / 3 \quad (\text{eq. 13})$$

where $k = F_{MMA} DP_n$, and DP_n is the number average degree of polymerization. The frequencies of the M-centered triads are related to the areas under the MMM, MMB+BMM, and BMB resonances (29) (the coisotacticity factor is 0.40).

The $^1\text{H-NMR}$ spectra for random St-MAH copolymers yielded an estimate of the copolymer composition (29), which was determined using the formula:

$$F_{st} = 0.2 I_{arom} (0.5 I_{alif} - 0.1 I_{arom})^{-1} \quad (\text{eq. 14})$$

where F_{st} is the molar fraction of styrene in the copolymer, I_{arom} is the area in the region 6-8 ppm, corresponding to styrene units, and I_{alif} is the area in the region 1-3 ppm. The overall variance of compositional distribution for styrene, σ^2 , was computed from the areas under the SSS, SSM+MSS, and MSM resonances in the DEPT subspectra, I_{SSS} , $I_{SSM+MSS}$, I_{MSM} , using the formula:

$$\sigma^2 = \{(3 I_{SSS} - k)^2 + (2 I_{SSM+MSS} - k)^2 + (I_{MSM} - k)^2\} / 3 \quad (\text{eq. 15})$$

where $k = F_{st} DP_n$, DP_n is the number average degree of polymerization and F_{st} is the molar fraction of styrene in the copolymer.

The weight of copolymer in each fraction, w_{copo} , was determined using the formula:

$$w_{copo} = (w_{TMS} / I_{TMS}) \tau_1 I_{copo} / M_{fra} \quad (\text{eq. 16})$$

where M_{fra} is the number-average molar mass of the fraction, I_{copo} is $I_{alif} + I_{arom}$, I_{TMS} is the area under the peak at 0 ppm, corresponding to tetramethylsilane (TMS), w_{TMS} is the weight of TMS in the NMR tube (0.136 mg) and where τ_1 is a dimensionless constant equal to 1466.2, which arises from the fact that St and MAH repeat unit possess 8 and 2 proton respectively, whereas TMS possesses 16 protons.

The assignments for the resonances in the $^1\text{H-NMR}$ spectra for random St-MMA copolymers have been reported (30). The molar fraction of MMA in the copolymer, F_{MMA} and the weight of copolymer in each fraction, w_{copo} , was determined using the formulas:

$$F_{MMA}(x) = 1/[1 + (3/5) A_{arom}/A_{mo}] \quad (\text{eq. 17})$$

$$w_{copo}(x) = (w_{TMS} / A_{TMS}) \tau_2 (A_{arom} + A_{mo}) / (\mu_{smid}) \quad (\text{eq. 18})$$

where A_{arom} is the area in the region 6-8 ppm, corresponding to styrene units and A_{mo} is the area in the region 1-3 ppm due to methoxy protons of MMA units, A_{TMS} is the area under the peak at 0 ppm, corresponding to TMS, w_{TMS} is the weight of TMS in the NMR tube and τ_2 is a numerical factor which is equal to 916. The overall variance of compositional distribution for styrene, σ^2 , for this copolymer sample was computed from the areas under the styrene-centered triads.

Table 1 SEC/MALDI and SEC/NMR data for copolymer sample MB41

Fraction	Ve ^a	C _{MMA} ^b	\overline{M}_n^c	\overline{M}_w^c	D ^c	weight ^d
30	27.75		173000	175000	1.01	0.157
31	28.25		133000	135000	1.03	0.234
36	29.11	0.39	89000	90000	1.01	0.282
40	30.01		72000	73500	1.02	0.298
41	30.25	0.35	64000	67000	1.04	0.291
42	30.52		55000	57000	1.04	0.274
43	30.75		50000	51500	1.03	0.252
44	31.01		45000	47700	1.06	0.223
45	31.25		39000	41400	1.06	0.194
46	31.52	0.42	34000	35400	1.04	0.164
47	31.75		31000	32860	1.06	0.139
48	32.01		28000	29400	1.05	0.107
49	32.25		25000	26000	1.04	0.099
50	32.51		23000	23920	1.04	0.084
51	32.75	0.42	21000	21840	1.04	0.073
54	33.51		17000	17900	1.05	0.046
56	34.01	0.65	13500	13800	1.02	0.036
58	34.51		11000	11400	1.03	0.031
61	35.25	0.78	7200	7800	1.08	0.024
62	35.51		6700	7250	1.08	0.022
65	36.25		5000	5400	1.08	0.018

a SEC elution volume (mL)

b molar fraction of MMA in the copolymer fraction derived from NMR data using eq. 12

c \overline{M}_n , \overline{M}_w , D of the SEC fraction as determined by MALDI

d weight fraction, as derived from the SEC trace

Table 2 SEC/MALDI and SEC/NMR data for copolymer SH91

Fraction	Ve ^a	C _{St} ^b	\overline{M}_n^c	\overline{M}_w^c	D ^c	weight ^c	Weight ^e
7	23.8	0.97				27	27
10	24.7	0.89				33	35
14	25.9	0.99				34	37
16	26.5		92000	97000	1.05	32	
18	27.1	0.78	71000	74000	1.04	29	31
20	27.7		54000	57000	1.05	26	
22	28.3	0.81	42000	45000	1.07	22	20
24	28.9		32000	34000	1.06	19	
25	29.2		28000	29000	1.04	18	
26	29.5	0.70	25000	26000	1.04	16	14
27	29.8		22000	23000	1.04	15	
28	30.1		19000	20000	1.05	13	
29	30.4	0.58	16700	17000	1.02	12	9
30	30.7		14700	15300	1.04	11	
31	31		12900	13500	1.05	10	
32	31.3	0.66	11300	11600	1.03	9	5
33	31.6		9900	10400	1.05	8	
34	31.9		8700	9200	1.06	7	
35	32.2	0.81	6600	7800	1.18	7	5
36	32.5		5700	6900	1.21	6	
37	32.8		5900	6200	1.05	6	

.a SEC elution volume (mL)

.b Molar fraction of St in the copolymer fraction, derived from NMR data using eq. 14

.c \overline{M}_n \overline{M}_w and D of the SEC fraction as determined by MALDI

.d Weight fraction, derived from the RI detector of the SEC apparatus without dn/dc correction

.e Weight fraction, derived from NMR data using eq. 16

MALDI-TOF Mass Spectra

A BRUKER REFLEX mass spectrometer was used to obtain the matrix assisted laser desorption/ionization (MALDI)-time of flight (TOF) mass spectra. The spectrometer is equipped with a nitrogen laser (337 nm., 5ns), a flash ADC (time base of 4ns) and a HIMAS detector. The laser irradiance was slightly above threshold (ca. 10^6 W/cm²). Ions below *m/z* 350 were removed with pulsed deflection and 100 transients were summed. The MALDI mass spectra of the SEC fractions were processed with the XMASS program from Bruker. The program uses mass spectral intensities to compute the quantities known as most-probable molar mass, number-average molar mass, weight-average molar mass, and polydispersity index (denoted as *M_p*, \overline{M}_n , \overline{M}_w and *D*, respectively) of each selected fraction.

A small amount (0.02 mL) of the chromatographic eluate in each fraction were added to 0.02 mL of a 0.7 M solution of 2-(4-hydroxyphenylazo)-benzoic acid (HABA) matrix. Probe tips were loaded with 1-2 microliters of the resulting solution and the solvent was slowly evaporated.

Results and Discussion

Copolymer sample MB41 is a high conversion (100%) random copolymer of methyl methacrylate (MMA) and butyl acrylate (BA) produced by radical initiation. The sample was injected into the SEC apparatus, and about 40 fractions were collected. Several SEC fractions were then subjected to off-line MALDI and NMR analysis, respectively.

The SEC fractions analyzed by MALDI-TOF yielded excellent spectra with narrow distributions up to high molar masses (170000 Daltons), and the mass spectra of these nearly monodisperse samples allowed the computation of reliable values of the molar masses corresponding to the fractions. The log(*M*) values of the fractions showed a linear correlation with the elution volume of each fraction and allowed the calibration of the SEC trace against *MM*, and the calibrated SEC trace could then be used to compute average molar mass and dispersion of the unfractionated copolymer ($\overline{M}_w = 91000$, $\overline{M}_n = 43000$, *D*=2.1).

The SEC fractions were also analyzed by 500MHz ¹H-NMR and the signal-to-noise ratio was acceptable for all spectra (it never fell below 13:1). Peaks in the region between 4.2- 3.5 ppm were considered and more specifically, the region 4.16-3.92 ppm, corresponding to MMA units, and the region 3.66-3.51 ppm, corresponding to butylacrylate units. The copolymer composition of each fraction was determined using eq 9.

Table 1 reports a summary of the MALDI and NMR results. From the data in Table 1, it can be seen that the composition varies, and the fractions taken in the SEC region close to the peak elution volumes possess compositional values close to the average ones (*F_{MMA}* = 0.41). At higher masses the composition

takes values up to 65% BA. At low masses, instead, the macromolecular chains are rich in MMA (about 78%, Table 1). Peaks belonging to the $^1\text{H-NMR}$ spectrum in the 3.66-3.51 ppm region turned out to be well resolved. For instance, Figure 1 reports a section (with the cited region) of the 500MHz $^1\text{H-NMR}$ spectrum for fractions 46 and 51, along with the spectrum of the unfractionated sample. Peaks in the cited region can be assigned to the M-centered triads and, from the inspection of the figure, it can be seen that the intensities of the peaks are different. This implies that the relative frequencies of M-centered triads in fraction 46 are different from the corresponding frequencies in fraction 51 and in the unfractionated copolymer.

Inserting peak intensities in eq 11, the variance of the compositional distribution (σ^2) was derived. The variance for fractions 46 and 51 turned out to be slightly lower than the variance for the unfractionated copolymer, but the order of magnitude is the same. This result does not come unexpected, since MALDI-TOF data on a series of high-conversion MMA-BA random copolymers indicate that σ^2 for SEC fractions is virtually identical to σ^2 for the unfractionated copolymer (22).

The computer program COPOFRAC was used to generate the compositional distribution histogram for sample MB41 and the result is shown in Figure 2. It can be seen that the weight is large in the region 0.2-0.5, and that the tallest value is for $F_{\text{MMA}} = 0.38$, which falls very close to the average ($F_{\text{MMA}} = 0.41$).

Copolymer samples SH91 and SH78 are random copolymer samples of styrene (St) and maleic-anhydride (MAH) obtained at high conversion from solution polymerization using AIBN as the initiator. The ^{13}C spectra of samples SH91 and SH78 (omitted for brevity) do not yield sequence information because the signals due to methine and methylene carbons are partially overlapped. However, sequence information can be obtained from DEPT experiments, by recording the spectra at $\pi/4$ and at $3\pi/4$ and then combining them together. The areas under the SSS, SSM+MSS, and MSM resonances are 0.32, 0.50 and 0.18 respectively. In a similar manner, the areas under the SSS, SSM+MSS, and MSM resonances for sample SH91 were 0.39, 0.47 and 0.13 respectively. Inserting the three values for the SSS, SSM+MSS, and MSM resonances in eq. 15, the overall variance of compositional distribution was found to be $\sigma^2=0.0844$ for sample S78 and $\sigma^2=0.0676$ for sample SH91. The theoretical variances for SH78 and SH91 are $\sigma^2=0.015$ and $\sigma^2=0.0097$ respectively, which are lower than the former ones. A knowledge of the average composition and of the variance around the average may give some hints on the abundance of chains which possess a composition that differs from the average, although this is not sufficient to reconstruct the compositional distribution. For this reason, it is necessary to adopt a different approach, based on fractionation.

Copolymers SH91 and SH78 were fractionated by SEC and 50-60 fractions collected for each copolymer. The SEC fractions yield excellent MALDI-TOF spectra with narrow distributions (the polydispersity index being often smaller

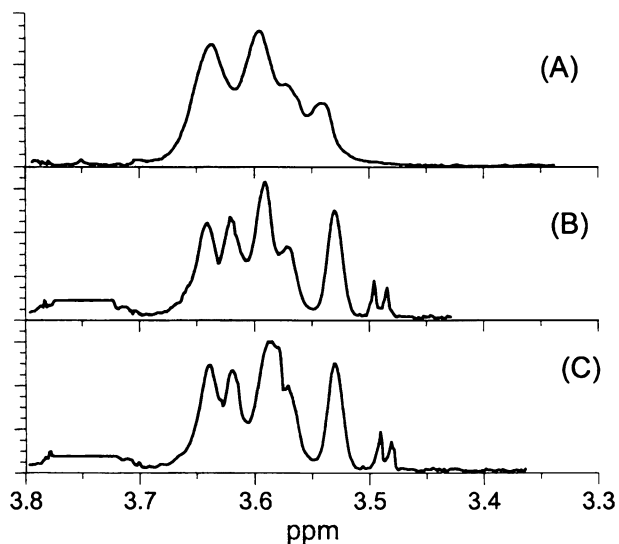


Figure 1: Expansion of the 3.3-3.8 ppm region of the 500MHz ^1H -NMR spectrum for sample MB41. (A): The unfractionated sample; (B): fraction 46; (C) fraction 51.

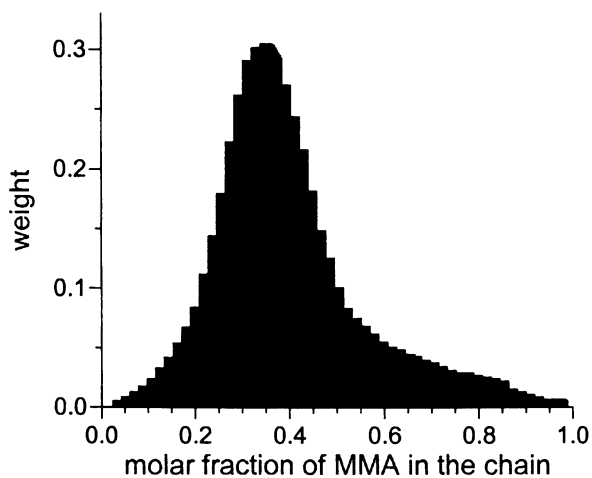


Figure 2: Compositional distribution for sample MB41

than 1.1, as reported in Table 2) up to high molar masses (96 kDa). Beyond that, MALDI spectra became very weak and molar mass could not be estimated.

The copolymer fractions were also analyzed by $^1\text{H-NMR}$. The copolymer composition of each fraction was determined measuring the area of the regions 6-8 ppm and 1-3ppm and combining them together as depicted in eq. 14. The composition values obtained by this procedure (see Table 2) imply that the molar fraction of styrene in both copolymer samples varies as the mass of the chain grows. In the case of sample SH91 the average molar fraction of styrene is in the range 0.58-0.99. Sample SH78 (data omitted for brevity) turned out to possess a more limited compositional heterogeneity since the average molar fraction of styrene is in the range 0.53-0.89.

The SEC data in Table 2 indicate that the copolymer fractions have a composition close to alternating (50%) for a molar mass of about 17-19 kDa. This molar mass corresponds to the kinetic chain length of the alternating copolymer and that lower and higher molar masses are subjected to higher percent of styrene inclusion.

Thereafter, $^1\text{H-NMR}$ data was used to measure the amount of copolymer contained in each fraction by measuring I_{TMS} (the area under the peak at 0 ppm, corresponding to TMS) and combining it with the quantities I_{arom} and I_{alif} defined in eq. 16. The resulting weight values are reported in Table 2 (column 8). In order to measure the amount of copolymer, one may rely on the SEC detector, which is a differential refractometer, and assume that the detector's response reflects the amount of copolymer. Table 2 (column 7) reports the amount of copolymer estimated using the latter method. There are some discrepancies between the cited (R.I.) values and the values obtained by $^1\text{H-NMR}$. The discrepancies between the two measurements are often small; however, in some cases they become large and cannot be neglected. For instance, the two values for the amount of copolymer in fraction 36 are 17 and 26, which implies a difference larger than 30%. This difference is due to the fact that we are dealing with compositionally heterogeneous copolymers; the response to styrene units and to maleic-anhydride units may be different and the refractometer response is therefore unreliable. An UV detector is commonly added to the apparatus and used to correct for the different values of the quantity dn/dc for the two monomers. However the time-lag estimation between the two detectors is cumbersome (1-5).

The average molar mass and dispersion of the unfractionated copolymers were then computed. The software for such calculations needs the calibration lines for the two samples and the abundances. The calibration data was taken from Table 2 (column 5), which reports the MALDI-TOF analysis of each fraction. The result was $M_n = 151000$, $M_w = 345000$, $D=2.28$. Computer program COPOFRAC was used to generate the compositional distribution histogram for sample SH91 and the result is shown in Figure 3. This histogram differs from the preceding one (see Fig. 2) in that it is almost flat, especially in the region 0.7-0.9, which implies that the compositional distribution is broad. This agrees with the results of the DEPT-NMR experiment, which indicated that

the overall variance of compositional distribution for sample SH78 is large. These results can be understood since the MAH monomer is consumed in the first part of the copolymer forming reaction. Therefore in the SH91 copolymer sample, when the conversion is above 50%, the compositional distribution becomes very rich in styrene units, showing a neat maximum at 95% in styrene units (Figure 3).

Copolymer sample M30 is a random copolymer with units of styrene (St) and methyl methacrylate (MMA) obtained at high conversion. The copolymer was injected in the SEC apparatus, the SEC fractions were collected and analyzed by ^1H -NMR and MALDI. Figure 4 reports a summary of the MALDI and NMR results. From data in Figure 4a, it can be seen that the composition varies dramatically as the molar mass increases. Specifically, the molar fraction of styrene is very high at low masses (14500), then it falls steadily (in an almost linear manner) and it reaches the value of 0.53 at high mass.

The weight of copolymer in each fraction was computed using eq. 18. Figure 4b reports the weight before correction (solid line) and after correction (dotted line). It can be seen that the values are different and this implies that the SEC chromatogram as resulting from the RI detector is misleading, since it takes its tallest value about 1 mL earlier, which corresponds to a 33% error in the determination of M_n and M_w .

Figure 4c reports the 200MHz ^1H -NMR spectrum of fraction 34. It can be seen that the signal-to-noise ratio is acceptable and this demonstrates that off-line SEC-NMR can be performed using medium-low field magnets (200MHz), a very attractive feature indeed!

SEC fractions of M30 yielded acceptable MALDI-TOF mass spectra (omitted for brevity) with a peculiar feature, namely strong signals due to doubly-charged ions. The calibration data were used to compute the molar mass averages, which turned out to be $M_n = 99000$, $M_w = 240000$, $D=2.4$. Computer program COPOFRAC was used to generate the compositional distribution histogram for sample M30 and the result is shown in Figure 4d. This histogram differs from the preceding ones (see Figs. 2,3) since there is a plateau in the styrene-poor region, which originates from long MMA-rich chains. When the molar fraction of styrene increases from 0.4 to 0.65, the weight increases, thereafter it bends downwards.

In the case of sample M30, four different fractionation experiments were performed and 50 fractions of 0.2 mL, 25 fractions of 0.4 mL, 15 fractions of 0.8 mL, 15 fractions of 1 mL were collected. The goal of these experiments is to find the optimal conditions, namely the largest volume of the fraction where the aforementioned loss of accuracy is small and to collect experimental data which can be used to test the model for copolymers obtained by SEC fractionation described in the theoretical section

Figure 5a-d reports the MALDI-TOF mass spectra of the fractions collected around 29 mL. The four spectra are bell-shaped, the tallest molar mass is about 46000) and it is quite apparent that the spectrum becomes broader as the volume of the fraction grows. The MALDI-TOF mass spectra of the fractions collected

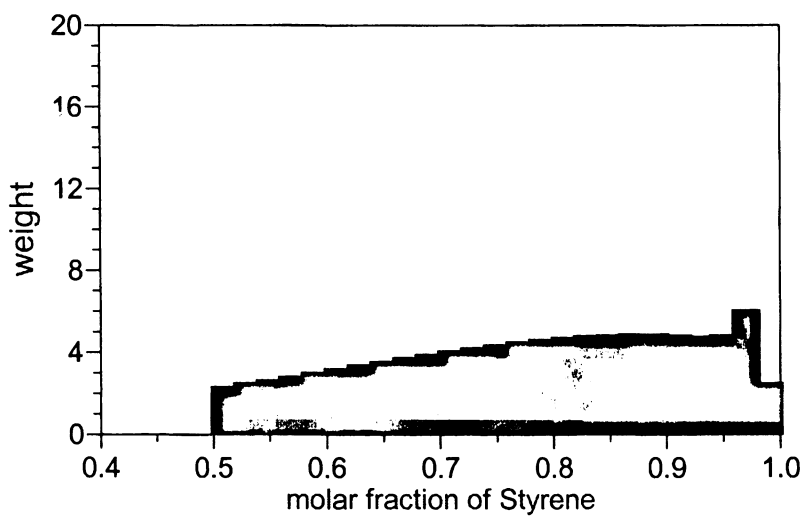
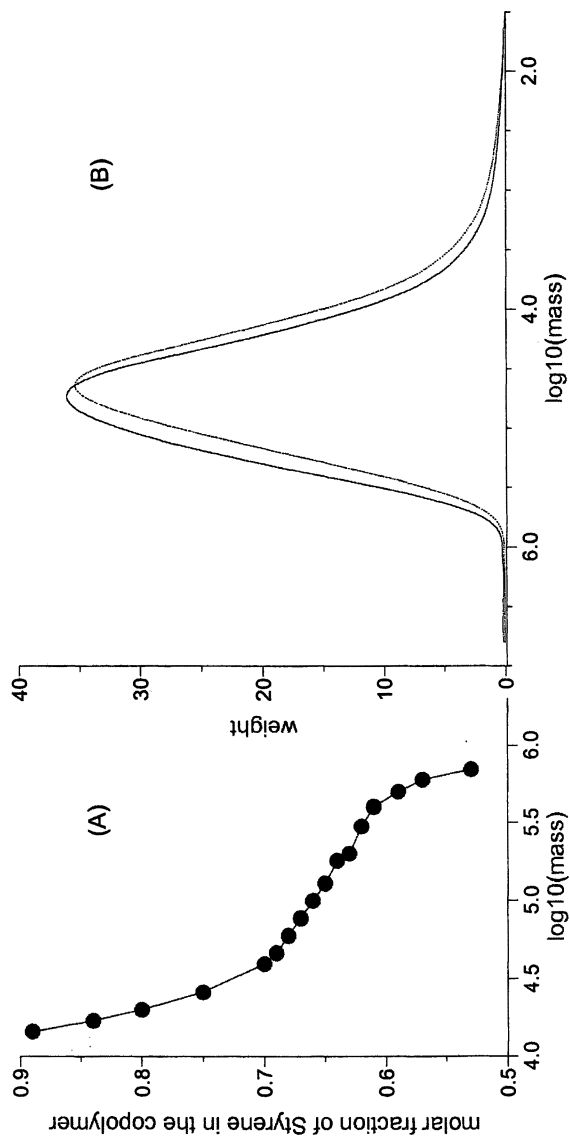


Figure 3: Compositional distribution for sample SH91



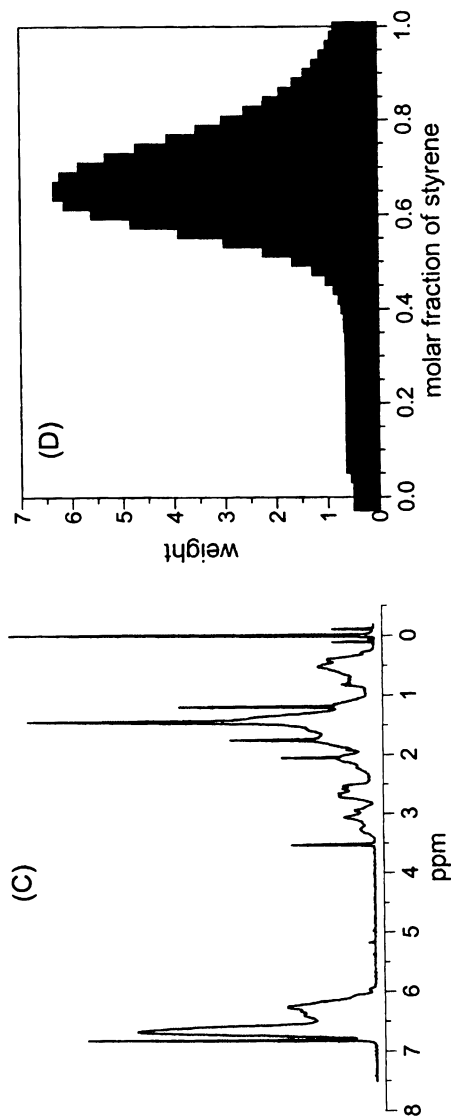


Figure 4: SEC fractionation for sample M30. (A): the compositional drift. (B): SEC traces before correction (full line), and after correction (dotted line). (C): the 250 MHz NMR spectrum of fraction 34. (D): compositional distribution for the sample.

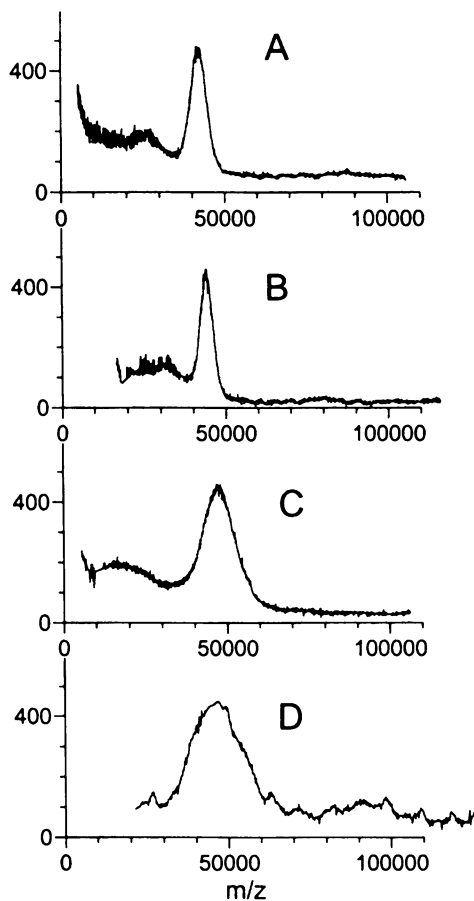


Figure 5 MALDI of fractions of sample M30 collected in four different experiments. The volume of the fraction is 0.2 ml (A) , 0.4 ml (B), 0.8 ml (C), 1.0 ml (D). The M_w/M_n ratio of the fractions is also displayed for fractions collected around 29 ml. (E), around 30 ml. (F).

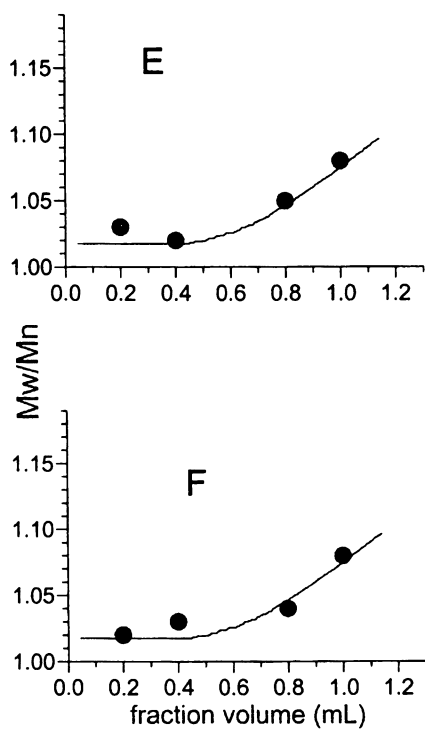


Figure 5. *Continued.*

around 30 mL (data omitted for brevity) are bell-shaped too, and the tallest molar mass is about 26000.

Computer program COPOFRAC was used to predict the polydispersity index (D) versus V_1 (the volume of the fraction) for this experiment. Figure 5e (full line) reports the result of the calculation and it can be seen that D scales in a non-linear manner (this implies that eq. 8 does not possess an analytical solution) and that when V_1 is larger than 0.6 mL, D becomes unacceptably large. On the other hand, when V_1 is smaller than 0.6 mL, D is unacceptable and thus these represent the optimal conditions. Figure 5f (full line) reports the result of a similar calculation for fractions collected around 30 mL. Again, the optimal conditions occur when V_1 is smaller than 0.6 mL. Figure 5e (points) reports the experimental data for D of fractions collected around 29 mL whereas Figure 5f (points) reports analogous for fractions collected around 30 mL. These data allow a comparison between theory and experiment and the agreement is good, demonstrating the validity of the model proposed.

Computer program COPOFRAC was used to predict the changes in composition as the volume of the fraction grows and, more specifically, the difference between the composition of the SEC fraction and the composition of the unfractionated copolymer, which is related to the quantity ϕ defined in eq. 6. Figure 6a (full line) reports the result of the calculation, and it can be seen that ϕ varies linearly with λ (which is defined by $\lambda = \log(V_1)$, see eq. 7) and that when V_1 becomes larger and larger, the composition of the SEC fraction becomes virtually coincident with that of the unfractionated copolymer (the difference drops to zero and the logarithm tends to minus infinity). Figure 6a (points) reports the experimental data for ϕ of fractions collected around 29 mL, plus an additional point, obtained from eq. 4 (which gives the composition when SEC fraction x is mixed together with SEC fraction y). Data in Figure 6a can be used to compare predicted and experimental ϕ values. There is a fair agreement, and the linear scaling of ϕ with λ is clearly confirmed.

An interesting feature of the model developed for copolymers obtained by SEC fractionation is that it predicts a compositionally homogeneous copolymer can yield a compositionally inhomogeneous fraction. This is caused by the "mass coelution" effect discussed in the Introduction. Specifically, when the quantities ρ_1 and ρ_2 in (eq. 5) are large the fraction possesses a drift and is therefore compositionally inhomogeneous

Computer program COPOFRAC was used to predict how the composition varies with chain length q in the case of SEC fractionation of a copolyester with units of butylene adipate and butylene sebacate(21) and more specifically the molar fraction of butylene adipate units for some SEC fractions. Figure 6b (full line) reports the result of the calculation for fraction 26 and it possesses three most evident features, namely the curve is more or less straight (a line), the molar fraction of butylene adipate units increases with chain size, and the slope is small but certainly not negligible. The MALDI-TOF mass spectra of fraction 26 was reported elsewhere (21) along with a thorough tabulation of mass spectral

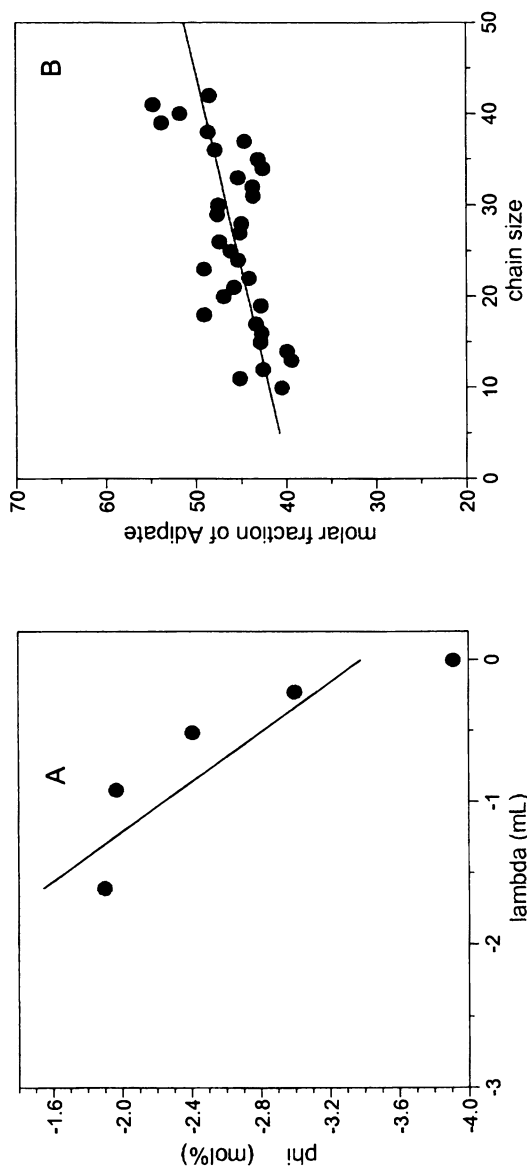


Figure 6. Comparison between theory (full lines) and experiment (points).
(A): ϕ versus λ in eq. 5; (B): molar fraction of adipate versus chain size

intensities. Using the intensities, we derived the molar fraction of butylene adipate units for each chain size as shown in Figure 6b (points). It can be seen that points are somehow scattered, but the fact that the molar fraction of butylene adipate units increases with chain size stands out clearly. This implies that the fraction is compositionally inhomogeneous, and it demonstrates that the prediction of the model is correct.

Conclusions

A method for full copolymer characterization is presented, which employs off-line SEC-NMR and SEC-MALDI. Examples are given of copolymers reacted at high conversions. Off-line SEC-NMR and SEC-MALDI can be performed using medium-low field magnets (200MHz), a very attractive feature since it allows the use of affordable equipment. A theoretical model is developed which allows us to predict the mass spectrum and the $^1\text{H-NMR}$ spectrum of each SEC fraction. It also generates the Bivariate Distribution (see eq. 10) and the compositional distribution histogram (see eq. 11) and predicts what happens when two (or more) SEC fractions are mixed together

Acknowledgments

Partial financial support from the Italian Ministry for University and for Scientific and Technological Research (MURST), from PROGETTO FINALIZZATO MATERIALI SPECIALI PER TECNOLOGIE AVANZATE II (CNR, Rome), and from the National Council of Research (CNR, Rome) is gratefully acknowledged. A special thank is due to Dr. G. Impallomeni for helpful discussion.

References and Notes

1. Gores et al. in Provder T (ed) "Chromatography of polymers", ACS Symp Ser 521, ACS Publ, Washington, 1993, chapter 10
2. Cooper AR in Bark LS, Allen NS, (eds), "Analysis of Polymer Systems", Applied Science, London 1982, chapter 8
3. Dawkins in Allen G, Bevington J, (eds) "Comprehensive Polymer Science", Pergamon, Oxford, 1989, Vol 1, Chapter 12
4. Meehan et al. in Protschka M, Dubin PL, (eds), "Strategies in Size Exclusion Chromatography", ACS Symp Ser 635, ACS Publ, Washington, 1993, Chapter 15
5. Trathnigg B, *J. Chrom.*, **507**, 552, 1991, see also Trathnigg B, Yan X, *Chromatographia*, **467**, 33, 1992
6. Albert K, *J. Chromatogr.* **A703**, 123, 1995,
7. Korhammer S, Bernreuther A, *Fresenius J. Anal. Chem.*, **354**, 131, 1996,

8. Ute K, Niimi R, Hongo H, Hatada K, *Polymer J.*, **30**, 439, 1998
9. Hatada K, Ute K, Okamoto Y, Imanari M, Fujii N, *Polymer Bull.*, **20**, 317, 1988
10. Hatada K, Ute K, Kitayama T, Nisimura T, Kashiyaama M, *Polymer Bull.*, **22**, 549, 1990
11. Ute K, Niimi R, Hatada K, Kolbert AC, *Int. J. Polym. Anal. Charact.*, **30**, 888, 1998
12. Hatada K, Ute K, Kitayama T, Yamamoto M, Nisimura T, Kashiyaama M, *Polymer Bull.*, **21**, 489, 1989
13. Kramer I, Pasch H, Handel H, Albert K, *Macromol. Chem. Phys.*, **200**, 1734, 1999
14. Montaudo G, Garozzo D, Montaudo M.S, Puglisi C, Samperi F, *Macromolecules*, **28**, 7983, 1995,
15. Montaudo G, Montaudo M.S, Puglisi C, Samperi F, *Rapid Commun. Mass Spectrom.*, **9**, 1158, 1995.
16. Montaudo G, Montaudo M.S, Puglisi C, Samperi F, *Int. J. Polym. Anal. & Charact.*, **3**, 177, 1997
17. Montaudo M.S, Puglisi C, Samperi F, Montaudo G, *Macromolecules*, **31**, 3839, 1998.
18. Carroccio S, Rizzarelli P, Puglisi C, *Rapid Commun. Mass Spectrom.*, **14**, 1513, 2000
19. Lou X, Van Dongen JLJ, Meijer EW, *J. Chromat.*, **A896**, 19, 2000,
20. Esser, E, Keil C, Braun D, Montag P, Pasch H, *Polymer*, **41**, 4039, 2000,
21. Montaudo M.S, Puglisi C, Samperi F, Montaudo G, *Rapid Commun. Mass Spectrom.*, **12**, 519, 1998.
22. Montaudo MS, Montaudo G, *Macromolecules*, **32**, 7015, 1999
23. Montaudo MS, *Macromolecules*, **34**, 2792, 2001
24. Murphy RE, Schure MR, Foley JP, *Anal. Chem.*, **70**, 1585, 1998
25. Ogawa T, *J. Appl. Pol. Sci.*, **23**, 3515, 1979
26. Kuchanov SI, *Adv. Polym. Sci.*, **52**, 157, 2001
27. Tobita H, *Polymer*, **39**, 2367, 1998
28. Aerdts AM, German AL, Van der Velden GPM, *Magnet. Reson. Chem.*, **580**, 32, 1994
29. Barron P.F., Hill D.J.H., O'Donnell J.H., Osullivan P.W. , *Macromolecules* **1984**, *17*, 1967.
30. Aerdts A, DeHaan JW, German AL, *Macromolecules*, **26**, 1965, 1993

Chapter 29

Coupled SEC-NMR Analysis of Alginates

Thomas G. Neiss¹ and H. N. Cheng²

¹Chemical Process R&D Division, Bristol-Myers Squibb Company,
Chambers Works, PRF (S1), Deepwater, NJ 08023

²Hercules Incorporated Research Center, 500 Hercules Road,
Wilmington, DE 19808-1599

Naturally produced polysaccharides tend to be heterogeneous both in composition and in molecular weight. Segregation of polymer chains through a separation method, followed by spectroscopic analysis, is often needed to provide information on polymer microstructure. We report the first coupled SEC-NMR analysis of alginates. The data can be fitted to 2-component 1st order Markovian models. The two components likely correspond to the actions of two epimerization enzymes, one enzyme predominantly producing blocks of G units, and the second enzyme producing single M→G epimerization or alternating MG units. Quantitative information about the components is obtained.

Introduction

Plant polysaccharides tend to be heterogeneous in nature, with distributions of molecular weight, composition, monomer sequence, and functional groups. Monomer sequence distribution is often a critical parameter in determining the functional properties of the polysaccharide. While the spectroscopic analysis of these materials may produce an accurate assessment of the monomer composition, the monomer sequence distribution is a statistical average of the

ensemble and NMR cannot discriminate intramolecular from intermolecular heterogeneity in polysaccharide systems. Sequence information is further compromised by degradative steps often used in sample preparation required to produce a sample for analysis. Physicochemical separation of the polymer chains becomes necessary to further characterize the distribution of monomers present in a sample.

Alginates are linear polysaccharides isolated from algae or produced through bacterial fermentation and used as rheology modifiers in aqueous systems, coatings, and stabilizing agents(1). They are composed of β -D-mannuronic acid, M, and its epimer, α -L-guluronic acid, G. These two monomer units are arranged in both homopolymeric and randomly distributed copolymer blocks. Alginates are typically described by their M/G ratio and are high M if $F_M \geq 0.7$ and high G when $F_M \leq 0.6$ (2,3). Other important structural parameters are the distribution of M and G units, and the molecular weight distribution of the polymer.

Solution NMR spectroscopy is an extremely powerful technique for the study of polymer microstructure including that of alginates. A significant amount of data on alginate microstructure from ^1H and ^{13}C NMR measurements is available in the literature(3-7). Spectral resonances of a given saccharide unit are sensitive to the identity of the saccharide units adjoining it in the polymer chain, with ^{13}C shifts of up to 1 ppm or more and ^1H shifts in the 0.1 to 0.4 ppm range. Diad and Triad sequence distributions are readily obtained using the higher field spectrometers ($B_0 \geq 9.4$ Tesla) and with degradation of molecular weight to reduce sample viscosity. Two distinct disadvantages which exist in the current NMR methods are the need to reduce molecular weight of the alginates and the need to address intermolecular polymer heterogeneity by separation or other physicochemical processes, e.g., fractionation or chromatography. The former can lead to a misrepresentation of the sequence distribution by favoring the loss of a particular structural moiety, that most sensitive to acid hydrolysis, the common method of molecular weight reduction, while absence of the latter relegates the NMR results to a statistical average of the entire chain ensemble.

Coupling of chromatographic separations with NMR spectroscopy is a well-established technique, including the use of both HPLC or SEC in separating samples based on hydrophobicity or molecular size(8-15). The focus of HPLC-NMR has been in the area of pharmaceutical analysis, primarily in discovery and in metabolism research, where the technique has been proven extremely valuable. In contrast, SEC-NMR has been implemented primarily for the analysis of synthetic polymers, with little or no reported results in the area of polysaccharides. We would like to report the first coupled SEC-NMR study of alginates to determine alginate monomer composition and sequence distribution as a function of molecular weight. Through a stop-flow hyphenated NMR technique, NMR spectra of alginates can be obtained at specific molecular

weights, revealing chemical composition and distribution at that particular point in the chromatograph.

Statistical analyses of alginate NMR data have been reported in the literature(1,3,4,7,16,17). Results obtained from both ^1H and ^{13}C spectra of diad and triad sequences are typically fitted to Bernoullian and Markovian statistical models. However, application of any statistical model to NMR data on whole alginate samples or those with minimal fractionation may provide deceptively simple results since the unrealistic assumption must be made that all polymer chains are identical, thereby ignoring intermolecular and intramolecular heterogeneity. Indeed, the use of (one-component) Bernoullian and Markovian models has been fraught with problems(1,3). A promising recent development is the use of discrete multicomponent models and continuous chemical composition distribution approaches to analyze alginate NMR data(16,17).

By coupling NMR directly with an appropriate separation technique, intermolecular heterogeneity can be investigated separately from the intramolecular distribution. The type of separation method (SEC, IC, HPLC) available for the analysis can provide several physicochemical methods of "sorting" polymer chain heterogeneity (molecular weight, charge density, hydrophobic interactions). The computational framework for this analysis has been reported previously(16,17), providing the background for this study, and will not be further elaborated here.

EXPERIMENTAL

Size Exclusion Chromatography (SEC)

SEC measurements were implemented and optimized based on those in the open literature(18,19). Separation was completed using a Hewlett-Packard 1100 Series LC system comprised of a binary pump, autosampler, thermostatted column oven, and variable wavelength detector. Control of the modules was achieved using Bruker Instruments HystarNT™ software and serial connections to each module. Molecular weight separation was completed using TosoHaas G3000PW_{XL} and G5000PW_{XL} columns, both 7.8 mm. x 30 cm., connected in series and protected using a 6.0 mm. x 4 cm. guard column. A G6000PW_{XL} column was also tested in place of the G5000PW_{XL} column, with no significant change in alginate chromatography. The mobile phase was 0.05 M NaCl in LC grade $\text{d}_2\text{-H}_2\text{O}$ at pH 6. Both pH and salt concentrations were investigated in this work. While changes in pH in the range from 4 to 7 had a negligible effect on the separation, the salt concentration was a critical parameter in controlling retention. A balance between chromatographic resolution, sensitivity of the NMR measurement and dielectric effects in the NMR probe was obtained at a

0.05 M concentration. This level of salt was sufficient to provide resolution in the SEC separation with enough material in the NMR probe to obtain a ^1H spectrum in a reasonable time period. A flow rate of 0.7 mL/min. and column temperature of 40°C were used for all separations. UV absorption was measured at 210 nm. for both the alginates and polystyrene sulfonate molecular weight standards and 205 nm. for pullulan standards. Polystyrene sulfonate narrow molecular weight standards (American Polymer Standards Corp.) were used to monitor system stability and reproducibility, but did not serve as suitable molecular weight calibrants owing to their structural differences from polysaccharides. Pullulans molecular weight standards (Shodex) were found to be weakly detectable in the UV region and were subsequently used as molecular weight calibrants. Both sets of standards were prepared as per manufacturer instructions. A 100 μL . injection of a 10 mg./mL. solution (1% w/v) of alginate, corresponding to 1 mg. of sample, was used for the SEC-NMR analysis. The chromatographic system was connected to a Bruker Instruments 4 mm. inverse detection probe with 3 axis gradients through a Bruker Peak Sampling Unit, BPSU-12, used to control flow from the system. The flow cell had an active volume of 120 μL . and a total volume of 240 μL . Control of the system during chromatogram acquisition, transfer and NMR measurement was completed using automated software features found in Bruker XWIN-NMR™ and HyStarNT™ software packages.

NMR Spectroscopy

All NMR measurements were completed on a Bruker Instruments DRX-500 FT NMR spectrometer with a ^1H observation frequency of 500.13 MHz at a field strength of 11.75 Tesla. The spectrometer was equipped with a variable temperature control unit, 3-axis gradient amplifier, a 300 W. X nucleus amplifier, 100 W. ^1H amplifier, and digital lock and receiver systems. ^1H spectra of the whole polymer samples were obtained using a 5 mm. inverse probe (Bruker). Spectra were acquired of 0.1% (w/v) solutions in $\text{d}_2\text{-H}_2\text{O}$ at pH 6 and 70°C. Sixty-four transients were acquired for each spectrum with a sweep width of 8169 Hz, 64k data points, a 90° excitation pulse and a pulse repetition time of 6 seconds, including the acquisition time. ^{13}C NMR spectra were acquired at 125.x MHz using a 10 mm. broadband probe (Nalorac). Whole polymer samples were analyzed as 5% (w/v) solutions in $\text{d}_2\text{-H}_2\text{O}$ at pH 6 at a probe temperature of 90°C. Spectra were acquired with a single pulse sequence with heteronuclear decoupling during both signal acquisition and relaxation delay periods. A sweep width of 29498 Hz was acquired with 64k data points, a 90° excitation pulse and a pulse repetition time of 4 seconds. A total of 12k transients were required for the Protonal and Manegel samples and 36k transients for the NaAlginate sample. ^1H SEC-NMR spectra were obtained using

the probe described in the SEC experimental section. Experimental parameters were the same as those for the whole polymer samples with the exception of a pulse repetition time of 4 seconds and a sweep width of 10 kHz. All ^1H NMR spectra used for diad and triad analysis were acquired without solvent suppression as rf suppression of the HOD resonance was found to alter resonance intensities of the signals of interest.

Diad and triad fractions were measured by fitting the data to Lorentzian lineshapes using PeakFitTM software (SPSS). Amplitude, width and position were fit for each peak without constraints. In some cases, particularly for the anomeric ^{13}C NMR signals, resonances had asymmetric lineshapes or inflection points indicative of unresolved structural information such as higher order sequence information. These lineshapes required fitting the signal in question to several lines that were combined for statistical analysis. Diad and triad data were analyzed following methods previously reported(16,17,20,21).

Results and Discussion

Three commercial samples of sodium alginate, Protonal LFR, Sigma NaAlginat, and Manegel LMW, were examined in this study. The SEC chromatogram of Protonal LFR is shown in Figure 1 and was typical of all three samples. The major signal is of the alginate polymer and shows a shift in maxima, dependent on the sample. A second smaller band with a retention time about 27 minutes was determined to be monomer sugar units and low molecular weight polyols, while a third band at 31 minutes has not been identified, but may be ionic species in the sample. Using the pullulan calibration shown in Figure 2, the number average molecular weights of each sample were determined to be 70 kD. for Protonal LFR, 212 kD. for NaAlginat, and 63 kD. for Manegel LMW. The data spread indicates a molecular weight range from ~2,000,000 Daltons to monomers of several hundred Daltons.

NMR Spectroscopy

A ^{13}C NMR spectrum of Manegel LMW is shown in Figure 3 and is typical for a high G alginate. The splitting of the anomeric carbon signals at ~101 ppm are of the most value as both diad and triad information is readily obtained. The carbonyl resonances also have a significant amount of sequence information, but assignments are not as well established and therefore not used in this work. Without acid hydrolysis of the polymer molecular weight, resolution limitations

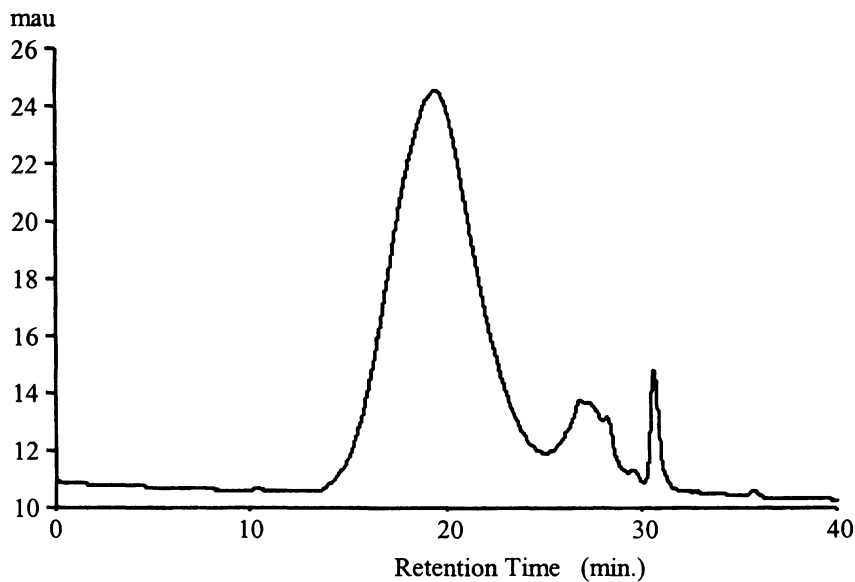


Figure 1. Aqueous SEC chromatogram of Protonal LFR

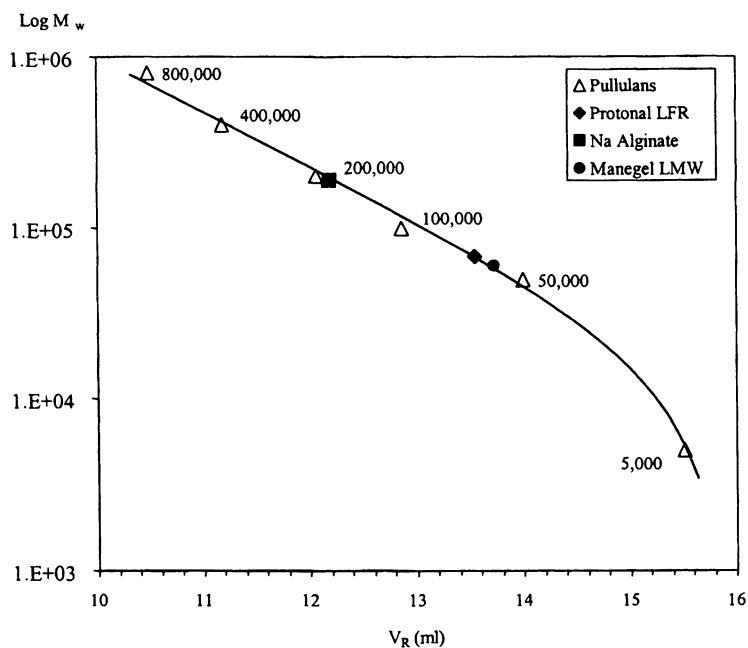


Figure 2. Pullulan calibration curve for SEC analysis of Alginates

permitted the observation of all diads and only the M centered triads in the ^{13}C spectra. Chemical shift assignments of Grasdalen et.al. were used in the assignment of signals(4,5).

The ^1H NMR spectrum of Protonal LFR is shown in Figure 4. All diads and the MGM and GGM triads could be directly measured from the ^1H spectrum, while MGG and GGG were calculated from diad and triad frequencies. Unfortunately the M triads could not be observed in either the whole polymer or SEC-NMR ^1H spectra and limited the extent of the statistical analysis. Assignments used were those of Grasdalen(6). The spectrum shown in Figure 4 was acquired with on-resonance water suppression, which is also affecting the H₅ GG diad signal. Suppression was not used in the spectra acquired for sequence analysis in order to prevent distortion of the resonance signals. Four or five spectra were acquired for each chromatogram.

Statistical Analysis

The diad and G-centered triad intensities measured for the whole polymers are reported in Table I. As expected, all three samples fitted poorly to one-component 1st order Markovian (or Bernoullian) models. The mean deviations in all three cases are larger than 1%. Instead, the data fitted reasonably well to two-component 1st order Markovian models. This finding is consistent with the latest NMR studies on alginates (16,17) which also indicated that alginates NMR data should be fitted not to one-component models, but to multicomponent models.

The diad and G-centered triad intensities as measured in the SEC-NMR experiment are reported in Table II. Again, the data did not fit well to one-component 1st order Markovian model, but gave satisfactory fits to the two-component 1st order Markovian model, with mean deviations all less than 1.0%.

A two-component 1st order Markovian model can be considered a mixture of two discrete components, each characterized by unique reaction probabilities P_{GM} and P_{MG} and a weight factor, w_1 or w_2 , such that the intensity of a particular diad or triad sequence is written as(21):

$$I_{i,\text{obsd}} = w_1 f_{1i} + w_2 f_{2i}$$

where $I_{i,\text{obsd}}$ is the observed diad or triad intensity and f_{ji} is the intensity for signal i and component j . Table III contains all of the reaction probabilities and weight factors calculated for this model and NMR data. Component 1 is almost completely a G homopolymeric block with a small amount of residual M as seen in the sum of the reaction probabilities. This component represents the region of highest epimerization in the alginate biosynthesis process. The second component of each data set is a high M containing region with an almost random

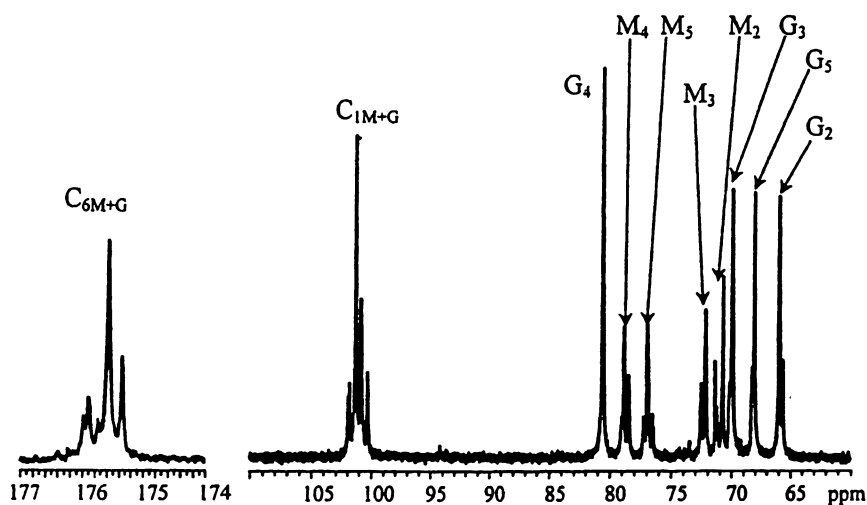


Figure 3. Solution ^{13}C NMR spectrum of Manegel LMW.

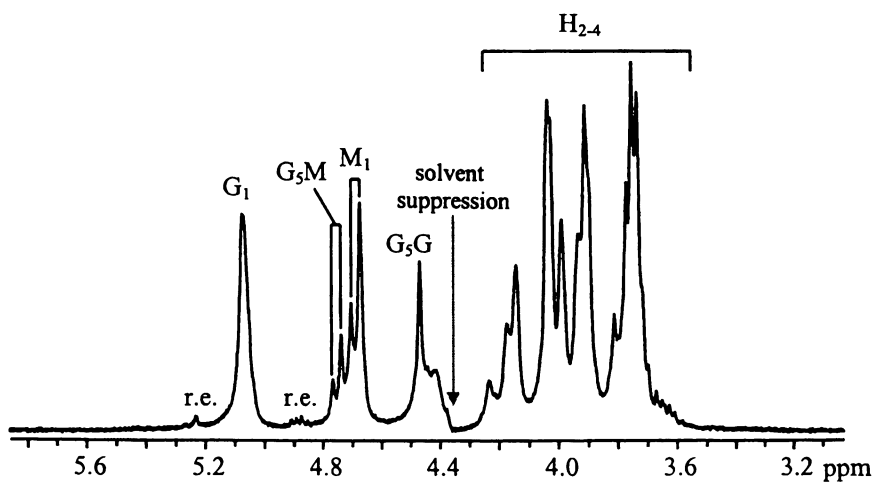


Figure 4. Solution ^1H NMR spectrum of Protonal LFR.

Table I. NMR analysis of whole (unfractionated) alginate samples

Sequence	Protonal			NaAlginate			Manegel		
	I_{obsd}	I_{calc}^a	I_{calc}^b	I_{obsd}	I_{calc}^a	I_{calc}^b	I_{obsd}	I_{calc}^a	I_{calc}^b
MM	19.1	19.1	19.1	32.4	32.4	32.4	20.9	20.9	20.9
MG	24.0	24.0	24.0	49.5	49.5	49.5	27.2	27.2	27.2
GG	56.9	56.9	56.9	18.1	18.1	18.1	51.9	51.9	51.9
MGM	5.9	2.1	8.8	19.9	14.3	19.1	9.1	2.8	9.1
GGM	6.4	19.8	6.4	11.3	20.9	11.3	9.0	21.6	9.0
GGG	56.4	47.0	53.7	11.7	7.6	12.4	44.2	41.1	47.4
One-component 1st order Markov model									
	P_{GM}	0.174			0.578			0.208	
	P_{MG}	0.386			0.433			0.394	
	MD^c	4.4			3.2			3.7	
Two-component 1st order Markov model									
component 1	P_{GM}	0.004			0.006			0.004	
	P_{MG}	0.991			0.998			0.984	
	w_1	0.533			0.110			0.459	
component 2	P_{GM}	0.745			0.774			0.678	
	P_{MG}	0.382			0.432			0.391	
	w_2	0.467			0.890			0.541	
	MD^c	0.9			0.3			0.5	

^a Fitted to 1-component 1st order Markovian model

^b Fitted to 2-component 1st order Markovian model

^c Mean deviation between observed and calculated intensities

sequence distribution of M and G for Protonal LFR and a tendency toward alternating sequences in the other two samples. The weight factors also present an interesting result in that w_2 increases as molecular weight decreases, and as the M content increases. This trend is pronounced in the Protonal and Manegel samples, but less so in the NaAlginate sample.

An estimate can be made of the contributions of the two components to the overall polymer. The appropriate weight of each SEC fraction can be estimated from the SEC curve. These are then multiplied by the component weight factors for each fraction. The contribution of the two components to each polymer is obtained by the sum (Table IV). Thus, for the Protonal and Manegel samples the contribution of component 1 is about 60%, whereas for NaAlginate the contribution of component 1 is about 29%. These numbers are approximate because only 4-5 fractions are used to represent each polymer.

Table II. Observed and (calculated)^a diad and triad intensities for alginate fractions of three samples examined using SEC-NMR.

<i>Sample</i>	Fr.	M_w^b	<i>MM</i>	<i>MG</i>	<i>GG</i>	<i>MGM</i>	<i>GGM</i>	<i>GGG</i>	MD^c
Protonal LFR	1	280	9.4	7.8	82.8	2.0	3.6	81.0	
			(9.4)	(7.8)	(82.8)	(2.1)	(3.6)	(81.0)	0.0
	2	150	12.8	11.3	75.9	3.5	2.4	74.7	
			(12.8)	(11.3)	(75.9)	(4.5)	(2.4)	(74.7)	0.2
	3	49	19.7	18.7	61.6	6.2	6.4	58.8	
			(19.7)	(18.7)	(61.6)	(6.2)	(6.4)	(58.8)	0.0
	4	14	21.9	24.5	53.6	7.4	8.0	49.6	
			(21.9)	(24.5)	(53.6)	(8.2)	(8.0)	(49.6)	0.1
NaAlginate	1	659	38.6	22.9	38.4	5.6	5.6	35.6	
			(38.6)	(22.9)	(38.4)	(8.7)	(5.6)	(35.6)	0.5
	2	297	33.4	31.3	35.3	14.7	1.8	34.4	
			(33.4)	(31.3)	(35.3)	(14.8)	(1.8)	(34.4)	0.0
	3	98	33.8	37.6	28.6	15.0	4.6	26.3	
			(33.8)	(37.6)	(28.6)	(16.5)	(4.6)	(26.3)	0.4
	4	32	34.5	44.6	20.9	19.0	4.6	18.6	
			(34.5)	(44.6)	(20.9)	(20.0)	(4.6)	(18.6)	0.2
	5	14	34.0	39.7	26.3	17.9	3.0	24.8	
			(34.0)	(39.7)	(26.3)	(17.9)	(3.0)	(24.8)	0.0
Manegel LMW	1	281	15.6	9.1	75.3	1.2	2.5	72.8	
			(15.6)	(9.1)	(75.3)	(2.8)	(3.5)	(73.5)	0.4
	2	136	14.3	13.9	71.7	3.9	3.0	70.2	
			(14.3)	(13.9)	(71.8)	(5.5)	(3.0)	(70.3)	0.3
	3	48	18.4	19.3	62.3	6.2	4.8	59.9	
			(18.4)	(19.3)	(62.3)	(7.3)	(4.8)	(59.9)	0.2
	4	18	21.8	22.4	55.8	7.0	4.6	53.5	
			(21.8)	(22.4)	(55.8)	(8.9)	(4.6)	(53.5)	0.3
	5	8	24.1	26.6	49.3	9.2	6.2	46.2	
			(24.1)	(26.6)	(49.3)	(10.2)	(6.2)	(46.2)	0.2

^a Calculation done with a two-component 1st Markovian model.

^b Weight-average molecular weight in Daltons $\times 10^3$.

^c Mean deviation between the observed and the calculated intensities.

Table III. Summary of two-component, 1st order Markovian statistical analysis of alginate fraction data obtained from SEC-NMR.

Sample	Fr.	M_w	Component 1		Component 2		Weight Factor	
			P_{GM}	P_{MG}	P_{GM}	P_{MG}	w_1	w_2
Protocal LFR	1	280	0.001	0.999	0.581	0.288	0.799	0.201
	2	150	0.001	0.999	0.790	0.306	0.744	0.256
	3	49	0.001	0.999	0.662	0.321	0.570	0.430
	4	14	0.001	0.999	0.676	0.358	0.479	0.521
NaAlginate	1	659	0.009	0.991	0.776	0.224	0.358	0.642
	2	297	0.004	0.999	0.951	0.317	0.348	0.652
	3	98	0.005	0.999	0.882	0.356	0.263	0.737
	4	32	0.085	1.000	0.972	0.372	0.241	0.759
	5	14	0.042	0.994	0.978	0.355	0.282	0.718
Manegel LMW	1	281	0.009	0.997	0.708	0.201	0.750	0.250
	2	136	0.008	0.994	0.854	0.308	0.718	0.282
	3	48	0.011	0.994	0.805	0.329	0.614	0.386
	4	18	0.009	0.992	0.829	0.330	0.545	0.455
	5	8	0.006	0.989	0.782	0.351	0.462	0.538

Table IV. Contributions of the components to each polymer

Sample	Fr.	% polymer	w_1	w_2	% polym.* w_1	% polym.* w_2
Protocal LFR	1	9.4	0.799	0.201	7.51	1.89
	2	21.9	0.744	0.256	16.29	5.61
	3	46.9	0.570	0.430	26.73	20.17
	4	21.8	0.479	0.521	<u>10.44</u>	<u>11.36</u>
Component weight % from all fractions					<u>60.97</u>	<u>39.03</u>
NaAlginate	1	8.6	0.358	0.642	3.08	5.52
	2	20.0	0.348	0.652	6.96	13.04
	3	42.9	0.263	0.737	11.28	31.62
	4	19.9	0.241	0.759	4.80	15.10
	5	8.6	0.282	0.718	<u>2.43</u>	<u>6.17</u>
Component weight % from all fractions					<u>28.55</u>	<u>71.45</u>
Manegel LMW	1	8.6	0.750	0.250	6.45	2.15
	2	20.0	0.718	0.282	14.36	5.64
	3	42.9	0.614	0.386	26.34	16.56
	4	19.9	0.545	0.455	10.85	9.05
	5	8.6	0.462	0.538	<u>3.97</u>	<u>4.63</u>
Component weight % from all fractions					<u>61.97</u>	<u>38.03</u>

Note that whereas the analysis has been accomplished satisfactorily through two-component analysis, equally satisfactory analysis can also be made using more components (e.g., 3-component 1st order Markovian model). However, further experimental evidence is needed to justify more complex models. For example, the P_{MG} values for component 2 for the NaAlginate fractions are not constant (Table III) and in fact increase from about 0.22 to 0.35. Moreover, the component weights (w_1 and w_2) in Table I (obtained from the whole polymer) are somewhat different from the component weights in Table IV (obtained from the fractions) for the same NaAlginate polymer. A similar observation may be made of the corresponding data for the other two alginate polymers, albeit to lesser extents. It is perhaps likely that component 2 may contain 2 sub-components, but more data would be needed to check this possibility (e.g., gathering more SEC fractions).

Enzymatic Action

It appears that there are at least two separate enzymes that carry out the epimerization reactions, corresponding to the two components uncovered in the NMR analysis. The first enzyme (corresponding to component 1) predominantly converts M units into blocks of G units. The second enzyme (corresponding to component 2) either produces single $M \rightarrow G$ epimerization or even favors the formation of alternating MG units. It is of interest that the component weights are different for the three samples. These probably reflect different enzyme actions or different biological origins of the alginates. The first enzymatic reaction contributes roughly 60% to the final polymer structure for Protanal and Manegel samples and about 29% to the NaAlginate sample.

The correlation of the fraction weight factors (w_1 and w_2) with molecular weight and with the M-content is intriguing. From the literature(1), there are at least three sources of molecular weight spread: 1) The enzyme(s) that synthesize the alginates may produce chains of variable lengths, 2) An endo alginate lyase (or another enzyme) may degrade the polymer, 3) The extraction process may depolymerize the polymer. Because the alginates are from commercial sources, it is difficult to speculate on the mechanism of such correlation. From the data, it appears that the epimerization reactions are not concomitant with the chain-breaking reaction. Thus, if the first reaction were to lead to chain breakage, a decrease in w_1 should result in a molecular weight increase, contrary to what is observed for the data on fractions (Table III). Similarly, if the second reaction were to lead to chain breakage, then the NaAlginate sample, with the highest w_2 , should have the lowest molecular weight, again contrary to the observed data (Table III).

Comments on Hyphenated NMR Analysis

The coupled SEC-NMR analysis appears to be very useful in an understanding of the alginate microstructure. The amount of information acquired for alginate samples, while substantial, is the limiting factor in the statistical analysis of alginate sequence distributions. Further analysis would be possible with the addition of M triad intensities and the collection of more spectra per SEC trace. Some experimental limitations need to be overcome, primarily improved sensitivity of the NMR measurement with a smaller volume flow cell and higher temperature capabilities. The latter would permit suppression of the HOD signal without distortion of signals containing sequence information. Suitable solvent suppression techniques such as WET and diffusion-based methods perhaps can be used which may significantly enhance sensitivity. Additional separation mechanisms, such as the use of ion chromatography, would provide a different perspective on the heterogeneity of alginates.

Conclusions

In this work, coupled SEC-NMR analysis has been demonstrated for three samples of alginates. The NMR data have been treated with two-component 1st order Markov statistical models. The first component reflects a mostly G homopolymer, and the second component is a MG copolymer with an almost random or alternating sequence distribution. The relevance of the two components to the epimerization reactions has been noted.

It is known that stretches of consecutive G units tend to produce a fairly stiff chain, whereas consecutive M or MG units produce more flexible chains. In addition, the gel-forming properties of alginates depend on the composition and the sequential arrangement of G. Thus, the microstructure of alginates and the modes of enzymatic action are important to the commercial application of alginates. The coupled SEC-NMR analysis (and other hyphenated separation-NMR techniques) appears to be very useful in this connection.

References

1. Moe, S.T.; Draget, K.I.; Skjak-Braek, G.; Smidsrod, O. In *Food Polysaccharides and Their Applications*; Stephen, A.M., Ed.; Dekker: New York, NY, 1998, pp 245-286.

2. Yalpani, M. *Polysaccharides. Synthesis, Modifications and Structure: Property Relations.*; Studies in Organic Chemistry 36; Elsevier: New York, NY, 1988.
3. Panikhar, R.; Brasch, D.J. *Carbohydr. Res.* **1997**, *300*, 228-238.
4. Grasdalen, H.; Larsen, B.; Smidsrod, O. *Carbohydr. Res.* **1981**, *89*, 175-191.
5. Grasdalen, H.; Larsen, B.; Smidsrod, O. *Carbohydr. Res.* **1977**, *56*, C11-C15.
6. Grasdalen, H. *Carbohydr. Res.* **1983**, *118*, 255-260.
7. Panikhar, R.; Brasch, D.J. *Carbohydr. Res.* **1996**, *293*, 119-132.
8. Peng, S.X. *Biomed. Chromatogr.* **2000**, *14*, 430-441.
9. Linton, J.C.; Nicholson, J.K.; Sidelmann, U.G.; Wilson, I.D. *Drug Metab. Rev.* **1997**, *29*, 705-746.
10. Albert, K.; Dachtler, M.; Glaser, T.; Handel, H.; Lacker, T.; Schlotterbeck, G.; Strohschein, S.; Tseng, L.-H.; Braumann, U. *J. High Resol. Chromatogr.* **1999**, *22*, 135-143.
11. Albert, K. *J. Chromatogr. A* **1999**, *856*, 199-211.
12. Montaudo, M.S.; Montaudo, G. *Macromolecules* **1999**, *32*, 7015-7022.
13. Kramer, I.; Pasch, H.; Handel, H.; Albert, K. *Macromol. Chem. Phys.* **1999**, *200*, 1734-1744.
14. Ute, K.; Niimi, R.; Hatada, K.; Kolbert, A.C. *Int. J. Polym. Anal. Charact.* **1999**, *5*, 47-59.
15. Ute, K.; Niimi, R.; Hongo, S.; Hatada, K. *Polym. J.* **1998**, *30*, 439-443.
16. Cheng, H.N. *Polym. Bull.* **1999**, *43*, 247-254.
17. Neiss, T.G.; Cheng, H.N. *ACS Polym. Prepr.*, **2001**, *42(1)*, 76.
18. Ci, S.X.; Huynh, T.H.; Louie, L.W.; Yang, A.; Beals, B.J.; Ron, N.; Tsang, W.-G.; Soon-Shiong, P.; Desai, N.P. *J. Chromatogr. A* **1999**, *864*, 199-210.
19. Martinsen, A.; Skjak-Braek, G.; Smidsrod, O.; Zanetti, F.; Paoletti, S. *Carbohydr. Res.* **1991**, *15*, 171-193.
20. Cheng, H.N. In *Encyclopedia of NMR*; Grant, D.M.; Harris, R.K., Eds.; Wiley: New York, NY, 1995, pp 3713-3721.
21. Cheng, H.N. *J. Appl. Polym. Sci.* **1988**, *35*, 1639.

Chapter 30

Local Segmental Dynamics of Polyacrylates in Concentrated Chloroform Solutions

Frank D. Blum¹ and Raj B. Durairaj²

¹Department of Chemistry and Materials Research Center, University
of Missouri at Rolla, Rolla, MO 65409-0010

²Indspec Chemical Corporation, 1010 William Pitt Way,
Pittsburgh, PA 15238

The behavior of methine-labeled poly(ethyl acrylate)-d₁ (PEA-d₁), poly(*iso*-propyl acrylate)-d₁ (PIPA-d₁), and poly(*n*-butyl acrylate)-d₁ (PNBA-d₁) has been studied with deuterium NMR relaxation time measurements in concentrated solutions with chloroform. PEA-d₁ and PNBA-d₁ behaved similarly in terms of solution dynamics, but PIPA-d₁ was found to reorient significantly faster at similar concentrations. The relaxation times were fitted to a log-normal distribution of correlation times and the resulting mean correlation times fit to Arrhenius behavior. The energies of activation were found to increase with increasing concentration from about 6 kJ/mol at lower concentrations to 10-20 kJ/mol from about 40 to 80 wt % polymer.

Introduction

Molecular motion in polymer solutions can have significant effects on the physical properties of the systems formed from these solutions. For example, the rates of drying polymer films can determine the film properties. We have shown that the drying of a polystyrene film from toluene solutions could be predicted with the knowledge of thermodynamic parameters, plus solvent diffusion data. (1) The ability of polymers to respond to changes in conditions is determined by the ability of the polymer and/or its segments to reorient. Solvent diffusion is also correlated to the segmental motions of the polymer chains. (2) The reason for this correlation appears to be that both molecules are coupled to the same fractional free volume.

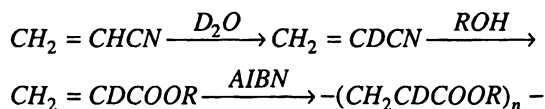
The characterization of the segmental motions of polymers is difficult, especially in concentrated solutions. One technique that is well suited to study polymer segmental motions is NMR relaxation measurement. (3,4) Studies have mostly focussed on the carbon or proton relaxation behavior at lower concentrations. Dipolar interactions among protons, or protons and ^{13}C , tie the relaxation phenomena to local motions of polymer segments. Proton and ^{13}C techniques have been of limited use in more concentrated solutions, which to some extent is the most important regime for the development of many polymer properties. In more concentrated solutions, the overlap of spectral features and/or the complexity of the interactions make extracting motional information difficult, even if the relaxation measurements can be made.

In our laboratory, we have found that the use of deuterium NMR relaxation times could provide a convenient probe of local segmental motions in concentrated solutions. The overlap of different moieties can be avoided through the use of specific labeling. The low natural abundance of deuterium means that only the labeled sites will give any appreciable amount of signal. The moderate size quadrupole moment of the deuteron means that the relaxation of deuterons attached to carbons can be interpreted in terms of the reorientation of the C-D bond vector. Additionally, the relaxation times of deuterons on polymers tend to be quite rapid so that the experiments can be done quickly.

In the present study, we report the relaxation of three acrylate polymers in concentrated solutions with chloroform. The polymers were labeled in the methine position so that the backbone motions of the molecules were probed. In order to probe the relaxation, T_1 and T_2 were used because they cover a wide range of spectra densities for the polymer. We have previously reported the behavior of poly(*iso*-propyl acrylate)- d_1 (PIPA- d_1) in chloroform (5) where we showed that the relaxation of the polymer could be probed at very high concentrations with one technique. We previously found that at higher concentrations, the relaxation data could not be adequately fit with existing models. However, the subsequent development and correction of models allowed us to extend the concentrations where meaningful interpretations could be made. (6) The present study extends this work so that a comparison can be made among a series of polymers in the same family.

Experimental

The polyacrylates were synthesized with deuterium labels on the methine position on the backbone. The monomeric acrylates were made by the exchange of the methine proton on acrylonitrile with D_2O , hydroquinone and CaO , as previously reported for *iso*-propyl acrylate.⁽⁵⁾ The nitrile group was converted to the appropriate ester with the appropriate alcohol and sulfuric acid. Since our first report, a more facile synthesis of these monomers has been reported.⁽⁷⁾ The polymerizations were carried out in toluene using azobis-*iso*-butyronitrile (AIBN) as an initiator. The reaction scheme is given below.



In the above equation the R group designates the particular acrylate. Ethyl, *iso*-propyl, and *n*-butyl acrylates were produced yielding the polymers poly(ethyl acrylate)- d_1 (PEA- d_1), poly(*iso*-propyl acrylate)- d_1 (PIPA- d_1) and poly(*n*-butyl acrylate)- d_1 . For PIPA the viscosity average molecular mass was measured to be 98,000 daltons.⁽⁵⁾ The molecular masses of the other polymers were not estimated directly because their Mark-Houwink coefficients were not known, but they had similar intrinsic viscosities. At these molecular weights, we expect the relaxation times to be independent of molecular mass.⁽³⁾

Deuterium NMR experiments were performed at 13.7 MHz on a JEOL FX 90Q spectrometer. The T_1 measurements were performed using an inversion recovery sequence and the T_2^* values were estimated from the line widths. Because the resonances are relatively broad for the polymers in concentrated solutions, the T_2 's measured were virtually the same as those measured from the Carr-Purcell-Meiboom-Gill (CPMG) method. In this case, measuring the line widths was much faster than measuring the T_2 's by the CPMG method. Thus the T_2^* measurements were taken to be equivalent to the T_2 's.

Results and Discussion

Relaxation measurements have been made for PEA- d_1 , PIPA- d_1 , and PNBA- d_1 . The T_1 and T_2 data were interpreted using a log-normal distribution of correlation times. The relaxation times are determined by:

$$\frac{1}{T_1} = \frac{3\pi^2}{20} (e^2 q Q / h)^2 [J(\omega_0) + 4J(2\omega_0)] \quad (1)$$

and

$$\frac{1}{T_2} = \frac{3\pi^2}{40} (e^2 qQ/h)^2 [3J(0) + 5J(\omega_0) + 2J(2\omega_0)] \quad (2)$$

where the first term ($e^2 qQ/h$) is the quadrupole coupling constant, taken to be 170 kHz for an aliphatic C-D, and the J 's are the spectral densities at different frequencies. We note that the spectral densities probe frequencies which are on the order of ω (13.7 MHz) for T_1 , and ω and 0 (indicative of slower motions) for T_2 . The spectral density is the relative amount of motion at a given frequency and is the Fourier transform of the autocorrelation function, $G(\tau, \sigma)$, or:

$$J(\omega) = \int_{-\infty}^{\infty} G(\tau, \sigma) e^{i\omega\tau} d\tau \quad (3)$$

The autocorrelation function embodies the complexity of the decay of motion in the system. We have chosen to represent this with the log-normal distribution of correlation times or:

$$G(\tau, \sigma) = \frac{1}{\pi^{1/2} \sigma \tau_r} e^{-(\ln \tau_r / \sigma + \sigma / 4)^2} \quad (4)$$

where $\tau_r = \tau/\tau_0$. This is the reduced correlation time and is scaled relative to the mean correlation time.

Our experience suggests that the log-normal distribution is suitable for the fitting of the polymer relaxation data. However, we have found that several other models would be similarly successful at fitting the data. Perhaps the original of these, the $\log\chi^2$ distribution, is a skewed distribution originally proposed by Schaefer.⁽⁸⁾ The model, as originally proposed, requires a modification identified by us.⁽⁶⁾ The Hall-Helfand model,⁽⁹⁾ with effectively a short and long correlation time feature, also fits a variety of data including those from adsorbed polymers in contact with solvent.⁽¹⁰⁾ Based on our experience, and the model's formulation, we suspect that the model of deJean de la Batie, et al.⁽¹¹⁾ would also fit the data well. We have stuck with the log-normal distribution because of its simplicity and also because of its apparent ability to fit the physical nature of the problem.

The results of the relaxation time measurements for PEA-d₁, PIPA-d₁, and PNBA-d₁ are shown in Figures 1-3. For PEA-d₁, it can be seen in Figure 1 that the T_1 relaxation times go through minima that move to lower temperatures as the concentrations are decreased. At the T_1 minima the motional rates should be roughly on the order of the Larmor frequency. The T_2 values monotonically decrease as expected with decreasing temperature or increasing concentration. We note that the T_2 data are always shorter than the corresponding T_1 's, as expected, suggesting that the motion of the polymer is neither isotropic or fast. For PIPA-d₁ the situation in Figure 2 is similar, with the relaxation times showing similar trends. For PIPA-d₁, a much broader range of concentrations

was studied. The relaxation times for PIPA-d₁ were also much longer than those corresponding to PEA-d₁. For PNBA-d₁, Figure 3, the same trends were observed with the magnitude of the relaxation times being more like PEA-d₁ than PIPA-d₁.

The results of fitting the relaxation times to the log-normal distribution of correlation times are shown in Figures 4-6. Since PEA-d₁ and PNBA-d₁ had similar relaxation times, we shall examine their behavior first. For PEA-d₁ and PNBA-d₁, the behavior of the mean correlation times (τ_0) shown in Figures 4 and 5 were quite similar in terms of both the correlation times and, consequently, the temperature dependence. In all cases, the temperature dependence is reasonably well described with an exponential function. For PEA-d₁ a different behavior can be seen from 60 to 70 wt % polymer. Above 60 wt%, the apparent energies of activation increase. The values for the width parameter (not shown), σ , were between 2 and 4 for these polymers.

The behavior for PIPA-d₁ was a little more complex, in part because a much wider temperature and concentration range were studied. We note that the scale in Figure 6 is different than in Figures 4 or 5. As expected from the raw relaxation time data, the correlation times for PIPA-d₁ segmental motions are significantly faster than the other two polymers. While a careful look at the data on a larger scale reveals that there is a systematic curvature of the $\log(\tau)$ data with $1/T$, for the purposes of comparison, it is quite reasonable to fit the data to an exponential. A clear demarcation between 40 and 50 wt % in terms of the energy of activation exists. We have previously noted that this concentration likely marks the changeover from semi-dilute to concentrated polymer behavior.⁽⁵⁾ In addition, the width parameters for PIPA-d₁ were in the range of 3 to 7, which is indicative of a narrower distribution.

A comparison of the exponential fits of the mean correlation times for all three polymers as a function of concentration is given in Figure 7. At low concentrations (PIPA-d₁ only) the energies of activation were relatively constant at about 6 kJ/mol. At higher concentrations these values generally increase with concentration in the 10-20 kJ/mol range. At the highest concentration, roughly 90 wt %, the highest energy of activation seems to belong to PIPA-d₁.

It is interesting to compare the current results with other studies. The measured glass transition temperatures (T_g) for the three polymers studied here are 219, 249 and 270 K for PNBA, PEA, and PIPA, respectively.⁽¹²⁾ These values do not seem to be useful for the ordering of the behavior in general. However, it is tempting to suggest that the energies of activation at the highest concentrations 90 wt % correlate with the glass transition temperatures of the bulk polymers. The higher the value of the T_g , the higher the energy barrier for segmental motions is. Thus it is possible that, at 90 wt % polymer, the solutions already appear to have a solid-like component.

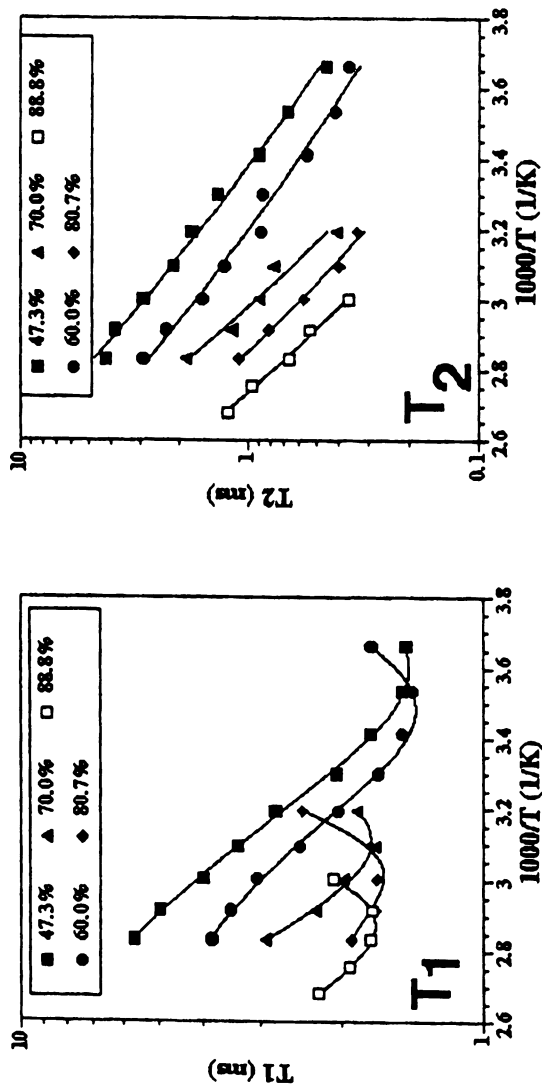


Figure 1. T_1 (\square) and T_2 (\square) relaxation behavior for PEA- d_1 as a function of temperature. Concentrations are given as wt % polymer. The curves are drawn to aid the eye.

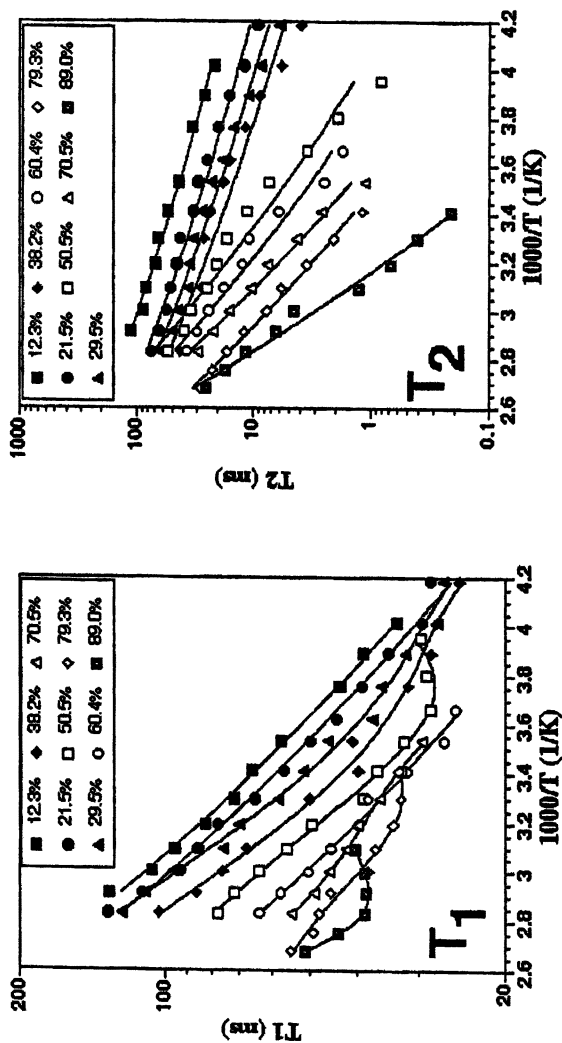


Figure 2. T_1 (t) and T_2 (t) relaxation behavior for PIPA- d_1 as a function of temperature. Concentrations are given as wt % polymer. The curves are drawn to aid the eye.

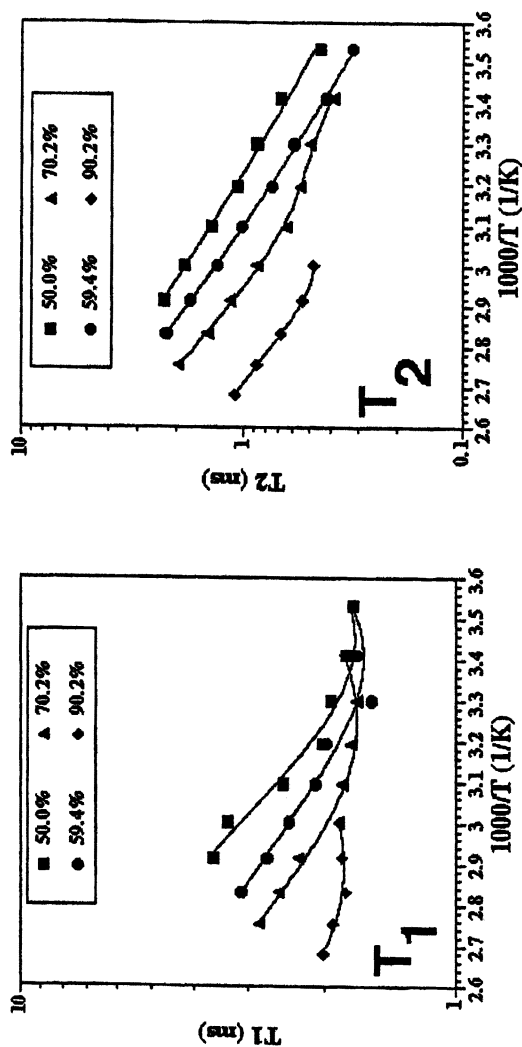


Figure 3. T_1 (μ) and T_2 (τ) relaxation behavior for PNBA- d_1 as a function of temperature. Concentrations are given as wt % polymer. The curves are drawn to aid the eye.

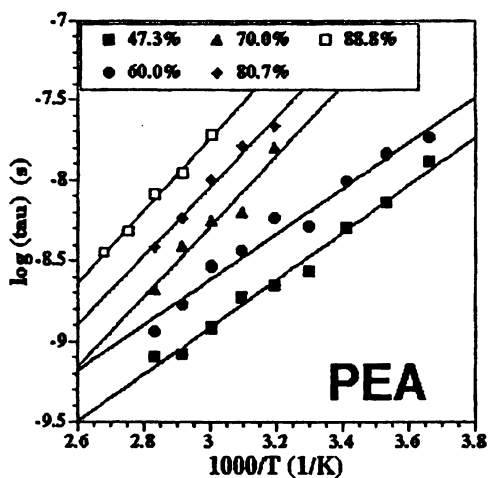


Figure 4. Correlation time results as a function of concentration and temperature for PEA- d_1 .

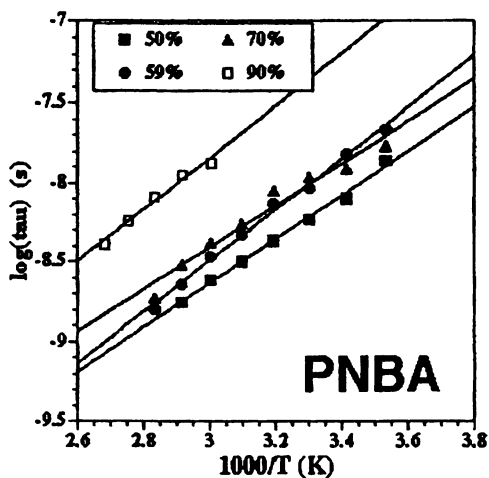


Figure 5. Correlation time results as a function of concentration and temperature for PNBA- d_1 in chloroform.

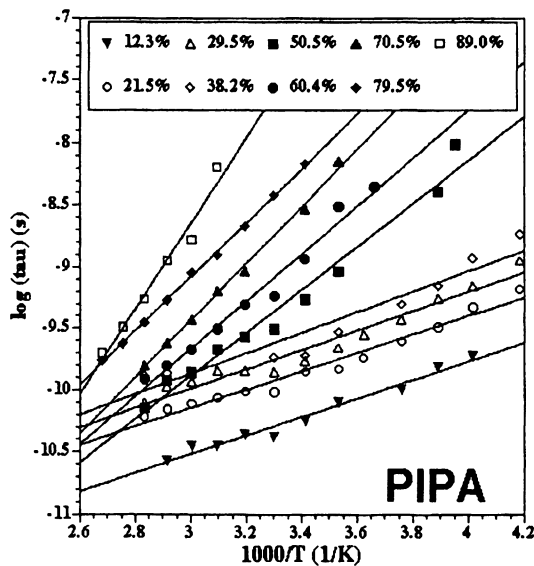


Figure 6. Correlation time results as a function of concentration and temperature for PIPA- d_1 in chloroform.

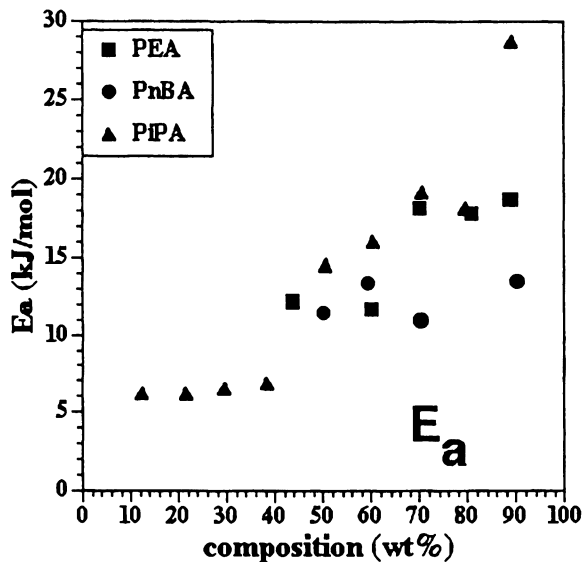


Figure 7. Energies of activation for the three acrylates as a function of composition (wt % polymer).

Conclusions

The log-normal distribution of correlation times can be used to fit the relaxation data from concentrated polymer solutions. The data provide reasonable variations of the mean correlation times with concentration and temperature. Of the systems studied, PIPA-d₁ was found to reorient much more rapidly than either PEA-d₁ or PNBA-d₁. Relatively low energies of activation were found for PIPA-d₁ in semi-dilute solution. These energies of activation increased with concentration and were similar for all three polymers until the highest concentration where the apparent energies of activation scaled with the glass transition temperature of the bulk polymers.

Acknowledgements

The authors acknowledge the financial support of the United States National Science Foundation. The authors also acknowledge the work of Dr. Robert O'Connor for writing the data reduction routines.

References

- 1 Waggoner, R. A.; Blum, F. D. *J. Coat. Technol.* **1989**, *61*(768), 51-56.
- 2 Blum, F. D.; Durairaj, B.; Padmanabhan, A. S. *J. Polym. Sci., Part B: Polym. Phys.* **1986**, *24*, 493-502.
- 3 Heatley, F. *Prog. Nucl. Magn. Reson. Spectrosc.* **1979**, *13*, 47-85.
- 4 Dais, P.; Spyros, A. *Prog. Nucl. Magn. Reson. Spectrosc.* **1995**, *27*, 555-633.
- 5 Blum, F. D.; Durairaj, B.; Padmanabhan, A. S. *Macromolecules* **1984**, *17*, 2837-2846.
- 6 O'Connor, R. D.; Blum, F. D. *Macromolecules* **1994**, *27*, 1654-1656.
- 7 Mathias, L. J.; Colletti, R. F. *Macromolecules* **1991**, *24*, 5515-5521.
- 8 Schaefer, J. *Macromolecules* **1973**, *6*, 882.
- 9 Hall, C. K.; Helfand, E. *Jouranal of Chemical Physics* **1982**, *77*, 3275.
- 10 Liang, M.; Blum, F. D. *Macromolecules* **1996**, *29*, 7374-7377.
- 11 DeJean de la Batie, R.; Laupretre, F.; Monnerie, L. *Macromolecules* **1988**, *21*, 2045-2052.
- 12 Brandup, J.; Immergut, E. H., Eds. *Polymer Handbook*; 3rd ed.; Wiley Interscience; 1989.

Chapter 31

NMR Spectroscopic Study of Ion-Conducting ^{15}N -Labeled Polyphosphazenes

Thomas A. Luther, Mason K. Harrup, and Frederick F. Stewart

Energy and Environmental Sciences, Idaho National Engineering and Environmental Laboratory, P.O. Box 1625, Idaho Falls, ID 83415-2208

To investigate the nitrogen nuclei involvement in metal ion complexation in polyphosphazenes, two ^{15}N labeled polyphosphazenes, ^{15}N poly-[bis(2-(2-methoxyethoxy)ethoxy)phosphazene] (^{15}N MEEP) and ^{15}N poly-[(2-allylphenoxy) $_{0.12}$ (4-methoxyphenoxy) $_{1.02}$ (2-(2-methoxyethoxy)ethoxy) $_{0.86}$]phosphazene] (^{15}N HPP), were studied by NMR spectroscopy (^1H , $^{13}\text{C}\{^1\text{H}\}$, ^{15}N , and ^{31}P) at magnetic field strengths of 7.04 and 17.63 Tesla. The complexation of lithium ion in the polymer matrix was probed by changes in chemical shifts and variable temperature spin-lattice relaxation (T_1) studies. After a 39 mol% addition of lithium trifluoromethanesulfonate (LiOTf), observable changes in chemical shifts are exhibited in the NMR spectra of ^{15}N MEEP in CDCl_3 . The NMR spectra of ^{15}N HPP in CDCl_3 only exhibit changes in the chemical shifts of resonances that correspond to 2-(2-methoxyethoxy)ethoxy pendant groups after addition of 39 mol% LiOTf. Most significantly, a sharp decrease in the ^{15}N NMR minimum T_1 value measured for ^{15}N MEEP reveals that significant lithium ion complexation occurs with the nitrogen nuclei.

Polyphosphazenes are a class of materials that have been studied as solid polymer electrolytes for the past 16 years. The first polyphosphazene shown to have ion conducting properties when complexed with a metal salt was poly[bis(2-(2-methoxyethoxy)ethoxy)phosphazene] (MEEP) (1). The proposed transport mechanism of the metal ions through the MEEP matrix has been modeled on the transport mechanism of metal ions through poly(ethylene oxide) (PEO) (2). This proposed model characterizes the ionic transport in terms of "jumps" between neighboring polymer strands utilizing the lone electron pairs of the oxygen atoms on the side chains and that the backbone nitrogen atoms are not significantly involved (3). This study set out to investigate metal ion complexation in polyphosphazenes by NMR spectroscopy. In particular, the involvement of the nitrogen atoms with the metal ions was explored through changes in chemical shift and variable temperature spin-lattice relaxation (T_1) NMR experiments. Unfortunately, the natural abundance of the spin active ^{15}N nuclei that can be observed by NMR spectroscopy is too low to be effectively studied (natural abundance ^{15}N is only 0.345%). To overcome the natural abundance deficiency, the polyphosphazenes in this study were synthesized from ^{15}N labeled precursors.

Experimental

NMR Spectroscopy. NMR data (^1H , ^{31}P , $^{13}\text{C}\{^1\text{H}\}$, and ^{15}N) were acquired on a Bruker DMX 300WB spectrometer with a magnetic field strength of 7.04 Tesla corresponding to operating frequencies of 300.13 MHz (^1H) 121.49 MHz (^{31}P), 75.48 MHz (^{13}C), and 30.41 MHz (^{15}N). Additional NMR spectra were acquired on a Bruker DMX 750 spectrometer with a magnetic field strength of 17.63 Tesla corresponding to operating frequencies of 750.13 MHz (^1H), 303.66 MHz (^{31}P), 188.64 MHz (^{13}C), and 76.01 MHz (^{15}N). The NMR spectra were referenced internally to TMS (^1H and $^{13}\text{C}\{^1\text{H}\}$) or externally to H_3PO_4 (^{31}P) or to $(^{15}\text{NH}_4)_2\text{SO}_4$ (^{15}N). Spin-lattice relaxation measurements were performed using standard inversion-recovery $180^\circ\text{-}\tau\text{-}90^\circ$ pulse sequence experiments. Variable temperature NMR experiments were conducted using a Bruker DMX 300WB spectrometer equipped with a Bruker BVT 3000 temperature control module. Temperature calibration was accomplished by following the Van Geet methanol calibration method (4).

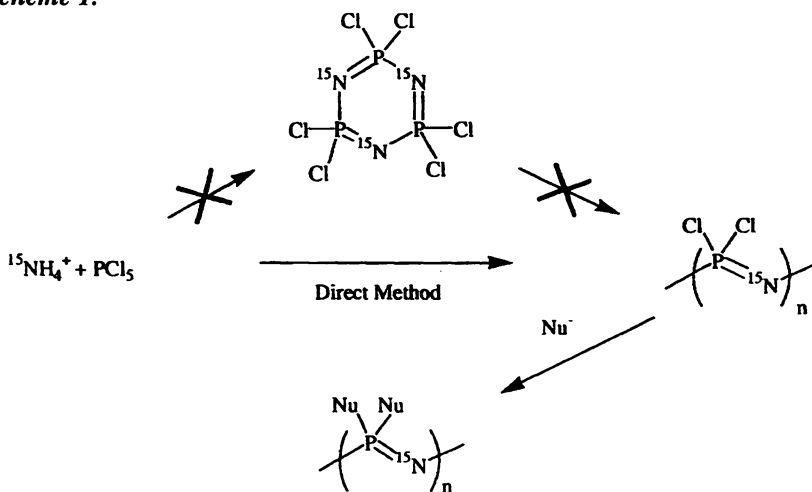
Materials. NMR solvents tetrahydrofuran- d_8 (THF- d_8), D_2O , and chloroform- d (CDCl_3) were obtained from Cambridge Isotope Laboratories. Lithium trifluoromethanesulfonate (LiOTf) was purchased from Aldrich Chemical Co. and used as received. The two isotopically ^{15}N labeled polyphosphazenes

investigated for this work, ^{15}N MEEP and ^{15}N poly(((2-allylphenoxy) $_{0.12}$ (4-methoxyphenoxy) $_{1.02}$ (2-(2-methoxyethoxy)ethoxy) $_{0.86}$)phosphazene] (^{15}N HPP), were prepared from ^{15}N labeled polydichlorophosphazene following published procedures for the unlabeled materials (5-7).

Results and Discussion

Synthesis of ^{15}N Labeled Polyphosphazenes. Linear polyphosphazenes are generally synthesized by a low yielding ring opening polymerization of hexachlorocyclotriphosphazene to generate polydichlorophosphazene followed by substitution reactions utilizing organic nucleophiles to displace the chlorine nuclei (8). The ^{15}N labeled polyphosphazenes in this study were synthesized using an alternate route to generate the polydichlorophosphazene with the backbone nitrogen nuclei fully ^{15}N labeled. The ^{15}N polydichlorophosphazene was formed directly from ammonium sulfate following published procedures using ^{15}N ammonium sulfate in place of ^{14}N ammonium sulfate (Scheme 1) (5). The ^{15}N MEEP and ^{15}N HPP were then prepared from ^{15}N polydichlorophosphazene using sodium salts of 2-(2-methoxyethoxy)ethanol (MEE), methoxyphenol (MeOP), and *o*-allylphenol (*o*-Al) following published procedures for similar unlabeled polyphosphazenes (6, 7).

Scheme 1.



NMR Characterization. The NMR samples were typically prepared with approximately 300 mg ^{15}N MEEP or ^{15}N HPP and 0.5 mL solvent in a 5 mm NMR tube. THF- d_8 , CDCl_3 , and D_2O (^{15}N MEEP only) were used as solvents.

As expected, some solvent effects are exhibited in the solution spectra primarily as a small change in the observed chemical shifts along with some minor resolution differences. The sharpness of the resonances in the ^1H NMR spectrum of ^{15}N MEEP, with THF-d_8 as the solvent, allows for measurable proton-proton coupling of 5.0 Hz.

The ^{15}N NMR spectrum of ^{15}N MEEP at an operating frequency of 30 MHz exhibits a major resonance at δ 63.1 (THF-d_8) with a full-width at half maximum linewidth ($\Delta\nu_{1/2}$) of 75 Hz (Figure 1). A minor resonance in the ^{31}P NMR spectra downfield (0 to -5 ppm region) of the major resonance is also observable in the ^{15}N NMR spectra (δ 71.9). Similar resonances are observed in the ^{31}P and ^{15}N NMR spectra of the related ^{15}N HPP. These downfield resonances are consistent with polymer chain-end effects.

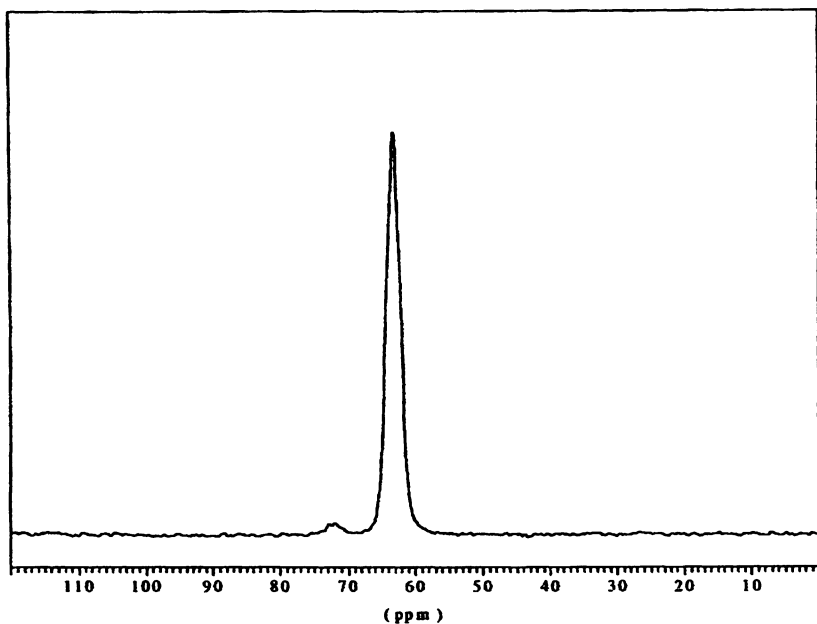


Figure 1. ^{15}N NMR spectrum of ^{15}N MEEP (THF-d_8).

(Reproduced from reference 13. Copyright 2002 American Chemical Society.)

Characterization of ^{15}N HPP as ^{15}N poly[$((2\text{-allylphenoxy})_{0.12}(4\text{-methoxyphenoxy})_{1.02}(2\text{-}(2\text{-methoxyethoxy})\text{ethoxy})_{0.86})\text{phosphazene}$] was accomplished by integration of the ^1H NMR spectrum to determine the relative ratios of the pendant groups (7). The ^{31}P NMR spectrum of ^{15}N HPP acquired at an operating frequency of 121 MHz exhibits three resonances that are due to the phosphorus nuclei that have 2 MEE, 1 MEE and 1 aryloxy (OAr), or 2 OAr pendant groups attached. The resolution of the spectrum at this operating frequency is such that OAr corresponds to either MeOP or *o*-Al. The ^{31}P NMR spectrum acquired at an operating frequency of 304 MHz exhibits further

resolution of these resonances. Two separate resonances are now observed for the phosphorus nuclei with 1 MEE and 1 MeOP versus 1 MEE and 1 *o*-Al pendant groups attached along with a distinct resonance for the phosphorus nuclei with 2 MeOP pendant groups. The only unresolved resonance at this frequency corresponds to the phosphorus nuclei with either 1 MeOP and 1 *o*-Al or 2 *o*-Al pendant groups.

The ^{15}N NMR spectrum of ^{15}N HPP at 30 MHz is a single very broad resonance ($\Delta\nu_{1/2} \sim 260$ Hz). However, the ^{15}N NMR spectrum acquired at 76 MHz exhibits five separate resonances. These resonances arise from the adjacent phosphorus environments that relate the number of OAr pendant groups versus the number of MEE pendant groups attached to the phosphorus nuclei. When both neighboring phosphorus nuclei have two OAr pendant groups attached, the ^{15}N resonance exhibits spin coupling of 40 Hz. As the number of aryloxy pendant groups decrease, the resolution decreases and the chemical shift of the resonance moves further upfield. The resonance that is the furthest upfield has the immediate phosphorus environment similar to MEEP and has an observed chemical shift at approximately 62.3 ppm.

^{13}C NMR Peak Assignment for ^{15}N MEEP. The use of THF- d_8 as a solvent for ^{15}N MEEP has a distinct advantage over the other solvents for structural determination by NMR spectroscopy experiments. The increased resolution and chemical shift dispersity that is evident in the ^1H NMR spectrum also occurs in the $^{13}\text{C}\{^1\text{H}\}$ NMR spectrum. This allows for the unambiguous assignment of the ^{13}C NMR resonances of ^{15}N MEEP via various NMR techniques including two-dimensional proton homonuclear (COSY) and proton-carbon heteronuclear (HETCOR) correlation experiments. The assignments are consistent with the results of NMR spin-lattice relaxation (T_1) experiments where the relaxation times of carbon atoms in flexible side chains increase with distance from the polymer backbone (Figure 2) (9). The assignments agree with published data for the unlabeled MEEP (3).

^{15}N MEEP/Lithium Trifluoromethanesulfonate Complexes. Lithium trifluoromethanesulfonate (LiOTf) was used to study metal ion complexation within the polymer matrices of the ^{15}N polyphosphazenes. LiOTf was added to ^{15}N MEEP in incremental amounts in an NMR tube. Additional NMR spectra were acquired to observe changes in the resonances of the $^{13}\text{C}\{^1\text{H}\}$, ^{31}P , and ^{15}N nuclei. The addition of approximately 100 mol% of LiOTf resulted in no significant change in the chemical shift of the resonance in the ^{31}P NMR spectra with THF- d_8 as the solvent. This indicated that, as expected, the THF- d_8 has the ability to out compete the polymer for solvation of the lithium ions. Since LiOTf is soluble in the polymer matrix but it is not appreciably soluble in CDCl_3 , further NMR experiments were conducted using CDCl_3 . Linear changes in the chemical shift in the resonances of the $^{13}\text{C}\{^1\text{H}\}$, ^{31}P , and ^{15}N NMR spectra were observed for the incremental addition of LiOTf. After a 39

mol% addition of LiOTf to ^{15}N MEEP, the $^{13}\text{C}\{^1\text{H}\}$ NMR chemical shift changes were 0.16 ppm for C1, -0.14 ppm for C2, 0.63 ppm for C3, -0.62 ppm for C4, and -0.01 ppm for C5 (Figure 3). The observed downfield ^{31}P and ^{15}N NMR chemical shift changes were 1.51 and 0.70 ppm respectively (Figures 4 and 5). Amounts greater than approximately 40 mol% addition of LiOTf to either ^{15}N MEEP or ^{15}N HPP in CDCl_3 resulted in incomplete solvation of the metal salt.

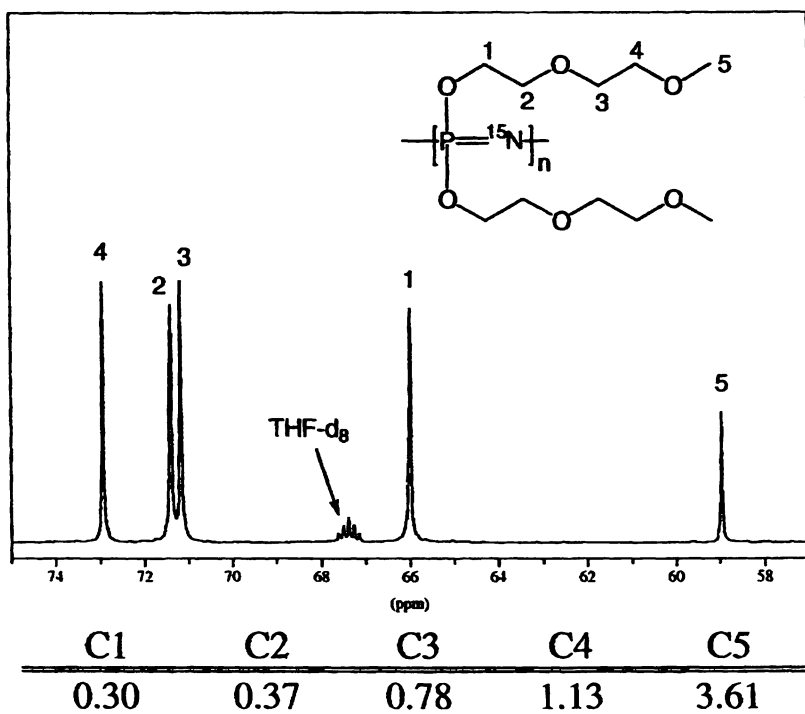


Figure 2. $^{13}\text{C}\{^1\text{H}\}$ NMR spectrum of ^{15}N MEEP (THF-d_8) with carbon peak assignments and $^{13}\text{C}\{^1\text{H}\}$ NMR (CDCl_3 , 75 MHz) room temperature spin-lattice relaxation times (T_1) of ^{15}N MEEP (seconds).

(Reproduced from reference 13. Copyright 2002 American Chemical Society.)

The $^{13}\text{C}\{^1\text{H}\}$ NMR spectra of ^{15}N HPP acquired at 75 and 189 MHz exhibit resolvable resonances for the carbon nuclei in the pendant groups. After a 39 mol% addition of LiOTf, only the C4 resonance of the MEE pendant groups shows a chemical shift change of -0.6 ppm. The other resonances of ^{15}N HPP exhibit smaller chemical shift changes, in the -0.2 to 0.2 ppm range.

After the 39 mol% addition of LiOTf to ^{15}N HPP, the ^{31}P NMR spectrum acquired at 121 MHz shows a chemical shift change of 0.39 ppm for the resonance corresponding to the phosphorus nuclei with 2 MEE pendant groups

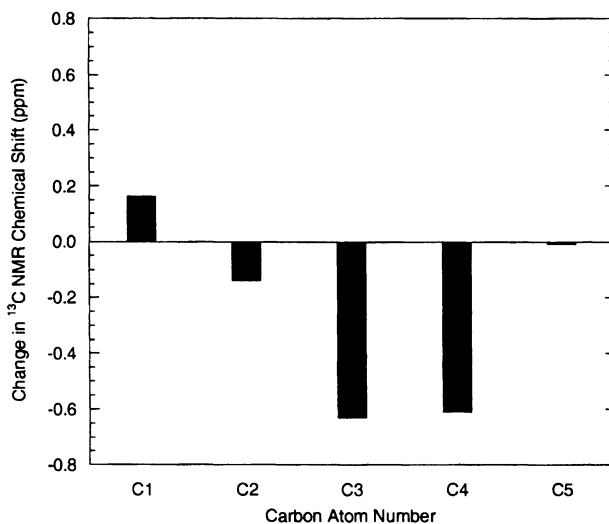


Figure 3. Change in ^{13}C NMR chemical shifts for ^{15}N MEEP in CDCl_3 after lithium ion complexation.

(Reproduced from reference 13. Copyright 2002 American Chemical Society.)

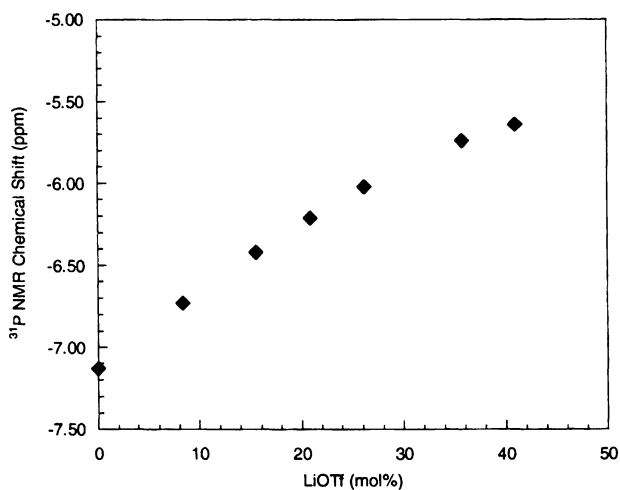


Figure 4. Change in the ^{31}P NMR chemical shift of ^{15}N MEEP (CDCl_3 , 121 MHz) with the addition of LiOTf.

(Reproduced from reference 13. Copyright 2002 American Chemical Society.)

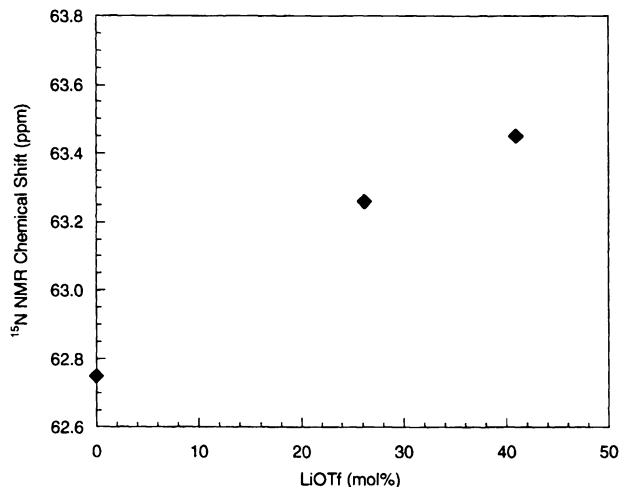


Figure 5. Change in the ^{15}N NMR chemical shift of ^{15}N MEEP (CDCl_3 , 30 MHz) with the addition of LiOTf.
(Reproduced from reference 13. Copyright 2002 American Chemical Society.)

attached (Figure 6). The resonance for the nuclei with 1 MEE and 1 OAr pendant groups exhibits a smaller chemical shift change of 0.17 ppm. There was no significant change in chemical shift for the resonances corresponding to the phosphorus nuclei with 2 OAr pendant groups attached.

In the ^{15}N NMR spectrum of ^{15}N HPP, the 39 mol% addition of LiOTf results in resonance E to shift downfield ~ 1 ppm and the resolution of resonances B-D decreases (Figure 7). The only resonance that does not undergo any observable change is resonance A, which has four OAr pendant groups attached to the two adjacent phosphorus nuclei.

Temperature Dependence of Spin-Lattice Relaxation. The spin-lattice relaxation rate (T_1^{-1}) is comprised of various contributions to the relaxation process, including homo- and heteronuclear dipolar interactions, quadrupolar interactions, chemical shift anisotropy, spin-rotation, and others (10). When the relaxation mechanism is dominated by inter- and intramolecular dipole-dipole interactions, the T_1^{-1} will increase with temperature, pass through a maximum, and decrease with increasing temperature. Since the relaxation rate is the inverse of the relaxation time, the T_1 will decrease, pass through a minimum ($T_{1\text{min}}$), and then increase with increasing temperature (11). The $T_{1\text{min}}$ values are proportional to the internuclear distances.

In the temperature range studied, the $^{13}\text{C}\{^1\text{H}\}$ NMR T_1 data of ^{15}N MEEP in CDCl_3 only exhibit distinct minimum values for carbons C1 and C2, which is approximately 0.11 seconds at 226 K for both nuclei. At the lowest

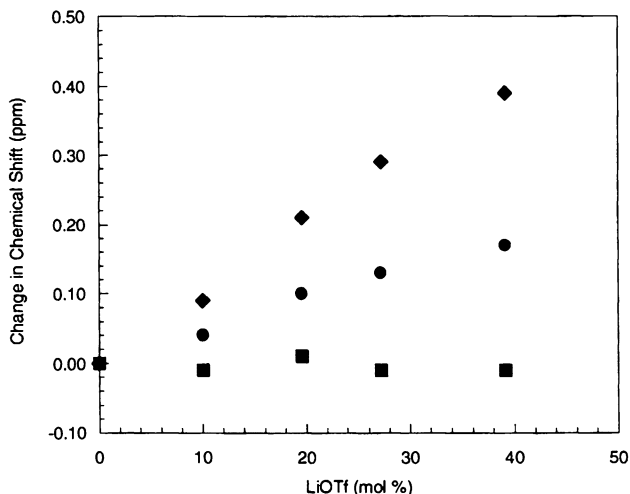


Figure 6. Change in ^{31}P NMR chemical shifts of ^{15}N HPP (CDCl_3 , 121 MHz) with increasing amounts of LiOTf added. The symbols correspond to the following pendant group configurations attached to the phosphorus nuclei: ◆ = $(\text{MEE})_2$, ● = $(\text{MEE})(\text{OAr})$, ■ = $(\text{OAr})_2$. (Reproduced from reference 13. Copyright 2002 American Chemical Society.)

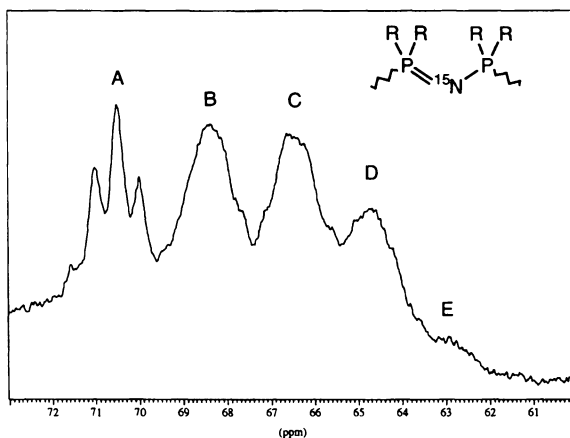


Figure 7. ^{15}N NMR spectrum of ^{15}N HPP after 39 mol% addition of LiOTf (CDCl_3 , 76 MHz). The pendant group assignments for the observed resonances are A: R = 4 OAr, B: R = 3 OAr and 1 MEE, C: R = 2 OAr and 2 MEE, D: R = 1 OAr and 3 MEE, E: R = 4 MEE. (Reproduced from reference 13. Copyright 2002 American Chemical Society.)

temperature recorded (215 K), the T_1 for C3 had reached a constant value of 0.15 seconds. The T_1 values for C4 and C5, 0.16 and 0.58 seconds respectively, were still decreasing with the decrease in temperature.

The complexation of LiOTf to the polymer matrix results in a decrease in the flexibility of the polymer. This decrease in flexibility is evidence by an increase in the glass transition temperature (T_g) values (12, 13). The decrease in flexibility is also observed as an increase in temperature where the $T_{1\min}$ occurs. After the 39 mol% addition of LiOTf, the $T_{1\min}$ values showed the expected increase in temperature, approximately 285 K for all the carbon resonances, except for the C5 resonance. The T_1 values for C5 were still decreasing at the lowest obtainable temperature (1.30 seconds at 262 K). The $T_{1\min}$ values showed increases in relaxation times of approximately 0.04 seconds for C1 and C2, and approximately 0.07 seconds for C3 and C4 (Table I).

Table I. $^{13}\text{C}\{^1\text{H}\}$ NMR $T_{1\min}$ Values of ^{15}N MEEP (CDCl_3 , 75 MHz) before and after LiOTf complexation (Seconds).

	C1	C2	C3	C4	C5
^{15}N MEEP	0.11	0.11	0.15 ^a	0.16 ^a	0.58 ^a
^{15}N MEEP/ Li^+	0.15	0.15	0.22	0.23	1.30 ^a

^a T_1 value still decreasing at the lowest temperature recorded (215 K).

SOURCE: Reproduced with permission from reference 13. Copyright 2002 American Chemical Society.

The ^{31}P NMR T_1 data indicate a $T_{1\min}$ value of 1.55 seconds at 256 K. After the addition of the LiOTf, the $T_{1\min}$ increases to 1.76 seconds at 309 K (Figure 8). The ^{15}N NMR $T_{1\min}$ value decreases with the addition of LiOTf, from approximately 7.5 seconds at 255 K to 5.0 seconds at 300 K (Figure 9). This relaxation rate increase, or $T_{1\min}$ decrease, is consistent with lithium ion coordinating to the nitrogen nuclei and the corresponding heteronuclear and quadrupolar interactions contributing to the relaxation process.

Conclusions

The NMR data for ^{15}N HPP indicate that the solvation energies of the less polar MeOP and *o*-AL pendant groups are not sufficient to successfully compete with the MEE pendant groups for complexation with the lithium ion. However, coordination of the lithium ion in the MEE environments is not limited to the oxygen nuclei on the etherial pendant groups as proposed by the PEO ion transport model for MEEP (3). Examination of the ^{31}P and ^{15}N NMR data reveal that when four MEE pendant groups are attached to the adjacent phosphorus nuclei, a pocket is formed that allows coordination of the lithium ion with the nitrogen nuclei.

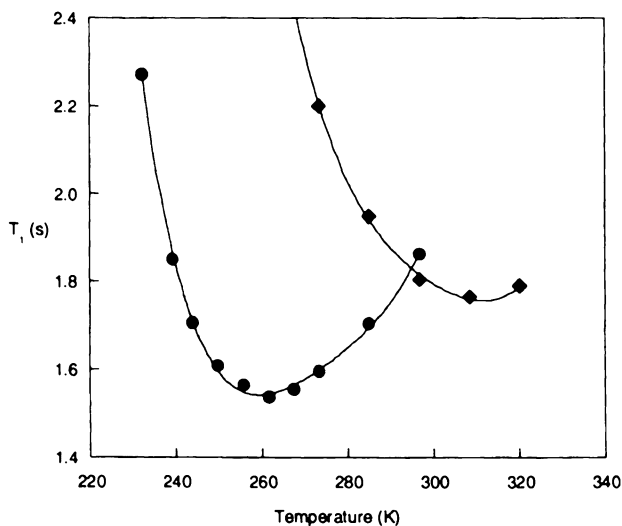


Figure 8. ^{31}P NMR spin-lattice relaxation times of ^{15}N MEEP (CDCl_3 , 121 MHz) before and after lithium ion complexation. The symbols correspond to: ● = ^{15}N MEEP, ◆ = ^{15}N MEEP + LiOTf. (Reproduced from reference 13. Copyright 2002 American Chemical Society.)

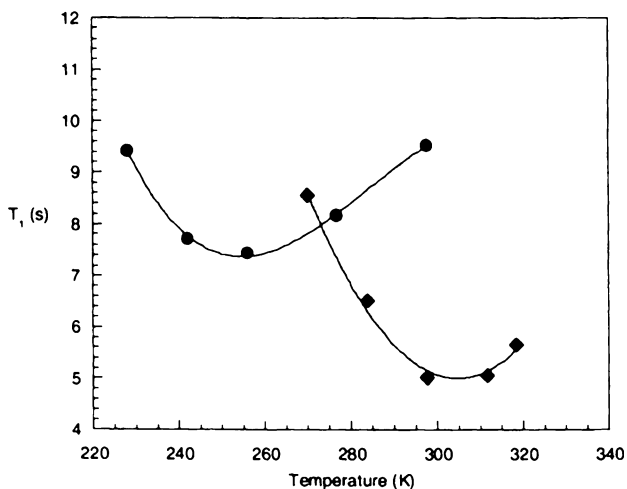


Figure 9. ^{15}N NMR spin-lattice relaxation times of ^{15}N MEEP (CDCl_3 , 30 MHz) before and after lithium ion complexation. The symbols correspond to: ● = ^{15}N MEEP, ◆ = ^{15}N MEEP + LiOTf. (Reproduced from reference 13. Copyright 2002 American Chemical Society.)

Changes in the chemical shifts in the ^{15}N and ^{31}P NMR spectra of ^{15}N MEEP following lithium ion addition are consistent with lithium ion complexation with the etherial oxygen nuclei or the nitrogen nuclei of the polyphosphazene backbone. The sharp decrease in the ^{15}N NMR $T_{1\text{min}}$ value measured for ^{15}N MEEP reveals that significant lithium ion complexation preferentially occurs with the nitrogen nuclei rather than the oxygen nuclei.

Acknowledgements

The authors thank Dr. Tom Pratum for his assistance with the Bruker DMX 750 NMR Spectrometer at the University of Washington. The work described in this paper was supported by the United States Department of Energy through contract DE-AC07-99ID13727.

References

- (1) Blonsky, P. M.; Shriver, D. F.; Austin, P.; Allcock, H. R. *J. Am. Chem. Soc.* **1984**, *106*, 6854-6855.
- (2) Ratner, M. A.; Shriver, D. F. *Chem. Rev.* **1988**, *88*, 109-124.
- (3) Allcock, H. R.; Napierala, M. E.; Olmeijer, D. L.; Best, S. A.; Merz, K. M. *Macromolecules* **1999**, *32*, 732-741.
- (4) Van Geet, A. L. *Analytical Chemistry* **1970**, *42*, 679-680.
- (5) Allen, C. W.; Hneihen, A. S. *Phosphorus Sulfur Silicon Relat. Elem.* **1999**, *146*, 213-216.
- (6) Harrup, M. K.; Stewart, F. F. *J. Appl. Polym. Sci.* **2000**, *78*, 1092-1099.
- (7) Stewart, F. F.; Harrup, M. K.; Luther, T. A.; Orme, C. J.; Lash, R. P. *J. Appl. Polym. Sci.* **2001**, *80*, 422-431.
- (8) Mark, J. E.; Allcock, H. R.; West, R. *Inorganic Polymers*; Prentice Hall: Englewood Cliffs, New Jersey, 1992.
- (9) Krajewski-Bertrand, M.-A.; Lauprêtre, F.; Monnerie, L. *Dynamics of Solutions and Fluid Mixtures by NMR*; John Wiley & Sons: Chichester, 1995.
- (10) Günther, H. *NMR Spectroscopy: Basic Principles, Concepts, and Applications in Chemistry*; Second ed.; John Wiley & Sons: Chichester, 1995.
- (11) Desrosiers, P. J.; Cai, L. H.; Lin, Z. R.; Richards, R.; Halpern, J. *J. Am. Chem. Soc.* **1991**, *113*, 4173-4184.
- (12) Allcock, H. R.; Napierala, M. E.; Cameron, C. G.; O'Connor, S. J. M. *Macromolecules* **1996**, *29*, 1951-1956.
- (13) Stewart, F. F.; Singler, R. E.; Harrup, M. K.; Peterson, E. S.; Lash, R. P. *J. Appl. Polym. Sci.* **2000**, *76*, 55-66.
- (14) Luther, T. A.; Stewart, F. F.; Budzien, J. L.; LaViolette, R. A.; Bauer, W. F.; Harrup, M. K.; Allen, C. W.; Elayan, A. "On the Mechanism of Ion Transport Through Polyphosphazene Solid Polymer Electrolytes I: NMR, IR, and Raman Spectroscopic Studies and Computational Analysis of ^{15}N -Labeled Polyphosphazenes," *J. Amer. Chem. Soc.*, Submitted for Publication, 2002.

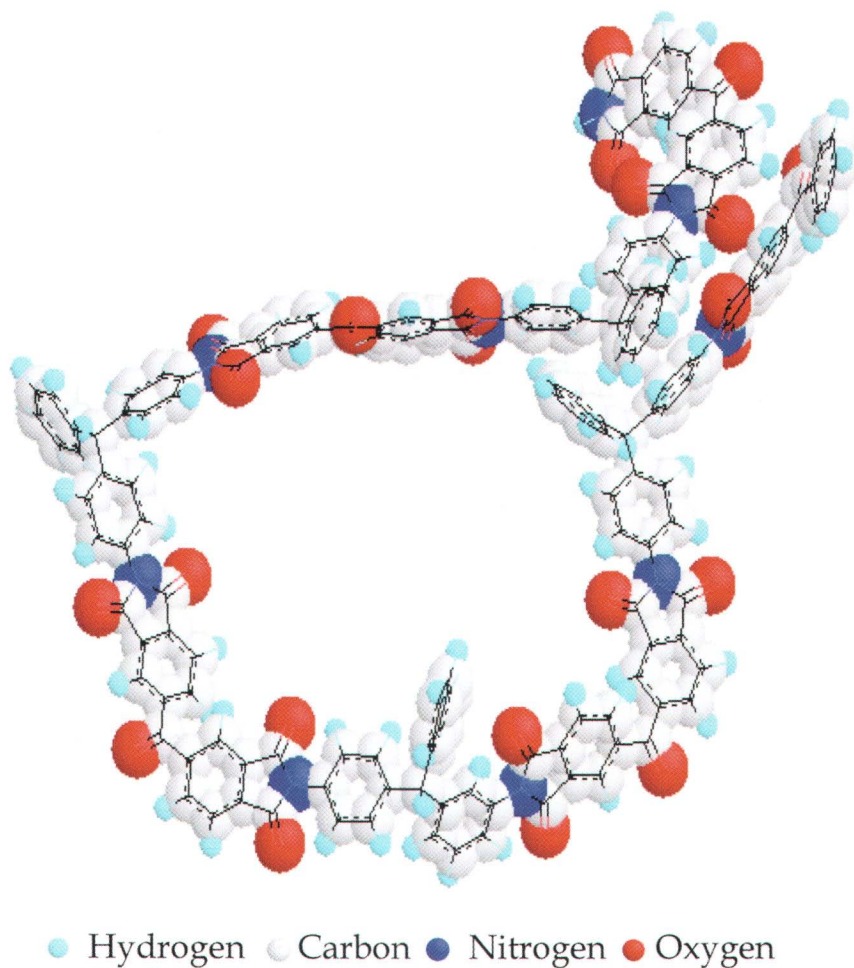


Plate 1. Minimum-energy geometry obtained after a geometry optimization for BZP-TPM with five repeating units.

Author Index

- Andrews, Gavin P., 216
Asakura, Tetsuo, 71
Ashida, Jun, 71
Assemat, Olivier, 123
Baianu, I. C., 298
Battiste, John L., 179
Bertoniere, Noelle R., 306
Beshah, Kebede, 344
Blum, Frank D., 398
Brar, A. S., 166, 174
Brickhouse, Mark, 325
Brown, Gavin M., 289
Bush, C. Allen, 272
Busico, V., 192
Chai, Minghui, 137, 147
Cheng, H. N., 3, 382
Cholli, Ashok L., 58, 258
Chûjô, Riichirô, 83, 208
Cui, Min-Hui, 228
Durairaj, Raj B., 398
English, Alan D., 3
Fawcett, Allan H., 216
Fenelli, Steven P., 228
Fukutani, Kyoko, 83
Grates, John A., 228
Hania, Majid I. M., 216
Harrup, Mason K., 409
Hiller, Wolf, 338
Hu, Sanlin, 137
Huckerby, Thomas N., 289
Jacob, Monsey M., 58
Kaur, M., 174
Koivula, Michael N., 179
Kumar, Jayant, 58, 258
Kumar, R., 174
Lauder, Robert M., 289
Li, Lian, 58
Likhatchev, Dmitri, 242
Liu, Wei, 258
Lu, J., 43
Luther, Thomas A., 409
Magoshi, Yoshiko, 83
Mannina, L., 192
Martínez-Richa, Antonio, 242
Maskos, Karol, 306
Mirau, Peter A., 22, 43
Montaudo, Maurizio S., 358
Neiss, Thomas G., 382
Newmark, Richard A., 179
Nieduszynski, Ian A., 289
Niemczura, Walter P., 306
Nojima, S., 43
Ozu, E. M., 298
Pasch, Harald, 338
Puapaiboon, Uraivan, 147
Rinaldi, Peter L., 94, 123, 137, 147
Sachinvala, Navzer (Nozar) D., 306
Sahoo, Sangrama K., 258
Saito, Masayoshi, 208
Samuelson, Lynne, 258
Segre, A. L., 192
Shimozawa, Kenichi, 208
Stewart, Frederick F., 409
Taylor, Richard T., 147

- Thakur, Khalid, 32
Tonelli, A. E., 43
Van Axel Castelli, V., 192
Vera-Graziano, Ricardo, 242
Vigo, Tyrone L., 306
Wang, Huiming, 325
Werner, Mark, 228
Winsor, David L., 306
- Wu, Jian, 344
Xu, Qiuwei, 325
Yadav, A., 174
Yamane, Tsutomu, 71
Yang, Nan-Loh, 228
Yang, Shu, 22
Yang, Suizhou, 58
Zhang, Yuli, 228

Subject Index

A

Acrylic acid. *See* Acrylonitrile

copolymers

Acrylonitrile copolymers

acrylonitrile/acrylic acid (A/B), 171, 173

acrylonitrile/glycidylmethacrylate (A/G), 169, 171

acrylonitrile/methyl methacrylate (A/M), 167, 169

2D double quantum filtered

correlated spectroscopy (DQFCOSY) spectrum of A/B in DMSO- d_6 , 172*f*

2D NMR techniques, 167

inverse-HETCOR spectrum of A/G, 170*f*

methylene region of inverse-HETCOR spectrum of A/M, 168*f*

Addition polymers, solution NMR, 9

Adonitol, ester oligomers, 223, 225*t*

Alginates

commercial samples Protonal LFR, Sigma NaAlginate, and Manegel LMW, 386

contributions of components to each polymer, 392*t*

coupling chromatographic separations with NMR, 383–384

description, 383

diad and G-centered triad intensities for unfractionated, 390*t*

diad and triad fractions measurement, 386

diad and triad intensities for, fractions using size exclusion chromatography (SEC)–NMR, 391*t*

enzymatic action, 393

equation for intensity of diad or triad sequences, 388

experimental, 384–386

hyphenated NMR analysis, 394

Markovian model, 388, 390*t*

microstructure by solution NMR, 383

NMR analysis of whole samples, 390*t*

NMR spectroscopy, 386, 388

NMR spectroscopy method, 385–386

pullulan calibration curve for SEC analysis of, 387*f*

SEC chromatogram of Protonal LFR, 387*f*

size exclusion chromatography (SEC), 384–385

solution ^{13}C NMR spectrum of Manegel LMW, 389*f*

solution ^1H NMR spectrum of Protonal LFR, 389*f*

statistical analysis, 388, 390, 393

two-component 1st order Markovian statistical analysis of fraction data, 392*t*

Allylcellulose, substituted. *See*

Cellulose ethers

Amorphophallus konjac K. Koch, gelling, 298

Archeological silk

composition, 84

correlation between initial compliance (A), initial tensile strength (B), A/B ratio, and reciprocal spin-lattice relaxation time (T_1) for fresh silk, 86*f*

correlation between ratio A/B with T_1 for fresh silk fabrics with and without dyestuff and mordant, 89*f*

- direct or indirect physical property measurements, 84
- effect of paramagnetic impurities on T_1 , 87
- estimation of physical properties of preserved silk fabrics, 91
- experimental verification of fluctuation-dissipation theorem, 85–87
- Konjikido hall in Chusonji Temple, 84–85
- left and right problem, 84–85, 91
- logarithmic free induction decay curve of fresh silk fabric and corresponding degraded sample, 88*f*
- relationship between temperature index and ratio A/B for samples preserved in Chusonji Temple, 90*f*
- samples from ancient times, 83–84
- Articles, NMR spectroscopy, 3–4
- Atomic bond distances, optimized polyimide, 255*t*
- Azocellulose polymers
- assignments for 4-cyanophenylazophenol in CP/MAS NMR, 62
 - assignments for cellulose samples, 62, 64
 - assignments for samples AZOEST21 and AZOEST49, 62–63
 - atomic force microscopy (AFM) images showing 3D views of SRGs, 68*f*, 69*f*
 - characteristic peaks of azocellulose from Mitsunobu reaction, 66–67
 - characterization methods, 61
 - CP/MAS spectra of cellulose, AZOVIS69, and 4-cyanophenylazophenol, 64*f*
 - cross polarization/magic angle spinning (CP/MAS) spectra of cellulose, AZOEST21, AZOEST49, and 4-cyanophenylazophenol, 63*f*
 - experimental conditions for synthesis via Mitsunobu, 62*t*
 - FTIR spectra of cellulose, AZOEST21, AZOEST49, and 4-cyanophenylazophenol, 65–66
 - low molecular weight cellulose and azocellulose vs. ultrahigh molecular weight cellulose and azocellulose, 65
 - materials, 59–60
 - photoinduced surface relief gratings (SRGs), 59
 - SRG fabrication, 61
 - SRG on films of, 67
 - synthesis by Mitsunobu reaction, 60
- B**
- Biopolymers. *See* Glucomannan polysaccharides (GP); Keratan sulfates; Polysaccharides
- Bipolar gradient pulses stimulated echo sequence (BPPSTE)
- diffusion, 348, 350
 - proton NMR of complex polymer mixture before and after BPPSTE, 349*f*
 - schematic, 349*f*
 - technique, 346–347
 - See also* On-line liquid chromatography–NMR (LC–NMR)
- Bis(cyclopentadienyl)TiCl₂, poly(propylene), 195, 196
- Block copolymers. *See* On-line liquid chromatography–NMR (LC–NMR); Poly(ϵ -caprolactone) (PCL) and inclusion complexes (ICs)
- Bombyx mori* silk fibroin
- ¹³C CP/MAS NMR of model compounds, 78*f*

- ^{13}C CP/MAS spectrum of (AlaGly)₁₅ 30 mer, 74f
- ^{13}C solution NMR spectrum, 74f
- circular dichroism (CD) spectra, 79f
- experimental, 72–73
- experimental and simulated 2D spin-diffusion NMR spectrum of labeled (AlaGly)₁₅ 30 mer, 75f
- ^1H -coupled and decoupled spectra of carbonyl carbons for Gly residue vs. concentration, 81f
- helical (silk I) content of, as function of concentration, 80f
- intramolecular hydrogen bonds, 76
- model compounds for characterizing structure of peptides, 77–78
- NMR methods, 73
- origin of stability of, in water, 77–79
- peptide synthesis, 72–73
- repeated β -turn type II-like structure, 76f
- silk I structure in solid state, 73, 76–77
- solution structure of silk fibroin, 79–81
- Bond distances, optimized polyimide, 255t
- Books, NMR spectroscopy, 3–4
- Branched polymers. *See* Polyesters
- Buddhist temple. *See* Archeological silk
- Butyl acrylate (BA). *See* Copolymer characterization; On-line liquid chromatography–NMR (LC–NMR); Polyacrylates
- C**
- Carbohydrate, numbering system, 314f, 315f
- Cartilage, 2D NMR of human fetal, 293–295
- Catalysts, poly(propylene), 193
- Cationic copolymerization. *See* Trioxane/1,3-dioxepane (TOX/DOP) copolymerization
- Cellulose
- commercial samples, 59–60
- cross polarization and magic angle spinning (CP/MAS) spectra, 62–65
- description, 59
- Mitsunobu reaction for azocellulose polymers, 60
- See also* Azocellulose polymers; Cellulose ethers; Ethylcellulose (EC)
- Cellulose acetate butyrate (CAB)
- chemical shifts, assignments, and relaxation times, 181t
- heteronuclear correlations, 180
- Cellulose ethers
- carbohydrate and ether appendage numbering system, 314f, 315f
- chemical shift assignments for 2,3,6-tri-O-methylcellulose (**2**), 316, 320f
- chemical shift assignments for tri-O-allyl- and tri-O-crotyl- celluloses, 321t
- comparing coupling constant in polymer **2** with other cellulose and glucose derivatives, 320t
- COSY spectrum of polymer **2**, 318f
- focus of research, 306–307
- ^1H and ^{13}C NMR of **2**, 317f
- HMBC spectrum of polymer **2**, 318f
- HMQC spectrum of polymer **2**, 319f
- methods for making chemical shift assignments, 316
- nomenclature system for chemical shift assignments, 313, 316
- opportunities, 322
- 6-phenyl-6-deoxy-2,3-di-O-methylcellulose (**9**) synthesis, 309–310
- physical characteristics, 310–314
- physical characteristics of **2**, 310

- physical characteristics of 2,3-di-O-methylcellulose (7), 313
- physical characteristics of tri-O-allylcellulose (3), 310, 312
- physical characteristics of tri-O-crotylcellulose (4), 312
- physical characteristics of 6-bromo-6-deoxy-2,3-di-O-methylcellulose (8), 313
- physical characteristics of 6-O-trityl-2,3-di-O-methylcellulose (6), 313
- physical characteristics of 6-O-tritylcellulose (5), 312
- physical characteristics of 9, 313
- physical properties of polymers 2–9, 311*t*
- proton and carbon assignments of 6-phenyl-6-deoxy-2,3-di-O-methyl-1,4-anhydroglucose repeat unit, 321*t*
- reagents and yields, 307
- scale-ups, 322
- syntheses of 3 and 4, 309
- synthesis, 308*f*
- synthesis of 2, 307
- synthesis highlights, 307, 309–310
- Chain-end structure
- 2D NMR spectra of polystyrene with phosphorus-containing chain ends, 16*f*
- identification, 95
- one-dimensional ^1H , ^{13}C , and ^{31}P NMR spectra of polystyrene with phosphorus-containing chain ends, 115*f*
- polybutadiene with Sn-containing chain ends, 113, 114*f*
- poly(propylene), 206
- three-dimensional NMR, 113, 114*f*
- See also* Polymer characterization
- Chemical shift anisotropy (CSA)
- lab frame orientation dependent CSA, 35*f*
- rigid and semi-rigid materials, 33
- Chemical shifts
- cellulose ether, 320*t*, 321*t*
- methods for making assignments, 316
- nomenclature system for assignments, 313, 316
- prediction, 8
- solution NMR, 33
- Chloroform. *See* Polyacrylates
- Chusonji Temple
- preserved silk fabrics, 84–85
- See also* Archeological silk
- Circular dichroism (CD), *Bombyx mori* silk fibroin, 79–80
- Coherence selection, pulsed field gradients (PFG), 101–102
- Combined rotation and multi-pulse (CRAMPS), NMR technique, 11
- Complex polymer mixtures. *See* On-line gel permeation chromatography–NMR (GPC–NMR); On-line liquid chromatography–NMR (LC–NMR)
- Composites
- studying formation, 24
- See also* Ethylene oxide/propylene oxide composites
- Computer-assisted methods, NMR, 7
- Condensation polymers, solution NMR, 9
- Conformation, polymer, NMR techniques, 11–12
- Conformational analysis
- NMR methods, 7
- polyimides, 247, 250–252
- COPOFRAC. *See* Copolymer characterization
- Copolymer characterization
- comparison between theory and experiment, 379*f*
- compositional distribution for sample MB41, 369, 370*f*
- compositional distribution for sample SH91, 371–372, 373*f*
- COPOFRAC computer program, 363

- COPOFRAC generating
compositional distribution, 371–372
- COPOFRAC predicting change in composition with chain length, 378
- COPOFRAC predicting change in composition with volume of fraction, 378
- COPOFRAC predicting polydispersity index vs. volume fraction, 377*f*, 378
- copolymer MB41 of methyl methacrylate (MMA) and butyl acrylate (BA), 368–369
- copolymer sample M30 of styrene (St) and MMA, 372
- copolymers SH91 and SH78 of St and maleic anhydride (MAH), 369, 371–372
- experimental, 363–365, 368
- ¹H NMR spectrum for sample MB41, 370*f*
- MALDI of fractions of sample M30, 376*f*
- mass coelution effect in size exclusion chromatography (SEC), 360–361
- materials, 363
- matrix assisted laser desorption/ionization–time of flight (MALDI–TOF) mass spectra method, 368
- NMR as detector for SEC, 359
- NMR calculations, 364–365
- NMR measurements, 364
- off-line SEC–NMR, 359, 360
- SEC fractionation for M30, 374*f*, 375*f*
- SEC fractionation method, 364
- SEC–MALDI and SEC–NMR data for copolymer MB41, 366*t*
- SEC–MALDI and SEC–NMR data for copolymer SH91, 367*t*
- SEC theory, 361–363
- Copolymers
HPLC–NMR of random styrene–ethyl acrylate, 340, 343*f*
See also Acrylonitrile copolymers; Ethylene oxide/propylene oxide composites; On-line liquid chromatography–NMR (LC–NMR); Poly(ε-caprolactone) (PCL) and inclusion complexes (ICs); Trioxane/1,3-dioxepane (TOX/DOP) copolymerization
- Correlation time. *See* Polyacrylates
- Coupling
dipolar, in polysaccharides, 282–284
scalar, in polysaccharides, 286
- p*-Cresol
¹H NMR spectrum of reaction mixture, 268*f*
polymerization, 266–267
residual monomer and dimers as function of H₂O₂, 268*f*
See also Poly(phenols)
- Crosslinked polymers
solid state NMR, 37–38
See also Solid state NMR, high temperature
- Cross polarization and magic angle spinning (CP/MAS)
cellulose, azocellulose polymers, and 4-cyanophenylazophenol, 62–65
NMR technique, 11–12
poly(ε-caprolactone) and inclusion complexes with cyclodextrin, 46*f*
See also Azocellulose polymers
- Crotylcellulose, substituted. *See* Cellulose ethers
- 4-Cyanophenylazophenol
cross polarization and magic angle spinning (CP/MAS) spectra, 62, 63*f*, 64*f*
See also Azocellulose polymers
- Cyclodextrins (CDs)
forming inclusion complexes, 44
See also Poly(ε-caprolactone) (PCL) and inclusion complexes (ICs)

D

Decoupling

comparing modulation schemes, 129, 130*f*

fluoropolymers, 127, 129

WURST sequence, 126

Dendrimers

slices of 3D NMR spectrum of carbosilane dendrimer using coherence transfer delays, 112*f*

structure by 3D NMR, 110

structure of second generation carbosilane-based, 111*f*

unique properties, 148

See also Polyurethane-based dendritic wedges

Deuterium labels. *See* Polyacrylates

4,4'-Diaminotriphenylmethane (DA-TPM). *See* Polyimides

Dielectric constant

applications for low, 22–23

designing films for low- k applications, 29–30

See also Ethylene oxide/propylene oxide composites

Diethylphthalate (DEP)

effect on α parameter, 210, 212*f*

effect on ω parameter, 212*f*, 214

internal donor, 211*t*

See also Propylene polymerization

Diffusion, NMR method, 8

Diffusion-ordered spectroscopy (DOSY), 2D NMR method, 8

1,1-Difluoroethylene. *See*

Fluoropolymers

Dimethyl malonate. *See* Polyesters

Di-*n*-butylphthalate (DBP)

effect on ω parameter, 213*f*, 214

internal donor, 211*t*

See also Propylene polymerization

1,3-Dioxepane (DOP). *See*

Trioxane/1,3-dioxepane

(TOX/DOP) copolymerization

Dioxolane (DOL). *See* Trioxane/1,3-dioxepane (TOX/DOP) copolymerization

Dipolar couplings

lab frame orientation dependent, 35*f*

polysaccharides, 282–284

rigid and semi-rigid materials, 33

Dipolar information, wideline

separation NMR (WISE), 13

Distortionless enhancement by polarization transfer (DEPT)

NMR technique, 167

pulse sequence, 182

Di-substituted cellulose ethers. *See*

Cellulose ethers

Double quantum filtered correlated spectroscopy (DQF-COSY)

acrylonitrile/acrylic acid copolymer, 172*f*

ethylcellulose, 329

experiment, 328

NMR technique, 166, 171

Dynamics

behavior of inclusion complexes, 48, 54

molecular motion in polymer solutions, 399

NMR techniques for polymer, 12–13

See also Polyacrylates

E

Enzymatic polymerization. *See*

Poly(phenols)

Enzymes

alginate, 393

cleavage of keratan sulfates, 291–292

routes to fragmentation, 292

See also Keratan sulfates

Erythritol

ester oligomers, 223, 225*t*

malonic ester system, 222–223, 224*f*

succinate system, 223, 224*f*

See also Polyesters

- Ester links
 chemistry, 217–219
See also Polyesters
- Ether appendage, numbering system, 314*f*, 315*f*
- Ethers. *See* Cellulose ethers
- Ethyl acrylate. *See* Polyacrylates;
 Styrene–ethyl acrylate copolymers
- Ethylcellulose (EC)
 annotated proton NMR spectrum, 327*f*
 applications and properties, 326
¹³C NMR spectra of acid hydrolyzed EC side chain methylene carbons, 332*f*
 degree of substitution (DS) by Sealed-Tube Zeisel (STZ) technique, 329
 2D NMR analysis of, 328–332
 2D NMR analysis of acid hydrolyzed EC, 332–333
 double quantum filtered correlated spectroscopy (DQF–COSY), 328
 experimental, 326, 328
 heteronuclear multiple bond correlation (HMBC), 328
 heteronuclear multiple quantum coherence (HMQC), 328
 HMQC and HMBC correlation spectra of acid catalyzed EC, 334*f*
 HMQC and HMBC spectra overlaid, 330*f*
 HOHAHA (homonuclear Hartmann–Hann) experiments, 328
 HOHAHA of EC polymer, 331*f*
 identification of proton correlation, 329, 330*f*
 NMR measurements, 326, 328
 preparation of acid hydrolyzed EC, 326
 relative ethyl substitution, 331
 relative positional DS of acid-catalyzed EC, 333, 335*f*
 relative positional DS of intact, 331*t*
 section of cross peaks in HOHAHA spectrum of EC hydrolysate, 335*f*
 structure, 327*f*
rac-Ethylenebis(4,5,6,7-tetrahydro-1-indenyl)-ZrCl₂, poly(propylene), 195, 196
- Ethylene oxide/propylene oxide composites
 2D exchange spectrum of 50:50 mix of methyl silsesquioxane:copolymer L101, 29*f*
 choosing polymer and matrix components, 24–25
 comparing 2D exchange spectra of methyl silsesquioxane cross peaks with equilibrium spectra, 30*f*
 copolymers (triblocks) L101, P103, and F88, 23
 designing films for low-*k* applications, 29–30
 effect of solvent loss, 27
 effect of temperature on proton NMR spectra of P103 in water, 26*f*
 intermolecular interactions, 28–29
 low-*k* film preparation, 26–27
 maintaining miscibility with cure, 27–28
 methods and materials, 23–24
 NMR spectra of neat methyl silsesquioxane, L101, and 50:50 mix, 28*f*
 precursors to ultra low-*k* films, 23
 schematic showing casting and curing of ultra low dielectric constant films, 24*f*
 self-assembly in solution, 25–26
 solution and solid state silicon NMR of methyl silsesquioxane, 25*f*
 solution NMR for composite formation in mixtures with methyl silsesquioxane, 24
 solution NMR spectrum of 50:50 methyl silsesquioxane:P103 mixture, 27*f*

structure formation and
intermolecular interactions, 30–31
External donors. *See* Propylene
polymerization

F

Fetal cartilage, 2D NMR of human,
293–295
Fibers. *See* Archeological silk
Flexibility
polypeptides, 273, 274*f*
See also Polysaccharides
Fluctuation-dissipation theorem
direct or indirect measurements,
84
experimental verification, 85–87
Fluoropolymers
applications and properties, 124
 ^{13}C NMR spectrum of PVH, CF_n
region, 130*f*
 ^{13}C NMR spectrum of PVH, CH_2
region, 132*f*
comparing decoupler modulation
schemes, 129, 130*f*
decoupling, 127, 129
decoupling sequence, 126
1,1-difluoroethylene (V) and
1,1,2,3,3,3-hexafluoropropylene
(H) monomers, 126
expansions from $^{19}\text{F}\{^{13}\text{C}\}$ -pulsed
field gradient heteronuclear single
quantum coherence (PFG–HSQC)
spectra of PVH, 133*f*
 ^{19}F NMR spectrum of PVH, 129*f*
HSQC experiment, 134
materials, 124
method for ^{19}F spectra using PFG–
HSQC sequence, 125–126
most probable structures from
polymerization of V and H, 128*f*
multidimensional NMR, 131, 134
NMR measurement methods, 125–
126

one-dimensional ^{19}F NMR spectrum,
127, 129*f*
one-dimensional NMR method, 125
polymer structure, 126–127
pulse sequence diagram from
 $^{19}\text{F}\{^{13}\text{C}\}$ -PFG–HSQC experiment,
132*f*

Fourier transform infrared (FTIR),
cellulose, azocellulose, and 4-
cyanophenylazophenol, 65–66

Fractals

^{13}C NMR spectrum of acetate-
fringed, 227*f*
 ^{13}C NMR spectrum of succinic acid-
fringed, 227*f*
forms of polyesters, 225–226
reaction with succinic anhydride, 226
See also Polyesters

Fragmentation, keratan sulfates, 292–
293

Free induction decay (FID), process
for generating, in FT–NMR, 34*f*

G

Gel permeation chromatography
(GPC). *See* On-line gel permeation
chromatography–NMR (GPC–
NMR)

Gelation

glucomannan polysaccharides (GP),
298–299, 301, 305
schematic of gel networks in GP,
303*f*

Glucomannan polysaccharides (GP)
addition of
ethylenediaminetetraacetic acid
(EDTA), 301

^{13}C chemical shift assignments of
oligosaccharides, 302*t*
gelling mechanisms, 301, 305
interaction with proteins, 301
infrared (IR) spectroscopy, 299
konnyaku flour, 298–299

- materials and methods, 299
 near IR (NIR) spectrum, 304*f*
 NMR spectroscopy and relaxation, 299
 oligosaccharides by partial hydrolysis, 300*t*
 pulsed NMR measurements of transverse water relaxation, 301
 schematic of gel networks, 303*f*
 Glutaric acid, ester oligomers, 223, 225*t*
 Glycerol
 ester oligomers, 223, 225*t*
 system with dimethyl malonate, 220, 221*f*
See also Polyesters
 Glycidyl methacrylate. *See* Acrylonitrile copolymers
 Glycosaminoglycan (GAG). *See* Keratan sulfates
 Gold Colored Hall
 preserved silk fabrics, 84–85
See also Archeological silk
 Gradient correlation spectroscopy (gCOSY), 2D spectrum of cellulose acetate butyrate (CAB), 184*f*
- H**
- HETCOR experiment
 NMR technique, 167
See also Acrylonitrile copolymers
 Heteronuclear correlation spectra
 α -CD/PCL-polystyrene (PS) complex, 51*f*
 α -cyclodextrin(CD)/polycaprolactone(PCL) complex, 49*f*
 γ -CD/PCL complex, 50*f*
 γ -CD/PCL-PS complex, 53*f*
 Heteronuclear multiple bond correlation (HMBC)
 accordion and normal gradient HMBC (gHMBC) spectra of
 poly(2-ethylhexyl acrylate), 185–186, 188
 acid hydrolyzed ethylcellulose, 334*f*
 cellulose ether, 318*f*
 ethylcellulose, 330*f*
 experiment, 328
 poly(urethane)-based dendritic wedges, 154*f*, 156*f*, 160*f*, 163*f*
 Heteronuclear multiple quantum coherence (HMQC)
 acid hydrolyzed ethylcellulose, 334*f*
 cellulose ether, 319*f*
 ethylcellulose, 330*f*
 fluoropolymers, 131
 gradient HMQC (gHMQC) of poly(2-ethylhexyl acrylate), 180, 187*f*
 poly(1-phenyl-1-silabutane) (PPSB), 108*f*
 poly(dimethylsiloxane), 141, 143
 poly(urethane)-based dendritic wedges, 153*f*, 159*f*, 162*f*
 Heteronuclear single quantum coherence (HSQC)
 expansions from spectra of fluoropolymer, 133*f*
 experiment for fluoropolymers, 131, 134
 HSQC–TOCSY of poly(vinyl alcohol), 175, 176*f*
 method using pulsed field gradient (PFG) HSQC sequence, 125–126
 pulse sequence diagram for experiment, 132*f*
 1,1,2,3,3,3-Hexafluoropropylene. *See* Fluoropolymers
 High molecular weight polymers, solid state NMR, 37–38
 High performance liquid chromatography (HPLC)
 coupling with NMR, 383–384
See also On-line high performance liquid chromatography–NMR (HPLC–NMR)

High pressure, high resolution ^1H NMR, NMR method, 8

Homonuclear Hartmann–Hahn (HOHAHA)
acid hydrolyzed ethylcellulose, 335*f*
ethylcellulose, 331*f*
experiment, 328

HPP. *See* Poly(phosphazenes)

Human fetal cartilage, 2D NMR, 293–295

Hydrogen peroxide. *See* Poly(phenols)

Hydrolysis
glucomannan oligosaccharides by partial, 300*t*
See also Glucomannan polysaccharides

Hyperbranched structures, fractal forms of polyesters, 225

Hyphenated techniques, solution NMR, 5

I

INADEQUATE experiment
assignment of CH in poly(propylene), 197–199
selective irradiation overlapped to ^{13}C spectra of syndiotactic polypropylene, 200*f*
See also Poly(propylene)

Inclusion complexes (ICs). *See* Poly(ϵ -caprolactone) (PCL) and inclusion complexes (ICs)

Insoluble polymers. *See* Solid state NMR, high temperature

Intermolecular interactions
strength evaluations, 28–29
studying in composites, 30–31

Internal donors. *See* Propylene polymerization

Inverse HETCOR
NMR technique, 167
See also Acrylonitrile copolymers

Iso-propyl acrylate. *See* Polyacrylates

Isotopic labeling, solution NMR, 6

K

Keratan sulfates
architecture, 296
2D NMR of human fetal cartilage, 294*f*
enzymatic routes, 292
enzymes for fragmentation, 291–292
family classifications, 290
fingerprints from fragments, 292–293
functions within cartilage, 296
geographical features, 292–293
glycosaminoglycan (GAG) family, 289
hydrazinolysis approach, 292
NMR approaches, 290–291
non-destructive examination of intact, 291
regulation of three-dimensional order, 295–296
spectra from intact polymers, 293, 295
structural studies, 290–292

Kinetics. *See* Trioxane/1,3-dioxepane (TOX/DOP) copolymerization

Konjikido hall
preserved silk fabrics, 84–85
See also Archeological silk

Konnyaku flour
gelling, 298, 301, 305
glucomannan polysaccharides, 298–299

L

Length scales
phase separation, 45, 47
solid state NMR, 10

- Line shape analysis, polymer dynamics, 13
- Linkages. *See* Polysaccharides
- Liquid chromatography (LC). *See* On-line liquid chromatography–NMR (LC–NMR)
- Lithium trifluoromethanesulfonate (LiOTf). *See* Poly(phosphazenes)
- M**
- Magic angle spinning (MAS)
- advantages of MAS NMR
 - acquisition of polymeric materials, 41–42
 - effect of temperature on MAS–NMR spectra of polymers, 34
 - rigid and semi-rigid materials, 33
 - schematic, 36*f*
 - See also* Solid state NMR, high temperature
- Main-chain structure
- monomer sequences, 96–97
 - See also* Polymer characterization
- Maleic anhydride (MAH). *See* Copolymer characterization
- Malonates. *See* Polyesters
- Markovian model, statistical analysis of alginates, 388, 390–393
- Mass coelution effect, size exclusion chromatography (SEC) of copolymers, 360–361
- Matrix assisted laser desorption/ionization (MALDI) copolymer of styrene and methyl methacrylate, 372, 376*f*, 378
- method, 368
 - sensitivity, 360
 - See also* Copolymer characterization
- Me₂C(3-Me-cyclopentadienyl)(9-fluorenyl)ZrCl₂, poly(propylene), 195, 196
- Me₂C(cyclopentadienyl)(9-fluorenyl)ZrCl₂, poly(propylene), 195, 196
- Mechanistic study, poly(propylene) catalysis, 193
- MEEP. *See* Poly(phosphazenes)
- Methylalumoxane (MAO), poly(propylene), 195, 196
- Methylcellulose, substituted. *See* Cellulose ethers
- Methyl methacrylate (MMA). *See* Acrylonitrile copolymers, Copolymer characterization
- Methyl silsesquioxane
- comparing 2D exchange spectra of cross peaks with equilibrium spectra, 30*f*
 - matrix material, 23
 - preparation of low-k films, 26–27
 - solution and solid state NMR before and after heating, 25*f*
 - See also* Ethylene oxide/propylene oxide composites
- Microstructure, polyester features, 218–219
- Mitsunobu reaction
- azocellulose synthesis, 60
 - experimental conditions, 61–62
 - See also* Azocellulose polymers
- Model
- Markovian, for statistical analysis of alginates, 388, 390–393
 - refinement of molecular, for polyimides, 253, 256
 - two-site, 209, 214
 - See also* Polyimides; Propylene polymerization
- Model polymers, poly(propylene), 194–195
- Molar mass, estimates by NMR, 359
- Molecular modeling
- computer-assisted, 7
 - polysaccharides, 285
 - See also* Polyimides

Molecular weight. *See*

Polysaccharides

Morphology, polymer, NMR techniques, 12

Multidimensional NMR

development, 94–95

fluoropolymers, 131, 134

polymers, 5

N

¹⁵N labeled polyphosphazenes. *See*

Poly(phosphazenes)

Nano-NMR method, 8

Natural polymers, solution NMR, 9–10

NMR spectroscopy publications, 3–4

Nomenclature, chemical shift assignments, 313, 316

Nonad sequences. *See* Trioxane/1,3-dioxepane (TOX/DOP) copolymerization

Nuclear Overhauser enhancement (NOE), polyimides, 252–253, 254*f*

O

Oligostyrene

HPLC–NMR analysis, 339–340

NMR on-flow run of, 341*f*

NMR spectra at different retention times, 342*f*

One-dimensional exchange

spectroscopy by sideband alternation (ODESSA), 13

On-line gel permeation

chromatography–NMR (GPC–NMR)

α -methyl protons of poly(methyl methacrylate) (pMMA) and aromatic protons of styrene (Sty) as function of GPC retention time, 356*f*

chemical composition and microstructure as function of molecular weight distribution, 354–355

GPC of pMMA, pSty, and p(Sty-*b*-MMA) mixture, 354*f*

See also On-line liquid chromatography–NMR (LC–NMR)

On-line high performance liquid chromatography–NMR (HPLC–NMR)

complex polymer systems, 338, 343 experimental, 339

HPLC chromatogram of styrene–ethyl acrylate copolymers, 343*f*

HPLC method, 339

NMR method, 339

NMR of polystyrene at different retention times, 342*f*

NMR on-flow run of oligostyrene, 341*f*

oligostyrene, 339–340

opportunities, 338

power, 339

random styrene–ethyl acrylate copolymers, 340

samples, 339

technical grade poly(ethylene oxide), 339

On-line liquid chromatography–NMR (LC–NMR)

bipolar gradient pulses stimulated echo sequence (BPPSTE), 346–347

BPPSTE diffusion, 348, 350

BPPSTE sequence, 349*f*

characterization of complex mixtures, 346

compositions and blockiness of various polymer mixtures, 352–353

experimental, 347–348

instrumentation, 347–348

material, 347

- mixture of poly(methyl methacrylate) (pMMA), poly(styrene-*b*-MMA) (p(Sty-*b*-MMA)), and pSty, 350–353
- proton NMR spectra of mixture of pMMA, poly(butyl acrylate) (pBA), and p(BA-*b*-MMA) block copolymer before and after BPPSTE solvent suppression, 349*f*
- pulsed field gradients (PFG) NMR solvent suppression approach, 355, 357
- reverse phase HPLC of mixture of pMMA, pBA, p(MMA/BA) and p(BA-*b*-MMA), 352*f*
- reverse phase HPLC of pMMA, pSty, p(Sty-*b*-MMA), 351*f*
- shortcoming of PFG NMR, 355
- stop-flow LC–NMR of pMMA, pBA, p(MMA/BA), and p(BA-*b*-MMA) mixture, 353*f*
- stop-flow LC–NMR of pMMA, pSty, and p(Sty-*b*-MMA) mixture, 351*f*
- WET approach, 346, 348
- WET approach vs. PFG NMR approach, 355, 357
- See also* On-line gel permeation chromatography–NMR (GPC–NMR)
- Oxidative coupling, phenolic monomers, 260
- P**
- Pentad sequences. *See* Trioxane/1,3-dioxepane (TOX/DOP) copolymerization
- Peptides, flexibility, 273, 274*f*
- Peroxides. *See* Poly(phenols)
- Phase coherence of spins, dissipation processes, 34
- Phenol
- ¹H NMR spectra of reaction mixture after H₂O₂ addition, 263*f*
- ¹H NMR spectra of reaction mixture before and after H₂O₂ addition, 262*f*
- polymerization, 260–264
- possible dimers from oxidative coupling, 261
- See also* Poly(phenols)
- Phosphazenes. *See* Poly(phosphazenes)
- Polyacrylates
- autocorrelation function, 401
- characterization of segmental motion, 399
- correlation time results as function of concentration and temperature, 406*f*, 407*f*
- deuterium labels on methine position for poly(ethyl acrylate) (PEA-*d*₁), poly(*iso*-propyl acrylate) (PIPA-*d*₁), and poly(*n*-butyl acrylate) (PNBA-*d*₁), 400
- deuterium NMR relaxation times, 399
- energies of activation for, as function of composition, 407*f*
- equations for relaxation times, 400–401
- experimental, 400
- fitting relaxation times to log-normal distribution of correlation times, 402
- relaxation behavior for PEA-*d*₁ as function of concentration, 403*f*
- relaxation behavior for PIPA-*d*₁ as function of concentration, 404*f*
- relaxation behavior for PNBA-*d*₁ as function of concentration, 405*f*
- relaxation in concentrated solutions, 399
- relaxation time measurements for deuterated PEA, PIPA, and PNBA, 401–402
- spectral density, 401
- synthesis with deuterium labels, 400

- Polybutadiene, Sn-containing chain ends, 113, 114*f*
- Poly(butyl acrylate) (pBA). *See* On-line liquid chromatography–NMR (LC–NMR)
- Poly(butyl methacrylate-*co*-2-ethylhexyl acrylate), magic angle spinning (MAS) proton-proton COSY, 40*f*
- Poly(butyl methacrylate) copolymers, chemical shifts, assignments, and relaxation times, 181*t*
- Poly(ϵ -caprolactone) (PCL) and inclusion complexes (ICs) comparing $T_{1\rho}(^1\text{H})$ relaxation times for PCL- α CD/IC and PCL- γ CD/IC, 47*t*
- CP/MAS spectra of PCL, PCL- α -CD, and α -CD, 46*f*
- diblock PCL-polystyrene (PS) ICs with α - and γ -CD, 48, 52
- 2D WIM/WISE experiments studying molecular dynamics, 54–55
- dynamic behavior of inclusion complexes, 54, 58
- experimental, 44–45
- heteronuclear correlation spectrum for α -CD/PCL complex, 49*f*
- heteronuclear correlation spectrum for α -CD/PCL-PS complex, 51*f*
- heteronuclear correlation spectrum for γ -CD/PCL complex, 50*f*
- heteronuclear correlation spectrum for γ -CD/PCL-PS, 53*f*
- ICs of α -cyclodextrins (CD) and γ -CD with PCL, 45
- length scale of phase separation, 45, 47
- materials, 44
- PCL-poly(ethylene oxide)-PCL chains in γ -CD channels vs. α -CD/IC channels, 55
- proton line widths for α -CD, γ -CD, PCL and ICs, 55*t*
- proton line widths for each PCL methylene carbon in PCL- α -CD-IC, 56*f*
- solid-state heteronuclear correlation experiment, 47–48
- solid state NMR spectroscopy, 44–45
- structure of PCL-PS diblock, 52
- $T_1(^{13}\text{C})$ values for α -CD, γ -CD, PCL and ICs, 54*t*
- Poly(1-chloro-1-fluoroethylene) slices from triple resonance 3D chemical shift correlation spectrum, 106*f*
- triple resonance 3D NMR, 104–105
- Poly(1-chloro-1-fluoroethylene-*co*-isobutylene) monomer sequences, 96–97
- one dimensional NMR spectra, 97*f*
- Poly(dimethylsiloxane) (PDMS) applications and properties, 138
- chemical shift assignments for $\text{MD}_3\text{M}^{\text{H}}$, 145*t*
- 1D NMR method, 139
- 1D NMR spectra, 140–141
- 2D NMR method, 139–140
- 2D NMR spectra, 141, 143
- 2D PFG–HMQC NMR spectra of $\text{MD}_3\text{M}^{\text{H}}$, 143*f*
- 3D NMR method, 140
- 3D NMR spectrum, 143
- experimental, 139–140
- NMR for structural analyses, 138
- nomenclature for defining, 138
- one-dimensional ^1H , ^{13}C , and ^{29}Si NMR spectra of $\text{MD}_3\text{M}^{\text{H}}$, 142*f*
- slices from 3D $^1\text{H}/^{13}\text{C}/^{29}\text{Si}$ spectrum of $\text{MD}_3\text{M}^{\text{H}}$, 144*f*
- structure of $\text{MD}_3\text{M}^{\text{H}}$, 139
- triple resonance, 138, 145
- Polyesters
acid-fringed fractal, 226

- ¹³C NMR shifts of glyceryl residues of malonate oligomers, 221*t*
- ¹³C NMR spectrum of acetate-fringed fractal, 227*f*
- ¹³C NMR spectrum of oligomers of erythritol and dimethyl malonate, 224*f*
- ¹³C NMR spectrum of oligomers of succinic anhydride and *meso*-erythritol, 224*f*
- ¹³C NMR spectrum of sample from glycerol and dimethylmalonate reaction, 221*f*
- ¹³C NMR spectrum of succinic acid-fringed fractal, 227*f*
- chemical shift parameters for substitutions at sites of glycerol, erythritol and adonitol, 225*t*
- chemistry for ester links, 217
- erythritol–malonic ester system, 222–223
- erythritol–succinate system, 223, 224*f*
- esterification reactions, 219
- experimental, 219
- fractal forms, 225–226
- glycerol–dimethyl malonate system, 220
- higher glycerol methyl malonate oligomers, 219
- hyperbranched structures, 225
- microstructure features, 218–219
- NMR spectral method, 219
- oligomer series, 223, 225*t*
- oligomeric malonic esters of erythritol, 222
- oligomers of glycerol and succinic acid, 218
- pattern of substitution, 218
- reaction of fractal with succinic anhydride, 226
- step growth polymerization, 217
- succession of glycerol oligomers in reaction with excess succinic anhydride, 218
- Polyethylene
- coherence selection, 101–102
- heteronuclear multiple bond correlation (HMBC) spectra, 101*f*
- Poly(ethylene oxide) (PEO)
- HPLC–NMR analysis, 339
- See also* Poly(ϵ -caprolactone) (PCL) and inclusion complexes (ICs)
- Poly(2-ethylhexyl acrylate)
- accordion 2D spectrum, 187*f*
- chemical shifts, assignments, and relaxation times, 181*t*
- gradient heteronuclear multiple quantum correlation (gHMQC) spectrum, 180, 187*f*
- Polyimides
- atomic bond distances for structure of BZP-TPM repeating unit after geometry optimization, 255*t*
- ¹³C NMR chemical shifts in solution, 250*t*
- conformational analysis, 247, 250–252
- equation for internuclear distance, 256
- experimental, 243, 246
- ¹H and ¹³C NMR spectroscopy, 246–247
- high-temperature polycondensation of diaminotriphenylmethane (DA-TPM) and aromatic dianhydrides, 243
- ¹H NMR chemical shifts in solution, 247*t*
- ¹H NMR spectrum of BZP-TPM, 248*f*, 249*f*
- model compound synthesis, 243
- molecular structure of minimum-energy conformers for PM-TPM and BZP-TPM, 251*f*
- NMR measurements, 246
- nuclear Overhauser enhancement (NOE) difference spectrum of BZP-TPM, 252–253, 254*f*
- preparation, 242–243

- refinement of model for, 253, 256
 structures of model and, 244*f*, 245*f*
 synthesis, 243
 theoretical calculations, 246
 torsion angles for model compound
 and repeating units, 252*t*
- Polymer characterization
 chain-end structure, 95, 113, 116,
 118
 coherence selection using pulsed
 field gradients (PFG), 101–102
 1D NMR spectra of poly(1-phenyl-1-
 silabutane) (PPSB), 107*f*
 2D experiments in literature, 99–100
 2D NMR spectra of polystyrene with
 phosphorus-containing chain ends,
 116*f*
 3D NMR experiment with C to Si
 coherence transfer delays, 110,
 112*f*
 diagram of relative intensities of
 different NMR signal components,
 100*f*
 double resonance 3D NMR
 experiments, 102–103
 factors determining feasibility of
 experiments, 104
 ^1H - ^{29}Si 2D heteronuclear multiple
 quantum coherence (HMQC)
 spectrum of PPSB, 108*f*
 heteronuclear multiple bond
 correlation (HMBC) spectra of
 polyethylene, 101*f*
 illustration of ^1H , ^{13}C and ^{31}P (HCP)
 3D NMR spectrum of phosphorus-
 containing chain-end structures,
 117*f*
 intensity of signals, 100–101
 main-chain structure, 96–97
 main-chain structure, monomer
 sequence, and stereosequence,
 104–105, 107, 110
 most probable structures from
 polymerization of isobutylene and
 1-chloro-1-fluoroethylene, 96*t*
- NMR as valuable tool, 94–95
 NMR spectra of poly(1-chloro-1-
 fluoroethylene) (PCFE), 105*f*
 one-dimensional HCP NMR spectra
 of phosphorus-containing chain-
 end structures, 115*f*
 one-dimensional NMR spectra of
 poly(1-chloro-1-fluoroethylene-
 co-isobutylene) (PCFEI), 97*f*
 pulse sequence diagram for triple
 resonance 3D NMR, 103*f*
 pulse sequence diagrams for 3D
 H(CA)P-CC-TOCSY and HCCH
 experiments, 119*f*
 relative stereochemistries in meso
 and racemic dyad and triad
 structures, 97*f*
 resonance assignments for
 phosphorus-containing chain-ends
 of polymer, 120*f*
 schematic of nD-NMR experiments,
 98*f*
 schematic of steps in producing 2D-
 NMR spectrum, 99*f*
 second pulse sequence (HCCH)
 providing detection of 2D-
 INADEQUATE spectra, 118, 119*f*
 slice of HCP, H(CA)P-CC-TOCSY
 and HCCH experiments, 120*f*
 slices from 3D NMR spectrum of
 PPSB, 109*f*
 slices from HCSi 3D NMR spectrum
 of carbosilane dendrimer using
 coherence transfer delays, 110,
 112*f*
 slices from HCSn 3D NMR spectrum
 of *n*-Bu₃Sn-terminated
 polybutadiene, 114*f*
 slices from triple resonance HCF 3D
 chemical shift correlation
 spectrum, 106*f*
 solution NMR, 4–5
 structure identification, 95
 structure of second generation
 carbosilane based dendrimer, 111*f*

- three dimensional NMR spectroscopy, 102–104
- two dimensional NMR, 98–101
- Polymer dynamics, NMR techniques, 12–13
- Polymer mixtures. *See* On-line gel permeation chromatography–NMR (GPC–NMR); On-line liquid chromatography–NMR (LC–NMR)
- Polymer morphology, NMR techniques, 12
- Polymer reactions, solution NMR, 10
- Polymer structure and conformation, NMR techniques, 11–12
- Polymerization
step growth, 217
See also Polyesters; Poly(phenols); Propylene polymerization
- Polymers
NMR literature, 3–4
 T_1 minima in viscous or viscoelastic state, 41*f*
See also On-line high performance liquid chromatography–NMR (HPLC–NMR)
- Poly(methyl methacrylate) (PMMA).
See Methyl methacrylate (MMA); On-line liquid chromatography–NMR (LC–NMR)
- Polypeptides. flexibility, 273, 274*f*
- Poly(phenols)
concerns, 259
coupling mechanism, 259
experimental, 259–260
 ^1H NMR spectra of phenol reaction mixture after H_2O_2 addition, 263*f*
 ^1H NMR spectra of phenol reaction mixture before and after H_2O_2 addition, 262*f*
 ^1H NMR spectra of *p*-sulfonated phenol reaction mixture before and after H_2O_2 addition, 264*f*
 ^1H NMR spectrum of *p*-cresol mixture after H_2O_2 addition, 268*f*
oxidative coupling reaction of phenolic monomers, 260
peroxidase-catalyzed polymerization of phenol, 259
plots of residual monomer and peak integrals as function of H_2O_2 , 265*f*
polymerization of *p*-cresol, 266–267
polymerization of phenol, 260–264
polymerization of *p*-sulfonated phenol, 264–266
possible dimers from oxidative coupling of phenol, 261
residual monomer and dimers as function of H_2O_2 , 268*f*
schematic of enzymatic polymerization, 260
structural characterization, 259
- Poly(1-phenyl-1-silabutane) (PPSB)
one dimensional NMR spectra, 107*f*
triple resonance 3D–NMR, 107, 108*f*, 109*f*
- Poly(phosphazenes)
change in ^{13}C NMR chemical shifts for ^{15}N MEEP (poly[bis(2-(2-methoxyethoxy)ethoxy)phosphazene]) after lithium ion complexation, 415*f*
change in ^{15}N NMR chemical shifts for ^{15}N MEEP after lithium trifluoromethanesulfonate (LiOTf) addition, 416*f*
change in ^{31}P NMR chemical shifts for ^{15}N poly[[(2-allylphenoxy) $_{0.12}$ (4-methoxyphenoxy) $_{1.02}$ (2-(2-methoxyethoxy)ethoxy) $_{0.86}$] phosphazene] (^{15}N HPP) with increasing LiOTf, 417*f*
change in ^{31}P NMR chemical shifts for ^{15}N MEEP after LiOTf addition, 415*f*
characterization of ^{15}N HPP, 412–413
 ^{13}C NMR peak assignment for ^{15}N MEEP, 413, 414*f*

- ^{13}C NMR room temperature spin-lattice relaxation times of ^{15}N MEEP, 414*f*
- ^{13}C NMR $T_{1\text{min}}$ values of ^{15}N MEEP before and after LiOTf complexation, 418*t*
- experimental, 410–411
- ion conducting of MEEP, 410
- materials, 410–411
- ^{15}N MEEP/LiOTf complexes, 413–416
- ^{15}N NMR spectrum of ^{15}N HPP after LiOTf addition, 417*f*
- ^{15}N NMR spectrum of ^{15}N MEEP, 412*f*
- ^{15}N NMR spin-lattice relaxation times of ^{15}N MEEP before and after lithium ion complexation, 419*f*
- NMR characterization, 411–413
- NMR spectroscopy method, 410
- ^{31}P NMR spin-lattice relaxation times of ^{15}N MEEP before and after lithium ion complexation, 419*f*
- synthesis of ^{15}N labeled, 411
- temperature dependence of spin-lattice relaxation, 416, 418
- Poly(propylene)
- assignment of CH, 197–199
- catalyst systems, 195, 196
- chain ends and terminations, 206
- CH–CH₃ region of INADEQUATE 2D NMR, 198*f*
- chemical shift values of ^{13}C
- resonances of terminal units, 206*t*
- choice of model polymers, 194–195
- ^{13}C NMR spectrum of low molecular weight, 204*f*, 205*f*
- 2D selective INADEQUATE spectra by selective irradiation overlapped to ^{13}C spectra of syndiotactic, 200*f*
- experimental, 193–194
- high field ^{13}C spectra, 199
- indirect mechanistic study, 193
- mechanistic study of catalysts, 193
- methine region of ^{13}C NMR spectra, 201*f*
- methine region of ^{13}C NMR spectrum of regioregular syndiotactic, 200*f*
- methyl region of ^{13}C NMR spectra, 202*f*, 203*f*
- methyl region of ^{13}C NMR spectrum, 195*f*
- methylene region of ^{13}C NMR spectra, 201*f*
- microstructure, 209
- proton magic angle spinning (MAS) NMR, 38*f*
- relaxation times in undegassed, 194*t*
- rotational isomeric state (RIS) approximation, 196
- rules of assignments of CH₃ and CH₂, 196–197
- statistical analysis of stereostructure, 193
- See also* Propylene polymerization
- Polysaccharides
- comparing relaxed maps for alanine dipeptide and disaccharide, 274*f*
- comparison of ^1H NMR spectra for three high molecular weight bacterial, 276*f*, 277*f*
- complications in complete structure determination by NMR, 275
- flexibility and internal motion of second kind, 278–279
- flexibility of high molecular weight, 279, 282
- flexibility of polypeptides vs., 273, 274*f*
- heptasaccharide subunit of, of *Streptococcus mitis*, 281*f*
- hexasaccharide subunit of capsular, of *Vibrio cholerae*, 280*f*
- ^1H NMR spectrum of, from *S. pneumoniae*, 277*f*
- ^1H NMR spectrum of, from *S. mitis*, 276*f*

- ^1H NMR spectrum of, from *V. cholerae*, 276*f*
- Lewis tetrasaccharide epitope, 280*f*
- methods for determining detailed models, 282
- methods for more flexible, 284–285
- molecular modeling, 285
- monomer sequence distribution, 382–383
- nature of flexibility, 272–273, 275, 278
- physical properties, 275
- residual dipolar coupling, 282–284
- rigid linkages and internal motion of first kind, 278
- scalar coupling, 286
- See also Alginates; Glucmannan polysaccharides (GP)
- Polystyrene (PS)
- chain end analysis, 113, 116
- HPLC–NMR analysis of oligostyrene, 339–340
- NMR on-flow run of oligostyrene, 341*f*
- NMR spectra at different retention times, 342*f*
- one-dimensional ^1H , ^{13}C , and ^{31}P NMR of, with phosphorus-containing chain ends, 115*f*
- pulse sequence diagrams for 3D experiments, 119*f*
- resonance assignments for phosphorus-containing chain ends, 118, 120*f*
- three-dimensional NMR of, with phosphorus-containing chain ends, 117*f*
- two-dimensional NMR of, with phosphorus-containing chain ends, 116*f*
- See also On-line liquid chromatography–NMR (LC–NMR); Poly(ϵ -caprolactone) (PCL) and inclusion complexes (ICs)
- Polyurethane-based dendritic wedges
- 1st, 2nd, and 3rd generation wedges, 149
- ^{13}C 1D NMR spectrum of partial structure 2, 158*f*
- ^{13}C NMR spectrum of partial structure 3, 162*f*
- ^{13}C NMR spectrum of partial structure 1, 152*f*
- chemical shift assignments for 1, 2, and 3, 164*t*
- 1D NMR experiments, 150
- 2D heteronuclear multiple bond correlation (HMBC) experiment, 153–154
- 2D heteronuclear multiple quantum coherence (HMQC) correlations, 153
- 2D NMR experiments, 150
- dendrimer synthesis, 149
- expansions of aliphatic regions from HMBC spectrum of 1, 156*f*
- experimental, 148, 150
- ^1H - ^{13}C PFG-HMBC 2D NMR spectrum of 2, 160*f*
- ^1H - ^{13}C PFG-HMBC 2D NMR spectrum of 3 expansions, 163*f*
- ^1H - ^{13}C PFG-HMQC 2D NMR spectrum of 2, 159*f*
- ^1H - ^{13}C PFG-HMQC 2D NMR spectrum of 3 expansions, 162*f*
- ^1H 1D NMR spectrum and partial structure 1, 151*f*
- ^1H 1D NMR spectrum and partial structure 2, 157*f*
- ^1H NMR spectrum of 3, 161*f*
- NMR measurements, 148, 150
- partial structures 1, 2, and 3, 149
- PFG–HMBC 2D NMR spectrum of partial structure 1, 154*f*
- PFG–HMQC 2D NMR spectrum of partial structure 1, 153*f*
- unique properties of dendrimers, 148
- Poly(vinyl alcohol)

experimental, 175
 heteronuclear single quantum
 coherence–total correlated
 spectroscopy (HSQC–TOCSY)
 spectrum, 175, 176*f*
 methine carbon crosspeaks and
 corresponding pentads, 177*t*
 peak assignments, 175, 177
 preparation, 175
 Preserved silk. *See* Archeological silk
 Propylene oxide. *See* Ethylene
 oxide/propylene oxide composites
 Propylene polymerization
 catalyst preparation, 209
 catalysts and internal donors,
 211*t*
¹³C NMR measurements, 210
 effects of internal and external
 donors on α parameter, 210
 effects of internal and external
 donors on ω parameter, 214
 experimental, 209–210
 external and internal donors, 209
 microstructure of polypropylene,
 209
 polymerization results, 211*t*
 procedure, 210
 relationship between α and molar
 ratio of internal donor to Ti (iD/Ti)
 in solid catalyst, 212*f*
 relationship between ω and iD/Ti in
 solid catalyst, 212*f*, 213*f*
 two-site model, 209, 214
See also Poly(propylene)
iso-Propyl acrylate. *See* Polyacrylates
 Proteins, addition to glucomannan
 polysaccharides, 301
 Publications, NMR spectroscopy,
 3–4
 Pullulan
 calibration curve, 387*f*
See also Alginates
 Pulsed field gradients (PFG),
 coherence selection, 101–102

R

Random copolymers. *See* Copolymer
 characterization
 Reactions, NMR for polymer, 10
 Relaxation studies
 equations for relaxation times, 400–
 401
 polymer solutions, 7–8
 times for various polymers, 180, 182
See also Polyacrylates
 Reviews, NMR spectroscopy, 3–4
 Rheo-NMR method, 8
 Rigid polymers
 magic angle spinning (MAS) NMR,
 38*f*
 NMR measurements, 33
 Rigidity, polysaccharides, 278
 Ring-opening polymers, solution
 NMR, 9
 Rotational-echo double resonance
 (REDOR), NMR technique, 12
 Rotational isomeric state (RIS),
 calculating chemical shift, 196

S

Saccharides. *See* Polysaccharides
 Scalar coupling, polysaccharides,
 286
 Segmental dynamics
 molecular motion in polymer
 solutions, 399
See also Polyacrylates
 Semi-crystalline polymer, NMR
 analysis, 40–41
 Semi-rigid polymers
 magic angle spinning (MAS) NMR,
 38*f*
 NMR measurements, 33
 Sequences. *See* Trioxane/1,3-
 dioxepane (TOX/DOP)
 copolymerization

- Silicon. *See* Poly(dimethylsiloxane) (PDMS)
- Silk
 structure and formation, 71–72
See also Archeological silk; *Bombyx mori* silk fibroin
- Simulations, polysaccharides, 285
- Size exclusion chromatography (SEC)
 configuration, 359
 COPOFRAC computer program, 363
 copolymer of styrene and methyl methacrylate, 372, 374*f*, 375*f*
 coupling with NMR, 383–384
 fractionation method, 364
 hyphenated NMR analysis, 394
 mass coelution effect for copolymers, 360–361
 measurement of alginates, 384–385
 NMR as detector, 359
 off-line SEC–NMR, 359, 360
 pullulan calibration curve, 387*f*
 theory, 361–363
See also Copolymer characterization
- Solid state NMR
 experimental techniques, 11–13
 length scales, 10
 line shape analysis, 13
 secondary or tertiary of polymers, 11
 structure and dynamics of polymers, 10–11
 techniques for polymer dynamics, 12–13
 techniques for polymer morphology, 12
 techniques for polymer structure and conformation, 11–12
See also Ethylene oxide/propylene oxide composites
- Solid state NMR, high temperature
 advantages of magic angle spinning (MAS) NMR acquisition in polymeric materials, 41–42
 broadening NMR spectral resonances, 36
 chemical shift anisotropy (CSA), 35–36
 crosslinked insoluble amorphous polymer, 39–40
 crosslinked polymers, 37–38
 crystallinity and morphology of insoluble materials, 37
 dissipation of phase coherence of spins, 34
 experimental, 33
 FT–NMR and magic angle spinning (MAS), 34–36
 high molecular weight polymers, 37–38
 lab frame orientation dependent chemical shift anisotropy (CSA), 35*f*
 Larmor frequency, 35
 line narrowing under MAS and high temperature, 39
 low variable temperature (VT) gas flow rate, 41
 magic angle spinning (MAS), 36*f*
 MAS NMR of polymers in various physical states, 38*f*
 MAS proton-proton COSY of poly(butyl methacrylate-*co*-2-ethylhexyl acrylate), 40*f*
 NMR spectra of amorphous polymer at various temperatures, 39*f*
 process of generating free induction decay (FID) in FT–NMR, 34*f*
 proton MAS NMR of poly(propylene), 38*f*
 semi-crystalline polymer, 40–41
 spin diffusion processes, 36
 T₁ minima in viscous or viscoelastic state, 41*f*
- Solubility, *Bombyx mori* silk fibroin in water, 77–79
- Solution NMR
 addition polymers, 9
 application areas, 8–10
 chemical shift predictions, 8
 chemical shifts, 33

- computer-aided methodologies, 7
- condensation polymers, 9
- diffusion measurements, 8
- high pressure and resolution, 8
- hyphenated techniques, 5
- isotopic labeling, 6
- microstructure of alginates, 383
- multidimensional NMR, 5
- nano-NMR, 8
- natural polymers, 9–10
- polymer analysis, 4–5
- polymer reactions, 10
- relaxation studies, 7–8
- rheo-NMR, 8
- ring-opening polymers, 9
- structure, 10–11, 37
- structure formation and intermolecular interactions in composites, 30–31
- theoretical modeling, 6–7
- See also* Ethylene oxide/propylene oxide composites
- Spin diffusion, processes, 36
- Spin-lattice relaxation temperature dependence, 416, 418
- See also* Poly(phosphazenes)
- Step growth polymerization, polyesters, 217
- Stereochemical structure
- 2D NMR techniques, 174–175
- See also* Poly(vinyl alcohol)
- Stereostructure, poly(propylene), 193
- Streptococcus mitis*, ^1H NMR spectrum of polysaccharide, 275, 276f
- Streptococcus pneumoniae*, ^1H NMR spectrum of polysaccharide, 275, 277f
- Structure
- ^{13}C NMR spectroscopy, 217
- complications of, determination of polysaccharides, 275
- fluoropolymers, 126–127
- microstructural features of polyesters, 218–219
- NMR techniques, 11–12, 138
- relative stereochemistries in meso and racemic dyad and triad structures, 97f
- solution NMR, 10–11, 37
- studying formation in composites, 30–31
- See also* *Bombyx mori* silk fibroin; Polymer characterization
- Styrene. *See* Copolymer characterization; Oligostyrene; Polystyrene (PS)
- Styrene–ethyl acrylate copolymers
- HPLC chromatogram, 343f
- HPLC–NMR of random, 340
- Substitution, pattern in polyesters, 218
- Succinic acid. *See* Polyesters
- Succinic anhydride. *See* Polyesters
- Sulfates, keratan. *See* Keratan sulfates
- p*-Sulfonated phenol polymerization, 264–266
- See also* Poly(phenols)
- Surface relief gratings (SRGs)
- atomic force microscopy (AFM) images of SRGs on azocellulose polymer films, 68f, 69f
- azocellulose films, 59, 67
- fabrication method, 61
- See also* Azocellulose polymers
- T**
- Temperature. *See* Solid state NMR, high temperature
- Terminations, poly(propylene), 206
- Theoretical modeling, solution NMR, 6–7
- Theory, size exclusion chromatography (SEC), 361–363
- Three-dimensional NMR
- double resonance, 102–103
- experiment construction, 102–104
- factors determining feasibility, 104
- polymers, 5

- polystyrene with phosphorus-containing chain ends, 116, 117*f*, 118, 120*f*
- pulse sequence diagram for triple resonance, 103*f*
- spectrum of poly(dimethylsiloxane), 143, 144*f*
- techniques for studying structure, 138
- See also* Poly(dimethylsiloxane) (PDMS); Polymer characterization
- Torsion angles, polyimides, 252*t*
- Total correlated spectroscopy (TOCSY)
- cellulose acetate butyrate (CAB), 184*f*
- heteronuclear single quantum coherence (HSQC)–TOCSY of poly(vinyl alcohol), 175, 176*f*
- NMR technique, 167
- See also* Two-dimensional NMR of polymers
- Triblock copolymers. *See* Ethylene oxide/propylene oxide composites
- Trifluoroacetic acid (TFA), ethylcellulose hydrolysis, 326
- Trioxane/1,3-dioxepane (TOX/DOP) copolymerization
- assignment of pentad sequences, 231–232
- ¹³C NMR spectra as function of time, 234*f*, 235*f*
- cationic copolymerization, 229, 230
- experimental, 230–231
- kinetic experiments, 231
- kinetic profiles of pentad sequences and central carbon of CH₂CH₂CH₂CH₂O co-unit, 236*f*
- kinetic study of initiating mechanism, 232–233, 237
- literature, 229
- materials, 230
- microstructure by NMR, 229
- NMR measurements, 230–231
- nonad sequences, 237–240
- nonad sequences as function of time, 238*f*
- procedure, 230
- proton and carbon chemical shifts of pentad sequences of TOX/DOP and TOX/DOL (dioxolane), 232*t*
- reaction, 229
- Triple resonance. *See* Fluoropolymers; Poly(dimethylsiloxane) (PDMS); Polymer characterization
- Tri-substituted cellulose ethers. *See* Cellulose ethers
- Tritylcellulose, substituted. *See* Cellulose ethers
- Two-dimensional NMR
- experiments, 98–99
- intensity of signals, 100–101
- keratan sulfates, 293–295
- literature, 99–100
- method for studying poly(dimethylsiloxane), 139–140
- polymers, 5
- schematic, 98*f*, 99*f*
- spectra of poly(dimethylsiloxane), 141, 143
- stereochemical structures, 174–175
- structures, 180
- See also* Acrylonitrile copolymers; Ethylcellulose (EC); Polymer characterization; Poly(vinyl alcohol)
- Two-dimensional NMR of polymers
- accordion and normal gradient heteronuclear multiple bond correlation (gHMBC) spectra of poly(2-ethylhexyl acrylate) (II), 185–186, 187*f*
- accordion 2D spectrum of (II), 187*f*
- assignments, 180–182
- chemical shifts, assignments and relaxation times for cellulose acetate butyrate (CAB, I), (II) and *i*-butyl/*n*-butyl methacrylate copolymers (III), 181*t*

2D gradient correlated spectroscopy (gCOSY) spectrum of CAB, 184*f*
 2D gradient heteronuclear multiple quantum coherence (gHMQC) spectrum of (II), 187*f*
 2D total correlated spectroscopy (TOCSY) spectrum of CAB, 184*f*, 185*f*
 heteronuclear correlation experiments, 183, 185–188
 homonuclear correlations, 182–183
 relaxation times, 180, 182
 signal/noise of long range gHMBC or accordion type intensities in copolymer (III), 186*t*
 signal/noise of long range gHMBC or accordion type intensities in (II), 186*t*
 Two-site model parameters, 214, 219
See also Propylene polymerization

U

Ultra low dielectric constant. *See* Ethylene oxide/propylene oxide composites

Unswellable polymers. *See* Solid state NMR, high temperature

V

Vibrio cholerae, ¹H NMR spectrum of polysaccharide, 275, 276*f*
 Viscous polymers, magic angle spinning (MAS) NMR, 38*f*
 Viscous state, T₁ minima, 41*f*

W

Wideline separation NMR (WISE), 2D experiment, 13

Z

Ziegler–Natta catalysts, poly(propylene), 193